STUDIA UNIVERSITATIS
BABEŞ-BOLYAI

UNIVERSITATEA BABEŞ-BOLYAI
BABEŞ-BOLYAI TUDOMÁNYEGYETEM
BABEŞ-BOLYAI UNIVERSITÄT
BABEŞ-BOLYAI UNIVERSITY
TRADITIO ET EXCELLENTIA

BIOLOGIA

Volume 70 (2025), June, No. 1/2025

STUDIA
UNIVERSITATIS BABEŞ-BOLYAI
BIOLOGIA

1 / 2025
January – June

EDITORIAL BOARD
STUDIA UNIVERSITATIS BABEŞ-BOLYAI BIOLOGIA

YEAR **Volume 70 (LXX), 2025**
MONTH **JUNE**
ISSUE **1**

PUBLISHED ONLINE: 2025-06-25
ISSUE DOI: 10.24193/subbbiol.2025.1
ISSN (online): 2065-9512
https://studiabiologia.reviste.ubbcluj.ro/

STUDIA UNIVERSITATIS BABEŞ-BOLYAI

BIOLOGIA

1

SUMAR – CONTENT – SOMMAIRE – INHALT

All authors are responsible for submitting manuscripts in comprehensible US or UK English and ensuring scientific accuracy.

Original picture on front cover:
A juvenile ball python (*Python regius*, Shaw 1802) © Cristina Craioveanu.

STUDIA UNIVERSITATIS BABEŞ-BOLYAI BIOLOGIA, 70, 1, 2025 (p. 7-18)
doi:10.24193/subbbiol.2025.1.01

Fumed silica-coated magnetic particles: DNA extraction application

Stanley Evander Emeltan Tjoa[1,4], Mudasir Mudasir[2], Edi Suharyadi[3], Budi Setiadi Daryono[1]✉

[1]Department of Tropical Biology, Universitas Gadjah Mada, Yogyakarta, Indonesia;
[2]Department of Chemistry, Universitas Gadjah Mada, Yogyakarta, Indonesia;
[3]Department of Physics, Universitas Gadjah Mada, Yogyakarta, Indonesia;
[4]Konimex Diagnostic Center, PT Konimex, Solo, Indonesia.
✉***Corresponding author, E-mail: bs_daryono@mail.ugm.ac.id.***

Article history: Received 15 January 2025; Revised 03 March 2025; Accepted 11 March 2025; Available online 25 June 2025

Abstract. Tetraethyl orthosilicate (TEOS) is widely used for preparing magnetic particles in DNA extraction kits, but it poses toxicity and safety concerns. To address this issue, we developed magnetic particles using fumed silica as a safer alternative to TEOS for magnetite particle preparation for DNA extraction. The method effectively extracts DNA from various biological matrices, including urine, serum, saliva, sputum, whole blood, and plasma, without detectable inhibitors. The extracted DNA is suitable for downstream molecular applications such as qPCR and sequencing. The proposed magnetic particles with fumed silica not only reduce chemical hazards but also provide a safer, efficient, and reliable method for routine DNA extraction in molecular biology laboratories.

Keywords: DNA extraction, fumed silica, magnetite

Introduction

DNA extraction is a routine procedure that has become essential in various molecular laboratories. The demand for DNA extraction kits has risen due to the need for a straightforward, simple procedure that can handle a wide range of samples. Many available kits are based on spin-column and magnetic

nanoparticle technologies, which offer reliable and efficient solutions for DNA extraction. Spin-column kits utilize a silica membrane to bind DNA, while magnetic nanoparticle kits use magnetic particles to isolate DNA.

Unlike spin-column kits, those using magnetic nanoparticles require relatively lower energy, as they utilize magnetic force to separate DNA from impurities. Besides magnetic nanoparticles, the materials used include coating agents to prevent Fe_3O_4 from oxidizing into Fe_2O_3, which has weaker ferromagnetic properties (Dzeranov *et al.,* 2023). Tetraethyl Orthosilicate (TEOS) is the most commonly used coating agent (Fan *et al.,* 2019; Torres-Rodríguez *et al.,* 2019; Alghuthaymi, 2020; Nguyen *et al.,* 2022; Firoozeh *et al.,* 2023).

TEOS has irritating properties to the eyes and respiratory tract, as stated in its material safety data sheet. TEOS serves as a source of silica. Another source of silica that lacks these irritant properties is fumed silica. Fumed silica is produced from the hydrolysis of silicon tetrachloride by forced evaporation with combustion (Flörke *et al.,* 2012). Consequently, fumed silica could be a safer alternative to TEOS.

This study aims to test fumed silica-coated magnetic particles for DNA extraction from various matrices, including serum, urine, saliva, sputum, whole blood, and plasma, and to evaluate the suitability of the extracted DNA for sequencing procedures.

Materials and methods

Material

The materials used in this study included $FeSO_4$ and $FeCl_3$ as precursors; tetraethyl orthosilicate (TEOS), ammonia solution, NaOH, Tris, and EDTA from Merck (Darmstadt, Germany); fumed silica from Wacker (Nünchritz, Germany); Triton-X from Vivantis (Selangor, Malaysia); SDS from BASF (Hong Kong); PEG 6000 from Clariant (Gendorf, Germany); NaCl from Dominion Salt (Mount Maunganui, New Zealand); and isopropanol and ethanol from Bratachem (Solo, Indonesia).

The bacterial strain used for DNA extraction was *Mycobacterium tuberculosis* ATCC 25177 from Microbiologics (United States). The media used for bacterial growth were Lowenstein Jensen and Trypticase Soy Broth (TSB), both purchased from Himedia (Mumbai, India). Specimens were obtained from the Konimex Diagnostic Center repository (Solo, Indonesia).

Magnetite synthesis

$FeSO_4$ and $FeCl_3$, with a molarity ratio of 1:2, were mixed in water. NaOH solution was added dropwise while stirring until the pH reached 8-10. The solution was then allowed to settle, and the supernatant was decanted. The

precipitate was washed twice with water. The washed precipitate was dried in the oven at 60-100°C for two hours. The dried magnetite was then coated with fumed silica using a previously defined protocol (Thangaraj *et al.,* 2019). In this protocol, TEOS was substituted with 20 µg/mg fumed silica per magnetite. The resulting particles are referred to as fumed silica-coated magnetic particles (FsMP).

FsMP regeneration test

FsMP was used to extract DNA using previously defined protocol (Tjoa *et al.,* 2025) from *M. tuberculosis* culture. The purity factor was measured using a nanophotometer at 260/280 nm. The DNA was also amplified using a quantitative Polymerase Chain Reaction (qPCR) CFP10 gene amplification kit from Konimex Diagnostic Center (Solo, Indonesia) using MicPCR machine to obtain the Cycle threshold (Ct) value. The used FsMP was washed with 500 µl elution buffer and reused for DNA extraction. DNA extraction using the same FsMP were repeated five times with three replications. The purity factors and Ct values from the repeated steps were compared.

Matrices suitability test

FsMP was used to extract DNA from *M. tuberculosis* culture spiked into urine, serum, saliva, sputum, whole blood, and plasma. The extracted DNA was diluted into three consecutive dilutions. Each dilution was then amplified using a qPCR CFP10 gene amplification kit to obtain Ct values. The Ct values and dilutions were plotted to create a regression equation, which was used to determine the PCR efficiency value. The ΔCt value was calculated by comparing the actual Ct result with the Ct value predicted by the regression equation. These values were used to assess inhibition in the PCR process.

Sequencing

The amplicon or PCR product, from *M. tuberculosis* obtained in the PCR step using qPCR CFP10 gene amplification kit from Konimex Diagnostic Center (Solo, Indonesia) using MicPCR machine underwent sequencing using the Sanger method, specifically the single-pass, two-reaction approach. The sequencing results were aligned with the *M. tuberculosis* reference genome and the nucleotide database using BLAST from NCBI

Results and Discussion

FsMP was successfully synthesized and evaluated for its potential use in repeated DNA extraction. The regeneration test was conducted to assess its

reusability and efficiency across multiple DNA extraction cycles, providing insight into the material's stability and consistent performance. The test was performed using one loop of *M. tuberculosis* in 1 ml of TSB media, with DNA extraction carried out five times in three independent repetitions. The extracted DNA was assessed for purity based on the A260/280 ratio and its suitability for PCR amplification. The results are presented in Fig. 1.

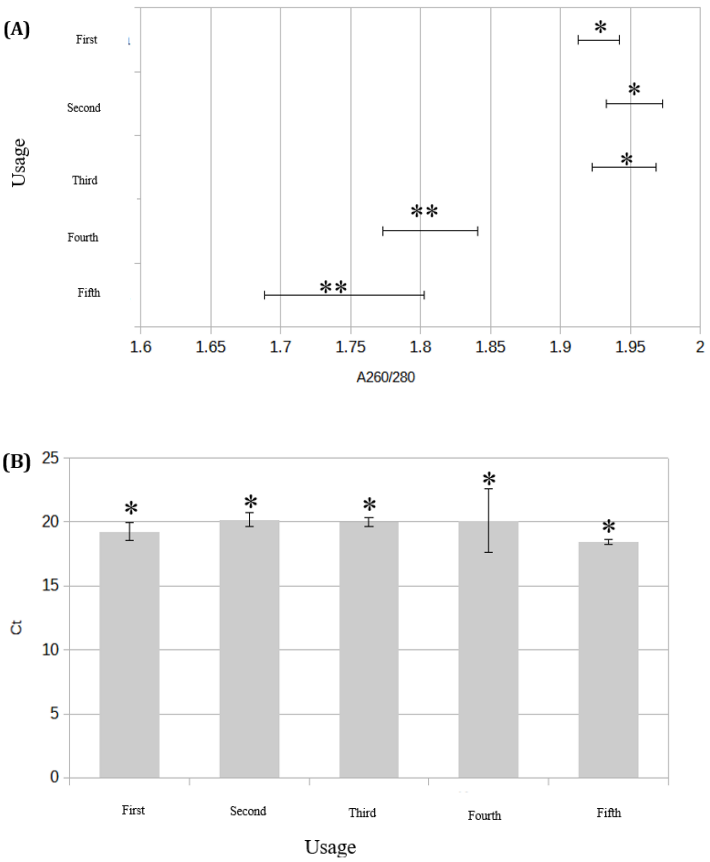

Figure 1. (A) A260/280 comparison and (B) Ct value comparison from extracted DNA using FsMP in 5 times repeatance. Notation (*) showed same group based on post-hoc analysis using Tukey with α value: 0.05.

Data analysis was performed by comparing the A260/280 ratios and Ct values from each repetition. The DNA purity values obtained from repeated FsMP extractions consistently fell within the range of 1.6 to 2.0, indicating acceptable purity. From the third repetition onward, the purity values slightly

differed from the initial use, though they remained within the acceptable range. The Ct value represents the relative concentration of DNA obtained based on the number of PCR amplification cycles required for detection. The Ct values remained consistent across all extractions, indicating that the DNA concentration did not vary significantly even after five consecutive uses of this particular preparation of FsMP.

A matrices suitability test was conducted using matrices spiked with *M. tuberculosis* culture at a 1:1 ratio. The extracted DNA was subsequently amplified using qPCR. The resulting qPCR amplicon was visualized on an electrophoresis gel, as shown in Fig. 2, revealing a DNA band of approximately 120 bp in length. This indicates successful amplification. Furthermore, the DNA extracted from the tested matrices did not introduce any inhibitors that could interfere with the PCR reaction.

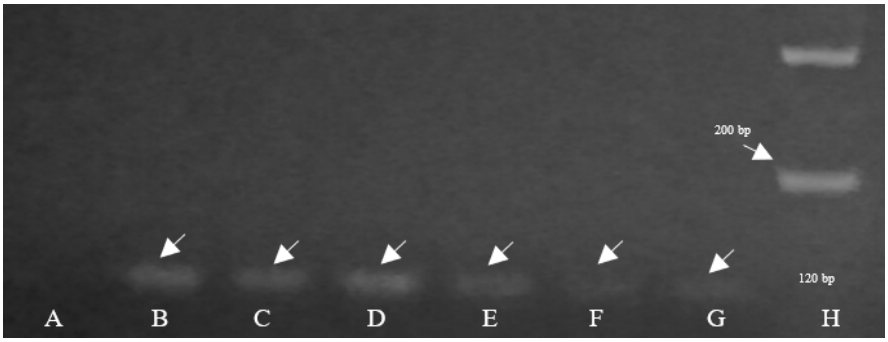

Figure 2. Amplicon visualization with electrophoresis. Amplicon size around 120 bp. (A) Negative. (B) Culture. (C) In urine. (D) In serum. (E) In saliva. (F) In whole blood. (G) In sputum. (H) Ladder.

Experiments using various types of specimens were also conducted to evaluate the efficiency of qPCR. qPCR efficiency reflects the capacity of all components in the reaction to amplify DNA. Ideally, each PCR cycle results in the duplication of DNA, producing two copies from a single DNA template, which corresponds to an efficiency value of 100%. The method for calculating DNA efficiency is presented in the following formula (Nybo, 2018).

$$PCR\ efficiency\ (\%) = 100\ x\ \left(10^{\left(\frac{-1}{a}\right)} - 1\right)$$

$a = slope.$
$y = ax + b$
$y = Ct$
$x = Log\ (concentration)$

PCR efficiency testing was performed on DNA extracts prepared in three dilutions. The results are presented in Fig. 3, which includes a normalized fluorescence versus cycle graph, an efficiency calculation plot, and a ΔCt comparison between the observed and calculated Ct values. PCR efficiency values approaching 100% (75% - 110%) with R^2 values ≥ 0.98 indicate that the PCR reactions are running efficiently, unaffected by inhibitors (which can lower efficiency) or activators (which can inflate efficiency beyond optimal levels) (Booth *et al.,* 2010).

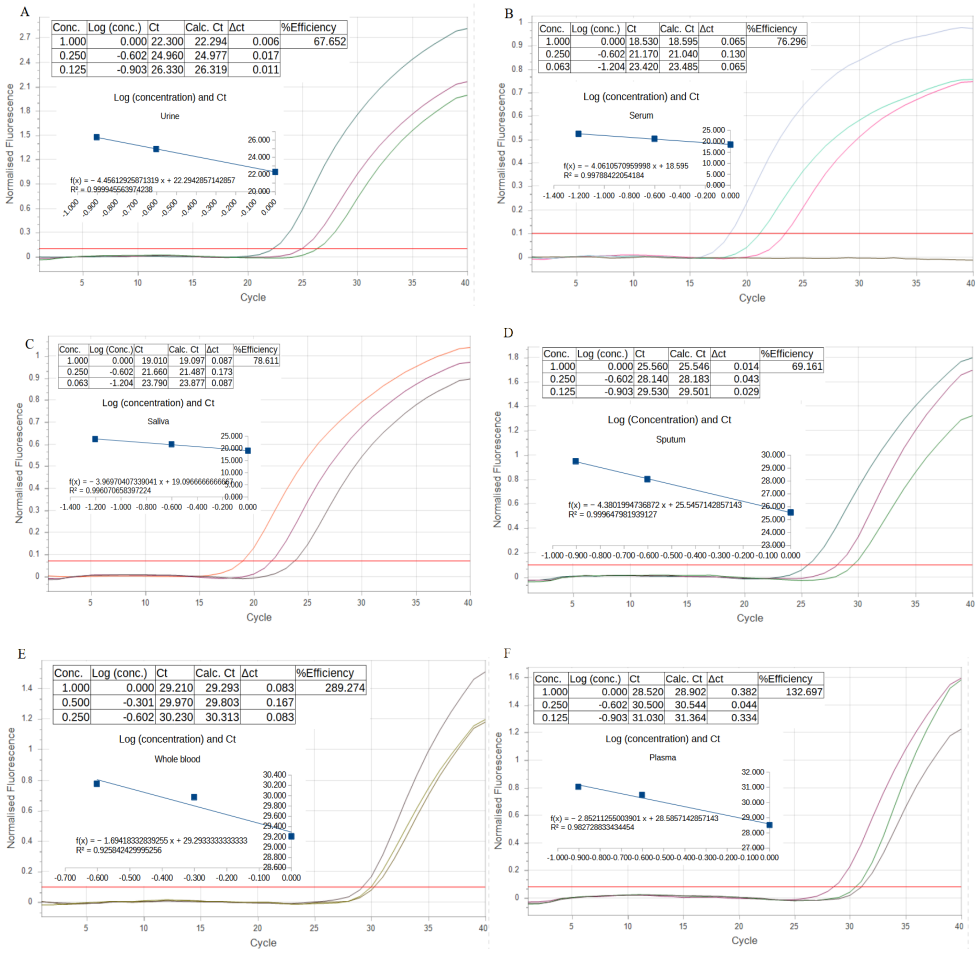

Figure 3. Normalised fluorescence and cycle graph, efficiency calculation graph, and ΔCt comparison of actual and calculated Ct for six matrices. (A) Urine. (B) Serum. (C) Saliva. (D) Sputum. (E) Whole blood. (F) Plasma.

The PCR efficiencies for *M. Tuberculosis* in urine, saliva, serum, sputum, whole blood, and plasma were 67.652% (R^2 = 1), 76.296% (R^2 = 0.998), 78.611% (R^2 = 0.996), 69.161% (R^2 = 1), 289.274% (R^2 = 0.926), and 132.697% (R^2 = 0.983), respectively. The PCR efficiencies ranged from 67.652% to 289.274%. Efficiency values for urine and sputum specimens were below 75%, indicating poor compatibility of the PCR process with the extracted DNA. To improve compatibility, an additional step to remove PCR inhibitors was necessary, such as the removal of urea and crystals from urine (Munch *et al.,* 2019) and biological factors from sputum (Reed *et al.,* 2016).

DNA extracted from whole blood and plasma exhibited efficiency values exceeding 110%, indicating that FsMP was ineffective in fully removing impurities that interfere with PCR. the excessive efficiency values likely result from PCR artifacts or altered reaction kinetics caused by residual contaminants. Potential interfering impurities in blood include heme, leukocytes, and anticoagulant compounds such as EDTA and heparin (Al-Soud and Rådström, 2001).

Plasma was included in the efficiency analysis to assess its impact on PCR performance. While separating plasma from red blood cells helps reduce interference by minimizing cellular components, plasma still contains residual contaminants such as such as immunoglobulin G, which can affect the PCR reaction (Al-Soud and Rådström, 2001). This persistent interference likely to contributes to the efficiency value exceeding 110%.

PCR efficiency is influenced by several factors beyond the quality of the DNA extract. It can be affected by the choice of primers, polymerase, and PCR parameters, as well as the compatibility of these components (Booth *et al.,* 2010; Louw *et al.,* 2011). DNA extracts can be considered free from inhibitors and activators if the ΔCt value is < 0.5 (Waiblinger and Grohmann, 2014).

The ΔCt value represents the difference between the actual Ct value and the Ct value predicted by the line equation. The ΔCt values for all specimens and their respective dilutions met the criteria for inhibitor-free DNA extracts. These results indicate that FsMP is capable of effectively extracting DNA from various specimens, including urine, serum, saliva, blood, sputum, and plasma.

PCR products were subsequently sequenced using the Sanger method, employing a single-pass DNA sequencing with two reactions. Two-direction sequencing was performed, using both forward and reverse primers. The sequencing results, presented in Fig. 4, show the CFP10 fragment gene chromatogram. The chromatogram reveals that at least one position in the forward sequence has an unreadable nucleotide, whereas all nucleotides in the reverse sequence are clearly readable. The differences observed between the forward and reverse sequences may be caused by sequence artifacts, PCR amplification inaccuracies, or DNA degradation during sample preparation (Al-Shuhaib & Hashim, 2023). However, the sequencing data remain reliable, as reads labeled with "N" account for less than 5% of the total reads (Crossley *et al*., 2020).

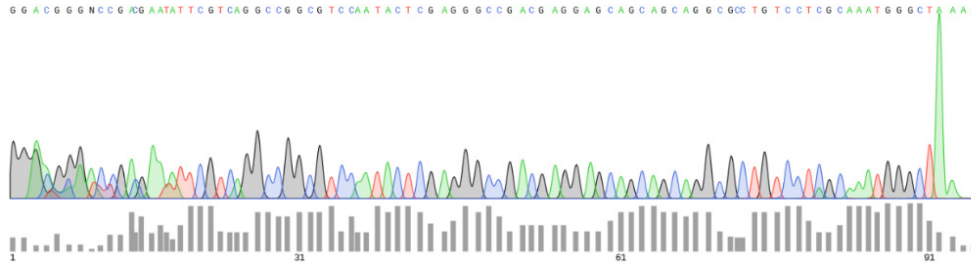

>Forward direction
GGACGGGNCCGACGAATATTCGTCAGGCCGGCGTCCAATACTCGAGGGCCGACGA
GGAGCAGCAGCAGGCGCCTGTCCTCGCAAATGGGCTAAAC

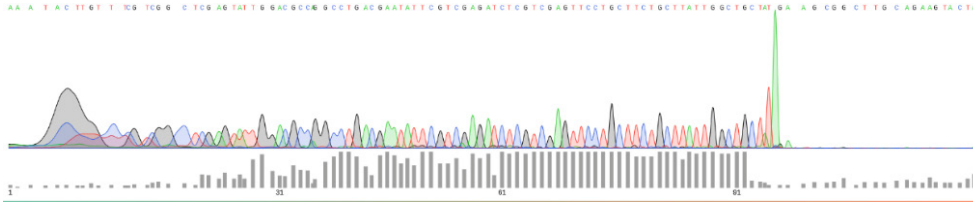

>Reverse direction
TCGTCGGCTCGAGTATTGGACGCCAGGCCTGACGAATATTCGTCGAGATCTCGTC
GAGTTCCTGCTTCTGCTTATTGGCTGCT

Figure 4. Chromatogram and FASTA format of the sequencing result for the CFP10 fragment gene.

Further analysis was performed using BLAST through the web services provided by NCBI (Zhang *et al.,* 2000). The reference genome used was NC_00962.3 from *Mycobacterium tuberculosis* H37Rv, a complete genome with a length of 4,411,532 bp. The BLAST results are presented in Fig. 5.

From the alignment results, both sequences showed a percentage identity (per ident) greater than 95%, with the largest gaps being 3%. These results indicate that the sequences produced from CFP10 gene fragment could be successfully read and identified as *Mycobacterium tuberculosis*, the organism from which the DNA was extracted. This finding is further supported by the BLAST results from the nucleotide database collection at NCBI, conducted on August 31, 2024, and presented in Fig. 6. Among the first 100 entries retrieved, 98 sequences were identified as *Mycobacterium tuberculosis* for both the forward and reverse sequences. The per ident values for the forward and reverse sequences were 98.74% and 96.74%, respectively.

(A)

Sequence ID: Query_4394065 Length: 95 Number of Matches: 1

Range 1: 10 to 91 Graphics ▼ Next Match ▲ Previous Match

Score	Expect	Identities	Gaps	Strand
145 bits(78)	3e-35	81/82(99%)	1/82(1%)	Plus/Plus

```
Query  4352491  CGACGAATATTCGTCAGGCCGGCGTCCAATACTCGAGGGCCGACGAGGAGCAGCAGCAGG  4352550
                ||||||||||||||||||||||||||||||||||||||||||||||||||||||||||
Sbjct  10       CGACGAATATTCGTCAGGCCGGCGTCCAATACTCGAGGGCCGACGAGGAGCAGCAGCAGG  69

Query  4352551  CG-CTGTCCTCGCAAATGGGCT  4352571
                || |||||||||||||||||||
Sbjct  70       CGCCTGTCCTCGCAAATGGGCT  91
```

Sequence ID: Query_4394064 Length: 83 Number of Matches: 1

(B)

Range 1: 1 to 83 Graphics ▼ Next Match ▲ Previous Matc

Score	Expect	Identities	Gaps	Strand
137 bits(74)	4e-33	82/85(96%)	3/85(3%)	Plus/Minus

```
Query  4352453  AGCAGCCAATAAGCAGAAGCAGGAACTCGACGAGATCTCGACGAATATTCGTCAGGCC-G  4352511
                |||||||||||||||||||||||||||||||||||||||||||||||||||||||| |
Sbjct  83       AGCAGCCAATAAGCAGAAGCAGGAACTCGACGAGATCTCGACGAATATTCGTCAGGCCTG  24

Query  4352512  GCGTCCAATACTCGAGGGCCGACGA  4352536
                |||||||||||||||  |||||||
Sbjct  23       GCGTCCAATACTCGAG--CCGACGA  1
```

Figure 5. (A) CFP10 gene fragment forward direction sequence alignment. (B) CFP10 gene fragment reverse direction sequence alignment.

(A)

Description	Scientific Name	Max Score	Total Score	Query Cover	E value	Per. Ident	Acc. Len	Accession
Mycobacterium tuberculosis strain 0B049XDR genome	Mycobacterium tuberculosis	147	147	86%	6e-31	98.78%	4539433	CP008971.1
Mycobacterium orygis strain NIAB_BDWBCSHFL_1 chromosome, complete genome	Mycobacterium orygis	145	145	86%	2e-30	98.78%	4347055	CP138660.1
Mutant Mycobacterium tuberculosis variant bovis isolate PHOPR KO3, partial genome	Mycobacterium tuberculosis variant bo…	145	145	86%	2e-30	98.78%	4349904	CP133601.1
Mutant Mycobacterium tuberculosis variant bovis isolate PHOPR KO1, partial genome	Mycobacterium tuberculosis variant bo…	145	145	86%	2e-30	98.78%	4349896	CP133603.1
Mycobacterium tuberculosis variant bovis strain AF2122/97 chromosome	Mycobacterium tuberculosis variant bo…	145	145	86%	2e-30	98.78%	4349904	CP133604.1
Mutant Mycobacterium tuberculosis variant bovis isolate PHOPR KO2, partial genome	Mycobacterium tuberculosis variant bo…	145	145	86%	2e-30	98.78%	4349904	CP133602.1
Mycobacterium tuberculosis strain AST-T7 chromosome, complete genome	Mycobacterium tuberculosis	145	145	86%	2e-30	98.78%	4399274	CP133045.1
Mycobacterium tuberculosis strain AST-T3 chromosome, complete genome	Mycobacterium tuberculosis	145	145	86%	2e-30	98.78%	4411248	CP133041.1
Mycobacterium tuberculosis strain AST-T4 chromosome, complete genome	Mycobacterium tuberculosis	145	145	86%	2e-30	98.78%	4412499	CP133042.1
Mycobacterium tuberculosis strain AST-T6 chromosome, complete genome	Mycobacterium tuberculosis	145	145	86%	2e-30	98.78%	4420361	CP133044.1

(B)

Description	Scientific Name	Max Score	Total Score	Query Cover	E value	Per. Ident	Acc. Len	Accession
Mycobacterium orygis strain NIAB_BDWBCSHFL_1 chromosome, complete genome	Mycobacterium orygis	137	137	100%	3e-28	96.47%	4347055	CP138660.1
Mycobacterium tuberculosis strain Beijing, complete genome	Mycobacterium tuberculosis	137	137	100%	3e-28	96.47%	4378588	CP011510.1
Mycobacterium tuberculosis strain MTBCR170941 chromosome, complete genome	Mycobacterium tuberculosis	137	137	100%	3e-28	96.47%	4396671	CP104271.1
Mycobacterium tuberculosis strain MTBCR170001 chromosome, complete genome	Mycobacterium tuberculosis	137	137	100%	3e-28	96.47%	4424759	CP097112.1
Mycobacterium tuberculosis strain MTBCR170020 chromosome, complete genome	Mycobacterium tuberculosis	137	137	100%	3e-28	96.47%	4442985	CP097111.1
Mycobacterium tuberculosis strain MTBCR170027 chromosome, complete genome	Mycobacterium tuberculosis	137	137	100%	3e-28	96.47%	4456234	CP097110.1
Mycobacterium tuberculosis strain MTBCR170031 chromosome, complete genome	Mycobacterium tuberculosis	137	137	100%	3e-28	96.47%	4417031	CP097109.1
Mycobacterium tuberculosis strain SCAID 252.0, complete genome	Mycobacterium tuberculosis	137	137	100%	3e-28	96.47%	4439387	CP016888.1
Mutant Mycobacterium tuberculosis variant bovis isolate PHOPR KO3, partial genome	Mycobacterium tuberculosis variant bo…	137	137	100%	3e-28	96.47%	4349904	CP133601.1
Mutant Mycobacterium tuberculosis variant bovis isolate PHOPR KO1, partial genome	Mycobacterium tuberculosis variant bo…	137	137	100%	3e-28	96.47%	4349896	CP133603.1

Figure 6. Ten first entries from BLAST in NCBI nucleotide collection. (A) Forward direction. (B) Reverse direction.

The sequencing analysis performed in this study utilized short-read sequencing. Overall, FsMP can be used to extract DNA suitable for downstream processes such as PCR and short-read sequencing.

For further exploration, the DNA extracted using FsMP can also be evaluated for its suitability in long-read sequencing, which may provide deeper insights and broaden its applications in genetic studies. Another recommendation is to compare different preparations of FsMP to assess batch-to-batch consistency in DNA extraction performance. This analysis will help determine the reproducibility and reliability of FsMP for downstream applications.

Conclusions

In this study, we successfully prepared magnet particles which coated with fumed silica. Fumed silica is a safer option than TEOS as the coating agent. FsMP could be used in the DNA extraction for several type of biological samples such as serum, saliva, urine, sputum, whole blood, and plasma. Extracted DNA from FsMP could be used in the downstream process like PCR and short-read sequencing.

Acknowledgements. We would like to thank PT Konimex for the funds.

References

Al-Shuhaib, M.B.S. & Hashim, H.O. (2023). Mastering DNA chromatogram analysis in Sanger sequencing for reliable clinical analysis. *J. Genet. Eng. Biotechnol. 21*, 115. https://doi.org/s43141-023-00587-6

Al-Soud, W.A. & Rådström, P. J. (2001). Purification and Characterization of PCR-Inhibitory Components in Blood Cells. *Clin. Microbiol. 39*, 2, 485-493. https://doi.org/10.1128/JCM.39.2.485-493.2001

Alghuthaymi, M. (2020). Magnetic-silica nanoshell for extraction of fungal genomic DNA from Rhizopus oryzae. *Biointerface Res. Appl. Chem. 10*, 2, 4972-4976. https://doi.org/0.33263/BRIAC102.972976

Booth, C.S., Pienaar, E., Termaat, J.R., Whitney, S.E., Louw, T.M., & Viljoen, H.J. (2010). Efficiency of the Polymerase Chain Reaction. *Chem. Eng. Sci. 65*, 17, 4996-5006 (2010) https://doi.org/10.1013/j.ces.2010.05.046

Crossley, B.M., Bai, J., Glaser, A., Maers, R., Porter, E., Killian, M.L, Clement, T., & Toohey-Kurth, K. (2020). Guidelines for Sanger sequencing and molecular assay monitoring. *J. Vet. Diagn. Invest. 32,* 6, 767-775. https://doi.org/10.1177/1040638720905833

Dzeranov, A., Bondarenko, L., Pankratov, D., Dzhardimalieva, G., Jorobekova, S., Saman, D., & Kydralieva, K. (2023). Impact of Silica-Modification and Oxidation on the Crystal Structure of Magnetite Nanoparticles. *Magnetochemistry. 2023*, 9, 18. https://doi.org/10.3390/magnetochemistry9010018

Fan, Q., Guan, Y., Zhang, Z., Xu, G., Yang, Y., & Guo, C. (2019). A new method of synthesis well-dispersion and dense Fe3O4@SiO2 magnetic nanoparticles for DNA extraction. *Chem. Phys. Lett. 715*, 7-13. https://doi.org/10.1016/j.cplett.2018.11.001

Firoozeh, F., Neshan, A., Khaledi, A., Zibaei, M., Amiri, A., Sobhani, A., Badmasti, F., & Nikbin, V.S. (2023). Evaluation of the effect of magnetic nanoparticles on extraction of genomic DNA of Escherichia coli. *Polym. Bull. 80*, 3153-3163. https://doi.org/10.1007/s00289-022-04196-0

Flörke, O.W., Graetsch, H.A., Brunk, F., Benda, L., Paschen, S., Bergna, H.E., Roberts, W.O., Welsh, W.A., Libanati, C., Ettlinger, M., Kerner, D., Maier, M., Meon, W., Schmoll, R., Gies, H., & Schiffmann, D. (2012). Silica.Ullmann's encyclopedia of industrial chemistry. *Wiley*, Weinheim. https://doi.org/10.1002/14356007.a23_583

Louw, T.M., Booth, C.S., Pienaar, E., TerMaat, J.R., Whitney, S.E., & Viljoen, H.J. (2011). Experimental Validation of a Fundamental Model for PCR Efficiency. *Chem. Eng. Sci. 66*, 1783-1789. https://doi.org/10.1016/j.ces.2011.01.029

Munch, M.M., Chambers, L.C., Manhart, L.E., Domogala, D., Lopez, A., Fredricks, D.N., & Srinivasan, S. (2019). Optimizing Bacterial DNA Extraction in Urine. *PLoS One. 14*, 9, e0222962. https://doi.org/10.1371/journal.pone.0222962

Nguyen, L.T., Le, N.T., Ta, H.K.T., & Nguyen, K.D. (2022). Isolation of DNA from Arthrospira platensis and whole blood using magnetic nanoparticles (Fe3O4@OA and Fe3O4@OA@SiO2). *J. Anal. Sci. Technol. 13*, 1, 28. https://doi.org/10.1186/s40543-022-00337-2

Nybo, K. (2011). qPCR Efficiency Calculations. *Biotechniques*, *51*, 401-402. https://doi.org/10.2144/000113776

Reed, J.L., Walker, Z.J., Basu, D., Allen, V., Nicol, M.P., Kelso, D.M., & McFall, S. (2016). Highly Sensitive Sequence Specific qPCR Detection of Mycobacterium tuberculosis Complex in Respiratory Specimens. *Tuberculosis. 101*, 114-124. https://doi.org/10.1016/j.tube.2016.09.002.

Thangaraj, B., Jia, Z., Dai, L., Liu, D., & Du, W. (2019). Effect of silica coating on Fe_3O_4 magnetic nanoparticles for lipase immobilization and their application for biodiesel production. *Arab. J. Chem. 12*, 8, 4694-4706. https://doi.org/10.1016/j.arabjc.2013.09.004

Tjoa, S.E.E., Mudasir, M., Suharyadi, E., & Daryono, B.S. (2025). DNA extraction procedure based on magnetite nanoparticle: A Plackett-Burman design optimization. *Res. J. Biotech. 20,* 3, 1-7. https://doi.org/10.25303/203rjbt0107

Torres-Rodríguez, J., Soto, G., Medina, J.L., Portillo-López, A., Hernández-López, E.L., Viveros, E.V., Galindo, J.T.E., Tiznado, H., Flores, D., & Muñoz-Muñoz, F. (2019). Cobalt–zinc ferrite and magnetite SiO2 nanocomposite powder for magnetic extraction of DNA. *J. Sol-Gel Sci. Technol. 91*, 33-43. https://doi.org/10.1007/s10971-019-05017-z

Waiblinger, H. & Grohmann, L. (2014). Guidelines for validation of DNA extraction methods applied in subsequent PCR analysis of food and feed products for the presence of genetically modified material. *J. Verbrauch. Lebensm. 9*, 183-190. https://doi.org/10.1007/s00003-014-0862-3

Zhang, Z., Schwartz, S., Wagner, L., & Miller, W. (2000). A greedy algorithm for aligning DNA sequences*. J. Comput. Biol. 7*, 1-2, 203-214. https://doi.org/10.1089/10665270050081478

STUDIA UNIVERSITATIS BABEŞ-BOLYAI BIOLOGIA, 70, 1, 2025 (p. 19-47)
doi:10.24193/subbbiol.2025.1.02

Charting the academic output on cyanobacterial exopolysaccharides and their industrial applications

Maricel Bocaneala[1,2]✉, Giovani M. Goron[3] and Elena Rakosy-Tican[1]

[1]Department of Molecular Biology and Biotechnology, Faculty of Biology and Geology, "Babeş-Bolyai" University, 5-7 Clinicilor St., 400006 Cluj-Napoca, Romania; [2]National Institute for Research and Development of Isotopic and Molecular Technologies, 67-103 Donat St., 400293 Cluj-Napoca, Romania; [3]Department of Public Health, College of Political, Administrative and Communication Sciences, Babes-Bolyai University, 71 General Traian Mosoiu St., 400132 Cluj-Napoca, Romania;
✉***Corresponding author, E-mail: maricel.bocaneala@ubbcluj.ro***

Article history: Received 4 February 2025; Revised 17 March 2025; Accepted 17 March 2025; Available online 25 June 2025

Abstract. Cyanobacterial exopolysaccharides (EPS) are diverse biopolymers with significant ecological roles and growing industrial potential due to their biocompatibility, biodegradability, and functional versatility. This study presents a bibliometric and patent analysis of cyanobacterial EPS research between 2004 and 2023, exploring academic and industrial advancements. The bibliometric analysis of 1,022 articles identified pharmaceuticals and environmental applications as dominant research themes, while the food, agriculture, and energy sectors showed emerging interest. A manually curated subset of 79 articles focusing on industrial applications highlighted EPS's potential in pollutant removal, drug development, and biofertilization. Patent analysis, with data from 618 entries, revealed a surge in filings post-2014, predominantly in the USA, reflecting growing industrial interest. While healthcare and environmental sectors lead in EPS applications, translational gaps between academic research and industrial adoption persist, particularly in underdeveloped domains. This study presents the multidisciplinary appeal of cyanobacterial EPS, striving to offer insights into future research directions and their potential for sustainable innovation across diverse sectors.

Keywords: bibliometric analysis; cyanobacterial EPS; exopolysaccharide; technological transfer

Introduction

Cyanobacterial exopolysaccharides (EPS) are a diverse group of biopolymers with remarkable structural and functional properties. These extracellular polysaccharides play important roles in ecological processes such as biofilm formation, nutrient cycling, and microbial interactions (Rossi & De Philippis, 2015; Potnis *et al.*, 2021; Nishanth *et al.*, 2021; Debnath *et al.*, 2024). Beyond their environmental significance, cyanobacterial EPS have garnered increasing attention for their potential industrial applications, covering diverse fields like healthcare, environmental remediation, food production, agriculture, and bioenergy (Kumar *et al.*, 2018; Laroche, 2022).

In recent decades, the expanding interest in sustainable and biotechnological innovations has driven research into cyanobacterial EPS. These biopolymers exhibit a range of desirable properties, including high biocompatibility, biodegradability, and functional versatility, making them attractive candidates for applications such as drug delivery systems, wound healing materials, biofertilizers, and biosorbents for pollutant removal. Advancements in analytical techniques and interdisciplinary approaches have enabled the exploration of novel cyanobacterial strains and optimized EPS production processes, further stimulating scientific inquiry and industrial interest (Li *et al.*, 2001; Mota *et al.*, 2020; Potnis *et al.*, 2021; Reignier *et al.*, 2023; Rodrigues *et al.*, 2024; Yousaf *et al.*, 2024).

The technological transfer of cyanobacterial EPS from research to industrial applications involves several critical steps, including strain selection, optimization of production parameters, and downstream processing. Selecting appropriate cyanobacterial strains is essential, as EPS yield and composition can vary significantly among species. Optimization of cultivation conditions, such as nutrient availability, light intensity, and temperature, can impact EPS production. Efficient downstream processing techniques, including extraction and purification methods, are crucial to obtaining high-quality EPS suitable for industrial use (Cruz *et al.*, 2020).

Cyanobacterial EPS have demonstrated potential in various industrial settings. In the food industry, they can serve as natural thickeners, stabilizers, and emulsifiers, improving the texture and shelf-life of products (Vicente-García *et al.*, 2004; Jindal *et al.*, 2013; Najdenski *et al.*, 2013; Nath *et al.*, 2021). In pharmaceuticals, their bioactive properties, such as antioxidant, antibacterial, and antiviral activities, make them suitable for developing new therapeutic agents (Gacheva *et al.*, 2013; Bhatnagar *et al.*, 2014; Shen *et al.*, 2018; Flores *et al.*, 2019; Ramachandran *et al.*, 2020). Environmental applications include bioremediation, where EPS can bind heavy metals and pollutants, facilitating their removal from contaminated sites (Colica *et al.*, 2010; Santos *et al.*, 2014; Mota *et al.*, 2016; Mohamed *et al.*, 2023). Additionally, in agriculture, EPS-

producing cyanobacteria contribute to soil stabilization and fertility, promoting sustainable farming practices (Van Camp *et al.*, 2022; Falsini *et al.*, 2023; Vinoth *et al.*, 2023).

The current study aims to map the academic and industrial landscapes of cyanobacterial EPS research through a bibliometric analysis of publication trends, prominent contributors, and thematic areas of research for potential industrial applications. Additionally, it explores the translational potential of this research through an analysis of patent filings, offering insights into the intersection of scientific discovery and technological application. While other studies have performed bibliometric analysis on cyanobacterial exopolysaccharides (Qi *et al.*, 2019; Kim *et al.*, 2024; Mugani *et al.*, 2024), to our knowledge none had approached this analysis through the concepts of technological transfer and had the scope of exploring the link between patent data and publication records for this research niche.

Materials and methods

Bibliometric data retrieval

The bibliometric data was retrieved from Clarivate's Web of Science and analyzed using Biblioshiny, a Bibliometrix R package (Aria & Cuccurullo, 2017).

The search was performed on Web of Science's Core Collection (edition: SCI-Expanded) using the following search string: (all fields) exopolysaccharide OR extracellular polysaccharide OR EPS OR exopolysaccharide-producing cyanobacteria OR exopolysaccharides OR extracellular polysaccharide EPS OR extracellular polysaccharides EPS OR exopolysaccharides OR released polysaccharides RPS AND (all fields; second row) cyanobacteria OR cyanobacterium. We then selected only the articles, in English, and published between 2004–2023. The specific year range was selected in order to explore publications within the past two decades, however, publications from 2024 are yet to be published and indexed, therefore we limited the search to 2023.

We obtained a query result of 1035 articles, based on the above-mentioned search, criteria, and filters. Data was exported in BIB format and imported into Bibliometrix. Further screening was performed using this tool - filtering out papers that were included in the WoS export, but that were flagged as indexed in 2024 issue releases. A total of 1022 articles met the inclusion criteria. In this paper, we will refer to this dataset as the "full dataset", to distinguish it from the filtered one. We proceeded to manually filter which papers out of the total 1022 report data on industrial or biotechnological application of cyanobacterial EPS (selection criteria listed in Section 2.1.1), and this dataset will be referred to as "filtered dataset" moving forward (Figure 1).

Articles selection criteria for the filtered dataset

The filtered dataset contains a subset of articles from the full dataset that reference information on possible technological applications of cyanobacterial EPS. In order to meet the selection criteria, articles must report direct or potential applications of cyanobacterial EPS that the authors have experimentally tested. Additionally, studies should relate these findings to potential industrial integration, either through proposed applications or by comparing EPS characteristics with those of existing products (e.g., gums, adhesives). Articles mentioning applications without presenting adequate methodological details were excluded from the dataset. Cyanobacterial EPS must either constitute the primary product or serve as a key ingredient within the product.

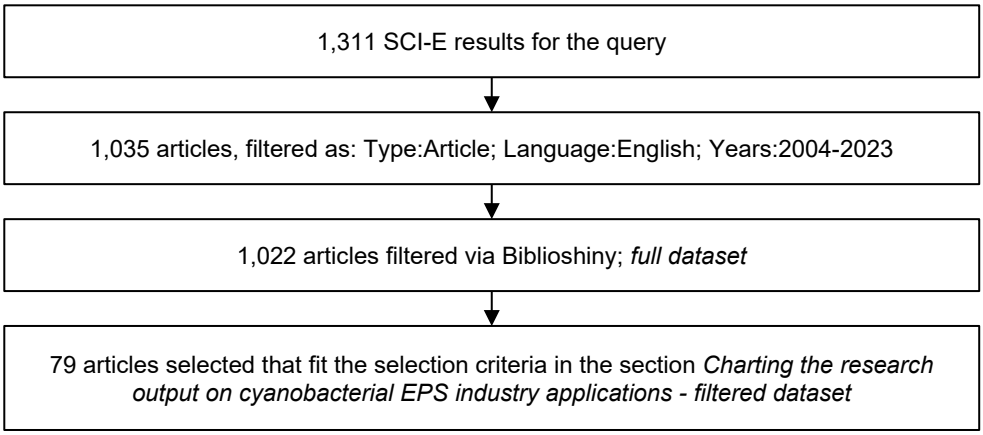

Figure 1. Chart presenting the filtering process of the articles from both the full dataset and the filtered one.

Filtered dataset

We conducted a manual screening of articles that report research on potential industrial applications of cyanobacterial EPS, following the selection criteria outlined in Section 2.1.1. From this process, 79 articles were identified and reviewed. For each selected article, we extracted and compiled relevant data into a dataset, which includes a rationale for inclusion based on the selection criteria, details on the methodologies reported or referenced, the specific properties of cyanobacterial EPS examined, potential industrial applications, industries mentioned, and the cyanobacterial organisms studied.

Espacenet patent data

In order to collect data on the patents published on cyanobacterial EPS, we performed a query on Espacenet (the European Patent Office) using the following search string: (nftxt = "cyanobacteria" OR nftxt = "cyanobacterium") AND (nftxt = "exopolysaccharide" OR nftxt = "extracellular polysaccharide" OR nftxt = "EPS"), and parameters: query language: en, filters: earliest publication date (family): 2004-01-01 — 2023-12-31. A total of 618 patents resulted. Data was exported and analyzed further using Microsoft Excel.

Results

Charting the research output on cyanobacterial EPS - full dataset

We analyzed the research output focused on cyanobacterial EPS from the full dataset. Using InCites, we determined that there are 4173 distinct authors that have contributed to the 1034 articles.

Annual scientific production

Figure 2 illustrates the annual production of articles from 2004 – 2023 on cyanobacterial EPS. Over this period, the research output has shown a steady increase, with an annual growth rate of 13.14%. This growth highlights an expanding interest and investment in the field, which can point towards potentially promising industrial and biotechnological applications of cyanobacterial EPS. The increasing volume of publications seen in almost every year suggests that researchers are actively exploring the potential of cyanobaterial EPS.

We note a dip in research output between 2014 and 2016, and then again between 2020 and 2022. In our opinion the first decrease in research output can be linked to a reduction of funds, which can be seen in the federal obligations for research and development reports for that time in the United States of America (National Center for Science and Engineering Statistics, 2021). The USA being one of the most prolific scientific outputs produced in this niche (Figure 3A), further strengthens this link. Additionally, in 2015 China launched the "Made in China 2025" initiative, a national strategic plan and industrial policy (Center for Strategic and International Studies, 2021). This marked a shift in its focus on supporting manufacturing capabilities. China also being the first country by affiliation frequency, appearing 1162 times in the full dataset (Figure 3B), can further point towards this research output dip. The reduced research output on this niche between 2020 and 2022 could be attributed in part to the COVID-19 Pandemic and/or limited access to on-site research facilities.

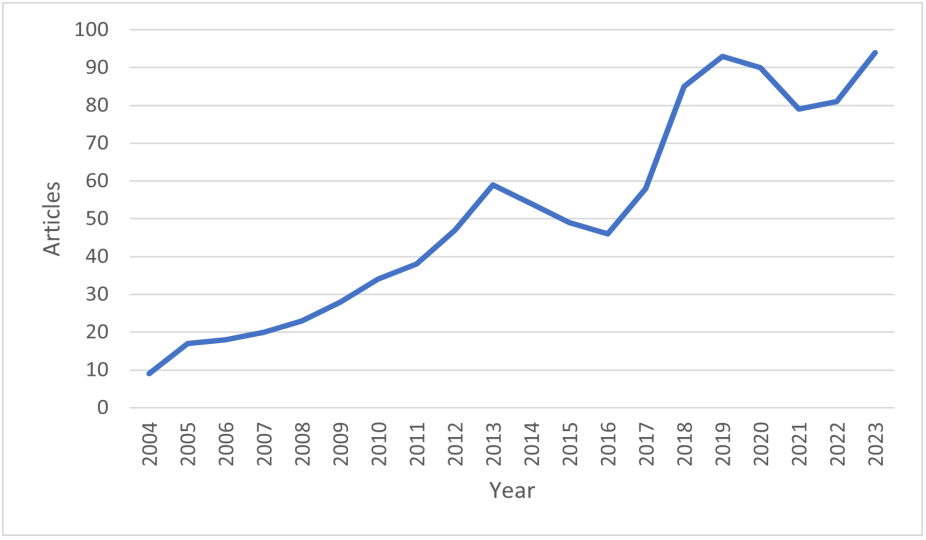

Figure 2. Annual scientific production, generated using Microsoft Excel, based on data analyzed in Bibliometrix.

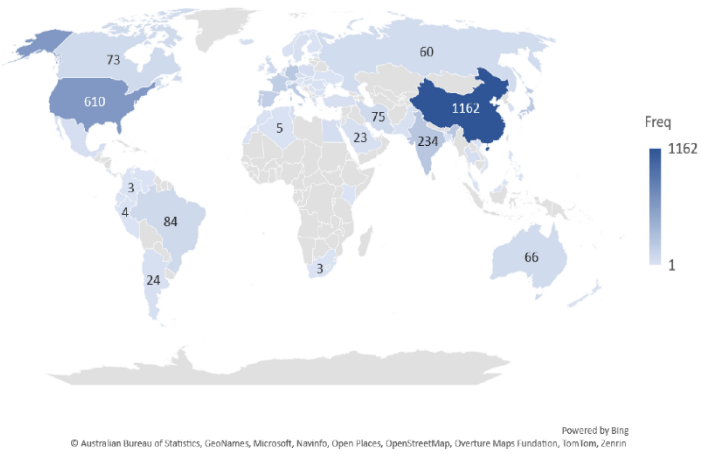

Country	Frequency
China	1162
USA	610
India	234
Germany	223
Japan	210
Italy	198
Portugal	190
France	176
Spain	173
Brazil	84

Figure 3. Top 10 most prolific countries in terms of scientific production from the full dataset. Data was analyzed with Bibliometrix and Excel.
A: World map with the frequency of country of origin attributed to each publication (generated in Microsoft Excel).
B: Figure legend containing the raw data of the frequency of publications attributed to each of the top 10 countries.

Regarding the top 10 most globally cited articles (Figure 4), leading this list is an article by Borowitzka, published in the *Journal of Applied Phycology* in 2013 (Borowitzka, 2013), which has accrued 936 total citations and stands out for its high annual citation rate of 78. This prominence highlights its significant influence on the field, likely due to its focus on practical applications of EPS in biotechnology. Ward's 2009 article in *Applied and Environmental Microbiology* (Ward *et al.*, 2009) follows, with 709 citations and a steady annual citation rate of 44.31, indicating its sustained relevance within environmental microbiology. Additonally, articles by Qu (Qu *et al.*, 2012) and Parikh (Parikh *et al.*, 2006) achieved high citation counts and annual rates. We note that most of the top 10 papers in this list are published in journals that focus on applied research.

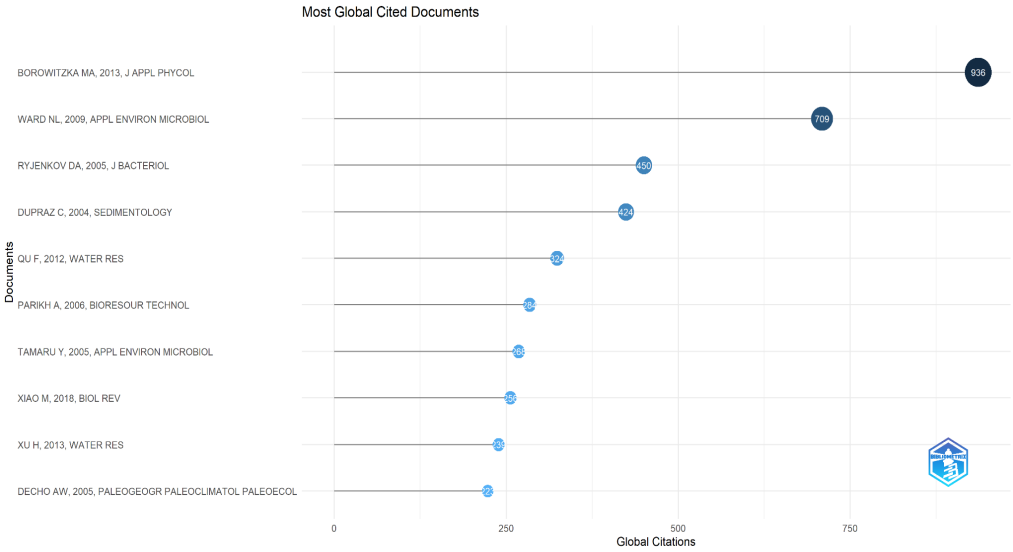

Figure 4. Top 10 most globally cited articles from the 1022 full dataset; figure generated in Bibliometrix.

Authorship and research networks

The analysis of the top 10 most prolific authors in cyanobacterial EPS research reveals a small group of researchers who have consistently contributed to advancing the field (Figure 5). Leading this group is Paula Tamagnini, with 22 articles published in the full dataset, followed closely by Roberto De Philippis with 21 articles. Both authors have significantly influenced the literature on

cyanobacterial EPS, likely focusing on key topics such as EPS characterization and its industrial applications. Ming Li also stands out with 16 articles, while Shi-Ru Jia and Rita Mota each contributed 12 articles. Other notable contributors include Peter Capek, Xiang Gao, Federico Rossi, and Li Wu, each with 11 publications, and Alessandra Adessi, who has published 10 articles. The collective work of these prolific authors points to a concentrated effort among a select few researchers who are driving the development and visibility of cyanobacterial EPS studies. Their sustained productivity likely aligns with the field's shift towards applied research and suggests a readiness for industry-related exploration, particularly in biotechnology and resource management contexts.

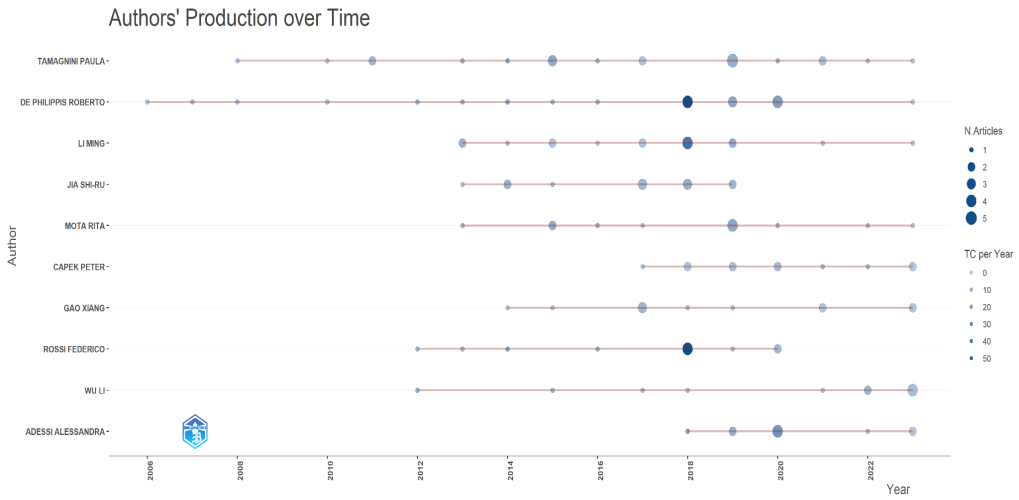

Figure 5. Top 10 most prolific authors based on the number of articles from the full dataset. Here we visualize using Bibliometrix the production over time of these authors.

In Figure 6, we visualize the collaborative efforts between countries related to publishing cyanobacterial EPS research. The United States emerges as the most collaborative nation, engaging in 132 recorded partnerships, followed by China (n=124), Germany (n=64) and Italy (n=54). This analysis illustrates a geographically diverse yet interconnected research ecosystem when it comes to exploring cyanobacterial EPS and its applications.

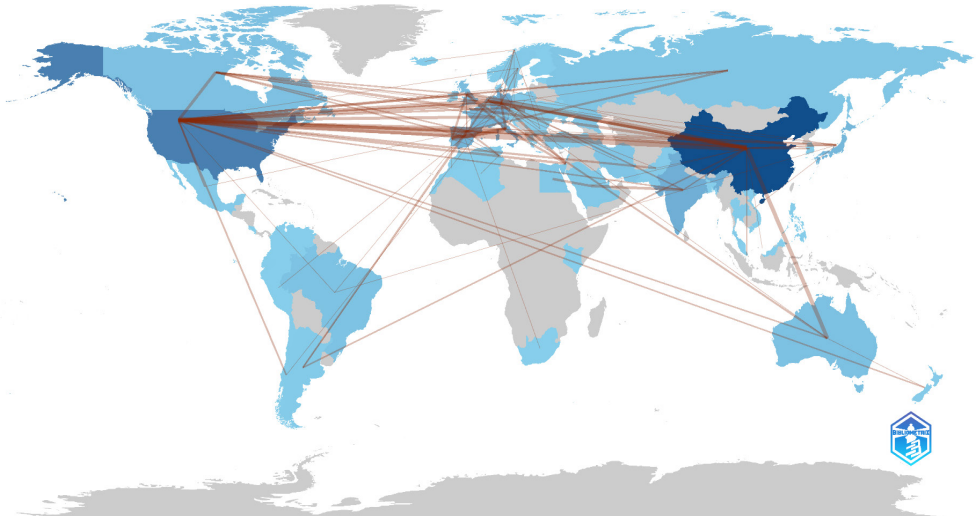

Figure 6. Countries' collaboration world map, generated using Bibliometrix.

Publishing avenues for cyanobacterial EPS research

The 1022 articles were published in 349 distinct sources (journals). Out of these, the top 10 in terms of the number of papers published from the full dataset are shown in Figure 7. This visualization indicates the core journals where cyanobacterial EPS research is most frequently published, the first being the *Journal of Applied Phycology*, with 48 published papers.

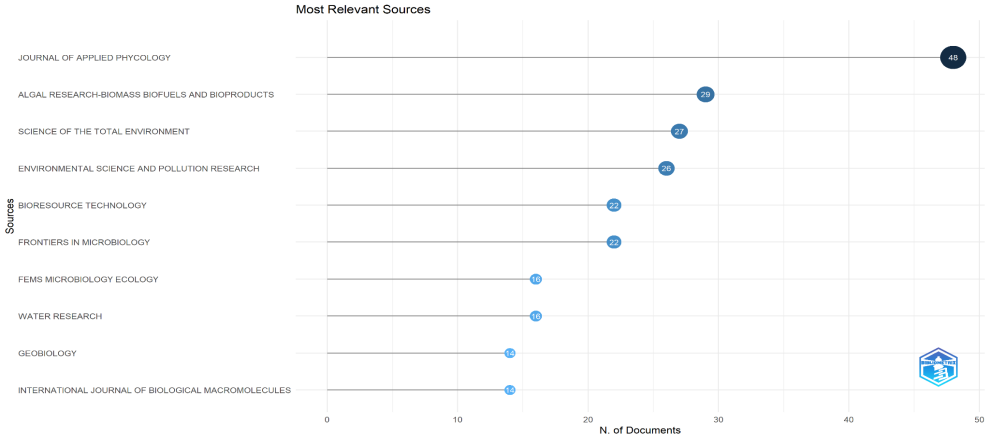

Figure 7. Top 10 most relevant journals publishing cyanobacterial EPS research, showing the distribution of the 1022 articles across the top 10 journals, highlighting the primary publication venues in this field, generated with Bibliometrix.

The growth of the number of articles published within each of the top 10 journals is highlighted in Figure 8. The analysis of publication trends across the top 10 journals for cyanobacterial EPS research reveals a distinct pattern that aligns with the hypothesis that this field is maturing toward technological transfer and industrial applications. Overall, journals with an applied focus, particularly those dedicated to biotechnology and resource management, have shown significant growth in publication counts over the years. This trend is led by the Journal of Applied Phycology and Bioresource Technology, where consistent increases in published articles indicate strong interest in potential practical applications of cyanobacterial EPS. The growth of the number of articles in these journals likely reflects a growing interest in finding solution that incorporate these polymers. In contrast, journals with a more general environmental or microbiological focus, such as Environmental Science and Pollution Research and FEMS Microbiology Ecology, maintained steady but modest publication output. These journals contribute to the fundamental understanding of EPS, particularly within environmental and ecological contexts, yet they do not exhibit the same dynamic growth as journals with applied orientations. This suggests that while cyanobacterial EPS remains a relevant topic within environmental studies, the current momentum is largely driven by its potential for practical application, which is better suited to journals emphasizing biotechnology and resource use.

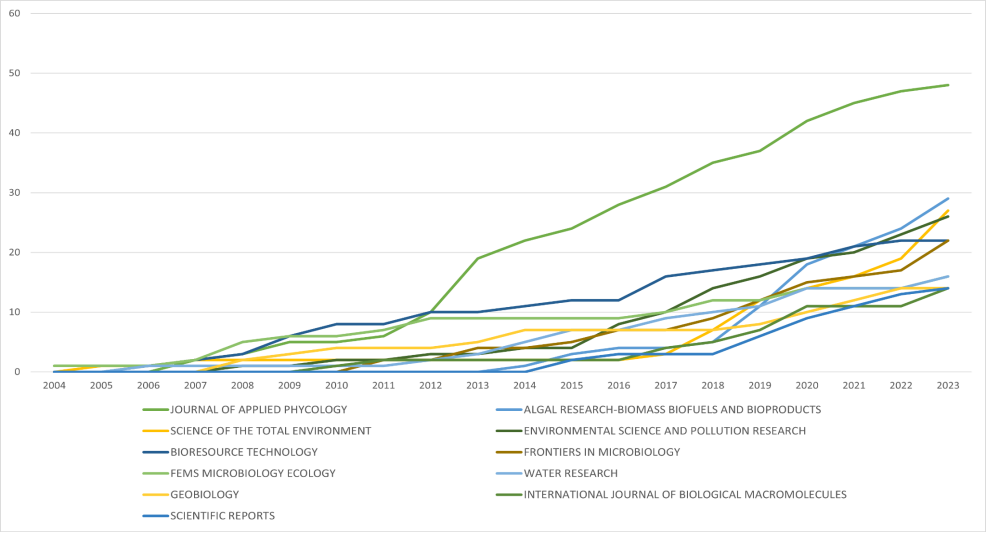

Figure 8. Annual publication growth of the number of articles on cyanobacterial EPS in the top 10 journals (2004–2023), generated using Bibliometrix data in Microsoft Excel.

Research interests

There are 2904 distinct author keywords in the full dataset. We illustrate a word cloud of the most prominent keywords used in Figure 9. This analysis reveals key research themes and concepts within cyanobacterial EPS studies. Unsurprisingly, the most frequently used term is "cyanobacteria" (179 occurrences). This is closely followed by "growth" (157), "polysaccharides" (119), and "exopolysaccharides" (108), indicating a strong emphasis on understanding both the general growth dynamics and specific biopolymer production by these organisms. Terms like "biosynthesis", "extracellular polymeric substances" and "extracellular polysaccharides" suggest ongoing interest in the biological processes and structural components that underpin EPS production, which are relevant for exploring practical applications.

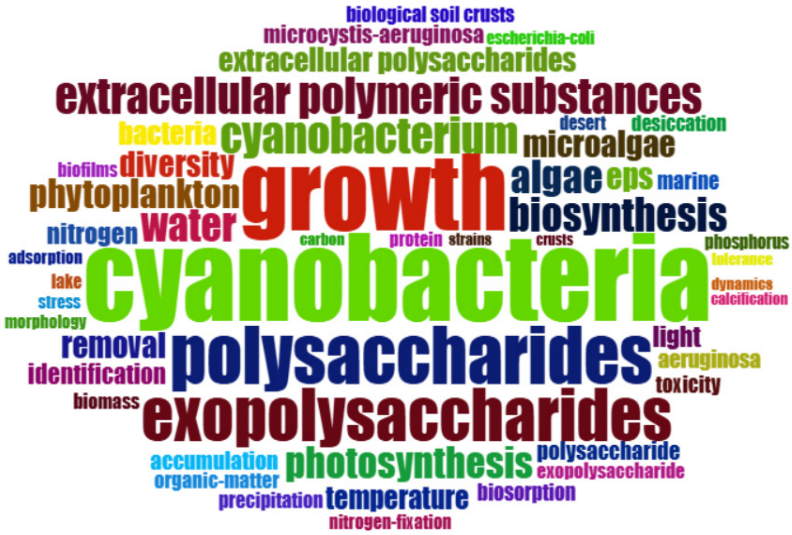

Figure 9. Word cloud generated in Bibliometrix using author keywords from the full dataset of 1022 published articles on cyanobacterial EPS.

Regarding how research trends evolved over time, in Figure 10 we visualize this concept using Bibliometrix and the author keywords. Some prominent and long-standing terms, such as "cyanobacteria", "exopolysaccharides" and "extracellular polymeric substances" while to be expected in the context of this specific dataset, reflect important concepts in this field, emphasizing them as core research areas. Notably, "microbial", "microalgae" and "biosynthesis"

have also shown continuous interest, pointing towards ongoing research into both EPS origins and production mechanisms. In recent years, there has been a rise in terms associated with applied and environmental applications, such as "adsorption", "removal" and "biosorption", which can indicate growing attention towards using cyanobacterial EPS for bioremediation, pollutant binding, and environmental cleanup. Additionally, terms like "ultrafiltration", "nitrate" and "diatoms", even though they might not be directly linked to cyanobacterial EPS on a first look, might reflect an applied focus, potentially linked to water treatment technologies and the use of EPS in managing specific environmental contaminants. Similarly, terms like "biocrusts", "phytoplankton" and "stromatolite" suggest a niche interest in studying EPS within ecological and geological contexts, connected to soil stabilization and their impact on geological history records.

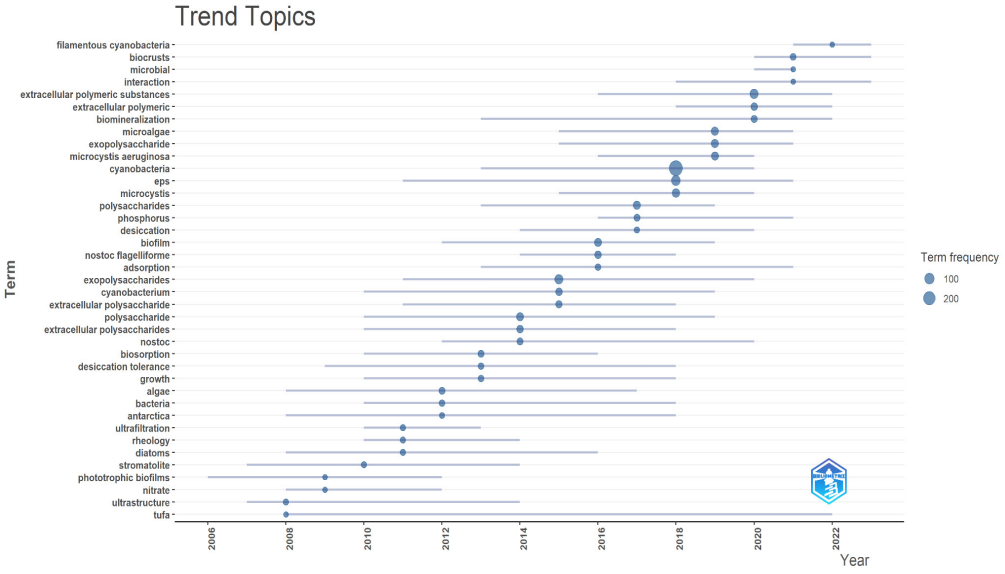

Figure 10. Author keywords are visualized as trends through time (2004-2023) and the frequency of use within the full dataset, generated with Bibliometrix. Horizontal axis: time; vertical axis: author keywords. The horizontal blue lines represent the time span in which each keyword was used within articles, while the circular dots and their dimensions are directly correlated with the frequency of use in the dataset.

The thematic map (Figure 11) highlights a few prominent trends within cyanobacterial EPS research. The Motor Themes quadrant contains terms like "extracellular polymeric substances" (EPS), "microbial mats" and "biomineralization."

These topics are relevant and well-developed, suggesting they are important to the field and involve complex, multidisciplinary applications. Their placement reflects an advanced understanding of EPS roles in environmental contexts, such as the formation of microbial mats and biomineral structures, which are key to ecological and industrial applications. In the Basic Themes quadrant, terms such as “cyanobacteria”, “exopolysaccharides”, “polysaccharide” and “microalgae” represent foundational areas that form the scientific basis of the field. These themes seem less intensively developed recently, indicating they serve as the foundation of cyanobacterial EPS research but may be more mature with fewer current innovations.

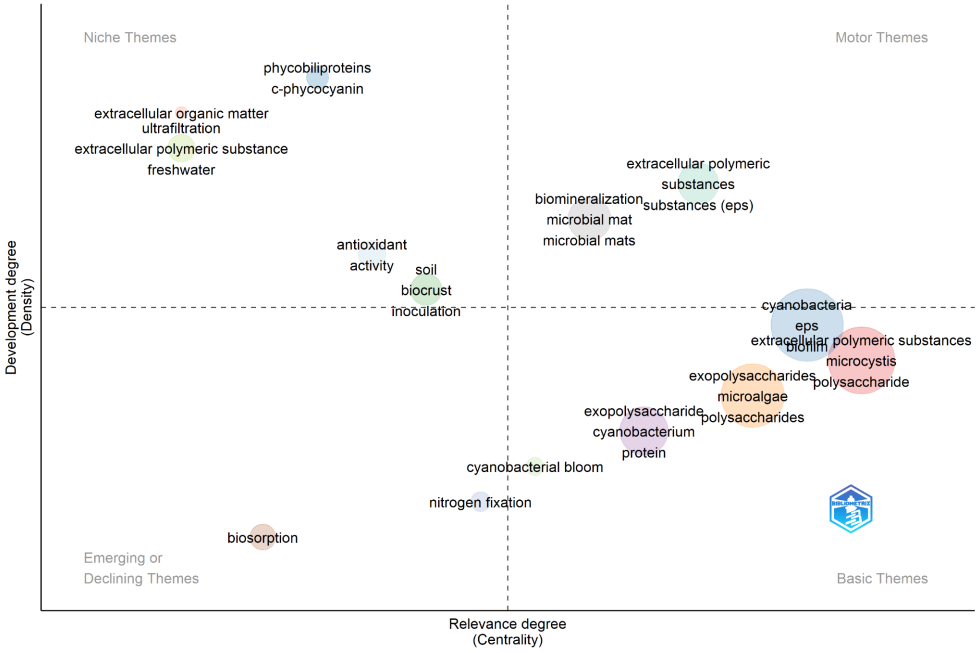

Figure 11. Thematic map of cyanobacterial EPS research showing four quadrants: Niche Themes, Motor Themes, Basic Themes, and Emerging or Declining Themes. Each term represents a distinct research focus, with its position on the map determined by relevance (centrality) and development (density). Topics in the Motor Themes quadrant are highly relevant and developed, indicating advanced and widely applicable research areas. Niche Themes are specialized but less central, focusing on specific applications or topics. Basic Themes represent foundational areas with broad importance but limited recent development. Emerging or Declining Themes are less relevant and show lower density, indicating potential areas of decreasing interest or nascent topics in need of further exploration; generated with Bibliometrix.

Niche Themes like “antioxidant activities” and “soil biocrust inoculation” occupy a specialized role within the field, showing strong development. These topics relate to particular applications, with reference to bioactive compounds derived from cyanobacteria or specific extraction techniques, pointing towards ongoing interest in specific technological and biochemical applications that may not be widely explored across the field. The presence of other types of molecules within this quadrant, namely “phycobiliproteins” also indicates the catalog of potentially useful molecules that cyanobacteria have to offer and the ability to be a multiple compound-producing organism without significant human intervention. Emerging or declining themes are represented by “biosorption” positioned with low density and centrality. This suggests that while biosorption may hold potential in applications like pollutant removal, it remains underdeveloped within the current EPS research framework, or it may be an area of declining interest as other approaches become more favorable.

The thematic evolution (Figure 12) is divided into three branches. During the 2004–2014 period, themes such as “cyanobacteria”, “extracellular polymeric substances” and “biological soil crust” are seen, laying the foundation for understanding EPS structures and their ecological roles. Themes such as “biosorption” and “phylogeny” also reflect an early interest in the environmental applications and genetic backgrounds of cyanobacteria. Then, in the 2015–2020 period, more diverse and application-oriented themes emerged, including “biofilm”, “antioxidant” and “biosynthesis”. This shift reflects a growing interest in the functional properties of EPS and its biochemical applications, aligning with industry-related uses in biotechnology. Topics like “16S rRNA gene” and “biomineralization” indicate increased focus on microbial community dynamics and EPS’s role in mineralization processes, suggesting that researchers were expanding their scope from basic characterization to more complex environmental interactions. The most recent period, 2021–2023, shows a further transition towards specialized applications and environmental relevance, with the emergence of terms like “microbial community”, “water quality”, “adsorption” and “biodeterioration”. These themes indicate a strong emphasis on EPS in ecological and environmental contexts, with applications in water treatment, pollutant removal, and microbial community interactions.

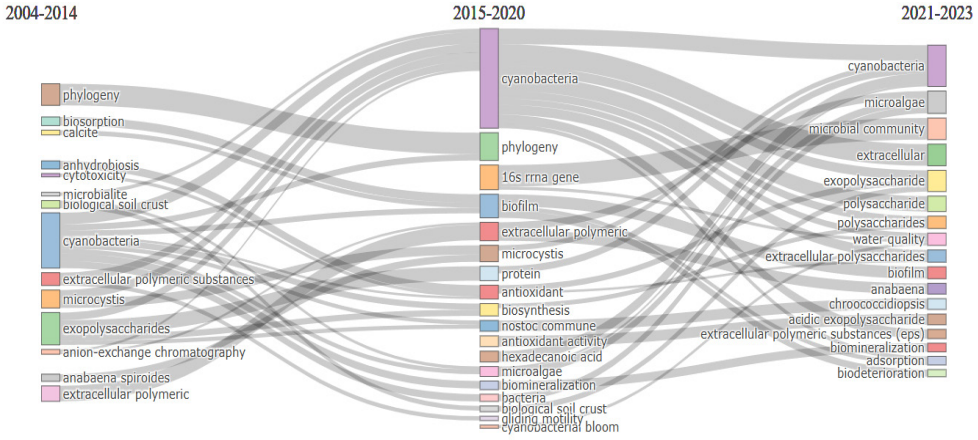

Figure 12. Thematic evolution of author keywords in cyanobacterial EPS research from 2004 to 2023. It illustrates the transition and development of major themes in 2004–2014, 2015–2020, and 2021–2023. Each colored block represents a research theme, with the size of each block indicating the relative focus on that theme. Lines between blocks connect related themes across periods, showing the continuity or emergence of research areas over time.

Charting the research output on cyanobacterial EPS industry applications - filtered dataset

There are 1022 articles in the full dataset and only 79 in the filtered one. The papers that focus specifically on industry applications of cyanobacterial EPS make up only 7.73% of the total articles in English that report research on cyanobacterial EPS indexed in Web of Science between 2004 and 2023. In this section, we analyze the industry-specific research applications of cyanobacterial EPS by examining the curated subset of 79 studies from the larger dataset. These papers were manually selected based on their explicit focus on potential industrial uses of cyanobacterial EPS. In this section we analyze these papers, providing a closer look at the specific industries that are emerging as key areas of interest for EPS applications, as well as the unique properties and functions driving their relevance.

In Figure 13 we visualize the analysis of the 79 studies from the perspective of industries mentioned as potential beneficiaries of each research. There seems to be a strong emphasis on healthcare and pharmaceutical applications for

cyanobacterial EPS, with 35 papers reporting potential uses in this sector. Of these, 29 studies specifically mention pharmacological applications, indicating a significant interest in EPS's bioactive properties for drug development, therapeutic interventions, immune modulation, and other related applications. A smaller subset (6 articles) highlights uses in general healthcare, most being related to the EPS's biocompatibility and potential in wound healing. Environmental applications constitute the second-largest category, with 20 studies focusing on sustainability-oriented uses. Metal removal is the primary environmental sub-category (12 articles), followed by wastewater treatment (8 articles), both being related to the potential of EPS's utilities in pollution control. In the food and agriculture field, 12 studies highlight applications, with food industries accounting for the majority (9 articles), most mentioning their potential uses in food preservation and additives. The agriculture subset includes 3 studies, with specific references to biofertilizers (2 articles) and biopesticides (1 article). Applications in the energy sector remain exploratory, with individual studies mentioning hydrogen production and energy production (bioethanol) as potential uses. Other applications make up a total of 16 mentions, with diverse fields represented. This distribution illustrates that, while healthcare and environmental applications dominate, there is emerging interest in other industrial uses of cyanobacterial EPS.

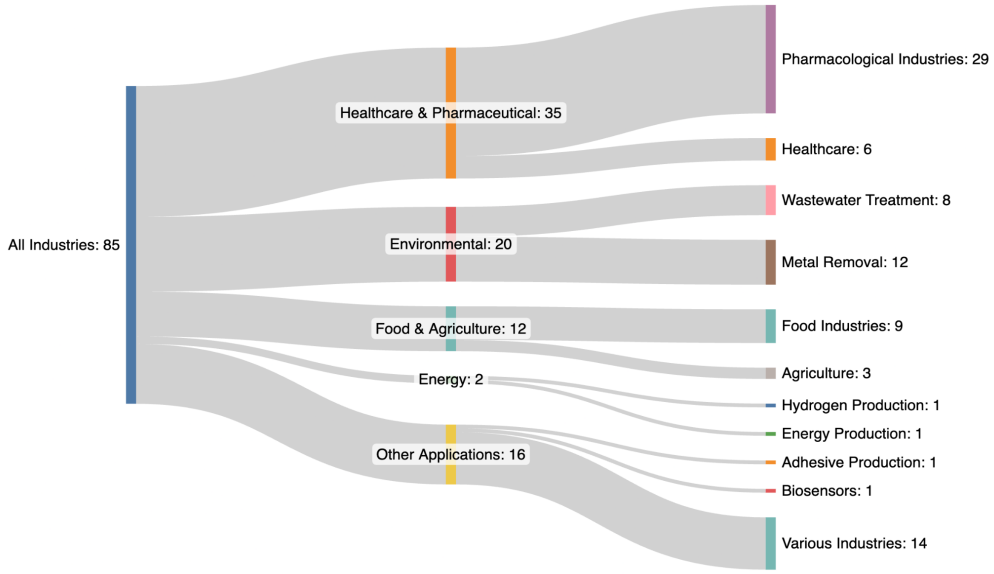

Figure 13. Potential applications for cyanobacterial EPS across various industries and sub-industries. Diagram created using SankeyMATIC.

We examined the publication trends across the main unified industries to identify potential distinct patterns that emerge over time, based on the publication year of the filtered dataset, as shown in Figure 14 (where x-axis represents the publication years, and the y-axis shows the publication count - each paper being counted once for each industry it mentions). Environmental applications, as well as healthcare and pharma-focused ones consistently exhibit high research activity, suggesting that these fields have maintained constant scientific interest, likely due to their relevance. In contrast, food and agriculture-related industries and other industries reveal sporadic peaks, which may correlate with periods of relevance, possibly driven by specific advancements or funding opportunities targeting these sectors. Energy-related industries show relatively low representation, indicating limited research in this direction or slower adoption of cyanobacterial EPS uses in this domain.

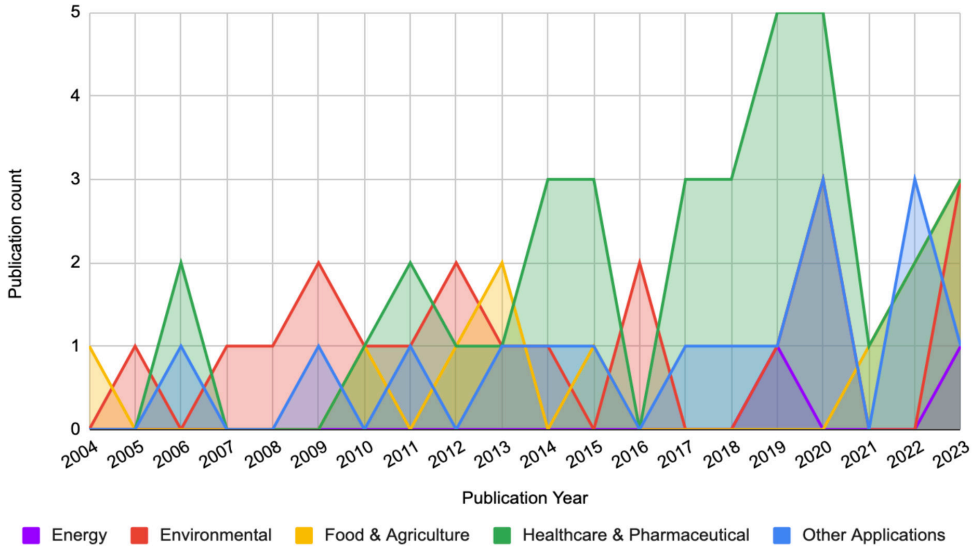

Figure 14. Distribution of publication counts across various main industries over time.

We also examined the distribution of cyanobacteria genera per main industry based on the data. We compiled this analysis in Figure 15. This heatmap reveals distinct patterns in the focus of cyanobacterial EPS research across industries. Healthcare and pharmaceutical, as well as environmental applications, dominate the distribution, with several genera such as *Cyanothece*, *Nostoc*, and *Synechocystis* frequently cited, reflecting these genera's known

benefits in therapeutic and ecological contexts (Colica *et al.*, 2010; Santos *et al.*, 2014; Leite *et al.*, 2017; Strieth *et al.*, 2020). Genera like *Phormidium* and *Spirulina*, which have established roles in nutritional and agricultural products (Vicente-García *et al.*, 2004; Li *et al.*, 2011; Ruangsomboon *et al.*, 2013; Vinoth *et al.*, 2023), were associated with applications in food and agriculture in our analysis. Notably, the top 10 genera mention in the filtered dataset (by the number of mentions) are *Nostoc* (23 occurrences), *Cyanothece* (11 occurrences), *Anabaena* (11 occurrences), *Synechocystis* (8 occurrences), *Oscillatoria* (5 occurrences), *Phormidium* (4 occurrences), *Gloeocapsa* (4 occurrences), *Lyngbya* (3 occurrences), *Aphanothece* (3 occurrences), *Cyanobacterium* (3 occurrences).

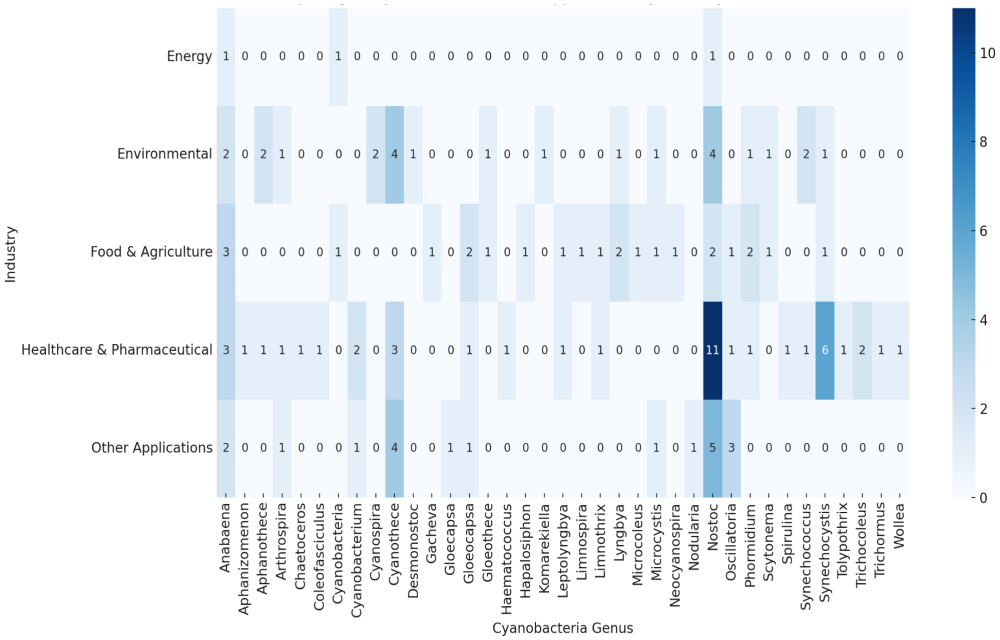

Figure 15. Heatmap that illustrates the distribution of unique genera (39) across the five main industries (Energy, Environmental, Healthcare & Pharmaceutical, Food & Agriculture, and Other Applications). Each cell indicates the count of unique publications where a specific genus is mentioned within a particular industry. Darker shades represent higher publication counts, showing which genera are most frequently associated with each industry.

Espacenet patent analysis

In this section, we analyze the patent landscape for cyanobacterial EPS using data extracted from the Espacenet database of the European Patent Office. This section highlights the industrial relevance and translational potential of cyanobacterial EPS. Our analysis aims to explore the connections between academic research output and industry adoption (through the intellectual property space) in the context of technological transfer.

Upon performing the search query as mentioned in the Materials and Methods (section 2.3), a total of 618 patents resulted.

Analyzing the geographical distribution of the patent document applications, we observe 59 distinct countries or jurisdictions for which a total of 2162 documents were filed. Here we mention that the discrepancy between the total number of patent documents (2162) and unique patent entries (618) reflects the grouping of related patents under a single patent family. Each patent family may include multiple filings across different jurisdictions for the same invention. For most countries (42 jurisdictions) there were between 1 and 12 documents filed. In Figure 16 we illustrate the distribution of the top 15 countries or entities for which intellectual property protection was sought based on the number of patent documents filed between 2004 and 2023 on cyanobacterial EPS. While we note some diversity in terms of the countries, it is clear that notable jurisdictions of interest where legal protection is of interest emerge. USA leads with the highest number of document filings (329), reflecting its interest in patenting potential industrial and research applications of the cyanobacterial EPS. This is closely followed by documents filed under the World Intellectual Property Organization (312), indicating international interest in securing broad patent protection, while China ranks third (286). Other jurisdictions, including the European Patent Office (205) and Canada (154), also demonstrate moderate interest.

When comparing the publication frequency of each country based on co-authors (Figure 3), China emerges as the leader. This aligns with China's growing interest in biotechnology and environmental sciences (Cao & Zhang, 2023; Xiao & Kerr, 2022). However, the majority of patents are filed in the USA and through the World Intellectual Property Organization (WO), with China coming in third (Figure 16). This discrepancy suggests a divergence between academic output and intellectual property strategies. Filing through WO under the Patent Cooperation Treaty (PCT) indicates a strategic approach to securing global intellectual property rights, while the USA's robust biotech industry incentivizes direct filings within its jurisdiction.

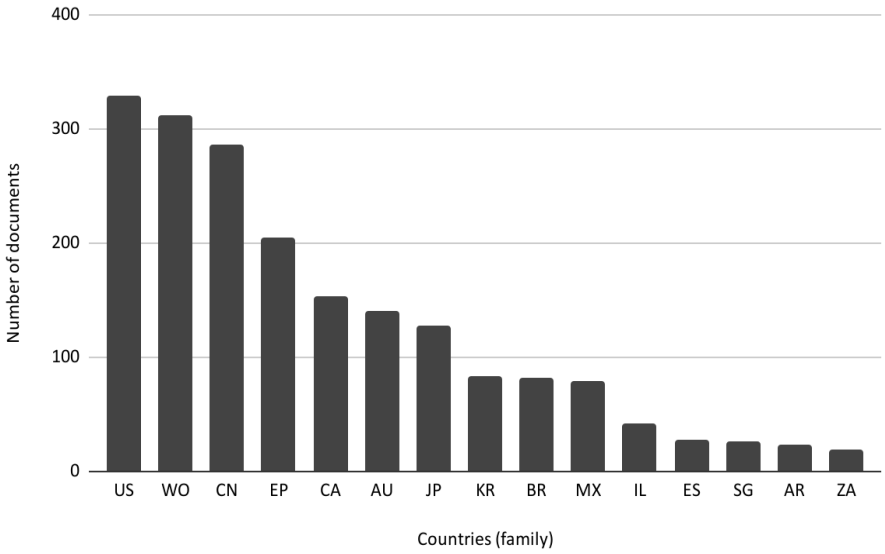

Figure 16. Geographical distribution of patent filings related to cyanobacterial EPS based on Espacenet data. The bar chart depicts the number of patent documents for the top 15 countries or jurisdictions (by the total number of documents filed between 2004 and 2023). OX-axis: countries (family) indicates the country or patent jurisdiction where the patent family was filed (e.g., US for the United States, CN for China, EP for European Patent Office, etc.). OY-axis: the number of documents represents the number of patent documents filed in that country or jurisdiction.

Next, we analyzed the temporal distribution of patent document filings for cyanobacterial EPS (Figure 17). Patent filings were sporadic between 2004 and 2010, with fewer than 15 patent documents published annually. This period likely represents the early stages of research and industrial interest in cyanobacterial EPS. Which matches the observations regarding the number of articles published in that period (Figure 2). A notable increase in patent activity began around 2011, with a sharp rise observed from 2014 onwards. This trend suggests a growing recognition of the commercial and biotechnological potential of cyanobacterial EPS. Additionally, the sustained high level of filings in recent years suggests an ongoing interest and active development in this field, which is confirmed by the growing number of articles published in the same time span (Figure 2).

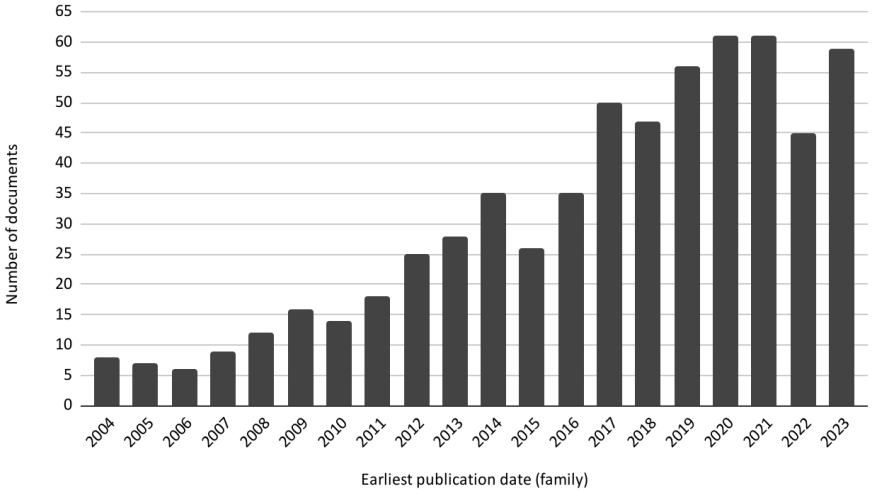

Figure 17. Temporal trends in patent filings for cyanobacterial EPS. Horizontal axis: the earliest publication date (family) refers to the year when the earliest patent in a family was published, representing the initial disclosure of the invention. Vertical axis: the number of documents represents the number of patent documents filed in that year.

In the dataset, between the 618 entities exported and the 2162 documents, there are 1000 distinct applicants. Most of the 1000 distinct applicants (971 applicants) have filed between 1 and 3 documents to be patented, and a select few have filed for more than that. Table 1 encompasses the top 10 applicants based on the total number of documents they have applied for, as well as the countries in which these entities are based, alongside a short description of their business focus based on publicly available information. The analysis of patent applicants highlights key players driving innovation in cyanobacterial EPS. Pivot Bio Inc leads with 26 patent documents, followed by Cool Planet Energy Systems Inc with 21 documents. The third player would be Native Microbials Inc with 20 documents - 10 plus the 10 from Ascus Biosciences Inc (company rebranded). Other notable applicants include Heliae Dev LLC (15 documents), Carbon Tech Holdings LLC (13 documents), and Algenol Biotech LLC (12 documents). The concentration of the number of patents among a few organizations suggests the presence of industry leaders heavily engaged in the research and commercialization of cyanobacterial EPS applications. Interestingly, the University of California seems to be the only educational-focused entity from the top applicants.

Table 1. The top 10 applicants filing patents related to cyanobacterial EPS, based on the total number of documents in the extracted Espacenet database.

Applicants	Documents	Focus	Country
Pivot Bio Inc	26	Specializes in developing microbial solutions to enhance nitrogen delivery to crops, aiming to reduce reliance on synthetic fertilizers.	USA
Cool Planet Energy Systems Inc	21	Developes engineered biocarbon technology designed to improve soil health while sequestering carbon. Their technology produced biochar-based agricultural products from biomass.	USA
Heliae Dev LLC	15	Focuses on developing microalgae-based technologies for agriculture, nutrition, and personal care products.	USA
Carbon Tech Holdings LLC	13	Involved in developing technologies for carbon capture and utilization, aiming to create sustainable materials and chemicals from carbon dioxide.	USA
Algenol Biotech LLC	12	Industrial biotechnology company that commercializes patented algae technology for the production of ethanol and other fuels. They utilize proprietary technologies to produce various products, including personal care items, food supplements, and industrial products, from a patented strain of cyanobacteria and a proprietary photobioreactor system.	USA
Univ California	2	US-based university.	USA
Sumitomo Chemical Co	11	Develops a wide range of products, including chemicals, petrochemicals, and agrochemicals. They invest in biotechnology research for applications in agriculture and materials science.	Japan
Ascus Biosciences Inc	10	Develops microbiome-based solutions for animal health and nutrition. It was later rebranded as *Native Microbials Inc.*	USA
Ecolab USA Inc	10	Develops solutions for water treatment, purification, cleaning, and hygiene across various industries, including food, healthcare, and hospitality.	USA
Native Microbials Inc	10	Rebrand of *Ascus Biosciences Inc*	USA

We observe that among the top 10 applicants, 9 are US-based companies, which explains why the majority of patent applications seek legal protection in the USA (Figure 16). This observation also somewhat explains the earlier discrepancy noted in this section that while China leads in the number of co-authors affiliated with publications, it ranks third in patent filings. This suggests that the robust academic collaboration in China does not yet fully translate into comparable levels of patent activity, unlike in the USA, where strong industry participation drives patent filings.

Discussion

Our study offers an analysis of the academic and industrial landscape surrounding cyanobacterial EPS between 2004 and 2023. By using bibliometric and patent analyses, we have identified key trends, contributors, and an increased potential for industrial applications of cyanobacterial EPS research. Below, we discuss the implications of these findings, their relevance to the scientific and industrial communities, and the limitations of this study.

Our findings reveal a steadily growing body of research on cyanobacterial EPS, with an annual growth rate of 13.14% over the study period (2004–2023). This growth shows an increased interest in this field. However, the thematic focus remains concentrated around healthcare, pharmaceuticals, and environmental applications, hence we understand that these industries dominate the research agenda.

The analysis of authorship and collaborative networks highlights the concentrated effort among a select group of researchers and institutions, particularly in China, the USA, India, and Europe. This collaboration aligns with the multidisciplinary nature of EPS applications but also indicates geographic and institutional disparities in research intensity and focus.

The filtered dataset illustrates a notable interest in the healthcare and environmental sectors, accounting for over half of the research focus. The bioactive and bioremediation properties of EPS have driven these trends, making them promising candidates for drug development, wound healing, and pollutant removal. Despite this focus, research on applications in the food, agriculture, and energy sectors remains sporadic and underdeveloped, possibly due to limited funding.

The positive annual growth rate of publications, dominance of leading global economies as top research producers, and the applied focus of top journals and highly cited articles highlight the field's translational orientation.

These findings point to the fact that cyanobacterial EPS research is oriented towards potential applications.

The increase in patent filings post-2014 mirrors the expansion of potential industrial interest, with the USA and China being prominent players. However, a disconnect between academic output and patent filings is evident, particularly in countries like China, which leads in publication frequency but lags in patent activity. This may suggest challenges in translating academic research into commercial products.

We note potential IP-related search limitations – the Espacenet search was done based on two terms: *cyanobacteria* and *exopolysaccharide*. It is possible that some patent filings would be more specific and name a particular cyanobacteria genus, species, strain, a particular extracellular polysaccharide, or process, and not necessarily use these relatively general terms. However, we have conducted the search using the "full text" filter, meaning all patents having the keywords within the documentation were included. While this does not guarantee all relevant patents were included, it brings the result closer to reality.

Regarding the publishing data collection – our study relies on WoS for bibliometric data, and we have included only English-language articles. We have used a relatively general search string, which should have included the majority of relevant research. We did not include in the search query specific cyanobacteria species names, but we used the "*all fields*" option. Since it is unlikely that papers focusing on specific cyanobacterial strains would not have used the term *cyanobacteria* or similar in any of the indexing fields, we believe all relevant results have been included.

Conclusions

Our study provides a bibliometric and patent analysis of cyanobacterial EPS, highlighting their academic and industrial significance. The growth in publications (13.14% annual growth), the active involvement of leading global economies, and the applied focus of top journals and cited articles underscore the increasing translational potential of these versatile biopolymers. Healthcare and environmental applications dominate the research landscape, reflecting the bioactive and bioremediation properties of EPS, while interest in other industries, such as food, agriculture, and energy, remains emergent. Patent data further supports the industrial readiness of EPS, with a growing number of filings and significant contributions from key players in biotechnology. Patent data further substantiates the industrial readiness of EPS, with a sharp increase

in filings post-2014 and a concentration of activity in the USA and globally through the Patent Cooperation Treaty. Leading contributors, including industry and some academic institutions, are driving innovation, with patents addressing diverse applications ranging from microbial solutions in agriculture to bio-based materials and energy production. These findings highlight the multidisciplinary appeal and industrial potential of cyanobacterial EPS. With sustained academic and industrial investment, EPS are positioned to contribute significantly to sustainable technologies and solutions across a range of sectors. This study provides a potential roadmap for future research and innovation, emphasizing the critical role of EPS in advancing biotechnology and sustainability.

Acknowledgements: Certain data included herein are derived from Clarivate™ (Web of Science™) and InCites.

Author Contributions: Conceptualization, M.B. and G.M.G.; methodology, M.B. and G.M.G.; software, G.M.G..; validation, E.R.-T., M.B. and G.M.G.; formal analysis, E.R.-T.; data curation, M.B.; writing—original draft preparation, M.B., G.M.G. and E.R.-T.; writing—review and editing, M.B., G.M.G. and E.R.-T.; visualization, G.M.G.; supervision, E.R.-T. All authors have read and agreed to the published version of the manuscript.

Funding: This work was supported through the "Nucleu" Program within the National Research Development and Innovation Plan 2022–2027, Romania, carried out with the support of MEC, project no. 27N/03.01.2023, component project code PN 23 24 01 02.

Data Availability Statement: Data is available upon request from authors.

References

Aria, M., & Cuccurullo, C. (2017). bibliometrix: An R-tool for comprehensive science mapping analysis. *J. Informetr. 11*(4), 959–975. https://doi.org/10.1016/j.joi.2017.08.007

Bhatnagar, M., Parwani, L., Sharma, V., Ganguly, J., & Bhatnagar, A. (2014). Exopolymers from *Tolypothrix tenuis* and three *Anabaena sp*. (Cyanobacteriaceae) as novel blood clotting agents for wound management. *Carbohyd. Polym. 99*, 692–699. https://doi.org/10.1016/j.carbpol.2013.09.005

Borowitzka, M. A. (2013). High-value products from microalgae—their development and commercialisation. *J. Appl. Phycol. 25*(3), 743–756. https://doi.org/10.1007/s10811-013-9983-9

Cao, X., & Zhang, Y. (2023). Environmental regulation, foreign investment, and green innovation: A case study from China. *Environ. Sci. Pollut. R. 30*(3), 7218–7235. https://doi.org/10.1007/s11356-022-22722-5.

Center for Strategic and International Studies (2021). China power project: Is China catching up to the United States in research and development (R&D) [Accessed 27 December 2024] https://chinapower.csis.org/china-research-and-development-rnd/

Colica, G., Mecarozzi, P. C., & De Philippis, R. (2010). Treatment of Cr(VI)-containing wastewaters with exopolysaccharide-producing cyanobacteria in pilot flow through and batch systems. *Appl. Microbiol. Biot. 87*(5), 1953–1961. https://doi.org/10.1007/s00253-010-2665-5

Cruz, D., Vasconcelos, V., Pierre, G., Michaud, P., & Delattre, C. (2020). Exopolysaccharides from cyanobacteria: strategies for bioprocess development. *Appl. Sci. 10*(11), Article 11. https://doi.org/10.3390/app10113763

Debnath, S., Muthuraj, M., Bandyopadhyay, T. K., Bobby, Md. N., Vanitha, K., Tiwari, O. N., & Bhunia, B. (2024). Engineering strategies and applications of cyanobacterial exopolysaccharides: A review on past achievements and recent perspectives. *Carbohyd. Polym.*, 328, 121686. https://doi.org/10.1016/j.carbpol.2023.121686

European Patent Office. (n.d.). Espacenet patent search. Retrieved November 2, 2024, from https://worldwide.espacenet.com/

Falsini, S., Rosi, M. C., Ravegnini, E., Schiff, S., Gonnelli, C., Papini, A., Adessi, A., Urciuoli, S., & Ristori, S. (2023). Nanoformulations with exopolysaccharides from cyanobacteria: Enhancing the efficacy of bioactive molecules in the Mediterranean fruit fly control. *Environ. Sci. Pollut. R. 30*(35), 83760–83770. https://doi.org/10.1007/s11356-023-28180-x

Flores, C., Lima, R. T., Adessi, A., Sousa, A., Pereira, S. B., Granja, P. L., De Philippis, R., Soares, P., & Tamagnini, P. (2019). Characterization and antitumor activity of the extracellular carbohydrate polymer from the cyanobacterium *Synechocystis* ΔsigF mutant. *Int. J. Biol. Macromol. 136*, 1219–1227. https://doi.org/10.1016/j.ijbiomac.2019.06.152

Gacheva, G., Gigova, L., Ivanova, N., Iliev, I., Toshkova, R., Gardeva, E., Kussovski, V., & Najdenski, H. (2013). Suboptimal growth temperatures enhance the biological activity of cultured cyanobacterium *Gloeocapsa sp*. *J. Appl. Phycol. 25*(1), 183–194. https://doi.org/10.1007/s10811-012-9852-y

Hyo Gyeom Kim, Kyung Hwa Cho, & Recknagel, F. (2024). Bibliometric network analysis of scientific research on early warning signals for cyanobacterial blooms in lakes and rivers. *Ecol. Inform.* 102503–102503. https://doi.org/10.1016/j.ecoinf.2024.102503

Jindal, N., Pal Singh, D., & Singh Khattar, J. (2013). Optimization, characterization, and flow properties of exopolysaccharides produced by the cyanobacterium *Lyngbya stagnina*. *J. Basic. Microb. 53*(11), 902–912. https://doi.org/10.1002/jobm.201200201

Kumar, D., Kaštánek, P., & Adhikary, S. P. (2018). Exopolysaccharides from cyanobacteria and microalgae and their commercial application. *Curr. Sci. 115*(2), 234–241

Laroche, C. (2022). Exopolysaccharides from microalgae and cyanobacteria: diversity of strains, production strategies, and applications. *Mar. Drugs 20*(5). https://doi.org/10.3390/md20050336

Leite, J. P., Mota, R., Durão, J., Neves, S. C., Barrias, C. C., Tamagnini, P., & Gales, L. (2017). Cyanobacterium-derived extracellular carbohydrate polymer for the controlled delivery of functional proteins. *Macromol. Biosci. 17*(2), 1600206. https://doi.org/10.1002/mabi.201600206

Li, H., Li, Z., Xiong, S., Zhang, H., Li, N., Zhou, S., Liu, Y., & Huang, Z. (2011). Pilot-scale isolation of bioactive extracellular polymeric substances from cell-free media of mass microalgal cultures using tangential-flow ultrafiltration. *Process Biochem. 46*(5), 1104–1109. https://doi.org/10.1016/j.procbio.2011.01.028

Li, P., Harding, S. E., & Liu, Z. (2001). Cyanobacterial exopolysaccharides: their nature and potential biotechnological applications. *Biotechnol. Genet. Eng. 18*(1), 375–404. https://doi.org/10.1080/02648725.2001.10648020

Mohamed, Z. A., Elnour, R. O., Alamri, S., & Hashem, M. (2023). Increased production of extracellular polysaccharides in *Arthrospira platensis* as a protective response against saxitoxin: Implications to outdoor mass production. *Algal Res. 74*, 103184. https://doi.org/10.1016/j.algal.2023.103184

Mota, R., Flores, C., & Tamagnini, P. (2020). Cyanobacterial extracellular polymeric substances (EPS). In J. M. Oliveira, H. Radhouani, & R. L. Reis (ed.), *Polysaccharides of Microbial Origin: Biomedical Applications* (pp. 1–28). Springer International Publishing. https://doi.org/10.1007/978-3-030-35734-4_11-1

Mota, R., Rossi, F., Andrenelli, L., Pereira, S. B., De Philippis, R., & Tamagnini, P. (2016). Released polysaccharides (RPS) from *Cyanothece sp*. CCY 0110 as biosorbent for heavy metals bioremediation: Interactions between metals and RPS binding sites. *Appl. Microbiol. Biot. 100*(17), 7765–7775. https://doi.org/10.1007/s00253-016-7602-9

Mugani, R., Fatima El Khalloufi, El Mahdi Redouane, Haida, M., Roseline Prisca Aba, Yasser Essadki, El, S., Abdessamad Hejjaj, Naaila Ouazzani, Campos, A., Hans-Peter Grossart, Mandi, L., Vasconcelos, V., & Brahim Oudra. (2024). Unlocking the potential of bacterioplankton-mediated microcystin degradation and removal: A bibliometric analysis of sustainable water treatment strategies. *Water Res. 255*, 121497–121497. https://doi.org/10.1016/j.watres.2024.121497

Najdenski, H. M., Gigova, L. G., Iliev, I. I., Pilarski, P. S., Lukavský, J., Tsvetkova, I. V., Ninova, M. S., & Kussovski, V. K. (2013). Antibacterial and antifungal activities of selected microalgae and cyanobacteria. *Int. J. Food Sci. Tech. 48*(7), 1533–1540. https://doi.org/10.1111/ijfs.12122

Nath, P. C., Tiwari, O. N., Devi, I., Bandyopadhyay, T. K., & Bhunia, B. (2021). Biochemical and morphological fingerprints of isolated *Anabaena sp*.: A precious feedstock for food additives. *Biomass Conversion and Biorefinery*, 11(6), 2723–2733. https://doi.org/10.1007/s13399-020-00651-y

National Center for Science and Engineering Statistics. Survey of federal funds for research and development, volume 70, FYs 2020–21. National Science Foundation (2021). [Accessed 27 December 2024]. https://ncses.nsf.gov/surveys/federal-funds-research-development/2021#data.

Nishanth, S., Bharti, A., Gupta, H., Gupta, K., Gulia, U., & Prasanna, R. (2021). Chapter 14 - Cyanobacterial extracellular polymeric substances (EPS): Biosynthesis and their potential applications. In: S. Das & H. R. Dash (Eds.), *Microbial and Natural Macromolecules*,pp. 349–369. Academic Press. https://doi.org/10.1016/B978-0-12-820084-1.00015-6

Parikh, A., Madamwar, D., & Patel, H. (2006). Aerobic decolorization of textile dyes by a mixed bacterial consortium DMC. *Bioresource Technol. 97*(16), 2193–2198. https://doi.org/10.1016/j.biortech.2005.09.008

Potnis, A. A., Raghavan, P. S., & Rajaram, H. (2021). Overview on cyanobacterial exopolysaccharides and biofilms: Role in bioremediation. *Rev. Environ. Sci. Bio. 20*(3), 781–794. https://doi.org/10.1007/s11157-021-09586-w

Qi, Y., Chen, X., Hu, Z., Song, C., & Cui, Y.-L. (2019). Bibliometric analysis of algal-bacterial symbiosis in wastewater treatment. *Int. J. Env. Res. Pub. He. 16*(6), 1077–1077. https://doi.org/10.3390/ijerph16061077

Qu, F., Zhu, A., Ma, Y., Zhang, L., & Ding, Y. (2012). Anaerobic digestion of rice straw in a constructed wetland for biogas and biofertilizer production. *Water Res. 46*(8), 2670–2676. https://doi.org/10.1016/j.watres.2012.02.045

Ramachandran, L., Marappa, N., Sethumadhavan, K., & Nooruddin, T. (2020). Glycoprotein prompted plausible bactericidal and antibiofilm outturn of extracellular polymers from *Nostoc microscopicum*. *Appl. Biochem. Biotech. 191*(1), 284–298. https://doi.org/10.1007/s12010-019-03179-8

Reignier, O., Bormans, M., Marchand, L., Sinquin, C., Amzil, Z., Zykwinska, A., & Briand, E. (2023). Production and composition of extracellular polymeric substances by a unicellular strain and natural colonies of Microcystis: Impact of salinity and nutrient stress. *Env. Microbiol. Rep. 15*(6), 783–796. https://doi.org/10.1111/1758-2229.13200

Rodrigues, F., Mendonça, I., Faria, M., Gomes, R., Pinchetti, J. L. G., Ferreira, A., & Cordeiro, N. (2024). Response surface methodology applied to cyanobacterial eps production: steps and statistical validations. *Processes 12*(8), Article 8. https://doi.org/10.3390/pr12081733

Rossi, F., & De Philippis, R. (2015). Role of cyanobacterial exopolysaccharides in phototrophic biofilms and in complex microbial mats. *Life 5*(2), Article 2. https://doi.org/10.3390/life5021218

Ruangsomboon, S., Wongrat, L., Choochote, S., Ganmanee, M., & Saparnklang, A. (2013). Effects of low pH and Pb2+ stress on living cyanobacterium, *Phormidium angustissimum* West & G.S.West: A test of its feasibility as a living biosorbent. *J. Appl. Phycol. 25*(3), 905–911. https://doi.org/10.1007/s10811-013-0004-9

SankeyMATIC. (n.d.). Sankey diagram builder. [Accessed 2 November 2024] http://sankeymatic.com

Santos, C., Silva, C. J., Büttel, Z., Guimarães, R., Pereira, S. B., Tamagnini, P., & Zille, A. (2014). Preparation and characterization of polysaccharides/PVA blend nanofibrous membranes by electrospinning method. *Carbohyd. Polym. 99*, 584–592. https://doi.org/10.1016/j.carbpol.2013.09.008

Shen, S., Jia, S., Wu, Y., Yan, R., Lin, Y.-H., Zhao, D., & Han, P. (2018). Effect of culture conditions on the physicochemical properties and antioxidant activities of polysaccharides from *Nostoc flagelliforme*. *Carbohyd. Polym. 198*, 426–433. https://doi.org/10.1016/j.carbpol.2018.06.111

Van Camp, C., Fraikin, C., Claverie, E., Onderwater, R., & Wattiez, R. (2022). Capsular polysaccharides and exopolysaccharides from *Gloeothece verrucosa* under various nitrogen regimes and their potential plant defence stimulation activity. *Algal Res. 64*, 102680. https://doi.org/10.1016/j.algal.2022.102680

Vicente-García, V., Ríos-Leal, E., Calderón-Domínguez, G., Cañizares-Villanueva, R. O., & Olvera-Ramírez, R. (2004). Detection, isolation, and characterization of exopolysaccharide produced by a strain of *Phormidium* 94a isolated from an arid zone of Mexico. *Biotechnol. Bioeng. 85*(3), 306–310. https://doi.org/10.1002/bit.10912

Vinoth, M., Sivasankari, S., Ahamed, A. K. K., Alsamhary, K. I., Al-enazi, N. M., Abdel-Raouf, N., Alharbi, R. M., Govindarajan, R. K., Ravi, G., Alarjani, K. M., & Sholkamy, E. N. (2023). Bio-characterization and liquid chromatography–mass spectrometry analysis of exopolysaccharides in biofilm-producing cyanobacteria isolated from soil crust: exploring the potential of microalgal biomolecules. *Biology 12*(8). https://doi.org/10.3390/biology12081065

Ward, N. L., Challacombe, J. F., Janssen, P. H., Henrissat, B., Coutinho, P. M., Wu, M., ... & Kuske, C. R. (2009). Three genomes from the phylum *Acidobacteria* provide insight into the lifestyles of these microorganisms in soils. *Appl. Environ. Microb. 75*(7), 2046–2056. https://doi.org/10.1128/aem.02294-08

Xiao, Z., & Kerr, W. A. (2022). Biotechnology in China – regulation, investment, and delayed commercialization. *GM Crops Food 13*(1), 86–96. https://doi.org/10.1080/21645698.2022.2068336

Yousaf, F., Bukhari, S. A. R., Shakir, H. A., Khan, M., Franco, M., & Irfan, M. (2024). Cyanobacterial exopolysaccharides: extraction, processing, and applications. In M. A. Mehmood, P. Verma, M. P. Shah, & M. J. Betenbaugh (Eds*.), Pharmaceutical and Nutraceutical Potential of Cyanobacteria*, pp. 277–309. Springer International Publishing. https://doi.org/10.1007/978-3-031-45523-0_11

STUDIA UNIVERSITATIS BABEŞ-BOLYAI BIOLOGIA, 70, 1, 2025 (p. 49-63)
doi:10.24193/subbbiol.2025.1.03

The effects of bulk, biologic and nano-form fertilizers on *Zea mays* growth under irrigated circumstances

Mohsen Janmohammadi[1], Soheila Samadi[2] and Naser Sabaghnia[1]✉

[1]*Department of Plant Production and Genetics, Faculty of Agriculture, University of Maragheh, Iran;* [2]*Department of Biology, Payame Noor University, PO BOX 19395-3697 Tehran, Iran;*
✉***Corresponding author, E-mail: sabaghnia@maragheh.ac.ir.***

Article history: Received 15 March 2024; Revised 16 December 2024; Accepted 5 May 2025; Available online 25 June 2025

Abstract. In practical plant biology, nanotechnology has involvements on every step of cropping, such as early growing, maintenance, harvesting and post harvesting and it has caused remarkable changes in findings solutions for facing problems. A trial was done to study the effects of different fertilizers on maize performance. The trial compared NPK bulk fertilizer, synthetic nano-sized fertilizers (boron, zinc, and complete), and biological fertilizers. Analyzing the data through principal component (PC) analysis indicated that the PC1 and PC2 explained for 56 and 27% of the variability in the dataset. Synthetic nano-zinc and nano-boron emerged as the most promising fertilizers, showcasing superior performance in terms of yield performance and yield components. A vector-tool biplot highlighted a robust positively correlation between chlorophyll content and straw yield, along with similar trends in grain yield and number of kernels per ear. Conventional bulk fertilizer (NPK) showed relatively lower efficiency across most evaluated traits. Based on ideal trait biplot, biological yield and stem diameter exhibited similar properties like to ideal trait, while oil percentage and hundred grain weight demonstrated unfavorable performance across treatments. This analysis underscores the efficacy of the treatment × trait biplot in elucidating relationships among traits and facilitating visual comparisons between different fertilizers. Overall, the findings underscore the significant enhancement of various maize cultivation traits through the application of synthetic nano-zinc and boron fertilizers, particularly in full irrigation condition.

Keywords: bulk fertilizer, nano-complete, nano-zinc, treatment by trait interaction

Introduction

Corn (*Zea mays* L.) is a versatile crop known for its adaptability to diverse production environments. It ranks as the third most significant crop globally, following wheat and rice, in terms of cultivation area, production output, and grain yield. However, in semi-arid regions, water scarcity and drought stress pose considerable challenges to crop productivity (Zou *et al.,* 2021). Food security in these regions relies heavily on the cultivation of plants that exhibit high tolerance to water deficits. Approximately 20-25 percent of maize-growing areas experience the harmful impacts of environmental stresses and the impact of water scarcity on maize grain yields varies across different stages of crop growth (Meng *et al.,* 2016). Nonetheless, selecting for stress tolerance remains challenging due to the complexity of genotype × environment interactions and insufficient understanding of tolerance mechanisms. Studies have shown that water scarcity negatively impacts phenological traits and root properties in maize. Grain yield and its components in maize are governed by a complex interplay of genes that respond to water scarcity with varying degrees of adaptability. Consequently, maize yield losses due to drought stress can range up to 76%, depending on the severity, timing, and stage of drought occurrence. Chukwudi *et al.* (2021) observed a decrease in grain yield of approximately 40% under drought stress, primarily attributable to reductions in kernel weight and kernel number.

Effective nutrient management stands out as a critical factor influencing maize performance, with responses to mineral fertilization varying depending on fertilizer type, application timing, and soil conditions. Moreover, the efficacy of fertilization is influenced by environmental factors such as climate and soil moisture content (Chen *et al.* 2018). While the conventional recommendation for maize typically involves the application of NPK (nitrogen, phosphorus, and potassium) fertilizers, their application under water-limited conditions remains inadequately explored. Biological fertilizers also play a pivotal role in crop production and soil fertility enhancement. These fertilizers, referred to as bio-fertilizers, because they contain living microorganisms that augment the providing of essential nutrients to host plants via nature-based ways such as fixing of nitrogen and solubilizing of phosphorus (Kumar *et al.,* 2018). However, the effects of biological fertilizers under water stress conditions are not yet fully understood. Micronutrients, required by plants in minute quantities, typically maintain concentrations below 100 parts per million (ppm). Among these micronutrients, zinc and boron are pivotal for various metabolic processes. Zinc, a constituent of numerous enzymes and proteins, plays crucial roles in growth hormone production and internode elongation (Rudani *et al.,* 2018). Boron, essential for both vegetative and reproductive growth, contributes to the integrity

of cell walls by binding to pectic polysaccharides. Additionally, it facilitates cell division, influences plasma membranes and phenol metabolism, and is indispensable for nitrogen fixation (Kohli *et al.,* 2023). However, boron can become toxic at levels slightly exceeding those necessary for normal growth.

In semi-arid regions, micronutrients tend to be readily adsorbed to soil particles, with their availability decreasing as soil pH rises, so nano-fertilizers offer a potential solution to this issue (Janmohammadi and Sabaghnia, 2023). These next-generation fertilizers contain nano-scaled active nutrients and controlled-release kinetics to target specific sites, effectively serving as smart issues. Nano fertilizers significantly enhance the efficiency of nutrient usage compared to conventional bulk fertilizers, primarily due to targeted delivery and slow or controlled release (Dimkpa *et al.,* 2020). The superiority of nano-based fertilizers lies in their novel and improved physical, chemical, and biological properties, driven by their high surface area-to-volume. While some information exists on the foliar application of certain nano-micronutrient fertilizers on specific crops, there remains a lack of sufficient data regarding the efficacy of soil-applied nano-fertilizers under conditions of limited irrigation. Hence, this study aims to assess the impacts of bio- and nano- based fertilizers on maize performance, its components, and some other morphological traits under limited irrigation conditions.

Materials and methods

Trial

The study took place at the research field of the Agricultural and Natural Resources College of Moghan, located in northwestern Iran (latitude 39° 41' N and longitude 47° 32' E). Situated in a Mediterranean-type climate zone, the region experiences rainfall predominantly from May to October. As per data from the ParsAbad, Moghan. Maximum temperatures reach 31.4 °C in August, while minimum temperatures drop to 1.4 °C in January. The average yearly precipitation stands at 389.5 mm. Planting was conducted manually, with two seeds per hole on flat ground, followed by thinning to achieve the desired population densities soon after emergence. To ensure uniform germination, emergence, and establishment, all trial plots received an initial irrigation. Each plot comprised seven rows, each 5 meters in length, with row spacing set at 65 cm and intra-row spacing at 20 cm, aligning with recommended commercial densities for the site. Surface normal irrigation, reaching up to 100% of field capacity, was administered on the vegetative step. Irrigation during this period was scheduled when half the depth of the root zone approached a 50% depletion level, with a net irrigation water depth of approximately 120 mm.

Treatments

The clay loamy soil in the area boasted sufficient depth, exceeding 1 meter, soil characteristics included a clay loam texture, pH of 7.5, electrical conductivity (EC) of 0.94 ds/m, and low nutrient content (0.03% nitrogen, 0.01% phosphorus, and 0.02% potassium). Treatments encompassed various options: a control group receiving no fertilizer (control), bio-fertilizers including nitrogen (Bio-N), and phosphorous (Bio-B). Additionally, nano-boron (Nano-B), nano-zinc (Nano-Zn), complete nano-fertilizer (Nano-C), and bulk NPK (180:100:50 kg ha^{-1} urea, superphosphate, and sulphate of potash) fertilizer were included (Table 1). Nitrogen bio-fertilizer composed of the promoting rhizobacteria consortium (107 CFU/ml; including *Azotobacter chroococcum* + *Azospirillum lipoferum* species. Also, phosphorus bio-fertilizer included phosphate solubilizing rhizobacteria such as *Pseudomonas* and *Bacillus*. Half of the nitrogen and all of the phosphorus and potassium were performed pre-sowing, while the second half of nitrogen was top-dressed after a sowing. Bio-fertilizers were applied via seed inoculation just before planting. The nano-chelated complete fertilizer contained several essential elements at specified concentrations. Nano-fertilizers were administered three times via foliar spray at a 2000 ppm rate during the 9-leaf stage, stem elongation, and heading stages. All farming managements were uniformly applied to all plots throughout the experimental period. The synthesized nano-fertilizers were obtained from the SepehrParmis Co., Iran.

Table 1. The applied fertilizer treatments on maize

#	Type	Code	Name
1	---	Control	No- fertilizer application
2	Bio-fertilizer	Bio-N	Nitrogen bio-fertilizer
3		Bio-B	Phosphorous bio-fertilizer
4	Nano-fertilizer	Nano-B	Boron nano-fertilizer
5		Nano-Zn	Zinc nano-fertilizer
6		Nano-C	Complete nano-fertilizer
7	Chemical-fertilizer	NPK	Nitrogen, phosphorous, and potassium

Traits

The About ten randomly selected plant samples were chosen from each plot to determine leaf area (LA), kernels per ear (KE), ear diameter (ED), ear length (EL) and stem diameter (SD). At the harvesting stage, three 4-meter rows of maize were harvested from the center of each plot to determine grain yield (GY), biomass yield (BY), straw yield (SY), hundred grain weight (HGW) and harvest index (HI). Relative water content (RWC) was recorded at the beginning

of the grain development stage. Oil percentage (OP) was recorded via a near-infrared tool while relative water content (RWC) and chlorophyll (CHL) were recorded at the starting of the grain formation time.

Data analysis

The biplot model as the treatment by trait (TT) interaction was applied with GGEbiplot application (Yan, 2001) via blow equation.

$$\frac{\alpha_{ij} - \beta_j}{\sigma_j} = \sum_{n=1}^{2} \lambda_n \xi_{in} \eta_{jn} + \varepsilon_{ij}$$

where $\alpha_{ij}$is the fertilizer i for character j, $\beta_j$is the average of fertilizers in character j, $\sigma_{ij}$is the standard deviation of character j, $\lambda_n$is the lambda for PC (principal component) n, ξ_{in} is score for fertilizer i on PCn, η_{jn} is score for character j on PCn, and $\varepsilon_{ij}$is the error term.

Results and discussion

The fitted TT biplot fourmula elucidated 83% of the variability in the data illustrating the performance of maize across various fertilizers. Notably, the first two PC models determined for 56% and 27% of this variability, respectively. This significant portion of variation underscores the intricate interplay among the measured traits across the different fertilizer treatments (Begam *et al.,* 2024). As emphasized by Janmohammadi *et al.* (2016), the key structure among the characteristics must be evident in the fitted model, and the success of the TT biplot model hinges on identifying the first two PC axes. However, in line with the report of Sabaghnia *et al.* (2016), and Porkabiri *et al.* (2019), it has been proposed that two PC axes are adequate for predictive modeling in analyses of two-way datasets such as the TT biplot model. Hence, the interaction between the seven fertilizers treatments and the thirteen traits in current investigation was most accurately predicted by the PC1 and PC2.

In the polygon-too (Fig. 1), the traits are regarded as the tester, while the treatments serve as the entries. This figure effectively showcases which treatment(s) excel in specific traits and in this biplot, the fertilizer(s) positioned at each vertex indicate the best or worst performers in terms of the characteristics found within the section. From Fig. 1, it's evident that the Nano-Zinc fertilizer (Nano-Zn) treatment outperformed others in all traits such as grain yield (GY), except straw yield (SY), chlorophyll content (CHL) and oil percentage (OP). This suggests that Nano-Zn can be deemed as the optimal fertilizer for maize production, particularly excelling in these traits. Suganya *et al.* (2020) corroborated that the usage of zinc can enhance maize performance and other characteristics.

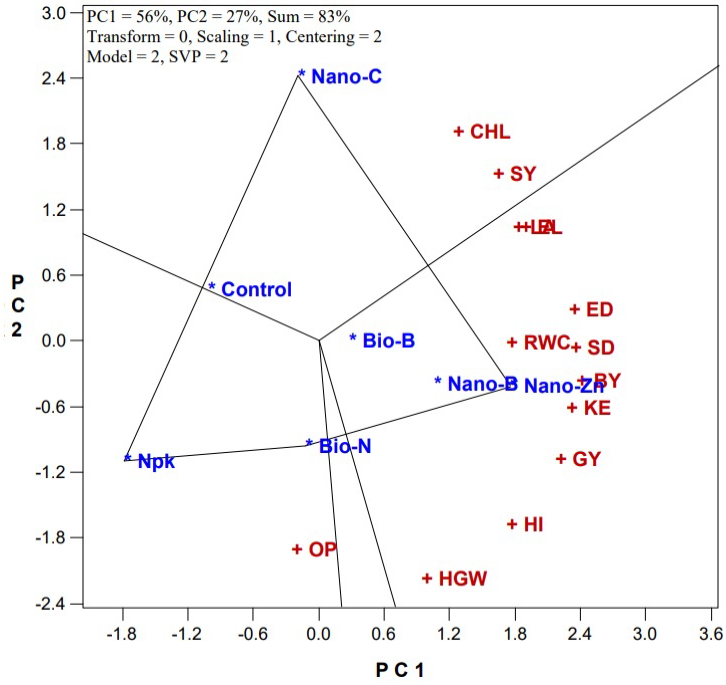

Figure 1. Which won where tool of treatment by trait (TT) biplot.
Traits are: leaf area (LA), kernels per ear (KE), chlorophyll content (CHL), ear diameter (ED), grain yield (GY), ear length (EL), stem diameter (SD), relative water content (RWC), biomass yield (BY), straw yield (SY), hundred grain weight (HGW), harvest index (HI) and oil percentage (OP).

Similarly, Ahmad *et al.* (2024) noted that maize grain yield increased with zinc fertilization, significantly boosting both nitrogen uptake and yield. The nano-complete fertilizer (Nano-C) emerged as the top-performing fertilizer for CHL and SY traits while conventional bulk NPK fertilizer (nitrogen + phosphorus + potassium) proved to be the best treatment for the oil percentage (OP) trait. Despite the Nano-Zn following to Nano-B demonstrating prowess in grain yield and yield component traits, they didn't excel in important traits like oil percentage and chlorophyll content. This suggests that yield properties may not necessarily correlate with oil percentage or chlorophyll content. Similarly, Farnia *et al.* (2015) found that nano-form fertilizers of zinc and boron improved yield components and performance in maize, aligning well with our findings.

In the vector-view TT biplot, vectors extend from the biplot origin approximate the association of traits by the angle cosine (Janmohammadi *et al.* 2017). The relative length of the vectors indicates the remarkable variability described by the model, with all measured traits contributing except for plant height (Fig. 2).

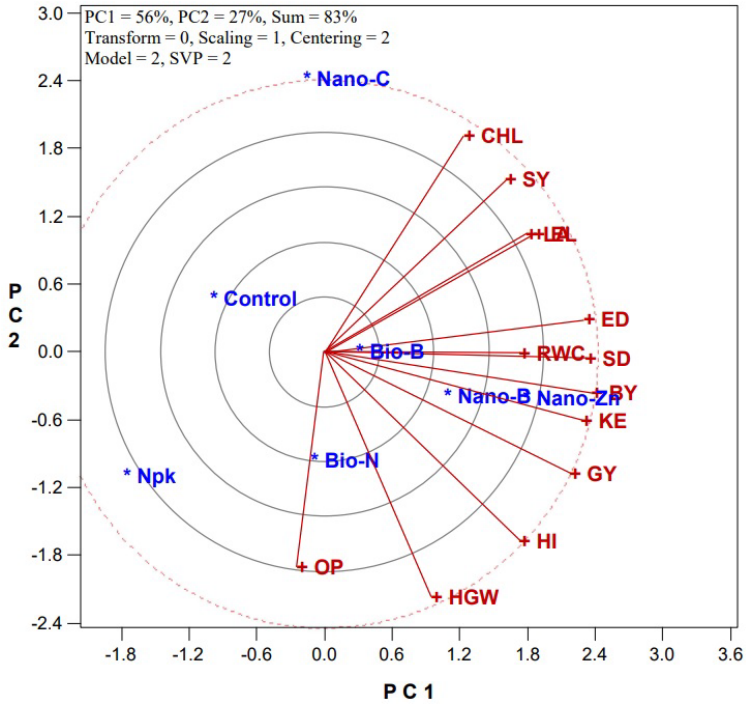

Figure 2. Vector tool of treatment by trait (TT).
Traits are: leaf area (LA), kernels per ear (KE), chlorophyll content (CHL), ear diameter (ED), grain yield (GY), ear length (EL), stem diameter (SD), relative water content (RWC), biomass yield (BY), straw yield (SY), hundred grain weight (HGW), harvest index (HI) and oil percentage (OP).

Notably, the relationships unveiled by this model include: (i) A positively association between CHL and SY, between ear length (EL) and leaf area (LA), between kernels per ear (KE) and biomass yield (BY), between grain yield (GY) and kernels per ear (KE), and between relative water content (RWC) with stem diameter (SD), evident from their angles. (ii) A relatively zero association between oil percentage (OP) with kernels per ear (KE) and biomass yield (BY), and between GY with SY and CHL, indicated by nearly perpendicular vectors. (iii) A negative association between chlorophyll content (CHL) and oil percentage (OP), illustrated by large obtuse angles (Fig. 2). While most of these predictions align with Pearson's correlation coefficients (Results are not shown), some discrepancies arise because the TT biplot method explains less than 100% of the total variation (in this study, 83%). Although, these conclusions contain minor errors, the TT biplot offers predictions on the overall dataset pattern, making them likely more reliable than individual observations (Yari *et al.,* 2018). Significant positive

correlations between yield performance and kernels per ear as well as significant positively correlation between ear length and leaf area have been reported (Zhang *et al.,* 2020).

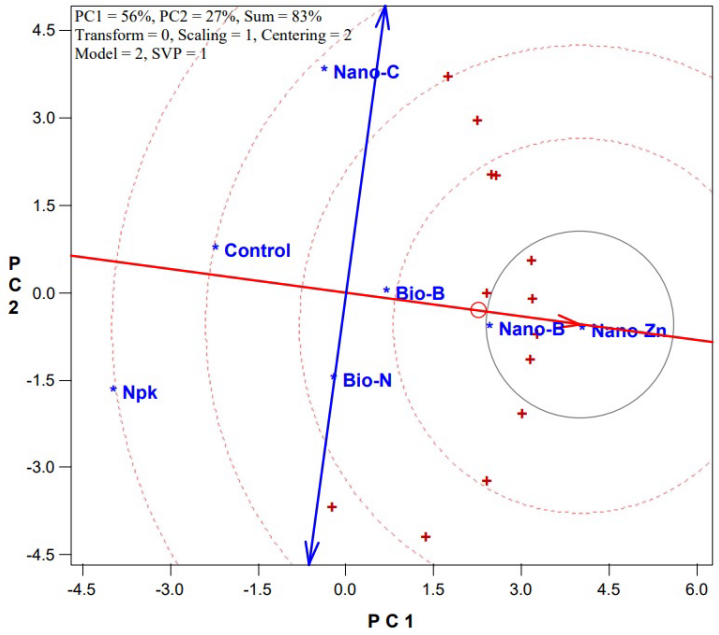

Figure 3. Ideal treatment tool of treatment by trait (TT) biplot.

For the quest for identifying an ideal treatment, it is generated as one that incorporates various favorable traits in its response. In Fig. 3, the single-arrow line represents the mean-trait axis, where fertilizers are ranked based on their trait response and divides this axis into two, with the right portion displaying fertilizers above mean and the left indicating those below mean (Mohammadi *et al.,* 2023). Based on this biplot (Fig. 3), Nano-Zn, Nano-B, and Bio-B exhibited above-average performance, while Bio-N, Nano-C, Control, and NPK (nitrogen + phosphorus + potassium) demonstrated below-average performance across traits.

The underperformance of NPK observed in this research aligns with the findings of Senthilkumar *et al.* (2021), who noted that micronutrient applications, such as zinc, outperformed NPK fertilizer. An ideal fertilizer should boast the high response for all traits, indicated by the long projection onto the mean trait axis and the short fertilizer vector. From Fig. 3, Nano-Zn and Nano-B fertilizer are close to the location of an ideal one, ranking as high regarding the response of traits due to their desirability across most traits. These treatments could serve as preferable alternatives to conventional fertilizers like NPK or other bulk fertilizers.

Current finding is supported by the study of Yousefzadeh *et al.* (2021), who highlighted that nano-forms of zinc and boron application yielded superior performance in various agronomic and yield traits of maize.

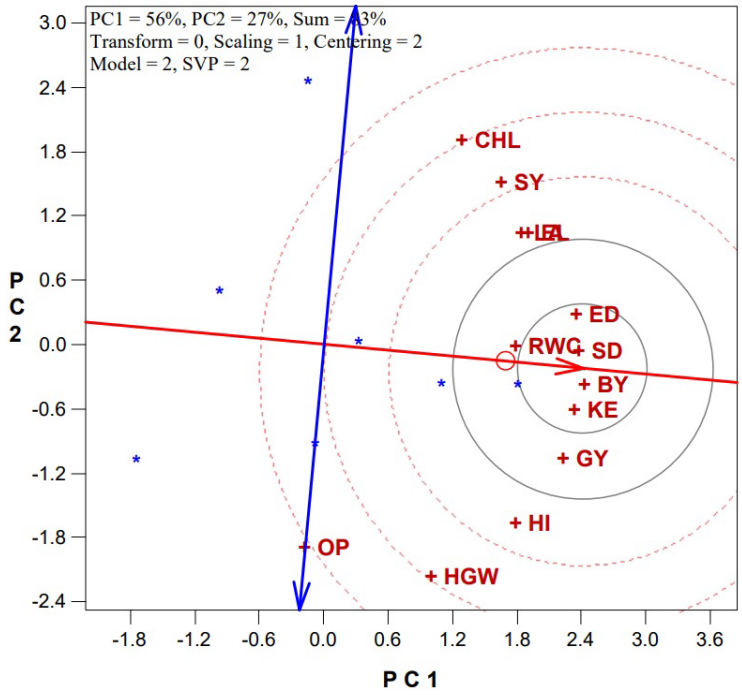

Figure 4. Ideal trait tool of treatment by trait (TT) biplot.
Traits are: leaf area (LA), kernels per ear (KE), chlorophyll content (CHL), ear diameter (ED), grain yield (GY), ear length (EL), stem diameter (SD), relative water content (RWC), biomass yield (BY), straw yield (SY), hundred grain weight (HGW), harvest index (HI) and oil percentage (OP).

In the TT biplot, the ideal trait incorporates various favorable treatments in its response. In Fig. 4, the single-arrow line represents the average-tester axis abscissa, where traits are ranked based on their response to treatments (Ebrahimi *et al.,* 2023). Based on this biplot (Fig. 4), biomass yield (BY) and stem diameter (SD) following to kernels per ear (KE), ear diameter (ED), relative water content (RWC) and grain yield (GY) exhibited similar properties like to ideal trait and indicated above-average performance, while oil percentage (OP), hundred grain weight (HGW), chlorophyll content (CHL) and straw yield (SY), demonstrated unfavorable performance across treatments. In the vector-tool of the model depicted in Fig. 5, treatments closely associated with the target trait of good grain yield

in maize are highlighted. Nano-Zn and Nano-B emerge as fertilizers good for achieving desirable yield performance, indicating that their usage is expected to enhance grain yield under drought stress conditions.

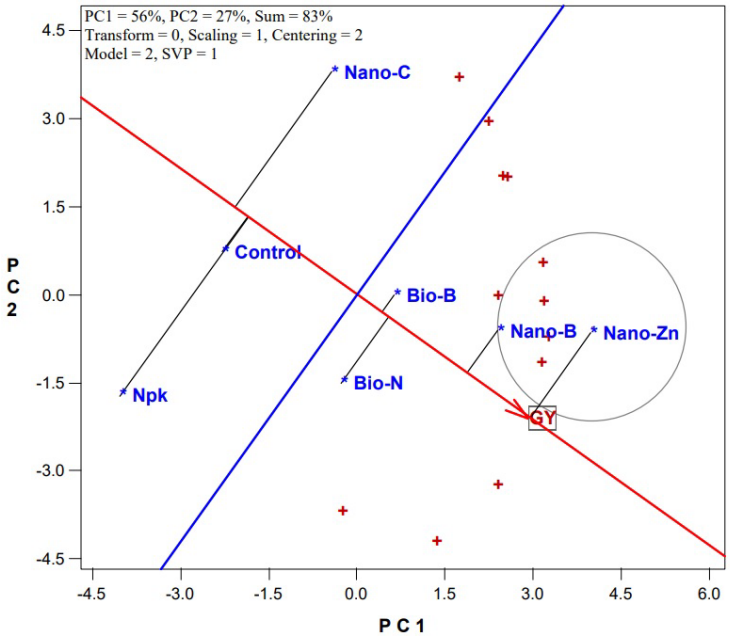

Figure 5. Examine a trait tool of treatment by trait (TT) biplot, for the selected trait (GY, grain yield).

This implies that the use of nano-sized micronutrient fertilizers not only promotes high yield perforamnce but also improves other agronomic characteristics, thereby enhancing the widespread adoption of such fertilizers. Azam *et al.* (2020) demonstrated the positive effect of zinc nano-fertilizer usage in plant growth and performance of maize, attributed to increased activity of growth hormones. Similarly, Al-Juthery and Al-Maamouri (2020) emphasized the positive effects of boron nano-fertilizer in improving potato traits. Saritha *et al.* (2022) found that nano-composites were safe for crop products, suggesting that the use of nano-sized fertilizers is not only beneficial for crop production but also offers economic advantages.

In corn genotypes, two yield components [kernels per ear (KE) and hundred grain weight (HGW)] are crucial for selecting genotypes with superior grain yield (GY) performance. Fig. 6 presents a biplot based on these traits, which captures significant variability; the first two principal components (PCs) account for 85% and 15% of this variation, respectively. The trait vectors illustrate the

interrelationships among them, a pattern consistent across various datasets. Notably, grain yield is more closely related to the number of kernels per ear than to the hundred grain weight. Other studies have also highlighted the importance of the number of kernels per ear (Liu *et al.,* 2020; Sabitha *et al.,* 2024). For optimal selection of corn genotypes, it is advisable to prioritize kernels per ear (KE) over hundred grain weight (HGW) in the selection indices. Moreover, selecting based solely on both traits is not recommended due to their weak positive correlation; focusing on kernels per ear alone yields satisfactory results. The TT biplot model demonstrates that selecting based on kernels per ear during the early stages of selection is not only logical but also efficient. Additionally, this model facilitates genotype assessment based on these two traits. The predominance of the number of seeds per plant over seed weight in various cereals has been documented by numerous researchers (Matsuyama and Ookawa, 2020; Tehulie and Eskezia, 2021).

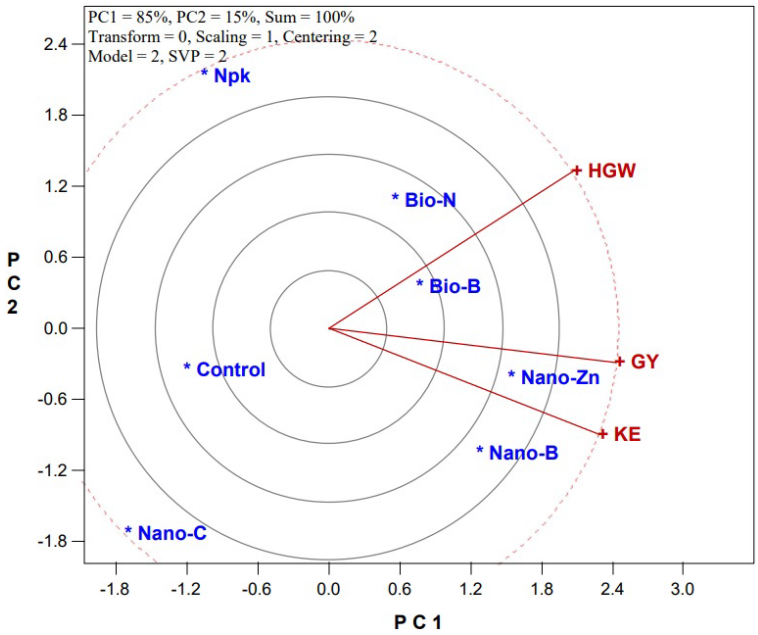

Figure 6. Vector tool of treatment by trait (TT) biplot, for kernels per ear (KE) and hundred grain weight (HGW) with grain yield (GY).

Studies have demonstrated that the utilization of nano-fertilizers leads to significant increased efficiency nutrient application, decreased toxicity in fields, mitigation of adverse impacts related with over-application, and reduced rates of usage. This is particularly significant for reaching the goals of sustainable farming, especially in undeveloped regions. The emergence of nanotechnology has introduced

a variety of nanomaterials with unique biologic as well as physical and chemical properties. Encapsulation of fertilizers within nanoparticles is one such innovation, which can be achieved through methods such as encapsulation inside nanopores, coating with thin polymer films, and delivery as emulsions of nano-scale dimensions (Konappa *et al.,* 2021). Nano-size fertilizers integrate nano-tools for synchronization the gradual delivery of fertilizers with crop uptake, thus preventing unfavorable fertilizer degradation in the field. The employed TT biplot model serves as an accomplished option for imaged analysis of dataset. In comparison to the routine numerical models, this procedure offers several benefits: (i) graphical presentation enhances understanding of dataset patterns, (ii) interpretative nature facilitates pairwise comparisons between treatments. However, a potential limitation of the biplot method is its failure to describe most of the variability in some conditions, thereby not displaying all structures of the data. Even in such instances, it can be ensured that this model of the PC1 and PC2 still captures the large portion significant data structures.

Conclusions

This study revealed notable disparities among various nano, bio, and bulk fertilizers concerning maize performance. Specifically, we found that two nano-fertilizers, namely nano-zinc and nano-boron, outperformed other fertilizers by enhancing the productivity of several key traits in maize, so their application emerges as a pivotal factor in maize production.

Conflict of interests. The authors declare that they have no conflict of interest.

Institutuinal Review Board and Ethics Committee Statement. Not applicable.

Informed Consent Statement. Not applicable.

Acknowledgements. We extend our sincere gratitude to Professor W. Yan of the Agriculture and Agri-Food Canada for providing access to the GGEbiplot.

Authors contributions. Conceptualization (Janmohammadi, M.); methodology (Samadi, S.); investigation (Janmohammadi, M.); data curation (Sabaghnia, N.); software (Sabaghnia, N.); writing Sabaghnia, N.); supervision (Janmohammadi, M.); funding acquisition (Samadi, S.); All authors have read and agreed the published version of the manuscript.

References

Ahmad, I., Ahmad, W., Nepal, J., Junaid, M. B., Bukhari, N. A., Usman, M., ... & Khan, R. N. (2024). Synergistic enhancement of maize crop yield and nutrient assimilation via ZnO nanoparticles and phosphorus fertilization. *J Sci Food Agric*, *104(11),* 6733-6745. https://doi.org/10.1002/jsfa.13500

Al-Juthery, WA H., & Hilal Obaid Al-Maamouri, E. (2020). Effect of urea and nano-nitrogen fertigation and foliar application of nano-boron and molybdenum on some growth and yield parameters of potato. *Al-Qadisiyah J Agric Sci, 10(1),* 253-263.

Azam, M., Bhatti, H. N., Khan, A., Zafar, L., & Iqbal, M. (2022). Zinc oxide nano-fertilizer application (foliar and soil) effect on the growth, photosynthetic pigments and antioxidant system of maize cultivar. *Biocat Agric Biotech, 42,* 102343. https://doi.org/10.1016/j.bcab.2022.102343

Begam, A., Pramanick, M., Dutta, S., Paramanik, B., Dutta, G., Patra, P. S., ... & Biswas, A. (2024). Inter-cropping patterns and nutrient management effects on maize growth, yield and quality. *Field Crops Res, 310,* 109363. https://doi.org/10.1016/j.fcr.2024.109363

Chen, J., Lü, S., Zhang, Z., Zhao, X., Li, X., Ning, P., & Liu, M. (2018). Environmentally friendly fertilizers: A review of materials used and their effects on the environment. *Sci Total Environ, 613,* 829-839. https://doi.org/10.1016/j.scitotenv.2017.09.186

Chukwudi, U. P., Kutu, F. R., & Mavengahama, S. (2021). Heat stress effect on the grain yield of three drought-tolerant maize varieties under varying growth conditions. *Plants, 10(8),* 1532. https://doi.org/10.3390/plants10081532

Dimkpa, C. O., Fugice, J., Singh, U., & Lewis, T. D. (2020). Development of fertilizers for enhanced nitrogen use efficiency–Trends and perspectives. *Sci Total Envirn, 731,* 139113. https://doi.org/10.1016/j.scitotenv.2020.139113

Ebrahimi, H., Sabaghnia, N., Javanmard, A., & Abbasi, A. (2023). Genotype by trait biplot analysis of trait relations in safflower. *Agrotech Indus Crops, 3(2),* 67-73. https://doi.org/10.22126/ATIC.2023.8906.1086

Farnia, A., Omidi, M. M., & Farnia, A. (2015). Effect of nano-zinc chelate and nano-biofertilizer on yield and yield components of maize (*Zea mays* L.), under water stress condition. *Indian J Nat Sci, 5(29),* 4614-4624.

Janmohammadi, M., & Sabaghnia, N. (2023). Strategies to alleviate the unusual effects of climate change on crop production: a thirsty and warm future, low crop quality. A review. *Biologija, 69(2),* 121–133. https://doi.org/10.6001/biologija.2023.69.2.1

Janmohammadi, M., Sabaghnia, N., Dashti, S., & Nouraein, M. (2016). Investigation of foliar application of nano-micronutrientfertilizers and nano-titanium dioxide on some traits of barley. *Biologija, 62(2),* 148-156. https://doi.org/10.6001/biologija.v62i2.3340

Janmohammadi, M., Yousefzadeh, S., Dashti, S., & Sabaghnia, N. (2017). Effects of exogenous application of nano particles and compatible organic solutes on sunflower (*Helianthus annuus* L.). *Bot Serb, 41(1),* 37-46. https://doi.org/10.5281/zenodo.453554

Kohli, S. K., Kaur, H., Khanna, K., Handa, N., Bhardwaj, R., Rinklebe, J., & Ahmad, P. (2023). Boron in plants: Uptake, deficiency and biological potential. *Plant Growth Reg, 100(2),* 267-282. https://doi.org/10.1007/s10725-022-00844-7

Konappa, N., Krishnamurthy, S., Arakere, U. C., Chowdappa, S., Akbarbasha, R., & Ramachandrappa, N. S. (2021). Nanofertilizers and nanopesticides: Recent trends, future prospects in agriculture. *Advances in Nano-Fertilizers and Nano-Pesticides in Agriculture,* 281-330. pp. 616. https://doi.org/10.1016/B978-0-12-820092-6.00012-4

Kumar, M. S., Reddy, G. C., Phogat, M., & Korav, S. (2018). Role of bio-fertilizers towards sustainable agricultural development: A review. *J Pharmacogn Phytochem, 7(6),* 1915-1921.

Liu, D. Y., Zhang, W., Liu, Y. M., Chen, X. P., & Zou, C. Q. (2020). Soil application of zinc fertilizer increases maize yield by enhancing the kernel number and kernel weight of inferior grains. *Front Plant Sci, 11,* 506596. https://doi.org/10.3389/fpls.2020.00188

Matsuyama, H., & Ookawa, T. (2020). The effects of seeding rate on yield, lodging resistance and culm strength in wheat. *Plant Prod Sci, 23(3),* 322-332. https://doi.org/10.1080/1343943X.2019.1702469

Meng, Q., Chen, X., Lobell, D. B., Cui, Z., Zhang, Y., Yang, H., & Zhang, F. (2016). Growing sensitivity of maize to water scarcity under climate change. *Sci Rep*, *6(1),* 19605. https://doi.org/10.1038/srep19605

Mohammadi, N., Gohari, A. M., Pouralibaba, H. R., Moradi, M., Mahmodi, F., Sabaghnia, N., & Maleki, H. H. (2023). Nonparametric stability analysis for disease properties of common bunt in wheat. *Iran J Genet Plant Breed, 12(1),* 53-75. https://doi.org/10.30479/ijgpb.2023.19395.1359

Porkabiri, Z., Sabaghnia, N., Ranjbar, R., & Maleki, H. H. (2019). Morphological traits and resistance to Egyptian broomrape weed (*Orobanche aegyptiaca* Pers.) in tobacco under greenhouse condition. Aust J Crop Sci, *13(2),* 287-293. https://doi.org/10.21475/ajcs.19.13.02.p1429

Rudani, K., Vishal, P., & Kalavati, P. (2018). The importance of zinc in plant growth-A review. *Inter Res J Nat Appl Sci*, *5(2),* 38-48.

Sabaghnia, N., & Janmohammadi, M. (2016). Biplot analysis of silicon dioxide on early growth of sunflower. *Plant Breed Seed Sci, 73(1),* 87. https://doi.org/10.1515/plass-2016-0008

Sabitha, N., Reddy, D. M., Reddy, D. L., Sudhakar, P., & Reddy, B. R. (2024). Association analysis over seasons among morphological, physiological and yield components with kernel yield in maize (*Zea mays* L.*). J Adv Bio Biotech, 27(5),* 151-156. https://doi.org/10.9734/jabb/2024/v27i5774

Saritha, G. N. G., Anju, T., & Kumar, A. (2022). Nanotechnology-Big impact: How nanotechnology is changing the future of agriculture?. *J Agric Food Res, 10,* 100457. https://doi.org/10.1016/j.jafr.2022.100457

Senthilkumar, K., Sillo, F. S., Rodenburg, J., Dimkpa, C., Saito, K., Dieng, I., & Bindraban, P. S. (2021). Rice yield and economic response to micronutrient application in Tanzania. *Field Crops Res, 270,* 108201. https://doi.org/10.1016/j.fcr.2021.108201

Suganya, A., Saravanan, A., & Manivannan, N. (2020). Role of zinc nutrition for increasing zinc availability, uptake, yield, and quality of maize (*Zea mays* L.) grains: An overview. *Commun Soil Sci Plant Ana, 51(15),* 2001-2021. https://doi.org/10.1080/00103624.2020.1820030

Tehulie, N. S., & Eskezia, H. (2021). Effects of nitrogen fertilizer rates on growth, yield components and yield of food barley (*Hordeum vulgare* L.): A Review. *Journal of Plant Sci Agric Res*, *5,* 46.

Yan, W. (2001). GGEbiplot—a Windows application for graphical analysis of multi-environment trial data and other types of two-way data. *Agron J, 93(5),* 1111–1118. https://doi.org/10.2134/agronj2001.9351111x

Yari, S., Sabaghnia, N., Pasandi, M., & Janmohammadi, M. (2018). Assessment of genotype× trait interaction of rye genotypes for some morphologic traits through GGE biplot methodology. *Ann. Univ. Mariae Curie-Skłodowska Bio*, *72,* 37-45. http://dx.doi.org/10.17951/c.2017.72.1.37-45

Yousefzadeh, S., Janmohammadi, M., & Sabaghnia, N. (2021). The effect of different nano-, bio-and conventional mineral fertilizers application on some morphological characteristics of maize. *Agric Fores, 67(3),* 135-145. http://doi.org/10.17707/AgricultForest.67.3.11

Zhang, L., Yu, P., Liu, J., Fu, Q., Chen, J., Wu, Y., & Wei, X. (2022). Spatial variability of maize leaf area and relationship with yield. Agron J, *114(1),* 461-470. https://doi.org/10.1002/agj2.20963

Zou, Y., Saddique, Q., Ali, A., Xu, J., Khan, M. I., Qing, M., ... & Siddique, K. H. (2021). Deficit irrigation improves maize yield and water use efficiency in a semi-arid environment. *Agric Water Manag, 243,* 106483. https://doi.org/10.1016/j.agwat.2020.106483

STUDIA UNIVERSITATIS BABEŞ-BOLYAI BIOLOGIA, 70, 1, 2025 (p. 65-83)
doi:10.24193/subbbiol.2025.1.04

Diversity of arthropods associated with sheep, cow, goat, and camel manure in the southeast of Algeria

Mohammed Ben Yahia Benchenna[1]✉, Wassima Dehliz-Lakhdari[2], Omar Guezoul[3], Faiza Marniche[4] and Abderrahmène Dehliz[2]

[1]Phoeniculture Research Laboratory Phoenix, Department of Agronomic Sciences, Faculty of Natural and Life Sciences, University of Ouargla, Ouargla, Algeria; [2]National Institute of Agronomic Research of Algeria, Sidi Mahdi, Touggourt, Algeria; [3]Laboratory of Saharan Bio-Resources: Preservation and Development, Department of Agronomic Sciences, Faculty of Natural and Life Sciences, University of Ouargla, Ouargla, Algeria; [4]Higher National Veterinary School, Laboratory of Zoology, El Alia, Algeria;
✉ ***Corresponding Author, E-mail: benchennamohammedbenyahia@gmail.com***

Article history: Received 02 August 2024; Revised 15 April 2025; Accepted 26 May 2025; Available online 25 June 2025

Abstract. Within the region of southeast Algeria, the Berlese method was utilized to conduct an inventory of the arthropods that were associated with four different types of manure: cow, sheep, goat, and camel. A total of 6,908 arthropods were collected, and they were categorized into four classes, 14 orders, and 37 families. The three families, *Histeridae, Sphaeroceridae,* and *Staphylinidae*, were found almost everywhere, with the relative abundance of each family varying according to the type of manure. The *Anthicidae* and *Scarabaeidae* families, which are the only two families remaining, were distributed selectively. The Shannon diversity index (H') for arthropod families obtained from the various types of manure reveals that sheep and goat manure display the highest level of diversity by (H' = 2.26 bits) and (H' = 2.23 bits), respectively. The frequency of the larval form (86.58%, NI = 5,981) compared to the adult form (13.42%, NI = 927) suggests that manure is an appropriate environment for incubating the immature stages of several arthropods. On occasion, members of certain families of pests were discovered. These families include *Bostrychidae, Dermestidae*, and *Gryllotalpidae.*

Keywords: Berlese, *Histeridae*, inventory, manure, *Scarabaeidae*

Introduction

Animal manure can increase soil fertility by providing N, P, K, and other mineral nutrients (Hoffmann *et al*., 2001; Lupwayi *et al*., 2000; Bayu *et al*., 2005). Livestock manure increases soil organic matter content and cation exchange capacity, as well as the pH of acid and calcareous soils. It also improves soil aggregate stability, infiltration, soil macrostructure, and erosion resistance (Bayu *et al*., 2005). The use of animal manure to increase crop yield and restore soil fertility is an age-old and important practice for nutrient recycling. Using livestock manure is an inexpensive way to fertilize crops (Radke *et al*., 1988).

Several studies (Bezanson and Floate, 2019; Buse *et al*., 2021; Heo *et al*., 2015; Mohr, 1943; Pecenka and Lundgren, 2019) have shown that animal dung is associated with a wide range of arthropod species. According to (Liu *et al*., 2019), animal manure can influence habitat selection for some insectivorous birds because it contains coleopteran adults and larvae, which serve as food indicators. The arthropod fauna associated with decaying animal manure has received significant attention in studies, with the majority of previous research focusing on Coleoptera and Diptera, which play critical roles in the dung decomposition process (Curry, 1979).

(Valiela, 1974) stated that the arthropod fauna of soil and vegetation invades fresh manure in an orderly pattern, with the number of taxa and complexity of the food web increasing as succession occurs. Fresh mammal manure is an important food source for many dung-breeding flies and beetles (Heo *et al*., 2015; Nichols *et al*., 2008). Coprophagous beetles play important ecological roles by feeding on animal manure both as adults and larvae (Nichols *et al*., 2008). Within this context, a comprehensive survey was undertaken to assess the arthropod population linked to diverse forms of organic fertilizer, which directly impacts agricultural practices in southeast Algeria. The manure originated from four different sources: cows, sheep, goats, and camels.

Materials and methods

Study area

The investigation was conducted in the Oued Righ region, located in the northeastern part of the Algerian Sahara. The longitude of the location is situated between 05°50’ and 05°75’ East, while its latitude ranges from 32°54’ to 39°9’ North. The geographical range spans from the southern to the northern regions (Lakhdari and Kherfi, 2010; Zahi *et al*., 2011). The Oued Righ region contains a number of oases. These oases are located along a 130 km canal that extends between the El Oued and Ouargla provinces (Lembarek and Remini, 2019). Oued

Righ exhibits a Saharan climate characterized by a hot summer and a temperate winter. The air is relatively dry, with an average annual humidity of approximately 48%. Precipitation is infrequent and irregular, seldom surpassing 17 mm in the most humid month, while maximum temperatures can reach 47 °C (Dehliz *et al*., 2018; Lembarek and Remini, 2019). Furthermore, this area is distinguished by the existence of wetlands that support a limited variety of plant life but are well suited to the challenging ecological conditions caused by the prevailing climate (drought) and soil (high salinity) (Koull and Chehma, 2013) (Fig. 1).

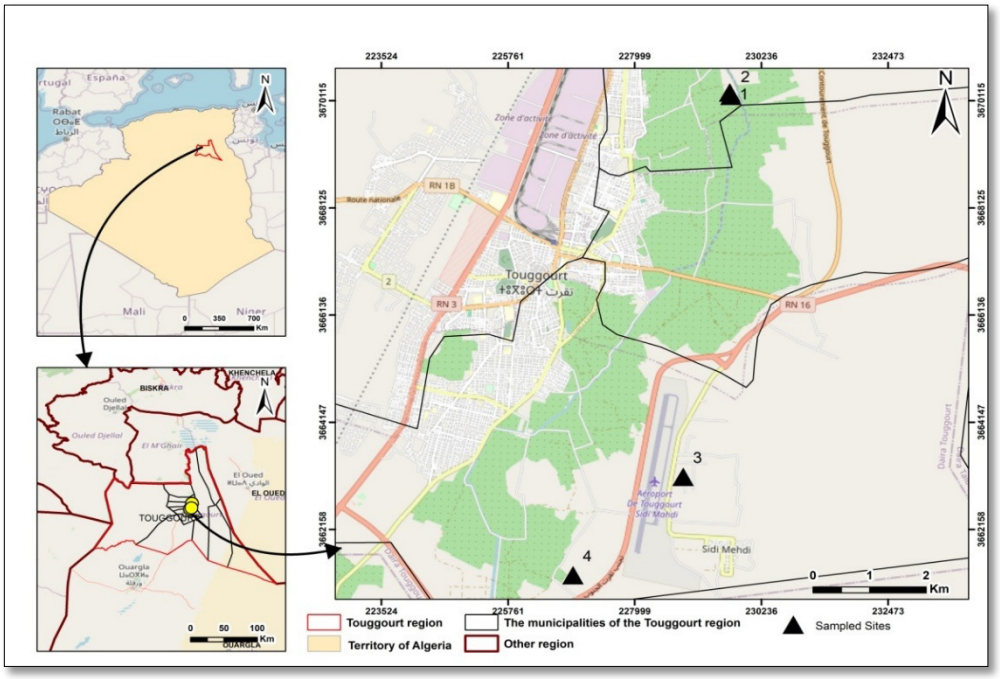

Figure 1. Study Area and Sampling Sites in Touggourt County, Algeria.

Experimental sites

The choice of investigation sites was determined by specific criteria, including the selection of well-structured farms with a significant number of animals and farms where only one livestock species was present to allow for the separate study of different manure types. Additionally, farms were chosen where the use of chemical products that could harm the manure fauna was avoided (Daam *et al*., 2019; Lumaret *et al*., 2012). Lastly, all selected farms had been

operational for at least two years, guaranteeing the presence of a substantial number of arthropods that interact with the manure, either directly or indirectly. For this study, we chose four farms situated in the southeast of Oued Righ that engage in distinct breeding activities (Fig. 2). The average distance between the four sampling sites is around three kilometers.

Figure 2. Sampling sites for different types of manure: A: Camel farm, B: Sheep farm, C: Goat farm, D: Cow farm.

The camel farm covers an area of 200 m^2 and is surrounded by date palm cultivation in all four directions. The facility accommodates a total of 10 dromedaries, primarily consisting of young males who are specifically bred for meat production. Additionally, the facility is situated in an area that is directly exposed to sunlight. The cow and sheep farms are located in close proximity and are also encompassed by date palm cultivation on three sides, with the Oued Righ channel acting as their northern boundary. The cow farm spans a 2-ha plot and houses 80 dairy cows, the majority of which are exposed to direct sunlight. The sheep farm spans an area of 50 square meters and houses a population of 15 individuals, with half of the area being shaded. The goat farm is situated within the INRAA (National Institute of Agronomic Research of Algeria) station of Touggourt. It spans an area of 320 m^2 and accommodates 35 goats. The farm is surrounded by open space in all directions.

Animal feeding

Throughout our research, we recorded the feeds provided for each type of animal at the various study sites. Cow feed consists primarily of corn silage, [69]uzern, and other grasses, whereas sheep, camels, and goats eat wheat bran, dried dates, barley, and hay. Camel breeders, in particular, use spontaneous plants from the Tamaricaceae family when there is a feed shortage.

Sampling method

Manure samples were collected monthly, three times per month, over six months, from January 2021 to June 2021. The manure sampling was conducted randomly, selecting samples from both the central and peripheral areas of each farm. All samples contained a mixture of fresh, moist, and dried manure. The sampling depth varied between 5 and 10 cm. Furthermore, samples were collected consistently between 9:30 AM and 2:00 PM on identical days.

Extraction of arthropods from manure

To remove arthropods that are linked to various forms of manure, we employed the Berlese funnel, a method that has been endorsed and utilized by multiple authors for the purpose of removing arthropods from different substrates (Anderson *et al*., 2013; Bousquet and Laplante, 2006). Prior to introducing the substrate into the funnels, arthropods of greater dimensions were collected. Two nets were employed: the initial one consisted of a rubber material with a pore size of 1.5 mm^2, reinforced by a rigid plastic net with a pore size of 2 mm^2. To ensure that manure samples were of the same volume, we used funnels of the same volume, 1400 cm^3, for all manure types. The collection container was filled with a solution of ethanol with a concentration of 70%. The samples were then kept in a controlled environment for five days.

Techniques for specimen conservation

The majority of the specimens collected using the Berlese funnel are diminutive and susceptible to harm. Hence, they are placed within tubes containing a 70% ethanol solution. Specimens of considerable size were affixed to entomological pins and stored in a desiccated state.

Identification of collected arthropods

The specimens were counted and classified under a stereomicroscope utilizing multiple taxonomic identification guides. We employed (Bertone's, 2019) key for Dipteran identification and Coleoptera. We consulted the keys

provided by (Arnett Jr and Thomas, 2001), (Hagstrum, 2016), and (Jameson, 2002). Furthermore, we employed the overarching principles outlined by (Borror *et al*., 1970). The unidentified samples were transported to the Zoology Laboratory at the National Veterinary School of El Alia. There, they were identified and verified in the Arthropod collection of the Forest and Agricultural Zoology Department (ENSA).

Data analysis

To assess the findings, we used the ecological composition indices of total richness (S) (Blondel, 1975), relative abundance (RA%) (Dajoz, 1971), and Shannon's ecological structure indices, which measure species diversity and relative abundance in a given sample. It accounts for both the number of species and their relative distribution. The diversity index indicates how diverse the sample is. The H' diversity index, 'H' = -∑ Pi log2 Pi (Blondel *et al*., 1973), ranges from 0 to H' max, where H' max represents the maximum theoretical value. H' max equals Log2 S. And Pielou's evenness index I E = H' / H' max measures the consistency with which species are distributed in the sample (Blondel, 1975). It accounts for both the number of species and their relative abundance. An equity index of 1 indicates a completely even distribution of species, whereas an index less than 1 indicates an uneven distribution. Correspondence factor analyses (CFA) were conducted on the number of families identified using PAST version 1.37 (Hammer and Harper, 2001) to investigate the distribution of families in the various types of manure examined. Additionally, variance analyses (ANOVA) and chi-square tests were performed using version 19 of Minitab software.

Results

By extracting arthropods from various forms of manure, we were able to classify them into four distinct categories: Entognatha, Arachnida, Crustacea, and Insecta. The latter is the most prevalent in all four types of manure (cow, goat, sheep, and camel), with relative abundances of 99.97%, 99.54%, 99.73%, and 93.53%, respectively. Additionally, it is the only class present in all manure types examined.

Larval and imaginal forms

Out of the collected Arthropods, 13.42% (NI = 927) were in their adult stage, while the larval stage was the most prevalent, accounting for 86.58% (NI = 5981). The second group consists of two orders, Diptera and Coleoptera,

with abundances of 93.04% (NI = 5565) and 6.96% (NI = 416), respectively. The number of Diptera larvae was highest in cow manure (NI = 3567), followed by sheep manure (NI = 1350), and lowest in camel manure (NI = 241). The abundance of Coleoptera larvae in all the types of manure studied was low, ranging from 54 to 197 individuals (54 ≤ NI ≤ 197) (Fig. 3).

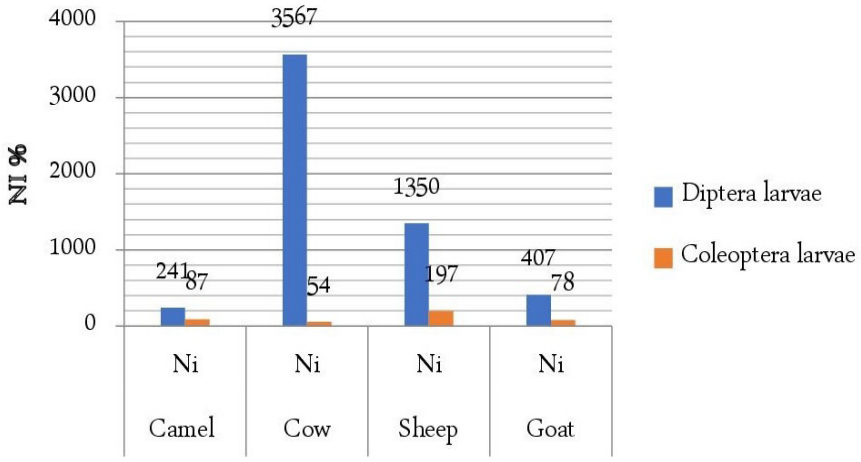

Figure 3. The number of individuals (NI) of Coleoptera and Diptera larvae counted in the four types of camel, cattle, sheep and goat manure.

The chi-square test was used to determine the distribution of Coleoptera and Diptera larvae in four different types of manure. The results revealed a highly significant (d =1, χ^2=4432.74, p < 0.0001) difference between the Diptera and Coleoptera orders, with the high dominance of Diptera larvae. Furthermore, the distribution of larvae by manure type was found to be highly significant (df=3, χ^2=503.4, p < 0.0001), indicating a heterogeneous distribution of larvae from both orders across the different types of manure.

After extracting various types of manure, 6,908 arthropods from 14 orders were recovered (Tab. 1). Diptera (25.76 ≤ RA%≤ 51.45), Coleoptera (25.76 ≤ RA% 52.20), and Hymenoptera (1.52 ≤ RA% ≤ 17.13) were the three most common orders among the four manure types (cow, goat, sheep, and camel). Five orders have a selective presence (recorded in a single type of manure): Collembola RA=38.64%, Thysanoptera RA=38.64% (camel manure), Isopoda RA=0.61%, Orthoptera RA=0.31% (goat manure), and Lepidoptera RA=0.34%. Six orders, Araneae, Hemiptera, Psocodea, Homoptera, Ombioptera and Pseudoscorpiones, share two to three types of manure and have low relative abundance (0.31 ≤ RA% ≤ 6.06).

Table 1. Results of a study on the distribution of arthropod orders in four different types of manure: camel, cow, sheep and goat.

Nr crt	Order	Camel		Cow		Sheep		Goat	
		Ni	AR %	Ni	AR %	Ni	AR %	Ni	AR %
1	Araneae	-	-	1	0.34	-	-	1	0.58
2	Pseudoscorpiones	-	-	-	-	3	0.92	2	1.16
3	Isopoda	-	-	-	-	2	0.61	-	-
4	Collembola	51	38.64	-	-	-	-	-	-
5	Diptera	34	25.76	111	37.63	122	37.31	89	51.45
6	Psocodea	8	6.06	1	0.34	-	-	-	-
7	Hymenoptera	2	1.52	17	5.76	56	17.13	3	1.73
8	Thysanoptera	2	1.52	-	-	-	-	-	-
9	Homoptera	1	0.76	2	0.68	-	-	-	-
10	Coleoptera	34	25.76	154	52.20	141	43.12	69	39.88
11	Lepidoptera	-	-	1	0.34	-	-	-	-
12	Hemiptera	-	-	7	2.37	1	0.31	9	5.20
13	Ombioptera	-	-	1	0.34	1	0.31	-	-
14	Orthoptera	-	-	-	-	1	0.31	-	-
	Total	132	100	295	100	327	100	173	100

The chi-square test was used to determine the most abundant orders in four types of manure. Results revealed highly significant differences between orders (χ^2 =444.51 *df*=15 $p < 0.0001$), with Coleoptera representing the most dominant order (43%), followed by Diptera (39%). The other four orders (Collembola, Hemiptera, Psocodea and Hymenoptera) had percentages below 10%. The distribution of arthropods on the four types of manure also proved highly significant (χ^2 =1032.88, df=5, $p < 0.0001$). Tab. 2 shows that the four manure types account for a total of 37 arthropod families. The findings show that their diversity, frequencies, and spatial distribution vary depending on habitat type but follow a relatively similar pattern. Goat and sheep manure have higher RA% values for some arthropod families compared to other manure types.

Goat manure

Goat manure exhibits the highest level of diversity, encompassing 24 distinct families. The *Sphaeroceridae* family has the highest abundance, accounting for 42.66% of the total. The families *Nitidulidae*, *Staphylinidae*, and *Scarabaeidae*, comprising 6.99% to 11.89% of the total, rank second in terms of abundance.

Camel manure

Camel manure exhibited the lowest diversity, with a recorded count of 15 families. Collombola was the most prevalent, accounting for 44.74% of the total. *Aphodiidae* followed with a prevalence of 12.28%. Psocodea, *Histeridae*, *Scarabaeidae*, and *Sphaeroceridae* were evenly distributed, with relative percentages ranging from 7.02% to 8.77%.

Sheep manure

Sheep manure contained 21 families, with the most common ones being *Staphylinidae* (accounting for 29.30% of the total) and *Histeridae* (accounting for 14.42% of the total). The next most frequent families were *Formicidae*, *Sphaeroceridae*, *Carabidae*, and *Tenebrionidae*, with relative abundances ranging from 7.44% to 11.63%.

Cow manure

Out of the 18 families collected, four families have a notable average presence: *Histeridae*, *Sphaeroceridae*, *Staphylinidae*, and *Anthicidae*, with relative abundances of 26.86%, 26.03%, 20.66%, and 10.33%, respectively. The results of the analysis of variance (ANOVA) (Tab. 2) indicate that the variations in the relative abundance of the families studied are not significantly influenced by the period and family parameters, nor by their interactions.

We performed a multivariate statistical analysis on the arthropod population data collected at four distinct stations throughout our investigation to gain a thorough picture of the distribution of the different families among the four types of manure. The findings are displayed in the Axis 1 and Axis 2 factorial design of the Correspondence Factorial Analysis (CFA) (Fig. 4), which encompasses 83.8% of the data.

Table 2. Analysis of variance: impact of manure, months, and families on variations in arthropod relative abundance.

Source	*df*	Sum of squares	Mean square	F-Values	P-Values
Manure	3	0.000084	0.000028	0.94	0.423
Months	5	0.000117	0.000023	0.78	0.563
Families	37	0.000885	0.000024	0.8	0.798
Manure* months	15	0.000627	0.000042	1.4	0.144
Manure* families	111	0.003368	0.00003	1.01	0.453
Months * families	185	0.00517	0.000028	0.93	0.709
Error	531	0.015907	0.00003		
Total	887	0.026187			

df: degree of freedom

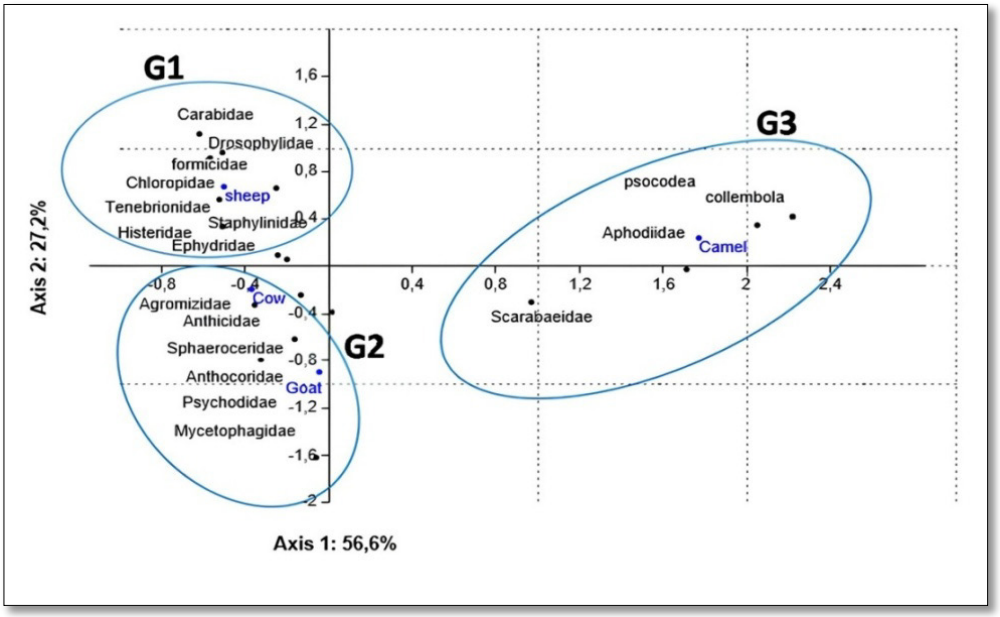

Figure 4. Factorial Correspondence Analysis (FCA) showing the association between arthropod families and four types of manure in the factorial plane (Axis 1 explains the largest portion of variance at 56.6%, and Axis 2 explains the second largest portion at 27.2%).

The CFA's factorial design yielded three distinct groups (G1, G2, G3) consisting of families linked to a specific type of manure, namely cow, sheep, camel, or goat. Group G1 features the eight families with the highest abundance in sheep manure, such as *Carabidae*, *Staphylinidae*, *Tenebrionidae* and *Histeridae*. In comparison, group G2 contains six families with the highest numbers in cow and goat manure, including *Sphaeroceridae*, *Anthocoridae* and *Anthicidae*. Group G3 features the most abundant families in camel manure, including *Aphodiidae*, *Scarabaeidae* and Collembola. The distance between families and manure type on the factorial plane decreases with the increasing workforce of individuals and vice versa. Regarding the arthropod population, it is evident that cow manure has the highest number of individuals (242) while camel manure has the lowest number (114) (Tab. 3). On the contrary, the total richness of goat manure is the highest at 24 species, while the other types of manure - sheep, cattle and camel have a total richness of 21, 18 and 15 species, respectively.

Table 3. Number of samples (NS), number of individuals (NI), and total richness (S) of arthropod families collected from four types of manure.

Parameter	Camel	Cow	Sheep	Goat
NS	90	90	90	90
NI	114	242	215	143
S	15	18	21	24

Table 4. Results of a study on the distribution of arthropod families in four different types of manure: camel, cow, sheep and goat.

No crt.	Family	Camel		Cow		Sheep		Goat	
		Ni	RA %	Ni	RA %	Ni	RA %	Ni	RA %
1	*Porcellionidae*	-	-	-	-	1	0.47	-	-
2	*Neobisiidae*	-	-	-	-	1	0.47	-	-
3	*Cheliferidae*	-	-	-	-	1	0.47	1	0.70
4	*Chernetidae*	-	-	-	-	-	-	1	0.70
5	*Sphaeroceridae*	9	7.89	63	26.033	20	9.30	61	42.66
6	*Psychodidae*	2	1.75	6	2.479	2	0.93	4	2.80
7	*Chloropidae*	2	1.75	2	0.826	13	6.05	2	1.40
8	*Agromizidae*	1	0.88	6	2.479	1	0.47	1	0.70
9	*Scatopsidae*	-	-	-	-	-	-	1	0.70

No crt.	Family	Camel		Cow		Sheep		Goat	
		Ni	RA %	Ni	RA %	Ni	RA %	Ni	RA %
10	*Sciaridae*	-	-	-	-	1	0.47	1	0.70
11	Collembola	51	44.74	-	-	-	-	-	-
12	*Drosophylidae*	-	-	-	-	9	4.19	1	0.70
13	*Phoridae*	1	0.88	-	-	-	-	-	-
14	*Ephydridae*	1	0.88	4	1.653	4	1.86	2	1.40
15	*Aphididae*	1	0.88	1	0.413	-	-	-	-
16	*Anthicidae*	1	0.88	25	10.331	1	0.47	1	0.70
17	*Aphodiidae*	14	12.28	-	-	-	-	4	2.80
18	*Scarabaeidae*	10	8.77	1	0.413	4	1.86	17	11.89
19	*Laemophloeidae*	2	1.75	-	-	-	-	3	2.10
20	*Histeridae*	10	8.77	65	26.860	31	14.42	5	3.50
21	*Corylophidae*	-	-	1	0.413	1	0.47	1	0.70
22	*Staphylinidae*	-	-	50	20.661	63	29.30	10	6.99
23	*Tenebrionidae*	-	-	4	1.653	16	7.44	3	2.10
24	*Carabidae*	-	-	1	0.413	18	8.37	-	-
25	*Bostrychidae*	-	-	1	0.413	-	-	-	-
26	*Dermestidae*	-	-	1	0.413	-	-	-	-
27	*Hybosoridae*	-	-	-	-	1	0.47	-	-
28	*Monotomidae*	-	-	-	-	1	0.47	2	1.40
29	*Cryptophagidae*	-	-	-	-	-	-	2	1.40
30	*Nitidulidae*	-	-	-	-	-	-	6	4.20
31	*Mycetophagidae*	-	-	-	-	-	-	10	6.99
32	*Ptiliidae*	-	-	-	-	-	-	1	0.70
33	Psocodea	8	7.02	-	-	-	-	-	-
34	*Formicidae*	1	0.88	4	1.653	25	11.63	-	-
35	*Anthocoridae*	-	-	6	2.479	-	-	3	2.10
36	*Liposcelididae*	-	-	1	0.413	-	-	-	-
37	*Gryllotalpidae*	-	-	-	-	1	0.47	-	-
	Total	114	100	242	100	215	100	143	100

The inventory yields two biodiversity indices, namely Shannon's diversity index (H') and Pielou's evenness index (E), as presented in (Tab. 5). Shannon's diversity index (H') was used to assess the diversity of arthropod families in various types of manure in southeastern Algeria. The results indicate that the H' values for the different types of manure range from 1.89 to 2.26 bits, suggesting a slight variation in arthropod diversity among the different types of manure. However, the H max values for the different samples suggest that the diversity has not been fully explored, and there may be other families present. Pielou's evenness index (E) for the various manure types varied between 0.67 and 0.74, indicating that the distribution of arthropods is relatively uniform within each manure type. However, the variations between the different manure types are not significant. The findings suggest a minor difference in arthropod diversity among the various types of manure but a consistent pattern in their distribution.

Table 5. Shannon index (H') and Pielou's evenness index (E) applied to arthropod families obtained from four types of manure.

Diversity	Camel	Cow	Sheep	Goat
H'	1.89	1.94	2.26	2.23
Hmax	2.71	2.89	3.04	3.18
E	0.70	0.67	0.74	0.70

Discussion

This study allowed the identification of the arthropods found in four different types of manure (cow, sheep, goat, and camel) in southeastern Algeria. Four classes of arthropods were identified: Entognatha, Arachnida, Crustacea, and Insecta. The latter, referring to a specific type, is the most prevalent, constituting over 90% of all analyzed manure samples. (Floate, 2011) stated that coprophagous insects exhibit a tendency towards being generalists and are drawn to the feces of various animal species, albeit with certain preferences.

Larval and imaginal forms

The preponderance of larval rather than adult forms can be attributed to the nature of manure, which provides a favorable developmental environment for the immature stages of certain species, particularly Diptera and Coleoptera

associated with various types of manure. According to (Hammer, 1941; Legner and Olton, 1970), the components and arrangements of domestic animal manure attract females of specific Diptera groups, who lay their eggs within the manure, where the larvae feed and develop. Furthermore, the technique used to extract arthropods is ineffective for capturing flying insects such as Diptera and Hymenoptera. As a result, all adult Diptera collected were submerged during the extraction period. Diptera larvae density varied according to manure type, with the highest abundance found in cow manure and the lowest in camel manure. This variation could be attributed to humidity, which is essential for Diptera larvae development.

According to (Fatchurochim *et al*., 1989), the amount of moisture in manure plays an important role in determining fly abundance. According to (Akbassova *et al*., 2016), of all manure types (cow, sheep, and camel), camel manure has the lowest odor, light structure, and moisture content (5-8%). According to Ali (Khan *et al*., 2012), cow manure has a very high moisture content of 75.9%. This moisture content is required for the incubation of *Musca domestica* (Linnaeus, 1758) larvae. Cow manure had the highest number of arthropod individuals (NI = 242), most likely due to the abundance of decomposer larvae (Diptera and Coleoptera) that attract other types of arthropods, including predators, as suggested by (Sladecek *et al*., 2021). Insects colonizing manure at the start of the succession encourage the establishment of other insects at the end, such as coprophagous beetles and coprophagous insect larvae, as demonstrated by (Sladecek *et al*., 2021).

Order dominance

The two predominant orders of arthropods, Diptera and Coleoptera, were the most frequently detected among the four types of manure examined. The prevalence of these two orders fluctuates, depending on the developmental stage of the individuals. Diptera exhibit greater dominance during their immature stage, whereas Coleoptera exhibit greater dominance during their adult stage. The variation in dominance observed may be attributed to the extraction method employed. Various researchers have documented the prevalence of Diptera and Coleoptera in various forms of manure (Blume, 1970; Fatchurochim *et al*., 1989; Lee and Wall, 2006; Legner and Olton, 1970; Sladecek *et al*., 2021).

Family distribution

Only three of the 37 arthropod families identified were present in the majority of the manure types examined. The *Sphaeroceridae* are associated with decomposing plant and animal organic matter such as dung, leaf litter, manure,

and vertebrate corpses, according to a study by (Papp *et al*., 2021). These various types of organic matter create an ideal environment for larval development. This information supports the findings, with the *Sphaeroceridae* family being the most extracted in the Berlese apparatus due to the high density of larvae in the various types of manure studied. The accumulation of eggs and larvae from this and other families makes the environment appealing to certain predators, who come second. (Arnett Jr and Thomas, 2001) and (Legner and Olton, 1970) considered *Histeridae* and *Staphylinidae* to be predators. (Arnett Jr and Thomas, 2001) discovered that *Histeridae* prefer large mammals' excrements, which are high in larvae, particularly those of certain dipteran families.

Other recorded species are from families such as *Tenebrionidae*, *Bostrychidae*, *Dermestidae* and Psocodea, which are primarily associated with animal feedstuffs like barley and wheat bran, which are commonly infested by stored-product insect pests. According to (Subramanyam, 1995), all important insect species that harm stored products belong to one of seven families: *Tenebrionidae*, *Silvanidae*, *Dermestidae*, *Curculionidae*, *Bostrichidae*, *Bruchidae* or *Cucujidae*. Some insects have a selective distribution, and their presence in certain types of manure may be related to the needs of their next generation or their feeding preferences. The *Scarabaeidae* and *Aphodiidae* families, for example, are found exclusively in camel and goat manure. *Scarabaeoidea* beetles in a semi-arid climate have mouthparts adapted to consume dry vertebrate pellets, according to a study by (Verdú and Galante, 2004).

Other families, like the *Anthicidae*, prefer cow manure because it contains more moisture than other types of manure. Adults in this family are omnivorous (Werner and Chandler, 1995), eating fungal hyphae, spores, and plant exudates, but they can also be opportunistic predators of small arthropods. The *Anthicidae* family includes predatory species as well as saprophagous ones. The *Nitidulidae* family has also been identified in this type of manure. Species in this family are predominantly mycetophagous (Jameson, 2002) and saprophagous. It should be noted that the *Anthicidae* and *Nitidulidae* families' use of cow manure is related to their trophic requirements for predatory species and their hyphae richness for mycetophagous species (Dickinson and Underhay, 1977). Of the 37 arthropod families recorded, 11 were only observed once. The families are *Aphididae*, *Dermestidae*, *Chernetidae*, *Neobisiidae*, *Liposcelididae*, and *Gryllotalpidae*. According to (Floate, 2011), some arthropod species may be present in manure despite having no direct relationship with it. Springtails, millipedes, spiders, ground beetles, and ants, for example, may pay them a passing visit.

Conclusions

The objective of this study was to enhance our comprehension of the arthropod fauna linked to various types of manure that are not well-documented in the Oued Righ region of southeastern Algeria. This endeavor has facilitated our comprehension of the various categories of arthropods, whether they are adversaries or allies in oasis agriculture, and has enhanced our approach to utilizing this prevalent organic material in agriculture in southeast Algeria. Four classes of arthropods were identified: Entognatha, Arachnida, Crustacea, and Insecta. Among the four types of manure examined, Insecta was found to be the most prevalent. While cow manure is highly fertile for coprophagous Diptera larvae, its abundance of larvae creates an appealing environment for specific predatory families, particularly *Histeridae* and *Staphylinidae*. The succession of different families highlights the impact of trophic requirements on the distribution of families. Conversely, specific families that are regarded as nuisances, such as *Gryllotalpidae*, *Bostrychidae*, and *Dermestidae*, are not linked to beneficial manure but can be introduced through contaminated cattle feed. Therefore, the farmer must exercise all essential measures prior to utilizing this particular organic matter.

Acknowledgments. The authors extend their gratitude to all the farmers across various cattle, sheep, goat, and camel farms for providing the facilities necessary to conduct this research work.

References

Akbassova, A. D., Sainova, G. A., Aimbetova, I. O., Sunakbaeva, D. K. & Akeshova, M. M. (2016). Impact of polyfunctional vermicompost on the productivity of vegetable root crops. *FEB*. 25(9), 3755–3759.

Ali Khan, H. A., Ali Shad, S. & Akram, W. (2012). Effect of livestock manures on the fitness of house fly, *Musca domestica* L. (Diptera: *Muscidae*). *Parasitol*. *Res*. 111(3), 1165–1171. https://doi.org/10.1007/s00436-012-2947-1

Anderson, J. T., Zilli, F. L., Montalto, L., Marchese, M. R., McKinney, M. & Park, Y. L. (2013). Sampling and processing aquatic and terrestrial invertebrates in wetlands. Wetland techniques: volume II: Organisms, 143-195. https://doi.org/10.1007/978-94-007-6931-1_5

Arnett Jr., R. H. & Thomas, M. C. (2001). American beetles. Volume I: Archostemata, Myxophaga, Adephaga, Polyphaga: Staphyliniformia. *In American beetles*.CRC Press, pp. 272. https://doi.org/10.1201/9781482274325

Bayu, W., Rethman, N. F. G. & Hammes, P. S. (2005). The role of animal manure in sustainable soil fertility management in Sub-Saharan Africa: *A review*. *J*. *Sustain*. *Agric*. 25(2), 113–136. https://doi.org/10.1300/J064v25n02_09

Bertone, M. A. (2019). Manual of afrotropical diptera, volume I: Introductory chapters and keys to diptera families, *Am*. *Entomol.* 65, 69–70. https://doi.org/10.1093/ae/tmz011

Bezanson, G. A. & Floate, K. D. (2019). An updated checklist of the coleoptera associated with livestock dung on pastures in America north of Mexico. *Coleopt*. *Bull* . 73, 655–683. https://doi.org/10.1649/0010-065X-73.3.655

Blondel, J., Ferry, C. & Frochot, B., (1973). Avifaune et végétation. essai d'analyse de la diversité. Inist-CNRS. 41, 63–84.

Blondel, Jacques. (1975). L'analyse des peuplementsd'oiseaux, éléments d'un diagnostic écologique I. la méthode des échantillonnages fréquentiels progressifs. *Rev Ecol-Terre Vie*. 4, 533–589.

Blume, R. R. (1970). Insects associated with bovine droppings in Kerr and Bexar counties, *Texas J*. *Econ*. *Entomol*. 63(3), 1023–1024. https://doi.org/10.1093/jee/63.3.1023

Borror, D.J. & White, R.E., (1970). A field guide to insects: America north of Mexico Volume XIX. Houghton Mifflin Harcourt, pp. 312.

Buse, J., Hoenselaar, G., Langenbach, F., Schleicher, P., Twietmeyer, S., Popa, F. & Heurich, M., (2021). Dung beetle richness is positively affected by the density of wild ungulate populations in forests. *Biodivers*. *Conserv*. 30, 3115-3131. https://doi.org/10.1007/s10531-021-02238-z

Curry, J. P. (1979). The arthropod fauna associated with cattle manure applied as slurry to grass land. Section b: biological, geological, and chemical science. *PRIA*, 79, 15–27. http://www.jstor.org/stable/20494325

Dajoz, R., (1971). Précis d'écologie. Ed. *Dunod*, Paris, pp 434.

Daam, M.A., Chelinho, S., Niemeyer, J.C., Owojori, O.J., De Silva, P.M.C., Sousa, J.P., van Gestel, C.A. & Römbke, J., (2019). Environmental risk assessment of pesticides in tropical terrestrial ecosystems: test procedures, current status and future perspectives. *Ecotoxicol Environ Saf*. 181, 534-547. https://doi.org/10.1016/j.ecoenv.2019.06.038

Dehliz, A., Lakhdari, W., Acheuk, F., Aoudjit, R., Benlamoudi, W., Mlik, R., Hammi, H., Chergui, S., Guermit, K. & Matallah, S. (2018). Euphorbia guyoniana aqueous extract efficiency against tomato leaf miner in southern east Algeria. *Org*. *Agric*. 8(4), 349–354. https://doi.org/10.1007/s13165-017-0201-y

Dickinson, C. H. & Underhay, V. H. S. (1977). Growth of fungi in cattle dung. *Trans*. *Br*. *Mycol*. *Soc*. 69(3), 473–477. https://doi.org/10.1016/S0007-1536(77)80086-7

Fatchurochim, S., Geden, C. J. & Axtell, R. C. (1989). Filth fly (Diptera) oviposition and larval development in poultry manure of various moisture levels. *J Entomol Sci*. 24(2), 224–231. https://doi.org/10.18474/0749-8004-24.2.224

Floate, K. D. (2011). Arthropods in cattle dung on canada's grasslands in arthropods of canadian grasslands Volume II: Inhabitants of a changing landscape. *Biol*. *Surv*. *Can*. *taxon*. *ser*. 2(4), 71-88. https://doi.org/10.3752/9780968932155.ch4

Hagstrum, D., (2016). Atlas of stored-product insects and mites. Elsevier, pp. 128.

Hammer, O. (1941). Biological and ecological investigations on flies associated with pasturing cattle and their excrement. *Vidensk*. *Mead*. *Dansk*. *Naturh*. *Foren*. 105.

Hammer, Ø. & Harper, D. A. T. (2001). Past: paleontological statistics software package for education and data analysis. *Palaeont*. *Electr*. 4(1), 1.

Haynes, R. J. & Francis, G. S. (1990). Effects of mixed cropping farming systems on changes in soil properties on the Canterbury Plains. *N*. *Z*. *J*. *Ecol*. 73–82. http://www.jstor.org/stable/24053313

Heo, C. C., Kurahashi, H., Hayashi, T., Nazni, W. A., Omar, B., Medicine, F., Mara, U. T., Campus, S. B., Hospital, J. & Buluh, S. (2015). Coprophilic dipteran community associated with horse dung in Malaysia. *Halteres*. 6, 33–50.

Hoffmann, I., Gerling, D., Kyiogwom, U. B. & Mané-Bielfeldt, A. (2001). Farmers' management strategies to maintain soil fertility in a remote area in northwest Nigeria. *Agric Ecosyst Environ*. 86, 263–275. https://doi.org/10.1016/S0167-8809(00)00288-7

Jameson, M. L. (2002). Trogidae MacLeay 1819. In: American beetles, Volume II: Polyphaga: *Scarabaeoidea* through *Curculionoidea*.1st Ed.CRC Press, pp.17-19.

Koull, N., and Chehma, A. (2013). diversite floristique des zones humides de la vallee de l'oued Righ (Sahara Septentrional Algerien). *Bio*. 3(2), 72–81. https://doi.org/10.12816/0008873

Lakhdari, K. & Kherfi, Y. (2010). L'agrobiodiversitéoasienne: un potentiel à promouvoir et à préserver. *J Arid Land*. 24, 142–152.

Lumaret, J. P., Errouissi, F., Floate, K., Rombke, J. & Wardhaugh, K. (2012). A review on the toxicity and non-target effects of macrocyclic lactones in terrestrial and aquatic environments. *Curr*. *Pharm*. *Biotechnol*. 13, 1004-1060. https://doi.org/10.2174/138920112800399257

Lee, C. M. & Wall, R. (2006). Cow-dung colonization and decomposition following insect exclusion. *Bull*. *Entomol*. *Res*. 96(3), 315–322. https://doi.org/10.1079/BER2006428

Legner, E. F. & Olton, G. S. (1970). Worldwide survey and comparison of adult predator and scavenger insect populations associated with domestic animal manure where livestock is artificially congregated. *Hilgardia*.40(9), 225–266.

Lembarek, M. S. & Remini, B. (2019). Evolution of the flow of drainage waters in the Oued Righ canal, *J*. *Water Land Dev*. 41(1), 133–138. https://doi.org/10.2478/jwld-2019-0036

Liu, W., Wu, Y., DuBay, S.G., Zhao, C., Wang, B. & Ran, J., (2019). Dung-associated arthropods influence foraging ecology and habitat selection in black-necked cranes (Grus nigricollis) on the Qinghai–Tibet plateau. *Ecol*. *Evol*. 9, 2096-2105. https://doi.org/10.1002/ece3.4904

Lupwayi, N. Z., Girma, M. & Haque, I. (2000). Plant nutrient contents of cattle manures from small-scale farms and experimental stations in the Ethiopian highlands. *Agric*. *Ecosyst*. *Environ*. 78(1), 57–63. https://doi.org/10.1016/S0167-8809(99)00113-9

Mohr, C. O. (1943). Cattle droppings as ecological units. *Ecol*. *Monogr*. 13(3), 275–298. https://doi.org/10.2307/1943223

Nichols, E., Spector, S., Louzada, J., Larsen, T., Amezquita, S. & Favila, M. E. (2008). Ecological functions and ecosystem services provided by Scarabaeinae dung beetles. *Biol*. *Conserv*., 6, 1461–1474. https://doi.org/10.1016/j.biocon.2008.04.011

Papp, L., Roháček, J., Kirk-Spriggs, A. H. & Sinclair, B. J. (2021): 99. *Sphaeroceridae* (Lesser dung flies). In: Kirk-Spriggs, A.H. and Sinclair, B.J., eds, manual of afrotropical diptera. VolumeIII. Brachycera–Cyclorrhapha, excluding Calyptratae. Suricata 8.1st Ed. *SANBI*, Pretoria, pp. 2145–2192.

Pecenka, J.R. & Lundgren, J.G., (2019). Effects of herd management and the use of ivermectin on dung arthropod communities in grasslands. *Basic Appl*. *Ecol*. 40, 19-29. https://doi.org/10.1016/j.baae.2019.07.006

Radke, J. K., Andrews, R. W., Janke, R. R. & Peters, S. E. (1988). low-input cropping systems and efficiency of water and nitrogen use. cropping strategies for efficient use of water and nitrogen. American society of agronomy. *SSSA*, *Inc*. 51, 193-218. https://doi.org/10.2134/asaspecpub51.c12

Ramade, F. (1984). Elément d'ecologie et ecologie fondamentale. *McGraw Hill*, Paris, pp.379.

Sladecek, F. X. J., Segar, S. T. & Konvicka, M. (2021). Early successional colonizers both facilitate and inhibit the late successional colonizers in communities of dung-inhabiting insects. *Eur*. *J*. *Entomol*. 118, 240–249. https://doi.org/10.14411/eje.2021.025

Subramanyam, B. (1995). Integrated management of insects in stored products. CRC Press, pp.48.

Telnov, D. (2008). Order coleoptera, family *Anthicidae*. Arthropod fauna of the UAE. 1(2), 270–292.

Valiela, I., (1974). Composition, food webs and population limitation in dung arthropod communities during invasion and succession. *Am*. *Midl*. *Nat*. 92(2),370-385. https://doi.org/10.2307/2424302

Verdú, J. R. & Galante, E. (2004). Behavioural and morphological adaptations for a low-quality resource in semi-arid environments: dung beetles (Coleoptera, Scarabaeoidea) associated with the European rabbit (Oryctolagus cuniculus L.). *J*. *Nat*. *Hist*. 38(6), 705–715. https://doi.org/10.1080/0022293021000041707

Werner, F. G. & Chandler, D. S. (1995). Anthicidae (Insecta: Coleoptera). *Fauna N*. *Z*. 34. https://doi.org/10.7931/J2/FNZ.34

Zahi, F., Drouichee, A., Bouchahm, N., Hamzaoui, W., Chaib, W. & Djabri, L. (2011). The water upwelling in Oued Righ valley : Inventory and caracterization. *J*. *Environ*. *Geogr*. 2, 445–450.

STUDIA UNIVERSITATIS BABEŞ-BOLYAI BIOLOGIA, 70, 1, 2025 (p. 85-120)
doi:10.24193/subbbiol.2025.1.05

Enhanced azo dye (Sudan G) decolorization and simultaneous electricity generation using a bacterial consortium in a dual-chamber microbial fuel cell

Chinwendu Jude Echejiuba[1], Chimezie Jason Ogugbue[1]✉ and Ifeyinwa Sarah Obuekwe[2]

[1]Department of Microbiology, Faculty of Science, University of Port Harcourt, Port Harcourt, Nigeria; [2]Department of Microbiology, Faculty of Life Sciences, University of Benin, Benin City, Nigeria
✉***Corresponding author, E-mail:*** *jason.ogugbue@uniport.edu.ng*

Article history: Received 7 August 2024; Revised 3 December 2024; Accepted 22 May 2025; Available online 25 June 2025

Abstract. Azo dyes are prevalent anthropogenic compounds, making their enhanced treatment crucial in our color-saturated world. This study examined the ability of a microbial consortium, comprising *Pseudomonas aeruginosa* (MW584979), *Enterobacter hormaechei* (MW584986), *Providencia stuartii* (MW584987), *Escherichia coli* (MZ394117), and *Pseudomonas xiamenensis* (MW585052), to decolorize Sudan orange G in a microbial fuel cell (MFC) after determining the optimal conditions for dye decoorization using response surface methodology (RSM) and the One Factor at a Time (OFAT) method. Degradation products were analyzed using the gas chromatography-mass spectroscopy technique. The consortium achieved an 88% decolorization rate within 24 hours under the optimal conditions identified by the Central Composite Design (CCD) of RSM. These conditions, pH 7.0, temperature 35, salinity 5 g/L, and glucose concentration 10 g/L, when applied in the MFC, resulted in an enhanced decolorization rate of 92% and simultaneous electricity generation of 130 mV within 24 hours. GC-MS analysis confirmed the breakdown of the azo dye into simpler, less toxic compounds. Metabolites produced through RSM and MFC processes were identified and compared with controls using chromatography-mass spectrometry. Degradation metabolites obtained after treatment of the dye wastewater in the MFC include Cyclopentane and cyclopropylidene-

2(1H)-naphthalenone which highlights the role of microbial enzymatic activity in converting complex azo dye structures into environmentally benign compounds. These results highlight the successful integration of RSM for process optimization and MFCs for enhanced biodegradation and renewable energy production. The scalability of this technique is promising, given the relatively simple and cost-effective setup of MFC systems. Moreover, the economic feasibility of large-scale deployment is enhanced by the dual benefits of wastewater treatment and renewable energy production, making it a sustainable solution for managing azo dye pollution.

Keywords: wastewater, biodegradation, 16srRNA, electricity generation, response surface methodology

Introduction

Synthetic dyes such as azo dyes have nitrogen-nitrogen double bond attached to the aromatic groups and are the main coloring agents in many industries including the textile industry (Cao *et al*., 2019; Firoozeh *et al*., 2022; Al-Tohamy *et al*., 2023). They make up most of the synthetic dyes used in industries since they are easy to synthesize and cost effective however, some are carcinogenic and mutagenic and have been reported to be biotoxic (Das and Mishra, 2017; Chen *et al*., 2021; Ngo and Tischler, 2022; Rafaqat *et al.,* 2022). Interestingly, about 10 to 15% of the synthetic dyes used in textile manufacturing are lost as wastewater effluent (Md *et al*., 2021). Hence, treatment of synthetic textile wastewater is desirable. However, since physicochemical methods such as membrane filtration is energy and cost intensive, biotreatment using microorganisms is a safer, cost effective and ecofriendly way to tackle these wastewaters (Das and Mishra, 2017; Trivedi *et al*., 2022; Al-Tohamy *et al*., 2023). Trivedi *et al*. (2022) reported increase in azo dye methyl orange decolorization with increase in biomass concentration under denitrifying conditions.

Enacted strict laws and regulations have made the textile wastewater treatment an extensive research area worldwide (Al-Tohamy *et al*., 2023), and bioremediation has been of great interest to researchers and industries, as the transition toward greener solutions has become more in demand in recent times (Cao *et al*., 2019; Gul *et al*., 2021; Ngo and Tischler, 2022; Al-Tohamy *et al*., 2023). For example, indigenous microbial consortium obtained from a textile factory sedimentation tank enhanced the decolorization of an azo dye on a broad range of temperature, pH, salinity and dye concentrations (Cao *et al*.,

2019). Similarly, a halotolerant yeast consortium (*Sterigmatomyces halophilus* SSA-1575 and *Meyerozyma guilliermondii* SSA-1547) exhibited 96.1% decolorization efficiency when exposed to 50 mg/L of a reactive azo dye (Al-Tohamy *et al*., 2023).

Microbial fuel cell (MFC) is an emerging and promising technology that addresses challenges of wastewater treatment while simultaneously incorporating bioelectricity production and CO2 emission reduction during microbial metabolism (Mittal and Kumar, 2022; Sikder and Rahman, 2023). This novel biological approach enhances the rate of anaerobic degradation of complex organics by introducing electrodes as an electron acceptor (Matteo, 2018). MFCs can enhance further the bioreduction of textile pollutants such as azo dyes as they have an infinite resource of terminal electron acceptors (anode) compared to exhaustible electron acceptors such as oxygen again, it has electricity generation as an additional advantage (Ilamathi and Jayapriya, 2017). Sikder and Rahman, (2023) demonstrated significant reduction in COD and TDS of municipal, textile and tannery wastewaters with better voltage and current generation from textile wastewater with MFC technology. Biodegradation of Remazol Brilliant Blue R (RBBR) was accompanied with electricity generation using fungal-based fuel cell (Umar *et al*., 2023). Nk and Rahman, (2020) showed 77.03% COD removal with concomitant current production of 4.8 MA and power density of 16.8 mW/m^2 from textile wastewater using single chambered microbial fuel cell. Similarly, enhanced anaerobic treatment of dyeing wastewater with microbial fuel cell was most effective with electrode area ratio of 1:1 (Hu *et al*., 2023).

The present study investigated the impact of different cultural conditions on the decolorization of an azo dye (Sudan G) with C.I. Number 11920 using five (5) azo dye degrading bacteria as well as MFC for enhanced decolorization.

Synthetic dyes, particularly azo dyes, are characterized by nitrogen-nitrogen double bonds attached to aromatic groups, and they serve as the primary coloring agents in various industries, including textiles (Cao *et al.*, 2019; Firoozeh *et al.*, 2022; Al-Tohamy *et al.*, 2023). These dyes dominate industrial applications due to their ease of synthesis and cost-effectiveness; however, many azo dyes are carcinogenic, mutagenic, and biotoxic, posing significant environmental and health risks (Das and Mishra, 2017; Chen *et al.*, 2021; Ngo and Tischler, 2022; Rafaqat *et al.*, 2022). Alarmingly, approximately 10 to 15% of synthetic dyes used in textile manufacturing are discharged as wastewater effluent, necessitating effective treatment strategies (Md *et al.*, 2021).

Traditional physicochemical methods for treating textile wastewater, such as membrane filtration, are often energy-intensive and expensive, making them less sustainable. In contrast, biotreatment using microorganisms offers a safer, cost-effective, and eco-friendly alternative to tackle these pollutants (Das

and Mishra, 2017; Trivedi *et al.*, 2022; Al-Tohamy *et al.*, 2023). For instance, Trivedi *et al.* (2022) reported enhanced decolorization of azo dye methyl orange with increasing biomass concentrations under denitrifying conditions. However, existing bioremediation techniques require optimization to address the limitations of efficiency and applicability across diverse environmental conditions.

Recent stringent laws and regulations governing textile wastewater discharge have driven extensive research into more sustainable and eco-friendly solutions (Al-Tohamy *et al*., 2023). Among these, bioremediation has garnered significant interest due to its alignment with the global transition toward greener technologies (Cao *et al.*, 2019; Gul *et al*., 2021; Ngo and Tischler, 2022). Microbial consortia derived from textile factory sedimentation tanks, for example, have demonstrated remarkable decolorization efficiencies for azo dyes under varying conditions of temperature, pH, salinity, and dye concentrations (Cao *et al*., 2019). Similarly, halotolerant yeast consortia have achieved impressive decolorization rates of reactive azo dyes, emphasizing the potential of microbial approaches in treating dye-laden wastewaters (Al-Tohamy *et al*., 2023).

However, despite the promise of bioremediation, the need for more efficient, scalable, and multifunctional systems has driven interest in microbial fuel cells. These systems combine wastewater treatment with the generation of bioelectricity and the reduction of CO_2 emissions during microbial metabolism, addressing environmental challenges on multiple fronts (Mittal and Kumar, 2022; Sikder and Rahman, 2023).

MFCs work by employing electrodes as terminal electron acceptors in microbial metabolism, enhancing the anaerobic degradation of complex organic pollutants such as azo dyes. Unlike traditional electron acceptors like oxygen, which are finite and location-dependent, the electrodes in MFCs provide a continuous and renewable alternative, supporting sustained microbial activity and degradation processes, as well as electricity generation (Ilamathi and Jayapriya, 2017; Matteo, 2018). This mechanism enables MFCs to significantly reduce chemical oxygen demand (COD) and total dissolved solids (TDS) in various types of wastewater, including municipal, textile, and tannery effluents. Notably, Sikder and Rahman (2023) observed superior voltage and current generation during the treatment of textile wastewater, highlighting the dual benefits of pollutant removal and energy production.

Furthermore, recent advances have demonstrated the potential for enhanced efficiency through system optimization. For instance, fungal-based MFCs successfully biodegraded Remazol Brilliant Blue R (RBBR) while generating electricity, showcasing the versatility of MFC technology (Umar *et al*., 2023).

Similarly, Hu *et al*. (2023) reported improved anaerobic treatment of dyeing wastewater by optimizing the electrode area ratio, emphasizing both the adaptability and scalability of MFCs for industrial applications. This dual functionality not only addresses wastewater treatment challenges but also supports the transition toward green energy and reduction in carbon emissions. Moreover, the high scalability and adaptability potentials of MFC make them practical for industrial wastewater applications, where they can contribute to cost-effective, large-scale solutions with significant environmental and economic benefits.

This study builds on these advancements by investigating the impact of different cultural conditions on the decolorization of an azo dye (Sudan orange G) using a microbial consortium and exploiting MFC technology to enhance treatment efficiency and electricity generation, thereby addressing the dual objectives of effective azo dye degradation and renewable energy production. The findings aim to contribute to the growing body of research on sustainable solutions for managing industrial dye pollution.

Materials and methods

Textile wastewater and isolation of azo dye reducing bacteria

Sudan orange G, a dye routinely used by local dyers was used as the azo dye for the preparation of simulated textile wastewater in this study. High purity Sudan orange G dye was purchased from Aldrich Chemical Co, USA and was used without prior purification. The chemical structure of Sudan orange G is shown in Figure 1. The textile effluent used for bacterial isolation was kindly donated by Sunflag Nigeria Limited, and Kofar Mata Dye Pits. The textile effluent samples were enriched by introducing 10 mL of samples into 90 mL of mineral salt broth enhanced with 0.01% of Sudan orange G dye and contained in 250 mL Erlenmeyer flask. Serial dilutions were made from the enriched culture of the textile effluent up to dilution 10^{-3}. Subsequently, mineral salt agar medium enhanced with 0.01% of Sudan orange G dye was inoculated with 0.1 mL of each suspension, spread with a glass spreader and incubated at 37 for 72 hrs. After incubation, zone of clearance around distinct colonies was taken as evidence of decolorization and organisms exhibiting dye decolorization potential were identified. The same medium was inoculated with a suspension derived from a stream water sample, which served as the control. No zones of clearing were observed on the control plates.

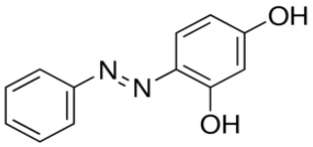

Figure 1. Chemical structure of Sudan orange G

Bacterial community identification

Identification of bacterial isolates were based on molecular technique and characterization using Polymerase chain reaction (PCR) with appropriate primers at Molecular Biology Unit, Medical laboratory Science Department, Niger Delta University (Bayelsa State).

DNA extraction. Five milliliters (5 mL) of an overnight broth culture of the bacterial isolate in Luria Bertani (LB) medium was spun at 14, 000 rpm for 3 mins. The cells were re-suspended in 500 µL of normal saline and heated at 95^{o}C for 20 mins. The heated bacterial suspension was cooled on ice and spun for 3 mins at 14, 000 rpm. The supernatant containing the DNA was transferred to a 1.5 mL microcentrifuge tube and stored at -20℃ for other downstream reactions. or Gram-positive bacteria with tougher cell walls, the boiling method was supplemented with additional steps to enhance lysis and improve DNA yield. One such step involved treating the bacterial cells with lysozyme, facilitating more effective DNA extraction.

DNA quantification. The extracted genomic DNA was quantified using the Nanodrop 1000 spectrophotometer. DNA purity was assessed by measuring the A260/A280 ratio, which provides an indication of protein contamination. A ratio within the range of 1.8–2.0 was considered acceptable, ensuring the DNA was of sufficient quality for downstream applications such as PCR amplification and sequencing.

The software of the equipment was launched by double clicking on the Nanodrop icon. The equipment was initialized with 2 µL of sterile distilled water and blanked using normal saline. Two microliters (2 µL) of the extracted DNA were loaded onto the lower pedestal; the upper pedestal was brought down to contact the extracted DNA on the lower pedestal. The DNA concentration was measured by clicking on the "measure" button.

16S rRNA amplification. The 16s rRNA region of the rRNA gene of the isolates were amplified using the 27F: 5'-AGAGTTTGATCMTGGCTCAG-3' and 1492R: 5'-CGGTTACCTTGTTACGACTT-3' primers on an ABI 9700 Applied Biosystems thermal cycler at a final volume of 40 microlitres for 35 cycles.

The PCR mix utilized for amplification included the X2 Dream Taq Master Mix supplied by Inqaba, South Africa, which contains Taq polymerase, dNTPs, and $MgCl_2$ at optimized concentrations suitable for standard PCR reactions. The final concentration of primers in the reaction was 0.5 μM, and the total reaction volume was 40 μL. While the precise concentrations of Taq polymerase, dNTPs, and $MgCl_2$ are proprietary to the master mix formulation, these are pre-optimized by the manufacturer to ensure reproducibility and efficient amplification. The PCR conditions were as follows: Initial denaturation, 95℃ for 5 minutes; denaturation, 95℃ for 30 seconds; annealing, 52℃ for 30 seconds; extension, 72℃ for 30 seconds for 35 cycles and final extension, 72℃for 5 mins. The product was resolved on a 1% agarose gel at 130 V for 30 mins and visualized on a blue light transilluminator.

*Sequencing.*Sequencing was done using the BigDye Terminator kit on a 3510 ABI sequencer by Inqaba Biotechnological, Pretoria South Africa. The sequencing was done at a final volume of 10 μL; the components included 0.25 μL BigDye® terminator v1.1/v3.1, 2.25 μL of 5 x BigDye sequencing buffer, 10 μM Primer PCR primer, and 2-10 μg PCR template per 100 bp. The sequencing condition were as follows; 32 cycles of 96 for 10s, 55 for 5s and 60 for 4 mins. Sequencing quality was assessed by reviewing chromatograms generated from the 3510 ABI sequencer using appropriate sequencing analysis software. Key metrics, such as the quality scores (Phred scores) and the clarity of the chromatogram peaks, were evaluated to ensure high-quality reads. Any low-quality sequences or ambiguous base calls were addressed by trimming the affected regions using sequence editing software such as BioEdit or MEGA. If significant issues persisted, such as incomplete reads or unclear chromatograms, re-sequencing was performed to obtain accurate data. These steps ensured the reliability of the sequences used for subsequent phylogenetic analysis.

Phylogenetic analysis. The obtained sequences were edited using the Trace Edit bioinformatics algorithm to ensure accuracy. Similar sequences were retrieved from the National Center for Biotechnology Information (NCBI) database using BLASTN. The BLAST search parameters included default settings for gap penalties and scoring, with the top hits selected based on sequence identity (≥97%), query coverage, and relevance to taxonomy. Only closely related sequences with high identity scores were chosen for downstream analysis. Sequences were aligned using the MAFFT software with default settings to ensure accurate multiple sequence alignment. The evolutionary history was inferred using the Neighbor-Joining method in MEGA 6.0, employing the Jukes-Cantor model for sequence evolution. The reliability of the phylogenetic tree was assessed through bootstrap analysis with 500 replicates, and bootstrap values were included to validate the confidence of the tree branches.

The sequences obtained in this study were submitted to the GenBank database and assigned the following accession numbers: *Pseudomonas aeruginosa* (MW584979), *Enterobacter hormaechei* (MW584986), *Providencia stuartii* (MW584987), *Escherichia coli* (MZ394117), and *Pseudomonas xiamenensis* (MW585052). This ensures transparency and facilitates accessibility for future research. The decolorization abilities of the bacterial isolates were evaluated using Sudan orange G and maintained in Bushnell Haas broth at 37 for routine experiments.

Azoreductase (azR) gene amplification

The azR gene of the isolates was amplified using the primers azRF (5'-GCGGATG(GC)G(GA)TTGTATTAT-3') and azRR (5'-ATCAAGCAC(AC)A(CG)(TC)TG(CT)TT-3') on an ABI 9700 Applied Biosystems thermal cycler in a 40 µL reaction volume for 35 cycles. These primers were sourced from literature and validated for specificity through initial PCR trials to ensure reliable amplification of the target gene in the bacterial species studied.

The PCR mix contained Taq polymerase for 5 minutes, followed by 35 cycles of denaturation at 95℃ for 30 seconds, annealing at 57℃for 30 seconds, and extension at 72℃for 30 seconds. A final extension step was performed at 72℃for 5 minutes.

The PCR products were resolved on a 1% agarose gel, which was run at 130 V for 30 minutes. A DNA ladder was included on the gel to determine the molecular sizes of the PCR products. The gel was stained with SYBR Green, and the bands were visualized using a blue light transilluminator. These steps ensured the successful amplification and confirmation of the azR gene for further analysis

Effect of cultural conditions on biodecolorization

The medium here contained mineral salt broth (10 mL) inoculated with 10 mL of azo dye reducing bacteria at 0.5 McFarland standard solution homogeneity of each of the bacterial species (*Pseudomonas aeruginosa* (MW584979), *Enterobacter hormaechei* (MW584986), *Providencia stuartii (*MW584987), *Escherichia coli* (MZ394117) and *Pseudomonas xiamenensis* (MW585052) with 0.1 cc g/L of the dye for 24 hrs. The 0.5 McFarland standard was chosen as it provides a consistent measure of bacterial density, approximately equivalent to 1.5×10^8 CFU/mL, which is commonly used in microbial assays for ensuring uniform inoculum size. It served as a general benchmark for the initial inoculum, ensuring comparable starting conditions for all isolates. Thereafter, microbial growth and decolorization were based on UV-visible light spectrophotometer (LaMotte Smart) at 600 nm and 388 nm respectively.

Effect of pH. The effect of pH on dye decolorization by bacterial isolates was determined using different regimes of pH (4, 5, 6, 7, 8, 9 and 10). The pH of the medium was adjusted using 1N solutions of HCl and NaOH to achieve the desired pH values (4, 5, 6, 7, 8, 9, and 10) before inoculation. Sets of Erlenmeyer flasks containing 20 mL each of mineral salt broth containing 0.1 g/L dye were prepared and inoculated with 10 mL of the respective bacterial isolates and incubated at 35 for 24 hrs. No inoculum was added in the control tube. Thereafter, the extent of decolorization in each flask was assessed by centrifuging each broth culture samples at 12,000 rpm for 15 mins after which the supernatant was analyzed using a UV-visible light spectrophotometer (Chen *et al.,*2003). During the experiment, the pH was not actively monitored or readjusted, as the focus was on assessing the initial pH's impact on dye decolorization.

Effect of temperature. Mineral salt broth (20 mL) containing 0.1 g/L dye was inoculated with 10 mL of the respective bacterial isolates at different temperatures (15, 20, 25, 30, 35, 40 and 45℃) and incubated for 24 hrs. The temperature of the incubation was controlled using thermostatically regulated incubators set to the desired temperatures. Each incubator was pre-calibrated to ensure accuracy, and the temperature was monitored periodically during the 24-hour incubation period using a thermometer placed inside the incubator. This ensured consistent temperature conditions throughout the experiment for all bacterial isolates. No inoculum was added in the control tube and dye concentration was same in all tubes. Thereafter, the extent of decolorization in each flask was assessed by centrifuging each broth culture samples at 12,000 rpm for 15 mins after which the supernatant was analyzed using a UV-visible light spectrophotometer (Chen *et al.,*2003).

Effect of glucose. To evaluate the effect of glucose concentration on microbial dye decolorization, different concentrations of glucose ranging from 0.1 g/L to 10 g/L were prepared in mineral salt broth, each containing 0.1 g/L of the dye. These glucose concentrations were selected based on prior experiments to assess the impact of carbon source availability on microbial activity, including dye decolorization.

A 20 mL volume of each glucose concentration was dispensed into Erlenmeyer flasks and sterilized by autoclaving. After sterilization, 10 mL of an 18-hour old microbial culture was added to each flask, and the flasks were incubated at 35 for 24 hours. Control tubes, in which no inoculum was added, were included to ensure that the dye concentration remained constant across all treatments. After the incubation period, the tubes were centrifuged at 12,000 rpm for 15 minutes to separate the cells from the supernatant.

The supernatants were then analyzed spectrophotometrically to determine the extent of dye decolorization. Dye reduction was measured by comparing the absorbance of the supernatants at the appropriate wavelength before and after the incubation period.

Effect of different sodium salts. Sodium chloride and sodium citrate were used at different concentrations (0-10 g/L) to determine their effect on dye decolorization. High sodium chloride levels can inhibit bacterial growth in non-halotolerant species, negatively impacting decolorization whereas, sodium citrate may enhance dye decolorization by chelating metal ions that inhibit enzymatic activity. Mineral salts broth (20 mL) containing dye concentration (0.1 g/L) and different concentrations (0 – 10 g/L) of sodium chloride and sodium citrate each was inoculated with 10 mL of the respective bacterial isolate and incubated at 35^{o}C for 24 hrs. Thereafter, the extent of decolorization in each flask was assessed by centrifuging each broth culture sample at 12,000 rpm for 15 mins after which the supernatant was analyzed using a UV-visible light spectrophotometer (Chen *et al.,*2003).

Effects of nitrogen sources. The effect of various nitrogen sources on dye decolorization by bacterial isolates was determined using urea and peptone as nitrogen sources. Urea and peptone were selected as nitrogen sources for this study due to their widespread use in microbial growth media and their ability to provide essential nitrogen for bacterial metabolism. Urea serves as a simple, inorganic nitrogen source, while peptone is a complex organic nitrogen source rich in amino acids and peptides. These distinct properties allow for the assessment of how different forms of nitrogen influence bacterial dye decolorization efficiency. Sets of Erlenmeyer flasks containing 70 mL each of sterile mineral salt broth containing 0.1g/L dye and 20 mL of different concentration (0 g/L to 10 g/L) of sterile urea or peptone were prepared and inoculated with 10 mL of the respective bacterial isolates. The chosen concentration range (0 g/L to 10 g/L) reflects conditions that encompass both nitrogen-limited and nitrogen-rich environments, ensuring a comprehensive evaluation of the bacterial isolates' response under varying nitrogen availability. After inoculation, the flasks were incubated at 35℃ for 24 hrs. Thereafter, the extent of decolorization in each flask was assessed by centrifuging each broth culture sample at 12,000 rpm for 15 mins after which the supernatant was analyzed using a UV-visible light spectrophotometer (Chen *et al.,* 2003).

*Effect of vitamins***.** Vitamins B_2 and B_{12} were used at different concentrations (0–10 g/L) to determine their effect on dye decolorization efficiency, thereby contributing to the optimization of bioremediation strategies. Vitamin B2 (riboflavin)

and vitamin B12 (cobalamin) were selected for this study due to their critical roles in microbial metabolism and enzymatic functions. vitamin B2 is a precursor for flavin adenine dinucleotide (FAD) and flavin mononucleotide (FMN), which are cofactors involved in various redox reactions essential for microbial energy production and enzymatic activities. Similarly, vitamin B12 is a cofactor for enzymes that facilitate key metabolic processes, such as methylation and reductive reactions, which may directly or indirectly influence the decolorization of dyes by supporting the enzymatic pathways responsible for breaking down azo bonds. The concentration range tested was selected based on preliminary experiments, ensuring that the concentrations covered a spectrum of physiological relevance without causing vitamin-induced toxicity or metabolic imbalance.

Mineral salts broth (20 mL) containing these different vitamin concentrations was each inoculated with 10 mL of the respective bacterial isolate and incubated at 35℃ for 24 hrs. Thereafter, the extent of decolorization in each flask was assessed by centrifuging each broth culture sample at 12,000 rpm for 15 mins after which the supernatant was analyzed using a UV-visible light spectrophotometer (Chen *et al.,* 2003).

Optimization of dye decolorization using response surface methodology

The central composite design of the response surface methodology (Design Expert-13) was used to optimize the decolorization of the dyes using the values in (Table 1) below. Response surface methodology (RSM) is an approach used to generate the best conditions for a system comprising many variables to calculate the combined effect of selected variables. In the present study, RSM was employed to identify the interaction between the operational variables such as pH, temperature, glucose concentration and salinity using the central composite design (Table 2).

Table 1. Range and levels of experimental variables for decolorization of Sudan orange G by consortium

Factors	**Levels**				
	-α	**-1**	**0**	**+1**	**+ α**
pH	5	6	7	8	9
Temperature (°C)	25	30	35	40	45
Glucose concentration	0.5	0.75	1	1.25	1.5
Salinity	1	3	5	7	9

Table 2. The number of runs and factors sed for the central composite design experiment

Std	Run	Factor 1 A: pH	Factor 2 B: Temp. (°C)	Factor 3 C; Glucose Conc. (g/L)	Factor 4 D: Salinity (%)	Response 1 % Decolorization	Response 2 Microbial Growth (600 nm)
22	1	7	35	14	5	62.65	1.42
19	2	7	25	10	5	44.02	0.38
6	3	8	30	12	3	51.02	0.53
2	4	8	30	8	3	54.12	0.69
25	5	7	35	10	5	74.14	1.78
16	6	8	40	12	7	56.74	0.76
9	7	6	30	8	7	52.81	0.62
12	8	8	40	8	7	54.89	0.73
15	9	6	40	12	7	68.25	1.61
14	10	8	30	12	7	60.86	0.98
17	11	5	35	10	5	61.02	1.09
1	12	6	30	8	3	54.78	0.71
27	13	7	35	10	5	81.73	2.12
8	14	8	40	12	3	70.12	1.73
18	15	9	35	10	5	69.18	1.71
13	16	6	30	12	7	62.74	1.48
21	17	7	35	6	5	62.64	1.38
26	18	7	35	10	5	75.47	1.89
20	19	7	45	10	5	39.87	0.34
4	20	8	40	8	3	67.85	1.58
5	21	6	30	12	3	51.81	0.58
11	22	6	40	8	7	48.89	0.48
23	23	7	35	10	1	47.28	0.43
3	24	6	40	8	3	58.98	0.89
10	25	8	30	8	7	51.02	0.53
7	26	6	40	12	3	57.87	0.83
24	27	7	35	10	9	68.81	1.64

Microbial fuel cell setup

A double chambered microbial fuel cell was used for enhanced decolorization of the dye (Sudan orange G). The set up comprised 0.1 g/L of the dye in 500 mL nutrient broth, two graphite rod electrodes (7.0 x 56.0 mm), copper wire conductor (1 mm diameter), multimeter and 2500 mL containers. The anode chamber of the MFC consisted of poultry dung mixed with sterile water to obtain a semi solid consistency. Poultry dung was used as the anode substrate

in this MFC setup due to its high organic matter content and diverse microbial population, which can facilitate the breakdown of organic compounds and generate electrons through microbial metabolism. The cathode chamber consisted of the dye inoculated with 1 mL of azo dye reducing bacteria at 0.5 McFarland standard solution homogeneity (*Pseudomonas aeruginosa* (MW584979), *Enterobacter hormaechei* (MW584986), *Providencia stuartii (*MW584987), *Escherichia coli* (MZ394117) and *Pseudomonas xiamenensis* (MW585052). Before use in the MFC, the electrodes were polished with fine sandpaper or abrasive material to remove surface oxidations and increase surface area for enhanced microbial attachment and electron transfer. The graphite rod electrodes were then carefully prepared to prevent contamination and ensure optimal performance. This preparation typically involves cleaning the electrodes with ethanol to remove oils or impurities, followed by rinsing them with distilled water. Both chambers were connected using a salt bridge (3 cm length; 1cm diameter) loaded with saline molten agar prepared by adding 10 g of sodium chloride in 100 mL of sterile water. Generation of electric current in the MFC was determined using a multimeter connected to the two graphite rods in each chamber via copper wire. Power (mv) produced were obtained at intervals of 12 hours for 3 days. Optimal conditions (as determined by RSM) were maintained in the cathode chamber during the experiment.

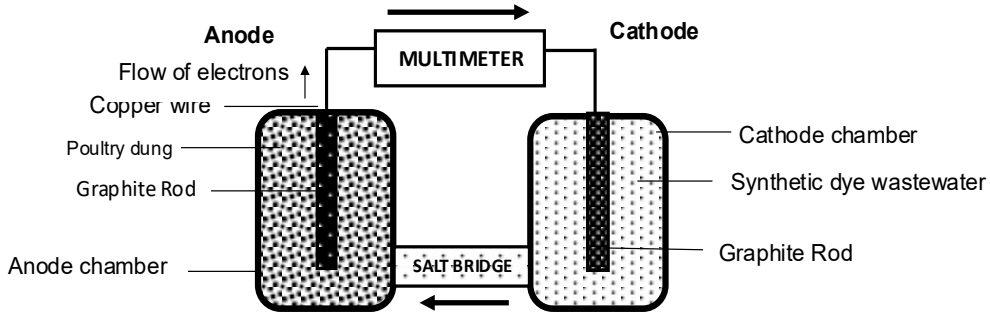

Figure 2. The microbial fuel cell

Bio decolorization, biodegradation and chemical analysis

Sudan orange G colour removal was monitored every 12 h using UV-visible light spectrophotometer at the maximum absorbance wavelength (λmax) of dye (i.e., 388 nm). Dye biodegradation was monitored by gas-chromatography-mass spectrometry (GC-MS). After dye degradation (3 days), the samples were centrifuged at 12,000 rpm for 5 min and the supernatants obtained were used

to extract metabolites. Thereafter, the absorbance of Sudan orange G broth was monitored in a UV-visible spectrophotometer at maximum absorption wavelength (388 nm). All the experiments were performed in triplicate and the results were expressed in terms of percentage decolorization as calculated using the formula (Eq.1) (Uppala *et al*., 2015).

$$\textbf{Eq. 1.}\ Decolorization\ \% = \frac{Initial\ Absorbance - Final\ Absorbance}{Initial\ Absorbance} \times 100$$

The chemical changes in the redox dyes during decolorization were analyzed using Gas Chromatography-Mass Spectrometry (GC-MS). For sample preparation, an aliquot of the decolorized dye was transferred into Erlenmeyer flasks, and 15 mL of methanol was added. The mixture was vigorously agitated and left to stand for 24 hours. Following this, the extract was filtered through No.1 Whatman filter paper using a funnel, and the filtrate was collected in a 100 mL conical flask. The resulting extract was then subjected to GC-MS analysis.

One microliter (1 µL) of the methanol extract was injected into the GC-MS instrument. The GC oven temperature program was as follows: an initial temperature of 60 for 2 minutes, followed by a ramp to 300 at a rate of 10 per minute, and held at 300 for 6 minutes. The mass spectrometer was operated with a transfer line temperature of 240, ion source temperature of 240, and an electron ionization energy of 70 eV. The scan interval was set at 0.1 seconds, with a scan time of 0.2 seconds, and a scan range from 50 to 600 Daltons. The GC-MS method was validated by assessing specificity, precision, and accuracy using standard reference compounds. The spectra obtained from the GC-MS were processed using TurboMass Ver 5.4.2 software and compared to the National Institute of Standards and Technology (NIST-2008) standard library database for compound identification.

Results and Discussion

The 16S rRNA sequence obtained from the isolate showed a 100% similarity with sequences in the NCBI non-redundant nucleotide (nr/nt) database, matching species such as *Providencia stuartii*, *Pseudomonas aeruginosa*, *Pseudomonas xiamenensis*, *Escherichia coli*, and *Enterobacter hormaechei*. Phylogenetic analysis using the Jukes-Cantor method revealed that the isolates are closely related to these species, with evolutionary distances supporting their placement within the genera *Providencia*, *Pseudomonas*, *Escherichia*, and *Enterobacter*. The sequences and their respective accession numbers were as follows: *Pseudomonas aeruginosa* (MW584979), *Enterobacter hormaechei* (MW584986),

Providencia stuartii (MW584987), *Escherichia coli* (MZ394117), and *Pseudomonas xiamenensis* (MW585052) (Table 2). This genetic analysis confirms the close evolutionary relationships of the isolates with these species, as shown in (Figure 3) and (Figure 4).

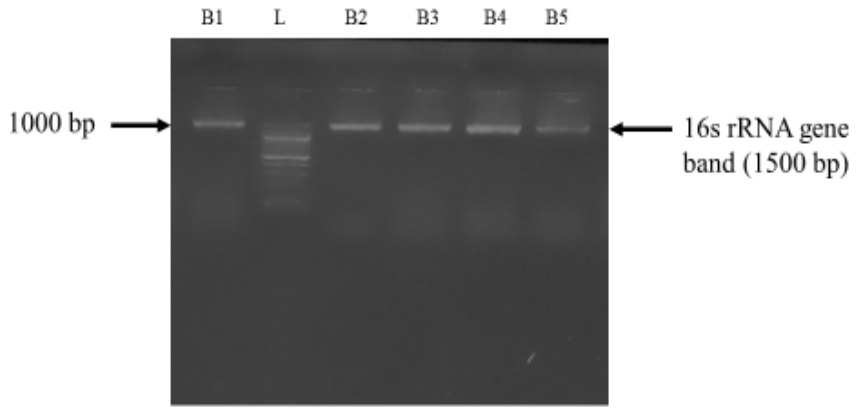

Figure 3. Agarose gel electrophoresis of the 16S rRNA gene of some selected bacterial isolates. Lanes B1-B5 represent the 16SrRNA gene bands (1500bp), lane L represents the 100bp molecular ladder**.** Key: B1= *Pseudomonas aeruginosa;* B2= *Enterobacter hormaechei*; B3= *Providencia stuartii;* B4= *Escherichia coli;* B5= *Pseudomonas xiamenensis.*

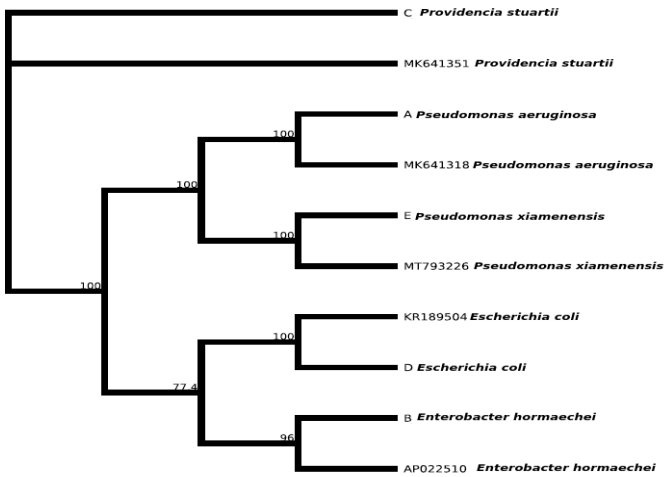

Figure 4. Neighbor-Joining tree based on 16S RNA gene sequence showing Relationship between *Providencia startii, Pseudomonas aeruginosa, Pseudomonas xiamenensis*, *Escherichia coli,* and *Enterobacter hormaechei.* Key: A= *Pseudomonas aeruginosa;* B= *Enterobacter hormaechei;* C= *Providencia stuartii;* D= *Escherichia coli;* E= *Pseudomonas xiamenensis*

The sequences obtained and their corresponding accession numbers were: *Pseudomonas aeruginosa* (MW584979), *Enterobacter hormaechei* (MW584986), *Providencia stuartii* (MW584987), *Escherichia coli* (MZ394117), and *Pseudomonas xiamenensis* (MW585052) (Table 2). This data provides a detailed genetic characterization, confirming the high similarity and close evolutionary relationships of the isolates with these known bacterial species. (Figure 5) depicts the agarose gel electrophoresis of the *azR* gene. Lanes A and C represent the *azR* at 500bp while lane L represents the 100 bp molecular ladder affirming that some of the bacterial species (*Pseudomonas aeruginosa* and *Provindencia stuartii*) possess the azoreductase enzyme gene in their chromosomes.

Table 3. Accession numbers of bacteria isolated from textile waste water

Isolate Code	Accession Number	Similarity Index (%)	Bacterial Species
A	MW584979	100	*Pseudomonas aeruginosa*
B	MW584986	96	*Enterobacter hormaechei*
C	MW584987	100	*Providencia stuartii*
D	MZ394117	100	*Escherichia coli*
E	MW585052	100	*Pseudomonas xiamenensis*

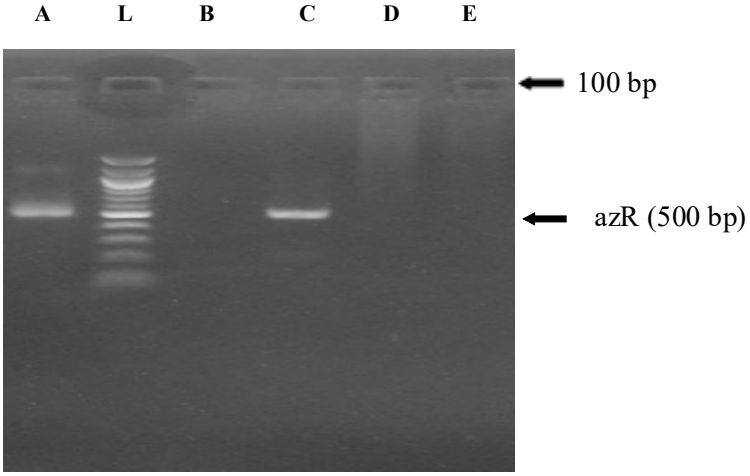

Figure 5. Agarose gel electrophoresis of the azR gene. Lanes A and C represent the azR at 500bp while lane L represents the 100 bp molecular ladder.Key: A= *Pseudomonas aeruginosa;* B= *Enterobacter hormaechei;* C= *Providencia stuartii;* D= *Escherichia coli;* E= *Pseudomonas xiamenensis*

Azoreductases play a crucial role in the bacterial degradation of azo dyes, a major class of synthetic dyes widely used in various industries. Azo dyes are characterized by the presence of one or more azo linkages (-N=N-). The *azr* gene encodes azoreductase enzymes, which catalyze the reductive cleavage of these azo bonds. This cleavage is a critical initial step in the biodegradation pathway of azo dyes, breaking down the complex dye molecule into smaller, less colored, and potentially less toxic aromatic amines. The general biochemical pathway involves the transfer of electrons from NADH or NADPH to the azo bond, resulting in its cleavage. This reaction typically occurs under anaerobic or microaerobic conditions.

The *azr* gene was chosen for investigation because azoreductase activity is a key indicator of a bacterium's ability to decolorize azo dyes. Detecting the presence of the *azr* gene provides direct evidence of the potential for azo dye degradation. Furthermore, the *azr* gene is a commonly studied marker in research on bacterial dye decolorization, allowing for comparisons with other studies.

The detection of the *azr* gene in *Pseudomonas aeruginosa* and *Providencia stuartii* in this study is consistent with previous research. Azoreductase activity has been widely reported in various bacterial species such as *Shewanella oneidensis*, *Rhodococcus opacus*, *Halomonas elongata*, and *Pseudomonas putida* (Qi *et al*., 2016; Mendes *et al*., 2011; Mugerfeld *et al*., 2009; Qi *et al*., 2017; Eslami *et al*., 2016).

The data on the effect of various pH levels on dye decolorization by isolates, as presented in (Figure 6), reveal critical insights into the process's sensitivity to this environmental factor. Optimal decolorization for both dyes was achieved at a neutral pH of 7. This suggests that the enzymes or other biological mechanisms responsible for dye breakdown within the bacterial isolates function most efficiently under these conditions. As the pH shifted towards acidity (pH 4), the decolorization efficiency significantly declined, with the lowest performance observed at this most acidic level. Similarly, as the pH increased towards alkalinity, the decolorization extent also decreased. These trends are consistently illustrated in Figure 4 for all dyes tested. The significant differences ($p < 0.05$) in the percentage of dye decolorization at various pH levels underscore the pronounced impact of pH on the decolorization process.

The strong pH dependence observed can be attributed to several factors. Firstly, pH significantly influences the activity and stability of enzymes. Many enzymes have specific pH optima, and deviations from this optimum can lead to conformational changes that reduce or abolish their catalytic activity. The enzymes involved in dye degradation within the bacterial isolates likely exhibit such pH sensitivity. Secondly, pH affects the surface charge of both the bacterial cells and the dye molecules. At extreme pH values, the charges on the bacterial

cell surface and the dye molecules might become similar, leading to electrostatic repulsion and hindering the interaction between the bacteria and the dye. This reduced interaction can limit dye adsorption onto the bacterial cells, a crucial initial step in the decolorization process. Thirdly, pH can impact the redox potential of the system, influencing the availability of electron donors and acceptors needed for enzymatic reactions involved in dye breakdown.

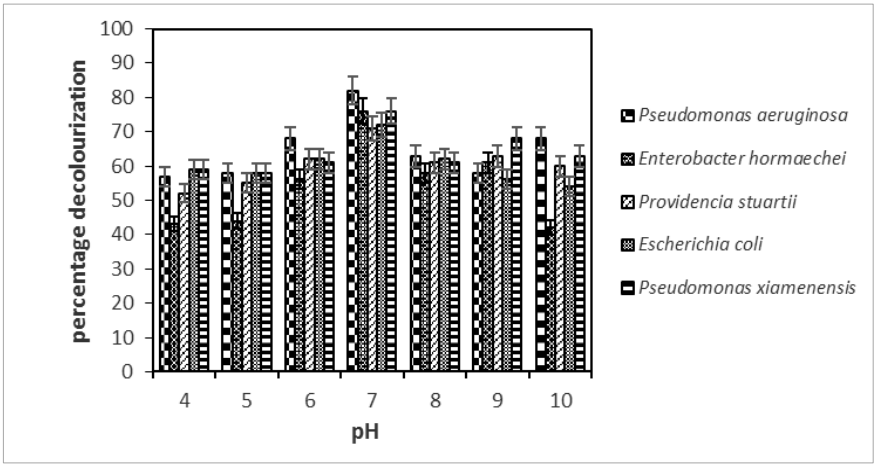

Figure 6. Effect of various pH on decolorization extent of Sudan orange G

These results are consistent with findings reported in the literature for other dye-decolorizing bacteria. For instance, studies on degradation of Malachite green by a bacterial culture have also demonstrated optimal dye decolorization at neutral or near-neutral pH, with decreased efficiency at both acidic and alkaline pH values (Etezad and Sadeghi-Kiakhani, 2021). Similarly, research on decolorization of Orange II by *Bacillus subtilis* has shown that pH affects the expression of dye-degrading enzymes, with optimal expression often observed around neutral pH (Ikram *et al*., 2022). The near-neutral pH range also aligns with the findings of Liu *et al*. (2017), who suggested that slightly acidic to neutral pH is generally optimal for bacterial dye degradation, although the specific range can vary depending on the microbial consortium. Deviations from this range can affect enzyme structure and activity, thus reducing decolorization efficiency, as well as impacting microbial growth and community dynamics, as highlighted by Lui *et al*. (2016).

However, it's important to note that the specific pH optima and the extent of pH influence can vary depending on the bacterial species, the type of dye, and the specific enzymatic mechanisms involved. For example, Methyl orange

decolorization has been shown to be optimal under slightly alkaline conditions (Trivedi *et al*., 2022), whereas Mordant Black 11 dye removal by *Staphylococcus* sp. MB377 is favored by acidic pH (Tahir *et al*., 2021). This variability highlights the importance of characterizing the pH dependence of dye decolorization for each specific bacterial isolate and dye combination.

The impact of various temperature regimes on dye decolorization by different bacterial isolates is illustrated in (Figure 7). The data clearly demonstrate that the highest level of dye decolorization was achieved at an optimal temperature of 35℃, highlighting the enhanced metabolic activity and efficiency of the isolates at this temperature. This optimal temperature suggests that the enzymes involved in the dye degradation pathways within these bacteria are most efficient around 35℃. Enzymes, being biological catalysts, typically have a temperature range within which they function optimally. Beyond this range, their activity can decrease due to denaturation or other conformational changes.

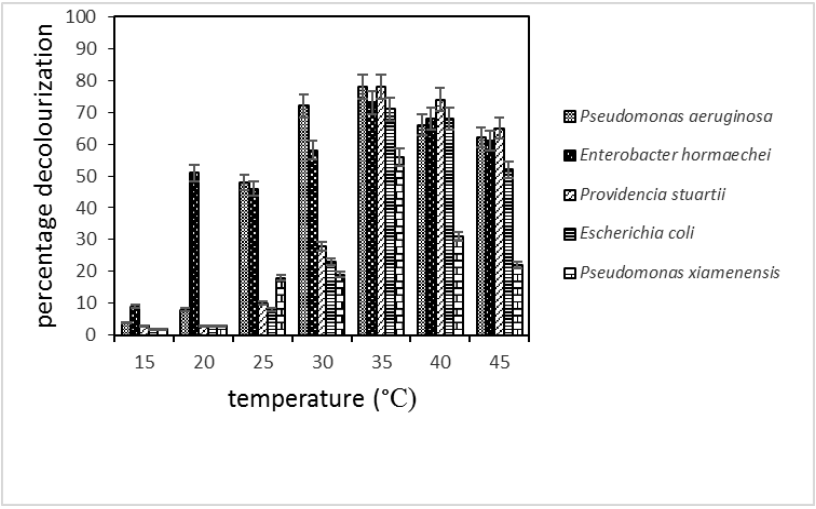

Figure 7. Effect of different temperature regimes on decolorization extent of Sudan orange G

Conversely, the lowest decolorization performance was recorded at 15, indicating that lower temperatures significantly impede the decolorization process. At lower temperatures, the metabolic activity of the bacteria slows down. This includes reduced enzyme activity, slower transport of molecules across cell membranes, and decreased rates of biochemical reactions essential for dye degradation. Essentially, the bacteria are less metabolically active and therefore less efficient at breaking down the dye molecules.

These findings underscore the importance of maintaining an optimal temperature to maximize the efficacy of bacterial dye decolorization, providing a direction for the development and optimization of bioremediation protocols. The 35 optimum observed in this study is consistent with the typical growth temperature range for many mesophilic bacteria, which thrive in moderate temperatures (20-45). Many studies have reported similar optimal temperatures for dye decolorization by various bacterial species. For example, in a study by Ikram *et al*. (2022) it was shown that optimal dye removal was at 35 during decolorization of Orange II by *Bacillus subtilis*. Similarly, a bacterium has also demonstrated enhanced Malachite green decolorization at temperatures close to 35 (Etezad and Sadeghi-Kiakhani, 2021). Dafale *et al*. (2016) also reported the moderate temperature range (25 to 35) as optimal for bacterial dye degradation. Taha *et al*. (2014) emphasized the importance of temperature control for optimizing microbial activity and minimizing the release of harmful intermediates during dye degradation.

However, it's important to note that the optimal temperature for dye decolorization can vary depending on the specific bacterial species, the type of dye, and other environmental factors. Some bacteria, such as *Proteus mirabilis*, can thrive and degrade pollutants at higher temperatures of 40 (Madhushika *et al*., 2021). Therefore, while 35 appears to be optimal for the isolates in this study, it's not a universal optimum for all dye-decolorizing bacteria.

The results on the effects of glucose concentration on dye decolorization by various bacterial Isolates are detailed in (Figure 8). The data reveal that the optimal decolorization of dyes was achieved at a glucose concentration of 10 g/L, showcasing the most efficient breakdown and removal of dye compounds under these conditions. In contrast, the lowest decolorization performance was observed at a glucose concentration of 0.1 g/L, indicating that insufficient glucose levels significantly hinder the decolorization process. This highlights the crucial role of glucose as a readily available carbon and energy source for the bacterial isolates, directly influencing their metabolic activity and, consequently, their ability to decolorize dyes.

Glucose influences the decolorization process at the microbial level in several key ways. Firstly, it serves as a primary carbon and energy source. Bacteria utilize glucose for essential metabolic processes, including growth, maintenance, and reproduction. Adequate glucose availability fuels these processes, providing the energy (ATP) and reducing equivalents (NADH) necessary for the enzymatic reactions involved in dye degradation. These reducing equivalents are particularly important in the reductive cleavage of azo dye bonds, a common mechanism for bacterial decolorization. Glucose acts as a crucial electron donor, promoting microbial growth and activity, which in turn enhances azo bond

reduction and dye decolorization (Keziban, 2019). Secondly, glucose can act as a co-metabolite. In some cases, the presence of glucose might be required for the bacteria to effectively utilize the dye as a secondary carbon source or for the enzymes involved in dye degradation to function optimally. While *Pseudomonas putida* WLY could utilize X-3B as its sole carbon source, its slow growth rate suggests that X-3B alone might not be an easily accessible carbon source. The addition of glucose significantly boosted both its growth and decolorization rate, indicating that glucose likely facilitated the utilization of the dye through co-metabolism or by providing an easily accessible form of carbon. Thirdly, glucose can influence the expression and activity of dye-degrading enzymes. It can stimulate the production of crucial enzymes like azoreductases, which are often involved in the initial steps of azo dye breakdown. Essentially, glucose acts as a metabolic trigger, enhancing the bacteria's overall metabolic machinery, including the specific enzymes needed for dye decolorization.

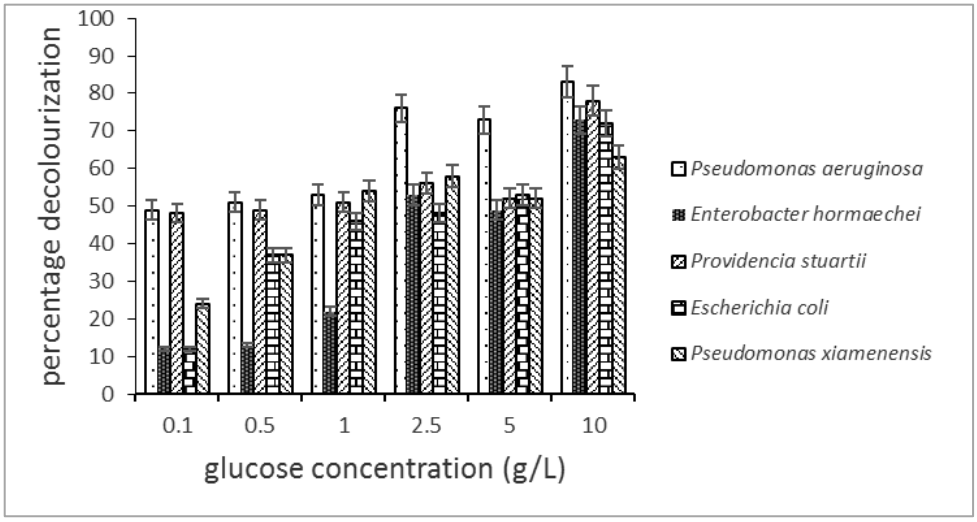

Figure 8. Effect of various glucose concentrations on decolorization extent of Sudan orange G

The importance of supplementary carbon sources for enhancing bacterial dye decolorization is well-documented. Our finding of 10 g/L glucose as optimal aligns with previous work. For example, Al-Ansari *et al*. (2022) observed improved Acid Orange decolorization by *Enterobacter aerogenes* ES014It with 1.5% glucose (equivalent to 15 g/L), while Sarkar *et al.* (2021) reported enhanced Congo Red removal by *Chryseobacterium geocarposphaerae* DD3 with 5 g/L glucose. Glucose's effectiveness is further supported by Kumaravel and Shanmugam (2024).

While glucose is often preferred, other carbon sources can also play a role. Zhang *et al*. (2021), for instance, showed that fructose co-metabolism enhanced Reactive Black 5 wastewater remediation by a *Pseudomonas aeruginosa* strain. This study reinforces the need to optimize carbon source availability for efficient bioremediation.

The effects of sodium chloride on dye decolorization by various bacterial isolates are detailed in (Figure 9). Optimal decolorization occurred at 5 g/L NaCl, suggesting this concentration promotes optimal microbial activity and efficiency. This aligns with studies suggesting that moderate salinity concentrations, around 5 g/L, are generally optimal for promoting microbial growth and enzyme activity (Hague *et al*., 2023). Tian *et al*. (2021) highlighted the importance of salinity control for effective dye degradation, as it influences microbial activity. Conversely, lower salt levels (0.1 g/L) significantly hindered decolorization. This indicates that while some salt is beneficial, too little can limit the bacteria's metabolic processes necessary for dye breakdown. Sodium chloride, at appropriate concentrations, can contribute to maintaining optimal osmotic pressure for bacterial cells, supporting enzyme activity and nutrient uptake. It can also influence the solubility and availability of the dye itself. However, excessively low salt concentrations can disrupt osmotic balance, potentially hindering cell growth and enzyme function. Our findings also align with Trivedi *et al.* (2022), who observed that Methyl Orange decolorization was unaffected by salinity up to 10 g/L NaCl, with an optimum between 5 and 8 g/L, further supporting the idea of an optimal range. While our study suggests 5 g/L as optimal, the difference may be due to the specific dye, bacterial isolates, or other experimental conditions.

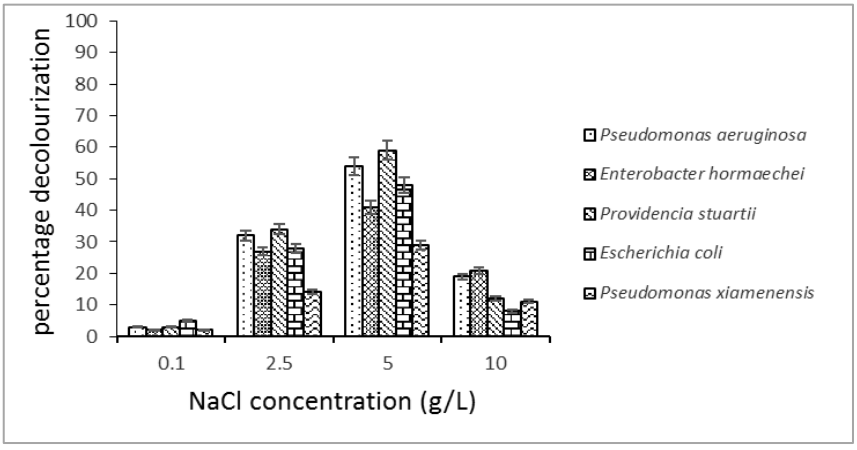

Figure 9. Effect of various sodium chloride concentrations on the decolorization extent of Sudan orange G

The halotolerance of the isolates, demonstrated by their ability to function in moderate salinity, makes them particularly promising for bioremediation in environments like textile wastewater, which often contains significant amounts of salt.

The impact of sodium citrate on dye decolorization is presented in (Figure 10). Optimal decolorization occurred at 5 g/L, while 10 g/L generally resulted in lower performance, particularly for *E. coli*. Sodium citrate, as a carbon source, can influence the metabolic pathways related to dye degradation. Citrate can be metabolized to provide energy and reducing equivalents, which are essential for the enzymatic breakdown of dyes. However, high concentrations might lead to substrate inhibition or competition for metabolic resources, thus hindering the decolorization process. This may be due to the phenomenon of catabolite repression, wherein the presence of a preferred carbon source (citrate) inhibits the expression of genes required for utilizing the dye. Our optimal concentration of 5 g/L suggests this is an effective concentration, where it promotes bacterial activity but not to an inhibitory extent. Georgiou *et al*. (2004) found that sodium salts can selectively promote the growth of bacteria with high azoreductase activity, which aligns with the observation of improved decolorization. Our results further emphasize the importance of optimizing sodium citrate concentrations, as both insufficient and excessive amounts can negatively impact dye removal.

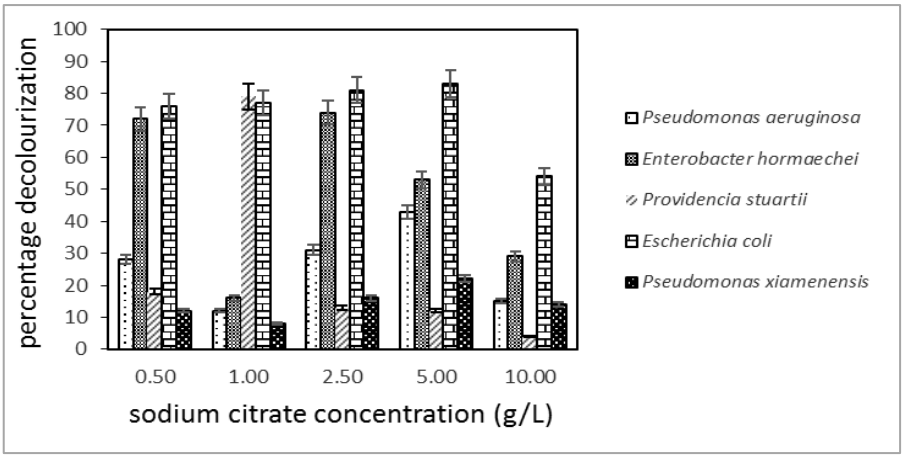

Figure 10. Effect of various sodium citrate concentrations on Sudan orange G

Data on effect of urea on dye decolorization are presented in (Figure 11). A concentration of 0.1 g/L proved optimal, whereas 8 g/L significantly reduced decolorization. Urea serves as a nitrogen source, which is crucial for bacterial

growth and protein synthesis, including the production of dye-degrading enzymes. However, excessively high urea concentrations could lead to ammonia toxicity, inhibiting bacterial growth and activity. High concentrations of urea may increase the pH of the environment, creating unfavorable conditions for the bacteria or the enzymes responsible for dye degradation, or both.

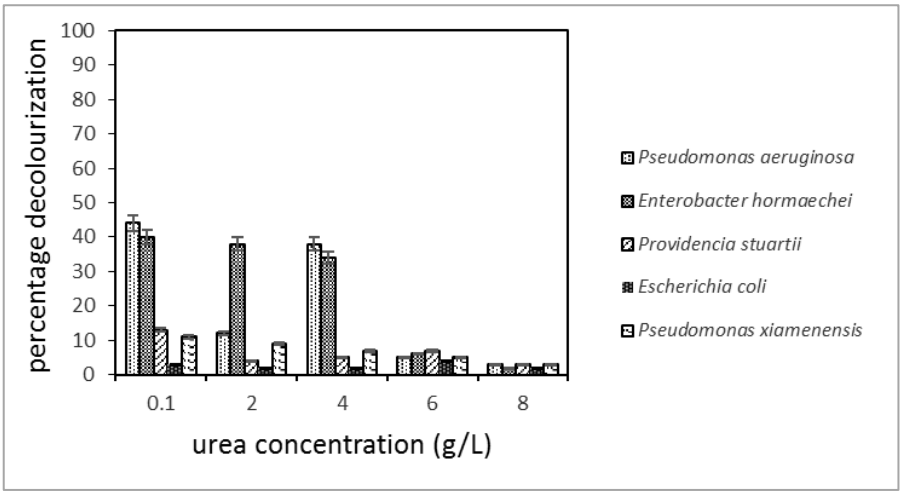

Figure 11. Effect of various urea concentrations on the decolorization extent of Sudan orange G

Fahad *et al*. (2020) reported that urea, as a nitrogen source, enhances microbial growth and activity, particularly in nitrogen-limited environments, which supports the concept that an optimized amount can be beneficial. Our findings demonstrate that the ideal urea level is low (0.1g/L), which suggests that only a minimal amount is necessary to support nitrogen requirements for efficient dye decolorization and that an excess might have the aforementioned inhibitory effects.

The data obtained on the effect of various peptone concentrations on dye decolorization by bacterial isolates are presented in (Figure 12). Generally, results indicate that there were no significant changes in the extent of decolorization of the azo dyes at different peptone concentrations. This suggests that peptone, a common nitrogen source, may not significantly influence the decolorization efficiency of these bacterial isolates under the conditions tested. Understanding the limited impact of peptone on decolorization is crucial for optimizing nutrient supplementation strategies in bioremediation processes.

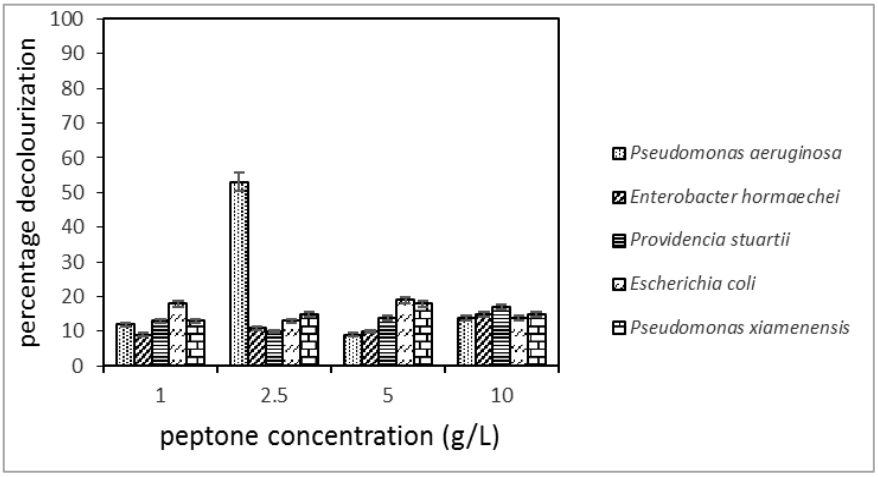

Figure 12. Effect of various peptone concentrations on decolorization extent of Sudan orange G.

The effect of vitamin B_2 on dye decolorization by various bacterial isolates is shown in (Figure 13). The data indicate that the optimal decolorization of the dyes was achieved at a vitamin B_2 concentration of 10 g/L. Conversely, the lowest decolorization performance was observed at a concentration of 0.5 g/L.

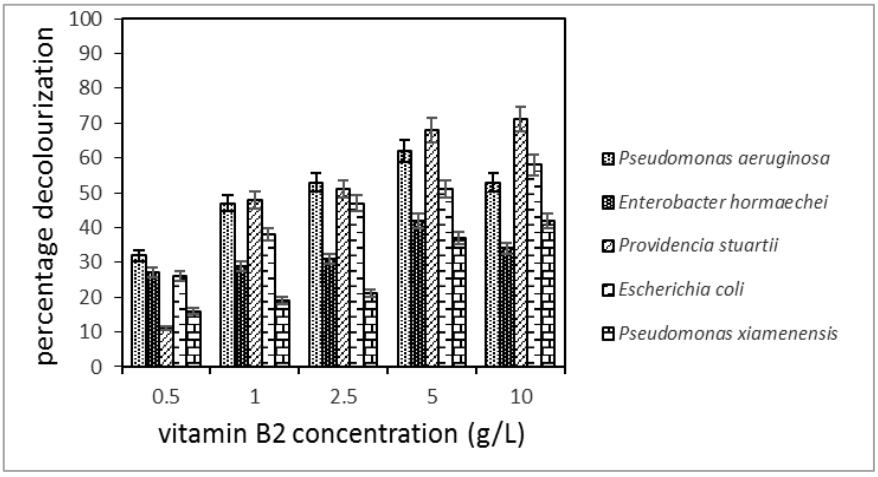

Figure 13. Effect of various vitamin B_2 concentrations on the decolorization extent of Sudan orange G

These findings highlight the importance of vitamin B_2 in enhancing microbial dye decolorization, potentially due to its role as a coenzyme in various biochemical reactions. Vitamin B_2 can selectively promote the growth of certain microbial populations that are more efficient in dye decolorization. This can lead to a more robust and efficient microbial community capable of higher decolorization rates. Sihang *et al.* (2013) in his study found that the addition of vitamin B_2 enriched specific microbial communities that were more effective at decolorizing textile dyes.

The results on the effects of vitamin B_{12} on dye decolorization by various bacterial isolates is presented in (Figure 14). This paper identified 0.5 mg/L as an optimal concentration for maximizing the decolorization efficiency of azo dyes without causing inhibitory effects. vitamin B_{12} likely enhances decolorization by acting as a cofactor in metabolic pathways critical for dye breakdown. vitamin B_{12} can enhance the decolorization process, however, its concentration must be optimized to avoid potential inhibitory effects.

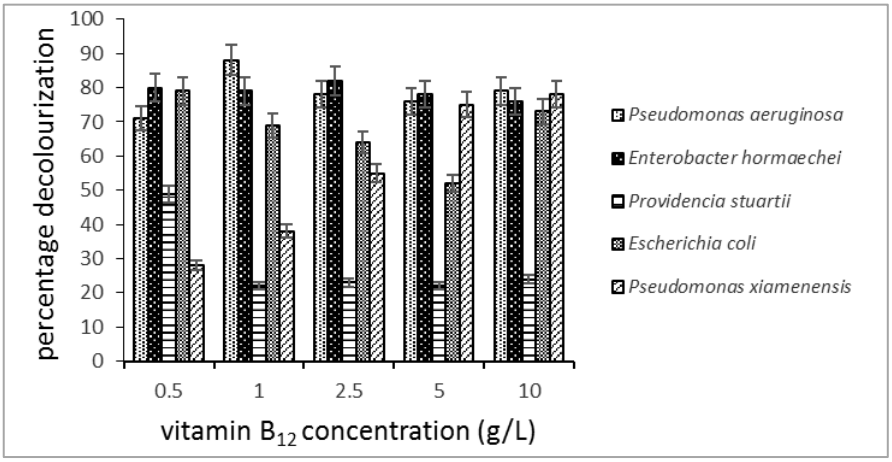

Figure 14. Effect of various vitamin B_{12} concentrations on the decolorization extent of Sudan orange G

Interactive effects of multiple variables on the percentage decolorization and microbial growth were investigated using 3-D surface plots (Figure 15), generated by varying two independent variables while holding others at their central levels. This approach, employing response surface methodology, allows visualization of the combined effects of the tested parameters. RSM typically involves statistically designed experiments to assess the influence of multiple factors and their interactions (Table 4). The data are then used to create response surfaces, which depict the relationship between the factors and the measured response (in this case, decolorization and microbial growth). This

allows for optimization of the process by identifying the factor combinations that yield the best results. RSM analysis identified the following ranges as having the greatest impact on both decolorization and microbial growth: pH 6.5-7, temperature 30-35°C, glucose 0.75-1 g/L, and salinity 4.5-5 g/L.

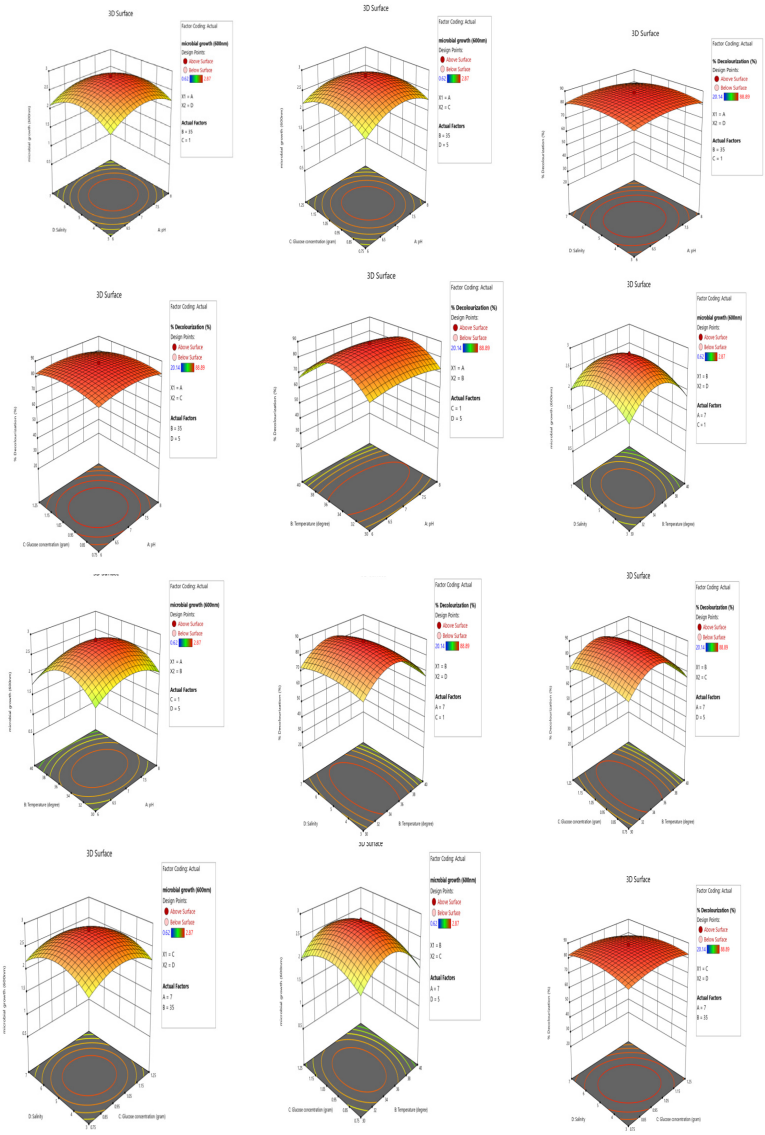

Figure 15. 3-D surface plot for the optimization of Sudan orange G decolorization by isolates in consortium of various parameters

Table 4. Composition of various experiments of the CCD for independent variables and responses (actual and predicted) by isolates in Consortium in Sudan orange G

Run	A; pH	B: Temp (t)	C: Glucose Conc. (g)	D: Salinity (g)	% Decolorization		Microbial Growth (600 nm)	
					Actual	Predicted	Actual	Predicted
1	5	35	1	5	73.45	76.58	1.52	1.50
2	6	30	0.75	3	66.81	64.97	1.38	1.37
3	8	40	1.25	7	53.07	52.88	0.96	0.99
4	8	30	0.75	7	68.98	67.33	1.48	1.51
5	8	40	0.75	7	58.45	59.15	0.98	1.20
6	8	30	0.75	3	65.14	66.01	1.38	1.50
7	8	30	1.25	7	63.89	62.02	1.32	1.32
8	7	35	1	1	75.78	75.16	1.68	1.54
9	6	30	1.25	7	66.82	65.07	1.42	1.42
10	7	35	1	9	67.88	71.26	1.44	1.36
11	8	40	1.25	3	58.78	59.37	0.97	1.22
12	7	35	1.5	5	70.75	72.78	1.58	1.56
13	6	40	0.75	7	62.14	60.30	0.99	1.22
14	6	30	1.25	3	69.84	68.41	1.49	1.46
15	7	45	1	5	20.14	19.69	0.62	0.30
16	7	35	1	5	87.81	88.25	2.78	2.82
17	9	35	1	5	74.01	73.64	1.78	1.58
18	7	35	1	5	88.04	88.25	2.81	2.82
19	7	25	1	5	31.01	34.22	0.72	0.83
20	6	30	0.75	7	68.89	67.57	1.47	1.41
21	6	40	1.25	7	58.45	56.85	0.98	1.05
22	6	40	1.25	3	62.45	62.07	1.24	1.24
23	7	35	1	5	88.89	88.25	2.87	2.82
24	8	30	1.25	3	66.81	66.62	1.48	1.42
25	7	35	0.5	5	74.89	75.62	1.87	1.67
26	6	40	0.75	3	58.45	59.59	0.98	1.17
27	8	40	0.75	3	59.98	59.70	1.31	1.34

Data obtained on power generation (Figure 16) show that the microbial consortium in the microbial fuel cell (MFC) generated 127 mV and achieved 90% decolorization of Sudan orange G within 24 hours. Following this peak, the electric power generation gradually declined. This demonstrates the potential of MFCs to effectively degrade dyes while simultaneously generating electricity, offering a sustainable, dual-benefit bioremediation approach. Optimizing MFC operating conditions can further enhance both decolorization efficiency and power generation, making this technology promising for environmental management. The observed correlation between power generation and dye decolorization suggests a direct link between microbial activity and electron release. As the bacteria degrade the dye, they release electrons, which contribute

to the increased power output. Microbial redox reactions release electrons, which are transferred to the MFC anode, generating a current. Efficient dye decolorization fuels electron release and thus power generation. However, as the dye substrate is depleted, electron release and power generation may decline. This dynamic interplay between power generation and dye decolorization in MFCs has been observed and studied by others, as highlighted by Li *et al*. (2021).

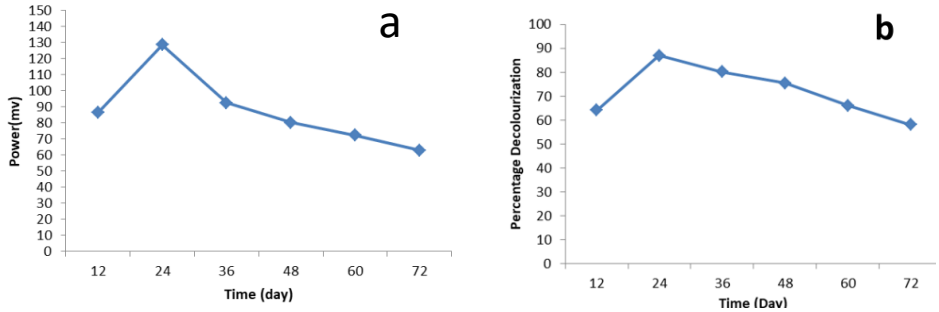

Figure 16. Changes in average daily power (**a**) generated with time and decolourization (**b**) of Sudan orange G by bacterial consortium coupled to MFC during bioremediation study

The GC-MS chromatograms (Figures 17-19) provide strong evidence of the azo dye's transformation after optimization and MFC treatment. The emergence of various degradation metabolites demonstrates the comprehensive breakdown of the dye into simpler compounds. Specifically, the identified metabolites post-MFC treatment were undecanoic acid, 10-methyl-, methyl ester, cyclopentane, and cyclopropylidene-2(1H)-naphthalenone. Undecanoic acid, 10-methyl-, methyl ester, a branched fatty acid ester, suggests bacterial utilization of dye components as carbon/energy sources. Cyclopentane, a simple alkane, indicates the breakdown of aromatic structures into smaller aliphatic components. Cyclopropylidene-2(1H)-naphthalenone, a cyclic ketone with a modified naphthalene ring, likely represents a degradation intermediate, suggesting further transformation is ongoing. These metabolites demonstrate the consortium's ability to degrade the dye into less complex, potentially less toxic compounds. This clearly illustrates the bacterial consortium's ability to not only decolorize but also effectively degrade the azo dye into potentially less harmful substances. This transformation highlights the efficacy of MFC technology for treating environmental contaminants and advancing sustainable wastewater treatment.

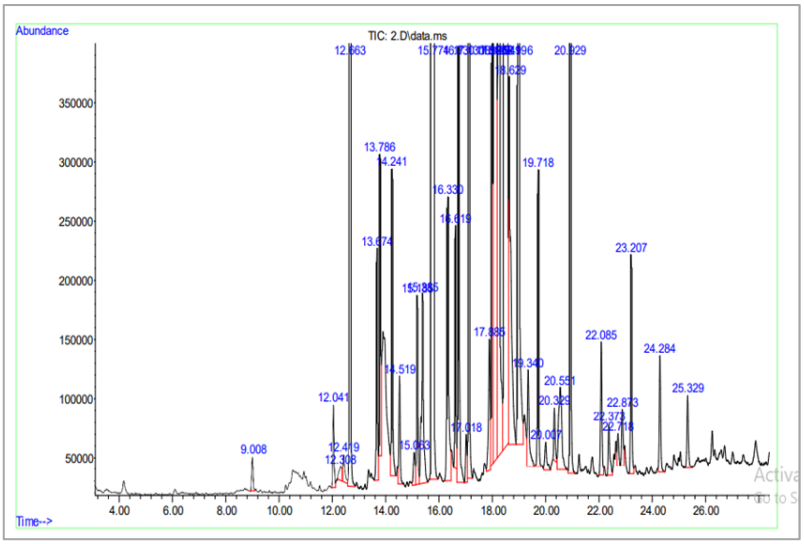

Figure 17. GC-MS chromatogram of the synthetic dye wastewater containing Sudan orange G before decolorization by bacterial consortium**.**

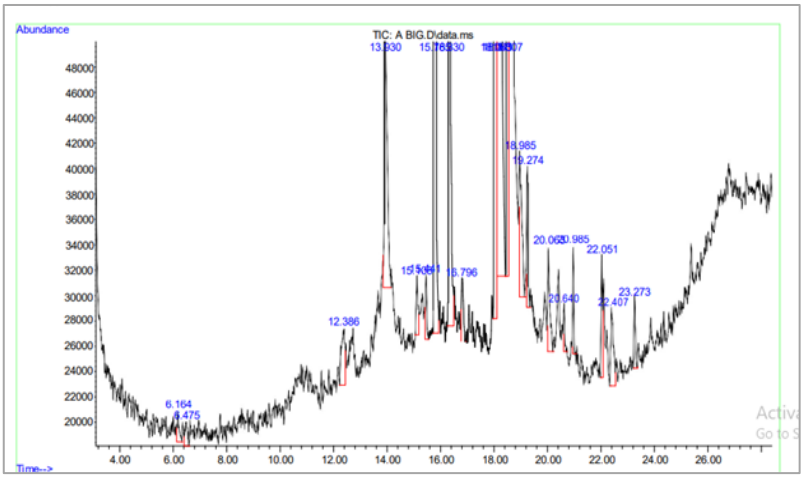

Figure 18. GC-MS chromatogram of decolorized Sudan orange G indicating degradation fractions after optimization of dye decolorization by bacterial consortium using RSM.

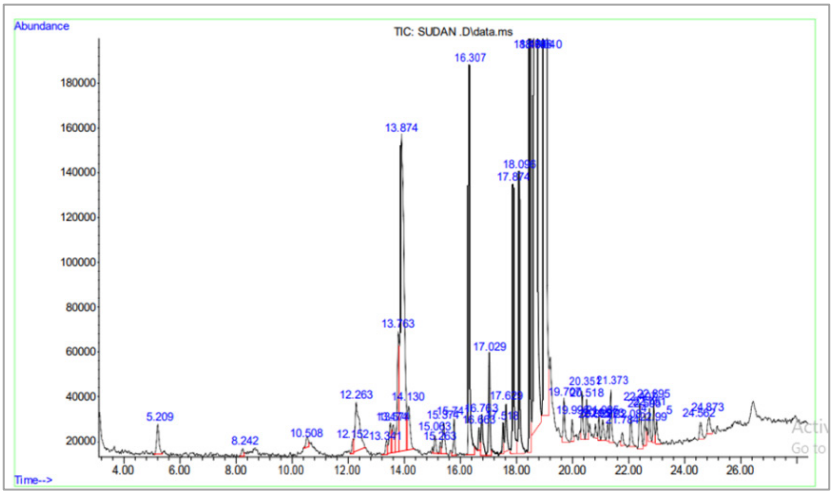

Figure 19. GC-MS chromatogram of decolorized Sudan orange G indicating degradation fractions after dye decolorization by bacterial consortium in the MFC.

Conclusion

The comprehensive dataset derived from this study substantiates the efficacy of *Pseudomonas aeruginosa* (MW584979), *Enterobacter hormaechei* (MW584986), *Providencia stuartii* (MW584987), *Escherichia coli* (MZ394117), and *Pseudomonas xiamenensis* (MW585052) in the degradation of azo dyes, particularly Sudan orange G. Notably, *Pseudomonas aeruginosa* (MW584979) and *Providencia stuartii* (MW584987) were found to harbor the azoreductase gene, further corroborating their ability to catalyze dye degradation processes. The utilization of a consortium approach, facilitated by response surface methodology, emerged as an effective strategy for optimizing culture conditions, as initially obtained through the One Factor at a Time (OFAT) method. This methodological synergy allowed for the maximization of dye decolorization, with experimental and predicted values demonstrating the practical utility of RSM. Remarkably, the manipulation of process variables resulted in a substantial enhancement of dye decolorization, reaching up to 88% within 24 hours. Furthermore, when integrated into a microbial fuel cell setup, this approach yielded a remarkable 92% decolorization efficiency alongside a notable power output of 130 mV. The metabolites produced during this process were further analyzed through GC-MS chromatography, revealing not only dye decolorization but also significant degradation, thereby underscoring the multifaceted remediation capabilities of

the microbial culture under investigation. Enhancing Sudan G decolorization and electricity generation in a dual-chambered MFC not only addresses the environmental issue of dye pollution but also contributes to sustainable energy production. Optimizing microbial activity, electrode materials, and operating conditions integrates environmental remediation with renewable energy generation, paving the way for practical applications of MFCs in wastewater treatment and energy production.

Conflict of Interest

The authors declare that they have no known competing financial interests or personal relationships that could have appeared to influence the work reported in this manuscript.

Authors' Contributions

Conceptualization and methodology were led by Prof. C.J. Ogugbue. Investigation and data curation were conducted by Mr. C.J. Echejiuba and Dr. I.S. Obuekwe. Supervision was provided by Prof. C.J. Ogugbue**.** Funding acquisition was secured by Mr. C.J Echejiuba. All authors have read and approved the final version of the manuscript for publication.

References

Al-Ansari, M.M., Li, Z., Masood, A. & Rajaselvam, J. (2022). Decolourization of azo dye using a batch bioreactor by an indigenous bacterium *Enterobacter aerogenes* ES014 from the waste water dye effluent and toxicity analysis. *Environ Res, 205*, 112189. https://doi.org/10.1016/j.envres.2021.112189

Al-Tohamy, R., Ali S. S., Xie, R., Schager, M., Khalil, M. A. & Sun, J. (2023). Decolorization of reactive azo dye using novel halotolerant yeast consortium HYC and proposed degradation pathway. *Ecotoxicol Environ Safe, 263,* 115258. https://doi.org/10.1016/j.ecoenv.2023.115258

Cao, J., Sanganyado, E., Liu, W., Zhang, W. & Liu, Y. (2019). Decolorization and detoxification of Direct Blue 2B by indigenous bacterial consortium. *J Environ Manage, 242,* 229-237. https://doi.org/10.1016/j.jenvman.2019.04.067

Chen, G., An, X., Li, H., Lai, F., Yuan, E., Xia, X. & Zhang, Q. (2021). Detoxification of azo dye Direct Black G by thermophilic *Anoxybacillus* sp. PDR2 and its application potential in bioremediation. *Ecotoxicol Environ Safe, 214,* 112084. https://doi.org/10.1016/j.ecoenv.2021.112084

Chen, K., Wua, J., Liou, D. H. & Sz-Chwun, J. (2003). Decolorization of the textile dyes by newly isolated bacterial strains. *J Biotechnol, 101*, 57–68. https://doi.org/10.1016/s0168-1656(02)00303-6

Dafale, N., Wate, S., Meshram, S. & Nandy, T. (2008). Kinetic study approach of 117emazol black-B use for the development of two-stage anoxic–oxic reactor for decolorization/ biodegradation of azo dyes by activated bacterial consortium. *J Hazard Mater*, *159*(2-3), 319–328. https://doi.org/10.1016/j.jhazmat.2008.02.058

Das, A. & Mishra, S. (2017). Removal of textile dye reactive green-19 using bacterial consortium: Process optimization using response surface methodology and kinetics study. *J Environ Chem Eng*, *5*(1), 612-627. https://doi.org/10.1016/j.jece.2016.10.005

Eslami, M., Amoozegar, M. A. & Asad, S. (2016). Isolation, cloning and characterization of an azoreductase from the halophilic bacterium *Halomonas elongata*. *Int. J. Biol. Macromol.*, *85*, 111–116.

Etezad, S. M., & Sadeghi-Kiakhani, M. (2021). Decolorization of malachite green dye solution by bacterial biodegradation. *Prog. Color Colorants Coat.*, *14*(2), 79-87.

Fahad, A. A., Abdulaziz, A.A., Hamdah, S.A., Amjad, A.A. & Naushad, A., (2020). Photocatalytic blue and rose bengal by using urea derived g-C_3N_4/ZnO nanocomposites. *Innov Catalytic Photocatalytic Systems Environ Remediation*, *10* (12), 1457. https://doi.org/10.3390/catal10121457

Felsenstein, J. (1985). Phylogenies and the comparative method. *Am. Nat, 125*(1),1–15. https://doi.org/10.1111/j.1558-5646.1985.tb00420.x

Firoozeh, F., Shahamat, Y. D., Rodríguez-Couto, S., Kouhsari, E. & Farhad, N. F. (2022). Bioremediation for the decolorization of textile dyes by bacterial strains isolated from dyeing wastewater. *Jordan J Biol Sci, 15*(2), 219-225. https://doi.org/10.54319/jjbs/150209

Georgiou, D., Metallinou, C., Aivasidis, A., Voudrias, E. & Gimouhopoulos, K. (2004). Decolorization of azo-reactive dyes and cotton-textile wastewater using anaerobic digestion and acetate-consuming bacteria. *Biochem Eng J*, *19*(1), 75–79. https://doi.org/10.1016/j.bej.2003.11.003

Gul, H., Raza, W., Lee, J., Azam, M., Ashraf, M. & Kim, K. (2021). Progress in microbial fuel cell technology for wastewater treatment and energy harvesting. *Chemosphere, 281*, 130828. https://doi.org/10.1016/j.chemosphere.2021.130828

Hague, M.M., Hague, M.K., Mosharaf, M.K., Rahman, A.,Islam, M.S., Nahar, K. & Molla, A.H. (2023). Enhanced biofilm-mediated degradation of carcinogenic and mutagenic azo dye by novel bacteria isolated from tannery wastewater. *J Environ Chem Eng, 11*(42), 110731. https://doi.org/10.1016/j.jece.2023.110731

Hu, L, Liu, N., Li, C., Mao, J., Li, M., Yun, Y. & Liu, W. (2023). Performance and response of coupled microbial fuel cells for enhanced anaerobic treatment of azo dye wastewater with simultaneous recovery of electrical energy. *Environ Sci Pollut Res Int, 30*(38), 89495-89509. https://doi.org/10.1007/s11356-023-28582-x

Ikram, M., Naeem, M., Zahoor, M., Hanafiah, M. M., Oyekanmi, A. A., Islam, N. U. & Sadiq, A. (2022). *Bacillus subtilis*: As an efficient bacterial strain for the reclamation of water loaded with textile azo dye, orange II. *Int J Mol Sci*, *23*(18), 10637.

Jukes, T.H. & Cantor, C.R. (1969). Evolution of protein molecules: Mammalian protein metabolism. *Academic Press, New York*, 21-132. http://dx.doi.org/10.1016/B978-1-4832-3211-9.50009-7

Kapdan, I.K., Kargi,F., McMullan, G. & Marchant, R. (2000). Decolorization of textile dyestuffs by a mixed bacterial consortium. *Biotechnol Lett, 22*, 1191181. http://dx.doi.org/10.1023/A:1005641430613

Keziban, A., Nuray, G., Soner, C. & Mahmut, O. (2019). Efficiency of glucose oxidase immobilized on tannin modified $NiFe_2O_4$ nanoparticles on decolorization of dye in the fenton and photo-biocatalyic processes. *J Photochem Photobiol*, *382,* 111935. https://doi.org/10.1016/j.jphotochem.2019.111935

Kumaravel, R. & Shanmugam, V. K. (2024). Biomimetic and ecological perspective towards decolorization of industrial important Azo dyes using bacterial cultures–A review. *Sustainable Chemistry for the Environment*, p. 100130. https://doi.org/10.1016/j.scenv.2024.100130

Ilamathi, R. & Jayapriya, J. (2017). Microbial fuel cells for dye decolorization. *Environ Chem Lett, 16,* 239-250 https://doi.org/10.1007/s10311-017-0669-4

Li, T., Song, H. L., Xu, H., Yang, X. L. & Chen, Q. L. (2021). Biological detoxification and decolorization enhancement of azo dye by introducing natural electron mediators in MFCs. *J Hazard Mater*, *416,* 125864. https://doi.org/10.1016/j.jhazmat.2021.125864

Liu, W., Liu, L., Liu, C., Hao, Y., Yang, H., Yuan, B. & Jiang, J. (2016). Methylene blue enhances the anaerobic decolorization and detoxication of azo dye by *Shewanella onediensis* MR-1. *Biochem Eng J*, *110*, 115–124. https://doi.org/10.1016/j.bej.2016.02.012

Liu, Y., Huang, L., Guo, W., Jia, L., Fu, Y., Gui, S. & Lu, F. (2017). Cloning, expression, and characterization of a thermostable and pH-stable laccase from *Klebsiella pneumoniae* and its application to dye decolorization. *Process Biochem*, *53,* 125–134. https://doi.org/10.1016/j.procbio.2016.11.015

Madhushika, H. G., Ariyadasa, T. U. & Gunawardena, S. H. P. (2021). Biodegradation of reactive yellow EXF dye: optimization of physiochemical parameters and analysis of degradation products. *Int J Environ Sci Technol*, 1-12.

Matteo, D., Anna, E. T., Barbara, L., Pierangela, C., Maddalena, P., Elham, J., Giuseppina, B. & Andrea, F. (2018). Bioelectrochemical BTEX removal at different voltages: assessment of the degradation and characterization of the microbial communities. *J Hazard Mater, 341*, 120-127. https://doi.org/10.1016/j.jhazmat.2017.07.054

Mendes, S., Pereira, L., Batista, C., & Martins, L. O. (2011). Molecular determinants of azo reduction activity in the strain *Pseudomonas putida* MET94. *Appl Microbiol Biotechnol*, *92*(2), 393–405.

Mittal, N. & Kumar, A. (2022). Microbial fuel cell as water-energy environment nexus: a relevant strategy for treating streamlined effluents. *Energy Nexus, 7*, 100097. https://doi.org/10.1016/j.nexus.2022.100097

Md Burhan Kabir Suhan, S.M. Tanveer Mahtab, Wafi Aziz, Sonia Akter, & Md Shahinoor Islam (2021). Sudan black B dye degradation in aqueous solution by fenton oxidation process: kinetics and cost analysis. *Case Stud Chem Environ Eng, 4,* 100126. https://doi.org/10.1016/j.cscee.2021.10012

Mugerfeld, I., Law, B. A., Wickham, G. S. & Thompson, D. K. (2009). A putative azoreductase gene is involved in the *Shewanella oneidensis* response to heavy metal stress. *Appl Microbiol Biotechnol*, *82*(6), 1131–1141.

Ngo, A. C. R. & Tischler, D. (2022). Microbial degradation of azo dyes: approaches and prospects for a hazard-free conversion by microorganisms. *J Environ Sci Pub Health*, *19*, 4740. https://doi.org/10.3390/ijerph19084740

NIST (2008). Glucose in Frozen Human Serum. National Institute of Standards & Technology Certificate of Analysis, In: Linstrom PJ, Mallard WG (eds). NIST Chemistry WebBook. NIST Standard Reference Database Number 965a. Gaithersburg, MD 20899 *National Institute of Standards and Technology*, 2011, 20899, http://webbook.nist.gov (retrieved April 27, 2011)

Nk, S. & Rahman, R. (2020). Microbial fuel cell an alternative for treatment of textile wastewater. *Int Res J Eng Technol*, *7*(4), 3962-3967.

OECD (2017), OECD Due Diligence Guidance for Responsible Supply Chains in the Garment and Footwear Sector, OECD Publishing, Paris. https://doi.org/10.1787/9789264290587-en

Qi, J., Paul, C. E., Hollmann, F. & Tischler, D. (2017). Changing the electron donor improves azoreductase dye degrading activity at neutral pH. *Enzyme Microb Technol*, *100*, 17–19.

Qi, J., Schlömann, M. & Tischler, D. (2016). Biochemical characterization of an azoreductase from *Rhodococcus opacus* 1CP possessing methyl red degradation ability. *Journal of Molecular Catalysis B: Enzymatic*, *130*, 9–17.

Rafaqat, S., Ali, N. Torres, C., C. & Rittmann, B. (2022). Recent progress in treatment of dyes wastewater using microbial-electro-Fenton technology. *RSC Advances*, *12,* 17104-17137. https://doi.org/10.1039/D2RA01831D

Sarkar, S., Echeverría-Vega, A., Banerjee, A. & Bandopadhyay, R. (2021). decolorisation and biodegradation of textile di-azo dye Congo red by chryseobacterium geocarposphaerae DD3. *Sustainability*, *13*(19), 10850.

Sihang, S, Pengfei, F. Yi, X. & Geng, Q. (2013). Experimental research of decoloring treatment on vitamin B_{12} wasterwater. *Appl Mech Mater, 295*-298:1209-1214 http://dx.doi.org/10.4028/www.scientific. net/AMM.295-298.1209

Sikder, S. & Rahman, M. M. (2023). Efficiency of microbial fuel cell in wastewater (municipal, textile and tannery) treatment and bioelectricity production. *Case Stud Chem Environ Eng, 8,* 100421. https://doi.org/10.1016/j.cscee.2023.100421

Saitou, N. & Nei, M. (1987). The neighbor-joining method: a new method for reconstructing phylogenetic trees. *Mol Biol Evol, 4*(4), 406-25. https://doi.org/ 10.1093/oxfordjournals.molbev.a040454. PMID: 3447015.

Taha, M., Adetutu, E.M., Shahsavari, E., Smith, A.t. & Ball, A.S., (2014). Azo and anthraquinone dye mixture decolorization at elevated temperature and concentration by a newly isolated thermophilic fungus, *Thermomucor indicae-seudaticae*. *J Environ Chem Eng, 2*(1), 415-423. https://doi.org/10.1016/j.jece.2014.01.015

Tahir, U., Nawaz, S., Hassan Khan, U. & Yasmin, A. (2021). Assessment of biodecolorization potentials of biofilm forming bacteria from two different genera for mordant black 11 dye. *Bioremediation Journal*, *25*(3), 252-270.

Tian, F., Wang, Y., Guo, G., Ding, K., Yang, F., Wang, H. & Liu, C. (2021). Enhanced azo dye biodegradation at high salinity by a halophilic bacterial consortium. *Bioresource Technol*., *326*, 124749. https://doi.org10.1016/j.biortech.2021.124749

Trivedi, A., Desireddy, S. & Chacko, S.P. (2022). Effect of pH, salinity, dye, and biomass concentration on decolorization of azo dye methyl orange in denitrifying conditions. *Water, 14,* 3747. https://doi.org/10.3390/w14223747

Umar, A., Abid, I., Antar, M., Dufossé, L., Hajji-Hedf, L., Elshikh, M. S., Abeer El Shahawy, A. & Abdel-Azeem, A. M. (2023). Electricity generation and oxidoreductase potential during dye discoloration by laccase-producing *Ganoderma gibbosum* in fungal fuel cell. *Microb cell fact, 22*, 258. https://doi.org/10.1186/s12934-023-02258-0

Uppala, R., Sundar, K. & Muthukumaran, A. (2015). Response surface methodology mediated optimization of decolorization of azo dye amido black 10B by *Kocuria kristinae* RC3. *Inter J Environ Sci Technol*, 2018, 1–12. https://doi.org/10.1007/s13762-018-1888-3

Zhang, Q., Xie, X., Xu, D., Hong, R., Wu, J., Zeng, X. & Liu, J. (2021). Accelerated azo dye biodegradation and detoxification by *Pseudomonas aeruginosa* DDMZ1-2 via fructose co-metabolism. *Environ Technol Innov*, *24*, 101878.

STUDIA UNIVERSITATIS BABEŞ-BOLYAI BIOLOGIA, 70, 1, 2025 (p. 121-132)
doi:10.24193/subbbiol.2025.1.06

Molecular detection of enterotoxin genes (*sea* and *sec*) in *Staphylococcus aureus* isolated from dairy products in Karaj, Alborz, Iran

Roudabeh Sadraei[1], Naser Harzandi[1]✉, Bahman Tabaraei[2]

[1]Department of Microbiology, Karaj Branch, Islamic Azad University, Karaj, Iran; [2] Bacterial Vaccines and Antigens Production Department, Pasteur Institute of Iran, Tehran, Iran;
✉***Corresponding author, E-mail:*** *Nasharzan@gmail.com*

Article history: Received 25 August 2024; Revised 25 October 2024; Accepted 17 January 2025; Available online 25 June 2025

Abstract. *Staphylococcus aureus,* a significant bacterial agent of food poisoning, particularly the strains producing enterotoxins, is a topic of paramount importance. The prevalence of these enterotoxins in the dairy industry, especially in regions like Karaj city, Alborz province, Iran, with its numerous industrial and traditional dairy companies, is a matter of great concern for public health. This study aims to evaluate the frequency of *sea* and *sec* genes among dairy products in Karaj, Iran. We collected 100 samples of industrial and traditional dairy products, including 25 samples of pasteurized milk, 25 samples of pasteurized ice cream, 25 samples of raw milk, and 25 samples of traditionally made ice cream, throughout Karaj, then transferred them into the laboratory, then cultured on the media containing mannitol salt agar and Brad Parker agar. Second, enzymatic tests, such as catalase and coagulase tests and biochemical and bacterial assessments, including mannitol fermentation and Gram staining methods, were employed to detect *S. aureus* contamination. Besides, the presence of *sea* and *sec* genes was assessed by PCR. Finally, the data were statistically analyzed using SPSS software. The results demonstrated that enzymatic and biochemical methods could detect 54 contaminated samples by *S. aureus* among 100 samples. However, as a reliable molecular technique, PCR detected 57 *S. aureus*-contaminated samples among all the tested samples. Moreover, it is indicated that 12 and 6 PCR-positive samples contained enterotoxin A and C types, respectively.

In brief, the huge amounts of dairy products in Karaj are significantly contaminated by enterotoxin-producing strains of *S. aureus*, especially type A and C.

Keywords: dairy products, enterotoxin A, enterotoxin C, polymerase chain reaction, *Staphylococcus aureus*.

Introduction

Food-borne diseases are considered the most vital issue in public health because millions of people are annually exposed to infections that could lead to hospitalization or death in severe cases. *Staphylococcus aureus* has been known as the second or third microbial agent of infections (Vargová *et al*., 2023), including secondary bacterial pneumonia following respiratory viral infections, bovine mastitis, vein inflammation, meningitis, urinary tract infection (UTI), and local inflammation of the bone endocarditis, and superficial skin lesion (Fabijan *et al*., 2020). *S. aureus* can grow quickly in different conditions, such as mammalian skin surface and mucous membranes. Besides, it can be found in various foods such as dairy, meat, vegetables, salads, and even cooked and salted food (Grispoldi *et al*., 2021). *S. aureus* contains several virulent factors causing pathogenicity and the colonization of different media. Two important virulence factors include bacterial enterotoxins and toxic shock syndrome toxin (TSST), classified as pyrogenic toxin superantigens (PTSAgs), which can significantly influence the host (Hu *et al*., 2021). Superantigens can specifically interact with major histocompatibility complex (MHC) molecules class II, producing extensive lymphocyte T proliferation and damage caused by high-level released cytokines. On the other hand, all the toxin-encoding genes can horizontally be transferred by mobile genetic elements (MGEs) such as phages and pathogenicity islands (PAIs). This could be really dangerous for people at risk, including the geriatric population, offspring, pregnant women, and patients with diabetes or immunocompromised diseases such as acquired immunodeficiency syndrome (AIDS) (Abdurrahman *et al*., 2020).

Staphylococcal enterotoxins can resist high-temperature stress, and the resistance is higher in food than *in vitro* environment. Also, the toxins are biologically active even after heating the food, although pasteurization can remove *S. aureus*. They are also resistant to stomachic and intestinal proteases, so the toxins are still active after digestion (Forouzani-Moghaddam *et al*., 2024). Many factors, such as the number of bacterial cells, salinity (higher than 7.5%), pH, temperature, and competition with other bacteria to achieve more food

resources, influence enterotoxin production in food (Al-Nabulsi *et al*., 2020). It has been demonstrated that there is a close correlation between enterotoxin production in dairy and food poisoning. Actually, 10^5-10^8 cfu/g of *S. aureus* can cause food poisoning (Vargová *et al*., 2023). Many studies have indicated that 15-80% of *S. aureus*, isolated from dairy products such as milk, cheese, ice cream, or even other protein-contained products, can biosynthesize enterotoxins. The symptoms of food poisoning caused by staphylococcal enterotoxins include nausea, vomiting, rarely diarrhea, and muscle and abdominal pain. There are also many significant economic losses from food poisoning caused by enterotoxigenic strains of *S. aureus* (Fabijan *et al*., 2020). This study aimed to evaluate the frequency of *sea* and *sec* genes in *Staphylococcus aureus* isolated from dairy products in Karaj, Alborz, Iran.

Materials and methods

Sampling

In the study, 100 samples of traditional and industrial dairy products, including 25 samples of raw milk, 25 samples of traditionally made ice cream, 25 samples of pasteurized milk, and 25 samples of pasteurized ice cream, were collected throughout Karaj. They were then transferred into the laboratory within sterilized tubes and incubated on mannitol salt agar and Brad Parker agar media at 37 °C for 48 hours. The phenotypic characteristics of the grown colonies were visually assessed.

Microbiological analyses

Biochemical analyses including Gram staining (Beveridge, 2001), fermentation of the mannitol (Lally *et al*., 1985), and culturing on Brad Parker (BP) medium (Parkor and Hewiit, 1970), as well as enzymatic assessment including catalase (Reiner, 2010) and coagulase tests (Sperber and Tatini, 1975), were used to detect *Staphylococcus spp*. and *S. aureus*, respectively. *S. aureus* can reduce potassium tellurite to metallic tellurium on the BP medium to form black colonies (Parkor and Hewiit, 1970).

Polymerase chain reaction

The bacterial DNA was extracted by DNG superscript –Plus kit (CinnaGen Co., Tehran, Iran). Specific primers were designed by Oligo v.7 software and then synthesized for *sea* and *sec* genes and *nuc* gene encoding deoxyribonuclease as an index to detect *S. aureus* (Tab. 1). *S. aureus* colonies were detected by PCR

using specific primers for the *nuc* gene. The positive samples with *S. aureus* were molecularly analyzed by PCR and the specific primers for *sea* and *sec* genes were used. Reference strains (Iranian Biological Resource Center, Tehran, Iran) were used as a positive control in PCR (Tab. 2). Gel electrophoresis (agarose 1.5%) was used to track the amplified DNA fragments.

Statistical analysis

Chi-square and t-tests were employed to statistically analyze the data, derived from PCR and the results from biochemical and enzymatic assessments by SPSS software (version 26.0.0.1).

Table 1. The primers used in the study

Gene	Sequence (5'-- 3')	Primer size (nt)	Product Size (bp)
nuc	F- GCG ATT GAT GGT GAT ACG GTT	21	279
	R- AGC CAA GCC TTG ACG AAC TAA AGC	24	
sea	F- GCA GGG AAC AGC TTT AGG C	19	520
	R- GTT CTG TAG AAG TAT GAA ACA CG	23	
sec	F- CTT GTA TGT ATG GAG GAA TAA CAA	24	283
	R- TGC AGG CAT CAT ATC ATA CCA	21	

Table 2. PCR programs used for amplification

Genes		*nuc*		*sea*		*sec*	
Steps		Temp. (˚C)	Time	Temp. (°C)	Time	Temp. (˚C)	Time
Initial denaturation		95	5 min	95	5 min	95	5 min
37 cycles	Denaturation	95	40 s	95	30 s	95	40 s
	Annealing	55	1 min	58	45 s	58	45 s
	Extension	72	80 s	72	1 min	72	1 min
Final extension		72	10 min	72	7 min	72	10 min

Temp. = temperature.

Results

Biochemical analyses

The results of mannitol fermentation on mannitol salt agar media (Fig. 1) indicated that 60 samples could grow on the media and form some bacterial and yeast colonies. Besides, raw milk contains more bacteria (17 samples), which could cause mannitol fermentation. Although the lowest rate of mannitol fermentation was observed in pasteurized ice cream (4 samples), there was statistically no significant difference between traditional ice cream (6 samples), pasteurized milk (5 samples), and ice cream (Tab. 3).

Interestingly, the number of black colonies was the highest for samples derived from raw milk (17 samples) on the Brad Parker media. Only two samples of pasteurized milk and ice cream formed black colonies, while six samples of traditional ice cream formed black colonies (Tab. 3; Fig 2).

Figure 1. Fermentation of mannitol salt agar

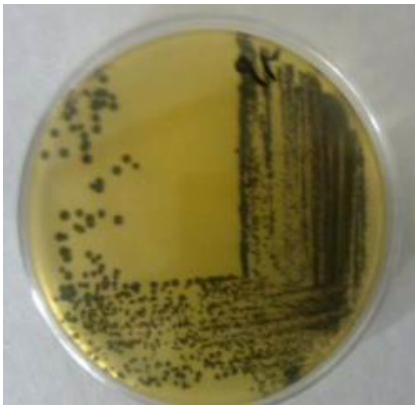

Figure 2. Black colonies formed by *S. aureus*

Table 3. The number of positive samples for each biochemical test

Test	Pasteurized milk	Pasteurized ice cream	Traditional ice cream	Raw milk
Mannitol salt agar	5	4	6	17
Brad Parker agar	2	2	6	17
Gram stain	5	2	8	17

It is also interesting that 17 raw milk samples contained Gram-positive bacteria that were expected to be *S. aureus* and 8, 5, and 2 samples for traditional ice cream, pasteurized milk, and ice cream, respectively (Tab. 1; Fig. 3).

Enzymatic analyses

Each colony grown on mannitol salt agar, suspected to contain *S. aureus*, was used for enzymatic analyses. As per the catalase test results, all 25 samples of raw milk and traditional ice cream were contaminated by *S. aureus*. There were also 23 and 24 *S. aureus*-infected samples for pasteurized milk and ice cream, respectively (Tab. 4).

For the coagulase test, 14 samples of the raw milk were coagulase-positive. In contrast, there was no coagulase-positive sample for pasteurized ice cream. Moreover, 2 coagulase-positive samples for pasteurized milk and 3 coagulase-positive samples for traditional ice cream were observed (Fig. 4; Tab. 4).

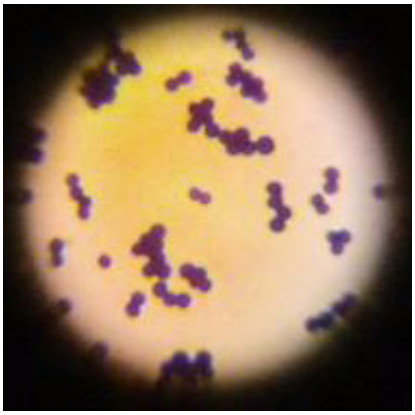

Figure 3. Grape-like clusters (cocci) arrangement of *S. aureus*

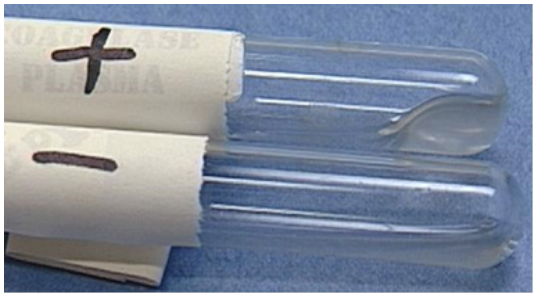

Figure 4. Positive and negative samples for the coagulase test

Table 4. The number of positive samples for each enzymatic test

Test	Pasteurized milk	Pasteurized ice cream	Traditional ice cream	Raw milk
Catalase	23	24	25	25
Coagulase	2	0	3	14

PCR

PCR by specific primer for the *nuc* gene detected 57 *S. aureus*-infected samples among all 100 samples. Also, using specific primers for *sea* and *sec* genes could repectively detect 11 and 6 many samples containing the genes encoding enterotoxins A and C on those 57 positive samples (Fig. 5). Details of the PCR test for each sample of the dairy products are in Tab. 5.

Table 5. The number of Positive-PCR samples for each gene

Gene	Pasteurized milk	Pasteurized ice cream	Traditional ice cream	Raw milk
nuc	17	7	14	19
sea	1	3	1	7
sec	0	2	1	3

Statistical analysis

The chi-square test of independence showed a significant difference between biochemical and enzymatic tests and PCR detection ($p<0.05$). The detection of *S. aureus* in samples by PCR containing specific primers for the nuc gene showed significant differences between pasteurized and traditional ice creams ($p<0.05$) but not between raw and pasteurized milk ($p>0.05$; Tab. 6).

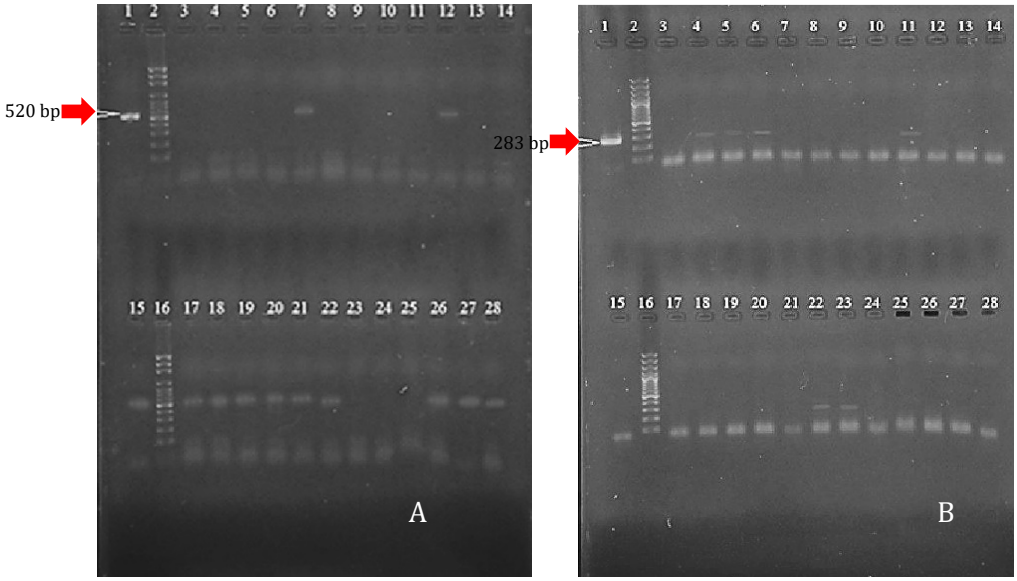

Figure 5. Gel electrophoresis of the PCR products, genes encoding: A) Enterotoxin A, 1: C+, 2 & 16: DNA molecular ladder, 3: C-, 4-8: Pasteurized milk, 9-14: Traditional ice cream, 15,17-22: Raw milk, 23-28: Pasteurized ice cream; B) Enterotoxin, 1:C+, 2 & 16: DNA molecular ladder, 3-7: Raw milk, 8-14: Traditional ice cream, 15: C-, 17-21: Pasteurized milk, 22-28: Pasteurized ice cream.

Table 6. Chi-Square Test for comparing biochemical and enzymatic tests and PCR

Statistical test	Value	df	P value	Exact Sig.	
				(2-sided)	(1-sided)
Pearson Chi-Square	11.636 a	1	.001		
Continuity Correction*	10.687	1	.001		
Likelihood Ratio	11.757	1	.001		
Fisher's Exact Test				.001	.001
Linear-by-Linear Association	11.578	1	.001		
N of Valid Cases	200				

a. 0 cells (0%) have an expected count of less than 5. The minimum expected count is 45.00. * Computed only for a 2x2 table

For detecting enterotoxin A using PCR containing specific primers for the *sea* gene, there is a significant difference among all samples derived from any studied dairy products ($p<0.05$). The difference is insignificant for the *sec* gene at the 5% level, while there is a difference between samples (Tab. 7).

Table 7. Chi-Square Test for PCR results

Bacteria	Statistical test	Value	Df	P value
Staphylococcus	Pearson Chi-Square	13.505 b	3	.004
	Likelihood Ratio	13.821	3	.003
	Linear-by-Linear Association	3.563	1	.059
	N of Valid Cases	100		
Enterotoxin A	Pearson Chi-Square	9.091 c	3	.028
	Likelihood Ratio	8.597	3	.035
	Linear-by-Linear Association	.300	1	.584
	N of Valid Cases	100		
Enterotoxin C	Pearson Chi-Square	3.546 d	3	.315
	Likelihood Ratio	4.712	3	.194
	Linear-by-Linear Association	.140	1	.708
	N of Valid Cases	100		
Total	Pearson Chi-Square	11.289 a	3	.010
	Likelihood Ratio	10.953	3	.012
	Linear-by-Linear Association	1.875	1	.171
	N of Valid Cases	300		

a. 0 cells (0.0%) have an expected count of less than 5. The minimum expected count is 18.75.
b. 0 cells (0.0%) have an expected count of less than 5. The minimum expected count is 10.75.
c. 4 cells (50.0%) have an expected count of less than 5. The minimum expected count is 3.00.
d. 4 cells (50.0%) have an expected count of less than 5. The minimum expected count is 1.50.

Discussion

S. aureus can be found as a resident bacteria on the skin and mucus of humans and animals, which are the initial resources of the bacteria. So, they can be transferred to the food during preparing, providing, packing, and storing food (Grispoldi *et al*., 2021). They can be found in a variety of foods, such as meat products, milk, and dairy products, fruit juice, as some proper media for the growth of the bacteria because they can grow independently in any conditions (Forouzani-Moghaddam *et al*., 2024). Notably, a lack of personal and environmental hygiene can facilitate food contamination by *S. aureus*, and consequently cause food poisoning (Vargová et al., 2023).

According to the universal standard, first-grade milk contains less than 100,000 microorganisms per ml. Also, the microbial load of milk should not be more than 750,000 microorganisms per ml (Tilocca *et al*., 2020; U.S. Department of Health and Human Services, Public Health Service and Food and Drug Administration, 2017). Although standard milk is retained in inappropriate conditions, *S. aureus* can quickly grow at the proper temperature and duration for bacterial growth and then infect the milk. Thus, the microbial load can be enhanced (El-Mokadem *et al*., 2020). If the milk is contaminated by *S. aureus*, pasteurization will be able to remove the bacteria; then, there is no bacterial risk to consumers' health. However, *S. aureus*, producing enterotoxin, could threaten consumers by causing food poisoning if the bacteria produced the toxins before pasteurization (Almutawif *et al*., 2019). Enterotoxins, particularly encoded by *sea* and *sec* genes, are the most crucial factors causing food poisoning (Forouzani-Moghaddam *et al*., 2024).

Staphylococcal enterotoxins can be detected by many important methods, including standard immunological techniques (Nouri *et al*., 2018). However, there are some disadvantages to using the methods, such as the long time needed to prepare the right conditions to produce toxins by the bacteria, cross-reactivity, and the probability of false results (Ali *et al*., 2020). On the other hand, the PCR test can detect enterotoxin-producing bacteria, even though the genes encoding the enterotoxins are not expressed. Thus, PCR could effectively detect *S. aureus*-producing enterotoxins A and C as the most crucial and common factors in food poisoning (Osman et al., 2020). Low concentrations of these types of enterotoxins can cause severe food poisoning. Thus, PCR is commonly used to detect enterotoxin-encoding genes. Many studies have used PCR to detect staphylococcal enterotoxins (Forouzani-Moghaddam *et al*., 2024). For example, Osman *et al*. utilized PCR to detect *S. aureus* and enterotoxins in buffalo milk (Osman *et al*., 2020).

Moreover, PCR detected the bacteria producing enterotoxins within milk and Coalho cheese in Brazil (Pereira *et al*., 2018). Wang *et al*. (2019) used PCR to detect *S. aureus* causing bovine mastitis and subsequent milk contamination. Finally, the molecular technique was employed to diagnose milk contamination by *S. aureus* and encode the gene for enterotoxin C in raw milk from several dairy farms in Java, Indonesia (Harijani *et al*., 2020).

In the present study, statistical analysis indicated that PCR is a significantly more precise technique than biochemical and enzymatic methods for diagnosing *S. aureus*-contaminated dairy products and detecting *S. aureus*-producing enterotoxins A and C.

Conclusions

According to the heat resistance of enterotoxins A and C, *S. aureus*-contaminated dairy products can be toxic and cause gastroenteritis in a short period even though they are heated. Therefore, Detecting genes encoding enterotoxins via PCR, a specific, sensitive, fast, and inexpensive molecular method, could be used instead of the conventional immunological assay techniques.

Acknowledgment: In memory of Dr. Bahman Tabaraei (RIP), Bacterial Vaccines and Antigens Production Department, Pasteur Institute of Iran, Tehran, Iran, advised the study.

References

Abdurrahman, G., Schmiedeke, F., Bachert, C., Bröker, B. M. & Holtfreter, S. (2020). Allergy—a new role for T cell superantigens of *Staphylococcus aureus*? *Toxins*, 12(3), 176. https://doi.org/10.3390/toxins12030176

Ali, A. A., Altemimi, A. B., Alhelfi, N. & Ibrahim, S. A. (2020). Application of biosensors for detection of pathogenic food bacteria: a review. *Biosens*., 10(6), 58. https://doi.org/10.3390/bios10060058

Almutawif, Y., Hartmann, B., Lloyd, M., Lai, C. T., Rea, A. & Geddes, D. (2019). *Staphylococcus aureus* enterotoxin production in raw and pasteurized milk: The effect of selected different storage durations and temperatures. Breastfeed. *Med*., 14(4), 256-261. https://doi.org/10.1089/bfm.2018.0227

Al-Nabulsi, A. A., Osaili, T. M., AbuNaser, R. A., Olaimat, A. N., Ayyash, M., Al-Holy, M. A. & Holley, R. A. (2020). Factors affecting the viability of *Staphylococcus aureus* and production of enterotoxin during processing and storage of white-brined cheese. *J. Dairy Sci*., 103(8), 6869-6881. https://doi.org/10.3168/jds.2020-18158

Beveridge, T. J (2001). Use of the Gram stain in microbiology. *Biotech. Histochem*., 76(3), 111-118. https://doi.org/10.1080/bih.76.3.111.118

El-Mokadem, E. A., El-Leboudy, A. A. & Amer, A. A. (2020). Occurrence of Enterobacteriaceae in Dairy Farm Milk. Alex. *J. Vet. Sci*., 64(2), 66-71. https://doi.org/10.5455/ajvs.254389

Fabijan, A. P., Lin, R. C., Ho, J., Maddocks, S., Ben Zakour, N. L. & Iredell, J. R. (2020). Safety of bacteriophage therapy in severe *Staphylococcus aureus* infection. *Nat. Microbiol*., 5(3), 465-472. https://doi.org/10.1038/s41564-019-0634-z

Forouzani-Moghaddam, M. J., Habibi, S., Hosseini-Safa, A., Khanaliha, K., Mokarinejad, R., Akhoundzadeh, F. & Oshaghi, M. (2024). Rapid detection of major enterotoxin genes and antibiotic resistance of *Staphylococcus aureus* isolated from raw milk in the Yazd province, Iran. *Vet. Med. Sci*., 10(3), e1407. https://doi.org/10.1002/vms3.1407

Grispoldi, L., Karama, M., Armani, A., Hadjicharalambous, C. & Cenci-Goga, B. T. (2021). *Staphylococcus aureus* enterotoxin in food of animal origin and staphylococcal food poisoning risk assessment from farm to table. *Ital. J. Anim. Sci*., 20(1), 677-690. https://doi.org/10.1080/1828051X.2020.1871428

Harijani, N., Wandari, A., Effendi, M. H. & Tyasningsih, W. (2020). Molecular Detection of Encoding Enterotoxin C Gene and Profile of Antibiotic Resistance on *Staphylococcus Aureus* Isolated from Several Dairy Farms in East Java, Indonesia. *Biochem. Cell. Arch*., 20(1), 3081-3085. http://repository.unair.ac.id/id/eprint/101305

Hu, D. L., Li, S., Fang, R. & Ono, H. K. (2021). Update on molecular diversity and multipathogenicity of staphylococcal superantigen toxins. *Anim. Dis.*, 1(1), 7. https://doi.org/10.1186/s44149-021-00007-7

Lally, R. T., Ederer, M. N. & Woolfrey, B. F. (1985). Evaluation of mannitol salt agar with oxacillin as a screening medium for methicillin-resistant *Staphylococcus aureus*. *J. Clin. Microbiol*., 22(4), 501-504. https://doi.org/10.1128/jcm.22.4.501-504.1985

Nouri, A., Ahari, H. & Shahbazzadeh, D. (2018). Designing a direct ELISA kit for the detection of *Staphylococcus aureus* enterotoxin A in raw milk samples. *Int. J. Biol. Macromol*., 107, 1732-1737. https://doi.org/10.1016/j.ijbiomac.2017.10.052

Osman, K. M., Pires, Á. D. S., Franco, O. L., Orabi, A., Hanafy, M. H., Marzouk, E. & Elbehiry, A. (2020). Enterotoxigenicity and antibiotic resistance of coagulase-negative staphylococci isolated from raw buffalo and cow milk. *Microb. Drug. Resist*., 26(5), 520-530. https://doi.org/10.1016/j.yclnex.2017.05.001

Parker, M. T. & Hewitt, J. H. (1970). Methicillin resistance in *Staphylococcus aureus*. *The Lancet*, 295(7651), 800-804. https://doi.org/10.1016/S0140-6736(70)92408-6

Pereira, C. T. M., de Oliveira, D. S. V., Veloso, V. S., Silva, S. D. S. P., Santos, L. S., Lima, A. F. & dos Santos Soares, M. J. (2018). Microbiology quality, detection of enterotoxin genes and antimicrobial resistance of *Staphylococcus aureus* isolated from milk and Coalho cheese. *Semin. Ciênc. Agrár*., 39(5), 1957-1967. https://doi.org/10.5433/1679-0359.2018v39n5p1957

Reiner, K. (2010), Catalase test protocol. American Society for Microbiology. https://asm.org/getattachment/72a871fc-ba92-4128-a194-6f1bab5c3ab7/Catalase

Sperber, W. Z. & Tatini, S. R. (1975). Interpretation of the tube coagulase test for identification of *Staphylococcus aureus*. *Appl. Microbiol*., 29(4), 502-505. https://doi.org/10.1128/am.29.4.502-505.1975

Tilocca, B., Costanzo, N., Morittu, V. M., Spina, A. A., Soggiu, A., Britti, D. & Piras, C. (2020). Milk microbiota: Characterization methods and role in cheese production. *J. Proteom*., 210, 103534. https://doi.org/10.1016/j.jprot.2019.103534

U.S. Dept. of Health and Human Services, Public Health Service and Food and Drug Admin. Grade "A" Pasteurized Milk Ordinance. 2017 Revision. https://www.fda.gov/media/114169/download

Vargová, M., Zigo, F., Výrostková, J., Farkašová, Z. & Rehan, I. F. (2023). The biofilm-producing ability of *Staphylococcus aureus* is obtained from the surfaces and milk of mastitic cows. *Vet. Sci.,* 10(6), 386. https://doi.org/10.3390/vetsci10060386

Wang, H., Hecht, S., Kline, D. & Leber, A. L. (2019). *Staphylococcus aureus* and methicillin resistance detection directly from pediatric samples using PCR assays with differential cycle threshold values for corroboration of methicillin resistance. *J. Microbiolog. Meth*., 159, 167-173. https://doi.org/10.1016/j.mimet.2019.01.009

STUDIA UNIVERSITATIS BABEŞ-BOLYAI BIOLOGIA, 70, 1, 2025 (p. 133-152)
doi:10.24193/subbbiol.2025.1.07

The control of *Cydia pomonella* (L.) (Lepidoptera, Tortricidae) population using sugars under semi-arid climate (Batna, Algeria)

Siham Zaaboubi[1], Imene Brahim[2]✉, Iness Brahim[3], Salah Neghmouche Nacer[4] and Younes Moussaoui[5,6]

[1]LAPAPEZA laboratory, Department of Agricultural Sciences, Institute of Veterinary and Agricultural Sciences, Batna 1 University, Batna, Algeria; [2]LAPAPEZA laboratory, Department of Agricultural Sciences, Institute of Veterinary and Agricultural Sciences, Batna 1 University, Batna, Algeria; [3]Barika Subdivision of Agriculture, Directorate of Agricultural Services, Batna, Algeria; [4]El Oued University, Faculty of Exact Sciences, Chemistry Department, P.O. Box 789, ElOued 39000, Algeria; [5]University of Sfax, Faculty of Sciences of Sfax, Organic Chemistry Laboratory (LR17ES08), Sfax 3029, Tunisia; [6]University of Gafsa, Faculty of Sciences of Gafsa, Gafsa 2112, Tunisia;
✉***Corresponding author, E-mail:*** *imene.brahim@univ-batna.dz*

Article history: Received 30 August 2024; Revised 2 April 2025; Accepted 26 May 2025; Available online 25 June 2025

Abstract. The codling moth remains the main pest of apples in the Batna region of Algeria and causes heavy damage to apple orchards. This paper aims to show the possibility of using insecticide (Thiacloprid which may provide selective control tools) and sugar (which may induce multiple systemic resistances) to control *Cydia pomonella*. The field trials were carried out on the "Anna" apple tree cultivar in Tilatou (Batna, Algeria). The efficacy of sucrose and fructose (100 ppm), in comparison to Thiacloprid (25 mL ha^{-1}), was assessed based on the proportion of fruits that larvae destroyed, the quantity of larvae gathered in corrugated cardboard, and the quantity of male moths trapped in pheromone traps. This study showed that all tested products reduced fruits damaged by *Cydia pomonella*. Treatments by sucrose and fructose provide percentages of damaged fruits at rates of 8.44±0.64 and 7.57±1.25, respectively, vs. 36.35±3.00 for untreated trees. The treatments also affected the number of larvae caught in bands of corrugated cardboard. Foliar spraying in the morning with sugar (every 20 days) can be an alternative method to manage the codling moth population. The use of sugars is a novel method in the plant protection

strategy. These results constitute an interesting alternative to classical approaches offered by the opportunity to reduce the rate of chemical insecticides required for effective pest management.

Keywords: codling-moth, fruit damage, apple, sucrose, fructose.

Introduction

The majority of control techniques used in apple orchards aim to combat the codling moth (*Cydia pomonella* L.). The cryptic *Cydia pomonella* (*C. pomonella*) larvae live inside the fruit throughout their feeding stages, leaving an unattractive hole that may encourage internal rotting (Unruh *et al.*, 2016; Garczynski *et al.*, 2019; Nelson *et al*., 2021; Ju *et al*., 2023). Besides apples, they also infest pears, apricots, and walnuts. If left unchecked, it can result in extremely large yield losses of more than 95% (Unruh *et al.*, 2016; Damos and Soulopoulou, 2019; Shayestehmehr *et al.*, 2021; Mahendiran *et al.*, 2022). Consumers will not allow even minimal surface damage to apples or pears, and fruit that has been infected cannot be sold. Control measures are necessary when the estimated cost of treating a pest is lower than the cost produced by the potential damage (Baranek *et al*., 2021; Cahill *et al*., 2022; Eliceche *et al.*, 2023). The increasing reliance on chemicals has been associated to a number of issues, including hazards for farmers and consumers health; outbreaks in secondary pests controlled by natural enemies under toxic pesticides; environmental pollution; biodiversity reduction and pesticide resistance (Arnault *et al*., 2016; Baranek *et al*., 2021; Rani *et al*., 2021; Ali *et al*., 2023). Insecticide resistance is a major issue in the control of *C. pomonella* all over the world. Insecticide efficacy reductions on codling moths have been tested in pome fruit production locations across Europe, the Middle East, North America and South America (Chouinard *et al*., 2016; Unruh *et al.*, 2016; Kadoić Balaško *et al*., 2020; Gomez *et al*., 2023; Kaplan, 2023; Shayestehmehr *et al.*, 2021).

Sugars can function as signaling molecules in the same way that classical plant hormones routinely do, modulating gene expression and development processes of plants (Ahmad, 2019; Choudhary *et al*., 2022; Xu *et al*., 2022; Guo *et al*., 2023; Xie *et al*., 2023). However, the regulatory networks underlying are still not clear due to many cell signaling pathways involved. Environmental stresses, including pathogen infection and wounding, induce a series of defence responses that also interfere with carbohydrate metabolism and sugar-responsive genes (Moghaddam and den Ende, 2012; Saddhe *et al*., 2021).

It was discovered a long time ago that damaged plants had a higher sugar tolerance or high sugar resistance. More research is being done about the role of sugar signaling in plant defense mechanisms against fungi (Trouvelot *et al*., 2014; Tun *et al*., 2023). This has led to the sweet-immunity and sugar-enhanced defense concepts (Moghaddam and den Ende, 2013; Arnault *et al*., 2016; Tarkowski *et al*., 2019). Moghaddam and den Ende (2012) reported that the concept of sweet immunity predicts specific key roles for saccharides in the control of biotic and abiotic stresses. Few researches have been done on sugar and sugar polyols on the leaf surface that Lepidoptera females use as signals when identifying the plant where they should lay their eggs (Bertea *et al*., 2020; Formela-Luboińska *et al*., 2020). It was therefore hypothesized that sugar spraying may also increase plant resistance, and indeed, several studies showed such positive effects. Spraying soluble carbohydrates (sucrose, fructose, glucose, and trehalose) on the leaves of maize, tomato, potato, bean plants, and apple trees could induce resistance to pests and diseases (Ahanger *et al*., 2013). Furthermore, soluble carbohydrates sprayed at low doses can penetrate the cuticle and end up on the plant surface, constituting signals perceived by the insect through contact, then influencing its behavior and selection of the host plant to lay eggs (Derridj *et al*., 2011). Sucrose and fructose have also been shown to have some potential in the management of different parasites under low to moderate pest loads and on perennial crops (vineyards, arboriculture). In organic orchards, they reduce *C. pomonella* larval attack by 55% (Costantini and La Torre, 2022; Eliceche *et al*., 2023). The objective of the present study is to show the possibility of using sucrose and fructose to control *C. pomonella* in one of the important apple tree-growing regions of Algeria. The efficacy of these two sugars (100 ppm) was assessed for control of *C. pomonella* in an Algerian apple orchard cultivated with the "Anna" cultivar.

Materials and methods

Field experiments

This study was conducted in 2019 in Tilatou (Batna, Algeria) in an apple orchard (864 m^2) "Anna" cultivar. Tilatou is situated in the south-west of Batna (35°19'57.30" N 5°47'57.23"E) located in a semi-arid bioclimatic zone with a cold winter and an average altitude of more than 760 m above sea level (Fig. 1).

Observations were made on one apple cultivar "Anna". Differences in the percentage of *C. pomonella* larval damage and the efficacy of sucrose, fructose and thiacloprid treatments were observed in this cultivar. Four blocks of sucrose-treated trees, 4 blocks of fructose-treated trees, 4 blocks of thiacloprid-

treated trees and 4 blocks of untreated trees. Each block comprises 4-7 trees. All modalities are then randomly distributed within each block (4) and each block comprises 4 to 7 trees (Table 1).

Figure 1. Exploitation and study orchard plan (Anna variety, Tilatou region)

Table 1. Experimental plan

Line 1	Line 2	Line 3	Line 4
I 1	II 3	III 2	IV 4
I 2	II 1	III 4	IV 3
I 3	II 4	III 1	IV 2
I 4	II 2	III 3	IV 1

Roman numbers represent different blocks; Arabic numbers correspond to the modalities. Were : (1) : Untreated modality, (2) : Sucrose, (3) : Fructose and (4) : Thiacloprid.

Foliar spraying

When the first codling moth males were captured in the pheromone traps that had been set up in the research orchard on April 25, 2019, the entire experimental plan was treated. An untreated orchard was used as a reference (Fig. 2), located in the same study region, Tilatou (35°26'52.26''N5°58'26.52''E).

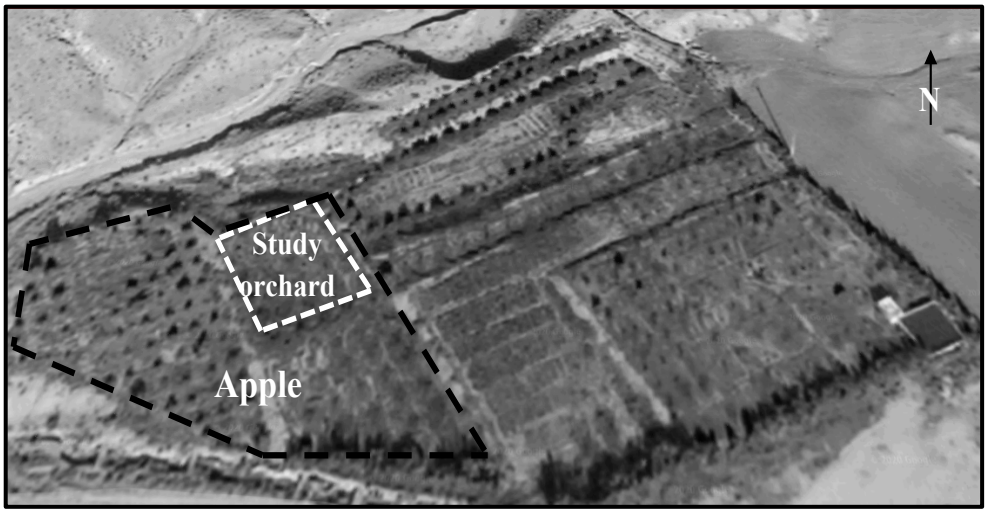

Figure 2. Exploitation and untreated orchard plan
(Golden delicious variety, Tilatou region)

In this orchard, *C. pomonella* dynamic flights were monitored by delta traps (Russell IPM, Algeria) baited with a standard pheromone capsule containing one mg of codlemone, installed at an approximate height of 1.70 m within the canopy of the tree, and checked every three days.

Treatment (= one foliar spray) was carried out very early in the morning, at the start of photosynthesis (Preininger *et al*., 2018), throughout the season during three insect generations, and until the harvest. The sucrose and fructose were sprayed every 20 days, and two applications with thiacloprid were done throughout the season on the whole tree (June 6th and 28th).

The sucrose used was from Fluka Biochemika (99% purity) used at 100 ppm (10 g 100 L^{-1}) dose. Previously weighted and brought into tubes for the amount of water sprayed. The use of sugar in the morning promotes its penetration when the apoplast (intercellular space) is poor. The chemical insecticide used is thiacloprid (Calypso480 SC, Bayer Crop Science), with a rate of 250 mL ha^{-1}. It is a specialty belonging to the chemical family of chloronicotinyls and neonicotinoids class. This insecticide was chosen because farmers in the region of Batna commonly use it. It is a systemic insecticide that acts by contact and ingestion on the insect nervous system (Gupta *et al*., 2019). This class of insecticide acts as agonists to acetylcholine, binding to postsynaptic nicotinic acetylcholine receptors, and causes paralysis and death of the insect, often within a few hours (Windley *et al*., 2017).

To perform different treatments, we used three backpacksprayers (Lion Mark), one sprayer for each modality, to avoid the risk of sugar contamination. The main material of the sprayer: plastic; power source: pressure, type; hand compression; pressure: 0.2-0.4 Mpa, (not dripping spray), capacity of 20 L (to spray the whole tree). To provide optimum security and prevent risks of intoxication during the execution of treatment with thiacloprid, personal protective equipment was used, including nitrile gloves, waterproof coveralls with hoods, boots, and a mask. The four modalities tested, as well as the doses administered for each modality, are represented in the Table (2).

Table 2. Modalities tested and doses used in the trial

Modalities	Formulated product	Active constituent	Dose
1	Untreated	Untreated	Untreated
2	Sugar	Sucrose	100 ppm (10g $100L^{-1}$)
3	Sugar	Fructose	100 ppm (10g $100L^{-1}$)
4	Calypso 480 SC	Thiacloprid	250 mL ha^{-1}

Estimation of diapausing larvae

On the tree trunk, bands of corrugated cardboard were positioned on May 6, to catch the larvae that were descending to overwinter under the tree (four to seven bands per block). These strips consist of two overlapping sheets of corrugated cardboard covered with a polyethylene mesh. The three layers are attached with wire. The mesh is designed to prevent birds from feeding on larvae. Trap bands are arranged around the base of the trunks of 76 experimental trees, close to the ground. Bands were removed on November 12.

Estimation of infested fruits

It consists of observing fallen and damaged fruits per tree during the fruiting period and damaged fruit at harvest per tree (August 7). Every week, the fallen fruits were collected from the ground and removed to distinguish those damaged by *C. pomonella* from those due to other causes. Observation and confirmation of codling moth damages on apples are made in the laboratory to distinguish between active, scarred or stopped damages.

Statistical analysis

The number of diapausing larvae and percentage of damaged fruit per tree were examined using ANOVA and Fisher's LSD test at $p<0.05$, respectively, to determine significant differences between means. Percentages of damaged fruits by larvae in the orchard were compared using the Abbott efficacy equation (Abbott, 1925):

$$\text{Efficacy} = 100 \times [(T0 - Tt)/T0].$$

where T0 is the total percentage of damaged fruits in the control block and Tt is the total percentage of damaged fruits in the treated block. All analyses were performed using STATISTICA 8 software v. 2008 (Stat Soft).

Results

The dynamic of C. pomonella flights

Flight of the codling moth began in first week of May in both these orchards (Fig. 3). In both the study and untreated orchard, catches in the *C. pomonella* pheromone traps dropped below detection levels after early November (Fig. 3). At these sites the codling moth went through three full generations and part of a fourth generation, and at least six moths co-existed during most months of research. In the studied test-orchard and the following non-sprayed one we confirmed the importance of catch for the first generation.

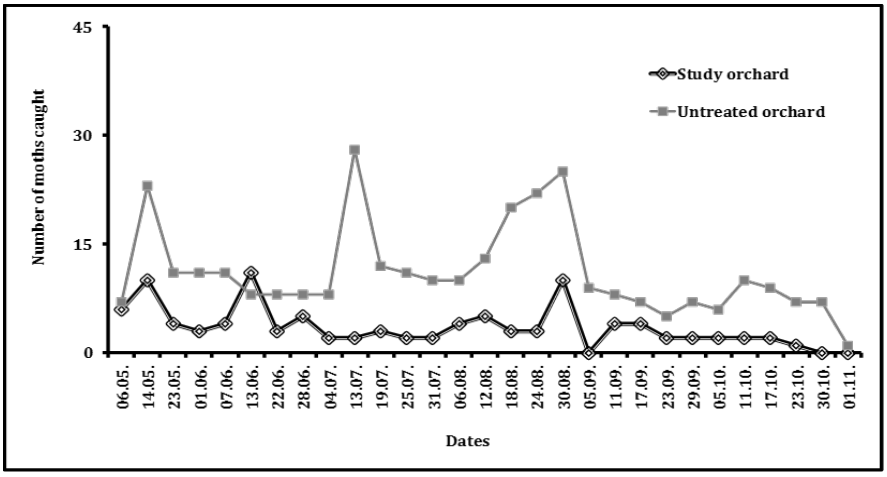

Figure 3. The dynamic of *C. pomonella* flights in the research orchard and the control orchard.

The first flight took place from May to the end of June; the second started in July and ran through the second week of August; and the third flight, began in second decade of August and runs until the first week of October. From there we can consider that the development of a fourth generation stopped. The dynamic of *C. pomonella* populations was related to the different phenological stages of the host plant (Fig. 4).

Estimation of diapausing larvae

A total of 205 larvae were observed and removed from bands of corrugated card board installed at the beginning of the experiment. Most of the larvae were located in untreated trees.

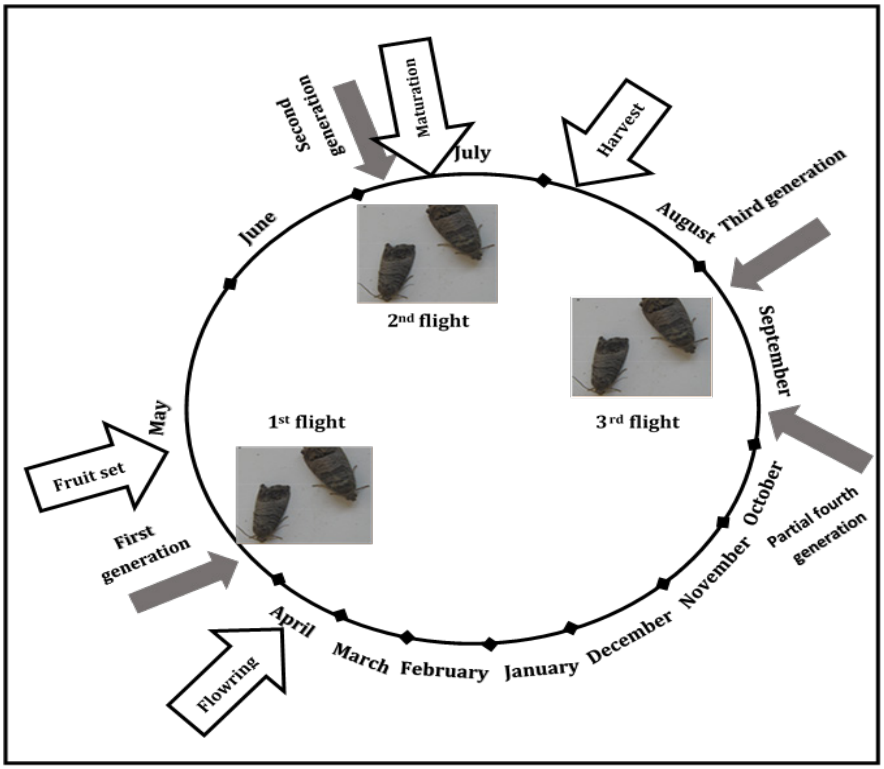

Figure 4. Life Cycle of the codling moth in an orchard that cultivates the "Anna" variety.

The greatest number of larvae per tree in treated blocks with thiacloprid, fructose and sucrose was, on average, 9.75%±0.69; 8.03%±0.77; and 9.25%±0.55, respectively. The average number of larvae collected in untreated blocks was 15.25±0.79. The numbers of larvae per tree band were similar for fructose and sucrose; there were highly significant differences between them and those untreated and treated with thiacloprid (ANOVA, Tukey's L.S.D. tests, $p< 0.05$) (Fig. 5).

On the other hand, the number of diapausing larvae captured in bands of trees sprayed with sucrose and fructose was approximately five and three times (in order) lower than those observed in untreated trees and, respectively, three and two times lower than those treated with thiacloprid (Fig. 5).

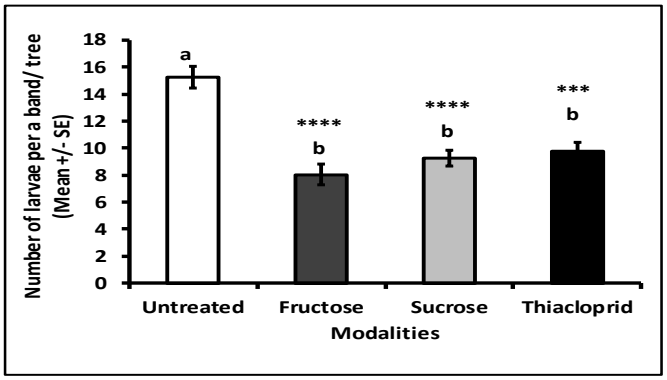

Figure 5. Average (±Standard Error) number of caterpillars per band or tree.
*ANOVA, Fisher's LSD tests, p<0.05; different letters show significant differences between treatments within each experiment. ****: p< 0.0001 and ***: p = 0.005.*

Damaged fruits

The counting at the end of the three generations on the attacked fruits of the trees of the experimental plan allows estimating the levels of efficiency of the tested modalities. The first falls were recorded in June. The losses increased over time and the most common attacks were caused by the second-generation caterpillars.

The percentage of damaged fruit at the end of the first generation was high. It reached 38.10%±9.33 in the untreated block, while the other modalities had a lower percentage of damaged fruit. Fructose, sucrose and thiacloprid showed a significant reduction in infestation levels of 14.01%±1.54, 13.38%±1.60 and 16.74±5.34% respectively, compared to the untreated modality (ANOVA, Fisher's tests, p< 0.001) (Fig. 6a).

For the second generation, the same assessments are recorded. Compared to the untreated trees we noted a higher significant reduction in the percentage of damaged fruit on trees treated with fructose (26.84%±9.53) and sucrose (28.33%±7.01). The application of thiacloprid showed also reduction in apple fruit damages, reaching 33.06%±4.39 compared to the untreated trees (59.77%±12.35) (ANOVA, Fisher's tests, p< 0.001) (Fig. 6a, 6b).

As for the first two generations, the third (partial) generation shows the same observations. Nevertheless, infestation levels are lower than those reported in the first (38.10%±9.33) and second generations (59.77%±12.35), where the latter has the highest percentage of infestation. The count at the end of the third generation shows an infestation level of 26.20%±5.77. Note that the tested modalities reduce the percentage of damaged fruits to 17.36%±4.62, 18.43%±3.20, and 19.88%±5.21 recorded by fructose, sucrose, and thiacloprid, respectively (Fig. 6c).

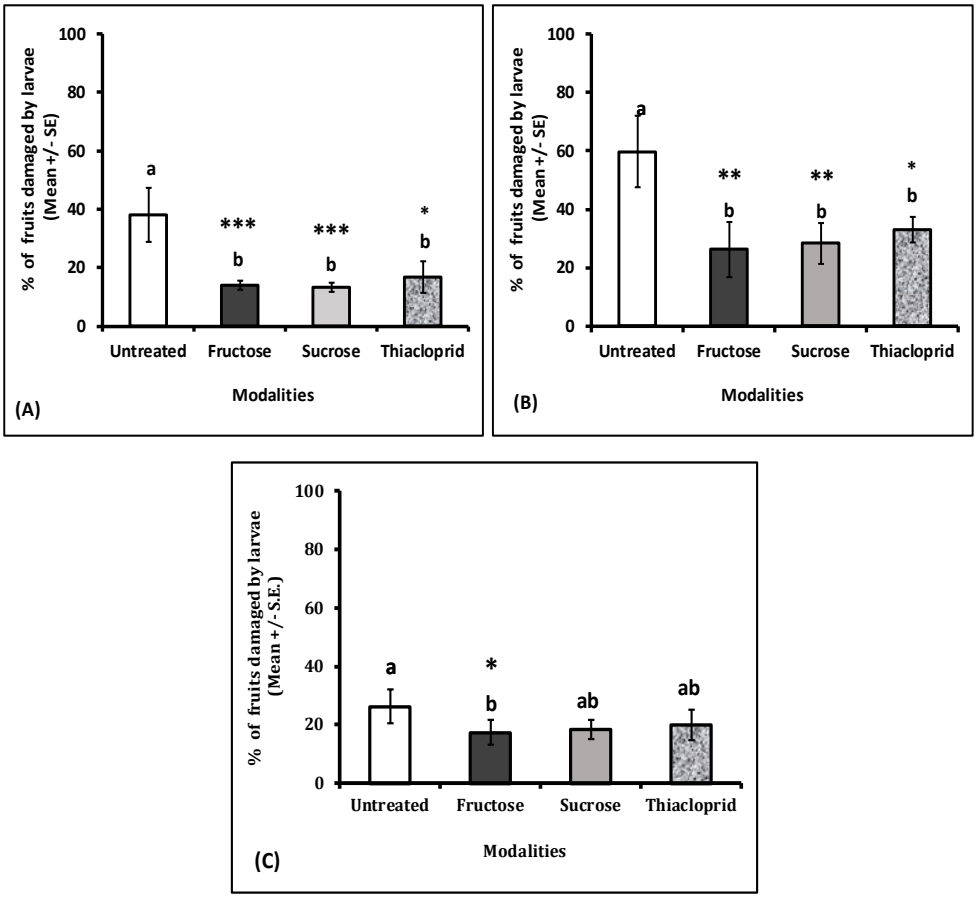

Figure 6. Mean (± SE) percentage of fruits damaged at the end of the first generation (A), the second generation (B), and the third generation (C) by larvae on "Anna" cultivar. *ANOVA, Fisher's LSD tests, p<0.05; different letters show significant differences between treatments within each experiment. *: p<0.05, **: p<0.01 and ***: p< 0.001.*

Fruit damage types

There were three types of fruit damage at harvest: scared, stopped, and active. The sucrose and fructose treatments had similar and significantly different percentages from trees that had not been treated ($p < 0.0001$) and from trees that had been treated with thiacloprid ($p < 0.01$) (Fig. 7a). For fallen fruit rates, they were similar and not significantly different between fructose and sucrose for any type of fruit damage and significantly different from untreated and thiacloprid-treated trees for scared and active fruit damage. For stopped fruit

damages, all modalities did not differ significantly. Treated trees with thiacloprid showed more active and scarred damages than treated trees with fructose and sucrose, whatever damaged or fallen fruits at harvest (Fig. 7b).

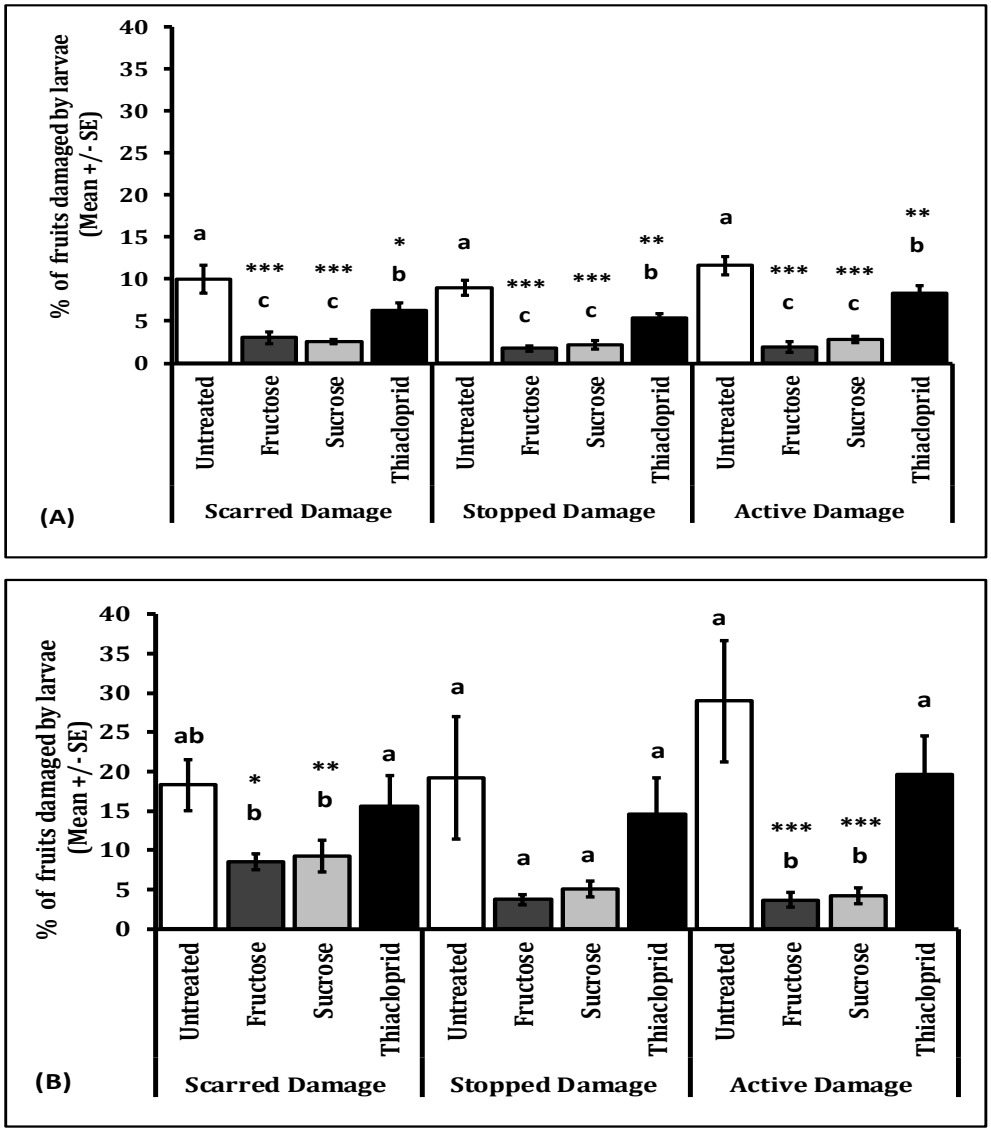

Figure 7. Mean (± SE) percentage of different fruits damaged at harvest (A) and fallen fruits (B) by larvae on "Anna" cultivar. *ANOVA, Fisher's LSD tests, p<0.05; different letters show significant differences between treatments within each experiment. ***: p <0.001, **: p ≤ 0.01 and *: p<0.05.*

Abbott efficacy

For the three generations, treatments based on infra-doses of sucrose, fructose, and thiacloprid allow to obtain a low to very important and significant efficiency between 22.95%±3.75 and 80.82%±2.59. Take note that thiacloprid, fructose, and sucrose all provide the best mean Abbot efficacy regardless of the generation. Figure (8) shows that the best results are recorded in the first generation by fructose (78.65%±2.17) and sucrose (80.82%±2.59), while thiacloprid has the highest efficiency in the second flight (32.3%±6.17) ($p<0.0001$, ANOVA, Fisher's L.S.D. tests, $p< 0.05$).

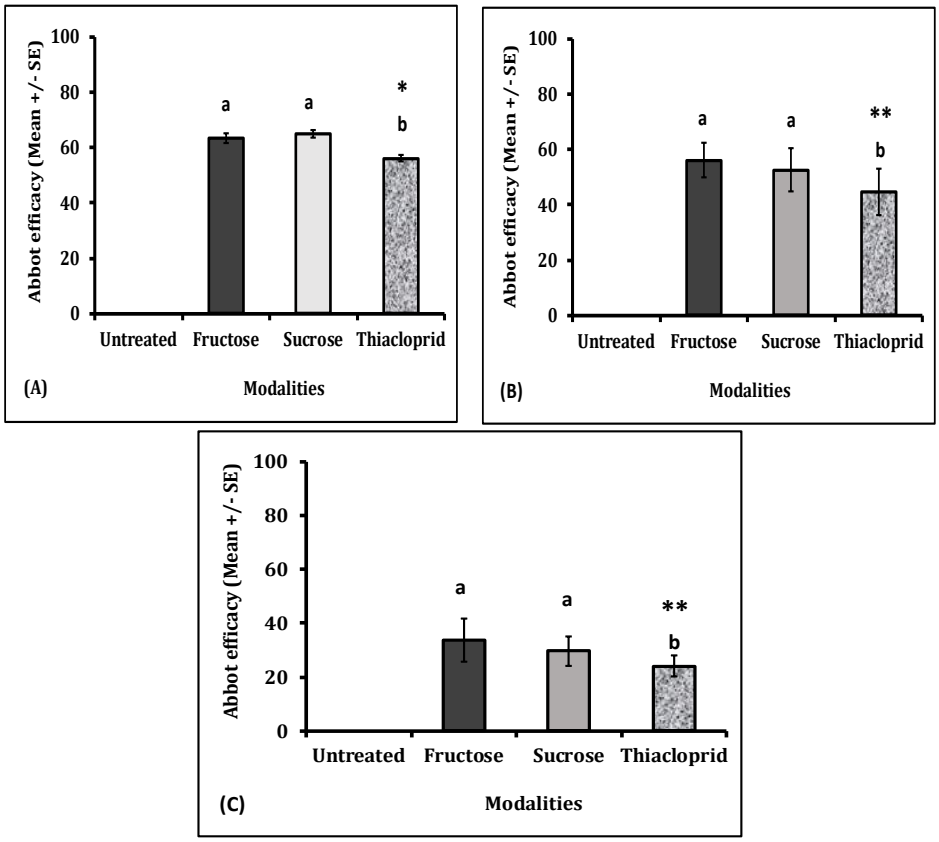

Figure 8. Mean Abbott effectiveness levels for sugar, insecticides (chemical and bio-insecticides), and damaged fruits at the end of the first generation (A), the second generation (B), and the third generation (C) by larvae on the cultivar "Anna" (Efficacy level in percent vs. untreated control damage level). *ANOVA, Fisher's LSD tests, $p <0.05$; different letters show significant differences between treatments within each experiment. *: $p<0.05$, and **: $p \leq 0.01$ are all present.*

Discussion

The dynamic of C. pomonella flights

The codling moth in Batna has three full generations and a partially developed a fourth generation, according to monitoring of its flight patterns conducted in two distinct orchards. In the research orchard, where male pheromone trap captures showed a total of 101 individuals and 322 individuals in the untreated orchard, the codling moth population density was rather low, according to the results that have been provided. The catches per trap were higher in the untreated orchard, confirming the permanent risk of this insect over the years. Work in most areas of Batna indicates that *C. pomonella* has two to three generations per year. For example, in Tazoult (altitude 1000 m) and Lambiridi (altitude 1075 m), there are three generations per year. In the Tizi-Ouzou area, there are three generations per year (Guermah and Medjdoub-Bensaad, 2016). And four generations in Morocco, with two full generations and two partial generations (El Iraqui and Hmimina, 2016a).

According to El Iraqui and Hmimina (2016b), the generation number changes depending on the altitude and is also related to temperature, which decreases by 3 degrees every 100 m of altitude (Gutiérrez-Gamboa *et al*., 2021). And it also comes from the spatial-temporal equation, related mainly to photoperiod and nutrition (El Iraqui and Hmimina, 2016a; 2016b; Hill *et al*., 2021).

Estimation of diapausing larvae

The sugar treatments and significantly reduce codling moth larval populations. Reduced codling moth larvae on corrugated cardboard bands suggests a decline in the adult population during the next few years. And its importance should not be underestimated given the role of these bands in the decreasing populations of codling moths (Arnault *et al*., 2015; 2016). It has been demonstrated that when the codling moth population density is relatively low, the sucrose and fructose treatments may be successful at controlling the pest.

The lower number of larvae in band traps, in both, tested modalities compared to the untreated modality indicates that they had a significant effect on larval populations. The reduction of the number of hibernating larvae in the two biological strategies is an encouraging result.

Damaged fruits

Chemical treatments (Calypso 480 SC Chloronicotinyls) showed that this product has a greater effect on reducing damage. In Morocco, a comparative study of thiachlorpid with other active ingredients showed a reduced sensitivity

of the field population for thiacloprid and deltamethrin, followed byazinphos-methyl and diflubenzuron (El Iraqui and Hmimina, 2016a).

The number of damaged fruits has decreased due to the application of sugars, whose effectiveness is enhanced when applied during the day.. It was also sufficient to preserve the fruits from attacking when the majority of the first-generation larvae emerged (Xi *et al*., 2021).

The induction of changing surface signals is necessary for host recognition and *C. pomonella* egg-laying. Foliar sprayings of maize with low concentrations of sucrose (1 to 10 mg L^{-1}) have a systemic impact on the plant and decrease *Ostrinia nubilalis* egg-laying (Derridj *et al.,* 2012). This could reduce the damage caused by *C. pomonella* and lepidopterans, to an apple. The trials conducted under semi-field circumstances revealed that the apple trees leaf surface composition and even the codling moth's egg distribution changed 20 days after being treated with sugar at 10 ppm (10 mg L^{-1}). Also, sugar-modified leaf surface signal recognition by the codling moth females and ABBOTT efficiency average on 4 years of experiments is 40+/-16.0% on the apple infests. Sugars can also reduce powdery mildew in melon cultures (Arnault *et al*., 2015). The significant reduction in larval damages can probably be explained by the fact that the sugar-induced systemic resistance vs. *C. pomonella* is due to the modification of metabolites present at the surface of leaves and fruits, some of which are signals for the insect that disrupt host recognition and egg-laying. According to the chemical examination of the metabolites on apple tree leaves, the sucrose treatment mostly caused changes (in terms of amounts and ratios) in metabolites, which altered the signals for the insect's host acceptance and egg-laying (Arnault *et al*., 2016).

Fruit damage types at harvest

Whatever damaged or fallen fruits were at harvest, the fructose treatments showed that scarred damages were much higher than stopped or active ones . Reporting that on an infected host, this delay may allow for continued feeding and producing healed fruits. According to Cabanat (1999), sucrose and fructose are phagostimulants that increase feeding by larvae at a dose of 100 ppm. In contrast, glucose has a repellent activity that diminishes at 100 ppm and induces a phagoinhibitory effect. In our case, we can say that the spraying of sugars alone, in mixtures, and in alternation induces a repellent activity on the larvae, which is reflected in a high percentage of stopped attacks.

In general, regardless of the type of damage and the fallen or harvested fruits, the reduction in infestation rates is explained by the fact that certain groups of plant-derived molecules. serve as signals perceived by the pest on the surface of the plants, influencing its behavior, stimulating oviposition in females, and affecting the feeding behavior of adults and larvae in several insects (Cabanat,

1999; Vrieling and Derridj, 2003; Derridj *et al.,* 2011). Additionally, the penetration of soluble substances (soluble sugars and polyols) in water deposited on the surface of the plant can stimulate defense reactions within the plant.

Few studies revealed that sugar foliar spray alone has interesting effects and when combined with chemical plant protection products, it allows reducing their doses while keeping a good efficiency. Sugars activate defense pathways but not always in the same way (Arnault *et al*., 2021).

Abbott efficacy

Regardless of any damaged or fallen fruit at harvest, sugar and the chemical treatments (Calypso 480 SC Chloronicotinyls) recorded Abbott's best average efficacy. This can be explained by several experiments conducted to test the efficacy of these modalities for the control of *C. pomonella* in apple orchards. Research results widely differ from one study to another, but generally, the application of the insecticide allows a significant decrease in the population of codling moths, as well as crop damage (Arnault *et al*., 2015).

The outcomes are in line with those of Arnault *et al*. (2016), who reported the findings of seven studies performed in apple orchards in Algeria and France between 2013 and 2014. After applying sucrose at 0.01%, the number of contaminated apples decreased. Sucrose had a mean Abbott effectiveness of 41.0%±10.0. Also, it was demonstrated that when sucrose was combined with the insecticide thiacloprid, it increased the effectiveness of the thiacloprid treatment by 18%. The researchers concluded that the interaction between sucrose and thiacloprid is not additive but rather synergistic and potentiating.

Conclusions

The employment of sucrose and fructose treatments as biological controls in agriculture holds a lot of promise for the environmentally friendly management of insect pests. According to the results, these two sugars can be used as a substitute for controlling codling moth populations and fruit damage levels in apple orchards. We also observed that it is an easy and safe method that benefits humans, wildlife, and the environment. By misting plants with little amounts of sugar, we were able to create plant resistance to *C. pomonella* behavior (antixenosis) (only 100 ppm). The occurrence appears to be widespread and repeatable. Additionally, it is administered easily with a standard sprayer, just like a chemical insecticide. This method of management should have the benefit of preventing plant damage brought on by neonate larvae. New directions in crop protection research will open up with the findings of the induced processes.

References

Abbott, W. S., (1925). A method of computing effectiveness of an insecticide. *J Econ Entomol, 18*, 265-267. https://doi.org/10.1093/jee/18.2.265a

Ahanger, M. A., Tyagi, S. R, Wani M.R., & Ahmad, P. (2013). Drought tolerance: role of organic osmolytes, growth regulators, and mineral nutrients. In: *Physiological Mechanisms and Adaptation Strategies in Plants Under Changing Environment, Volume* 1, Parvaiz A. and Wani M. R. (ed.), Springer, pp. 25-55. https://doi.org/10.1007/978-1-4614-8591-9_2

Ahmad, I. Z. (2019). Role of sugars in abiotic stress signaling in plants. In: *Plant Signaling Molecules*, Woodhead Publishing (ed.), pp. 207-217. https://doi.org/10.1016/B978-0-12-816451-8.00039-3

Ali, M.A., Abdellah, I.M., & Eletmany, M.R. (2023). Towards Sustainable Management of Insect Pests: Protecting Food Security through Ecological Intensification. *IJCBS, 24(4)*, 386-394.

Arnault, I., Aveline, N., Bardin, M., Brisset, M.N., Carriere, J., Chovelon, M., Delanoue, G., Furet, A., Frérot, B., Lambion, J., Ondet, S., Marchand, P., Desmoucaux, N., Romet, L., Thibord, J.B., & Trouvelot, S. (2021). Optimisation des stratégies de bio contrôle par la stimulation de l'immunité des plantes avec des applications d'infra-doses de sucres simples. [in Frensh]. *Innovations Agronomiques, 82*, 411-423.

Arnault, I., Bardin, M., Ondet, S., Furet, A., Chovelon, M., Kasprick, A.C., Marchand, P., Clerc, H., Davy, M., Roy, G., Romet, L., Auger, J., Mançois, A. & Derridj, S. (2015). Utilisation de micro-doses de sucres en protection des plantes. [in Frensh]. *Innovations Agronomiques, 46*, 1-10.

Arnault, I., Lombarkia, N., Joy-Ondet, S., Romet, L., Brahim, I., Meradi, R., Nasri, A., Auger, J., & Derridj, S. (2016). Foliar application of microdoses of sucrose to reduce codling moth *Cydia pomonella* L. (Lepidoptera: Tortricidae) damage to apple trees. *Pest Manage Sci, 72,* 1901–1909. https://doi.org/10.1002/ps.4228

Baranek, J., Banaszak, M., Kaznowski, A., & Lorent, D. (2021). A novel Bacillus thuringiensis Cry9Ea-like protein with high insecticidal activity towards *Cydia pomonella* larvae. *Pest Manage Sci, 77*, 1401-1408. https://doi.org/10.1002/ps.6157

Bertea, C., M., Casacci, L., P., Bonelli, S., Zampollo, A., & Barbero, F. (2020). Chemical, physiological and molecular responses of host plants to lepidopteran egg-laying. *Front Plant Sci, 10*, 1768. https://doi.org/10.3389/fpls.2019.01768

Cabanat, I. (1999). Étude du comportement de recherche du site alimentaire par les chenilles néonates de *Cydia pomonella* L. lépidoptère ravageur des pommes et des poires en relation avec les médiateurs biochimiques présents à la surface des organes végétaux du pommier. [in Frensh]. Mémoire de DEA. Université Paris-Nord. France, 25p.

Cahill, P.L., Davidson, I.C., Atalah, J.A., Cornelisen, C., & Hopkins, G. A. (2022). Toward integrated pest management in bivalve aquaculture. *Pest Manage Sci, 78*, 4427-4437. https://doi.org/10.1002/ps.7057

Choudhary, A., Kumar, A., Kaur, N., & Kaur, H. (2022). Molecular cues of sugar signaling in plants. *Physiol Plant, 174(1)*, e13630. https://doi.org/10.1111/ppl.13630

Chouinard, G., Firlej, A. ,& Cormier, D. (2016). Going beyond sprays and killing agents: Exclusion, sterilization anddisruption for insect pest control in pome and stone fruit orchards. *Sci Hortic, 208*, 13–27. https://doi.org/10.1016/j.scienta.2016.03.014

Costantini, E., & La Torre, A. (2022). Regulatory framework in the European Union governing the use of basic substances in conventional and organic production. *J Plant Dis Prot, 129*, 715-743. https://doi.org/10.1007/s41348-022-00569-9

Damos, P., & Soulopoulou, P. (2019). Stage-specific probabilistic phenology model of *Cydia pomonella* (Lepidoptera: Tortricidae) using laboratory maximum likelihood parameter estimates. *J Appl Entomol, 143*, 250-261. https://doi.org/10.1111/jen.12589

Derridj, S., Arnault, I., Lombakia, N., Ferre, E., Galy, H., Lambion, J., & Auger, J. (2011). Les sucres solubles utilisés comme inducteurs de résistance de la plante aux bio-agresseurs. [in Frensh]. *Quatrième conférence internationale sur les méthodes alternatives en protection des cultures, Lille - 8, 9, 10 mars 2011,* 383-388.

Derridj, S., Lombarkia, N., Garrec, J. P., Galy, H., & Ferre, E. (2012). Sugars on leaf surfaces used as signals by the insect and the plant: implications in orchard protection against *Cydia pomonella* L. (Lepidoptera, Tortricidae). In: Moths: Types, Ecological Significance and Control, ed. By Cauterrucio L. Nova Science Publishers Inc., Hauppage, NY, pp. 1–38.

El Iraqui, S., & Hmimina, M. (2016a). Assessment of control strategies against *Cydia pomonella* (L.) in Morocco*. J Plant Prot Res, 56(1)*, 82-88. https://doi.org/10.1515/jppr-2016-0012

El Iraqui, S., & Hmimina, M. (2016b). Impact of temperatures on the voltinism of *Cydia pomonella* (Lepidoptera: Tortricidae). *Ann Entomol Soc Am, 109*, 698–704. https://doi.org/10.1093/aesa/saw046

Eliceche, D., Rusconi, M., Rosales, M., Rossi, J., Salas, A., Macagno, C., D'Hervé, F., Silvestre, C., & Achinelly, F. (2023). The efficacy of *Steinernema feltiae* in the control of *Cydia pomonella* in organic apple and pear orchards of Patagonia Argentina and its impact on local populations of entomopathogenic nematodes. *BioControl,* 68, 459-470. https://doi.org/10.1007/s10526-023-10198-2

Formela-Luboińska, M., Remlein-Starosta, D., Waskiewicz, A.,Karolewski, Z., Bocianowski, J., Stepien, L., Labudda, M., Jeandet, P., & Morkunas, I. (2020). The role of saccharides in the mechanisms of pathogenicity of *Fusarium oxysporum f. sp*. lupini in yellow lupine (*Lupinus luteus* L.). *Int J Mol Sci*, 21, 7258. https://doi.org/10.3390/ijms21197258

Garczynski, S.F., Hendrickson, C.A., Harper, A., Unruh, T.R., Dhingra, A., Ahn, S.J., & Choi, M.Y. (2019). Neuropeptides and peptide hormones identified in codling moth, *Cydia pomonella* (Lepidoptera: Tortricidae). *Arch. Insect Biochem. Physiol, 101*, e21587. https://doi.org/10.1002/arch.21587

Gomez, M.P., Barud, F.J., Diaz, A., & Lopez, M.L. (2023). Oviposition and olfactometry response of codling moth (*Cydia pomonella*) to quince (*Cydonia oblonga*) cultivars. *J Appl Entomol, 147*, 307-312. https://doi.org/10.1111/jen.13113

Guo, W.J., Pommerrenig, B., Neuhaus, H.E., & Keller, I. (2023). Interaction between sugar transport and plant development. *J Plant Physiol, 288*, 154073. https://doi.org/10.1016/j.jplph.2023.154073

Guermah, D., & Medjdoub-Bensaad, F. (2016). Population dynamics of the codling moth Cydia pomonella (Lepidoptera: Tortricidae) on two apple varieties in Algeria. *Int J Bio Res Dev, 6*, 1-8.

Gupta, R.C., Mukherjee, I.R.M., Malik, J.K., Doss, R.B., Dettbarn, W.-D., & Milatovic, D. (2019). Insecticides. In: *Biomarkers in toxicology*, Ramesh C. Gupta (eds.), Academic Press, 455–475. https://doi.org/10.1016/B978-0-12-814655-2.00026-8

Gutiérrez-Gamboa, G., Zheng, W., & Martinez de Toda, F. (2021). Strategies in vineyard establishment to face global warming in viticulture: A mini review. *J Sci Food Agric, 101*, 1261-1269. https://doi.org/10.1002/jsfa.10813

Hill, G.M., Kawahara, A.Y., Daniels, J.C., Bateman, C.C., & Scheffers, B.R. (2021). Climate change effects on animal ecology: butterflies and moths as a case study. *Biol Rev, 96*, 2113-2126. https://doi.org/10.1111/brv.12746

Ju, D., Liu, Y.-X., Liu, X., Dewer, Y., Mota-Sanchez, D., & Yang, X.-Q. (2023). Exposure to lambda-cyhalothrin and abamectin drives sublethal and transgenerational effects on the development and reproduction of *Cydia pomonella*. *Ecotoxicol Environ Saf,* 252, 114581. https://doi.org/10.1016/j.ecoenv.2023.114581

Kadoić Balaško, M., Bažok, R., Mikac, K.M., Lemic, D., & Pajac Zivkovic, I. (2020). Pest management challenges and control practices in codling moth: A review. *Insects, 11(38)*, 1-22. https://doi.org/10.3390%2Finsects11010038

Kaplan, M. (2023). Determination of population change and damage rate of the harmful codling moth (*Cydia pomonella* Linnaeus) (Lepidoptera: Tortricidae) in apple orchards in malatya province, Türkiye. *Erwerbs-Obstbau, 65*, 1285-1290. https://doi.org/10.1007/s10341-023-00882-z

Mahendiran, G., Lal, S., & Sharma, O. (2022). Pests and Their Management on Temperate Fruits: (Apple, Pear, Peach, Apricot, Cherry, Persimmon, Walnut, Olive, Kiwifruit and Strawberry). In: *Trends in Horticultural Entomology*, Springer Singapore, pp. 891-941. https://doi.org/10.1007/978-981-19-0343-4_36

Moghaddam, M.R.B., & den Ende, W.V. (2013). Sweet immunity in the plant circadian regulatory network. *J Exp Bot, 64*, 1439-1449. https://doi.org/10.1093/jxb/ert046

Moghaddam, M.R.B., & den Ende, W.V. (2012). Sugars and plant innate immunity. *J Exp Bot, 63*, 3989-3998. https://doi.org/10.1093/jxb/ers129

Nelson, C., Esch, E., Kimmie, S., Tesche, M., Philip, H., & Arthur, S. (2021). Putting the sterile insect technique into the modern integrated pest management toolbox to control the codling moth in Canada. [in Frensh]. In: *Area-Wide Integrated Pest Management*, J. Hendrichs, R. Pereira and M. J. B. Vreysen (eds.), CRC, Boca-Raton, pp. 111-127. doi:10.1201/9781003169239-7

Preininger, C., Sauer, U., Bejarano, A., & Berninger, T. (2018). Concepts and applications of foliar spray for microbial inoculants. *Appl Microbiol Biotechnol, 102*, 7265-7282. https://doi.org/10.1007/s00253-018-9173-4

Rani, L., Thapa, K., Kanojia, N., Sharma, N., Singh, S., Grewal, A.S., Srivastav, A.L., & Kaushal, J. (2021). An extensive review on the consequences of chemical pesticides on human health and environment. *J Cleaner Prod, 283*, 124657. https://doi.org/10.1016/j.jclepro.2020.124657

Saddhe, A.A., Manuka, R., & Penna, S. (2021). Plant sugars: Homeostasis and transport under abiotic stress in plants. *Physiol Plant, 171*, 739-755. https://doi.org/10.1111/ppl.13283

Shayestehmehr, H., Karimzadeh, R., Feizizadeh, B. & Iranipour, S. (2021). Spatial distribution of *Cydia pomonella* (Lepidoptera: Tortricidae) populations and its relation with topographic variables. *Appl Entomol Zool. 56*, 187-197. https://doi.org/10.1007/s13355-020-00722-6

Tarkowski L.P., Poel B.V., Hofte M., & Ende W.V. (2019). Sweet Immunity: Inulin Boosts Resistance of Lettuce (*Lactuca sativa*) against Grey Mold (*Botrytis cinerea*) in an Ethylene-Dependent Manner. *Int J Mol Sci, 20,* 1052. https://doi.org/10.3390/ijms20051052

Trouvelot, S., Héloir M.C., Poinssot B., Gauthier A., Paris, F., Guillier, C., Combier, M., Trda, L., Daire X., & Adrian M. (2014). Carbohydrates in plant immunity and plant protection: roles and potential application as foliar sprays. *Front Plant Sci,* 4, 1-14.

Tun, W., Yoon, J., Vo, K.T.X., Cho, L.-H., Hoang, T.V., Peng, X., Kim, E.-J., Win, K.T.Y.S., Lee, S.-W., & Jung, K.-H. (2023). Sucrose preferentially promotes expression of OsWRKY7 and OsPR10a to enhance defense response to blast fungus in rice. *Front Plant Sci, 14*, 1117023. https://doi.org/10.3389/fpls.2023.1117023

Unruh, T.R., Miliczky, E.R., Horton, D.R., Thomsen-Archer, K., Rehfield-Ray, L., & Jones, V.P. (2016). Gut content analysis of arthropod predators of codling moth in Washington apple orchards. *Biol Control, 102*, 85-92. https://doi.org/10.1016/j.biocontrol.2016.05.014

Vrieling, K., & Derridj, S. (2003). Pyrrolizidine alkaloids in and on the leaf surface of *Senecio jacobaea* L. *Phytochemistry, 64*, 1223-1228.

Windley, M.J., Vetter, I., Lewis, R.J., & Nicholson, G.M. (2017). Lethal effects of an insecticidal spider venom peptide involve positive allosteric modulation of insect nicotinic acetylcholine receptors. *Neuropharmacology, 127*, 224-242. https://doi.org/10.1016/j.neuropharm.2017.04.008

Xi, Y., Xing, L., Wennmann, J. T., Fan, J., Li, Z., Wu, Q., Lu, S., Liu, B., Guo, J., Qiao, X., Huang, C., Qian, W., Jehle, J. A., & Wan, F., (2021). Gene expression patterns of *Cydia pomonella* granulovirus in codling moth larvae revealed by RNAseq analysis. *Virology, 558*, 110-118. https://doi.org/10.1016/j.virol.2021.02.015

Xie, J., Deng, B., Wang, W., & Zhang, H. (2023). Changes in sugar, organic acid and free amino acid levels and the expression of genes involved in the primary metabolism of oleocellosis in citrus peels. *J Plant Physiol, 280*, 153-877. https://doi.org/10.1016/j.jplph.2022.153877

Xu, Z., Xu, L., & Hu, X. (2022). Genomic analysis of sugar transporter genes in peanut (Arachis hypogaea): Characteristic, evolution and expression profiles during development and stress. *Oil Crop Science, 7*, 189-199. https://doi.org/10.1016/j.ocsci.2022.11.002

STUDIA UNIVERSITATIS BABEŞ-BOLYAI BIOLOGIA, 70, 1, 2025 (p. 153-172)
doi:10.24193/subbbiol.2025.1.08

Biochar soil amendments affect mycorrhizal colonization, root nodulation and dry matter accumulation in cowpeas (*Vigna unguiculata* (L.) Walp.)

Ifeyinwa Monica Uzoh[1,2], Keabetswe Chriscellda Ramadile[1], Uchechukwu Paschal Chukwudi[1,3], Ozede Nicholas Igiehon[1], Akinlolu Olalekan Akanmu[1] and Olubukola Oluranti Babalola[1] ✉

[1]Food Security and Safety Focus Area, Faculty of Natural and Agricultural Sciences, North-West University, Mmabatho 2735, South Africa; [2]Department of Soil Science, Faculty of Agriculture, University of Nigeria, Nsukka; [3]Department of Crop Science, Faculty of Agriculture, University of Nigeria, Nsukka
✉***Corresponding author, E-mail:*** *Olubukola.babalola@nwu.ac.za*

Article history: Received 24 September 2024; Revised 14 December 2024; Accepted 15 January 2025; Available online 25 June 2025

Abstract. There is increasing demand for renewable inputs to improve soil productivity to satisfy the ever-growing human population. Biochar as a renewable resource has attracted attention over the years as soil amendment, notable for climate change mitigation and crop improvement. This study assessed the impact of pine wood biochar soil amendments on mycorrhizal root colonization, root nodulation, growth and yield of cowpeas in 2017 and 2018. The experimental design was a randomized complete block design with three replications. Biochar was applied with or without inorganic fertilizer ($NPK_{15:15:15}$), cattle dung and nutrient source control two weeks before planting cowpea. Data on growth parameters, number of nodules, and plant dry matter accumulation were collected. Mycorrhizal colonization and spore counts associated with root nodules were determined under laboratory conditions. The results revealed that biochar amendments significantly affected nodulation, vine length, root length and weight. Percentage improvement was as follows: vine length by 8.8%, number of nodules by 14%, root length by 9.5%, root weight by 5.2% and dry matter accumulation by 92%. Application of NPK improved root length and weight over the control. Stereomicroscopic visualization of the roots

indicated high presence of arbuscules in the biochar treatment over the control. Biochar addition is essential for improvement of rhizosphere traits essential for plant growth enhancement.

Keywords: arbuscules, glomus species, mycorrhizal spore count, pine wood biochar, vesicles.

Introduction

Mycorrhizal colonization and root nodulation by rhizobia are important plant-microbe symbiotic interactions that benefit both plants and mycorrhizal fungi. Microorganisms in symbiotic association with plants are known for enhancing plant growth and increasing crop yield. Through mycorrhizal associations, plants obtain phosphorus from soil that is otherwise difficult for plants to reach (Igiehon and Babalola, 2017; Emmanuel *et al*., 2021). This access to extra nutrients enhances plant performance. Symbiotic relationships between leguminous plants and rhizobia stimulate nodule formation, offering the plant an additional source of nitrogen. Beyond access to nutrients, microorganisms offer protection against pathogens while producing growth-promoting hormones (Omomowo & Babalola, 2023). Plants attract these beneficial microorganisms through the secretion of root exudates, which include sugars, amino acids, and organic acids that act as chemical signals and energy sources, thereby creating a suitable environment for microbial colonization in the rhizosphere (Uzoh & Babalola, 2020; Akanmu *et al*., 2021). Cowpea (V*igna unguiculata*), a leguminous plant, owes its rich protein content to the microbial colonization in its rhizosphere (Agbodjato and Babalola, 2024).

Cowpea is a source of protein for rural and urban dwellers in sub-Saharan Africa, where it is widely grown (Omomowo & Babalola, 2021; Atugwu *et al*., 2023). It is commonly cultivated in the West and Central Africa. Cowpea contains 20 - 25% protein in their dry seed (Ddamulira *et al*., 2015). The fresh leaves and young pods are consumed as vegetables; the dry seeds are used for different food preparations, while the leaves are fed to livestock as fodder. It can tolerate drought and poor soil (Chinma *et al*., 2008). Cowpeas are important part of agricultural production systems since nitrogen fixation makes agricultural systems sustainable. Nitrogen requirement of subsequent crop or intercrop is thereby reduced. In addition, cowpeas' canopy protects the soil from the harmful effect of winds and runoff, thus preventing erosion.se of cowpea in cropping systems has increased farmers adoption of legume-based cropping systems.

Despite the roles cowpea plays in agricultural diversification of cropping systems, cowpea yield is still below expectation (Atugwu *et al*.,2023). A contributory factor to this poor yield is the low fertility of soils of savannah and semi-arid zones where cowpeas are prominently grown (Emmanuel *et al*., 2020; Ayangbenro *et al*., 2023). The misconception that cowpea does not need soil amendments due to its nitrogen fixing potential exacerbates the low yield. The study by Atugwu *et al*. (2023) demonstrates that cowpea responds well to soil amendments. Hence, any agronomic practice that improves soil fertility can improve the yield of cowpea.

Biochar, a product of organic matter pyrolysis, has the ability to improve soil health and sequence carbon when applied as soil amendments (Atkinson *et al*., 2010; Lehmann and Joseph, 2015). In addition, biochar improves crop yield, and enhances soil productivity (Chibuike-Ezepue *et al*. (2019)). The use of biochar has gained increasingly acceptance especially in the tropics, where the soils are highly weathered and low in productivity.

Crop improvements as a result of biochar application to the soil are attributed mainly to the biochar as soil conditioner, nutrient addition directly from the applied biochar and/or improvement of nutrient utilization efficiency, especially when combined with other organic or inorganic amendments (Chibuike-Ezepue *et al*., 2019). Research on biochar alone or combined with other fertilizers as a soil amendment for crop yield improvement reported positive effects on crop growth (Chen *et al*., 2010; Shen *et al*., 2016; Solaiman *et al*., 2010). However, information on the relationship between changes in soil properties, particularly biological properties, after biochar addition and the subsequent effect on crop growth is still lacking (Chibuike-Ezepue *et al*., 2019). Such biological properties include symbiotic relationships between plants and microorganisms (Babalola *et al*., 2007). There is a need to decipher the effect of biochar on nitrogen-fixing organisms and mycorrhiza root colonization, which are pivotal in N and P nutrition in tropical soils. Root nodules, which harbor rhizobia that fix nitrogen, could be used as a measure of the effect of biochar on nitrogen fixation and on the rhizobia growth (Xin *et al*., 2022).

Despite the growing interest in sustainable agriculture, a significant gap remains in our understanding of the effects of biochar on microbial symbioses, particularly in relation to root nodules, mycorrhizal colonization, and spore count. This study aims to address this gap by investigating the impact of biochar, both alone and in combination with NPK (15:15:15) or cattle dung, on cowpea. By exploring these interactions, we can enhance our knowledge of biochar's role in promoting plant health and productivity, which is crucial for developing more effective agricultural practices.

Materials and methods

Site description for the field experiment

The fieldwork was done in Faculty of Natural and Agricultural Science Farmland in North-West University, Mafikeng campus (longitude 25° 48' S, latitude 25° 38' E; 1218 m asl) in North West Province, South Africa. Mafikeng has a typical semi-arid tropical savanna climate and receives summer annual mean rainfall of 571 mm. The surface (0-20 cm) soil at the site is brown to dark reddish brown sandy loam classified as Hutton form according to the South African soil classification system (Soil Classification Working Group, 1991).

Experimental design and treatments

The experimental design used in this study was a randomized complete block design with three replications. Land area measuring 210 m^2 (15 m x 14 m) was mechanically ploughed and harrowed before being demarcated into 18 plots (6 treatments by 3 replications/blocks). The plot size was 3.75 m x 1.25 m with intra- and inter-block spacing of 1 m. Three cowpea seeds were planted per hole at a spacing of 0.75 m x 0.25 m, which were thinned down to one per hole three weeks after germination. The final plant population was 20 plants per plot. The experimental plots were manually kept weed free, while irrigation was applied using the sprinkler method.

The six treatments evaluated in this study are (i) sole application of biochar produced from pine wood at the rate of 5 tonnes per hectare, (ii) sole application of cattle dung at the rate of 5 tonnes per hectare, (iii) sole application of mineral fertilizer $NPK_{15:15:15,}$ at the rate of 60 kg per hectare (iv) combined application of biochar and cattle dung at half the rate of the sole applications, (v) combined application of biochar and cattle dung at half the rate of the sole applications, and (vi) control (no soil amendment).

The cattle dung was applied two weeks before planting to allow for mineralization, while the biochar and NPK were applied at planting. The experiment was established in October 2017 and terminated in February 2018. To assess the residual impact of the treatments on soil fertility, cowpeas were planted on the plots without applying other treatments. The second field planting was established in February 2018 after harvesting the initial planting was harvested and was terminated in June 2018.

Sample/Data collection

The chlorophyll content, vine length and girth, leaf length and girth, number of root nodules, shoot and root fresh/dry weight and mycorrhizal colonization were determined as detailed below: The chlorophyll meter (CCM-200 plus) was

used to measure chlorophyll content in cowpea leaves. The measurements were done 3 times in the first cultivation, while in residual biochar evaluation, measurements were done twice. The first measurement for each cropping period was carried out one month after treatment application and subsequently at monthly intervals. A measuring tape was used to estimate vine length, girth, and leaf length before and after the cowpea legume was uprooted. The measurements were recorded.

Root harvesting and nodule count

A day before root harvesting, the plot was irrigated to wet the soil for root harvesting so that root nodules would not be lost in the soil. After root harvesting, roots were washed in a basin under running water. The nodules from washed roots were counted.

Yield parameters

The fresh roots and shoots were air-dried inside the screen house, and their weight was obtained by weighing them on a weighing balance (RADWAG WagiElektroniczne, Poland).

Laboratory analysis

Cowpea root mycorrhizal colonization. The roots were cut into pieces and cleared in 2% (w/v) KOH for 15 min at 120°C in an autoclave. Using a fine sieve, the roots were rinsed with water three times and then covered with 2% (v/v) hydrogen chloride (HCl) for 30 min. After 30 min, the HCl was thrown away, and the roots were covered with 0.05% (w/v) trypan blue in lacto glycerol for 15 mins in an autoclave. The roots were then placed onto a petri dish with 50% (v/v) glycerol for de-staining and were viewed under a stereomicroscope.

Mycorrhiza spore extraction and characterization. Mycorrhiza spores were extracted by the sucrose floatation method. After extraction, microscopic slides were prepared, and different mycorrhiza species were identified, counted and photographed.

Statistical analysis

Data generated from this study were subjected to analysis of variance using GenStat discovery 4 edition software. The significant means were separated using Fischer's least significant difference at 5% probability level. Correlation coefficient analysis was performed to understand the relationships among the measured parameters. The GGE Biplot was used to rank the performance of the treatments.

Results

Effect of soil amendments with biochar on root nodules and root properties

The nodule number was significantly ($p<0.05$) affected by the treatments in both years (Table 1). In the first year, the highest number of nodules was obtained from roots of plants grown on biochar + cattle dung applied plots (32) and the least was from the control and NPK plots (15). Roots of plants grown on the sole biochar amended plot had 25 nodules. Combine the application of biochar with either cattle dung or NPK improved the number of nodules over the sole application. In the second cultivation, the highest nodule number was obtained from control and biochar.

Cowpea root length in the first year of cultivation was not significantly ($p<0.05$) affected by the treatments, while root weight in the second year of cultivation was not significantly ($p<0.05$) affected by treatments. Root weight in the first year of cultivation was significantly affected by the treatments, with biochar + cattle dung having the highest root weight (7.12 g); following by biochar + NPK (5.66 g). Control plots had the least root weight (3.80 g). In the second cultivation, root length was significantly ($p<0.05$) affected by the treatments. Control had the least root length (14.37 cm). NPK amended plot had the highest root length (24.20 cm), followed by biochar + NPK (23.27 cm), following by biochar + cattle dung (22.53).

The coefficient of variation (CV) ranged from low to moderate in all the parameters (1 to 50%) except root weight, which had a high CV% (55.7). This shows that the treatment effect varied most in root weight.

Table 1. Effect of soil amendment on root nodulation and root parameters

Soil treatment	First planting			Residual planting		
	Nodule number	Root length (cm)	Root weight (g)	Nodule number	Root length (cm)	Root weight (g)
Control (0 tha^{-1})	15	29.7	3.80	7	14.37	3.37
Biochar (5 tha^{-1})	25	27.7	5.46	5	16.40	5.40
NPK (60 kg ha^{-1})	15	26.0	4.31	4	24.20	5.76
Cattle dung (5 tha^{-1})	16	26.3	5.32	4	17.10	4.76
Biochar +NPK	19	34.7	5.66	4	23.27	5.50
Biochar +cattle dung	32	27.4	7.12	7	22.53	3.72
Cv (%)	36.4	19.4	30.2	27.2	12.9	55.7
F-LSD	13.61	Ns	2.99	2.77	4.59	Ns

Note: CV = coefficient of variation, ns = means not significant at 5%

Effect of biochar soil amendments, including on cowpea growth parameters and dry matter yield

Most of the growth parameters had low to moderate coefficient of variation (1 to 50%). Of all the parameters, only leaf lengths at 1MAP (month after planting) and 2MAP during the second-year planting were not significantly ($p<0.05$) affected by the treatments (Table 2). Biochar + cattle dung had the highest vine length 1MAP (38.80 cm) during the first year of planting. Sole cattle dung was recorded 33.33 cm vine length 1MAP, while biochar + NPK had the highest vine length 2MAP (63.1 cm). This was followed by biochar + cattle dung (50 cm). Among the sole applications, cattle dung produced the highest vine length 2MAP (48.7 cm) followed by biochar (47.7 cm), and the least vine length was from NPK-amended plots (39.3 cm). All the values obtained in the treatment's variants were higher than that of control. In the second-year planting, similar trend was observed.

Regarding leaf length, biochar + cattle dung had miniature leaf lengths at 1MAP and 2MAP (7.27 cm, 9.17 cm), followed by the control (7.33 cm, 9.33 cm). Amendment with biochar ensured the highest initial plant leaf length (9.50 cm), while the highest subsequent leaf length II was obtained from the NPK amended plot (11.23 cm). In the second year of cultivation, although the treatments did not significantly affect the leaf lengths, control had the least value. The highest leaf length during the second cultivation was obtained on plant cultivated on biochar + cattle dung plot (10.03 cm), followed by sole biochar (10.0 cm).

Table 2. Soil amendments, plant growth properties and dry matter yield

Soil treatment	First planting					Residual planting				
	Vine length 1MAP (cm)	Vine length 2MAP (cm)	Leaf length 1MAP (cm)	Leaf length 2MAP (cm)	Dry matter Yield (g)	Vine length 1MAP (cm)	Vine length 2MAP (cm)	Leaf length 1MAP (cm)	Leaf length 2MAP (cm)	Dry matter yield (g)
Control (0 tha^{-1})	28.3	34.7	7.33	9.33	53	23.0	31.6	6.40	7.87	3.06
Biochar (5 tha^{-1})	31.57	47.7	9.50	10.87	214	34.4	44.6	8.27	10.00	5.33
NPK (60 kg ha^{-1})	30.78	39.3	8.70	11.23	87	27.23	33.9	7.57	8.07	4.75
Cattle dung (5 tha^{-1})	33.33	48.7	9.30	10.60	125	38.07	44.4	8.7	9.07	6.67
Biochar +NPK	30.67	63.1	9.33	10.50	176	38.67	46.1	8.27	9.33	5.78
Biochar +cattle dung	38.80	50.0	7.27	9.17	123	33.47	42.2	8.53	10.03	7.07
Cv (%)	11.3	50.7	10.5	9.2	39.8	11.9	12	22.3	24.5	32.9
F-LSD	6.65	23.88	1.64	1.73	4.10	7.02	8.94	Ns	ns	3.25

Note: MAP = months after treatment application, CV = coefficient of variation, ns means not significant at 5%

The difference in dry matter yield between the first year and the second year was most likely because of winter that caught with the second cultivation, terminated the growth processes, and finally dried the plant. In the first year of planting, the highest dry matter yield was obtained from sole biochar (214 g), this result was followed by that of biochar + NPK (176 g). The least dry matter yield was obtained from control plots (53 g), followed by sole NPK amended plots (87 g). In the second year of planting, biochar + cattle dung ensured the highest dry matter yield (7.07 g) and the least was equally from the control plot (3.06 g).

Treatment effects on chlorophyll content of the plants

The treatments significantly affected chlorophyll content (Table 3). At one month after treatment application leaf chlorophyll content was as follows: NPK (84.7) > biochar + NPK (76.7) > cattle dung (66) >biochar (60.3) > biochar +cattle dung > control (36.6). The last measurement in the first year of planting showed that the results obtained from all treatments, were the same except biochar + cattle dung, which was significantly higher and different from all other treatments.

In the second year of planting, the chlorophyll content was generally lower than the first. And only two measurements were possible during the second year of cultivation. In the first year of planting, control had the least chlorophyll content (8.9), while in the second year, biochar + NPK had the least value (12.5). The first measurement showed that NPK amended plot had the highest chlorophyll content (45.9) > biochar + cattle dung (32.7) > biochar +NPK (32.3). In the second measurement, chlorophyll content order in plants cultivated with biochar treatment (49.7) > NPK (34.4) >cattle dung (27.8) >control (18.4) >biochar +cattle dung (15.3) >biochar +NPK (12.5).

Table 3. Effect of soil amendments on chlorophyll content of cowpea leaves

Soil treatment	First planting		Residual planting		Residual biochar application
	One Month after treatment application	Two Month after treatment application	One Month after treatment apllication	Two Month after treatment application	
Control (0 tha^{-1})	36.6	89.1	81.4	8.9	18.4
Biochar (5 tha^{-1})	60.3	105.1	122	17.3	49.7
NPK(60 kg ha^{-1})	84.7	87.8	101	45.9	34.4
Cattle dung (5 tha^{-1})	66	91.6	103.6	18.7	27.8
Biochar +NPK	76.7	107	82.4	32.3	12.5
Biochar +cattle dung	52.3	77.8	142.5	32.7	15.3
Cv	19.6	19	21.9	33.2	27.2
F-LSD	22.37	32.20 (ns)	42.04	15.95	13.02

Correlation analysis of the combination of the parameters of the two years of planting

The analysis reveals that dry matter yield (DMY) exhibits strong and significant positive correlations with several parameters, indicating its close relationship with these traits (Table 4). DMY is strongly correlated with root length (RL) ($r = 0.554$, $p < 0.01$), highlighting the importance of robust root development in contributing to biomass production. Furthermore, leaf chlorophyll content, measured at two stages (LC1MAP and LC2MAP), shows significant positive relationships with DMY, with LC2MAP having a particularly strong correlation ($r = 0.751$, $p < 0.01$). This suggests that higher chlorophyll content, especially during later growth stages, is a critical factor for achieving greater dry matter accumulation.

Leaf length at two stages (LL1MAP and LL2MAP) also contributes positively to DMY, as indicated by their significant correlations with LC2MAP ($r = 0.644$, $p < 0.01$) and RL. Interestingly, vine length at an earlier stage (PH1MAP) has a significant negative correlation with DMY ($r = -0.368$, $p < 0.05$), implying that early vigorous growth in height may not necessarily translate to higher dry matter yield, potentially due to resource allocation dynamics.

Table 4. Correlation coefficient of cowpea growth and yield parameters

	PH1MAP	PH2MAP	LL1MAP	LL2MAP	RL	NOS	WOR	NON	LC1MAP	LC2MAP	DMY
PH1MAP	1	0.246	0.212	0.024	-0.180	-0.091	-0.027	-0.232	-0.114	-.359*	-.368*
PH2MAP		1	.443**	.356*	0.152	-0.213	0.006	0.070	0.130	0.225	0.061
LL1MAP			1	.796**	0.203	0.006	0.202	-0.019	.385*	.367*	0.283
LL2MAP				1	0.201	0.072	0.244	0.097	.329*	.440**	0.300
RL					1	0.145	.573**	0.117	.508**	.613**	.554**
NOS						1	.460**	0.061	-0.007	-0.015	0.016
WOR							1	0.184	0.220	0.134	0.318
NON								1	0.142	.389*	.451**
LC1MAP									1	.676**	.644**
LC2MAP										1	.751**
DMY											1

Note: **.and * Correlation is significant at the 0.01 and 0.05 levels (2- tailed), 1MAP = one month after treatment application, 2MAP = two months after treatment application, PH = vine length, LL = leaf length, RL = root length, NOOS = number of offshoots. WOR = weight of roots, NON = number of nodules, LC = leaf chlorophyll, and DMY = dry matter yield

The biplot graph indicates that principal components (PC)1 and 2 explained 71.7% of the variation among the parameters measured (Figure 1). The biplot has five sections with five out of the six treatments occupying the vertex of the polygon. The section occupied by biochar + NPK (B1fnpk) contained most of the parameters (dry matter yield, vine length, root weight, root length, and number of nodules) while the leaf length and number of offshoots were housed in the biochar alone section (B1). The position of the control (B0) opposite the best performing treatment (biochar + NPK) indicates its poor performance in the selected parameters.

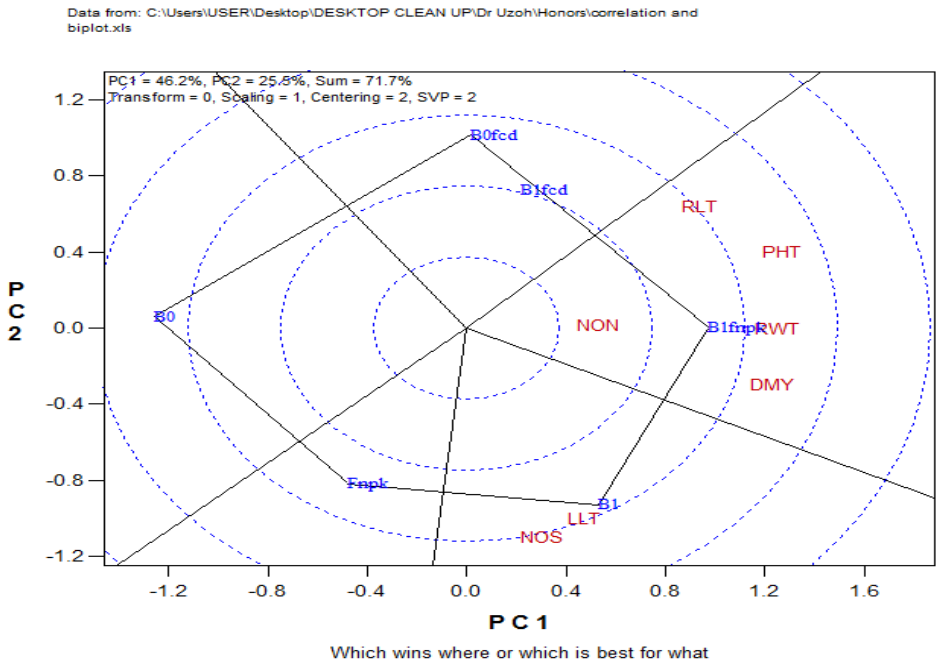

Figure 1. Graph of which-wins-where of the soil amendment treatments

Mycorrhizal colonization

The fungal mycorrhizal analysis under stereomicroscope resulted in visualization of hyphae, vesicles and arbuscules (Figures 2-5). Amendment with biochar gave the highest arbuscules, but hyphae was less visible, while in cattle dung-treated soil, there were more hyphae but fewer arbuscules. Cattle dung and biochar gave higher arbuscules than the control.

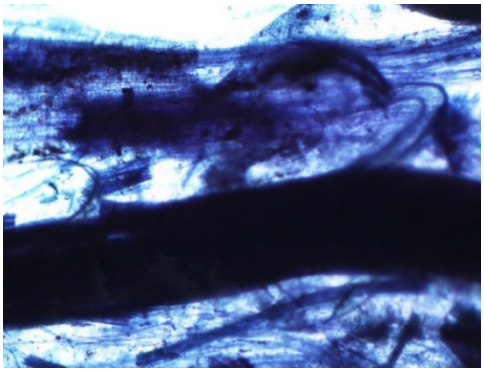

Figure 2. Cowpea roots treated with biochar alone (B1) showing darker arbuscules (38 visible arbuscules).

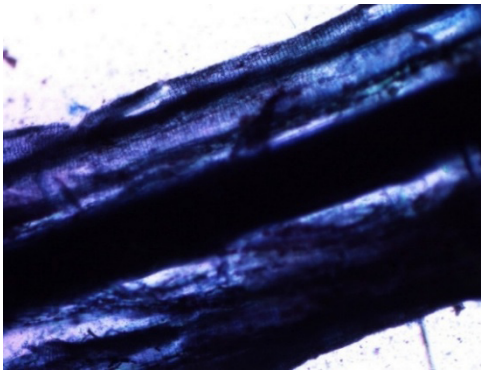

Figure 3. Cowpea roots treated with biochar + cattle dung with less arbuscules (10 visible arbuscules)

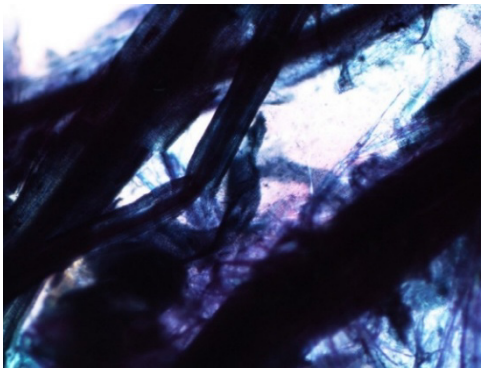

Figure 4. Cowpea roots of control had no visible arbuscules, but the hyphae observed were turbid.

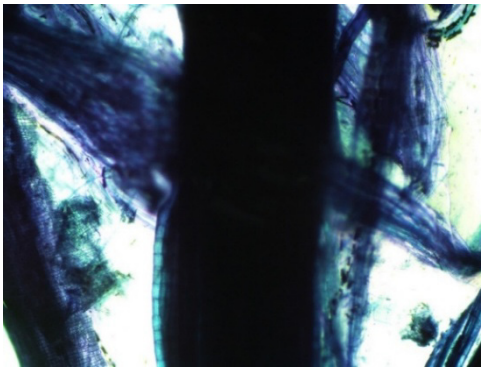

Figure 5. Cowpea roots treated with cattle dung showing both the arbuscules (16 visible arbuscules) and hyphae.

Mycorrhiza spore count in the soil

Effect of the treatments was evaluated on the mycorrhiza spore count in the soil after cultivation of cowpeas. Five mycorrhizae species were isolated from most of the treated soil, which include *Acaulospora, Glomus, Scutelospora, Gigaspora* and *Entrophospora*. Among these isolates, three namely, *Acaulospora, Glomus* and *Entrophospora* were significantly affected by the treatments. There was variability in the overall occurrence and the sequence of occurrence in both treated and untreated soils. Glomus had the highest number of spores in all the soils. It had hundreds of spores in almost all the treatment variants. *Acaulospora*

also had hundreds of spores, *Entrophospora* occurred in tens while *Scutelospora* was also in tens but fewer than *Entrophospora. Gigaspora* spores were found only in control, biochar plus NPK and NPK amended plots in few numbers. Apart from *Acaulospora*, which was higher in biochar amended plot, the control plot had higher spores than the amended plots. In control plots, Glomus and *Entrophospora* had the highest soil spores (365, 100). Sole biochar amended plots and biochar plus NPK amended plots had the next highest *Entrophospora* (232) and Glomus (268) spores, respectively. The biochar plus cattle dung amended plots had the least spores of all the mycorrhiza species. Sole biochar amended plots had the highest *Acaulospora* spores (308), which was significantly ($p < 0.05$) the same as control plots (289). Considering the amended organic and inorganic soils, apart from sole biochar, NPK or biochar plus NPK had higher mycorrhiza spores than cattle dung or biochar plus cattle dung in most of the isolates. Figure 6 shows the mycorrhiza spores while Figures 7 – 11 shows the different species with their characteristic features.

Table 5. Effect of soil amendment on soil mycorrhiza spore count

Soil Treatment	*Acaulospora*	*Glomus*	*Scutelospora*	*Gigaspora*	*Entrophospora*
Control (0 tha^{-1})	289^{a}	365^{a}	11^{a}	6^{a}	100^{a}
Biochar (5 tha^{-1})	308^{a}	232^{ab}	11^{a}	0^{a}	83^{ab}
Cattle dung (5 tha^{-1})	243^{a}	177^{b}	17^{a}	0^{a}	62^{abc}
NPK (60 kg ha^{-1})	243^{a}	198^{ab}	23^{a}	13^{a}	29^{bc}
Biochar +cattle dung	82^{b}	90^{b}	0^{a}	0^{a}	20^{c}
Biochar +NPK	209^{a}	268^{ab}	19^{a}	14^{a}	58^{abc}

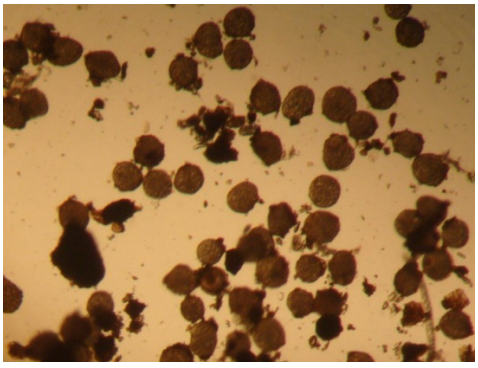

Figure 6. Mycorrhiza spores

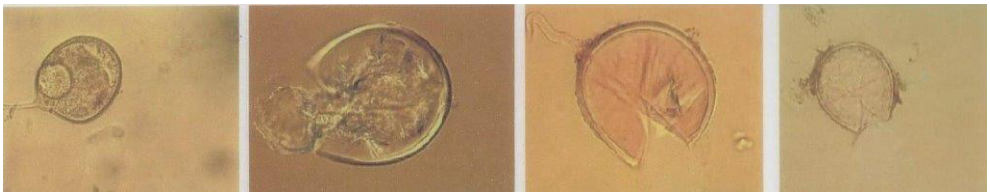

Figure 7. *Glomus intradices*

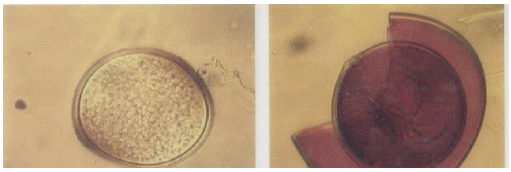

Figure 8. *Scutelospora calospora*

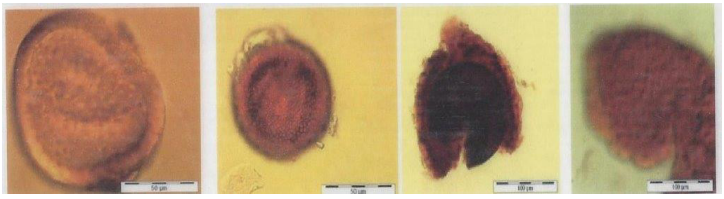

Figure 9. *Entrophospora colombiana*

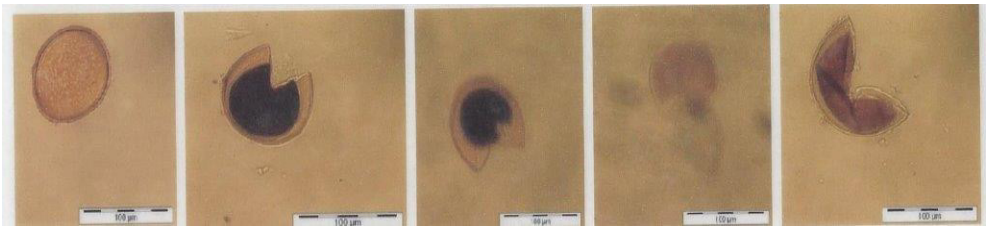

Figure 10. *Acaulospora mellea*

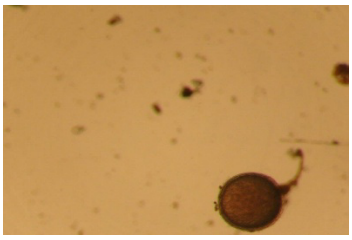

Figure 11. *Gigaspora* species

Discussion

Effect of soil amendments with biochar on root nodules and root properties

Roots are a significant part of a plant because it is an interface between nutrient and water absorption from the soil and any amendment added to it and the crop growth and development. Properties of the root are therefore very vital because these affect how the root accomplishes its task of nutrient and water absorption into the plant. Biochar soil amendment, according to Xiang *et al*. (2017) may change root development and properties, which inevitably affect crop performance. In this research, the sole application of biochar or in combination with NPK or cattle dung soil amendments increased root length and weight over the control. Xiang *et al*. (2017) found that responses of root traits associated with 13 variables under biochar application had increased root biomass (+32%), root volume (+29%) and surface area (+39%). They also found that biochar increased the number of root nodules, just as was confirmed with findings of this research. In both years, soil amendment increased the number of root nodules. The reason for observed increase in root properties was likely as a result of improvement in soil properties by those soil amendments. Biochar increases soil pH, nutrient status and cation exchange capacity (CEC) (Vanek and Lehmann, 2015), which invariably should improve root properties in biochar-applied plots (Macdonald *et al*., 2014; Olmo *et al*., 2016). Integration of NPK or cattle dung into biochar amendment enhanced root length and weight. Alburquerque *et al*. (2015) observed that biochar applied with NPK was found to interactively influence root growth.

Effect of soil amendments on growth parameters and dry matter yield

Amendments used in this research improved cowpea growth parameters and, most significantly, the dry matter yield. All the amendments had higher dry matter yield than the control. Applying biochar to soil can increase crop yields (Quilliam *et al*., 2013) and biochar applications may be helpful in developing more sustainable food production systems (Liu *et al*., 2017). In this study, biochar, cattle dung, NPK or their combination positively affected cowpea growth parameters and dry matter yields. This agrees with the result of Suthar (2012).

The combined insights from the correlation analysis and the GGE biplot reveal key relationships between dry matter yield and other agronomic parameters, as well as the differential performance of treatments in promoting specific traits. The correlation analysis underscores the importance of traits like root length and leaf chlorophyll content in driving DMY. The strong positive correlation between DMY and RL highlights the critical role of robust root

development in cowpea biomass production. Longer roots likely improve water and nutrient uptake, particularly under stress conditions, which translates to greater dry matter accumulation (Santos *et al*., 2020). Similarly, the significant positive correlations between DMY and LC, particularly at two months after treatment application, suggest that maintaining higher chlorophyll content during later growth stages is crucial for enhanced photosynthetic efficiency and biomass production. Wanjiku *et al* (2023) observed a significant increase in cowpea leaf chlorophyll content as the plant advances in age.

Leaf length at different growth stages also contributes positively to DMY, with LL1MAP and LL2MAP correlating significantly with RL and LC2MAP. This indicates that leaf expansion, coupled with enhanced chlorophyll content, optimizes photosynthetic capacity and resource capture, thereby supporting higher biomass yield. These findings align with Atugwu *et al*. (2023), who observed a significant correlation between cowpea leaf length and dry matter yield. Interestingly, vine length at an earlier stage shows a negative correlation with DMY, suggesting that excessive early vegetative growth in height may divert resources from other processes critical for dry matter accumulation.

The GGE biplot analysis further complements these findings, explaining 71.7% of the variation among parameters and showcasing the distinct performance of treatments. The "which-won-where" result identifies biochar + NPK as the most effective treatment, with DMY, RL, LC, root weight, and number of nodules all grouped within its polygon section. This indicates that biochar + NPK amendment promotes traits that directly contribute to enhanced biomass production, likely due to the synergistic effects of biochar and NPK in improving soil fertility, nutrient availability, and root-soil interactions. In contrast, the control was ranked low in the biplot analysis which indicates that cowpea responds to soil amendments even though it can fix nitrogen through its symbiotic relationship (Atugwu *et al*., 2023; Nkaa *et al*., 2014). The findings suggest that treatments that enhance both root system development and chlorophyll content are most effective in boosting biomass production. Yield is a polygenic trait that can be enhanced by identifying and modifying the morphological qualities that influence it (Chukwudi, 2021). Root traits, including RL and NON, appear to play pivotal roles in supporting nutrient and water uptake, which are critical for dry matter accumulation. Similarly, the strong relationship between LC and DMY highlights the importance of maintaining photosynthetic efficiency during later growth stages for maximizing yield.

Mycorrhizal colonization

The mycorrhizal colonization results showed the presence of hyphae, arbuscules and nodules in the roots. Biochar treated soil had the highest arbuscules showing high mycorrhizal colonization. Solaiman *et al*. (2010) also

showed that addition of biochar increases mycorrhizal colonization. In addition, cattle dung treated soil also had arbuscules showing mycorrhizal colonization. Although cattle dung treated soil had less arbuscules than biochar-treated soil. This also is in consonance with Muthukumar and Udaiyan (2002), who noted that the effect of organic manure on mycorrhizal colonization depends on the organic manure used. The combined application, which shows evidence of mycorrhizal colonization. Gryndler *et al*. (2001) observed that organic manure and mineral fertilization increases mycorrhizal colonization by increasing hyphal length. The hyphae help in the absorption of nutrients from the soil and transport them to the rest of the plant and arbuscules penetrate the cortical cells.

Mycorrhiza spore count in the soil

Spores of *Glomus* species was found in both amended and non-amended plots and in greatest number. Several studies of agricultural soil have shown dominance of Glomus species (Gunwal *et al*., 2014; Mathimaran *et al*., 2005) in such soils. The reason for the above observation was as result of the higher colonization efficiency of Glomus species than other mycorrhiza species. The five isolates reported from this study have also been indicated to be found in agricultural soils (Jansa *et al*., 2005). Except for amended soil, organic manure-amended plots showed lower spores of mycorrhiza than inorganic fertilizer amended plots. It's assumed that in organic fertilizer-amended plots phosphorus availability is higher than in inorganic fertilizer-amended plots (Xin *et al*., 2022). And as such leads to lower mycorrhiza colonization (Garcia and Zimmermann, 2014). Johnson (2010) observed that nutrient-stressed plants release more soluble carbohydrates in root exudates, which support more mycorrhiza than plants with sufficient nutrients. It has been noted that in high availability of phosphorus, that mycorrhiza colonization or sporulation is low. Other findings of mycorrhizal response in organic amended soils have shown diverse opinions. Aleklett and Wallander (2012) reported an increase in AMF growth from adding N-rich organic residue. Organic residue with low N didn't affect AMF colonization while Hammer *et al*. (2011) and Gryndler *et al*. (2009) found an increase in plant response to mycorrhiza and spore count.

Conclusion

Biochar soil amendments significantly improved mycorrhiza root colonization and spore count, root nodulation, root properties and cowpea dry matter yield when compared either to control or, in some cases, the other treatments that were added to the soil. The study was able to explain the

beneficial effect on yield attributed to biochar soil amendment. Correlation analyses show that the factors with a high correlation to dry matter yield mainly were improved by biochar soil amendment.

References

Abayomi, Y., Ajibade, T., Sammuel, O. & Saadudeen, B. (2008). Growth and yield responses of cowpea (*Vigna unguiculata* (L.) Walp) genotypes to nitrogen fertilizer (NPK) application in the Southern Guinea Savanna zone of Nigeria. *Asian J. Plant Sci.* 7, 170-176. https://scialert.net/abstract/?doi=ajps.2008.170.176

Abdel-Fattah, G. M. & Asrar, A.-W. A. (2012). Arbuscular mycorrhizal fungal application to improve growth and tolerance of wheat (*Triticum aestivum* L.) plants grown in saline soil. *Acta Physiol. Plant.* 34, 267-277. https://link.springer.com/article/10.1007/s11738-011-0825-6

Agbodjato, N. A. & Babalola, O. O. (2024). Promoting sustainable agriculture by exploiting plant growth-promoting rhizobacteria (PGPR) to improve maize and cowpea crops. *Peer J.* 12, e16836. https://doi.org/10.7717/peerj.16836.

Akanmu, A.O., Babalola, O.O., Venturi, V., Ayilara, M.S., Adeleke, B.S., Amoo, A.E., Sobowale, A.A., Fadiji, A.E. and Glick, B.R., 2021. Plant disease management: leveraging on the plant-microbe-soil interface in the biorational use of organic amendments. *Front. Plant Sci.* 12, p.700507. https://www.frontiersin.org/journals/plant-science/articles/10.3389/fpls.2021.700507/full

Alburquerque, J. A., Cabello, M., Avelino, R., Barrón, V., del Campillo, M. C. & Torrent, J. (2015). Plant growth responses to biochar amendment of Mediterranean soils deficient in iron and phosphorus. *J. Plant Nutr. Soil Sci.* 178, 567-575. https://doi.org/10.1002/jpln.201400653

Aleklett, K. & Wallander, H. (2012). Effects of organic amendments with various nitrogen levels on arbuscular mycorrhizal fungal growth. A *Appl. Soil Ecol.* 60, 71-76. https://doi.org/10.1016/j.apsoil.2012.03.007

Atkinson, C. J., Fitzgerald, J. D. & Hipps, N. A. (2010). Potential mechanisms for achieving agricultural benefits from biochar application to temperate soils: A review. *Plant Soil* 337, 1-18. https://rdcu.be/eqIpw

Atugwu, A. I., Chukwudi, U. P., Eze, E. I., Ugwu, M. O. & Enyi, J. I. (2023). Growth and yield attributes of cowpea accessions grown under different soil amendments in a derived Savannah zone. *AIMS Agric. Food* 8(4), 932-943. https://doi.org/10.3934/agrfood.2023049

Ayangbenro, A. S., Odelade, K. A. & Babalola, O. O. (2023). Seasonal variation drives microbial diversity in cowpea rhizosphere in a semi-arid region. *Int. J. Agric. Biol.* 29, 201–208. https://doi.org/10.17957/IJAB/15.2020

Babalola, O. O., Sanni, A. I., Odhiambo, G. D. & Torto, B. (2007). Plant growth-promoting rhizobacteria do not pose any deleterious effect on cowpea, and detectable amounts of ethylene are produced. *World J. Microbiol. Biotechnol.* 23(6), 747–752. https://doi.org/10.1007/s11274-006-9290-6

Chen, Y., Shinogi, Y. & Taira, M. (2010). Influence of biochar use on sugarcane growth, soil parameters, and groundwater quality. *Soil Res*. 48, 526-530. https://doi.org/10.1071/SR10011

Chibuike-Ezepue, G., Uzoh, I. & Unagwu, B. (2019). Biochar-induced modification of soil properties and the effect on crop production. *Adv. Agric. Sci.* 7, 59-87. https://aagri.org/file/journals/1/articles/153/submission/proof/153-1-769-3-10-20190614.pdf

Chinma, C., Alemede, I. & Emelife, I. (2008). Physicochemical and functional properties of some Nigerian cowpea varieties. *Pak. J. Nutr*. 7, 186-190. https://www.cabidigitallibrary.org/doi/full/10.5555/20083153188

Chukwudi, U. P. (2023). Ginger germplasm classification and identification of morphological markers related to rhizome yield. *Crop Sci*. 63, 248–254. https://doi.org/10.1002/csc2.20850

Ddamulira, G., Santos, C. A. F., Obuo, P., Alanyo, M. & Lwanga, C. K. (2015). Grain yield and protein content of Brazilian cowpea genotypes under diverse Ugandan environments. *Am. J. Plant Sci*. 6, 2074. https://www.scirp.org/journal/paperinformation?paperid=59175

Emmanuel, O. C., Akintola, O. A., Tetteh, F. M. & Babalola, O. O. (2021). Combined application of inoculant, phosphorus, and potassium enhances cowpea yield in Savanna soils. *Agronomy* 11, 15. https://doi.org/10.3390/agronomy11010015

Garcia, K. & Zimmermann, S. D. (2014). The role of mycorrhizal associations in plant potassium nutrition. *Front. Plant Sci*. 5, 337.

Gryndler, M., Hršelová, H., Cajthaml, T., Havránková, M., Řezáčová, V., Gryndlerová, H. & Larsen, J. (2009). Influence of soil organic matter decomposition on arbuscular mycorrhizal fungi in terms of asymbiotic hyphal growth and root colonization. *Mycorrhiza*, 19, 255-266. https://doi.org/10.1007/s00572-008-0217-y

Gryndler, M., Hršelová, H., Vosatka, M., Votruba, J. & Klir, J. (2001). Organic fertilization changes the response of mycelium of arbuscular mycorrhizal fungi and their sporulation to mineral NPK supply. *Folia Microbiol*. 46, 540-542. https://doi.org/10.1007/BF02817999

Gunwal, I., Sharma, K. & Mago, P. (2014). Spore density and root colonization by arbuscular mycorrhizal fungi in heavy-metal-contaminated soils. *IOSR J. Pharm. Biol. Sci*. 49-53. https://www.iosrjournals.org/iosr-jpbs/papers/Vol9-issue3/Version-3/K09334953.pdf

Hammer, E. C., Nasr, H. & Wallander, H. (2011). Effects of different organic materials and mineral nutrients on arbuscular mycorrhizal fungal growth in a Mediterranean saline dryland. *FEMS Microbiol. Ecol*. 43, 2332-2337. https://doi.org/10.1016/j.soilbio.2011.07.004

Igiehon, N. O. & Babalola, O. O. (2017). Biofertilizers and sustainable agriculture: Exploring arbuscular mycorrhizal fungi. *Appl. Microbiol. Biotechnol.* 101, 4871-4881. https://doi.org/10.1007/s00253-017-8344-z

Jansa, J., Mozafar, A. & Frossard, E. (2005). Phosphorus acquisition strategies within arbuscular mycorrhizal fungal community of a single field site. *Plant Soil* 276, 163-176. https://doi.org/10.1007/s11104-005-4274-0

Johnson, N. C. (2010). Resource stoichiometry elucidates the structure and function of arbuscular mycorrhizas across scales. *New Phytol.* 185, 631-647. https://doi.org/10.1111/j.1469-8137.2009.03110.x

Lehmann, J. & Joseph, S. (2015). Biochar for environmental management: An introduction. In: Biochar for environmental management (pp. 33-46). Routledge. https://doi.org/10.4324/9780203762264

Liu, L., Wang, Y., Yan, X., Li, J., Jiao, N. & Hu, S. (2017). Biochar amendments increase the yield advantage of legume-based intercropping systems over monoculture. *Agric. Ecosyst. Environ*. 237, 16-23. https://doi.org/10.1016/j.agee.2016.12.026

Macdonald, L. M., Farrell, M., Van Zwieten, L. & Krull, E. S. (2014). Plant growth responses to biochar addition: An Australian soils perspective. *Biol. Fertil. Soils* 50, 1035-1045. https://doi.org/10.1007/s00374-014-0921-z

Mathimaran, N., Ruh, R., Vullioud, P., Frossard, E. & Jansa, J. (2005). Glomus intraradices dominates arbuscular mycorrhizal communities in a heavy textured agricultural soil. *Mycorrhiza* 16, 61-66. https://doi.org/10.1007/s00572-005-0014-9

Muthukumar, T. & Udaiyan, K. (2002). Growth and yield of cowpea as influenced by changes in arbuscular mycorrhiza in response to organic manuring. *J. Agron. Crop Sci.* 188, 123-132. https://doi.org/10.1046/j.1439-037X.2002.00544.x

Nkaa, F. A., Nwokeocha, O. W. & Ihuoma, O. (2014). Effect of Phosphorus fertilizer on growth and yield of cowpea (*Vigna unguiculata*). *J. Pharm. Biol. Sci.* 9(5), 74–82. https://www.iosrjournals.org/iosr-jpbs/papers/Vol9-issue5/Version-4/N09547482.pdf

Ojo, A. O., Akinbode, O. A. & Adediran, J. A. (2011). Comparative study of different organic manures and NPK fertilizer for improvement of soil chemical properties and dry matter yield of maize in two different soils. *J. Soil Sci. Environ. Manage*. 2(1), 9-13. https://academicjournals.org/journal/JSSEM/article-full-text-pdf/0573C6210248

Omomowo, O. I. & Babalola, O. O. (2021). Constraints and prospects of improving cowpea productivity to ensure food, nutritional security, and environmental sustainability. *Front. Plant Sci.* 12, Article 751731. https://doi.org/10.3389/fpls.2021.751731.

Omomowo, W. & Babalola, O. O. (2023). Bioassessment of phylogenetic relatedness and plant growth enhancement of endophytic bacterial isolates from cowpea (*Vigna unguiculata*) plant tissues. *Horticulturae* 9(3), 332. https://doi.org/10.3390/horticulturae9030332.

Olmo, M., Lozano, A. M., Barrón, V. & Villar, R. (2016). Spatial heterogeneity of soil biochar content affects soil quality and wheat growth and yield. *Sci. Total Environ.* 562, 690-700. https://doi.org/10.1016/j.scitotenv.2016.04.089

Quilliam, R. S., DeLuca, T. H. & Jones, D. L. (2013). Biochar application reduces nodulation but increases nitrogenase activity in clover. *Plant Soil* 366, 83-92. . https://doi.org/10.1007/s11104-012-1411-4

Santos, R., Carvalho, M., Rosa, E., Carnide, V. & Castro, I. (2020). Root and agro-morphological traits performance in cowpea under drought stress. *Agronomy* 10(10), 1604. https://www.mdpi.com/2073-4395/10/10/1604

Shen, Q., Hedley, M., Camps Arbestain, M. & Kirschbaum, M. (2016). Can biochar increase the bioavailability of phosphorus? *J. Soil Sci. Plant Nutr.* 16, 268-286. http://dx.doi.org/10.4067/S0718-95162016005000022

Soil Classification Working Group. (1991). *Soil classification: A taxonomic system for South Africa* (2nd ed.). Department of Agricultural Development, Pretoria, South Africa. https://search.worldcat.org/title/1050392627.

Solaiman, Z. M., Blackwell, P., Abbott, L. K. & Storer, P. (2010). Direct and residual effect of biochar application on mycorrhizal root colonisation, growth and nutrition of wheat. *Soil Res.* 48, 546-554. https://www.publish.csiro.au/sr/sr10002

Suthar, S. (2012). Impact of vermicompost and composted farmyard manure on growth and yield of garlic (*Allium sativum* L.) field crop. *Int. J. Plant Prod*. 3, 27-38. http://www.gau.ac.ir/Jm/Programs/JurnalMgr/VolumArticle/EN_127_8.pdf

Vanek, S. J. & Lehmann, J. (2015). Phosphorus availability to beans via interactions between mycorrhizas and biochar. *Plant Soil* 395, 105-123. https://doi.org/10.1007/s11104-014-2246-y

Wanjiku, G. J., Kingori, G. G. & K. J. Kirimi (2023). Effect of harvesting stage on cowpea leaf nutrient composition. *Plant* 11(2), 50-59. https://doi.org.10.11648/j.plant.20231102.12

Xiang, Y., Deng, Q., Duan, H. & Guo, Y. (2017). Effects of biochar application on root traits: A meta-analysis. *GCB Bioenergy* 9, 1563-1572. https://doi.org/10.1111/gcbb.12449

Xin, Y., Fan, Y., Babalola, O. O., Zhang, X. & Yang, W. (2022). Legacy effects of biochar and compost addition on arbuscular mycorrhizal fungal community and co-occurrence network in black soil. *Microorganisms* 10, 2137. https://doi.org/10.3390/microorganisms10112137

STUDIA UNIVERSITATIS BABEŞ-BOLYAI BIOLOGIA, 70, 1, 2025 (p. 173-211)
doi:10.24193/subbbiol.2025.1.09

Tomato powder processing involving different pretreatments: its effect on quality of the product packaged in polyethylene terephthalate pouches

Faith Chidera Ekeh[1], Ihuoma Ahaotu[1], and Ndukwe Maduka[2]✉

[1]*Department of Microbiology, Faculty of Science, University of Port Harcourt, Choba, Rivers State, Nigeria;*
[2]*Department of Microbiology, Faculty of Science, Federal University Otuoke, Bayelsa State, Nigeria.*
✉***Corresponding author, E-mail:*** *madukann@fuotuoke.edu.ng*

Article history: Received 14 October 2024; Revised 02 December 2024; Accepted 04 March 2025; Available online 25 June 2025

Abstract. The method of drying fresh tomato (*Lycopersicon esculentum* mill) to prevent quick spoilage, could affect the quality of the product, and influence consumer acceptability. This study is focused on determining the effect of different pretreatments on the quality of tomato powders packaged in polyethylene terephthalate pouches, and stored for 16 weeks at room temperature (25±2 °C). A total of six tomato powder samples, which include the blanched ascorbic acid pretreated (BAAP), unblanched ascorbic acid pretreated (UAAP), blanched lime juice pretreated (BLJP), unblanched lime juice pretreated (ULJP), sundried without pretreatment (SDTP), and the control (without pretreatment; dehydrator used for drying), was prepared. The total viable counts (TVC) of the stored tomato powders were within the range of 4.40-7.31 $\log_{10}$CFU/g. Although the TVC of the samples increased within the first few weeks, the values reduced as the storage period increased. The SDTP tomato powder maintained a higher TVC compared with other stored samples. There was a reduction in pH, moisture, ash, titratable acidity, and vitamin C content of the powdered tomatoes. The lycopene content of tomato powders was within the range of 102.13±1.53-132.70±1.46 mg/100g, while the fruit tomato was 18.96±1.27 mg/100g. There were significant differences ($p<0.05$) in the functional properties of the tomato powders, with few exceptions. Different pretreatments increased the water absorption capacity and bulk density of the samples, but reduced their emulsion

stability. The BLJP and BAAP tomato powders had a very high sensory rating, whereas the SDTP sample was the least. Based on the overall results, blanched ascorbic acid pretreatment is recommended for the production of good quality tomato powder.

Keywords: ascorbic acid, blanching, lycopene, postharvest losses, shelf life.

Introduction

Tomatoes typically share the characteristics of fruit and vegetable (Degwale *et al*., 2022; Agada *et al.,* 2023). In some literature, tomato is assigned the scientific name *Solanum lycopersicum* L. (Zambare and Kulkarni, 2023; Obajemihi *et al*., 2024), while others refer to it as *Lycopersicon esculentum* mill (Kumar *et al*., 2016; Adedire *et al*., 2022). Tomato is recognized by the family it belongs to called Solanaceae, while the genus which it is also a member is referred as *Lycopersicon* (Farooq *et al*., 2020). Historical data provided useful evidence that made scientists to believe that tomatoes originated in South America, specifically in the Andean region of the continent. Agriculturists reported that the subtropical and tropical regions are conducive geographical regions for cultivating tomatoes in abundant (Oladipupo *et al.,* 2020).

A ripe fresh tomato can be eaten raw after it has been properly washed with clean water. This is applicable to a lot of fruits and vegetables. Millions of people across the world consume fruit tomatoes in various ways. Further processing of fruit tomatoes has led to the production of a range of products (paste, juice, puree, canned tomatoes, ketchup, dried powders, and pasta sauces) (Kumar *et al.,* 2021; Dūma *et al*., 2022).

It is estimated that tomatoes produced across the world is more than 171 million metric tons, annually. In 2018, 2020, and 2021, the global output of fruit tomato was 182, 186, and 189 million tons, respectively. After taken a lot of factors into consideration, experts projected that 220 million tons of tomatoes will be produced in the year 2030 (Collins *et al*., 2022; Silva *et al*., 2023; Chabi *et al*., 2024). The countries globally recognized as the major producers of tomatoes are China, the USA, Turkey, Egypt, and India (Dube *et al*., 2020; Ogunsola and Ogunsina, 2021). Since the five countries are self-sufficient in tomato production, they usually export the excess to foreign countries in need of the product. In West Africa, Nigeria is a leading country in tomato production. About 6 million tons of tomatoes are produced annually in Nigeria, (Aderibigbe *et al*., 2018; Agada *et al*., 2023). According to Alabi *et al*. (2023), the quantity of tomatoes produced in 2019 and 2020 in Nigeria is 3,798,939 and 3,693,722

tons, respectively. Although Nigeria is not among the top ten tomato producers globally, the country occupies the 13th position. The country accounts for 1.3% and 10.8% of the global and African total tomato output, respectively (Tafida *et al*., 2023).

The skin of tomatoes is reddish in colour when the fruit is ripe. Studies carried out by researchers have linked the reddish colour of ripe tomato to lycopene found in the skin of the fruit (Aguda *et al*., 2021). Fruit tomato is enriched with antioxidant compounds beneficial to human health. They include phenolic compounds, carotenoids, vitamins C, and D (Xu *et al*., 2018). Also found in fresh tomatoes are phenolic compounds which include phenolic acid and flavonoids. It has been well-reported that tomatoes contain carotenoids which include lycopene, α- and, β-carotenes (Hirata *et al*., 2024). Carotene, folate, niacin, vitamin A, B_1, B_2, B_6, B_{12}, C, E, K, and H are the vitamins present in tomato fruit in varying quantities (Yegrem and Dagnaw, 2022; Chabi *et al.,* 2024). Several bioactive compounds which include kaempferol, cholin, lutein, naringenin, and quercetin have been reported in fruit tomatoes (Abdusalam *et al.,* 2023). Minerals such as calcium, sodium, magnesium, phosphorus, zinc, iron, copper, manganese, potassium, boron, and sulfur are also found in tomatoes in varying quantities (Aggarwal *et al*., 2016; Farid *et al*., 2022; Chabi *et al*., 2024). Beta-carotene and lycopene found in tomatoes are linked to health benefits. That is why people who eat tomatoes regularly have reduced risk to suffer from prostate cancer and cardiovascular diseases (Aderibigbe *et al*., 2018; Collins *et al*., 2022). Prevention of certain diseases such as diabetes, atherosclerosis, asthma, and colon cancer are associated with consumption of fruit tomato (Aggarwal *et al*., 2016).

The moisture content of fruit tomato is usually above 90 %. Freshly harvested tomatoes deteriorate very fast as a result of increased activities of spoilage microorganisms favoured by high moisture content. Consequently, the market value of the fruit tomato depreciates as the days go by (Adejo *et al*., 2015; Aderibigbe *et al*., 2018; Farooq *et al*., 2020; Ahmad *et al*., 2022; Degwale *et al*., 2022). Without taking any concrete action after harvesting ripe fruit tomato to preserve it, spoilage of the fruits will take place within two weeks (Anisuzzaman *et al*., 2022).

Massive production of fruit tomato happens during the appropriate season in the year. It largely influences tomato output in many countries (Oboulbiga *et al*., 2022). During the season of plenty, the market is flooded with fresh tomatoes. The prices drop due to market forces of demand and supply. The period fresh tomato is abundant in the market is shorter than the off-season, when tomato scarcity persist and prices skyrocket, until the arrival of another season of harvest. This cycle is usually experienced in many African

countries, including Nigeria. In order to meet high demand for tomato especially during the off-season, importation of tomato concentrate mainly from China, Italy, and Singapore becomes a lucrative business (Oboulbiga *et al.,* 2022; Ossamulu *et al*., 2023). On yearly basis, it is estimated that Nigeria business owners import tomatoes worth US$70 million. This development is pathetic because the country produces enough quantity of tomatoes to feed her population (Amurtiya and Adewuyi, 2020).

With the intention of extending the shelf life of ripe fruit tomato, modern drying methods have been adopted by some researchers different from the traditional practice (Kumar *et al.,* 2016; Ladi *et al*., 2017; Yegrem and Ababele, 2022). The use of solar dryers, microwave drying, sun tunnel drying, and freeze-drying are some of the improved drying methods (Yadav and Ali, 2023; Zambare and Kulkarni, 2023; Gameh *et al*., 2024; Obajemihi *et al*., 2024). Despite the benefits of drying fresh tomatoes, the quality of the product is affected. Some researchers have noted that the application of various physical or chemical pretreatments before drying tomatoes could minimize or resist the reduction in quality of the product attributed to the usual drying process. Other benefits of pretreatments include reduction in the energy requirement, and length of time required for tomato to be properly dried (Yegrem and Dagnaw, 2022). It has been reported that the functional properties of tomato powder is affected during drying. A strategy to cushion the effect of functional property loss of dried tomato powder suggested by some researchers is the use of preservatives and weak acids prior to drying of tomato powder (Chawafambira and Maramba, 2022). The osmotic agents commonly used for pretreatment of tomatoes include NaCl, sucrose, potassium metabisulphate, sodium metabisulphite, sodium benzoate, calcium chloride, weak acids, and sugar. Thermal blanching is another pretreatment fresh tomato could be subjected to before drying. It involves the use of hot water or steam. After drying of tomato is properly done, the product could be stored in polyethylene bags, high density polyethylene (HDPE) bags, aluminum foil pouches, vacuum-packed using a nylon-polyethylene bag, polystyrene cups, polyvinylchloride (PVC) trays, metalized polyester film, low density polyethylene (LDPE), glass jars, and plastic containers (Yegrem and Ababele, 2022). The quality of tomato powder is significantly affected by different pretreatments and drying methods (Aderibigbe *et al*., 2018; Farooq *et al*., 2020; Yegrem and Ababele, 2022). A study was carried out by Sarker *et al*. (2014) to determine the effect of using a cabinet drier to dry sliced tomatoes at 60 ^{o}C. The researchers went further to store the pretreated samples in different wrapping materials for six months at ambient temperature. The various wrapping materials include (i) medium density polyethylene, (ii) HDPE, and (iii) laminated aluminum foil (LAF) pouches. After considering the overall

results from the study, the use of LAF pouches to store tomato powder and pretreatment of dried tomato powder using a salt solution of 1% $CaCl_2$ and 0.2% potassium metabisulphite was recommended.

The traditional method used by rural dwellers in developing countries to reduce drastically the moisture content of sliced fruit tomato is to expose the raw foodstuff under the sun. This drying method is affordable. The product becomes dehydrated after several days of sun-drying. Hot air is another cheap drying method adopted by rural dwellers to dehydrate fresh tomatoes (Farid *et al*., 2022). In addition to obvious benefit of drying fresh tomatoes which usually extend the shelf life of the product, the process also reduces its bulky size which has cost implications of transporting fresh tomato to the final consumer. One of the ingredients used in preparing ketchup, canned products, soup premixes, and sauces is dried tomatoes (Farooq *et al*., 2020; Zambare and Kulkarni, 2023).

Instead of discarding tomatoes that have started spoiling, it can be used to produce a highly soluble powder which has a useful application as a functional food ingredient. In the last few years, food industries are increasingly using tomato powder as a natural food colorant and nutritional additive (Hirata *et al*., 2024; Lyu *et al*., 2024).

Microorganisms are present in intact fruit tomatoes harvested from the farm. Several factors could influence the microbial population and diversity in fruit tomatoes. *Bacillus subtilis*, *Pseudomonas aeruginosa, Klebsiella* sp., and *Proteus mirabilis* are bacterial isolates, while fungal isolates which include *Penicillium* sp., *Rhizopus* sp., *Mucor* sp., *Aspergillus niger*, and *Rhizopus stolonifer* have been isolated from the so called "healthy tomatoes". Some of these bacterial and fungal species are involved in the spoilage of tomatoes (Aguda *et al*., 2021). Currently, there is limited information with regards to the bacterial and fungal species present in stored tomato powder, subjected to different pretreatments before drying, and packaged in different types of materials. Published works on tomato powder reported the population of microorganisms in the samples, but the researchers did not go further to identify the isolates (Sarker *et al*., 2014; Adejo *et al*., 2015, Ladi *et al*., 2017; Obadina *et al*., 2018; Aderibigbe *et al*., 2018; Leke and Bembur, 2023). Identification of microorganisms isolated from stored tomato powder is important because, the presence of pathogens in the product is a potential risk to consumers' health. It is wrong to assume that dried tomato powder is free from microbial contaminants that are pathogenic. Bawa *et al*. (2023) reported the presence of *Escherichia coli* which is a coliform bacteria and *Salmonella* sp. (ubiquitous in the environment) in the tomato powder meant for human consumption, but the researchers did not identify the yeasts and mold isolated from the samples. In this study, bacterial and fungal species isolated from tomato powder subjected to different pretreatments

was identified. The effect of different pretreatments and drying methods on the quality (physicochemical, nutritional, functional, and sensory properties) of tomato powder packaged inside polyethylene terephthalate pouches, and stored for 16 weeks at room temperature was determined.

Materials and methods

Source of tomatoes

About 200 kg of fruit tomatoes were purchased from Fruit Garden Market in Port Harcourt, Rivers state. The selection of tomato samples was based on ripeness and hardness. Soft and damaged tomatoes were separated and discarded from good ones. Each fruit tomato was cleaned three to four times with tap water and rinsed with distilled water.

Preparation of pretreatment solutions

The method describing how pretreatment solutions are prepared as earlier stated by Abano and Sam-Amoah (2011) was slightly modified and adopted in the present study. Preparation of fresh lime juice solution involved mixing 500 mL of lime juice and 500 mL of distilled water. 10% ascorbic acid solution was obtained by dissolving 100 g of food grade ascorbic acid powder (Heilongjiang NHU Biotechnologies, Europe) in 10 L of distilled water.

Sample preparation

Pretreatment of the tomato fruits

The tomato purchased from the Fruit garden were divided into six (6) equal parts. Each of the portions weigh 20 kg. The tomatoes were sliced into small irregular slices using a clean kitchen knife sterilized with 90% alcohol. The sliced tomato fruits were pretreated as follows:

(i) Control (CTRL): The sample was not pretreated. It was dried in a food dehydrator (model LY-FG2).

(ii) Sundried tomato powder (SDTP): The sample was not pretreated. It was dried under the sun.

(iii) Blanched lime juice pretreated (BLJP) sample: Tomato fruits was blanched with hot water for 1 minute, pretreated with lime juice (soaked for 10 minutes), and dried in a food dehydrator.

(iv) Unblanched lime juice pretreated (ULJP) sample: The tomato fruits were not blanched. It was pretreated by soaking it in a lime juice for 10 minutes, and dried in a dehydrator.

(v) Blanched ascorbic acid pretreated (BAAP) sample: The tomato fruits were blanched with hot water for 1 minute, pretreated by soaking it in a 10% ascorbic acid solution for 10 minutes, and dried in a dehydrator.

(vi) Unblanched ascorbic acid pretreated (UAAP) sample: The tomato fruits were not blanched. It was pretreated by soaking it in a 10% ascorbic acid solution for 10 minutes, and dried in a dehydrator.

Drying of samples

The portion of sliced fruit tomato which was sundried involved exposing the sample to direct sunlight for 8 hours. Other portions of sliced fruit tomato (i, iii-vi) were dried using a dehydrator sterilized with 90% alcohol. The temperature of the dehydrator was adjusted to 55 ^{o}C to dry the sliced tomatoes. The dried samples of tomato were milled to powder using a sterilized hammer mill machine. After milling each portion of the sliced and dried tomatoes, they were allowed to cool to room temperature. Without delay, each of the samples were packaged in polyethylene terephthalate pouches for storage, and further analysis. Each of the samples was properly labeled.

Serial dilution

Dilution of each sample of dried tomato powder was carried out (ten-fold serial dilution) by weighing 5 g of the sample in 45 mL of 0.1% sterile peptone water to yield a stock solution. The dilution was performed under aseptic conditions. Stepwise dilution of each sample of dried tomato powder was performed from the 10^{-1} dilution until 10^{-5} dilution was reached. Each stepwise transfer was performed using a sterile pipette.

Microbiological analysis

Isolation of bacteria and fungi

Under aseptic conditions, 0.1 mL of dilution 10^{-2} to 10^{-5} of the tomato powder samples was inoculated into freshly prepared plate count agar (PCA) and MacConkey agar (MCA) plates in accordance with manufacturer's instruction. To inoculate the samples on the agar plates, the spread plate method was used. Similarly, the diluted samples was aseptically inoculated onto Sabouraud dextrose agar (SDA) plates for the isolation of fungal species. The plates intended to isolate bacteria from the tomato powder samples were incubated at 37 ^{o}C in

a Memmert incubator (West Germany) for 48 hours. A longer incubation period of another set of plates (SDA) intended to isolate fungi from the samples lasted for 5 days at ambient temperature (28±2 °C). The colonies that appeared in each culture plate was totaled after counting was done manually and recorded. The total viable count (TVC) of each tomato powder sample was calculated and expressed in $\log_{10}$CFU/g. Monitoring of bacterial population of the tomato powder samples stored at room temperature (25±2 °C) was performed biweekly for 16 weeks.

Determination of pure cultures

Based on unique morphological characteristics of bacteria and fungi that appeared in the culture plates (MCA, SDA, PCA) after the incubation period, a wire loop sterilized by flaming it in a Bunsen burner was used to pick the isolates and subcultured using appropriate agar plates and incubation conditions maintained. Nutrient agar (NA) was used to subculture bacterial isolates. Pure isolates were identified using standard microbiological methods and molecular characterization. Sabouraud dextrose agar (SDA) plates were incorporated with antibiotics to prevent the growth of bacterial species which are contaminants. Repeated subculturing of each isolate was carried out using freshly prepared media until discrete colonies were obtained and transferred into slants. The slants were maintained until proper identification, and characterization of the isolates were concluded.

Identification of bacterial and fungal isolates

Distinct bacterial and fungal colonies that appeared on NA and SDA culture plates were picked based on the uniqueness of colonial characteristics, respectively. Each bacterial colony was characterized based on the colonial morphology, pigmentation, Gram reaction, motility, and biochemical tests performed using standard methods. The fungal isolates were identified based on lactophenol cotton blue stain, and morphological characteristics (Cruickshank *et al*., 1975; Harrigan and McCance, 1976; Samson and Hocstra, 1988; Ire *et al*., 2020).

Molecular identification

DNA extraction

In order to extract the deoxyribonucleic acid (DNA) present in the isolates, a ZR fungal/bacterial DNA mini prep extraction kit was used. The kit was imported from Inqaba, South Africa. A pure culture of each isolate that grew very well was aseptically transferred into e a ZR bashing bead lysis tube that contain

200 µL of isotonic buffer. 750 µL lysis solution was accurately measured and poured inside the lysis tube. Afterwards, the lysis tube was placed in a bead beater (it has a 2 mL tube holder). To achieve the purpose of releasing the lysed DNA inside the cell, machine carrying the lysis tube was operated at full speed for 5 minutes. Afterwards, the ZR bashing bead lysis tube was transferred to a centrifuge and spun for 1 minute at 10,000 x g. After centrifuging the sample, the supernatant measuring 400 µL was poured in a collection tube with an orange-top Zymo-Spin IV spin filter and spun at 8000 x g for 1 minute. The filtrate in the collection tubes was mixed with 1200 µL of fungal/bacterial DNA binding buffer. The total volume of the solution is 1600 µL. Eight hundred microliter (800 µL) of the solution was moved to a Zymo-Spin IIC column which has a collection tube and spun at 10,000 x g for 60 seconds. Coming from the collection tube is a flow that was discarded. What was left in the collection tube was placed on Zymo-spin. Thereafter, it was turned. Two hundred microliter (200 µL) of the DNA prewash buffer was added to the Zymo-spin IIC using a collection tube that is new. The content of the tube was spun at 10,000 x g for 1 minute. Afterwards, 500 µL of the fungal/bacterial DNA Wash Buffer was added, and the tube was spun at 10,000 x g for 1 minute. The Zymo-spin IIC column was moved to a clean 1.5 µL centrifuge tube. Exactly 100 µL of DNA elution buffer was added to the column matrix, and the column was spun at 10,000 x g for 30 seconds to bring out the DNA. The ultra-pure DNA extracted from the isolates was put in a freezer that maintained a temperature as low as -20 ^{o}C. The DNA sample was used in subsequent steps that involves quantification and sequencing.

DNA quantification

After the genomic DNA from the isolates were successful extracted, each of them was quantified using a Nanodrop 1000 spectrophotometer. Double-clicking of the Nanodrop icon automatically launched the software installed in the equipment. A sterile distilled water measuring 2 µL was used to set up the equipment, while normal saline was used to clear it. Two microliters (2 µL) of the genomic DNA extracted was put on the lower pedestal in the equipment. Thereafter, the upper pedestal was adjusted downwards in order to touch the extracted DNA in the lower pedestal.

16S rRNA amplification

The 16S rRNA region of the rRNA gene of the isolates was amplified. It involved the use of two primers namely 27F: 5'-AGAGTTTGATCMTGGCTCAG-3' and 1492R: 5'-CGGTTACCTTGTTACGACTT-3'. ABI 9700 Applied Biosystems thermal cycler is the equipment used for the amplification. A final volume of 40

µL was analysed by the thermal cycler for 35 cycles. A combination of Taq polymerase, dNTPs, and $MgCl_2$ referred as X2 Dream Taq Master mix was used as the PCR mix. The PCR mix was supplied by Inqaba Biotech., South Africa. The concentration of the primers is 0.5 µM, while the template used is the extracted DNA. The following PCR conditions were maintained during amplification of 16S rRNA: temperature of 95 °C was maintained for a period of 5 minutes for initial denaturation; the same temperature (95 °C) was maintained for 40 seconds for denaturation to occur; a lower temperature (52 °C) was maintained for 40 seconds for annealing to occur; extension occurred when a temperature of 72 °C was maintained for 40 seconds for 35 cycles; and final extension occurred within 5 minutes when the temperature was maintained for 72 °C. Separation of the product was carried out using a 1% agarose gel operated at 130 V for 30 minutes. Visualization of the product is made possible and could be seen on a blue light transilluminator.

Internal Transcribed Spacer (ITS) amplification

The ITS region of the isolate was amplified using the ITS1F: 5'-CTTGGTCATTTAGAGGAAGTAA-3' and ITS4: 5'-TCCTCCGCTTATTGATATGC-3' primers on an ABI 9700 Applied Biosystems thermal cycler at a final volume of 30 µL for 35 cycles. A combination of Taq polymerase, dNTPs, and $MgCl_2$ referred as the X2 Dream Taq Master mix was obtained from Inqaba Biotech., South Africa. The concentration of the primers used was 0.5 µM, while the extracted DNA is the template. The PCR conditions were as follows: temperature of 95 °C was maintained for a period of 5 minutes for initial denaturation; the same temperature (95 °C) was maintained for 40 seconds for denaturation to occur; a lower temperature (53 °C) was maintained for 40 seconds for annealing to occur; extension occurred when a temperature of 68 °C was maintained for 40 seconds for 35 cycles; and final extension occurred in 5 minutes when the temperature was maintained for 68 °C. For a 600bp product, the amplicon product was resolved on a 1% agarose gel. The operational condition is 200 V for exactly 15 minutes. Viewing of the amplicon was done using a blue light transilluminator.

Sequencing of 16S rRNA and ITS

A BigDye Terminator kit on a 3510 ABI sequencer manufactured by Inqaba Biotechnological of Pretoria, South Africa was used for sequencing of 16S rRNA and ITS. The final volume used for the sequencing was 10 µL. The components were as follows: 0.25 µL BigDye® terminator v1.1/v3.1, 2.25 µL of

5 x BigDye sequencing buffer, 10 µL of 10 µM Primer PCR primer, 2-10 ng PCR template per 100 bp. The following describes the sequencing conditions: 32 cycles of 96 °C for 10 seconds, 55 °C for 5 seconds, and 60 °C for 4 minutes.

Physicochemical analysis

Determination of pH

The pH values of tomato powder and fruit tomato samples was ascertained with the aid of a calibrated pH meter (Hanna model). It is a portable device which is carried around with a palm. Before using the pH meter to determine the pH of the fruit tomato, the sample was pulverized without adding water to it. A blender was used to pulverize the sample and poured into a 100 mL beaker. The six tomato powder samples were separately weighed into 100 mL beakers. Fifty millilitre (50 mL) of distilled water was added to each of the tomato powders inside a beaker to form solutions. The pH of all the samples was determined after the digital device was inserted into the solution as instructed by the manufacturer. The pH measurements were performed for all the samples. The analysis was carried out immediately after the tomato powder samples were produced and fresh tomato sampled. Ten replicate samples for each tomato preparation were analyzed. The analysis was repeated after the samples were stored for 16 weeks, at room temperature (25±2 ºC).

Determination of the vitamin C content

The vitamin C content of tomato powder and fruit tomato samples was determined using the AOAC (2000) titrimetric method. The solution used for the analysis was 0.01 g of 2, 6, dichlorophenol-indo-phenol in 100 mL of distilled water. Accurately measured 2 mL and 10 mL of glacial acetic acid were added to 5 mL of standard ascorbic acid and 25 mL of the sample solutions, respectively. While titrating both the standard ascorbic acid and the sample's solutions, indo-phenol was added. Titration continued until a pink colouration of the solution was noticed. Immediately it happened, the titre value was noted. The analysis was performed immediately after the tomato powder samples were produced and fresh tomato sampled. Ten replicate samples for each tomato preparation were analyzed. A repeat analysis was carried out for all the samples stored for 16 weeks, at room temperature (25±2 ºC).

Determination of the moisture content

The air oven drying method described by AOAC (2000) was used as a guide to perform the analysis. The samples involved were tomato powder and fruit tomatoes. Accurate weighing of the samples and empty crucibles used for

the analysis was performed using a calibrated analytical balance. The samples was heated at 100 °C for 10 hours. Afterwards, the samples were allowed to cool in a desiccator. The moisture analysis was performed immediately after the tomato powder was produced and fresh tomato sampled. After storing the tomato powder samples for 16 weeks at room temperature (25±2 °C), the moisture content of the samples was determined. The percentage moisture content of each sample was calculated using the formula overleaf:

$$\% \text{ Moisture content} = \frac{Crucible + Sample\ weight - Final\ weight\ of\ dried\ sample + crucible}{Crucible + Sample\ weight - Empty\ crucible\ weight} \times 100$$

Determination of the ash content

The furnace method described by AOAC (2000) was used as a guide to perform the test. The samples analyzed were tomato powder and fruit tomatoes. Each sample was weighed into an empty crucible which has been polished by flame. The sample inside the crucible was heated to ash in a muffle furnace at 630 °C for 3 hours. The crucible containing the ash was brought out from the muffle furnace and transferred into a desiccator to cool. Afterwards, the crucible containing ash was reweighed. The ash content of the sample was calculated. The analysis was performed immediately after the tomato powder was produced and fresh tomato sampled. Ten replicate samples for each tomato preparation were analyzed. After the samples were stored for 16 weeks at room temperature (25±2 °C), their ash content were also determined. The calculation of percentage ash content of each sample involves the formula:

$$\% \text{ Ash content} = \frac{Weight\ of\ crucible + sample - Weight\ of\ crucible + Sample\ after\ ashing}{Crucible + Weight\ of\ sample - Weight\ of\ empty\ crucible} \times 100$$

Determination of the titratable acidity

The titratable acidity as ascorbic acid of tomato powder samples and fruit tomato, were determined using the AOAC (2000) titrimetric method. Accurately weighed 0.1 g of each sample was transferred into a 250 mL conical flask. Afterwards, 100 mL of distilled water was added to the sample inside the conical flask. Twenty five milliliters (25 mL) of the solution was dispensed into beakers. The solution inside the beaker was used for titration. One drop of phenolphthalein that function as an indicator was added to the sample's solution. The solution was

titrated with 0.1 M sodium hydroxide. The titre value was noted immediately a pink color change appeared in the solution. The titratable acidity of each sample was performed immediately after the production of the tomato powder samples and fresh tomato. Ten replicate samples for each tomato preparation were analyzed. The analysis was repeated after the samples were stored for 16 weeks at room temperature (25±2 ^{o}C).

Determination of the functional properties

Water absorption capacity

The capacity of tomato powder to absorb water is reported as water absorption capacity. The test was performed using the stepwise procedure described by Sosulski *et al.* (1976). One gram (1 g) of the tomato powder was mixed with 10 mL of distilled water. The mixture was kept at room temperature (25±2 ^{o}C) for 30 minutes. The mixture was poured in tubes and centrifuged at 3,000 revolutions per minute. The percentage of water bound per gram of tomato powder was determined and the value(s) was used to calculate the water absorption rate. Ten replicate samples for each dehydrated tomato preparation were analyzed.

Oil absorption capacity

The procedure for determination of oil absorption capacity as described by Sosulski *et al.* (1976) was adopted. Tomato powder were the samples analyzed. One gram (1 g) of the sample was accurately weighed using a calibrated analytical balance. The weighed sample was mixed with 10 mL of soybean oil (Sp. Gravity: 0.9092). The mixture was left undisturbed for 30 minutes at room temperature (25±2 ^{o}C). Afterwards, the mixture was transferred in a test tube and spun in a centrifuge operated for 30 minutes at 300 rpm (2000 x g). Ten replicate samples for each dehydrated tomato preparation were analyzed.

Emulsion stability

The method described by Yasumatsu *et al*. (1972) for measuring the emulsion activity of food samples was adopted. In this experiment, an emulsion was created by adding 1 g of each tomato powder sample to 10 mL of distilled water and 10 mL of soybean oil in a calibrated centrifuge tube. The mixture was centrifuged at 2, 000 g for 5 minutes. The emulsion activity in the sample was calculated by dividing the emulsion layer height by the entire mixture height and expressed in percentage. The emulsion inside a calibrated centrifuge tube was heated at 80 °C in a water bath for 30 minutes. Afterwards, it was chilled

for 15 minutes under running tap water. The centrifuge tube containing the emulsion was transferred to a centrifuge and operated at 2, 000 g for 15 minutes. Thereafter, the emulsion stability was measured. A ratio of the emulsified layer's height to the whole mixture's height was used to estimate the stability of the emulsion. The result was expressed in percentage. Ten replicate samples for each dehydrated tomato preparation were analyzed.

$$\text{Emulsion stability} = \frac{Height\ of\ emulsion\ layer}{Total\ height} \text{ x } 100$$

Foaming capacity

The foaming capacity (FC) of tomato powder samples was determined by using the procedure described by Narayana and Narsinga (1982). Analytical balance was used to weigh 1 g of the sample. It was poured in a graduated measuring cylinder containing 50 mL of distilled water. The mixture was mixed at 30.2 °C. In order to create foam inside the measuring cylinder, the suspension was shaken vigorously for 5 minutes. The foam capacity of the sample was calculated by measuring the volume of foam, 30 seconds after whipping. Ten replicate samples for each dehydrated tomato preparation were analyzed.

$$\text{Foam capacity (FC)} = \frac{Volume\ of\ foam\ (AW) - Volume\ of\ foam\ (BW)}{Volume\ of\ foam\ (Bw)} \text{ x } 100$$

Where: AW = after whipping
BW = before whipping

After whipping the sample for 1 hour, the volume of foam formed was recorded. The result was used to calculate the stability of the foam, which is the percentage of the original volume of foam.

Bulk density

The procedure described by Jones *et al*. (2000) was used as a guide to perform the test. A calibrated analytical balance was used to weigh 20 g of tomato powder sample. It was poured in a 250 mL cylinder. The cylinder containing the sample was placed on a wooden board, and tapped several times. It continued until visible loss in volume was not observed any longer. The apparent (bulk) density was then determined using the weight and volume. Ten replicate samples for each dehydrated tomato preparation were analyzed.

Determination of the lycopene content

The quantity of lycopene present in the tomato powder samples was extracted using the procedure earlier described by Fish *et al.* (2002). One gram (1 g) of tomato powder was accurately weighed using a calibrated analytical balance. The sample was mixed with 5 mL of butylated hydroxytoluene (BHT) dissolved in acetone, 5 mL of ethanol, and 10 mL of hexane (Darmstard, Germany). The same procedure was repeated using fruit tomatoes. The ingredients were added to a bowl of ice. A magnetic stirring plate was used to swirl the content of the bowl for 15 minutes. Exactly 3 mL of deionized water was measured. Immediately after adding the deionized water to each sample vial, the solution was shaken on ice for 5 minutes at room temperature. Thereafter, it was noticed that the samples had been successfully separated into their respective phases. The absorbance of the hexane layer (upper layer) was measured at 503 nm in a spectrophotometer (UV-visible 754, Siemens, China). Estimated concentration of lycopene in the samples was obtained using the Beer-Lambert law that involves making the appropriate substitution for the molar extinction coefficient of lycopene in hexane. The equation is thus:

$$\text{Lycopene content (mg/100g)} = A_{503} \times 31.2/\text{g tissue}$$

Sensory evaluation

Sensory evaluation of the tomato powder without pretreatment, pretreated samples, and the control wrapped in polyethylene terephthalate pouches, was carried out before storage (week 0). Twenty (20) untrained panelists selected among the students of the University of Port Harcourt, evaluated the sensory properties of the coded samples (BAAP, UAAP, BLJP, ULJP, SDTP, and CTRL) of tomato powder for colour, smell, and handfeel, on a 9-point Hedonic scale. On this scale, the numbers 1-9 represent the following: 9 = like extremely, 8 = like very much, 7 = like moderately, 6 = like slightly, 5 = neither like nor dislike, 4 = dislike slightly, 3 = dislike moderately, 2 = dislike very much, and 1 = dislike extremely.

Statistical analysis

Analysis of Variance (ANOVA) was deployed in statistical analysis of the data emanating from the study. In addition, a Duncan's Multiple Range Test (DMRT) was carried out to test for a significant difference at $P<0.05$, between the treatment combinations. In order to carry out the statistical analysis of the data with ease, the Statistical Package for the Social Sciences (SPSS) version 23 software was used. Box plot and regression analysis were carried out using R Programming Software for Statistical Analysis.

Results

Bacterial population

The range of total viable count (TVC) of the stored samples include tomato blanched lime juice pretreated tomato powder (4.41-6.64 log_{10}CFU/g), unblanched lime juice pretreated tomato powder (4.45-4.95 log_{10}CFU/g), sundried tomato powder (5.99-7.31 log_{10}CFU/g), blanched ascorbic acid pretreated tomato powder (4.41-4.95 log_{10}CFU/g), unblanched ascorbic acid pretreated tomato powder (4.43-5.13 log_{10}CFU/g), and the control (4.57-5.17 log_{10}CFU/g). The TVC of the fruit tomato was 4.02 log_{10}CFU/g. The regression analysis shows that all the samples experienced a decrease in the total viable count, as indicated by the negative slope values (Fig. 1). The rate at which the TVC declined vary among the stored tomato powder subjected to different pretreatments, samples without pretreatment, including the control, with each sample showing a different slope. The SDTP and BLJP tomato powder showed stronger relationships, with R^2 values of 0.602 and 0.329, respectively. This suggests that the effect of sun-drying and pretreatment on the TVC of the SDTP and ULJP tomato powder, respectively, were more predictable and stable throughout the storage period (Fig. 2). On the other hand, the Control (R^2=0.054), ULJP (R^2=0.198), BAAP (R^2=0.231), and UAAP (R^2=0.264) tomato powder showed a weaker relationships, as evidenced by their low R^2 values.

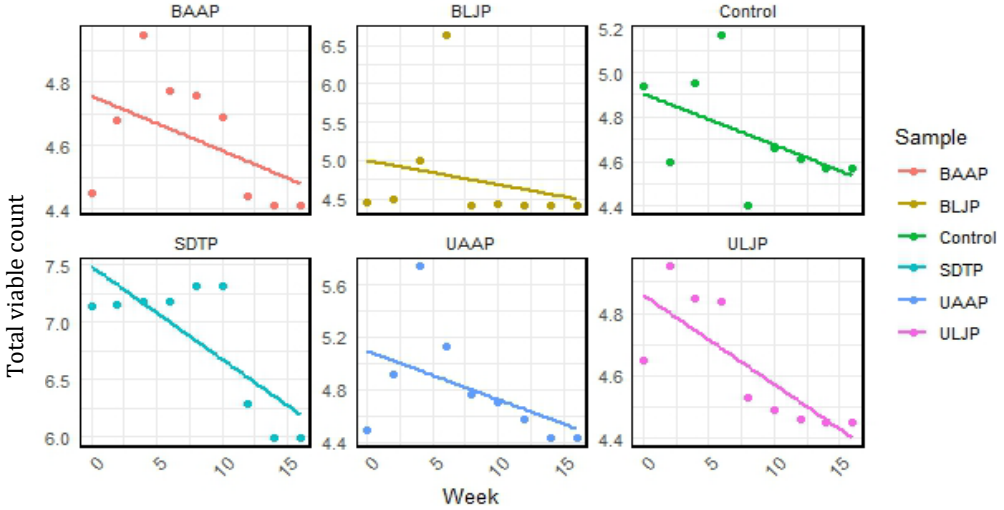

Figure 1. Linear regression of total viable count of tomato powder stored for 16 weeks at room temperature. Keys: BAAP - Blanched ascorbic acid pretreatment; BLJP - Blanched lime juice pretreatment; ULJP - Unblanched lime juice pretreatment; UAAP - Unblanched ascorbic acid pretreatment; CTRL - Control sample, without pretreatment, dried with a dehydrator; SDTP - Sundried, without pretreatment.

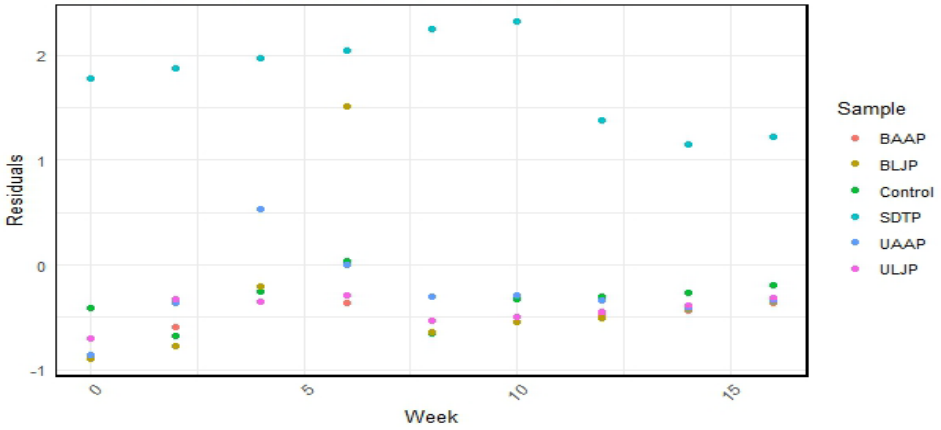

Figure 2. Residuals of linear regression for each sample of stored tomato powder for 16 weeks. Keys: BAAP - Blanched ascorbic acid pretreatment; BLJP - Blanched lime juice pretreatment; ULJP - Unblanched lime juice pretreatment; UAAP - Unblanched ascorbic acid pretreatment; CTRL - Control sample, without pretreatment, dried with a dehydrator; SDTP - Sundried, without pretreatment.

Microbial species

The bacterial species isolated from the tomato samples were *Bacillus cereus, B. anthracis, Proteus mirabilis, Acinetobacter calcoaceticus,* and *Klebsiella pneumonia* (Tab. 1), while the fungal isolates were *Pichia kudriavzevii, Trametes polyzona, Aspergillus foetidus,* and *Aspergillus novoparasiticus* (Tab. 2). The agarose gel electrophoresis and accession numbers of the bacterial isolates are presented in Fig. 3 and Tab. 2, while the results for the fungal isolates are depicted in Fig. 4 and Tab. 3, respectively. Fig. 5 depicts the tomato powder without pretreatment, pretreated samples, and the control, stored inside polyethylene terephthalate pouches for 16 weeks, at room temperature (25±2 ºC).

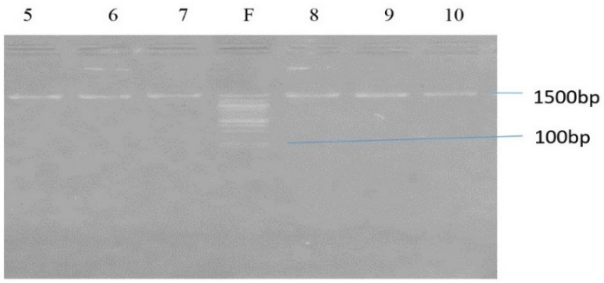

Figure 3. Agarose gel electrophoresis of the 16 S rRNA gene of the bacterial isolates. Lanes 5, 6, 7, 8, 9, and 10 represent the 16*S* rRNA gene band (1500 bp). Lane F represents the 100 bp molecular ladder of 1500 bp.

Table 1. Accession number for the bacteria isolated from the tomato powder samples.

Isolate code	Accession number	Similarity index	Bacterial species
F5	0N763797	99	*Bacillus cereus*
F6	CP073248	96	*Proteus mirabilis*
F7	CP101560	70	*Klebsiella pneumoniae*
F8	KT362717	100	*Bacillus anthracis*
F9	OP160033	58	*Acinetobacter calcoaceticus*
F10	OP160033	58	*Acinetobacter calcoaceticus*

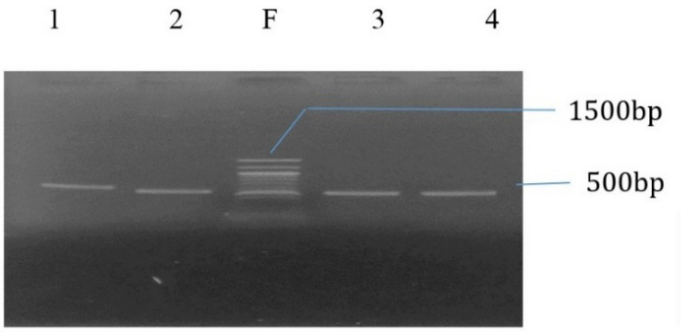

Figure 4. Agarose gel electrophoresis showing ITS gene of the fungal isolates. Lane 1 represents 600 bp; Lane 2 is 550 bp; and Lanes 3 and 4 are 500 bp of the ITS gene. F represents a100 bp DNA ladder of 1500 bp.

Table 2. Accession number for the fungi isolated from the tomato powder samples.

Isolate code	Accession number	Similarity index	Fungal species
F1	MK294305	100	*Pichia kudriavzevii*
F2	OP482406	100	*Aspergillus foetidus*
F3	OL685335	100	*Trametes polyzona*
F4	OL711681	100	*Aspergillus novoparasiticus*

Figure 5. Tomato powder without pretreatment, pretreated samples, and the control, stored inside polyethylene terephthalate pouches for 16 weeks, at room temperature. Keys: BAAP - Blanched ascorbic acid pretreatment; BLJP - Blanched lime juice pretreatment; ULJP - Unblanched lime juice pretreatment; UAAP - Unblanched ascorbic acid pretreatment; CTRL - Control, without pretreatment, dried with a dehydrator; SDTP - Sundried, without pretreatment.

Physicochemical parameters and nutritional content

Fig. 6 shows the box plot for the pH, titratable acidity, moisture, ash, and vitamin C content of the fruit tomato, tomato powder without pretreatment, pretreated tomato powder, and the control, at week 0. Also presented as a box plot (Fig. 7) is the pH, titratable acidity, moisture, ash, and vitamin C content of the tomato powder without pretreatment, pretreated tomato samples, and the control, stored for 16 weeks, at room temperature (25±2 ºC).

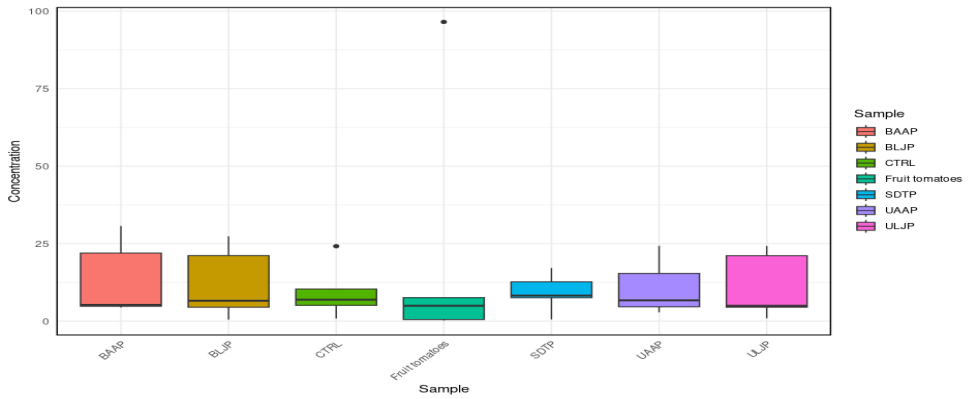

Figure 6. Boxplot of physicochemical, proximate composition, and vitamin C content of fruit tomato, tomato powder without pretreatment, pretreated samples, and the control, at week 0. Keys: BAAP - Blanched ascorbic acid pretreatment; BLJP - Blanched lime juice pretreatment; ULJP - Unblanched lime juice pretreatment; UAAP - Unblanched ascorbic acid pretreatment; CTRL – Control, without pretreatment, dried with a dehydrator; SDTP – Sundried, without pretreatment.

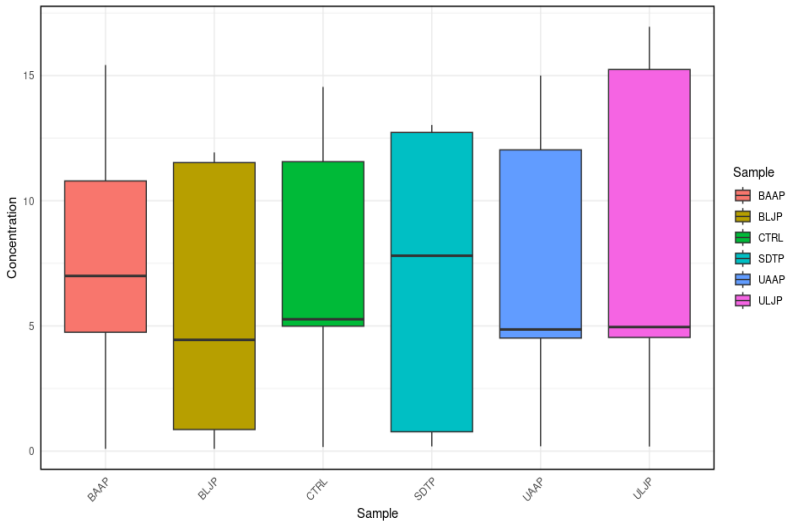

Figure 7. Boxplot of physicochemical, proximate composition, and vitamin C content of tomato powder without pretreatment, pretreated samples, and the control at week 16. Keys: BAAP - Blanched ascorbic acid pretreatment; BLJP - Blanched lime juice pretreatment; ULJP - Unblanched lime juice pretreatment; UAAP - Unblanched ascorbic acid pretreatment; CTRL – Control, without pretreatment, dried with a dehydrator; SDTP - Sundried, without pretreatment.

At week 0, the pH of fruit tomato was 4.96±0.02, while the tomato powder samples was within the range of 4.50±0.02-8.25±0.01. The BLJP and ULJP tomato powder samples had the least pH, whereas the sundried tomato powder (SDTP) had the highest. At week 16, the pH of the stored tomato samples was within the range of 4.42±0.10-7.8±0.06. A slight reduction in pH was reported in the stored tomato powder samples, with the exception of the control (pH 5.10).

The moisture content of the fruit tomato was 96.53±0.38%, while the tomato powder without pretreatment and the pretreated samples was within the range of 12.70±0.30-27.37±0.34%, at week 0. Meanwhile, the moisture content of the control sample was 24.18±0.26%. At week 16, the moisture content of all the samples of tomato powder within the range of 10.79±0.07-15.24±0.09% decreased from their initial values at week 0. The moisture content of the control sample was 14.55±0.10%.

The ash content of the tomato powder without pretreatment and the pretreated samples at week 0, were within the range of 4.95±0.11-17.15±0.12%. Meanwhile, the ash content of fruit tomato and control sample was 0.53±0.06% and 6.92±0.10%, respectively. Among the tomato powder samples, sundried

tomato powder (SDTP) had the highest ash content, whereas the unblanched lime juice pretreated (ULJP) tomato had the least. At week 16, the ash content of stored tomato powder samples were within the range of 0.86±0.06-13.02±0.11%. SDTP sample also had the highest ash content, whereas the BLJP tomato powder had the lowest. The ash content of the control sample was 5.27±0.11%.

At week 0, the vitamin C content of the fruit tomato, sundried tomato powder, and control sample was 0.20±0.03%, 0.56±0.09%, 0.85±0.07%, respectively. The vitamin C content of the pretreated tomato powder samples was within the range of 0.52±0.05-4.41±0.09%. BLJP and BAAP tomato powder had the lowest and highest vitamin C content, respectively. At week 16, the vitamin C content of all the samples of stored tomato powder was below 1%.

The titratable acidity (TA) of fruit tomato was 7.60±0.14%, while the tomato powder without pretreatment and pretreated samples was within the range of 7.57±0.30-30.73±0.10%. The TA of the control sample was 10.37±0.10%. Fruit tomato and SDTP sample had relatively the same titratable acidity (7.60%). After the tomato samples were stored for 16 weeks, the TA of the products decreased from their initial values, with the exception of the control. The TA of the stored tomato powder samples were within the range of 0.77±0.08-16.94±0.09%.

Lycopene content

The lycopene content of the fruit tomatoes, tomato powder without pretreatment, the pretreated samples, and the control are presented in Tab. 3.

Table 3. Lycopene content (mg/100g) of fruit tomatoes, tomato powder without pretreatment, pretreated samples, and the control at week 0.

Sample	BAAP	BLJP	CTRL	UAAP	ULJP	SDTP	Fruit tomato
R1	129.84	123.11	134.11	123.15	113.23	100.45	19.90
R2	130.45	120.45	130.05	121.04	112.45	101.67	16.83
R3	127.85	119.84	131.66	120.67	108.84	103.80	19.84
R4	128.34	121.07	132.49	118.85	109.25	101.29	19.17
R5	131.11	122.21	133.78	121.00	110.43	100.58	19.54
R6	128.14	121.53	130.99	117.59	111.95	99.99	18.94
R7	131.02	123.11	132.35	118.77	108.47	104.13	20.34
R8	129.23	120.89	133.11	119.48	112.80	103.49	19.04
R9	129.99	118.34	134.39	122.22	112.29	103.33	16.55
R10	130.14	120.23	134.08	117.11	108.99	102.54	19.48
Mean	129.61±1.75^{e}	121.08±1.49^{d}	132.70±1.46^{f}	119.11±1.96^{d}	110.87±1.86^{c}	102.13±1.53^{b}	18.96 ±1.27^{a}

Values in the last row represent the mean of ten samples ± standard error. Means with different superscripts along the row are significantly different at $p<0.05$. Keys: BAAP - Blanched ascorbic acid pretreatment; UAAP - Unblanched ascorbic acid pretreatment; BLJP - Blanched lime juice pretreatment; ULJP - Unblanched lime juice pretreatment; CTRL - Control without pretreatment, dried with a dehydrator; SDTP - Sundried, without pretreatment; R-Replicate.

Ten replicate samples for fruit tomato and dehydrated tomato preparations were analyzed. The mean lycopene content of the fruit tomatoes was 18.96±1.27 mg/100 g, while the tomato powder samples were within the range of 102.13±1.53-132.70±1.46 mg/100g. On average, the control sample had the highest lycopene content. There is a significant difference ($p<0.05$) in the lycopene content of the tomato samples, with the exception of BLJP and UAAP tomato powder.

Functional properties

Tab. 4 shows the functional properties of the tomato powder without pretreatment, the pretreated samples, and the control, at week 0. Among the samples, the blanched ascorbic acid pretreated (BAAP) tomato powder, had the highest water absorption capacity (WAC), bulk density, and foaming capacity reported as 15.53±1.70%, 1.17±0.32 g/cc, and 61.05±1.70%, respectively. The control sample had the lowest WAC (12.05±1.81%) and bulk density (0.64±0.07 g/cc), whereas its emulsion stability (55.62±1.88%) was the highest among the tomato powder samples.

The water absorption capacity (WAC) of the tomato powder samples was within the range of 12.05±1.81- 15.85±1.45%. The unblanched ascorbic acid pretreated tomato powder had the highest WAC, whereas the control sample had the least. There is a significant difference ($p<0.05$) in the WAC of the tomato powder samples.

The oil absorption capacity (OAC) of the tomato powder without pretreatment, the pretreated samples, and the control, was within the range of 12.53±1.57-16.66±1.40%. Among all the samples, the highest and lowest OAC were reported in the unblanched ascorbic acid pretreated (UAAP) and blanched lime juice pretreated (BLJP) tomato powder, respectively. The OAC of the control was 14.25±1.71%. There is no significant difference ($p>0.05$) in the OAC of the control and ULJP tomato samples; BAAP and UAAP tomato powder samples.

The emulsion stability of the tomato powder without pretreatment, the pretreated samples, and the control was within the range of 10.67±1.88-55.62±1.88%. The sample that had the highest and lowest emulsion stability was the control and blanched lime juice pretreated (BLJP) tomato powder, respectively. There is a significant difference ($p<0.05$) in the emulsion stability of the samples, with the exception of BLJP tomato powder and sundried tomato powder (SDTP).

The bulk density of the tomato powder without pretreatment, the pretreated samples, and the control was within the range of 0.64±0.07-1.17±0.32 g/cc. The control and blanched ascorbic acid pretreated (BAAP) tomato powder sample had the lowest and highest bulk densities, respectively. There is a significant difference ($p<0.05$) in the bulk density of the tomato samples.

The foaming capacity of the tomato powder without pretreatment, the pretreated samples, and the control was within the range of 26.02±0.10-61.05±1.70%. Among the tomato powder samples, blanched ascorbic acid pretreatment (BAAP) tomato powder had the highest foaming capacity, whereas the sundried tomato powder (SDTP) had the least. There is a significant difference ($p < 0.05$) in the foaming capacity among the samples, with the exception of the BLJP and the ULJP tomato powder samples.

Table 4. Functional properties of tomato powder without pretreatment, pretreated samples, and the control at week 0.

Functional property	Samples					
	BAAP	BLJP	CTRL	UAAP	ULJP	SDTP
Water absorption capacity (%)	15.53±1.70^{d}	14.27±1.09^{bc}	12.05±1.81^{a}	15.85±1.45^{d}	14.02±1.30^{b}	14.87±1.23^{cd}
Oil absorption capacity (%)	15.73±1.17^{c}	12.53±1.57^{a}	14.25±1.71^{b}	16.66±1.40^{c}	14.12±1.38^{b}	13.58±1.45^{a}
Emulsion stability (%)	14.78±1.62^{b}	10.67±1.88^{a}	55.62±1.88^{e}	49.81±1.78^{d}	25.42±1.80^{c}	11.37±1.43^{a}
Bulk density (g/cc)	1.17±0.32^{d}	0.73±0.11^{a,b}	0.64±0.07^{a}	0.84±0.09^{b,c}	0.88±0.09^{c}	0.75±0.09^{a,b,c}
Foaming capacity (%)	61.05±1.70^{e}	30.14±1.10^{b}	41.06±1.50^{d}	32.24±1.80^{c}	26.61±1.46^{b}	26.02±0.10^{a}

Values represent the mean of ten samples± standard error. The means with different superscripts in the same row are significantly different at $p<0.05$. Keys: BAAP - blanched ascorbic acid pretreatment; UAAP - Unblanched ascorbic acid pretreatment; BLJP - Blanched lime juice pretreatment; ULJP - Unblanched lime juice pretreatment; CTRL - Control without pretreatment, dried with a dehydrator; SDTP - Sundried, without pretreatment.

Sensory evaluation

Tab. 5 shows the results of the sensory evaluation of the tomato powder without pretreatment, the pretreated samples, and the control, at week 0. In terms of colour, the blanched lime juice pretreated (BLJP) tomato powder had the highest average sensory score (8.85±0.00), whereas the sundried tomato powder (SDTP) had the least score (3.40±0.82). There is a significant difference ($p<0.05$) in the colour rating of the tomato powder samples, with the exception of the unblanched lime juice pretreated (ULJP) and unblanched ascorbic acid pretreated (UAAP) tomato powder samples. The sensory rating of handfeel of the blanched lime juice pretreated tomato powder (8.30±0.82) was the highest among all the tomato samples, whereas the control was the least (6.10±1.20). All the tomato powder samples were not significantly different ($p>0.05$) in

terms of handfeel, with the exception of the control. With regards to smell as a sensory attribute of a product, the blanched lime juice pretreated (BLJP) tomato powder was assigned an average sensory score of 8.40±1.07. It is the highest sensory score among all the samples, whereas the sundried tomato powder (SDTP) was the least (2.40±1.00). There is no significant difference ($p>0.05$) between the control, ULJP, and UAAP tomato powder samples.

Table 5. Sensory evaluation of tomato powder without pretreatment, pretreated samples, and the control at week 0.

Parameter	Samples					
	BAAP	CTRL	BLJP	ULJP	SDTP	UAAP
Colour	8.0 ± 0.92^{d}	6.05 ± 0.89^{b}	8.85 ± 0.00^{e}	7.25 ± 0.85^{c}	3.40 ± 0.82^{a}	7.45 ± 1.0^{c}
Handfeel	8.10 ± 0.99^{b}	6.10 ± 1.20^{a}	8.30 ± 0.82^{b}	7.40 ± 0.97^{b}	7.30 ± 1.16^{b}	7.40 ± 1.35^{b}
Smell	$8.10\pm1.00^{b, c}$	7.20 ± 1.72^{b}	8.40 ± 1.07^{c}	7.20 ± 1.60^{b}	2.40 ± 1.00^{a}	7.40 ± 1.38^{b}

Values represent the mean of ten samples$\pm$standard error. The means with different superscripts in the same row are significantly different at $p<0.05$. Keys: BAAP - Blanched ascorbic acid pretreatment; UAAP - Unblanched ascorbic acid pretreatment; BLJP - Blanched lime juice pretreatment; ULJP - Unblanched lime juice pretreatment; CTRL - Control without pretreatment, dried with a dehydrator; SDTP – Sundried, without pretreatment.

Discussion

Bacterial population of the stored tomato powder

The result from this study shows that the blanched ascorbic acid pretreated (BAAP) tomato powder and unblanched lime juice pretreated (ULJP) tomato powder stored for 16 weeks at room temperature (25±2 ºC), met the International Commission on Microbiological Specification for Foods (ICMSF) standard. Stored samples of the blanched lime juice (BLJP) and unblanched ascorbic acid pretreated tomato powders (UAAP) also met the ICMSF standard, except at weeks 4 and 6. The ICMSF standard was met by the control sample, except at week 6. The bacterial population in 3 out of 6 samples of stored tomato powders that exceeded the limit stipulated by the ICMSF at week 4 and 6 could be attributed to the initial level of microbial contamination of the samples, availability of nutrients, and storage condition. In contrast, the stored sample of the sundried tomato powder (SDTP) did not meet the ICMSF standard. The ICMSF stipulates that the total bacterial count (TBC) of acceptable food should be $< 10^5$ (Adejo *et al.,* 2015).

Exposure of tomatoes to the environment during sun-drying could be responsible for high bacterial population in the stored samples. Bacteria surviving in the air and dust particles especially spore formers could settle on the exposed tomato slices during sun-drying. Under a favourable condition, the spores would germinate as vegetative cells and increase the bacterial load of the product during storage. Consequently, the microbial load of the product is most likely to exceed the limit permissible by the ICMSF. The sundried tomato powder (SDTP) did not undergo pretreatment which could have reduced the microbial population in the product (Obadina *et al*., 2018; Owureku-Asare *et al*., 2022). The control sample which did not undergo pretreatment before a dehydrator was used instead of drying it under the sun had a lower bacterial count than the SDTP sample. This result is an indication that the use of dehydrator to dry tomato was more effective in reducing the bacterial population in the samples than the pretreatments. In a related study, Ladi *et al*. (2017) reported that the total bacterial count of the sundried tomato powder stored for 3 and 6 months is 7.7 x 10^5 and 7.3 x 10^5 CFU/g, respectively. Obadina *et al.* (2018) reported that during ambient temperature storage of cherry and plum tomato powder which were not pretreated before drying, the population of microorganisms in the products steadily increased. The total aerobic count in both varieties of dried tomato powder were lower than the results reported in this study. This could be as a result of a higher temperature (60 ^oC, 65 ^oC, and 70 ^oC) used by the researchers to dry the tomato slices compared with 55 ^oC used in this study. Generally, dehydrated food products have a lower microbial load, compare with fresh products. The level of microbial load in the product that is being dried could be influenced by temperature and other factors. Jayathunge *et al.* (2012) reported that the total plate count (TPC) of tomato powder stored inside polypropylene (PP), polystyrene (PS), polyvinyl chloride (PVC), and triple laminated aluminum (PET/Al/PE), for six months is within the range of 1.06 x10^2-4.45 x10^2 CFU/g. The result is lower than the total viable count (TVC) of tomato samples reported in this study. Differences in packaging material, pretreatment prior to drying, and drying method could be responsible for the differences in the TVC of the stored tomato powder.

Microbial species isolated from the tomato samples

Two species of *Bacillus,* one species of *Proteus, Acinetobacter,* and *Klebsiella* each were isolated from tomato powder without pretreatment, pretreated samples, and the control. In a related study, Garg *et al*. (2013) reported the presence of *Proteus mirabilis* and *Klebsiella* sp. and other bacterial species in tomato puree sold in India. Among the bacterial species isolated from selected commercial brands of tomato paste sold in Katsina metropolis, Nigeria, it was

reported that *Bacillus* sp. had the highest percentage occurrence (Dabai *et al*., 2020). *Bacillus* sp. is characterized by its ability to form spores. It gives the organism ability to survive in a harsh environmental condition. The bacterium is present everywhere. That is why *Bacillus* species frequently contaminate various food products including stored tomato powder. *Bacillus* sp. is capable of surviving in acidic foods such as tomatoes. Possible sources of contamination of tomato powder with *Bacillus cereus* and *B. anthracis* include, air, soil, water, and food handlers (Ire *et al*., 2020; Akpaetok *et al*., 2023). According to Ahaotu *et al.* (2021a), ingestion of food contaminated with large population of *Bacillus cereus* and *B. anthracis* could manifest severe symptoms of foodborne illness. In humans and animals, *Klebsiella pneumoniae* could be isolated from their respiratory and intestinal tracts. The bacterium is commonly encountered in foods such as powder foods specially prepared for babies. Consumption of food contaminated with *K. pneumoniae* could cause infections in humans. Findings from this study shows that two species of *Aspergillus*, one species of *Pichia* and *Trametes* each were also isolated from the tomato samples. The environment where the tomato samples were prepared could be the source of the fungal species isolated from the samples. In a related study, Aliyu *et al*. (2018) isolated *Aspergillus fumigatus, A. flavus, A. oryzae, A. niger,* and a few other fungal species from the sundried tomato chips sold in Sokoto metropolis, Nigeria. Suleiman *et al.* (2023) tested the capability of fungi isolated from dry tomato chips sold in Keffi, Nigeria, to produce mycotoxins. The study reported that some of the fungal species produced aflatoxin, fumonisins, patulin, ochratoxin, and cyclopiazonic acid toxin. The presence of *Aspergillus* sp. and other fungal species in tomato paste were reported by Dabai *et al.* (2020). Going by the information currently available on dried tomato powder, this report could be considered as the first time microorganisms isolated from dehydrated tomato powder, subjected to different pretreatments, was identified using molecular methods. With this information, the health risk of consuming tomato powder contaminated with potential pathogenic microorganisms have been brought to the knowledge of tomato farmers, consumers, and the relevant regulatory bodies.

Vitamin C content of the tomato samples

A striking result from this study is that the quantity of vitamin C in the fresh tomato was lower than the dried tomato powder without pretreatment and the pretreated samples prior to storage. Low moisture content and pretreatment of the dried tomato powder could be responsible for higher vitamin C content of the product compared with the fresh fruit. The temperature of drying could also influence the quantity of vitamin C in the tomato powder. Ranjan and Shankar (2024) reported that the amount of vitamin C in the tomato

powder dried using a dehydrator set at 60 and 100 ^{o}C is 15 mg/100g and 10 mg/100g, respectively. Meanwhile the vitamin C content of the sample dried under the sun for 2 weeks is 13mg/100g. The use of ascorbic acid in the pretreatment of tomato powder could be responsible for high vitamin C content of the BAPP (4.37±0.0%) and UAAP (2.82±0.1%) tomato powder samples. In a related study, Farooq *et al*. (2020) reported that the pretreatment of tomato powder with 0.5% ascorbic acid and 0.5% citric acid could be responsible for the increase in quantity of ascorbic acid (mg/100g) present in the product. At week 16 of storage, the UAAP tomato powder had the highest vitamin C content (0.19±0.0 %), whereas the blanched ascorbic acid pretreated (0.09±0.0 %) and blanched lime juice pretreated (0.09±0.0 %) tomato powder were the least. This result suggest that blanching of the tomato slices before drying it affected the vitamin C content of the product. Notably, the vitamin C content of all the tomato powder samples decreased during the period of storage. This is in agreement with the findings from a related study by Dufera *et al*. (2023). Vitamin C is highly sensitive to oxidation when it is stored (Caritá *et al.,* 2020). This could be the reason for the reduction in the vitamin C content of the tomato samples during storage at room temperature. The sample with the least capability to retain vitamin C during storage, was the sundried tomato powder (SDTP). In contrast, the blanched lime juice pretreated (BLJP) tomato powder had the greatest ability to retain vitamin C among all the tomato powder samples. According to Dufera *et al.* (2023), the ability of any food to retain vitamin C shows the extent the food can also retain other nutrients. The researchers reported that the vitamin C content of tomato powder stored inside low density polyethylene bags for six months is within the range of 31.84±3.4-50.57±0.025 mg/100 g DM.

pH and titratable acidity of the tomato samples

The pH of all the tomato powder samples including the control were slightly acidic, with the exception of the sundried tomato powder (SDTP) which was non-acidic. It was also observed that the pH of fresh tomato was higher than the dried pretreated samples. This result is in agreement with a similar study by Degwale *et al*. (2022). The researchers reported that the pH of fresh tomato (4.567±0.10408) is higher than the tomato powder (4.55±0.05-4.267±0.05774). The use of lime during pretreatment could have contributed to the slight reduction in the pH of the BLJP and ULJP tomato powder samples. Farooq *et al.* (2020) reported that the pH of hot-air and freeze-dried tomato powder (with or without pretreatment), monitored for 30 days is within the range of 4.39±0.25-5.53±0.25. According to Sarker *et al*. (2014), the pH requirement that makes it most suitable for tomatoes to be processed into different products is 3.77. The researchers used 1% calcium chloride and 0.2%

potassium metabisulphite as a salt solution to pretreat tomato slices before it was dried, and packaged using three different packaging materials (LAF, HDPE, and MDPE). Each of the packaged tomato powder was stored at ambient temperature for six months. The pH of the samples is within the range of 3.58-4.30. This result is lower than the pH of stored tomato samples reported in this study. The variety of tomato, the osmotic agent used for the pretreatment, the activities of microorganisms present in the tomato, and the type of packaging material used for storing the product, could be responsible for the variations in pH. During industrial processing of tomatoes, it is recommended that the final pH of the product should not exceed 4.7. This condition will inhibit the growth of spoilage microorganisms, and extend the shelf life of the product (Sarker *et al*., 2014). The samples that met the requirement (pH > 4.7) were BLJP, UAAP, and ULJP tomato powder. Pretreatment of the tomato powder samples with lime and ascorbic acid could be partly responsible for the reduction in pH.

Most of the dried tomato powder samples had a relatively high values of titratable acidity (TA). This observation could be attributed to the concentration of organic acids in the tomato samples due to drying. A similar result was reported by Aderibigbe *et al.* (2018) and Obadina *et al.* (2018) from related studies. The observation that the TA of fresh tomato was lower than the pretreated tomato powder samples is in agreement with the findings from a related study by Degwale *et al*. (2022). The researchers reported that the TA of fresh tomato is 0.1433±0.00577%, while the dehydrated tomato powder samples were within the range of 0.2867±0.01528-0.4933±0.05508%. The breakdown of organic acids during storage of tomato powder could be the reason why the stored samples had a lower TA compared with the freshly prepared tomato powder samples. According to Aderibigbe *et al.* (2018), TA influences the taste, quality, and flavour of food products.

Ash and moisture content of the tomato samples

The ash content of sundried tomato powder (17.15±0.12%) at week 0 reported as the highest among all the samples could be attributed to mineral concentration due to the drying process. The fact that the fresh tomato (0.53±0.06%) had the least ash content compared to the dried tomato samples could be as a result of not drying the sample. Drying of tomatoes at different temperatures could also affect the ash content of the product. A study carried out by Ranjan and Shankar (2024) reported that the tomato powder dried under the sun; using a dehydrator set at 60 ^{o}C, and 100 ^{o}C is 5.00%, 5.20%, and 4.80%, respectively. Oladipupo *et al.* (2020) reported that the ash content of tomato powder stored for 6 weeks, using a black polyethylene and white polyethylene bag, is within the range of 10.2 to 10.80%. This result is partly in

agreement with our findings. Sarker *et al.* (2014) reported that the ash content of the tomato powder prepared using a salt solution (1% calcium chloride and 0.2% potassium metabisulphite) to pretreat the sample before it was dried, and stored inside a high density polyethylene (HDPE), medium density polyethylene (MDPE), and laminated aluminum foil (LAF) for 6 weeks is within the range of 9.22-9.52, 9.22-9.55 and 9.22-9.45%, respectively.

The moisture content (MC) of the fruit tomato was quite higher than the tomato powder samples (without pretreatment, the pretreated samples, and the control). Generally, freshly harvested fruits and vegetables have a high MC. It is one of the reasons fruits and vegetables have a short shelf life (Obiaocha-Nwaogwugwu *et al.,* 2024). Low MC of the tomato powder samples could be attributed to the effect of drying, which resulted in moisture loss of the fruit tomato. It has been reported that the temperature of drying could influence the MC of tomato power. Ranjan and Shankar (2024) reported that the MC of sundried tomato powder is 10%, while the samples dried at 60 ^{o}C and 100 ^{o}C is 10% and 20%, respectively. According to Nanelo and José (2023), the MC of dried tomatoes that ranges from 50-55% is acceptable. The MC of the tomato powder samples partially met the Commission économique pour l´Europe des Nations unies (CEE-ONU) standard which ranges from 12 to 18%. A very firm texture is one of the physical properties of the dried tomatoes that met the standard (Oboulbiga *et al*., 2022). In a related study that involved subjecting tomatoes to different pretreatments and storage conditions for a period of 60 days, Nanelo and José (2023) reported that the MC of the samples is within the range of 20.30±2.61-94.24±1.29%. The reduction in the MC of the stored samples of tomatoes, could be attributed to the metabolic activities of microorganisms present in the samples during storage. Moisture content within the range of 12.5 to 14.5% was reported by Oladipupo *et al*. (2020), in a study that involved storing the tomato powder pretreated with 1% $CaCl_2$ solution and 1% KMS, before it was dried and stored inside a laminated aluminum foil, black polyethylene, and white polyethylene bags, for 6 weeks. Sarker *et al*. (2014) reported that the MC of the tomato powder prepared using a salt solution (1% calcium chloride and 0.2% potassium metabisulphite) to pretreat the sample for 10 minutes, before it was dried, is 8.12%.

Lycopene content of the tomato samples

The lycopene content of the sundried tomato without pretreatment and tomato powder subjected to different pretreatments using weak acids were higher than the fruit tomato. This result is in agreement with the report by Degwale *et al*. (2022). According to the researchers, the increase in the lycopene content of the dehydrated tomatoes could be attributed to water loss. They also noted that the amount of lycopene in the tomato powder is concentrated after

the moisture content in the product is reduced. The lycopene content of the control sample was higher than other tomato powder samples subjected to different pretreatments. This result could be attributed to the leaching effect of nutrients caused by blanching and soaking the samples in the pretreatment solutions. Nishizono *et al*. (2023) reported that the lycopene content of three varieties of raw tomato fruit is within the range of 6.69±0.885 to 10.03±1.711 mg/100g. The lycopene content of the tomato powder stored in low density polyethylene bags for six months is within the range of 58.487±5.25 to 102.5±0.057 mg/100 g DM (Dufera *et al*., 2023). The lycopene content of the fruit tomato (18.96±1.27 mg/100g) evaluated in this study is lower than 85.33 mg/100g reported by Chen (2005) in the Tau-tai-lan T93 tomato variety. Studies have shown that different varieties of tomatoes have varying quantities of lycopene. The differences in lycopene content could be attributed to environmental factors and farming practices (Abushita *et al.,* 2000).

The lycopene content of tomatoes is influenced by the variety, growing area, varying temperature conditions, and agricultural methods, and equipment. According to Dūma *et al.* (2022), the lycopene content in the cherry tomato is higher than the big sized tomato. Drying of fruit tomato or subjecting the tomato slices to pretreatments before drying, could be responsible for the increase in lycopene content of tomato powder. Low moisture content of tomato powder compared with the fruit tomatoes could be responsible for "concentration effect", which increased the lycopene content of the product. The lycopene content of the sundried tomato powder was lower than other pretreated tomato powder, and the control samples. This result could be attributed to long period of sun-drying of tomato at an uncontrolled temperature, compared with quick drying of samples using a dehydrator at a high temperature (55 ^{o}C). According to Yusuf *et al.* (2013), the increase in temperature and duration of heat treatment of tomatoes could be responsible for lycopene degradation.

Functional properties of the tomato powders

It was observed that the bulk density of tomato powder without pretreatment, pretreated samples, and the control was low. Furthermore, the result indicate that pretreatment of the tomato powder samples dried in a dehydrator increased its bulk density. The way a food product is packaged is influenced by its bulk density. Packaging of any food product influences the final cost of the product. Bulk density is a parameter that determines the extent dried food products or powder will occupy space. Low bulk density is an indicator that a particular food is suitable to use in formulating a complementary food that is rich in nutrients. Therefore, tomato powder that were subjected to different pretreatments is more valuable than the fresh tomato. The size of particle,

protein, and starch content of a food substance influences its bulk density (Hussein *et al.,* 2016; Ahmad *et al*., 2022). Low bulk density of tomato powder reported in this study is an indication that during handling, storage, and distribution of the product, reduction in its volume, will not occur. This is in agreement with the report by Ahmad *et al*. (2022). The researchers reported that the bulk density of the sundried tomato and the tomato powder packaged in a polyethylene bag is 0.61±0.01 mg/100 g each.

The water absorption capacity (WAC) of pretreated tomato powder and the control indicate that pretreatment improved the WAC of the samples. According to Hussein *et al*. (2016), 'juiciness' of a food material could be rated using the parameter referred as water absorption index (WAI). Ahmad *et al.* (2022) reported that the WAC of sundried tomato and tomato powder packaged in polyethylene bags is 2.26±0.23 and 2.30±0.0.35 mg/100 g, respectively. The result is far lower than the WAC of tomato powder without pretreatment, pretreated samples, and the control. According to Ahmad et al. (2022), high WAC translate to low moisture content of a food product. In essence, the product shelf life is prolonged due to very slow activities of spoilage microorganisms. The ingredients that possess high water hydration capacity are recommended for food manufacturers to use as a thickening agent. Such ingredients can also be added to foods that contain too much water in order to reduce syneresis (Bhat *et al*., 2023).

According to Ahaotu *et al*. (2021b), oil absorption capacity (OAC) indicate the level of entrapment of oil by a food material. It is not only the mouth feel of a food product that is improved when the capacity of the food to absorb oil is increased, but also its flavour. Therefore, the unblanched ascorbic acid pretreated (UAAP) tomato powder ought to have the best sensory rating in terms of mouthfeel and flavour because the sample had the highest OAC compared with other tomato powders. A contrary sensory rating should involve the blanched lime juice pretreated (BLJP) tomato powder.

The blanched ascorbic acid pretreated (BAAP) tomato powder had the highest foaming capacity, whereas the least involved sundried tomato powder (SDTP). This result could be attributed to higher nutritional composition of the BAAP tomato powder, which caused the surface tension between water and air to reduce (Kaushal *et al.,* 2012). The unfolded protein that assemble at the boundary that separate the aqueous phase from the air phase is referred to as foams. Some researchers have suggested that the improvement in the foaming capacity (FC) and foaming stability (FS) by the formation of bubbles that are more uniform in size and adsorb faster, could be achieved with higher protein concentrations (1% w/w) (Mateo-Roque *et al*., 2024).

Our result indicate that pretreatment of tomato powder reduced the emulsion stability of the samples compared with the control. The emulsion stability of powders is an important functional property taken into consideration, while making and keeping emulsions stable in many food products (cake, coffee whiteners, and frozen desserts etc.). Owing to different components which they are made up of, the preparation of the above listed food products require different processes; their emulsifying and stabilizing requirements varies (Adebowale *et al.,* 2005).

Sensory report of the tomato powders

Blanched lime juice pretreated (BLJP) tomato powder was assigned the highest sensory score with regards to colour, smell, and handfeel of the samples, followed by the blanched ascorbic acid pretreated (BAAP) tomato powder. It is important to note that the three sensory attributes of BLJP and BAAP tomato powder samples were assigned average sensory scores interpreted as like very much. This sensory rating could be attributed to the combined effects of blanching, the use of ascorbic acid or lime juice during processing of the tomato powder, which contributed in stabilizing the colour and appearance of the product. Our sensory result is in agreement with the report by Latapi and Barrette (2005). According to the researchers, dipping tomatoes in 6% or 8% sodium metabisulphite for 5 minutes before drying, tremendously improved the colour of the product. Masamba *et al*. (2013) also reported that the fruit samples exposed to 1% sodium metabisulphite and lemon juice pretreatment before dying, had a better colour than the control sample. In terms of handfeel, the panelists recruited to carry out sensory evaluation of the samples regarded BLJP tomato powder as the most preferable product. In a related study, Panagiotou (1998) reported that the texture of vitamin C and honey-treated fruit samples were assigned a higher sensory score than the control sample. Overall sensory result from this study indicate that the sundried tomato powder (SDTP) was the least preferred sample. The sensory panelists had a moderate dislike for the colour of the SDTP, while the smell was disliked very much. Lack of pretreatment and exposure of the tomato sample to direct heat from the sun probably affected the sensory attribute of the product. According to Ramya *et al.* (2017), the ability of any dried food product to retain the original colour when it is still fresh, influences the choice of consumers and the market price of the product. Poor sensory rating of the SDTP sample could be attributed to higher fermentative activities of spoilage microorganisms from the environment on the sliced tomato during sun-drying. In addition, sun-drying of tomato powder could degrade the colour of the product by browning (Hameed *et al*., 2018; Degwale *et al*., 2022; Leke and Bembur, 2023). Our result clearly shows that the different pretreatments

applied during the production of tomato powder positively impacted the sensory attributes of the product. To some extent, the method of drying also played a role in the sensory attributes of the dehydrated tomato powder. In a related study, Ladi *et al*. (2017) reported that the oven-dried tomato powder had a better sensory rating in terms of colour, consistency, taste, flavour, and overall acceptability, compared with the sundried tomato powder.

Conclusions

Drying of the sliced tomato under the sun or the use of a dehydrator significantly reduced the moisture content of the fresh fruit tomato. It also influenced the nutrient composition, functional properties, and sensory attributes of the tomato samples. Blanched ascorbic acid pretreatment, unblanched ascorbic acid pretreatment, blanched lime juice pretreatment, and unblanched lime juice pretreatment, influenced the reduction in the microbial load of the dehydrated tomato powder, and reasonably improved the sensory attributes, functional properties, and quantity of lycopene and vitamin C in the product. Notably, different pretreatments of tomatoes affected the quantity of lycopene content in the dehydrated tomato powder, while exposure of sliced tomato to the environment during sun-drying is largely responsible for high bacterial load of the product. Although all the samples of stored tomato powders were packaged in polyethylene terephthalate pouches, there is possibility that the packaging material also influenced the quality of the product during storage. Based on the overall results, blanched ascorbic acid pretreatment is recommended for tomato slices, before drying the food material.

Acknowledgements: The authors are grateful to the Chief Laboratory Technologist, Department of Microbiology, University of Port Harcourt, for providing the technical support needed during the laboratory analyses involved in this study.

References

Abano, E. E. & Sam-Amoah, L. (2011). Effects of different pretreatments on drying characteristics of banana slices*. ARPN J Eng Appl Sci,* 6(3), 121-129.

Abdulsalam, R. A., Ijabadenyi, O. A., Cason, E. D. & Sabiu, S. (2023). Characterization of microbial diversity of two tomato cultivars through targeted next-generation 16S rRNA and ITS technique. *Microorganisms*, 11, 2337. https://doi.org/10.3390/microorganisms11092337

Abushita, A. A., Davoodi, H. G. & Biacs, P. A. (2000). Change in carotenoids and antioxidant vitamins in tomato as a function of varietal and technological factors. *J Agric Food Chem,* 48, 2075-2081.

Adebowale, Y. A., Adeyemi, I. A. & Oshodi, A. A. (2005). Functional and physicochemical properties of six *Mucuna* species. *Afr J Biotech,* 4(12), 1461-1468.

Adedire, O., Oladejo, A. O., Mbah, J. J., Popoola, A. S., Sadiku, Y., Onuwa, G. C. & Sikiru, G. K. (2022). Analysis of spoilage and storage of fresh tomato in Plateau Nigeria. *Food Agribusiness Mgt,* 3(2), 37-41. http://doi.org/10.26480/fabm.02.2022.37.41

Adejo, G. O., Agbali, F. A. & Otokpa, O. S. (2015). Antioxidant, total lycopene, ascorbic acid and microbial load estimation in powdered tomato varieties sold in Dutsin-Ma market. *Open Access Lib J,* 2, 1-7. http://dx.doi.org/10.4236/oalib.1101768

Aderibigbe, O. R., Owolade, O. S., Egbekunle, K. O., Popoola, F. O. & Jiboku, O. O. (2018). Quality attributes of tomato powder as affected by different pre-drying treatments. *Int Food Res J,* 25(3), 1126-1132.

Agada, E. O., Mohammed, S. S. & Nurudeen, A. O. (2023): Isolation and identification of bacteria associated with selected canned tomatoes sold in Utako market, Abuja. *FUW Trends Sci Tech J,* 8(2), 319-325.

Aggarwal, P., Goyal, P. & Kpoor, S. (2016). Effect of drying methods and pre-treatments on phytonutrients of tomato slices. *Int J Food Ferm Tech* 6(2), 421-432. http://dx.doi.org/10.5958/2277-9396.2016.00068.4

Aguda, O. Y., Faola, D. B., Oyedeji, M. B., Adegboyega, D. A., Akala, A. O. & Omotoso, T. P. (2021). Microorganism associated with the deterioration of tomato fruits (*Lycopersicon esculentum*) in Shasha market, Akure, Ondo State. *J Adv Microbiol Resear,* 2(1), 01-06.

Ahaotu, I., Wondikom, M. & Maduka N. (2021a). A preliminary study on the effect of storage temperatures on the population of *Bacillus cereus* in dry ginger powder. *J Biosci Biotech Discov,* 6(5), 53-57.

Ahaotu, I., Eze, O. & Maduka, N. (2021b). Quality assessment of corn-breadfruit-date flour and sensory evaluation of chin-chin prepared using the composite flours. *Adv Biotech Microbiol,* 16(3), 35-53.

Ahmad, A., Gungula, D. T., Tame, V. T., Kapsiya, J., Ilesanmi, J. O. & Kirawa, D. M. A. (2022). Effects of different drying methods and packaging materials on the physical and sensory qualities of tomato (*Lycopersicon lycopersicum* L.). *Intl J Agric Policy Resear,* 10(1), 26-30. https://doi.org/10.15739/IJAPR.22.004

Akpaetok, D. E., Ahaotu, I. & Maduka, N. (2023). Effect of pasteurization and storage temperatures on the quality of carrot juices. *Asian J Bio Sci,* 16(4), 600-613.

Alabi, O. O., Abdulazeez, I., Anekwe, C. E., Sambo, S. B., Alabuja, F. O., Drisu, T., Safugha, G. F., Obinna-Nwandikom, C. O., Abdullahi, M. & Aluwong, S. J. (2023). Technical efficiency differentials of tomato (*Solanum lycopersicum*) production under traditional and improved technologies in Nigeria. *Nepalese J Agric Sci*, 24, 186-198. http://esjindex.org/search.php?id=6279

Aliyu, L. S., Usman, A. Y., Musa, A. & Mani, U. (2018). Fungi isolated from dried tomato chips marketed in Sokoto metropolis. *J Adv Botany Zool,* 6(2), 1-3. http://dx.doi.org/10.5281/zendo.1210138

Amurtiya, M. & Adewuyi, K. A. (2020). Analysis of tomato production in some selected local government areas of Kano State, Nigeria. Proceedings of the 3rd International Network for Economic Research Symposium on Agri-Tech Economics for Sustainable Futures, 80-88pp.

Anisuzzaman, S. M., Joseph, C. G., Nga, J. L. H. & Ismail, F. N. (2022). Effect of carrier agents and operational parameters on the physical quality of spray-dried tomato powder: a review. *ASEAN J Chem Eng,* 22(2), 228-247. http://dx.doi.org/10.22146/ajche.71487

AOAC (2000). Official Methods of Analysis of Association of Official Analytical Chemists International, 17th edition. Washington, USA.

Bawa, F. M. (2023). Evaluating the quality of swish oven dried tomato powder. *Int J Home Sci,* 9(3), 87-92.

Bhat, I. M., Wani, S. M., Mir, S. A. & Nssem, Z. (2023): Effect of microwave-assisted vacuum and hot air ovendrying methods on quality characteristics of apple pomace powder. *Food Prod, Proc Nutri* 5, 26. https://doi.org/10.1186/s43014-023-00141-4

Caritá, A. C., Fonseca-Santos, B., Shultz, J. D., Michniak-Kohn, B., Chorilli, M. & Leonardi, G. R. (2020). Vitamin C: one compound, several uses. Advances for delivery, efficiency and stability. *Nanomedicine: Nanotech, Bio Med,* 24, 1-15. https://doi.org/10.1016/j.nano.2019.102117

Chabi, I. B., Zannou, O., Dedehou, E. S. C. A., Ayegnon, B. P., Odouaro, O. B. O., Maqsoos, S., Galanakis, C. M. & Kayodé, A. P. P. (2024): Tomato pomace as a source of valuable functional ingredients for improving physicochemical and sensory properties and extending the shelf life of foods: a review. *Heliyon,* 10, 1-16. https://doi.org/10.1016/j.heliyon.2024.e25261

Chawafambira, A. & Maramba, B. B. (2022). Use of sodium metabisulphite and citric acid to control degradation of nutraceutical compounds in dried tomato powder during prolonged storage. *J Food Proc Preserv,* 46, e16149. https://doi.org/10.1111/jfpp.16149

Chen, C. H. L. B. H. (2005). Stability of carotenoids in tomato juice during processing. *Eur Food Resear Tech,* 221, 274-280.

Collins, E. J., Bowyer, C., Tsouza, A. & Chopra, M. (2022). Tomatoes: an extensive review of the associated health impacts of tomatoes and factors that can affect their cultivation. *Bio,* 11, 1-44. https://doi.org/10.3390/biology11020239

Cruickshank, R., Duguid, J. R., Mermin, B. P. & Swain, R. H. A. (1975). Medical Microbiology. Churchill Livingstone Edinburg, London.

Dabai, S. M., Hindatu, H., Buhari, Y., Mubarak, I. & Mukhtar, G. (2020). Determination of pH and microbiological quality of commonly used tomato pastes in Katsina metropolis, Katsina state, Nigeria. *Int J Sc Tech,* 8(6), 53-62. http://dx.doi.org/10.24940/theijst/2020/v8/i6/ST2006-021

Degwale, A., Asrat, F., Eniyew, K., Asres, D., Tesfa, T. & Ayalew, A. (2022). Influence of dehydration temperature and time on physicochemical properties of tomato (*Solanum lycopersicum* L.) powder. *Front Sustainable Food Syst,* 6, 1-9. http://dx.doi.org/10.3389/fsufs.2022.839385

Dube, J., Ddamulira, G. & Maphosa, M. (2020). Tomato breeding in Sub-Saharan Africa-challenges and opportunities: a review. *Afr Crop Sc J,* 28(1), 131-140. DOI: https://dx.doi.org/10.4314/acsj.v28i1.10

Dufera, L. T., Hofacker, W. & Esper, A. (2023). Effect of packaging materials on lycopene vitamin C and water activity of dried tomato (*Lycopersicon esculentum* Mill.) powder during storage. *Food Sci Nutri,* 11, 6223-6230. http://dx.doi.org/10.1002/fsn3.3562

Dūma, M., Alsina, I., Dubova, L., Gavare, D., & Erdberga, L. (2022). Quality of different coloured tomatoes depending on the growing season. *Proceedings of the Latvian Acad Sci,* 76(1), 89-95. http://dx.doi.org/10.2478/prolas-2022-0014

Farid, E., Mounir, S., Talaat, E., Elnemr, S. & Siliha, H. (2022). Effect of foaming parameters on the physical and phytochemical properties of tomato powder. *Food Sci Biotech,* 31, 1423-1431. https://doi.org/10.1007/s10068-022-01125-9

Farooq, S., Rather, S. A., Gull, A., Ganai, S. A., Masoodi, F. A., Wani, S. M. & Ganaie, T. A. (2020). Physicochemical and nutraceutical properties of tomato powder as affected by pretreatments, drying methods, and storage period. *Intl J Food Propert,* 23(1), 797-808. https://doi.org/10.1080/10942912.2020.1758716

Fish, W. W., Perkins-Veazie, & Collins, J. K. (2002). A quantitative assay for lycopene that utilizes reduced volumes of organic solvents. *J Food Comp Analyses,* 15, 309-317.

Gameh, M. A., Elwakeel, A. E., Eissa, A. S. & Mostafa, N. B. (2024): Recent advances in solar drying technologies for tomato fruits: a comprehensive review. *Intl J Appli Energ Syst,* 6(1), 37-44.

Garg, R. K., Batav, N., Silawat, N. & Singh, R. K. (2013). Isolation and identification of pathogenic microbes from tomato puree and their delineation of distinctness by molecular techniques. *J Appli Bio Biotech,* 1(04), 024-031.

Hameed, O. B., Ahsan, H. & Nissar, N. (2018). Influence of pre-treatments, packaging material and storage on the crude and dietary fiber content of dried tomato slices (variety Punjab Chuhra). *Intl J Adv Resear Sci Eng,* 7(4), 1913-1918.

Harrigan, W. F. & McCance, M. E. (1976). Laboratory Methods in Food and Diary Microbiology, 2nd Edition, Academic Press Inc. London, 322pp.

Hirata, R., Kojima, K., Teramoto, Y. & Saigusa, N. (2024). Effect of conditions in the production of highly soluble powder from tomatoes using microbial enzyme preparation. *Afri J Biochem Resear,* 18(1), 1-9. http://dx.doi.org/10.5897/AJBR2024.1182

Hussein, J. B., Usman, M. A. & Filli, K. B. (2016). Effect of hybrid solar drying method on the functional and sensory properties of tomato. *Am J Food Sci Tech,* 4(5), 141-148. http://dx.doi.org/10.12691/ajfst-4-5-4

Ire, F. S., Benneth, G. K. & Maduka, N. (2020). Evaluation of ready-to-drink tigernut drinks sold within Port Harcourt metropolis, Rivers state, Nigeria. *Asian Food Sci J,* 16(1), 45-58.

Jayathunge, K. G. L. R., Kapilarathne, R. A. N. S., Thilakarathne, B. M. K. S., Fernando, M. D., Palipane, K. B. & Prasanna, P. H. P. (2012). Development of a methodology for production of dehydrated tomato powder and study the acceptability of the product. *J Agric Tech,* 8(2), 765-773.

Jones, D., Chinnaswamy, R., Tan, Y. & Hanna, M. (2000). Physiochemical properties of ready-to-eat breakfast cereals. *Cereal Foods World,* 45, 164-166.

Kaushal, P., Kumar, V. & Sharma, H. K. (2012). Comparative study of physicochemical, functional, anti-nutritional and pasting properties of taro *(Colocasia esculenta),* rice *(Oryza sativa),* pigeon pea *(Cajanus cajan)* flour and their blends. *LWT-Food Sci Tech,* 48, 59-68.

Kumar, M., Tomar, M., Bhuyan, D. J., Punia, S., Grasso, S., Sá, A. G. A., Carciofi, B. A. M., Arrutia, F., Changan, S., Radha, S. S., Dhumal, S., Senapathy, M., Satankar, V., Anitha, T., Sharma, A., Pandiselvam, R., Amarowicz, R. & Mekhemar, M. (2021). Tomato (*Solanum lycopersicum* L.) seed: a review on bioactives and biomedical activities. *Biomed Pharmacotherapy,* 142, 1-18. https://doi.org/10.1016/j.biopha.2021.112018

Kumar, V., Singh, S., Chandra, S., Singh, B. R. & Yadav, A. (2016). Effect of microbial growth on dehydrated tomato powder during different drying conditions. *J Pure Appli Microbiol,* 10(4), 2997-3002. http://dx.doi.org/10.22207/JPAM.10.4.69

Ladi, O. J., Awod, Y. P., Obogeh, K. A. & Alfa, I. N. (2017). Effect of drying methods and storage conditions on nutritional value and sensory properties of dehydrated tomato powder (*Lycopersicon esculentum*). *Int J Biochem Resear Rev,* 19(1), 1-7. http://dx.doi.org/10.9734/IJBCRR/2017/33103

Latapi, G. & Barrett, D. M. (2006). Influence of pre-drying treatments on quality and safety of sun-dried tomatoes. Part I: Use of steam blanching, boiling brine blanching and dips in salt or sodium metabisulphite. *J Food Sci,* 71, 1-20.

Leke, L. & Bembur, K. (2023). Effect of pre-treatment methods on the quality attributes of tomato powder. *Nig Annals Pure Appli Sci,* 6(1), 29-41.

Lyu, X., Ying, D., Zhang, P. & Fang, Z. (2024). Effect of whole tomato powder or tomato peel powder incorporation on the colour, nutritional, and textural properties of extruded high moisture meat analogues. *Food Bioproc Tech,* 17, 231-244. . https://doi.org/10.1007/s11947-023-03133-x

Masamba, K. G., Mkandawire, M., Chiputula, J. & Nyirenda, K. S. (2013). Evaluation of sensory quality attributes and extent of vitamin C degradation in dried pineapple, mango, and banana fruit pieces pre–treated with sodium metabisulphite and lemon juice. *Int Res J Agric Sc Soil Sci,* 3(3), 75-80.

Mateo-Roque, P., Morales-Camacho, J. I., Jara-Romero, G. J., Rosas-Cárdenas, F. F., Huerta-González, L. & Luna-Suárez (2024): Supercritical CO_2 treatment to modify techno-functional properties of proteins extracted from tomato seeds. *Foods*, 13, 1045. https://doi.org/10.3390/foods13071045

Nanelo, R. F. & José, A. E. (2023). Variation of physicochemical characteristics of tomato under different traditional forms of conservation. *Int J Food Studies,* 12, 112-122. http://dx.doi.org/10.7455/ijfs/12.1.2023.a8

Narayana, K. & Narsinga, R. M. S. (1982). Functional properties of war and heat processed winged bean (*Psophocarpus tetragonolobus*) flour. *J Food Sci,* 42, 534-538.

Nishizono, M., Issasi, C. S. C., Agutaya, J. K. C. N., Sasaki, M. & Mizukami, H. (2023). Production of dried tomato powder with a high concentration of functional components and nutrients. *J Antioxid Act,* 2(4), 1-21. http://dx.doi.org/10.14302/issn.2471-2140.jaa-23-4426

Obadina, A., Ibrahim, J. & Adekoya, I. (2018). Influence of drying temperature and storage period on the quality of cherry and plum tomato powder. *Food Sci Nutri,* 6, 1146-1153. https://dx.doi.org/10.1002/fsn3.658

Obajemihi, O. I., Cheng, J. H. & Sun, D. W. (2024). Novel cold plasma functionalized water pretreatment for improving drying performance and physicochemical properties of tomato (*Solanum lycopersicum* L.) fruits during infrared-accelerated pulsed vacuum drying. *J Food Eng,* 379, 1-13. https://doi.org/10.1016/j.jfoodeng.2024.112050

Obiaocha-Nwaogwugwu, C. N., Eruteya, O. C. & Ahaotu, I. (2024). Shelf-life extension of tomatoes (*Solanum lycopersicum*), okra (*Abelmoschus esculentus*) and eggplant (*Solanum melongena*) using edible coating. *Scientia Africana,* 23(2), 375-388. https://dx.doi.org/10.4314/sa.v23i2.35

Oboulbiga, E. B., Parkouda, C., Dabiré, C., Aimée, W. D., Guissou, B., Traore, K., Semde, Z., Douamba, Z., Sawadogo-Lingani, H. & Dicko, M. H. (2022). Storage stability of dried tomato slices during storage as affected by salt and lemon pretreatments. *Intl J Food Properties,* 25(1), 450-462. https://doi.org/10.1080/10942912.2022.2046051

Ogunsola, O. A. & Ogunsina, G. A. (2021). Tomato production and associated stress: a case of African climate. *Single Cell Bio,* 10(4), 1-5.

Oladipupo, R. A., Yusuf, K. A. & Salawu, G. (2020). Effect of storage materials on the proximate composition of tomato (*Lycopersicon esculentum*) powder. *FUDMA J Sci,* 4(2), 203-206. https://dx.doi.org/10.33003/fjs-2020-0402-212

Ossamulu, I. F., Akanya, H. O., Egwim, E. C. & Kabiru, A. Y. (2023). Improvement of shelf-life and nutrient quality of tomatoes and eggplant fruits using chitosan-starch composite coat. *Acta Sci Pol Technol Aliment,* 22(1), 43-55. http://dx.doi.org/10.17306/J.AFS.2023.1092

Owureku-Asare, M., Oduro, I., Saalia, F. K., Tortoe, C., Ampah, J. & Ambrose, K. (2022). Drying characteristics and microbiological quality assessment of sun-dried tomato. *Intl J Food Sci,* 1-13. https://doi.org/10.1155/2022/2352327

Panagiotou, N. M., Karathanos, V. T. & Maroulis, Z. B. (1998). Mass transfer modeling of the osmotic dehydration of some fruits. *Int. J Food Sci Tech,* 33(3), 267-284.

Ramya, H. N., Ashwini, A., Veena, B., Fazal, A. A. & Hanumanthraju, K. N. (2017): Influence of different drying techniques on dehydrated tomato powder. *Int. J Creative Resear Thoughts,* 5(3), 474-482.

Ranjan, S. K. & Shankar, P. (2024). Study on physiochemical and nutritional properties of tomato powder dried in solar dryer and dehydrator. *Int J Res Publ Rev*, 5(7), 1512-1517.

Samson, R. A. & Van-Reenen-Hockstra (1988). Introduction of Food Borne Fungi, 2nd Edition, Centroalbureau Voor Schimmel cultures, Baam. The Netherlands, pp. 299.

Sarker, M., Hannan, M. A., Quamruzzaman, M. A. A. & Khatun, H. (2014). Storage of tomato powder in different packaging materials. *J Agri Tech,* 10(3), 595-605.

Silva, F. D., Garcia, V. A. S., Vanin, F. M., Yoshida, C. M. P. & Carvalho, R. A. (2023). Application of tomato byproduct in food products-a review. *Food Sci Eng,* 4(1), 103-115. http://ojs.wiserpub.com/index.php/FSE/

Sosulski, F. W., Garatt, M. O. & Slinkard, A. E. (1976). Functional properties of ten legume flours. *Intl J Food Sci Tech,* 9, 66-69.

Suleiman, H. A., Owuna, J. E., Makut, M. D., Yahaya, I., Ekeleme, I. K., Abdullahi, Z. T. (2023): Assessment of mycotoxin producing fungi isolated from dried tomato chips sold in Keffi, Nigeria. *World J Adv Eng Tech Sci,* 9(02), 235-241. https://doi.org/10.30574/wjaets.2023.9.0222

Tafida, I., Idris, A. A., Ashura, B. A. & Nasiru, A. (2023). Analysis of adoption of tomato post-harvest technologies among smallholder farmers in Katsina State, Nigeria. *FUW Trends Sci Tech J,* 8(2), 413-418.

Xu, Q., Adyatni, I. & Reuhs, B. (2018). Effect of processing methods on the quality of tomato products. *Food Nutri Sci,* 9, 86-98. http://www.scirp.org/journal/fns

Yadav, A. K. & Ali, Z. (2023). Modern drying techniques in fruits and vegetables to reduce postharvest losses. *Indian Farmer,* 10(03), 101-104.

Yasumatsu, K., Sawada, K., Maritaka, S., Toda, J., Wada, T. & Ishi, K. (1972). Whipping and emulsifying properties of soy bean products. *Agric Bio Chem,* 36, 719-727.

Yegrem, L. & Dagnaw, L. A. (2022). Pretreatments, dehydration methods and packaging materials: effects on the nutritional quality of tomato powder: a review. *Archive Food Nutri Sci,* 6:050-061. https://dx.doi.org/10.29328/journal.afns.1001038

Yegrem, L. & Ababele, L. (2022). Pretreatments, dehydration methods and packaging materials: effects on the nutritional quality of tomato powder. *Austin J Nutri Food Sci,* 10(2), 1-11.

Yusuf, Y., Engin, D. & Yahya, T. (2013). Degradation kinetics of lycopene, β-carotene and ascorbic acid in tomatoes during hot air drying. *LWT-Food Sci Tech,* 50, 172-176.

Zambare, A. V. & Kulkarni, D. A. (2023). Experimental investigation on drying of tomato slices. *J Pharmacog Phytochem,* 12(6), 11-19.

STUDIA UNIVERSITATIS BABEŞ-BOLYAI BIOLOGIA, 70, 1, 2025 (p. 213-230)
doi:10.24193/subbbiol.2025.1.10

Influence of soil depth on seedling growth and development of *Amaranthus viridis* L. after amendment with organic fertilizer

Beckley Ikhajiagbe[1]✉, Augustine W. Ojanikele[2], Barka P. Mshelmbula[3], Gloria O. Omoregie[4], and Moteniola C. Adebiyi[1]

[1]Dept of Plant Biology and Biotechnology, University of Benin, Benin City, Nigeria; [2]Department of Surveying and Geoinformatics, Delta State University of Science and Technology, Ozoro, Delta State, Nigeria; [3]Dept of Botany, Federal University, Lafia, Nigeria; [4]Department of Environmental Management and Toxicology, Federal University of Petroleum Resources Effunrun, Delta State, Nigeria
✉***Corresponding author, E-mail: beckley.ikhajiagbe@uniben.edu***

Article history: Received 24 November 2024; Revised 26 April 2025; Accepted 26 April 2025; Available online 25 June 2025

Abstract. The implications of applying organic fertilizers made from dried cow dung and food waste on the seedling development and growth of *Amaranthus viridis* at different soil horizons was examined in the current study. The experiment was set up in a completely randomized design, with 6 profile depths x 3 fertilizer treatments x 3 replicates each, totaling 54 bowls. The set up was left for 5 weeks. The findings demonstrated that cow dung manure provided adequate plant nutrients for enhancing seedling growth *A. viridis*. Although 0.05 g seeds of *A. viridis* was sown in the bowls, emergence capacities under varying soil conditions differed. Amending the soils with food waste manure hampered emergence capacities of the test plant. There were only six (06) sprouts at the first week compared to 46 in the control. Despite the observation that soil horizon and organic fertilizer application had no discernible effect on the root length of 5 - week - old seedlings (which varied between 1.3 cm and 2.3 cm), the use of manure was associated with a decrease in foliar chlorosis incidence. Without manure, foliar chlorotic incidence was 58 % in the 61 – 75 cm soil profile depth, compared to 35.0 – 35.2 % when soils were

amended with either cow - dung or dried food waste manure. Ultimately, while deeper soil horizons initially posed challenges for growth, soil amendment successfully alleviated these unfavorable conditions.

Keywords: *soil horison, food waste manure, cow dung manure, nutrient availability, foliar chlorosis*

Introduction

Soil composition is dynamic and varies significantly across different levels due to various factors, including organisms, plants, microbes, and human activities (Kumar, 2020). This variability affects soil structure, fertility, and overall productivity. Human activities, such as deforestation, intensive farming, and urbanization, have profound impacts on soil health. Urbanization, in particular, has led to widespread soil degradation, erosion, and loss of arable land.

The consequences of human population expansion and urbanization on farmland are alarming. Farmlands intended for agricultural use have been rapidly taken over by estate developers and mining support businesses, resulting in soil excavation, environmental harm, and decreased food production (Oluwatosin and OjoAtere, 2001). This trend is exacerbated by the growing demand for housing, infrastructure, and natural resources. As a result, fertile soils are being irreversibly damaged, threatening food security and sustainable development.

Ensuring sustainable food production and soil management presents formidable challenges globally. The continuous expansion of the world's population is expected to intensify the strain on already burdened food systems (United Nations, 2020). Additionally, the increasing conversion of land due to urbanization, which involves significant topsoil removal for construction, contributes substantially to soil degradation and erosion (Wainaina *et al*., 2022; Pimentel, 2006).

Healthy soil is essential for the maintenance of vital ecosystem services, such as the filtering of water and the sequestration of carbon (Gong & Chen, 2011; Lal, 2015). However, the processes of soil excavation and erosion can severely compromise soil quality and fertility, negatively affecting agricultural productivity and disrupting these critical ecosystem services (Zhao *et al*., 2021; Kumar, 2020). In Nigeria's peri-urban areas, the practice of unmanaged soil excavation has resulted in substantial environmental deterioration, a decline in biodiversity, and adverse impacts on the livelihoods of local communities (Wainaina *et al*., 2022).

This study aims to address the urgent problems of soil degradation, diminished crop productivity, and the need for environmental sustainability by examining how different soil horizons influence crop development, with a specific focus on *Amaranthus viridis*. Specifically, the research will investigate the effects of varying soil horizons on the growth, yield, and nutritional value of *A. viridis*, a crop of significant importance for food security and nutrition in numerous communities. Furthermore, by evaluating the potential of organic fertilizer formulations derived from common household waste, this research seeks to contribute to the enhancement of agricultural output, the promotion of longterm food security, and the strengthening of ecosystem resilience.

Materials and methods

Study location

This research was conducted at the University of Benin's Ugbowo campus, specifically near the Department of Plant Biology and Biotechnology's screen house, located in Benin City, Edo State, Nigeria.

Experimental design

The study employed a completely randomized design (CRD) to investigate the effects of different soil profiles and organic amendments on crop development. The treatments consisted of soils from different profiles amended with cow dung manure (CDM), soils from different profiles amended with food waste manure (FWM), and a control group without any amendments. Each treatment was replicated three times.

Soil sampling

Soil samples were collected from three random farm locations in Ovia North-East Local Government, Edo State, Nigeria (Figure 1). The sampling area was carefully selected, and surface litter was removed. When soils were collected, all soils were pooled to obtain a composite sample, which was thereafter used for the experiment.

For profile soil sampling, four profile pits were dug using a shovel and digger, and composite sampling was carried out to mix the same horizon from different pits. Samples were taken from the first horizon to avoid contamination.

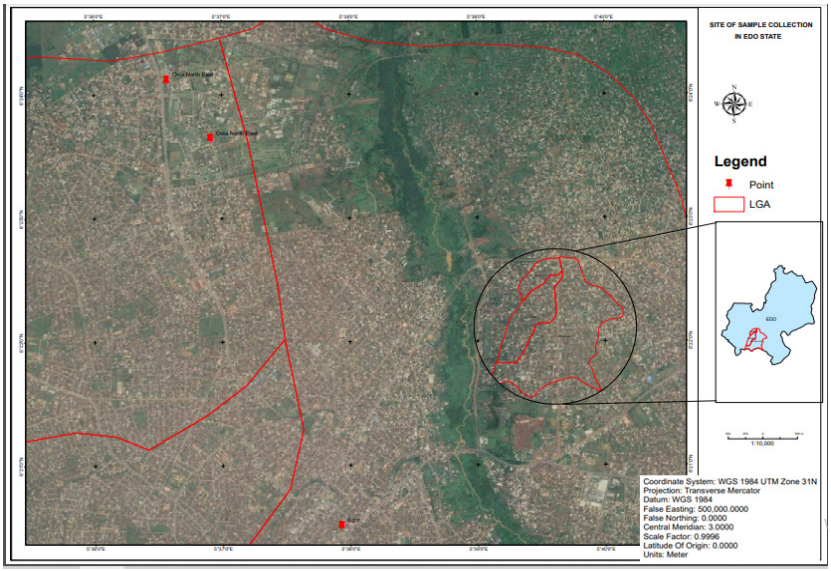

Figure 1. Map of soil collection locations

Each soil horizon was extracted and transferred into labelled nylon bags. Soil samples were collected from 0 to 75 cm depth, with 15 cm intervals, except for the topmost soil (0-10 cm and 11-15 cm). This resulted in six samples each, representing different horizons within the soil profile (Figures 2 and 3).

(a) **(b)**

Figure 2. Excavating one of the pits to obtain soil samples from various profile depths

(a) **(b)**

Figure 3. Image capturing the pit and its profiles

Development of organic fertilizers

This section outlines the procedures for developing two organic fertilizers used in the study.

Cow dung manure

Dried cow dung was sourced from the Aduduwa Cattle Market in Edo State. The dung was sun - dried to constant weight to ensure optimal moisture removal and readiness for use.

Dry food waste manure

The development of dry food waste manure (FWM) involved several key steps. Initially, food waste was collected from various locations, including Ekosodin and Uselu markets in Benin City, as well as local vendors. The collected waste was then sorted to separate different components. The composition of the dried food waste consisted of various organic materials, including orange peels (1800 g),

onion peels (500 g), plantain peels (1000 g), pineapple peel (400 g), watermelon (200 g), yam peels (300 g), potato peels (180 g), vegetables (300 g), eggshells (50 g), and dried leaves (200 g).

The food waste components underwent further processing to create the FWM. Each component was sun - dried to constant weight for 30 days to ensure optimal moisture removal. The dried components were then blended into a fine powder using a local mill. Finally, the powdered components were mixed together to create a homogeneous blend. This resulting FWM, along with CDM, was used as an organic fertilizer to amend the soil samples in the experiment, providing a nutrient - rich medium for plant growth.

Separation into bowls

The soil from each horizon was divided among three bowls, labeled A, B, and C, and then replicated. This resulted in a total of 54 bowls, based on the experimental design: 6 profile depths × 3 fertilizer treatments × 3 replicates each. The bowls, with a total surface area of 304.84 cm^2, were modified to prevent waterlogging. Five evenly spaced perforations were made in the bottom of each bowl using a nail, allowing for adequate percolation and drainage.

Treatment application

This research utilized 54 bowls, divided into three categories: A, B, and C. Categories A and B consisted of six bowls each, with different soil profiles mixed with CDM and dry FWM, respectively. Category C comprised 18 unamended soil profiles as controls. For the amended bowls (A and B), organic fertilizers were added on a weight/weight basis at a 10 % w/w concentration, with 1.6 kg of CDM or FWM added to 16 kg of soil dry weight per bowl.

Sowing

Following a one - week period, *A. viridis* seeds were broadcast - sown at 0.05 g per treatment. To facilitate even seed distribution and prevent overcrowding, this method was chosen. The bowls, with a surface area of 304.84 cm^2, received 1000ml of water after seeding and were then moved to their permanent locations. The resulting seed application density was 0.048 g per 304.84 cm^2, equivalent to 0.164 mg/cm^2.

Cultural practices and parameter measurement

The bowls were watered every two days for the first two weeks, then daily thereafter. Regular hand weeding was performed at intervals. To assess plant growth and development, several parameters were measured: plant height, chlorosis, leaf color, number of leaves, root length, and biomass. Specifically, plant height was measured using a meter rule on an index plant in each bowl. Chlorosis was evaluated by observing yellowing foliage as plants aged. Leaf color was assessed visually using a physical color namer map. The number of leaves in each bowl was counted and recorded. Root length was measured by carefully removing the index plant from each bowl and using a meter rule.

Determination of soil physico - chemical characteristics

Soil samples were collected at 3 random areas within pooled random depths (0 – 15 cm) within the area where soil was obtained, just before determination of plant identification and determination for soil seed bank assessment. Top soil was collected. Soils were analyzed for soil physico - chemical parameters according to methods described by Hanway and Heidel (1952); Metson (1961); Nelson and Sommers (1982); APHA (1985).

Isolation of bacterial and fungal isolates

Bacterial and fungal isolates were isolated using established microbiological protocols (Cheesebrough, 2000). Soil samples from each treatment underwent serial dilution and plating on selective media (nutrient agar for bacteria and potato dextrose agar for fungi). Following incubation at optimal temperatures (28 °C for bacteria and 25 °C for fungi) for 24 - 48 hours, colonies were counted and isolated based on distinct morphological features. Isolated microorganisms were purified through successive subculturing and preserved on agar slants at 4 °C for subsequent identification and analysis (Cheesebrough, 2000).

Data analysis

Results are reported as means of three replicates. Single- - factor analysis of variance (ANOVA) was employed to evaluate treatment effects. Statistical analysis was performed using IBM SPSS Statistics version 23 and Paleontological Statistics (PAST) software version 2.17c, where necessary, to assess significant differences between treatments and provide a comprehensive understanding of the data.

Results

The microbial populations in the organic fertilizers used in the study, analyzed just prior to soil application, are presented in Figure 4. Notably, the bacterial counts differed significantly between the two fertilizers. The dry FWM harbored a mean bacterial count of 6.50 ± 2.12 x 10^4 CFU/g, whereas the CDM had a significantly higher count of 11.75 ± 1.06 x 10^4 CFU/g. In contrast, fungal counts were relatively similar, with FWM exhibiting 1.07 ± 0.42 x 10^4 CFU/g and CDM showing 0.93 ± 0.36 x 10^4 CFU/g.

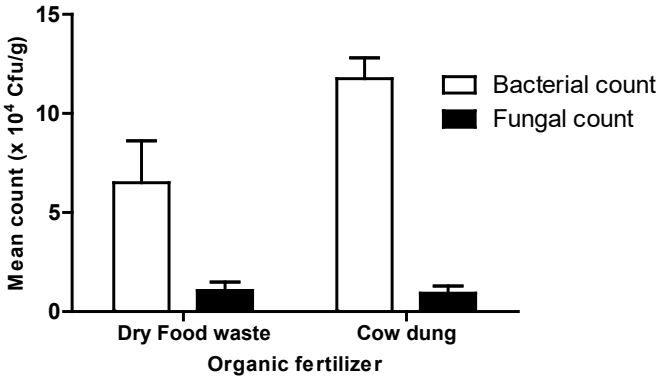

Figure 4. Bacterial and fungal counts in the materials used as organic fertilizer just before application to soil

The culturable bacterial and fungal composition of organic fertilizers used in the study, analyzed just before soil application, is presented in Table 1. The comparative analysis revealed a higher diversity of bacterial isolates in cow dung compared to dried food waste. Specifically, *Proteus mirabilis* was the predominant bacterial isolate in cow dung. In contrast, *Serratia marcescens* emerged as the dominant bacterial species in dried food waste. Regarding fungal composition, *Aspergillus fumigatus* and *Rhizopus stolonifer* were the predominant species in the organic fertilizers. Nutrient analysis, illustrated in Figure 5, showed significant differences between the two organic fertilizers. Cow dung exhibited a higher nitrogen content (12.43 %) compared to dried food waste. Conversely, dried food waste contained more potassium (36.34 %) than cow dung (28.12 %). These variations in microbial and nutrient composition may influence soil fertility and plant growth.

Table 1. Culturable bacterial and fungal composition of materials used as organic fertilizer just before application to soil

Isolates	Cow dung	Dry Food waste
Bacterial Isolates		
Bacillus subtillis	-	+
Proteus mirabilis	+++	-
Serratia marcescens	+	+++
Escherichia coli	+	+
Pseudomonas aeruginosa	+	-
Klebsiella oxytoca	+	-
Fungal Isolates		
Aspergillus niger	-	+
Aspergillus fumigatus	+	+
Rhizopus stolonifer	+	+
Trichoderma sp.	+	-
Penicillium sp.	-	+

Legend: + present; - absent

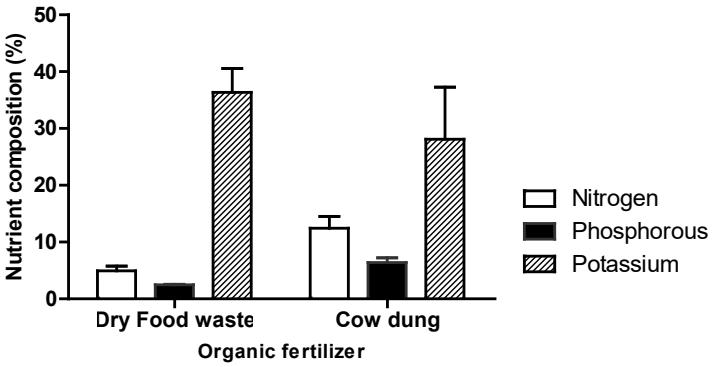

Figure 5. Nutrient composition of materials used as organic fertilizer just before application to soil

The emergence capacity of *A. viridis* seeds varied significantly under different soil conditions, as shown in Figure 6(a - c). Initially, 0.05 g of seeds were sown in each bowl. In unamended soils, collected from a depth of 0 - 10 cm, seed emergence was moderate, with 46 sprouts observed within the first week of

observation. This number increased to 69 sprouts by the third week, indicating continued germination and growth. In contrast, amending the soil of the same depth with CDM resulted in enhanced seed emergence, with 67 sprouts recorded in the first week (Figure 3).

However, amending the soil with FWM had a detrimental effect on seed emergence. After the first week, only six sprouts emerged in FWM - amended soil collected from 0 - 10 cm depth, and merely one sprout was observed in FWM - amended soil collected from 46 - 60 cm depth. This suggests that FWM may inhibit initial seed germination. Nevertheless, by the third week, rapid growth was observed in FWM - amended soils, indicating potential for delayed but accelerated development (Figure 6).

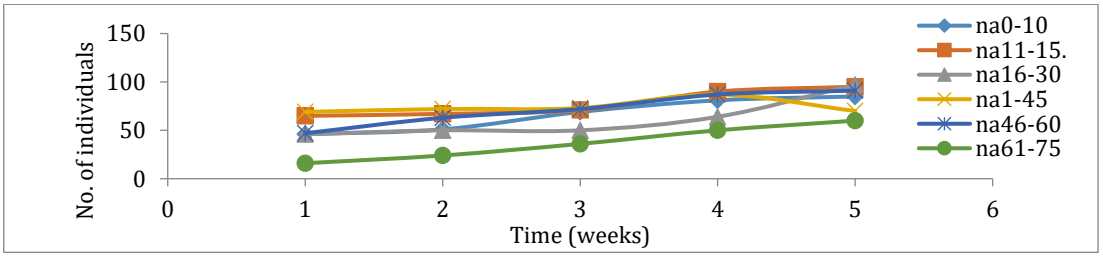

(a)

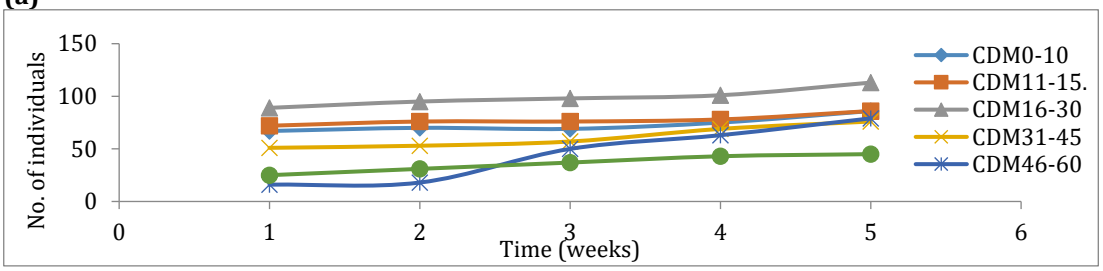

(b)

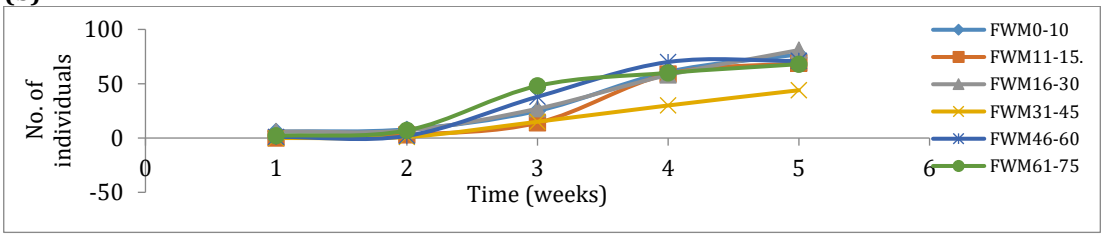

(c)

Figure 6. Amount of sprouts of *Amaranthus viridis* sown from 0.05 g seeds by broadcast on soils collected at different depth profiles 0 - 10, 11 - 15, 16 - 30, 31 - 45, 46 - 60 and 61 - 75cm respectively and amended with food waste manure (FMW), cow dung manure (CDM), and unamended (na).

Figure 7. Plants grown on soils obtained from the various horizons

Figure 8 illustrates the growth of *A. viridis* seedlings in soils of varying profile depths at 5 weeks post - sowing. Notably, unamended soils supported the growth of 85 individual seedlings from 0.05 g of seeds. In contrast, soils amended with dried CDM exhibited depth - dependent effects. At the 0 - 10 cm depth, CDM - amended soils yielded 86 sprouts, while the 31 - 45 cm depth profile produced 97 sprouts. Remarkably, the same depth profile with CDM amendment resulted in 113 sprouts, indicating optimal growth conditions.

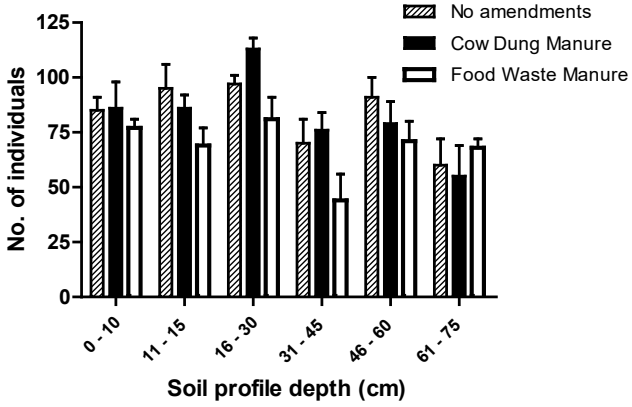

Figure 8. Number of individual *Amaranthus* seedlings grown in soils of differing profile depth at 5 weeks after sowing and soil amendments

The impact of soil depth on seedling growth was further underscored by the poor performance of seeds sown in deeper profiles (61 - 70 cm), regardless of amendment type. This depth range yielded only 55 - 68 sprouts, suggesting potential limitations in soil fertility, aeration, or moisture retention. In contrast, shallower depths (0 - 45 cm) demonstrated improved growth, particularly when amended with CDM.

Figure 9 illustrates the percentage of *A. viridis* seedlings with chlorotic foliage, indicating potential stress incidence. Notably, plants in deeper soil profiles (61 - 75 cm) exhibited higher foliar chlorosis (58 %) compared to those near the surface. However, manure application significantly reduced chlorotic incidence, with CDM and FWM amendments lowering rates to 35.0 - 35.2 %.

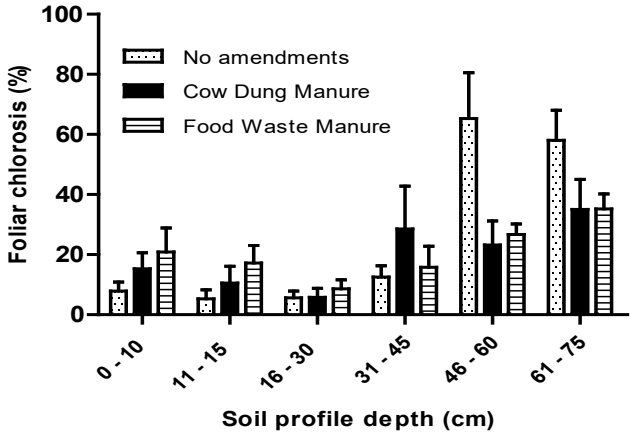

Figure 9. Percentage of leaves with chlorosis at 5 weeks after sowing and soil amendments.

The impact of soil amendments on seedling growth was further investigated. Without manure, leaf production remained stagnant (4 - 6 leaves per plant) across various soil profile depths. In contrast, adding CDM increased leaf production to 7 - 10 leaves per plant (Figure 10). This enhancement underscores the benefits of organic fertilizers on plant development. Root length, measured at 5 weeks, remained relatively consistent (1.3 - 2.3 cm) across soil horizons and fertilizer treatments (Figure 11). This suggests that root growth was not significantly influenced by soil depth or organic fertilizer application. Additional visual documentation of the experiment's setup at 3 weeks is provided in Figure 7.

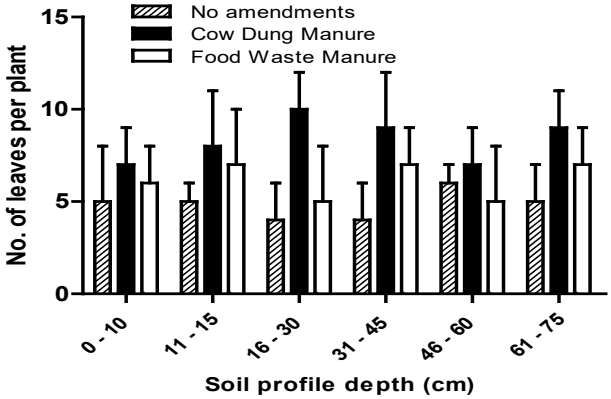

Figure 10. Number of leaves per plant at 5 weeks after sowing and soil amendments.

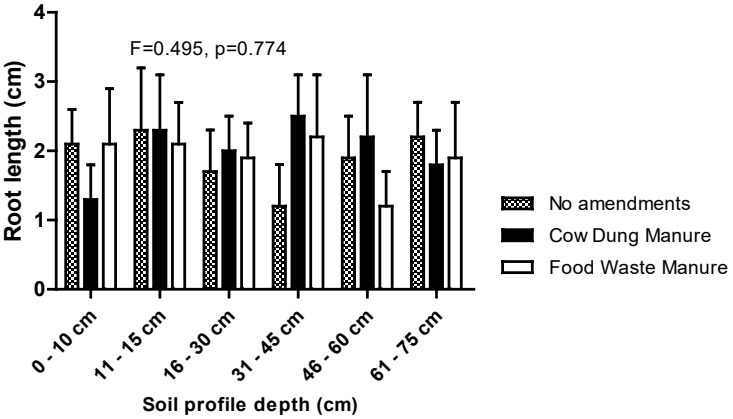

Figure 11. Root length of *Amaranthus viridis* seedlings at 5 weeks after sowing and soil amendments.

Figure 12 presents the total seedling dry weight of *A. viridis* after 5 weeks, originating from 0.05 g seeds. The data reveals significant effects of soil amendment and depth on biomass production. At the 0 - 10 cm horizon, seedlings without soil amendment had a biomass of 0.74 g, which increased to 0.89 g with cow dung amendment. Notably, the mean biomass across all amendment regimens within this horizon was 0.87 g. In contrast, seedlings in the 11 - 15 cm horizon exhibited higher biomass (1.05 g), while those in the deepest horizon (61 - 75 cm) had lower biomass (0.76 g).

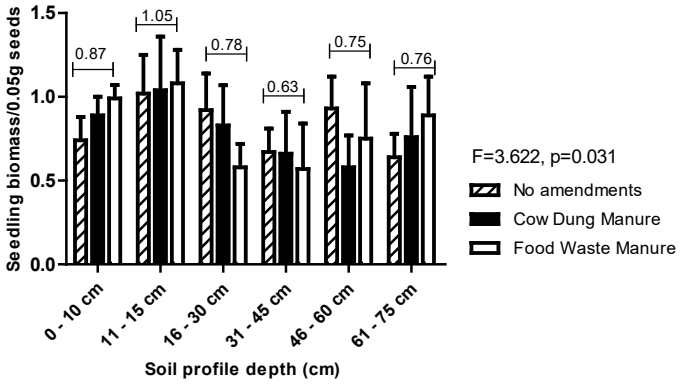

Figure 12. Total seedling biomass

Discussion

This study focused on the impact of soil depth on the growth of *A. viridis* after amendment with organic fertilizer. A primary role of soils is to provide plant roots with the nutrients required for growth and productivity (Miki *et al*., 2010). Soil is the largest pool of terrestrial organic carbon in the biosphere, storing more carbon than is contained in plants and the atmosphere combined (Schlesinger 1997).

The abundance of organic carbon in the soil affects and is affected by plant production, and its role as a key control of soil fertility and agricultural production has been recognized for more than a century. In agricultural production systems, plant roots grow below 25 cm and the deeper soils are important for crop yield, because top soils may dry out quickly during summer months, limiting the ability of roots to absorb water and nutrients in the upper layers of the soil profile. (Perkons *et al.,* 2014). Since plant growth is dependent on edaphic factors, the plant - soil interactions at different soil depths play a role in the abundance and composition of soil microbial communities. Although most studies have focused on nutrient rich topsoil, the roots of agricultural crops can grow as deep as 200 cm (Perkons *et al.,* 2014).

The subsoil which is also known as the B horizon contains some nutrients thereby making it capable of plant growth. Subsoils range in texture from gravel to heavy clay, in reaction from very acid to strongly alkaline, in fertility from very low to very high, and in structure and consistence from granular and friable to blocky, hard and plastic, or even cemented (Winters and Simonson, 1959; Reuss and Campbell, 1961).

Soils require nitrogen and phosphorus, with manure applications further enhancing response. Microbial abundance and diversity typically decrease with soil depth; this decrease can alter soil properties, while fertilizer incorporation improves crop yields, soil organic matter, and nutrient content (Gao *et al.,* 2015; Choudhary *et al.,* 2018).

Agboola and Unama (1991) emphasized the importance of maintaining soil organic matter in agricultural systems through practices that prevent its destruction or by consistently adding organic materials. Soil contains essential nutrients, and organic fertilizers enhance their availability for increased plant uptake and yield (Ref…). Applying organic fertilizers to the soil surface can provide a rich food source for microorganisms, significantly increasing microbial community composition and diversity (Chang *et al.,* 2007; Diacono and Montemurro, 2010).

Organic wastes such as animal manures, by - products of several kinds and composted residues can be used as amendments to increase soil fertility, since they are important sources of nutrients for growing crops and means for enhancing the overall soil quality (Davies and Lennartsson, 2005). Managing agricultural nutrients to provide a safe food supply and secure the environment remains one of the immense challenges of the 21st century. Crop nutrient uptake and crop yields are the principal factors that determine optimal fertilization practices. Therefore, it is very important to apply fertilizers in an efficient way to minimize loss and to improve the nutrient use efficiency.

Soil organic matter plays an important role in long - term soil conservation and/or restoration by sustaining its fertility, and hence in sustainable agricultural production, due to the improvement of physical, chemical and biological properties of soils (Sequi, 1989). The organic matter content is the result of the inputs by plant, animal and microbial residues, and the rate of decomposition through mineralization of both added and existing organic matter. Fertilization with manure improves soil's physical, chemical, and biological qualities, primarily by decreasing soil bulk density and improving structure (Ullah *et al.,* 2020; Du *et al.,* 2020). Organic fertilizers are applied to soil in precise amounts to increase soil organic carbon (SOC) and other vital plant nutrients, particularly N - P - K and micronutrients (Akhtar *et al.,* 2018; Iqbal *et al.,* 2021).

Soil organic carbon sequestration can be enhanced by fertilization such as incorporation of crop residues or the direct application of manure, which implies by high carbon inputs (Cai *et al.,* 2016). Based on 153 field experiments in China, Chen *et al*. (2014) observed an increase in crop yields of approximately 8.5 - 14.2 Mg ha^{-1} following fertilization with manure without any increase in nitrogen (N) fertilizer. According to literature, food waste cannot be used directly as a fertilizer. When food waste is used as a raw material for fertilization, various problems such as excessive salt content, mixing of impurities and odor arise (Chen *et al.,* 2021).

Conclusions

This study investigated the impact of soil horizons on the growth of *Amaranthus viridis* and the effects of organic fertilizer amendments. The results indicate that deeper soil horizons present less favorable conditions for seedling development. Seedling emergence and overall growth were notably influenced by soil depth, with shallower soil profiles generally supporting better development. The application of organic fertilizers, particularly cow dung manure, enhanced seedling growth and reduced foliar chlorosis. While food waste manure initially hampered seed emergence, it supported growth at later stages. These findings underscore the potential of organic amendments to improve soil conditions and promote *Amaranthus viridis* growth, particularly in less fertile soil horizons.

Acknowledgements. The authors are grateful to the students from the Department of Soil Science for their support in site identification.

References

Baxter, N.M., Williamson, J.R. (2001). *Know your Soils - Part 1: Introduction to Soils.* State of Victoria, Department of Natural Resources and Environment, Bendigo.

Bensch, E.A. (2003). Interference of redroot pigweed (*Amaranthus retroflexus*), Palmer amaranth (*Amaranthus palmeri*) and common waterhemp (*Amaranthus rudis*) in soybean. *Weed Sci., 51*(1), 37 - 43.

Blum, W.E.H., Warkentin, B.P. (2006). Soil, human society and the environment. In: Frossard, E. (eds.). Functions of Soils for Human Societies and the Environment. *Geol. Soc. Spec. Publ.*, London, 1 - 8. https://doi.org/10.1144/GSL.SP.2006.266.01.01

Blunden, G., Yang, M., Janicsak, G., Mathe, I., Carabot Cuervo, A. (1999). Betaine distribution in the Amaranthaceae. *Biochem. Syst. Ecol.*, *27*(1), 87 - 92.

Bratovcic, A., Zohorovic, M., Odobasic, A., Sestan, I. (2018). Efficiency of food waste as an organic fertilizer. *Int. J. Eng. Sci. Res. Technol., 7*(6), 527 - 530. https://doi.org/10.5281/zenodo.1299043

Brenan, J.P.M. (1981). The genus *Amaranthus* in southern Africa. J. S. Afr. Bot., *47*(3), 451 - 492. https://www.cabidigitallibrary.org/doi/full/10.5555/19812335778

Cheesebrough, M. (2000). Medical laboratory Manual for Tropical Countries (Vol. 2). Butterworth - Heinemann. ISBN: 0750646336

Dalziel, J.M. (1937). *The Useful Plants of West Tropical Africa.* Whitefriars Press Ltd, London.

Diacono, M., Montemurro, F. (2010). Long - term effects of organic amendments on soil fertility: A review. *Agron. Sustain. Dev., 30*(2), 401 - 422. https://doi.org/10.1051/agro/2009064

Diacono, M., Montemurro, F. (2011). Long - term effects of organic amendments on soil fertility. In: Lichtfouse, E., Hamelin, M., Navarrete, M., Debaeke, P. (eds.). *Sustainable Agriculture*. Springer, Dordrecht, 2 - 5. https://doi.org/10.1007/978-94-007-0394-0

Eluwa, M.C. (1977). Studies on *G. rhomboidalis* (Boheman) (Coleoptera: Curculionidae), a pest of African spinach. *J. Nat. Hist., 11*(3), 417 - 424. https://doi.org/10.1080/00222937700770191

Girotto, F., Alibardi, L., Cossu, R. (2015). Food waste generation and industrial uses: A review. *Waste Manag.*, *77*, 98 - 113. https://doi.org/10.1016/j.wasman.2015.07.002

Gong, B., Chen, B. (2011). The regulation analysis of low - carbon orientation for China land use. In: Li, D., Liu, Y. (eds.). *Computer and Computing Technologies in Agriculture.* Springer, Berlin/Heidelberg, 602 - 609.

Gong, Z., Chen, X. (2011). Soil science and sustainable development. *J. Integr. Agric., 10*(2), 147 - 155.

Grubben, G.J.H., Denton, O.A. (2004). *Plant Genetic Resources of Tropical Africa 2: Vegetable.* PROTA Foundation, Wageningen, 205 - 213.

Jiang, H., Han, X., Zou, W., Hao, X., Zhang, B. (2018). Seasonal and long - term changes in soil properties and organic carbon fractions as affected by manure application rates in the Mollisol Region of Northeast China. *Agric. Ecosyst. Environ.*, *268*, 133 - 143. https://doi.org/10.1016/j.agee.2018.09.003

Jin, C., Zheng, S., He, Y., Di, Z., Zhou, Z. (2005). Lead contamination in tea garden soils and factors affecting its bioavailability. *Chemosphere*, *59*(8), 51 - 90. https://doi.org/10.1016/j.chemosphere.2005.01.066

Joffe, J.S. (1929). Soil profile studies: Soil as an independent body and soil morphology. *Soil Sci*., *28*(1), 39 - 54.

Kumar, A. (2020). Organic fertilizers for sustainable agriculture. *J. Clean. Prod., 286*, 122193. https://doi.org/10.1016/j.jclepro.2020.122193

Kutílek, M. (1978). *Vodohospodářská pedologie [Water pedology].* 2. ed. Praha: SNTL/ ALFA, 296 pp.

Lal, R. (2015). Soil erosion and carbon dynamics. *Soil Tillage Res., 153*, 43 - 54. https://doi.org/10.1016/j.still.2015.04.002

Lee, J.R., Hong, G.Y., Dixit, A., Chung, J.W., Ma, K.H., Lee, J.H., Park, Y.J. (2008). Characterization of microsatellite loci developed for *Amaranthus hypochondriacus* and their cross - amplification in wild species. *Conserv. Genet.*, *9*(1), 243 - 246. https://doi.org/10.1007/s10592-007-9364-5

Morton, J.F. (1981). *Atlas of Medicinal Plants of Middle America, Bahamas to Yucatan.* Charles C Thomas. ISBN: 0398038223

Oluwatosin, G.A., Ojo Atere, J.O. (2001). Influence of topographic position on crop responses to different rates of fertilizers in south western Nigeria. *Moor J. Agric*., 1 - 7.

Papargyropoulou, E., Lozano, R., Steinberger, J.K., Wright, N., Ujang, Z. (2014). The food waste hierarchy as a framework for the management of food surplus and food waste. *J. Clean. Prod., 76*, 106 - 115. https://doi.org/10.1016/j.jclepro.2014.04.020

Pepper, I.L., Gerba, C.P., Newby, D.T., Rice, C.W. (2009). Soil: A public health threat or savior? *Crit. Rev. Environ. Sci. Technol., 39*, 416 - 423. https://doi.org/10.1080/10643380802004066

Pimentel, D. (2006). Soil erosion: A food and environmental threat. *Environ. Dev. Sustain., 8*(1), 119 - 137.

Rice, T.D. (1928). What is a soil series? *Soil Sci*., *9*, 125 - 130.

Rodriguez, B.J.I., Paz, O., Verdecia, G.J.L. (1983). Study of possible agents in the dissemination of weed seeds. *Centro Agricola*, *10*(1), 55 - 65.

Salles, M.S., Lombardo de Barros, C.S., Lemos, R.A., Pilati, C. (1991). Perirenal edema associated with *Amaranthus* spp poisoning in Brazilian swine. *Vet. Hum. Toxicol., 33*(6), 616 - 617.

Schoonover, J., Crim, J. (2015). An introduction to soil concepts and role of soils in watershed management. *J. Contemp. Water Res. Educ.*, *154*(1), 21 - 47.

Simbolon, H., Sutarno, H. (1986). Response of *Amaranthus* species to various light intensities. *Buletin Penelitian Hortikultura, 13*(3), 33 - 42. https://agris.fao.org/search/en/providers/122456/records/6471c71777fd37171a6f1a97

Simonson, R.W. (1959). Outline of a generalized theory of soil genesis. *Soil Sci. Soc. Am. J., 23*, 152 - 156. https://doi.org/10.2136/sssaj1959.03615995002300020007x

United Nations. (2020). *World population prospects 2019*. Department of Economic and Social Affairs. https://www.un.org/development/desa/pd/news/world-population-prospects-2019-0

Uphof, T.C.T. (1968). *Dictionary of Economic Plants*. Verlag von J. Cramer.

Wainaina, P., Minang, P.A., Nzyoka, J. (2022). *Negative environmental externalities within cocoa, coffee and oil palm value chains in Africa.* Tree Commodities and Resilient Green Economies in Africa, World Agroforestry (ICRAF).

Wainaina, P., Muthoni, J., Gicheru, P. (2022). Effects of soil erosion on agricultural productivity in peri - urban areas of Kenya. *J. Environ. Sci. Health*, Part B, *57*, 1 - 13. https://doi.org/10.1080/03601234.2022.2027929

Wunderlin, R.P., Hansen, B.F., Franck, A.R., Essig, F.B. (2023). *Atlas of Florida Plants.* [Online] [Available at: https://florida.plantatlas.usf.edu/] [Accessed: 15/08/2023]

Zhang, M., Fang, L. (2007). Tea plantation–induced activation of soil heavy metals. Commun. *Soil Sci. Plant Anal.*, *38*(12), 67 - 78. https://doi.org/10.1080/00103620701378593

Zhao, C., Liu, B., Wang, Y. (2021). Effects of organic amendments on soil fertility and crop yield. *J. Soil Sci. Plant Nutr.*, *21*(2), 533 - 544.

STUDIA UNIVERSITATIS BABEŞ-BOLYAI BIOLOGIA, 70, 1, 2025 (p. 231-244)
doi:10.24193/subbbiol.2025.1.11

Hunger-induced convergence of personality traits towards ambush-predatory behavior in ball pythons (*Python regius*, Shaw 1802)

Octavian Craioveanu[1], Elisabeth Spataro[2], and Cristina Craioveanu[2,3]✉

[1]Academic Cultural Heritage Department – Vivarium, Babeş-Bolyai University, Clinicilor 5-7, Cluj-Napoca, Romania; [2]Department of Taxonomy and Ecology, Faculty for Biology and Geology, Babeş-Bolyai University, Clinicilor 5-7, Cluj-Napoca, Romania; [3]Babeş-Bolyai University, Centre 3B, Sociobiology and Insect Ecology Lab, Clinicilor 5-7, Cluj-Napoca, Romania
✉***Corresponding author, E-mail: cristina.craioveanu@ubbcluj.ro***

Article history: Received 13 January 2025; Revised 25 March 2025; Accepted 03 April 2025; Available online 25 June 2025

Abstract. Personality traits have been shown to be influenced by environmental and internal factors, hunger being one of the most important. The resulting behavior fluctuates greatly depending on the feeding ecology of the different species and intraspecific individual variation.

In this study, we used eight captive-born juvenile ball pythons to examine the relationship between personality traits, namely shyness and exploratory tendencies, and the chronological postprandial-induced psychobiological effects on a seven-day interval that concluded with the installation of hunger.

We found a strong correlation between shyness and hunger. Regarding exploratory predispositions, we found high individual variation at the beginning and middle of the postprandial cycle that evened out as hunger's influence started to be perceived.

Notably, this study's outcomes have the potential to enhance our understanding of captive animal management techniques and contribute to improving zoo animal welfare.

Keywords: juvenile ball pythons, behavior experiment, reptile welfare, feeding strategy

Introduction

Although concepts like animal personality and animal personality traits are nowadays widely accepted as cutting-edge topics of the behavioral sciences (Gosling, 2001; Thaler *et al.*, 2022; Knight *et al.*, 2013; Wilson *et al.*, 2019; Stamps and Groothuis, 2010), reptiles and particularly snakes have seldom received the attention of the scientific community. This gap in the literature contains only a few existing studies (Thaler *et al.*, 2022; Skinner *et al.*, 2022; Waters *et al.*, 2017; Šimková *et al.*, 2017), all of which suggest that snakes display consistent personality differences that profoundly affect their behavior. However, empirical documentation about the personality trait-behavior relation is extremely sparse. Beyond its fundamental approach, the potential application of this research topic in conservation management and captive animal welfare (Nagabaskaran *et al.*, 2022; MacKinlay and Shaw, 2022) makes it even more relevant in the future.

Due to its high adaptability, relaxed temper, and low aggressiveness, *Python regius*, Shaw 1802, is one of the most popular snakes in the pet trade and has long been kept and bred in captivity (Toudonou *et al.*, 2022). In addition, the ball python is an important species for teaching, education, and raising awareness about herpetofauna conservation.

A personality trait can be considered a relatively consistent bias, habit, or disposition that, when combined with various environmental factors, causes individuals to behave in a certain way (Skinner *et al.*, 2022). However, these traits can sometimes be challenging to comprehend in terms of variation and evolution, as they may consistently differ on individual and group levels. Stamps and Groothuis suggest (2007) that a better way to understand these variations is to consider the functional connections between those traits and physiological processes.

The foraging behavior of snakes is typically predatory, and their individual and species-specific personality is highly affected by intrinsic physiological factors. Of these physiological factors, hunger is one of the more important (Perry and Pianka, 1997; Vitt and Pianka, 2007).

Studies on the postprandial behavior of snakes are rare and are mostly field experiments (*Crotalus spp* - Beck, 1996; *Elaphe obsoleta* - Blouin-Demers and Weatherhead, 2001; *Boiga irregularis* - Seirs *et al.*, 2018). In addition, we are unaware of any study that has formally examined post-prandial personality trait variation and its expression in behavior. Given the strong psychobiological effect of hunger (Beaulieu and Blundell, 2020; Ramond, 1954; Cooper, 2000), we expect to see a consistent correlation between hunger and behavior, especially in the risk aversion/risk tolerance region.

Indirect evidence and anecdotal observations suggest that Boidae and Pythonidae are ambush-hunting predators. However, using a direct technique (radiotelemetry, videography) to prove that ambush hunting is their primary feeding strategy is a complicated process covered by only a few studies (*Morelia spilota* - Slip and Shine, 1988; *Corallus hortulanus* - Esberad and Vrcibradic, 2007; *Morelia viridis* - Wilson *et al.*, 2007). There is no extensive documentation to prove that the ball python is an exclusive ambush predator (Hanscom *et al.*, 2023), but according to Waas *et al.* (2010), the species is more on the sit-and-wait side of the specter. Therefore, a drop in activity levels with increasing hunger is expected as a sign of foraging activity initiation. However, ambush/active hunter is a broad behavioral classification; therefore, we would like to see if the ambush predation strategy is a strong, preprogrammed, instinctual behavioral pattern and it overwrites the individual personality trait variation or is more a personality-driven activity, with different personality individuals reacting in a slightly different manner to hunger (i.e., the reaction to hunger differs across individuals in the expression of the studied personality traits and the corresponding behaviors).

Therefore, the present study investigates the post-feeding personality trait variation of *Phyton regius* in controlled laboratory conditions, with the experiment focusing on two hypothetical questions:

1. Where is the ball python located on the ambush-active hunting scale? More precisely, we wanted to find out if hungry snakes are more prone to risky behavior or if they will lower their activity levels and go into ambush mode.

2. How flexible is the ball python´s hunting strategy? Is there a group-consistent, preprogrammed, instinctual behavioral response to hunger? And if there is one, to what extent will it take over the individual personality trait variation?

We conclude by discussing the results of the study and its possible applications in captive reptile management and welfare.

Materials and methods

The study was conducted between July and August 2023 in the herpetology laboratory of the Babeș-Bolyai University`s Vivarium. The study was conducted in accord with the highest humane and ethical principles, according to the ARRIVE guidelines for In Vivo Experiments and WAZA (World Association of Zoos and Aquariums, 2023) code of ethics and animal welfare.

To test our hypotheses, we used eight juvenile (2 months old) ball pythons (*Python regius*, IUCN near threatened, numbered P1-P8), a constrictor species native to West and Central Africa (D'Cruze *et al.* 2020), obtained by captive breeding.

To create a more compact experimental group, we used only females with no significant variation in size and weight (mean length ± SD = 528.50 ± 12.78 mm and mean mass ± SD = 64.12 ± 1.96 g).

For a seven-day acclimation period and during the next seven-day experiment, the subjects were housed separately in opaque, Tupperware-type plastic containers (27 cm x 17 cm x 8 cm) provided with bark mulch substrate, a hiding place, and a water bowl, indirect ambient sunlight illumination, and night-time/day-time temperature variation of 20/27° C (Westhoff, 2005).

Before the experiment and during the acclimation period, the snakes were fed once a week (Martinez, 2020) and provided with water *ad libitum*.

During the seven-day experiment, we performed four tests (on days 1, 3, 5, and 7) for two personality trait values: shyness and exploratory tendencies. Although these parameters are considered personality traits, in our experiment, they are foremost the expression of the measurement of a specific behavior.

The shyness test measured the time (seconds) the animals took to emerge from the shelter in a novel arena. Each animal was placed in a roughly 200 ml half-sphere shelter with a 2 x 2 cm covered opening on the side. The shelter was then positioned in the center of a 55 cm L x 45 cm W x 40 cm H arena, high enough so the snakes could not escape during testing. After a 1-minute settling period, the opening was uncovered, and the timing began while the experimenter quietly withdrew his hand from the test area.

The tests were filmed with a GoPro 7 camera placed 40 cm above the arena. Playing back the videos (Windows Media Player), we measured the elapsed time between the beginning of the trial and the complete emergence of the head from the shelter ("complete head out") – an indication of how soon the animal starts to investigate the arena.

The exploratory tendencies test used the open field method (Bergeron *et al.*, 2013; Montiglio *et al.*, 2010; Gould *et al.*, 2009) and was a continuation of the shyness test in which we examined a 10 minutes time-frame with the "complete head out" being the T0 moment. With an alcohol-based permanent marker, we drew three concentric rectangles: 1, 2, and 3, so that we delimited four areas (the limit for area no. 4 was the external wall of the arena) in increasing order, with one being the closest and four the furthest from the shelter. The rectangles had the following dimensions: 10 cm x 25 cm, 20 cm x 33 cm, 27 cm x 42 cm, and 55 cm x 45 cm, respectively. We considered that the snake entered one area when the total length of its head was located inside that area.

To record and measure the snake`s exploratory tendencies, we recorded the distance covered in terms of all areas visited and the number of transitions between areas. For both variables, we computed their median. We used the

median of the area numbers instead of their mean, because it is a better indicator for overall movement and for the distance traveled from the center.

While designing the arena, we faced the problem of arena size. Theoretically, we should have used an arena as large as the distance a snake would cover in a straight line at maximum speed within 10 minutes (testing time). However, such an area is technically impossible to provide in laboratory conditions. To compensate for this shortcoming, we introduced a variable – total time spent in area 4 (TR4). We considered a high value of this variable to be a strong indicator that the test animal would have gone further than the limits of the arena and has a greater propensity for exploration. The arena was cleaned with water and soap to remove the scent and thoroughly rinsed after each trial.

Both personality trait value tests were repeated four times, at two-day intervals, to allow the changes in the animal`s motivational state to impact their reaction. Day one of the experiment was the first day after feeding, and the snakes were considered satiated. Seven days after their last meal (in test no. 4 – day seven of the experiment), the animals were considered hungry but not post-absorptive (McCue, 2007; Spencer *et al.*, 2020).

Data analyses

First, we tested the distribution of the four variables we recorded: shyness (s), distance covered – D (median of areas visited), number of transitions between areas, and time spent in area 4 – TR4 (s), with the help of the Shapiro-Wilk test. We subsequently used non-parametric comparison methods for variables that were not normally distributed. We log-transformed the values for shyness and obtained a normal distribution. For all normally distributed values, we subsequently used one-way ANOVA.

To check for the influence of hunger on shyness, we checked for the influence of trials (equivalent to time since the last feeding) with the help of a linear mixed effect model (lmer, RStudio 2023). We tested the effect of the trial (time since feeding, corresponding to day 1, 3, 5, or 7 after feeding) on shyness as a fixed effect and "individual" as a random effect.

To analyze the exploratory tendencies in terms of distance covered, the number of transitions between areas, and the time spent in the fourth area (TR4), we used the Kruskal-Wallis rank sum test (Kruskal.test, RStudio 2023), followed in case of significant differences by a Dunn-test (dunnTest, RStudio 2023) with P-values adjusted with the Benjamini-Hochberg method to compare trials and individuals separately. All analyses and plots were performed in RStudio (RStudio, 2023).

Results

Shyness significantly increased with time in each of the four trials. The mixed effect model indicated that the fixed effect trial (time) had a strong influence on the shyness parameter ($Estimate_{23}$ = 0.17, SE = 0.07, t = 2.64, P = 0.015, Fig. 1), and the random effect explained only 5.49% of the total variation in the shyness-value (Variance Random Effect „Individual" (intercept) = 0.04, SD = 0.21; Variance Random Effect of residuals = 0.79, SD = 0.83).

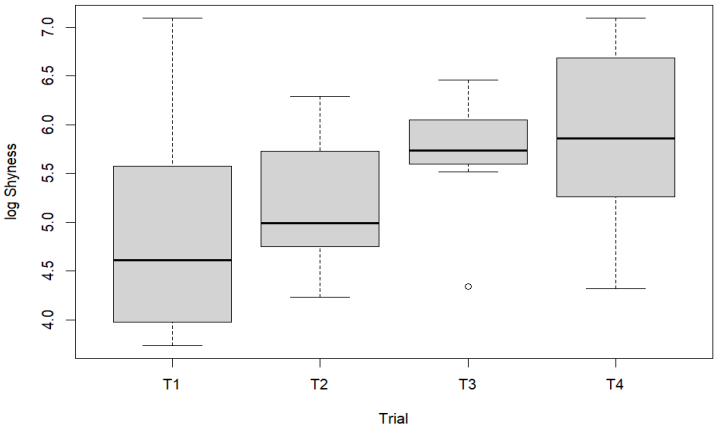

Figure 1. Log-transformed values of the Shyness parameter (time the animals took to emerge from the shelter) in each experimental trial (T1-T4). Boxplots represent median values (thick line inside the box), interquartile range (the box), maximum and minimum values (whiskers), and outliers (empty circles).

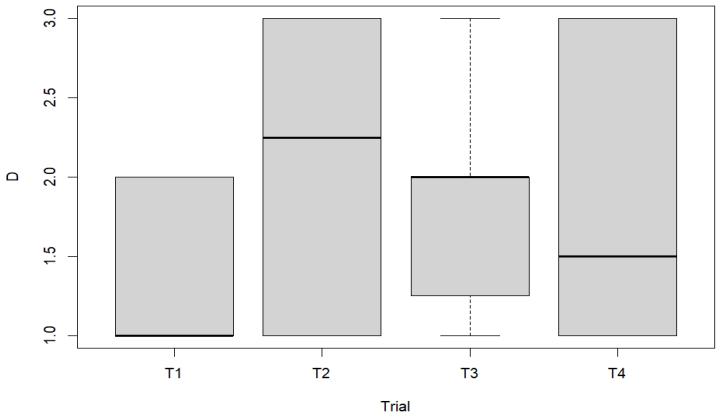

Figure 2. Median distance covered by individuals in different areas of the arena during the four Trials. Boxplots represent median values (thick line inside the box), interquartile range (the box), maximum and minimum values (whiskers), and outliers (empty circles).

We found no significant differences between the distances covered by the individuals in the four trials (Kruskal-Wallis test: χ^2_3= 1.85, P = 0.603). However, the median distance covered in the first trial by all individuals was shorter than the distance covered in the following two trials. In trial T4, the distance was slightly longer than in T1 but shorter than in T2 and T3, indicating a tendency to decrease from T2 towards T4 (Fig. 2).

We found significant differences between distances covered by individuals in the first three trials but not in the fourth (Table 1). However, when Benjamini-Hochberg-adjusted P-values were consulted, only the second trial showed a truly high variation of distances covered by each individual (Fig.3.). Some individuals tended to explore only the first area of the arena most of the trials, whereas others were more explorative. Individuals P6, P7, and P8 did not leave the shelter for the whole length of two trials (P8 in T1 and P6 and P7 in T4).

Table 1. Results of the comparisons between median distances (D) covered by individuals in each trial (individual Pythons are numbered P1-P8).

Trial	Kruskal-Wallis test result	Significant differences in D found between individuals Benjamini-Hochberg-adjusted *P*-values of the Dunn posthoc test
T1	χ^2_7 = 22.02 *P* = 0.003	-
T2	χ^2_7= 31.37 *P* < 0.001	P1-P2: *P* = 0.012 P1-P5: *P* = 0.010 P1-P7: *P* = 0.011 P1-P8: *P* = 0.010 P2-P4: *P* = 0.009 P3-P5: *P* = 0.009 P3-P7: *P* = 0.018 P3-P8: *P* = 0.011 P4-P7: *P* = 0.011 P4-P8: *P* = 0.014
T3	χ^2_7 = 19.09 *P* = 0.008	P2-P4: *P* = 0.016
T4	χ^2_7 = 13.57 *P* = 0.059	-

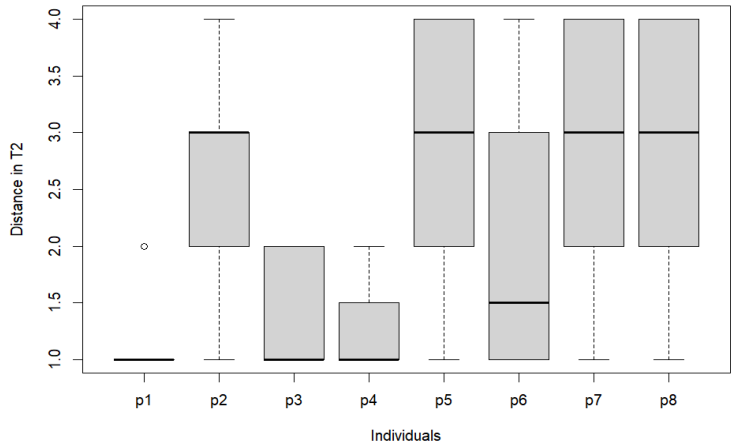

Figure 3. Distances covered by individual pythons in the second trial (T2). Boxplots represent median values (thick line inside the box), interquartile range (the box), maximum and minimum values (whiskers), and outliers (empty circles).

The number of transitions between areas of the arena did not differ significantly between trials (one-way ANOVA: $F_3 = 2.22$, $P = 0.108$) and between individuals (one-way ANOVA: $F_7 = 0.47$, $P = 0.844$). However, in the fourth trial, the individuals tended to make fewer transitions between areas (Fig. 4).

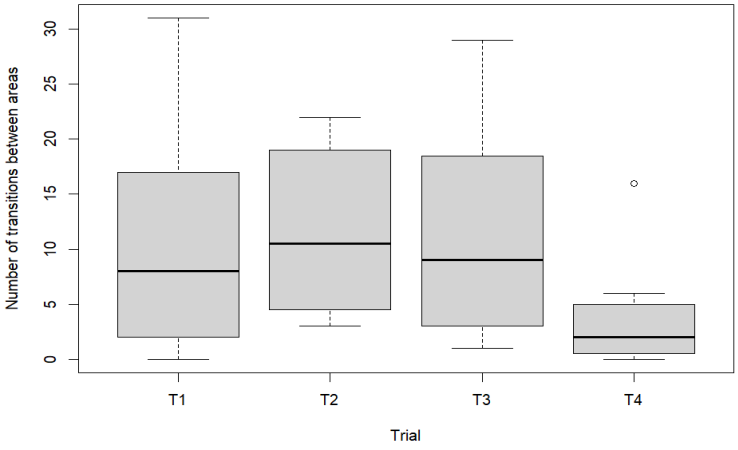

Figure 4. The number of transitions between areas of the arena recorded for all python individuals in the four trials. Boxplots represent median values (thick line inside the box), interquartile range (the box), maximum and minimum values (whiskers), and outliers (empty circles).

We found no significant differences between the times spent by all python individuals in the fourth area of the arena – TR4 (Kruskal-Wallis test: $\chi^2_3 = 4.28$, P = 0.233) per trial. We can, however, notice that most of the time spent by pythons in the fourth area of the arena was in the second and third trials (Fig. 5). Similarly, there were no significant differences detected between the time spent in the fourth area between individuals (Kruskal-Wallis test: $\chi^2_7 = 8.72$, P = 0.274). Considering individuals, we could notice that P1, P3, and P6 had a median of 0 time spent in the fourth region in all trials, whereas the other individuals spent between 25 and 444 s in the fourth region.

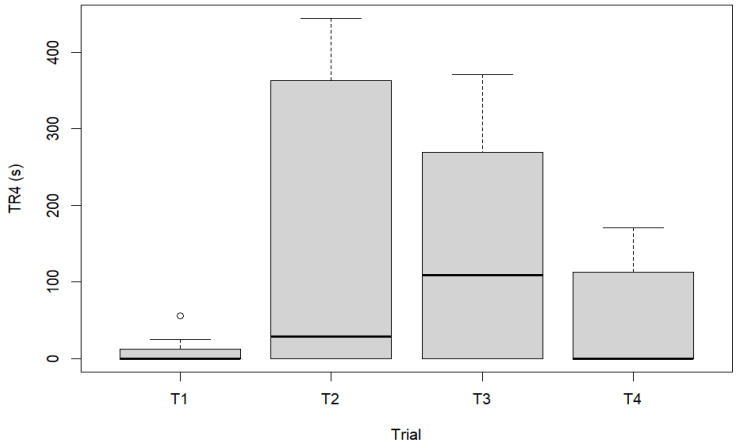

Figure 5. Time spent in the fourth area of the arena (TR4) by all python individuals in each trial. Boxplots represent median values (thick line inside the box), interquartile range (the box), maximum and minimum values (whiskers), and outliers (empty circles).

Discussion

Personality is what the animals are, behavior is what the animals do, and what they do is an intricate mesh between personality and the environment, internal or external. Therefore, we will interpret our results in behavioral terms primarily for practical purposes.

If we look at the statistical results, it becomes evident that there are two ways of interpretation.

First, if we consider only statistical significance, it is clear that shyness increases with time (Fig. 1) and consequently with hunger. Strictly speaking, animals take more and more time to stick their heads out of the shelter. This result describes the typical ambush predator behavior, in which the animals slowly and progressively adopt a sit-and-wait attitude perfectly correlated with

hunger. This interpretation would also answer our initial hypothetical question No. 1. And we would more or less leave out of the discussion the exploratory tendencies of the animals (distance covered, number of transitions between areas of the arena, and time spent in the fourth area of the arena) because there were no statistically significant differences found between the four trials.

However, if we look beyond the statistical significance, it becomes evident that there are also important, even pattern-like, differences between the activity in the four testing sessions and that these should be addressed in this discussion.

So, in this alternative way of interpretation, we emphasize that shyness significantly increased with hunger, but the activity and exploration of the animals decreased. Not linearly, like shyness, but more like an unimodal distribution pattern found in all three measured exploratory variables (Fig. 2, 4, and 5). According to Hanscom *et al.* (2023), a true ambush-hunting snake has three distinct behavioral stages: 1) an initial search for an ambush site, 2) a prolonged wait while remaining cryptic, and 3) the actual targeting and striking of potential prey.

A common characteristic of the behavioral patterns found in our experimental lot is that in T1, T2, and T3, the animals were more prone to exploration (T1, however, with lower values). They were at peak energy after digestion and before hunger, and they became relatively familiar with the arena after the first trial. Even though they were shyer than in T1, they ventured further and explored more of the arena than in T1 and T4.

The behavior of our experimental animals in T2 and T3 contradicts Clark`s asset protection principle (Clark, 1994), so at high energetics, they do not exhibit low activity and high levels of shyness but rather the opposite. However, the behavior mentioned above corresponds with stage 1 of the ambush behavioral pattern (Hanscom *et al.*, 2023) and, most likely, has to do with an active search for a suitable ambush site (small mammal pathways and nodes in the pathway networks, Clark, 2004), with a high probability of predation success.

Another characteristic of this second way of interpretation is the further increase in shyness (Fig. 1) and the decrease in exploratory activities in T4, compared with T2 and T3 (Fig. 2, 4, and 5). Again, this behavior opposes Clark's asset protection principle, which stipulates that at a low energy budget, they should be very bold and embark on risky activities to avoid starvation. However, it corresponds fully with stage 3 of the ambush behavioral pattern described by Hanscom *et al.* (2023).

When analyzing the data, we noticed that the initial levels of exploratory behavior (particularly in T2, see Table 1) varied significantly between individuals. However, later in T4, it looks like suddenly, abruptly, all individual variation stopped, and they all became very shy. Although the name of the personality trait test is shyness, this is a manifestation of the species' ambush foraging behavior.

The values recorded in the first testing session, T1, turned out to be quite puzzling and challenging to explain in terms of this species' ecology and life history. The animals were freshly fed, so a typical digestion behavior was expected, with low exploratory activity and high shyness. The exploratory activity was indeed low (Fig. 2, 4, and 5), or at least lower than in T2 and T3, but also the levels of shyness were at the lowest level (fig 1). They were more curious but less explorative, a very counterintuitive combination. They were sticking their head out of the shelter quicker but staying close to the shelter. It was their first testing trial; they were in unknown territory; maybe they were curious, but not that curious to explore further than the immediate vicinity of the shelter. Overall, we found no reasonable explanation for this personality-trait value association in the formal or anecdotic literature and got stuck in the realm of speculation. Nevertheless, one thing is for sure: all eight experimental animals exhibited the same low shyness levels in the digestion stage.

Besides the fundamental aspect of our research, there are also practical ways in which our results can be helpful. The personality trait-based technique described here can be used as a complementary tool, besides the more direct but difficult ones (telemetry, videography), in assessing the feeding strategies applied by different snake species. More precisely, it can be a more accessible method of pinpointing the snake species´ location on the ambush-active hunting scale.

The ball python is one of the most popular pet reptiles, with many captive specimens and well-known captive management techniques. However, there is always room for continual improvement; this is where our study could have another practical use and make a significant difference. Concerning enclosure design, the low activity in T4 emphasizes the importance of a shelter so the animal can behave as closely as possible to its instincts. The presence of the shelter will not only increase the feeding/hunting efficiency but will most certainly be very beneficial for the psychological welfare of the animal. It is common knowledge that handling any snake species right after feeding is not recommended because of the risk of vomiting up the food. Our results propose that another such time is just before eating, at least in ambush species. Causing discomfort in the prandial cycle's ambush phase may easily detour the snake from eating. The stubborn refuse of food and lengthy fasts the ball pythons are known for (Barten and Mader, 2013) may also be a direct result of unrestricted handling. So, if the animal is shyer and less active than usual, we recommend disturbing it as little as possible. Besides solving some of the fasting issues, this will also decrease the risk of getting bit. Any ambush snake species in captivity can benefit from the information mentioned above.

Time spent in the outer ring of the experimental arena suggests that even if they seem to get by in a smaller enclosure (McCurley, 2006; Rizzo, 2014; Hollandt *et al.*, 2021), ball pythons have a higher exploratory inclination (Fig. 5)

before entering the ambush foraging mode (T3 in our experiment). Setting up a larger terrarium is not always possible, so a multi-level enclosure design could be a solution to meet the animal´s exploration needs.

Conclusion

From the perspective of our starting hypotheses, there is a group-consistent response to hunger, and the significant personality trait variation between individuals is only visible in the satiated state. In other words, the feeding strategy is not driven by personality. Once hunger sets in, the ambush-foraging state of mind overrides all personality variation, and there is no individual inclination towards a more active hunting style.

References

Barten, S., Mader, D. (2013). *Ball pythons: natural history, husbandry, diseases, and techniques.* CABI Digital Library, https://cabidigitallibrary.org

Beaulieu, K., Blundell, J. (2021). The Psychobiology of Hunger – A Scientific Perspective. *Topoi (Rio.J),* 40, 565–574. https://doi.org/10.1007/s11245-020-09724-z

Beck, D.D. (1996). Effects of feeding on body temperatures of rattlesnakes: a field experiment. *Physiol. Zool,* 69(6), 1442–1455. http://www.jstor.org/stable/30164268

Bergeron, P., Montiglio, P.-O., Réale, D., Humphries, M.M., Gimenez, O., Garant, D. (2013). Disruptive viability selection on adult exploratory behavior in eastern chipmunks. *J. Evol. Biol.,* 26(4), 766–774.

Blouin-Demers, G., Weatherhead, P.J. (2001). An experimental test of the link between foraging, habitat selection and thermoregulation in black rat snakes *Elaphe obsoleta obsoleta*. *J. Anim. Ecol,* 70, 1006-1013. https://doi.org/10.1046/j.0021-8790.2001.00554.x

Clark, C. W. (1994). Antipredator behavior and the asset-protection principle. *Behav. Ecol,* 5, 159-170. https://doi.org/10.1093/beheco/5.2.159

Clark, R. W. (2004). Timber rattlesnakes (*Crotalus horridus*) use chemical cues to select ambush sites. *J. Chem. Ecol*., 30 (3), 607-17. https://doi.org/10.1023/B:JOEC.0000018632.27010.1e

Cooper, W. (2000). Tradeoffs between predation risk and feeding in a lizard, the broad-headed skink (*Eumeces laticeps*). *Behav*., 137(9), 1175–1189. https://doi.org/10.1163/156853900502583

D'Cruze, N., Harrington, L. A., Assou, D., Green, J., Macdonald, D. W., Ronfot, D., Segniagbeto, G. H., Auliya, M. (2020). Betting the farm: A review of ball python and other reptile trade from Togo, West Africa. *Nature Conservation,* 40, 65–91. https://doi.org/10.3897/natureconservation.40.48046

Esbérard, C. E. L., Vrcibradic, D. (2007). Snakes preying on bats: new records from Brazil and a review of recorded cases in the Neotropical Region. *Rev. Bras. Zool.,* 24, 848 853. https://doi.org/10.1590/S0101-81752007000300036

Gosling, S. D. (2001). From mice to men: What can we learn about personality from animal research? *Psychol. Bull.,* 127(1), 45–86.

Gould, T.D., Dao, D.T., Kovacsics, C.E. (2009). The Open Field Test, In: *Mood and Anxiety Related Phenotypes in Mice*, Gould, T. (ed). *Neuromethods*, 42, Humana Press, Totowa, NJ. https://doi.org/10.1007/978-1-60761-303-9_1

Hanscom, R.J., Higham, T.E., Ryan, D.S., Clark, R.W. (2023). Ambush hunting in snakes: behavior, function, and diversity. In: *Snakes: Morphology, Function, and Ecology*, Penning D, (ed). Nova Science Publishers, Inc. p. 279–311.

Hollandt, T., Baur, M., Wohr, A.C. (2021). Animal-appropriate housing of ball pythons (*Python regius*) - Behaviour-based evaluation of two types of housing systems. *PLoS ONE.* 16, e0247082. https://doi.org/10.1371/journal.pone.0247082

Kight, C., Morgan, D., Dall, S. (2013). *The Evolution of Animal Personality Variation.* eLS. John Wiley & Sons Ltd, Chichester. https://doi.org/10.1002/9780470015902.a0024662

MacKinlay, R.D., Shaw, R.C. (2022). A systematic review of animal personality in conservation science. *Conserv. Biol*., 37(1), e13935.

Martinez, M. (2020). Growth and Feeding Response in *Python regius* in Ambient Temperature vs. Hot-Spot. *Environmental Studies Undergraduate Student Theses.* 265. https://digitalcommons.unl.edu/envstudtheses/265

McCue, M. D. (2007). Snakes survive starvation by employing supply- and demand-side economic strategies. *Zoology* (Jena), 110(4), 318–327. https://doi.org/10.1016/j.zool.2007.02.004

McCurley, K. (2006). *Ball pythons in captivity* (*Professional breeders series*). ECO/Serpent's Tale NHBD, pp. 101.

Montiglio, P-O., Garant, D., Thomas, D., Réale, D. (2010). Individual variation in temporal activity patterns in open-field tests. *Anim. Behav.,* 80(5), 905-912. https://doi.org/10.1016/j.anbehav.2010.08.014

Nagabaskaran, G., Skinner, M., Miller, N. (2022). Western Hognose Snakes (*Heterodon nasicus*) Prefer Environmental Enrichment. *Animals*, 12, 3347. https://doi.org/10.3390/ani12233347

Perry, G., Pianka, E.R. (1997). Animal foraging: past, present and future. *Trends Ecol. Evol.,* 12, 360–364. https://doi.org/10.1016/S0169-5347(97)01097-5

Ramond, C. K. (1954). Performance in selective learning as a function of hunger. *J. Exp. Psychol*., 48(4), 265–270. https://doi.org/10.1037/h0053643

Rizzo, J. M. (2014). Captive Care and Husbandry of Ball Pythons (*Python regius*). *J. Herpetol. Med. Surg.*, 24 (1-2), 48–52. https://doi.org/10.5818/1529-9651-24.1.48

Siers, S.R., Yackel Adams, A.A., Reed R.N. (2018). Behavioral differences following ingestion of large meals and consequences for management of a harmful invasive snake: A field experiment. *Ecol. Evol.,* 8 (20), 10075 - 10093. https://doi.org/10.1002/ece3.4480

Šimková, O., Frýdlová, P., Žampachová, B., Frynta, D., Landová, E. (2017). Development of behavioural profile in the northern common boa (*Boa imperator*): Repeatable independent traits or personality? *PLoS ONE,* 12, https://doi.org/10.1002/ece3.4480

Skinner, M., Brown, S., Kumpan, L.T. (2022). Snake personality: Differential effects of development and social experience. *Behav. Ecol. Sociobiol.,* 76, 135. https://doi.org/10.1007/s00265-022-03227-0

Slip, D. J., Shine, R. (1988). Feeding habits of the diamond python, *Morelia s. spilota*: ambush predation by a boid snake. *J. Herpetol,* 22 (3), 323-330. https://doi.org/10.2307/1564156

Stamps, J., Groothuis, T.G.G. (2010). The development of animal personality: relevance, concepts and perspectives. *Biol. Rev.,* 85, 301-325. https://doi.org/10.1111/j.1469-185X.2009.00103.x

Stamps, J. A. (2007). Growth-mortality tradeoffs and ''personality traits'' in animals. *Ecol. Lett.,* 10 (5), 355-363. https://doi.org/10.1111/j.1461-0248.2007.01034.x

Spencer, M.M., Pierson, M.T., Gienger, C.M. (2020). Comparative energetics and thermal responses to feeding in allied *Agkistrodon* snakes with contrasting diet and habitat use. *J. Comp. Physiol. B*, 190 (3), 329–339. https://doi.org/10.1007/s00360-020-01267-4

Thaler, R., Ortega, Z., Ferreira, V.L. (2022). Extrinsic traits consistently drive microhabitat decisions of an arboreal snake, independently of sex and personality. *Behav. Process,* 199. https://doi.org/104649. 10.1016/j.beproc.2022.104649

Toudonou, C., Elwin, A., Penner, J., Coulthard, E., Norrey, J. D., Megson, D., Rödel, M-O., Sinsin, B., Harrington, L., Auliya, M., D'Cruze, N. (2022). Seeking serpents: Ball python trade in Benin, West Africa. *J. Nat. Conserv.*, 50**,** 85-114. https://doi.org/10.3897/natureconservation.50.86352

Vitt, L. J., Pianka, E.R. (2007). Feeding ecology in the natural world, In: *Lizard Ecology: The Evolutionary Consequences of Foraging Mode*, S. M. Reilly, L. D. McBrayer, and D. B. Miles (eds.). Cambridge University Press, Cambridge, pp. 141–172.

Waas, S., Werner, R.A., Starck, J.M. (2010). Fuel switching and energy partitioning during the postprandial metabolic response in the ball python (*Python regius*). *J. Exp. Biol.,* 213 (8), 1266–1271. https://doi.org/10.1242/jeb.033662

Waters, R.M., Bowers, B.B., Burghardt, G.M. (2017). Personality and Individuality in Reptile Behavior, In: *Personality in Nonhuman Animals*, Vonk, J., Weiss, A., Kuczaj, S. (eds), Springer, Cham, https://doi.org/10.1007/978-3-319-59300-5_8

Westhoff, G. (2005). Expert report on the suitability of Geo Rack I systems (manufacturer: Lanzo Herp Cages) for species-appropriate husbandry and rearing of the ball python (*Python regius*). https://www.lanzo-herp.de/Gutachten/Expertises.

Wilson, D. R., Henderson, W., Powell, R. (2007). Foraging ecology and diet of an ambush predator: the Green Python (*Morelia viridis*). Biology of the Boas and Pythons, 141-150.

Wilson, V., Guenther, A., Øverli, Ø., Seltmann, M.W., Altschul, D. (2019). Future Directions for Personality Research: Contributing New Insights to the Understanding of Animal Behavior. *Animals* (Basel), 9(5), 240. https://doi.org/10.3390/ani9050240

World Association of Zoos and Aquariums (WAZA) (2023). [Accessed 11 January 2025] https://www.waza.org/wp-content/uploads/2024/03/FINAL_WAZA-Code-of-Ethics-and-Complaints-Process.pdf?_cord_id=133db430-8a04-425a-be76-b25b643b3619

STUDIA UNIVERSITATIS BABEŞ-BOLYAI BIOLOGIA, 70, 1, 2025 (p. 245-286)
doi:10.24193/subbbiol.2025.1.12

Community-level physiological profiling of carbon substrate metabolization by microbial communities associated to sediments and water in karstic caves from Romania

Diana Felicia Panait[1,2,3]✉, Andrei Marian Panait[4], Adorján Cristea[5], Erika Andrea Levei[6], Oana Teodora Moldovan[7], Horia Leonard Banciu[8]✉

1. Institute for Research, Development in Applied Natural Sciences, Babeş-Bolyai University, Cluj-Napoca, Romania; 2. Electron Microscopy Center, Faculty of Biology and Geology, Babeş-Bolyai University, Cluj-Napoca, Romania; 3. Doctoral School of Integrative Biology, Faculty of Biology and Geology, Babeş-Bolyai University, Cluj-Napoca, Romania; 4. S.C. Brillio Romania SRL, Cluj-Napoca, Romania; 5. Department of Ecology and Taxonomy, Faculty of Biology and Geology, Babeş-Bolyai University, Cluj-Napoca, Romania; 6. INCDO-INOE 2000, Research Institute for Analytical Instrumentation, Cluj-Napoca, Romania; 7. Emil Racoviță Institute of Speleology, Cluj-Napoca Department, Cluj-Napoca, Romania; 8. Department of Molecular Biology and Biotechnology, Faculty of Biology and Geology, Babeş-Bolyai University.

✉***Corresponding authors, E-mail:*** *diana.bogdan@ubbcluj.ro, horia.banciu@ubbcluj.ro*

Article history: Received 28 February 2025; Revised 30 April 2025; Accepted 18 May 2025; Available online 25 June 2025

Abstract. Cave ecosystems comprise specialized microbial communities that play essential roles in biogeochemical cycles; yet their metabolic capabilities and ecological functions are not fully understood. As conventional cultivation techniques provide limited insights into the metabolic capabilities, methods based on direct functionality screening may improve our knowledge of cave microbial activity. In this study, the Community-Level Physiological Profiling (CLPP) based on Biolog® EcoPlate™ approach was applied to assess carbon (C) substrate utilization by microbial communities associated with 36 environamental samples collected from five karstic caves (Cloşani, Ferice, Leşu, Muierilor, and Topolniţa) in Romania. Principal Component Analysis (PCA) and Generalized Additive Models (GAMs) statistics were employed to infer the patterns of C substrate metabolization and their environmental drivers. Environmental variables such as sodium (Na) and

electrical conductivity (EC) significantly impacted C substrate utilization capabilities as indicated by both PCA and GAM. The latter analysis elucidated non-linear relationships between variables, such as EC, Na, and Mg, and microbial metabolic diversity indices. However, distinct C substrate utilization patterns were detected among sampled sites and chemical types. Unlike moonmilk samples where associated microbial communities appeared as exhibiting low C substrate utilization, the highest activity was shown in cave pool water samples with the associated microbial communities extensively consuming D-galacturonic acid and Tween 80. Conversely, substrates like L-threonine and α-ketobutyric acid showed limited utilization across all cave samples. Average Well Color Development (AWCD) and Shannon diversity indices indicated that microbial communities associated to samples from Cloșani and Muierilor caves demonstrated the highest metabolic diversity. Our findings suggested that metabolic profiling using Biolog® EcoPlate™ method combined with multivariate statistical methods might prove a suitable analysis approach to effectively screen for cave microbial functionality and the probable environmental drivers. Besides, this work distinguishes from similar studies by relying on GAM analysis to predict the environmental factors governing the microbially-mediated organic carbon degradation in subterranean ecosystems.

Keywords: caves, community-level physiological profile, generalized additive models, microbial communities, organic carbon substrates.

Introduction

The nutrient-limited subterranean ecosystems are inhabited by microorganisms with slow metabolism and growth rates (Epure *et al*., 2014). These cave-dwelling microbes are assumedly involved in biogeochemical cycles of major elements such as C, N, P or S. Therefore, investigation of taxonomic and metabolic diversity is crucial in enlarging our understanding of the interactions and ecological roles of cave microorganisms (Barton and Northup., 2007). Yet, investigating the microbial taxonomic and functional diversity in cave ecosystems poses significant challenges, including the limitations of the traditional culturing techniques, which recover only a small fraction of the members of microbial communities (Jones *et al*., 2015). Additionally, culture-dependent techniques provide limited understanding of microbial activity *in situ*, failing to capture the complexity of functional relationships within microbial communities. Therefore, complementary rapid and effective methods to directly assess the metabolic

potential of cave microbial communities are beneficial. For example, the Community-Level Physiological Profiles (CLPP) using EcoPlate™ plates (Biolog® Inc., Hayward, CA, USA) approach may be useful in characterizing the community functionality, offering a clearer view of microbial functional diversity and ecological potential in cave environment. The Biolog® EcoPlate™ is a time- and cost-effective tool that has been used to monitor the spatio-temporal carbon substrate preferences of microbial communities inhabiting a diverse range of habitats including groundwater (Melita *et al*., 2023), surface freshwater (Boteva *et al*., 2024), brackish-to-saline waters (Cristea *et al*., 2014), wetlands (Teng *et al*., 2020), agricultural soils (Rutgers et al., 2015), rhizosphere (Cacchio and Del Gallo, 2019), volcanic soils and mud (Amaresan *et al*., 2018; Asif *et al*., 2024), and limestone monuments (Andrei *et al*., 2017). Moreover, this versatile approach has been applied to assess the carbon utilization by bacterial communities in karst caves (Yun *et al*., 2018) and lava tube ice caves (O'Connor *et al*., 2021). Overall, the noteworthy benefit of this method is that it is comparable to high-resolution, yet more resource-consuming molecular techniques such as metagenomics. Although the Biolog® EcoPlate™ method provides a limited information on microbial metabolic capabilities, its rapidity in profiling the community-wide metabolic activity makes it a valuable complementary tool for metabolic fingerprinting with potential to enhance our understanding of functional diversity within cave ecosystems.

Despite the increasing interest in exploring cave microbial communities, considerable gaps remain in understanding both individual and community-driven microbial metabolic processes in caves. Present limitations result from focusing on taxonomy rather than functionality, scarcity of in situ studies, metabolite profiling, and a poor understanding of biogeochemical processes in caves or other subterranean environments. Here, we aimed to employ the Biolog® EcoPlate™ tool to survey the carbon substrate utilization patterns of microbial communities inhabiting cave pool water, water sediment (limon), dry sediments, and moonmilk (white precipitate with aggregates of fine carbonate crystals) from five Romanian caves, thereby addressing the diversity of carbon metabolization traits and the delineation of their main environmental drivers.

Materials and methods

Sampling sites

Five karstic caves (Cloşani, Ferice, Leşu, Muierilor, and Topolniţa) were sampled in this study (Figure 1). A brief description of sampled caves is provided below.

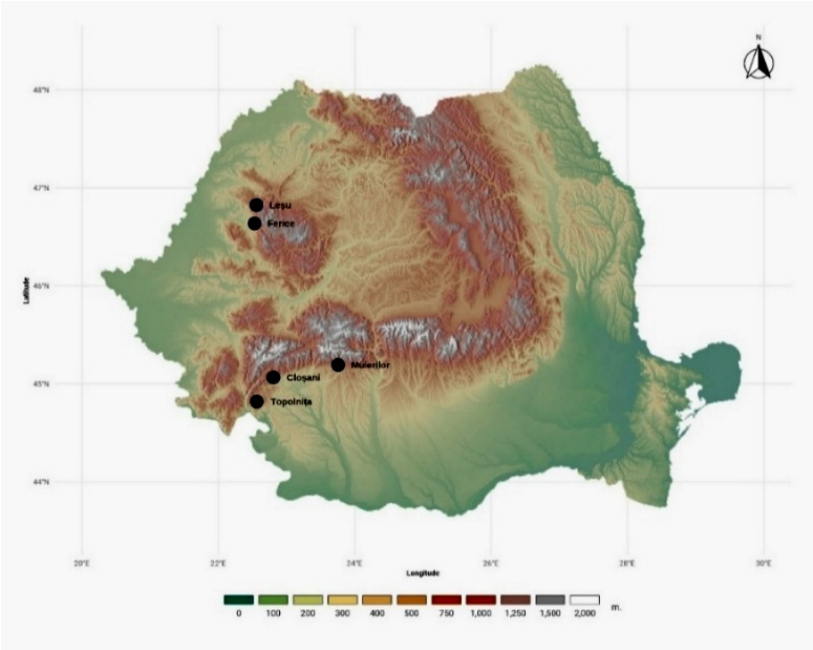

Figure 1. Geographic and altitudinal distribution of the sampled karstic Romanian caves. The map was generated using R Studio with topographic data using the 'geodata' package with the data source from Shuttle Radar Topography Mission (SRTM), specifically the hole-filled CGIAR-SRTM (90 m resolution) from https://srtm.csi.cgiar.org/.

Cloșani Cave is located in Southern Carpathians (near Cloșani village). It has a narrow entrance found at an altitude of 443 m above sea level (a.s.l). The two galleries have a length of 1100 m, and temperatures of about 11°C in the depth of the cave, increased humidity and a lack of air currents (Bleahu *et al*., 1976).

Ferice Cave is located in North-Western Romania, Apuseni Mountains at an elevation of 410 m a.s.l. in a region with oceanic climate influences. A low-flow stream crosses the main horizontal passage, which measures around 260 meters in length. During the winter season a small number of bats frequent the cave. The temperature within the cave ranges from 11.4°C to 12.7°C and the humidity from 80% (lowest value during May) to 95% (November) (Moldovan *et al*., 2023).

Leşu Cave (Peştera cu Apă din Valea Leşului) is situated in the Apuseni Mountains and designated protected area classified as a natural reserve (type IV IUCN). The Leşu cave system features a primary gallery approximately 1 km long, traversed by a meandering water stream for the initial 300 m, forming

alluvial terraces. The annual air temperature within the cave averages between 8.5° and 10°C. The cave has a significant hibernation colony of multiple bat species, primarily near the entrance (Zoltan and Szántó, 2003; Bücs *et al*., 2012).

Muierilor Cave is located in the Southern Carpathians near Baia de Fier, Gorj County, at approximately 645 m a.s.l. Its karstic system has multiple chambers and a total length of over 8000 m. The cave system includes pristine sections and a show cave (Level 2 – accessible for visitors). It is a protected natural monument with designated scientific reserves (Mirea *et al*., 2021).

Topolniţa Cave is located in the Southern Carpathians, at an elevation of ~400 m a.s.l. It is distinguishable by its extensive karst system covering more than 20 km^2 and by significant bat colonies that produce large guano deposits (Cleary *et al*., 2019; Moldovan *et al*., 2023).

Sample collection and Biolog® EcoPlate™ assay

Environmental samples were collected from the studied cave sites, including cave water and substrate (limon), dry sediment, and moonmilk (Table 1). Pool substrate samples (limon) were further considered and processed as 'sediment' samples. All samples were collected from areas free from human impact, including samples from show caves like Muierilor. Five grams of fresh sediment (including limon and moonmilk samples) were suspended in 50 mL NaCl 0.85% solution and stirred for about 30 minutes on a water-bath shaker (150-200 rpm) at 23°C. After one hour of on-the-table sedimentation, 100 µL of the resulted cellular suspension was inoculated in each well from the EcoPlate™ plates (Biolog® Inc., Hayward, CA, USA) under a laminar airflow hood, ensuring the prevention of contamination throughout all procedures. The 96-well Biolog® EcoPlate™ contains a total of 31 carbon substrates in triplicate and three wells without substrate serving as a control. One plate was used for each sample. No additional biological or technical replicates were included beyond the plate's built-in triplicates.

The optical density measurements at 590 nm (OD590) were performed on a plate reader (FLUOstar® Omega, BMG Labtech, Offenburg, Germany). Plates were incubated up to 8 days (200 hours) at 16 °C (chosen as near-environmental value) and specific intervals of time between readings were established based on the literature review which mostly depends on the color development on plates (Garland, 1997; Iţcuş *et al*., 2016). A 12-hour interval between measurements was established and carried out until no changes in both color development and OD_{590} values were detected. Variability in microbial inoculum size, inherent to environmental samples, may contribute to the observed differences in metabolic profiles.

Table 1. Summary of the sampled caves and sample types used in this study.

Sample nr.	Cave	Sample ID	Sample type
1	Cloşani	PCDF2-APA	water
2		PCDF3-APA	water
3		LAB1	sediment
4		LAB2	sediment
5		LAB3	sediment
6		GHICA1	sediment
7		GHICA2	sediment
8		GHICA3	sediment
9		PCDF1	sediment
10		PCDF2-LIMON	limon (sediment)
11		PCDF3-LIMON	limon (sediment)
12	Ferice	PFDF1	sediment
13		PFDF2	sediment
14		PFDF3	sediment
15		PFDF4-SOL	sediment
16		PFDF2MM	moonmilk
17		PFDFMMC	moonmilk
18		PFDF4-APA	water
19		PFDF4-LIMON	limon (sediment)
20	Muierilor	PMDF9-APA	water
21		PMDF10-APA	water
22		PMDF2	sediment
23		PMDF5	sediment
24		PMDF11	sediment
25		PMDF5A	sediment
26	Leşu	PLDF1	sediment
27		PLDF1A	sediment
28		PLDF1B	sediment
29		PLDF4	sediment
30		PLDF2	sediment
31		PLDF1B-APA	water
32		PLDF2-APA	water
33		PLDF3-APA	water
34	Topolniţa	PTDF1	sediment
35		PTDF2	sediment
36		PTDF3	sediment

Physico-chemical analyses

The pH and electrical conductivity (EC) were assessed in water samples and 1/5 sediment-to-water extracts using the Seven Excellence multiparameter (Mettler Toledo, Greifensee, Switzerland). To measure the concentration of elements, one gram of dried sediment was digested with aqua regia (21 mL of 12 M HCl and 7 mL of 15.8 M HNO_3), subsequently filtered and diluted to 100 mL with 0.5 M HNO_3. The *aqua regia*-extractable fraction includes both physiologically available and unavailable metals. Water samples were acidified with 15.8 M HNO_3 and filtered using cellulose acetate membrane filters with a pore size of 0.45 μm for the determination of dissolved metals and phosphorus contents. The concentrations of Na, Mg, K, Ca, and P in water, as well as Na, Mg, K, Ca, P, Al, Fe, S, and Mn in sediments, limon and moomilk were quantified using inductively coupled plasma optical emission spectrometry with an Optima 5300DV (Perkin Elmer, Waltham, MA, USA) spectrometer. Additionally, the concentrations of Al, Fe, As, Cr, Mn, Co, Ni, Cu, and Zn in water, along with As, Cr, Co, Ni, Cu, and Zn in sediments, were determined via inductively coupled mass spectrometry utilizing an Elan DRC II (Perkin Elmer, Waltham, MA, USA). The carbon, and nitrogen contents in sediments were quantified using a Flash 2000 CHNS/O analyzer (ThermoFisher Scientific, Waltham, MA, USA). Total nitrogen (TN) in water was quantified using catalytic combustion, followed by the oxidation of nitrogen monoxide to nitrogen dioxide using ozone, and subsequent detection via chemiluminescence with a Multi N/C 2100S Analyser (Analytik Jena, Jena, Germany). Dissolved carbon (DC) and dissolved inorganic carbon (DIC) were measured in water samples filtered via 0.45 μm PTFE syringe filters using catalytic combustion and infrared detection of CO2 utilizing a Multi N/C 2100S Analyser (Analytik Jena, Jena, Germany). Dissolved organic carbon (DOC) was derived by subtracting dissolved inorganic carbon (DIC) from total carbon (DC). Sulfate (SO_4^{2-}), nitrate (NO^{3-}), chloride (Cl^-), and phosphate (PO_4^{3-}) were quantified using ion chromatography on a 761 Compact IC (Metrohm, Switzerland).

Data acquisition, preprocessing and processing

Data from OD_{590} measurements were extracted from individual .xlsx files using **readxl** package. Data from some samples from Lesu Cave described in Bogdan *et al.* (2023) were reanalyzed in a comparative context and with a more comprehensive statistical analysis. Each sample was identified by its unique sampling site, sample type and the hour of incubation. The absorbance (OD_{590}) values were corrected against water blanks using designated wells and averaged across triplicate measurements for each carbon substrate. Further, the dataset

was processed to remove negative values after correction. Some samples were read up to 360 hours, but given that no changes were detected in the color development or OD_{590} measurements we excluded the timepoints after 204 hours. All analyses were performed using R (R Core Team, 2020) and key packages included the following: readxl version 1.4.3, dplyr version 1.1.4 and tidyr version 1.3.1 for data processing; mgcy version 1.9-1 for GAMs; factoextra version 1.0.7 for PCA; ggplot2 version 3.5.1 and pheatmap version 1.0.12 for data visualization.

Calculation of microbial metabolic diversity metrics

Microbial metabolic diversity metrics were calculated for each sample based on the formulas and indices from the literature (Zak *et al.*, 1994; Feigl *et al.*, 2017) (Table 2). The principal microbial metabolic diversity metrics provide insights into both the metabolic capacity and functional evenness of the microbial communities.

Table 2. Microbial metabolic diversity indices and equations used for calculations

Index	Equations	Definition
Average Well Color Development (AWCD)	AWCD= $\Sigma\frac{C-R}{N}$, C-OD_{590} values of each well R-OD_{590} values of the control well N-number of substrates (31)	Calculated by the differences between the OD_{590} of the wells containing individual carbon sources and the control wells
Richness	-	Represents the number of substrates utilized, defined as those with an absorbance greater than 0.25
Shannon diversity (H index)	$H = -\sum p_i \, log(p_i)$ pi-proportion of each substrate's utilization	Quantifies the diversity of microbial communities by considering both the richness and the proportional utilization of carbon substrates; higher values of H indicate greater diversity, as more substrates are being used more evenly across the microbial community.
Shannon evenness (E)	E=H/log (R) R – substrate richness	Measures how evenly the carbon substrates are utilized by the microbial community, and is derived by dividing the Shannon diversity (H) by the logarithm of substrate richness (R); values close to 1 indicate a more uniform distribution of substrate utilization, while values closer to 0 suggest that a few substrates dominate the activity.

Statistical analyses

Generalized Additive Models (GAMs)

Generalized Additive Models (Simpson, 2024) were employed to explore the link between microbial metabolic diversity metrics and geochemical factors. GAMs allow for non-linear relationships between predictor variables (e.g. values of geochemical or physico-chemical parameters) and response variables (e.g. microbial metrics). These models were fitted using the mgcy package, which applies smooth functions to each predictor. The microbial metrics, including richness, Shannon diversity, and Shannon evenness, were modeled as response variables with smooth terms for key geochemical predictors: pH, EC, and the concentrations of N, C, Na, Mg, K, Ca, P (Equation 1).

Equation 1. The formula for the GAMs which was applies smooth functions to each predictor.

$$Y = \beta_0 + s(pH) + s(EC) + s(N) + s(C) + s(Na) + \cdots + \epsilon$$

Where:

- Y is the microbial metric (Richness, Shannon Diversity, or Evenness),
- s(·) denotes a smooth function applied to each geochemical predictor.

These models allowed us to capture non-linear effects and interactions between environmental conditions and microbial diversity. Moreover, the GAMs were visually inspected for their goodness of fit using residual diagnostics. Model checks and plots of the smooth functions for each predictor were generated to assess the relationship between diversity and geochemical factors.

Principal Component Analysis (PCA)

The Principal Component Analysis (PCA) was used to investigate the joint variation in microbial community metabolic metrics and environmental geochemistry, by reducing the dimensionality of the dataset by identifying the principal components (PCs) that capture most of the variation in the datasets. Particularly, this is a powerful tool for identifying correlations between microbial metabolism (community-physiological profiles) and geochemical properties. In this case, PCA was applied to the combined dataset of microbial metrics such as AWCD, richness, Shannon diversity, Shannon evenness and physico-chemical variables (pH, EC, N, C, Na, Mg, K, Ca, P) using the factoextra package. These variables were scaled to ensure the comparability between measurements with different units for which the relationship between the principal components and

the original standardized variables was established with the equation presented below (Equation 2), in which, Z represents the matrix of principal components, W is the weight matrix that defines the linear combination of the original variables, and X denotes the matrix of original standardized variables which includes microbial metrics and chemical parameters.

Equation 2. The formula used to reduce the dimensionality of the dataset while capturing the most significant variance, facilitating the interpretation of underlying patterns in microbial and chemical interactions.

$$Z = W \times X,$$

Biplots were created to visualize the relationship between microbial metrics and geochemical factors, displaying the sample clustering and contribution of variables.

Data visualization

Boxplots and line plots were used for the representation of microbial activity (AWCD and diversity metrics) across sample types and time points. Heatmaps coupled with hierarchical clustering were created to display metabolic activity patterns across carbon sources, samples and hours. The PCA biplot was used to explore the relationship between microbial metrics and geochemical factors. At the same time, the results of the GAMs depict the non-linear trend between chemistry and microbial diversity.

Results

Physico-chemical characteristics of cave water and sediment samples

Physico-chemical parameters, including pH, EC and the concentration of major elements (N, C, Na, Mg, K, Ca, P) were measured from sediment (limon and moonmilk included here) and water samples, with total nitrogen (TN) and total carbon (TC) considered for N, and C respectively (Table 3). Sediments show high calcium (Ca) concentrations, particularly in LAB3 (454,682 mg/kg) and LAB2 (226,206 mg/kg), reflecting the limestone-rich environment. The phosphorus (P) levels were highly variable, with some sediments, such as PMDF11 (41167 mg/kg) showing higher concentrations compared to PFDF2MM (104 mg/kg). On the other hand, in water samples, the electrical conductivity (EC) was notably higher, specifically PFDF4-APA showing the highest value (359 µS/cm). Overall, the pH of all the samples was basic with variations from 7.8 in sediment sample GHICA2 to

9.3 in LAB1 (sediment) and PFDFMMC (moonmilk). Carbon concentrations varied widely in sediments, ranging from < 100 mg/kg (e.g., PTDF1, LAB1) to 98,400 mg/kg (PMDF2), highlighting localized carbon hotspots. In water, concentrations were more consistent, ranging from 17.3 mg/L to 50.0 mg/L, reflecting its role in transporting dissolved carbon species. Sediments consistently exhibited higher concentrations of elements compared to water, indicating their function as nutrient and mineral reservoirs. The geochemical data were merged with the microbial metabolic diversity metrics by sample ID, allowing for a combined analysis of microbial community structure and environmental chemistry. However, certain elements (Al, Fe, S, Mn, As, Cr, Co, Ni, Cu, Zn) and water-specific parameters (TN, DC, DIC, DOC, SO_4^{2-}, NO_3^-, Cl^-, PO_4^{3-}) were excluded from the PCA due to either their low concentrations or the inability to integrate both sediment and water sample data in the same PCA. Nevertheless, aluminum (Al) and iron (Fe) dominated the sediment samples, with maximum concentrations of 63,089 mg/kg and 55,572 mg/kg, respectively. At the same time, sulfur (S) and trace metals like copper (Cu) and zinc (Zn) showed localized enrichment. In contrast, water samples exhibited significantly lower and more uniform concentrations, with aluminum peaking at 7.84 μg/L and sulfate reaching 48.6 mg/L, reflecting dilution effects and contrasting physico-chemical attributes between sediments and water (Table S2).

Patterns of carbon source utilization in cave samples

The carbon substrate metabolization patterns significantly varied across all assayed cave samples (Figure 2). A higher OD_{590} was recorded for the samples inoculated in the wells containing Tween 40, putrescine and D-xylose, indicating a higher rate of microbial activity toward degradation of these compounds. Conversely, lower OD_{590} values after substrate consumption were exhibited in the wells containing 2-hydroxy benzoic acid and L-threonine suggesting limited microbial capacity to metabolize these compounds. The compounds such as pyruvic acid methyl ester and D-galacturonic acid were overall metabolized in most samples, though with considerable variation in OD values, suggesting functional redundancy in the community.

The average OD for selected carbon substrates indicated that the microbial community from the water samples exhibited the highest metabolic activity for a wide range of carbon sources (Table 4). D-galacturonic acid (mean OD_{590} = 1.22 ± 0.75), D-mannitol (1.05 ± 0.85), N-acetyl-D-glucosamine (1.03 ± 0.72), and Tween 80 (1.03 ± 0.79). In contrast, the microbial communities associated to the moonmilk samples showed the lowest ability to utilize organic C-substrates, with OD_{590} values remaining below 0.5 for most carbon sources.

Table 3. Physico-chemical parameters measured in cave sediment (including limon and moonmilk) and water samples. Total nitrogen (TN) was considered as N, and total carbon (TC) as C, for water samples.

Sample ID	pH	EC	N	C	Na	Mg	K	Ca	P
Sediments									
		µS/cm	mg/kg	mg/kg	mg/kg	mg/kg	mg/kg	mg/kg	mg/kg
PMDF2	8.80	69.0	< 100	98359	79	2833	1336	322967	4843
PMDF5	8.40	73.6	3500	18700	65	1123	2918	29137	9803
PMDF11	8.40	120.5	3180	19086	452	1850	3321	194933	41167
PMDF5A	8.59	102	2452.31	29280	182	6386	2395	112533	14963
PTDF1	8.50	49.7	< 100	417	161	6590	3407	11583	1135
PTDF2	8.80	57.6	< 100	< 100	125	6383	3298	10997	293
PTDF3	8.98	110.7	< 100	16636	170	6820	1806	113666	2022
LAB1	9.30	64.8	< 100	< 100	380	13578	3676	189052	739
LAB2	8.50	112.3	< 100	76500	235	1406	2209	226206	420
LAB3	8.60	104.6	< 100	85700	201	1313	3634	454682	346
GHICA1	8.00	73.9	< 100	1000	444	1810	5557	13265	276
GHICA2	7.80	160.2	< 100	3800	466	1809	5609	16741	501
GHICA3	8.10	89.9	1200	19900	441	1817	5202	65313	498
PCDF1	8.20	40.9	< 100	< 100	111	5873	3433	10023	9990
PFDF1	8.72	77.4	7839	9810	95	17307	5437	31733	879
PFDF2	8.62	69.3	7012	< 100	119	13847	6863	9400	1267
PFDF3	8.34	121.6	7300	3500	157	50533	4653	31757	7107
PFDFMMC	9.30	67.2	2800	97600	329	78570	921	150947	451
PFDF2MM	9.20	58.9	1600	121000	188	85871	518	211096	104
PLDF1	8.67	53.4	2686	37876	60	32210	1248	63833	1367
PLDF1A	8.60	83.9	5550	50429	123	5134	2192	110933	4247
PLDF1B	8.48	80.1	5339	17015	73	2950	2992	60733	1870
PLDF4	8.58	83.5	3079	11243	62	2143	1851	49667	3380
PLDF2	8.12	114.5	6584	34213	125	4297	1982	69000	8930
Water									
		µS/cm	mg/L	mg/L	mg/L	mg/L	mg/L	mg/L	mg/L
PMDF9-APA	8.20	287.5	15.1	18.0	1.625	1.346	5.734	55.90	0.31
PMDF10-APA	8.60	353.3	17.7	19.9	1.686	2.305	8.213	69.72	0.453
PCDF2-APA	8.10	168.4	<0.7	17.3	0.585	2.151	1.036	69.17	48.88
PCDF3-APA	7.90	189.4	<0.7	19.2	0.515	0.742	0.225	45.40	0.17
PFDF4-APA	8.30	359.2	<0.7	50.0	0.642	24.12	0.389	43.64	0.016
PLDF1B-APA	8.10	147.5	0.94	19.1	0.572	0.476	0.398	35.41	0.014
PLDF2-APA	8.10	171.3	0.86	22.2	0.487	0.451	0.373	40.64	0.032
PLDF3-APA	7.90	209.2	<0.7	26.4	0.493	0.873	0.483	48.97	0.004

Table 4. Average OD_{590} (± standard deviation) for selected carbon sources measured using the Biolog® EcoPlate™ method in water and sediment cave sample.

Carbon Source	Water (Mean ± SD)	Sediment (Mean ± SD)	Moonmilk (Mean ± SD)
D-mannitol	1.05 ± 0.85	0.63 ± 0.82	0.05 ± 0.03
N-acetyl-D-glucosamine	1.03 ± 0.72	0.42 ± 0.60	0.02 ± 0.01
L-serine	0.80 ± 0.68	0.55 ± 0.68	0.00 ± 0.00
Tween 80	1.03 ± 0.79	0.49 ± 0.60	0.20 ± 0.24
D-galacturonic acid	1.22 ± 0.75	0.60 ± 0.63	0.13 ± 0.13

Further on, the temporal dynamics based on median absorbance values for the carbon source utilization was assessed across the sample types (Figure 2). An overall higher C substrate utilization compared to the other samples was noted in water samples, specifically for substrates such as D-galacturonic acid, pyruvic acid methyl ester, Tween 40 and N-acetyl-D-glucosamine (Table 4). Certain C-sources, like putrescine and L-arginine, represent substrates for bacterial enzymatic activity, indicating similar patterns in sediment and water, but with generally higher utilization by water-associated communities. The moonmilk microbial communities overall show the lowest C-substrate utilization with many substrates exhibiting little to no increase in absorbance over time (e.g., γ-amino butyric acid, β-methyl-D-glucoside, D-cellobiose), except for D-xylose and 2-hydroxy benzoic acid which depict a higher median absorbance compared to sediment and water samples.

Similarly, the differences in temporal dynamics of median absorbances across the carbon substrates were assessed between sampling sites. The samples from Muierilor Cave showed the highest microbial-driven C-substrate utilization with preference for D-galacturonic acid, L-serine, D-malic acid, L-asparagine, and D-mannitol, suggesting that the communities from this sampling site can utilize a wide variety of substrates. On the other hand, the microbial communities associated to samples from Topolniţa Cave generally show the lowest activity, except for 2-hydroxy benzoic acid. To illustrate differences between samples and the metabolic capabilities of their microbial communities, separate graphs were generated for each sample type (Figures S2–S4). For example, microbial communities in Cloşani water samples exhibit notably high OD values over 1, for 19 carbon sources (Figure S2), suggesting that Cloşani water is the most metabolically active among the water samples. In contrast, the utilization of organic C sources by the microbial communities associated to the Muierilor Cave water samples has a lower activity (OD_{590} values < 0.5) with a few exceptions for substrates like 2-hydroxy benzoic acid, D-malic acid,

D-xylose, L-arginine, L-asparagine, Tween 40 and Tween 80. The sediment samples (Figure S3) show almost similar activity in samples from Leşu and Muierilor caves, yet higher in Leşu, whereas Cloşani, Ferice and Topolniţa caves depict approximately similar lower activity except for 2-hydroxy benzoic acid (Topolniţa), α-keto-butyric Acid (Cloşani) and L-serine (Ferice). In the moonmilk samples from a single sampling point (Ferice; Figure S4), median absorbance indicates that Tween 80 was the most rapidly consumed substrate, followed by Tween 40 and L-phenylalanine.

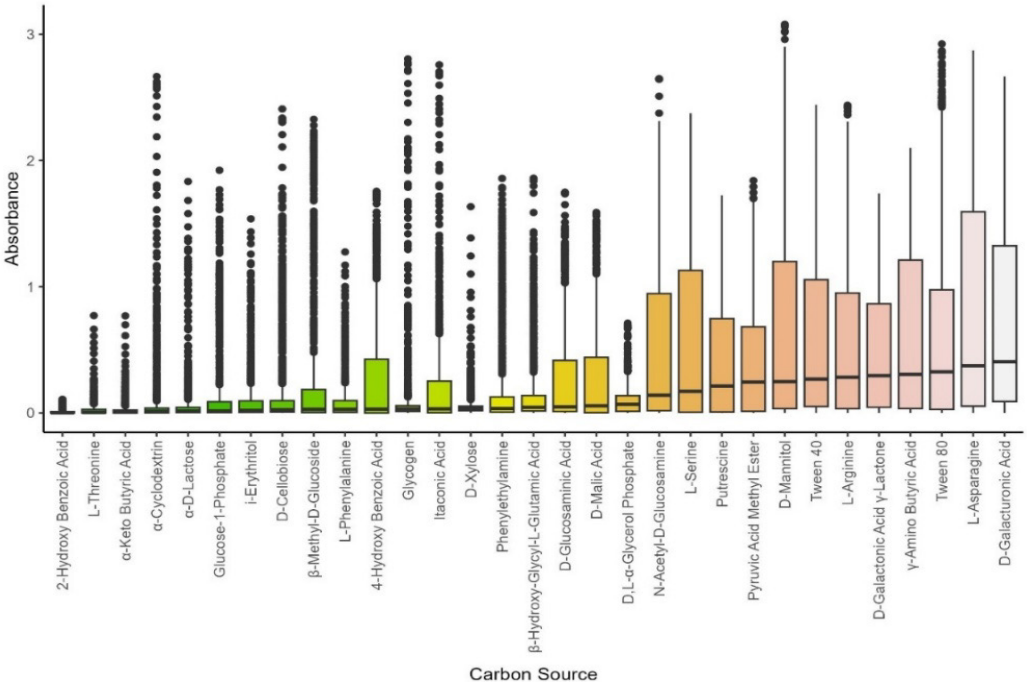

Figure 2. Box plot showing the median absorbance for the metabolization of 31 carbon substrates by microbial communities, highlighting differences in organic carbon substrate utilization and associated metabolic activity. Each box represents the interquartile range (IQR), with whiskers extending to 1.5 times the IQR, and individual dots showing outlier data points. The color coding differentiates the substrates but does not carry a specific meaning.

Estimation of overall carbon metabolization by Average-Well Color Development (AWCD)

The average-well color development (AWCD) at each sampling point for 200 hours provides information on the rates of organic carbon substrate consumption, thus insights into the overall metabolic activity. The overall trend across all sampling locations showed increased substrate utilization after 50 hours of incubation, with site-specific differences in utilization rates. Samples from Muierilor Cave exhibited the fastest changes and highest AWCD values, followed by those from Leșu, Cloșani, Ferice, and Topolnița caves (Figure 3).

The overall substrate metabolization patterns among the three different cave sample types (water, sediment, and moonmilk) were also investigated by the AWCD parameter (Figure 4 and Table S1).

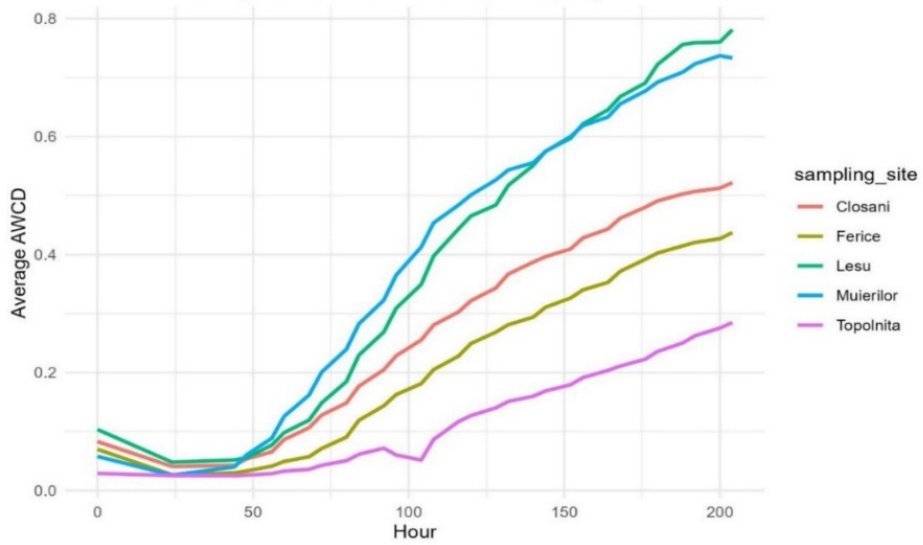

Figure 3. Average-well color development (AWCD) over time for all samples across five sampling sites: Closani, Ferice, Lesu, Muierilor, and Topolnița.

Water samples displayed the highest C-substrate utilizing activity, with a sharp increase in AWCD after 50 hours, reaching a final value of 0.8. The AWCD measured in sediment samples showed moderate, steady increase, reaching approximately 0.5 by the end of the incubation. Moonmilk samples exhibited the lowest AWCD, with a minimal and gradual increase. The overall AWCD patterns across the sample types might reflect significant differences in microbially-mediated organic substrate utilization across these distinct cave niches.

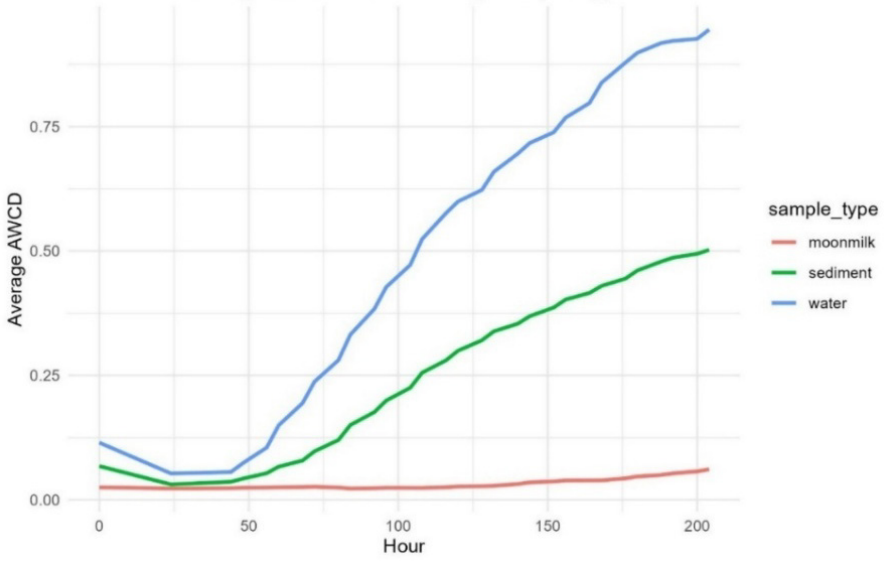

Figure 4. Average-well color development (AWCD) over time measured for the three cave sample types (water, sediment, and moonmilk).

Microbial metabolic diversity metrics across cave samples

Temporal dynamics of metabolic richness and diversity

Shannon diversity metrics were used to assess microbial metabolic diversity for each sampling location (Figure 5) and sample type (Figure S3), whereas maximum richness and H index by sample type were also calculated (Table 5). The Cloşani cave samples showed the highest median values of Shannon diversity metrics (2.83) among all sampled caves (Figure 5), which might indicate that both water and sediment samples likely support the most metabolically diverse microbial communities among tested caves. When comparing sample types, the water samples showed the highest median values of diversity indices (2.9), indicating that the cave aquatic communities are likely more metabolically diverse (i.e. with a broad C-substrate preference) than their sediment or moonmilk counterparts that exhibited lower median values of metabolic diversity indices of 2.75 (sediments), and 2.67 (moonmilk) (Figure S3).

Noteworthy, the moonmilk samples collected from Ferice Cave had the lowest calculated indices (Table S1 and Figure S3), possibly due to a more specialized or less diverse community. The samples from Leşu and Muierilor caves showed moderate metabolic diversity metrics with a median value for Shannon diversity of 2.81 (Leşu) and 2.82 (Muierilor) (Figure 5) with a higher

C-substrate metabolization diversity in sediments compared to water (Table S1). The lowest Shannon diversity values (~2.6) was calculated for samples collected from Topolnița (2.66) and Ferice (2.61) caves. Overall, these findings revealed that metabolic diversity toward organic carbon substrate use differed significantly among sampling locations and sample types, with Cloșani cave samples and water-associated communities, respectively, exhibiting the greatest metabolic diversity.

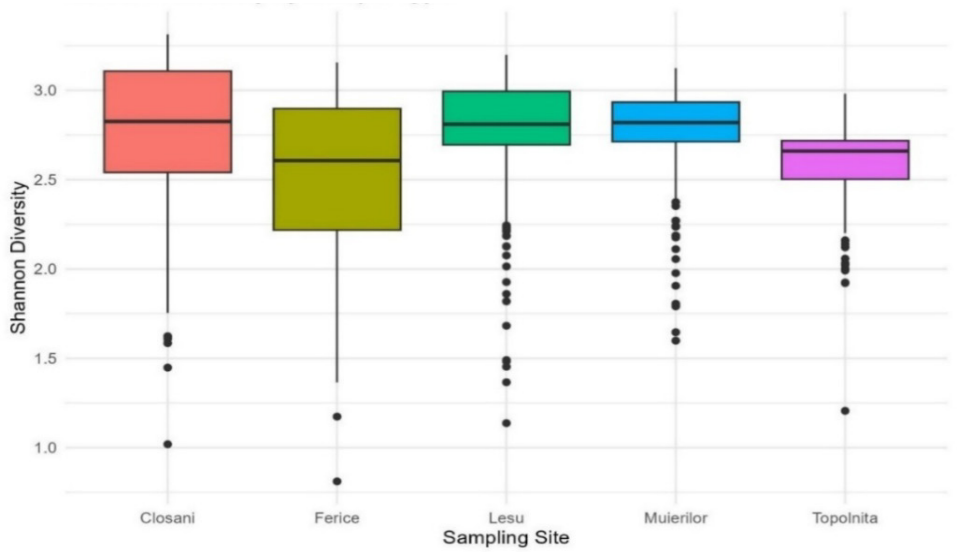

Figure 5. Box plot of Shannon diversity indices based on substrate utilization patterns for microbial communities across sampling sites (Cloșani, Ferice, Lesu, Muierilor, and Topolnița caves). The box colors correspond to different sampling sites, while the black dots represent outliers in Shannon diversity values.

Table 5. Maximum richness and Shannon diversity index by sample type across sampling sites. Richness represents the total number of substrates metabolized, while the Shannon diversity index reflects both the richness and evenness of substrate utilization.

Sample location	Max Richness (Water)	Max Richness (Sediment)	Max Richness (Moonmilk)	Shannon Diversity (Water)	Shannon Diversity (Sediment)	Shannon Diversity (Moonmilk)
Closani	54	76	-	6.45	26.98	-
Ferice	24	78	4	3.16	14.28	6.13
Lesu	56	101	-	8.64	14.94	-
Muierilor	49	62	-	6.19	11.84	-
Topolnita	-	29	-	-	8.62	-

Correlation of the AWCD and richness values

To illustrate both temporal dynamics of C-substrate utilization and diversity of substrate utilization a scatter plot combining AWCD and richness values associated with each sampling site and sample type was generated (Figure 6). The observed values and ranges are reported to illustrate variability across sampling sites and sample types than measures of central tendency (mean or median). Despite some site-specific variations, AWCD was positively correlated with richness (Figure 6). The results indicated that Cloșani Cave may support communities with greater metabolic versatility and a broader diversity of consumed substrates than the other cave sites. Richness values converged at lower AWCD values (0.0-0.5), suggesting baseline diversity despite limited activity. For AWCD values between 0.5 – 1.0, richness increased more consistently among sites (e.g., Leșu, Muierilor, Ferice) and a broader spread can be seen. Interestingly, Cloșani Cave had a wider spread in terms of both AWCD and richness with a positive trend, but mostly extended to the highest AWCD values (1.0 – 1.5) and maximum richness (close to 30). Also, a few samples from Ferice Cave also showed a positive trend, but this site actually depicted an intermediate metabolic activity and metabolic diversity richness. The widest range of richness and AWCD values have been counted for sediment, followed by water samples (Figure S4) the latter encountering the highest richness values. On the opposite, the moonmilk samples showed the lowest richness (< 10) and metabolic activity (< 0.1).

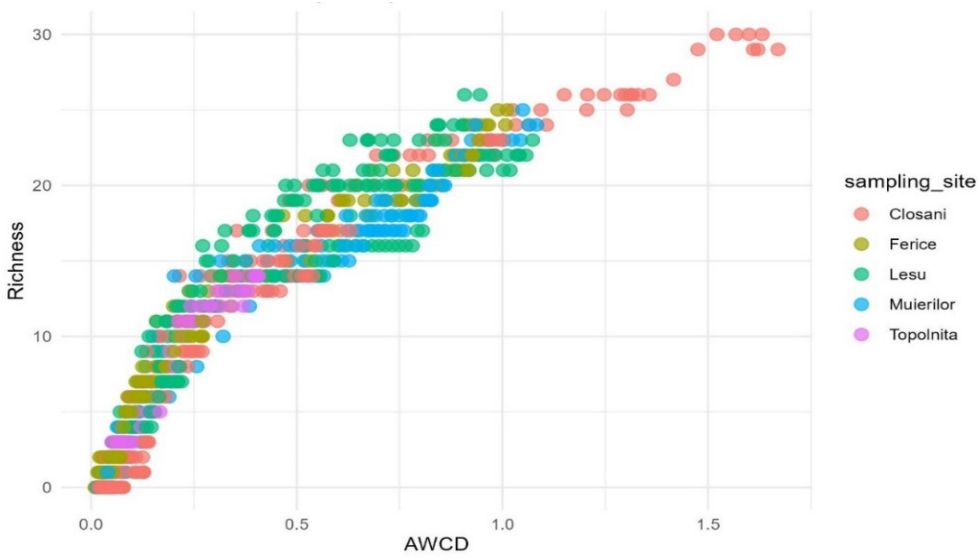

Figure 6. The scatter plot of AWCD and richness values measured at different time points over a total duration of 0-204 hours for all samples and sampling site.

Correlations between microbial metrics and chemistry

Correlation analysis identified key relationships between microbial activity metrics and environmental chemistry. AWCD correlated significantly with sodium ($r = 0.56$, $p < 0.01$) and phosphorus ($r = 0.45$, $p < 0.05$), while Shannon diversity correlated with electrical conductivity - EC ($r = 0.49$, $p < 0.05$) and magnesium ($r = 0.55$, $p < 0.05$). These results suggest that Na and P are positively associated with overall carbon substrate utilization rates (as indicated by AWCD), while EC, Na, and Mg contribute to shaping substrate preference patterns across microbial communities, as seen in the multivariate PCA analysis (Table 6, Figure 8).

Table 6. Pearson correlation coefficients for microbial activity metrics and environmental chemistry parameters. A single asterisk (*) denotes significance at the $p < 0.05$ level, and a double asterisk (**) denotes significance at the $p < 0.01$ level.

Metric	Na	P	EC	Mg	K
AWCD	0.56**	0.45*	0.39	0.55*	0.37
Richness	0.44*	0.32	0.48*	0.49*	0.30
Shannon Diversity	0.50*	0.40	0.49*	0.55*	0.41*

Analysis of microbial activity and carbon utilization in cave sediments

To assess microbial metabolic diversity across cave samples, hierarchical clustering and heatmaps were generated (Figure 7). These analyses revealed distinct metabolic profiles among sediment, water, and moonmilk samples.

Hierarchical AWCD clustering identified four microbial activity clusters (Supplementary Figure S5). Sediment samples from Cloşani and Muierilor caves showed consistently lower AWCD values, while water samples (e.g., PCDF2-APA, PLDF1B-APA) formed separate clusters with higher values, indicating greater microbial activity. Moonmilk samples (e.g., PFDF2MM and PFDFMMC) clustered with sediments, suggesting similar metabolic constraints. Similarly, substrate richness clustering highlighted high diversity in water samples (e.g. PCDF2-APA, PMDF9-APA, and PMDF10-APA) especially at later time points (116–204 hours), while samples like PFDF1 and PFDFMMC exhibited persistently low richness. High diversity was observed in GHICA2, PCDF2-APA, PMDF9-APA, and PMDF10-APA, whereas PFDF2, GHICA1, and PLDF3-APA displayed lower metabolic diversity, reflecting reduced microbial evenness.

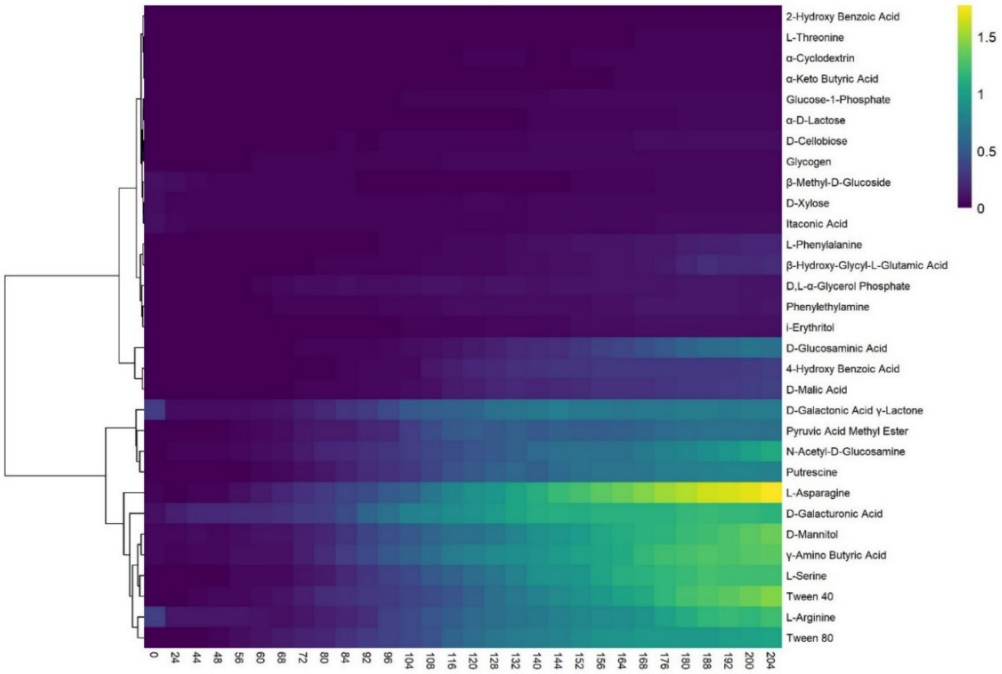

Figure 7. Heatmap plot of the median absorbance of microbial metabolic diversity across the carbon source types over time. The color scale represents absorbance values, with yellow indicating higher metabolic activity and purple indicating lower activity. Hierarchical clustering was applied to both carbon sources (rows) and time points (columns), revealing patterns of substrate utilization by the microbial communities over time.

Hierarchical clustering analysis was performed to examine microbial activity patterns based on carbon source utilization over time (Figure S7). Key findings indicated that L-asparagine and D-galacturonic acid show the highest metabolic activity after 120 hours (Figure S7). Noteworthy, Tween 40 and Tween 80 displayed increasing absorbance between 80 and 204 hours, suggesting delayed metabolism, likely due to shifts in microbial community structure or composition (Figure S7). Other carbon sources, including L-threonine, α-cyclodextrin, and α-keto butyric acid, exhibit minimal metabolic activity throughout the entire time period.

L-asparagine, Tween 80, and D-galacturonic acid were widely utilized across most of the samples, while L-threonine and α-keto butyric acid showed minimal microbial metabolization. Samples of sediment and moonmilk exhibit diminished overall metabolic activity, with the majority of carbon sources presenting low absorbance values, indicating a more restricted range of substrate use relative to water.

Environmental drivers of carbon substrate utilization

PCA was employed to examine the relationships between microbial metrics, including richness, Shannon diversity, and evenness along with several physico-chemical variables such as pH, EC, N, C, Na, Mg, K, Ca, and P. The first two components (PC1 and PC2) explained a significant proportion (>53%) of the data variation. The third component (PC3) gave an additional 10.9%, resulting in a cumulative explained variance of 64.6%. Water samples were strongly associated with higher microbial activity and substrate utilization diversity metrics (AWCD, richness, and Shannon diversity), driven primarily by EC. In contrast, sediment and moonmilk exhibited weak associations with all variables. An inverse correlation of Na and K with richness and AWCD suggests that increased concentrations of these ions may inhibit microbial activity and substrate utilization diversity (Figure 8).

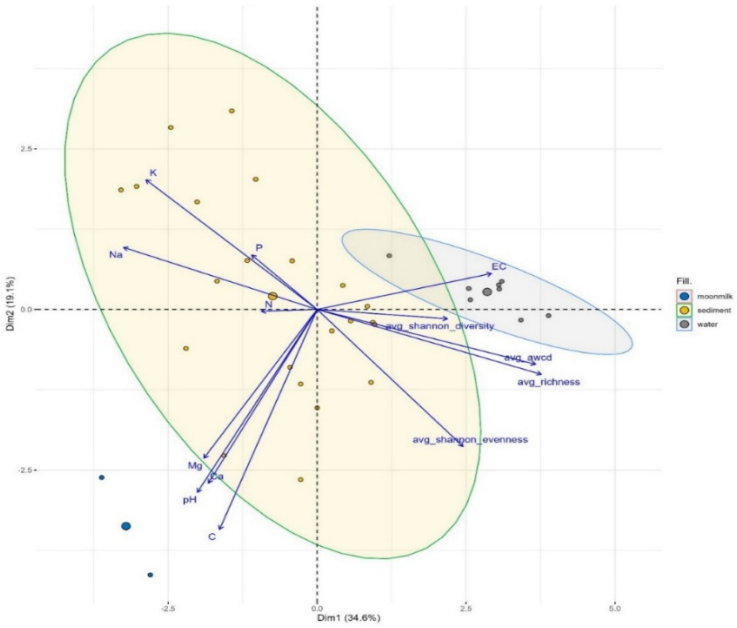

Figure 8. Principal Component Analysis (PCA) biplot showing the relationships between microbial metrics and cave chemistry variables across sample types. The first two principal components explain 34.6% and 19.1% of the variance, respectively. Microbial metrics such as average richness and AWCD are positively associated with EC, while pH, Ca, and Mg are negatively associated with microbial diversity metrics. The grouping of samples highlights distinct clustering based on sample type, with water samples clustering along higher EC values and sediment samples more spread out based on nutrient concentrations (Na, P, N, K).

Generalized Additive Models (GAMs) analysis

To capture complex, non-linear relationships between environmental variables and diversity metrics that usually evade the simpler PCA, GAMs have been employed to improve the accuracy of ecological predictions. The GAMs revealed that richness (Figure 9) and Shannon diversity (Figure 10) are strongly influenced by chemical variables, explaining 89.1% (first model) and 91.2% (second model) of the deviance. Richness showed nonlinear relationships with pH, K, and P ($p < 0.05$), while N and C had significant linear effects. Shannon diversity was significantly influenced by the nonlinear effects of EC and K ($p < 0.005$), while phophorus (P) was showing an exploratory trend toward significance ($p = 0.077$). A minor negative correlation was noticed between pH and Shannon diversity, suggesting that more basic environments may result in a slight decrease in diversity of consumed substrates (Figures 9 and 10).

Electrical conductivity (EC) emerged as a key factor influencing Shannon diversity (microbial substrate consumption diversity), showing a distinct nonlinear relationship (Figure 10). Shannon diversity peaked at intermediate EC levels (100–150 μS/cm) but declined at both lower and higher extremes. This aligns with the idea that intermediate ionic strength supports microbial functional diversity by optimizing nutrient transport without imposing osmotic stress. This suggests that EC below 100 may enhance substrate preference diversity, while fluctuations at higher levels (120–200) could have a negative impact. However, EC did not significantly affect Shannon evenness, suggesting its influence is more pronounced in shaping functional diversity in terms of microbial carbon substrate utilization rather than the uniformity of substrate preferences across the microbial community.

Phosphorus (P) had a strong negative effect on richness and evenness, but its relationship with Shannon diversity was non-linear, which peaked at intermediate P levels before declining at higher concentrations, suggesting that phosphorus may support certain taxa while reducing overall richness and evenness (Figures 9 and 10). The impact of chemical variables on Shannon evenness was investigated (Figure 11). The adjusted R^2 was 0.87, with 94.4% of the deviance explained. For example, variables such as sodium (Na) and magnesium (Mg), showed weak effects on richness (Figure 9) and Shannon diversity (Figure 10). However, Na displayed a non-linear relationship with Shannon evenness (Figure 11), suggesting that concentrations around 100 mg/kg may support a more even distribution of microbial substrate utilization preference, while extreme levels (<50 mg/kg or >200 mg/kg) could lead to disruption of evenness. Magnesium (Mg) did not show a strong effect on evenness (Figure 11). Potassium (K) had a strong negative effect on richness,

showing with increasing K levels (Figure 11), while with Shannon diversity it showed a non-linear relationship, peaking at intermediate levels before declining (Figure 10), suggesting that excessive K levels might reduce microbial metabolic C-utilization preferences. Lastly, calcium (Ca) was positively correlated with evenness (Figure 11), suggesting that elevated levels might promote a more even distribution of substrate utilization preference, whereas carbon (C) exhibited a slight decline with Shannon evenness, suggesting that higher concentrations might affect the distribution negatively.

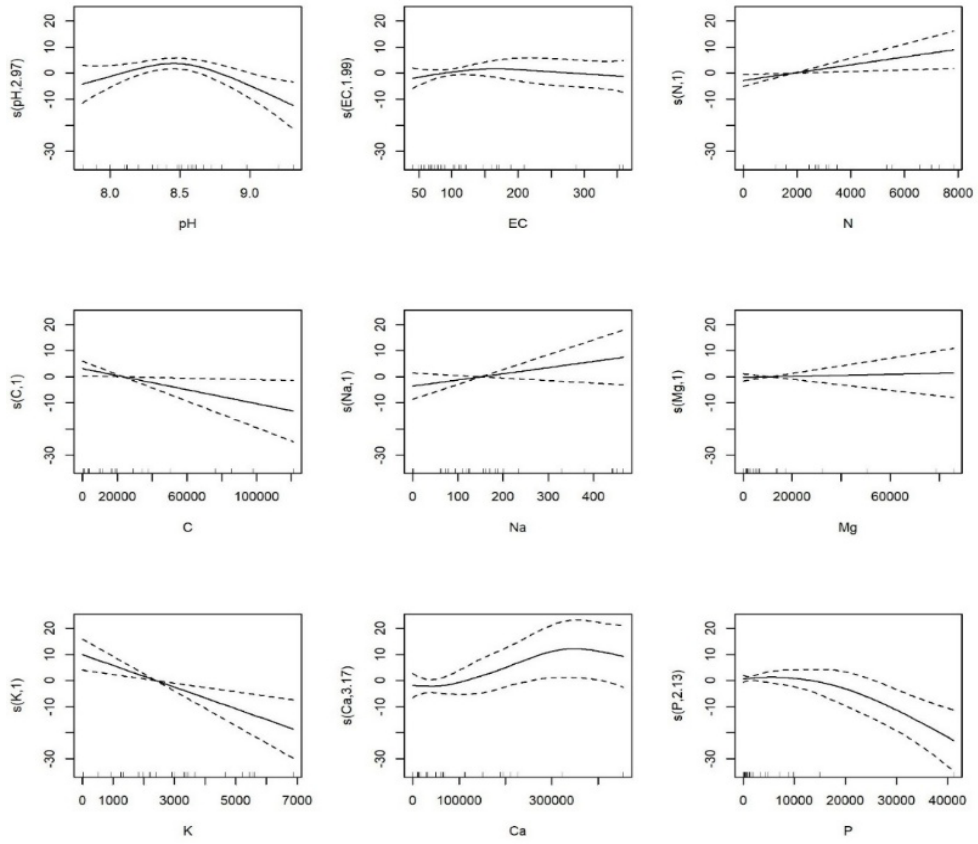

Figure 9. Generalized Additive Model plots showing the relationship between average richness and chemical factors (pH, EC, N, C, Na, Mg, K, Ca and P) in the analyzed cave samples. The solid lines represent the fitted smooths for each variable, while the dashed lines indicate the 95% confidence intervals. Variables with statistically significant relationships ($p < 0.05$) include pH, K, and P; variables with non-significant or marginal effects are included for completeness.

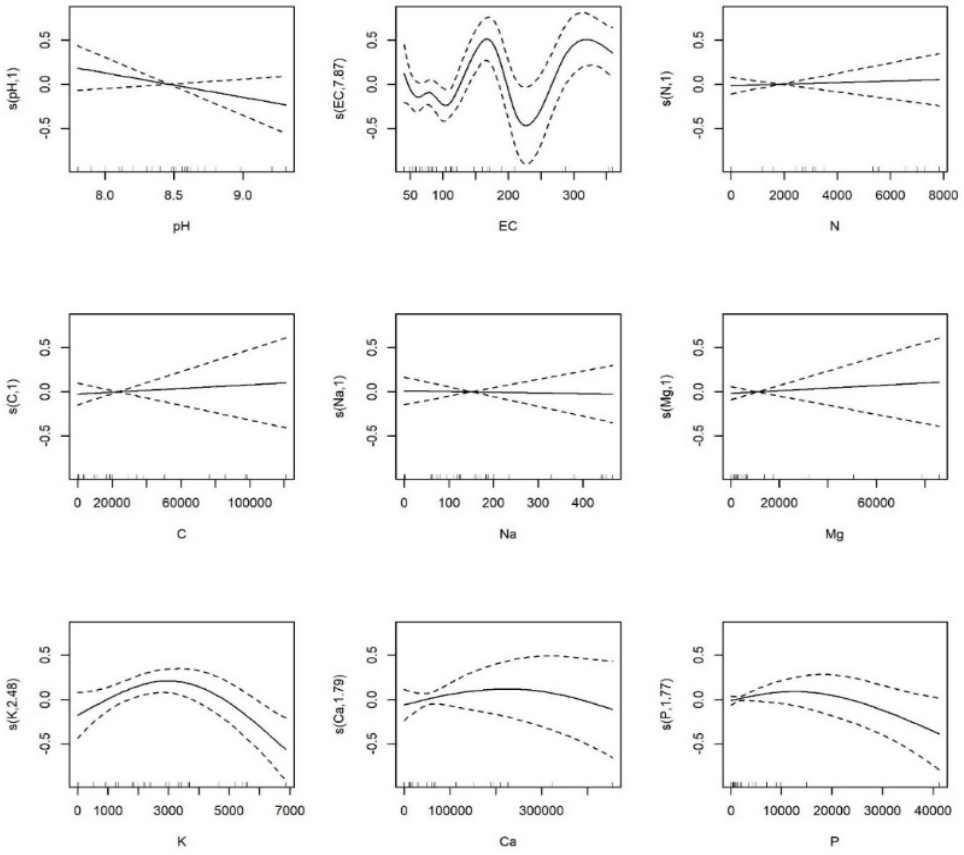

Figure 10. GAM plots showing the links between Shannon diversity and chemical factors (pH, EC, N, C, Na, Mg, K, Ca, and P). Solid lines represent the fitted smooths for each variable, while dashed lines indicate the 95% confidence intervals. Statistically significant relationships ($p < 0.05$) were found for EC and K; phosphorus (P) exhibited an exploratory trend toward significance ($p \approx 0.077$), while the other variables were not significant.

Besides sodium (Na), potassium (K) and carbon (C) which exhibited negative trends with evenness, EC, pH and N did not significantly influence evenness (Figure 11), suggesting that while some chemical variables might drive shifts in the distribution of microbial substrate utilization patterns, others have a more direct role in shaping the overall functional diversity.

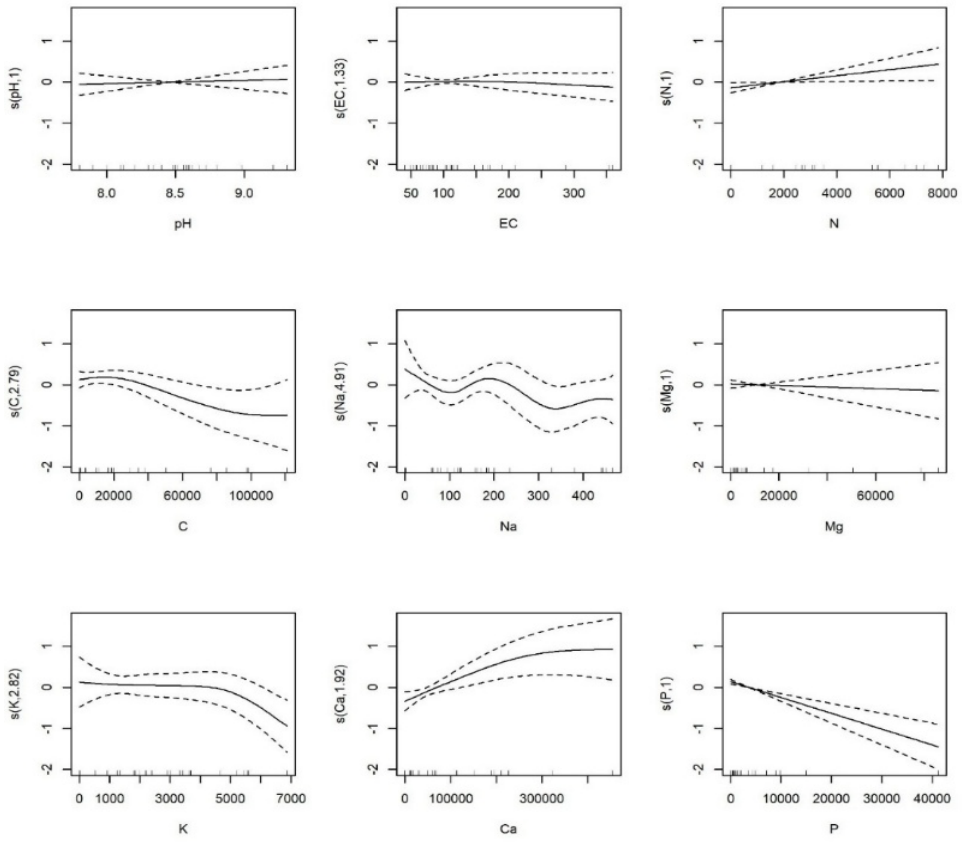

Figure 11. GAM plots of average Shannon evenness and different chemical factors (pH, EC, N, C, Na, Mg, K, Ca, and P). Solid lines represent the fitted smooths for each variable, while dashed lines indicate the 95% confidence intervals. No statistically significant relationships ($p < 0.05$) were observed; variables are shown for exploratory purposes.

Discussion

Variability and constraints in the analysis of carbon substrates utilization

After 200 hours of incubation, the C-substrate degradation patterns differed across water, sediment and moonmilk samples from Cloşani, Ferice, Muierilor, Leşu and Topolniţa caves. Although the same volume of inoculum was applied to

each well, we must take into consideration that there might be a variability in microbial inoculum size which may introduce inconsistencies in the results. Variability in microbial inoculum size likely contributed to discrepancies in optical density values, as showed by variations in wells containing the same substrate (Figure S1). Water samples showed greater C-substrate utilization potential and thus in microbial activity compared to sediment and moonmilk samples, supporting previous studies indicating that aquatic environments rich in organic matter support metabolically diverse communities (Obusan, 2023; Tobias-Hünefeldt *et al.*, 2023). Aquatic microbial communities are shaped by dynamic factors, including temperature and availability of organic carbon, which enhance their metabolic capabilities (Zheng *et al.*, 2014; Li *et al.*, 2021), suggesting that water environments can support a broader range of microbial taxa that can utilize diverse carbon sources. Thus, we could reasonably speculate on the relevance of aquatic microbial communities as key contributors to cave organic carbon degradation. Conversely, the stability of sediment and moonmilk geochemistry may restrain microbial diversity and its derived activity, with moonmilk samples displaying certain organic substrate degrading versatility. To the best of our knowledge, the present study is the first to evaluate the organic substrate utilization in moonmilk based on Biolog®EcoPlate™ approach and the few investigations on the metabolic potential of microorganisms associated with moonmilk formations prevent us from further assumptions.

The measurement of optical density in the Biolog®EcoPlate™ involves repeated handling and exposure to external environments, which increases the risk of contamination, especially for the plates incubated at temperatures higher than the room temperature (e.g., 37°C). Incubation was performed at 16°C to mitigate contamination risks and mimic cave conditions. Lower temperatures maintain microbial community structure while potentially decreasing metabolic activity, thereby improving the reliability of experimental outcomes (Akbari and Ghoshal, 2015; Tang *et al.*, 2017; Adekanmbi *et al.*, 2022).

Diversity analysis based on organic substrate metabolization

Despite the individual sample variation there are more metabolically active communities associated with higher microbial metabolic richness (Figure 5). Substrate utilization patterns varied by sample type, indicating variations in nutrient availability and environmental conditions. Sediment and water samples demonstrated greater microbial community-based substrate utilization diversity, whereas moonmilk associated microbial communities displayed intermediate richness. The findings correspond with research that associates substrate richness with improved metabolic functionality across various environmental conditions (Li *et al.*, 2017; Patsch *et al.*, 2018; Zhang *et al.*, 2020).

Hierarchical clustering and temporal analysis of substrate utilization showed distinct differentiation among sample types with distinct patterns across water, sediment, and moonmilk samples. Sediment samples demonstrated significant microbial metabolic versatility, employing various carbon sources as a result of the community heterogeneous composition (Meyer *et al.*, 2022). D-galacturonic acid, a major constituent of of pectin, is preferentially metabolized by microorganisms that colonize plant-associated environments. For instance, studies in Antarctic soils have revealed that the capacity to utilize D-galacturonic acid contributes to the metabolic diversity of resident microbiota, underscoring its ecological relevance in nutrient-poor and extreme environments (Pop *et al.*, 2025). Also, *Agrobacterium tumefaciens* have been demonstrated to possess dehydrogenases specific for D-galacturonic acid, facilitating its oxidation and subsequent use in central meteabolic pathways (Boer *et al.*, 2009; Parkkinen *et al.*, 2011). Here, sediment samples showed moderate C-substrate utilization with clear preferences for L-serine and L-arginine, but compared to water samples indicated a much lower metabolic efficiency. Koner *et al.* (2021) evaluated carbon substrate use patterns in limestone caves, demonstrating that microbial communities in sediment samples exhibited diverse metabolic activity. Their findings indicate that nutrient availability affects microbial growth, with sediment samples demonstrating greater richness and diversity than water samples, which contained more specialized communities. The clustering pattern of water samples exhibited selective carbon utilization, likely influenced by nutrient-rich yet special conditions (Pašić *et al.*, 2010; Power *et al.*, 2018; Tobias-Hünefeldt *et al.*, 2021). Additionally, members of the Fusobacteria have shown differential utilization of amino acids. Specifically, *Fusobacterium varium* has been reported to metabolize L-arginine, a capacity that distinguishes it from closely related species such as *Fusobacterium nucleatum*, which exhibit alternative substrate specificities (Ramezani *et al.*, 1999).

The microbial communities from moonmilk samples exhibited distinct substrate utilization patterns, especially for amino acids and amides, probably influenced by geological conditions such as high calcium carbonate content, low organic matter availabitlity, and stable microclimatic conditions chracateristic of moonmilk deposits (Nyyssönen *et al.*, 2014).

The broad range of metabolic activity inferred to Cloşani and Muierilor caves sediments underscores their microbial diversity and metabolic potential, aligning with findings from aquifer microbiome research (Wu *et al.*, 2015). Again, the separation of moonmilk samples in the dendrogram suggests that their distinct chemistry and environmental conditions support a specialized microbial community. Zheng and Gong (2019) and Theodorescu *et al.* (2023) evaluated niche differentiation within microbial communities and discovered that varying

environmental conditions can result in differences in microbial diversity and composition. Their findings support the idea that microbial communities within the moonmilk samples may have distinct metabolic requirements shaped by their environmental settings.

Moreover, it is important to consider that the findings of this study provide valuable insight into the functional potential of microbial communities but represent a temporal snapshot from a single season, spring. Despite the relative temperature of the caves it might be of interest to capture seasonal variations in microbial metabolic dynamics. Additionally, the set of carbon sources of Biolog® EcoPlates™ may not fully encompass the range of substrates utilized by the microbial communities, limiting insights into specific metabolic pathways or microbial identities. Future research combining metagenomics and broader substrate profiling could offer a more comprehensive understanding of the ecological roles of these communities.

Influence of environmental chemistry on C-substrate utilization capability

The Principal Component Analysis (PCA) illustrates clustering based on sample type, associating water samples with microbial metabolic diversity metrics (Shannon diversity, evenness, richness) and electrical conductivity, whereas sediment samples showed correlation with nutrient gradients, including potassium (K), phosphorus (P), and nitrogen (N). Moonmilk samples exhibited decreased associations, indicating unique microbial responses. The findings correspond with research emphasizing the impact of dissolved ions and nutrient gradients on microbial community structure and metabolic activity (Shaw *et al.*, 2008; Haegeman *et al.*, 2013; Park *et al.*, 2020).

Nutrient availability facilitated microbial growth in sediments, whereas elevated sodium concentrations were inhibitory, aligning with findings from cave and reservoir systems (Mandal *et al.*, 2017; D'Angeli *et al.*, 2019). Electrical conductivity influenced microbial metrics in water, influencing both diversity and activity (Shen *et al.*, 2022).

Generalized Additive Models (GAMs) further illustrated both linear (e.g., N, Na) and non-linear (e.g., K, P, Ca) influences of chemical variables on microbial metabolic diversity indices. Additionally, pH and electrical conductivity also showed non-linear effects. This underscores the significant impact of chemical environments on richness and metabolic potential of the microbial communities, similar to the study of Liu *et al.* (2023) in which GAMs were employed to examine the impact of different environmental variables on communities inhabiting the macrobenthos near Xiaoqing Estuary (Laizhou Bay, China) and their findings indicated that chemical factors, including salinity, organic matter, and nutrient

concentrations, significantly impacted biodiversity indices that are presumably linked to the metabolic activity, revealing both linear and non-linear relationships. Moreover, the study of the phytoplankton community structure in Lake Longhu (Jiang *et al.*, 2023) and the study of spatial patterns of biodiversity in a large marine ecosystem (Dencker *et al.*, 2017) revealed that environmental factors, including nutrient concentrations, had significant effects on the community variability.

Conclusions

In this study, we assessed the microbial metabolic diversity in cave sediment, water, and moonmilk samples using the Biolog® EcoPlate™ method, which enables rapid screening of carbon substrate utilization. Hierarchical clustering revealed significant differences between sample groups, with distinct functional profiles based on the sample's origin and geochemistry. Notably, this study is the first to apply Biolog® EcoPlates™ to moonmilk samples from karstic caves, highlighting the significance of employing novel approaches to explore the metabolic potential of microbial communities in cave environments.

The results revealed that microbial communities populating the cave water samples were the most metabolically versatile, utilizing a broad range of carbon substrates compared to those in sediment and moonmilk samples. D-galacturonic acid, L-asparagine, and Tween 80 were the most readily degraded C-substrates. Cave water hosted the most metabolically diverse microbial communities, playing a critical role in carbon turnover in studied cave systems, suggesting an important role in priming organic matter and facilitating nutrient cycling within the aquatic compartments of the caves. Sediment-associated communities exhibited more restricted metabolic profiles, favoring specific substrates like L-serine and L-arginine, reflecting potential specialization for recycling available organic substrates under more stable geochemical conditions. In contrast, moonmilk samples showed the least metabolic activity, with a narrow substrate range, indicating a specialized microbial community. Additionally, the application of Generalized Additive Models (GAMs) in cave microbiology is novel, providing a powerful approach for analyzing complex relationships between microbial metabolic diversity and environmental factors. GAMs revealed a positive correlation between Shannon diversity and intermediate values of electrical conductivity, indicating that moderate EC levels enhance microbial C-utilization.

Overall, this work offers fresh insights into the metabolic capacities of cave microbial communities and their adaptation to environmental variables, shedding light on their ecological significance in carbon cycling in cave environments. The observed patterns suggest that microbial communities might play key roles in carbon cycling in these subterranean karst ecosystems.

Acknowledgements and funding: This work was supported by a grant of the Ministry of Research, Innovation and Digitization, CNCS/CCCDI – UEFISCDI, project number 2/2019 (DARKFOOD), within PNCDI III. DFP has received financial support through the project: Entrepreneurship for innovation through doctoral and postdoctoral research, POCU/380/6/13/123886 co-financed by the European Social Fund, through the Operational Program for Human Capital 2014-2020. We thank to Ruxandra Bucur, Cristian Sitar, Alexandru Petculescu, Ionuț Cornel Mirea and Răzvan Arghir for their contribution to sampling campaigns.

Conflict of interest: The authors declare that the research was conducted in the absence of any commercial or financial relationships that could be construed as a potential conflict of interest.

Author contributions: DFP, HLB, OTM designed the research and drafted the manuscript; DFP and AC conducted the research; AMP performed the statistical analyses; OTM performed the sampling; EAL performed the chemical analyses. All authors contributed, verified, and approved the contents of the manuscript.

References

Adekanmbi, A. A., Shu, X., Zou, Y. & Sizmur, T. (2022). Legacy effect of constant and diurnally oscillating temperatures on soil respiration & microbial community structure. *Eur J Soil Sci.* 73(6), e13319, https://doi.org/10.1111/ejss.13319

Akbari, A., & Ghoshal, S. (2015). Effects of diurnal temperature variation on microbial community & petroleum hydrocarbon biodegradation in contaminated soils from a sub-Arctic site. Env. Micro., 17(12), 4916-4928, https://doi.org/10.1111/1462-2920.12846

Amaresan, N., Kumar, K., Venkadesaperumal, G., & Srivathsa, N. C. (2018). Microbial community level physiological profiles of active mud volcano soils in &aman & Nicobar Islands. *Nat. Acad. Sci. Lett.*, 41, 161-164, https://doi.org/10.25083/rbl/25.4/1731.1736

Asif, A., Koner, S., Chen, J. S., Hussain, A., Huang, S. W., Hussain, B., & Hsu, B. M. (2024). Uncovering the microbial community structure & physiological profiles of terrestrial mud volcanoes: a comprehensive metagenomic insight towards their Trichloroethylene biodegradation potentiality. *Env. Res.*, 119457, https://doi.org/10.1016/j.envres.2024.119457

Barton, H. A., and Northup, D. E. (2007). Geomicrobiology in cave environments: past, current and future perspectives. *J. Cave Karst Stud*., 69(1), 163-178.

Barton, H. A., Giarrizzo, J. G., Suarez, P., Robertson, C. E., Broering, M. J., Banks, E. D., & Venkateswaran, K. (2014). Microbial diversity in a Venezuelan orthoquartzite cave is dominated by the *Chloroflexi* (Class Ktedonobacterales) and *Thaumarchaeota* Group I. 1c. *Front. Microbiol*., 5, 615, https://doi.org/10.3389/fmicb.2014.00615

Bleahu, M., Decu, V., Negrea, S., Pleşa, C., Povară, I., &Viehmann, I. (1976). Caves from Romania. Editura Ştiinţifică şi Enciclopedică, Bucharest.

Boer, H., Maaheimo, H., Koivula, A., Penttilä, M., &Richard, P. (2009). Identification in *Agrobacterium tumefaciens* of the D-galacturonic acid dehydrogenase gene. *App. Microbio. Biotech*., 86(3), 901-909. https://doi.org/10.1007/s00253-009-2333-9

Bogdan D.F., Baricz A.I., Chiciudean I., Bulzu P.A., Cristea A., Năstase-Bucur R., Levei E.A., Cadar O., Sitar C., Banciu H.L. & Moldovan O.T., (2023), Diversity, distribution and organic substrates preferences of microbial communities of a low anthropic activity cave in North-Western Romania. *Front. Microbiol*. 14:962452, https://doi.org/10.3389/fmicb.2023.962452

Boteva, S., Stanachkova, M., Traykov, I., Angelova, B., & Kenarova, A. (2024). Bacterial functional responses to environmental variability: a case study in three distinct mountain lakes within a single watershed. *Biotechnol. Biotechnol. Equip*., 38(1), 2418549, https://doi.org/10.1080/13102818.2024.2418549

Bücs, S. L., Jére, C., Csősz, I., Barti, L., &Szodoray-Parády, F. (2012). Distribution and conservation status of cave-dwelling bats in the Romanian Western Carpathians. Vespertilio 16, 97–113.

Cacchio, P., &Del Gallo, M. (2019). A novel approach to isolation and screening of calcifying bacteria for biotechnological applications. *Geosci*., 9(11), 479, https://doi.org/10.3390/geosciences9110479

Cristea, A., Andrei, A. Ş., Baricz, A., Muntean, V., Banciu, H. L. (2014): Rapid assessment of carbon substrate utilization in the epilimnion of meromictic Ursu Lake (Sovata, Romania) by the Biolog Eco Plate™ approach. *Stud. Univ. Babes-Bolyai, Biol*. 59(1): 41-53

D'Angeli, I. M., Ghezzi, D., Leuko, S., Firrincieli, A., Parise, M., Fiorucci, A., & Cappelletti, M. (2019). Geomicrobiology of a seawater-influenced active sulfuric acid cave. *PLoS One*, 14(8), e0220706, https://doi.org/10.1371/journal.pone.0220706.

De Mandal, S., Chatterjee, R., &Kumar, N. S. (2017). Dominant bacterial phyla in caves and their predicted functional roles in C and N cycle. *BMC Microbio*., 17:90. https://doi.org/10.1186/s12866-017-1002-x

Dencker, T. S., Pecuchet, L., Beukhof, E., Richardson, K., Payne, M. R., & Lindegren, M. (2017). Temporal and spatial differences between taxonomic and trait biodiversity in a large marine ecosystem: Causes and consequences. *PLoS One*, 12(12), e0189731, https://doi.org/10.1371/journal.pone.0189731

Epure, L., Meleg, I. N., Munteanu, C. M., Roban, R. D., & Moldovan, O. T. (2014). Bacterial and fungal diversity of quaternary cave sediment deposits. *Geomicrobio. J*. 31, 116–127, https://doi.org/10.1080/01490451.2013.815292

Feigl, V., Ujaczki, É., Vaszita, E., &Molnár, M. (2017). Influence of red mud on soil microbial communities: Application and comprehensive evaluation of the Biolog® EcoPlate™ approach as a tool in soil microbiological studies. *Sci. Tot. Env*., 595, 903-911, https://doi.org/10.1016/j.scitotenv.2017.03.266

Garland, J. L. (1997). Analysis and interpretation of community-level physiological profiles in microbial ecology. *FEMS Microbio. Eco.*, 24(4), 289-300, https://doi.org/10.1111/j.1574-6941.1997.tb00446.x

Ghaly, T. M., Focardi, A., Elbourne, L. D. H., *et al.* (2023). Stratified microbial communities in Australia's only anchialine cave are taxonomically novel and drive chemotrophic energy production via coupled nitrogen-sulphur cycling. *Microbiome*, 11, 190. https://doi.org/10.1186/s40168-023-01633-8

Gryta, A., Frąc, M., &Oszust, K. (2014). The application of the Biolog EcoPlate approach in ecotoxicological evaluation of dairy sewage sludge. Applied biochemistry and biotechnology, 174, 1434-1443, https://doi.org/10.1007/s12010-014-1131-8

Gryta, A., Frąc, M., &Oszust, K. (2014). The application of the Biolog EcoPlate approach in ecotoxicological evaluation of dairy sewage sludge. *App. Biochem. Biotech*., 174, 1434-1443, https://doi.org/10.1007/s12010-014-1131-8

Haegeman, B., Hamelin, J., Moriarty, J., Neal, P., Dushoff, J., &Weitz, J. S. (2013). Robust estimation of microbial diversity in theory and in practice. *The ISME journal*, 7(6), 1092-1101, https://doi.org.10.1038/ismej.2013.10

Inskeep, W. P., Jay, Z. J., Tringe, S. G., Herrgård, M. J., Rusch, D. B., &YNP Metagenome Project Steering Committee and Working Group Members. (2013). The YNP metagenome project: environmental parameters responsible for microbial distribution in the Yellowstone geothermal ecosystem. *Front. Microbiol*., 4, 67, https://doi.org. 10.3389/fmicb.2013.00067

Iţcuş, C., Pascu, M. D., Brad, T., Perşoiu, A., &Purcarea, C. (2016). Diversity of cultured bacteria from the perennial ice block of Scarisoara Ice Cave, Romania. *Int. J. Speleo*., 45(1), 9, http://dx.doi.org/10.5038/1827-806X.45.1.1948

Jałowiecki, Ł., Chojniak, J. M., Dorgeloh, E., Hegedusova, B., Ejhed, H., Magnér, J., &Płaza, G. A. (2016). Microbial community profiles in wastewaters from onsite wastewater treatment systems technology. *PloS one*, 11(1), e0147725, https://doi.org/10.1371/journal.pone.0147725

Jiang, Y., Wang, Y., Huang, Z., Zheng, B., Wen, Y., &Liu, G. (2023). Investigation of phytoplankton community structure and formation mechanism: a case study of Lake Longhu in Jinjiang. *Front. Microbiol*., 14, 1267299, https://doi.org.10.3389/fmicb.2023.1267299

Jin, Q., Black, A., Kales, S. N., Vattem, D., Ruiz-Canela, M., &Sotos-Prieto, M. (2019). Metabolomics and Microbiomes as Potential Tools to Evaluate the Effects of the Mediterranean Diet. *Nutrients*, 11(1), 207, https://doi.org/10.3390/nu11010207

Jones, D. (2015). 2. Methods for Characterizing Microbial Communities in Caves &Karst: A Review. In A. Summers Engel (Ed.), Microbial Life of Cave Systems (pp. 23-46). Berlin, München, Boston: De Gruyter, https://doi.org/10.1515/9783110339888-004

Koner, S., Chen, J. S., Hsu, B. M., Rathod, J., Huang, S. W., Chien, H. Y., ... &Chan, M. W. (2022). Depth-resolved microbial diversity and functional profiles of trichloroethylene-contaminated soils for Biolog EcoPlate-based biostimulation strategy. *J. Hazard. Mater.*, 424, 127266, https://doi.org/10.1016/j.jhazmat.2021.127266

Koner, S., Chen, J. S., Hsu, B. M., Tan, C. W., Fan, C. W., Chen, T. H., &Nagarajan, V. (2021). Assessment of Carbon substrate catabolism pattern and functional metabolic pathway for Microbiota of Limestone Caves. *Microorganisms*, 9, https://doi.org/10.3390/microorganisms9081789

Li, H., Xu, Z., Yan, Q., Yang, S., Van Nostrand, J. D., Wang, Z., &Deng, Y. (2018). Soil microbial beta-diversity is linked with compositional variation in aboveground plant biomass in a semi-arid grassland. *PLANTSOIL*, 423, 465-480, https://doi.org/10.1007/s11104-017-3524-2

Li, X., Liu, L., Zhu, Y., Zhu, T., Wu, X., &Yang, D. (2021). Microbial community structure and its driving environmental factors in black carp (Mylopharyngodon piceus) aquaculture pond. Water, 13(21), 3089, https://doi.org/10.3390/w13213089

Liu, F., Giometto, A., &Wu, M. (2021). Microfluidic and mathematical modeling of aquatic microbial communities. *Anal. Bioanal. Chem*., 413, 2331–2344, https://doi.org/10.1007/s00216-020-03085-7

Liu, L., Li, A., Zhu, L., Xue, S., Li, J., Zhang, C., &Mao, Y. (2023). The Application of the Generalized Additive Model to Represent Macrobenthos near Xiaoqing Estuary, Laizhou Bay. *Biology*, 12(8), 1146, https://doi.org/10.3390/biology12081146

Martin-Pozas, T., Gonzalez-Pimentel, J. L., Jurado, V., Cuezva, S., Dominguez-Moñino, I., Fernandez-Cortes, A., &Saiz-Jimenez, C. (2020). Microbial activity in subterranean ecosystems: Recent advances. *Appl. Sci.*, 10(22), 8130, https://doi.org/10.3390/app10228130

Melita, M., Amalfitano, S., Preziosi, E., Ghergo, S., Frollini, E., Parrone, D., &Zoppini, A. (2023). Redox conditions and a moderate anthropogenic impairment of groundwater quality reflected on the microbial functional traits in a volcanic aquifer. *Aquat. Sci*., 85(1), 3, https://doi.org/10.1007/s00027-022-00899-8

Meyer, N. R., Parada, A. E., Kapili, B. J., Fortney, J. L., &Dekas, A. E. (2022). Rates and physico-chemical drivers of microbial anabolic activity in deep-sea sediments and implications for deep time. *Environ. Microbiol.*, 24(11), 5188-5201, https://doi.org/10.1111/1462-2920.16183

Moldovan, O. T., Carrell, A. A., Bulzu, P. A., Levei, E., Bucur, R., Sitar, C., &Podar, M. (2023). The gut microbiome mediates adaptation to scarce food in Coleoptera. *Environ. Microbiol.*, 18(1), 80, https://doi.org/10.1186/s40793-023-00537-2

Moretti, G., Matteucci, F., Ercole, C., Vegliò, F., &Del Gallo, M. (2016). Microbial community distribution and genetic analysis in a sludge active treatment for a complex industrial wastewater: A study using microbiological and molecular analysis and principal component analysis. *Ann. Microbiol.*, 66, 397-405, https://doi.org/10.1007/s13213-015-1122-1

Morita, N., Toma, Y., &Ueno, H. (2024). Microbial diversity and community structure in co-composted bamboo powder and tea leaves based on carbon substrate utilization patterns of the BIOLOG EcoPlate method. *Adv. Bamboo Sci*., 8, 100101, https://doi.org/10.1016/j.bamboo.2024.100101

Musat, N., Musat, F., Weber, P. K., &Pett-Ridge, J. (2016). Tracking microbial interactions with NanoSIMS. *COBIOT*, 41, 114–121, https://doi.org/10.1016/j.copbio.2016.06.007

Nyyssönen, M., Hultman, J., Ahonen, L., Kukkonen, I., Paulin, L., Laine, P., &Auvinen, P. (2014). Taxonomically and functionally diverse microbial communities in deep crystalline rocks of the Fennoscandian shield. *The ISME journal*, 8(1), 126-138, https://doi.org/10.1038/ismej.2013.125

Obusan, M. C. M., Castro, A. E., Villanueva, R. M. D., Isagan, M. D. E., Caras, J. A. A., &Simbahan, J. F. (2023). Physico-Chemical Quality and Physiological Profiles of Microbial Communities in Freshwater Systems of Mega Manila, Philippines. *Data*, 8(6), 103, https://doi.org/10.3390/data8060103

O'Connor, B. R., Fernández-Martínez, M. Á., Léveillé, R. J., & Whyte, L. G. (2021). Taxonomic characterization and microbial activity determination of cold-adapted microbial communities in Lava Tube Ice Caves from Lava Beds National Monument, a high-fidelity Mars analogue environment. *Astrobio.*, 21(5), 613-627, https://doi.org/10.1089/ast.2020.2327

Park, S., Cho, Y. J., Jung, D. Y., Jo, K. N., Lee, E. J., &Lee, J. S. (2020). Microbial diversity in moonmilk of Baeg-nyong Cave, Korean CZO. Front. Microbiol., 11, 613, https://doi.org/10.3389/fmicb.2020.00613

Pašić, L., Kovče, B., Sket, B., and Herzog-Velikonja, B. (2009). Diversity of microbial communities colonizing the walls of a Karstic cave in Slovenia. *FEMS Microbio. Eco.*, 71(1), 50-60, https://doi.org/10.1111/j.1574-6941.2009.00789.x

Parkkinen, T., Boer, H., Jänis, J., Andberg, M., Penttilä, M., Koivula, A., & Rouvinen, J. (2011). Crystal structure of uronate dehydrogenase from *Agrobacterium tumefaciens*. *JBC*, 286(31), 27294-27300. https://doi.org/10.1074/jbc.m111.254854

Patsch, D., van Vliet, S., Marcantini, L. G., &Johnson, D. R. (2018). Generality of associations between biological richness and the rates of metabolic processes across microbial communities. *Environ. Microbiol.*, 20(12), 4356-4368, https://doi.org/10.1111/1462-2920.14352

Paula, C. C. P. D., Bichuette, M. E., &Seleghim, M. H. R. (2020). Nutrient availability in tropical caves influences the dynamics of microbial biomass. *MicrobiologyOpen*, 9(7), e1044, https://doi.org/10.1002/mbo3.1044

Pedersen, K. (2012). Subterranean microbial populations metabolize hydrogen and acetate under in situ conditions in granitic groundwater at 450 m depth in the Äspö Hard Rock Laboratory, Sweden. *FEMS Microbio. Eco*., 81(1), 217–229. https://doi.org/10.1111/j.1574-6941.2012.01370.x

Pop, C.-E., Fendrihan, S., Crăciun, N., Vasilighean, G., Chifor, D. E., Topârceanu, F., Florea, A., Mihăilescu, D. F., &Mernea, M. (2025). Antarctic Soil and Viable Microbiota After Long-Term Storage at Constant −20 °C. *Biology*, *14*(3), 222. https://doi.org/10.3390/biology14030222

Power, J. F., Carere, C. R., Lee, C. K., Wakerley, G. L., Evans, D. W., Button, M., &Stott, M. B. (2018). Microbial biogeography of 925 geothermal springs in New Zealand. *Nature communications,* 9(1), 2876, https://doi.org/10.1038/s41467-018-05020-y

Ramezani, M., MacIntosh, S., &White, R. L. (1999). Utilization of d-amino acids by *Fusobacterium nucleatum* and *Fusobacterium varium*. *Amino Acids*, 17(2), 185-193. https://doi.org/10.1007/bf01361881

Rutgers, M., Wouterse, M., Drost, S. M., Breure, A. M., Mulder, C., Stone, D., &Bloem, J. (2016). Monitoring soil bacteria with community-level physiological profiles using Biolog™ Ecoplates in the Netherlands and Europe. *Appl. Soil Ecol.*, 97, 23-35, https://doi.org/10.1016/j.apsoil.2015.06.007

Shaw, A. K., Halpern, A. L., Beeson, K., Tran, B., Venter, J. C., &Martiny, J. B. (2008). It's all relative: ranking the diversity of aquatic bacterial communities. *Environ. Microbiol*, 10(9), 2200-2210, https://doi.org.10.1111/j.1462-2920.2008.01626.x

Shen, J., Smith, A. C., Barnett, M. J., Morgan, A., & Wynn, P. M. (2022). Distinct microbial communities in the soils, waters, and speleothems of a hyperalkaline cave system. Journal of Geophysical Research: *Biogeosciences*, 127(9), e2022JG006866, https://doi.org/10.3390/microorganisms9081789

Simpson, G. L., (2024). gratia: An R package for exploring generalized additive models. *J Open Source Software*, 9(104), 6962, https://doi.org/10.21105/joss.06962

Sofo, A., & Ricciuti, P. (2019). A standardized method for estimating the functional diversity of soil bacterial community by Biolog® EcoPlatesTM assay—the case study of a sustainable olive orchard. *App. Sci.*, 9(19), 4035, https://doi.org/10.3390/app9194035

Stefanowicz, A. (2006). The Biolog plates technique as a tool in ecological studies of microbial communities. *Pol. J. Environ. Stud*., 15(5).

Tang, Z., Sun, X., Luo, Z., He, N., & Sun, O. J. (2018). Effects of temperature, soil substrate, and microbial community on carbon mineralization across three climatically contrasting forest sites. *Eco. Evo.*, 8(2), 879-891, https://doi.org/10.1002/ece3.3708

Teng, Z., Fan, W., Wang, H., Cao, X., & Xu, X. (2020). Monitoring soil microorganisms with community-level physiological profiles using Biolog EcoPlates™ in Chaohu lakeside wetland, East China. *Eurasian J. Soil Sci.*, 53, 1142-1153, https://doi.org/10.1134/S1064229320080141

Theodorescu, M., Bucur, R., Bulzu, PA., Faur L., Levei EA., Mirea IC, Cadar O., Ferreira R, Souza-Silva M., & Moldovan OT. (2023). Environmental Drivers of the Moonmilk Microbiome Diversity in Some Temperate and Tropical Caves. *Microb Ecol*, 86,2847-2857, https://doi.org/10.1007/s00248-023-02286-8

Thompson, H. F., & Gutierrez, T. (2021). Detection of hydrocarbon-degrading bacteria on deepwater corals of the northeast Atlantic using CARD-FISH. *J. Microbiol. Methods*., 187, 106277, https://doi.org/10.1016/j.mimet.2021.106277

Tobias-Hünefeldt, S. P., Wing, S. R., Baltar, F., & Morales, S. E. (2021). Changes in microbial community phylogeny and metabolic activity along the water column uncouple at near sediment aphotic layers in fjords. *Sci. Rep*., 11(1), 19303, https://doi.org/10.1038/s41598-021-98519-2

Wu, X., Holmfeldt, K., Hubalek, V., Lundin, D., Åström, M., Bertilsson, S., & Dopson, M. (2016). Microbial metagenomes from three aquifers in the Fennoscandian shield terrestrial deep biosphere reveal metabolic partitioning among populations. *The ISME Journal*, 10(5), 1192-1203, https://doi.org/10.1038/ismej.2015.185

Yu, K., Yi, S., Li, B., *et al.* (2019). An integrated meta-omics approach reveals substrates involved in synergistic interactions in a bisphenol A (BPA)-degrading microbial community. *Microbiome*, 7(1), 16. https://doi.org/10.1186/s40168-019-0634-5

Yu, Z., Yang, J., Amalfitano, S., Yu, X., & Liu, L. (2014). Effects of water stratification and mixing on microbial community structure in a subtropical deep reservoir. *Sci. Rep*., 4(1), 5821, https://doi.org/10.1038/srep05821

Yun, Y., Cheng, X., Wang, W., & Wang, H. (2018). Seasonal variation of bacterial community and their functional diversity in drip water from a karst cave. *Chinese Science Bulletin*, 63(36), 3932-3944, https://doi.org/10.1360/N972018-00627

Zak, J. C., Willig, M. R., Moorhead, D. L., & Wildman, H. G. (1994). Functional diversity of microbial communities: a quantitative approach. *Soil Biol. Biochem*., 26(9), 1101-1108, https://doi.org/10.1016/0038-0717(94)90131-7

Zhang, P., Cui, Z., Guo, M., & Xi, R. (2020). Characteristics of the soil microbial community in the forestland of Camellia oleifera. *Peer J* 8: e9117, https://doi.org.10.7717/peerj.9117

Zheng, Y., & Gong, X. (2019). Niche differentiation rather than biogeography shapes the diversity and composition of microbiome of Cycas panzhihuaensis. *Microbiome*, 7, 1-19, https://doi.org/10.1186/s40168-019-0770-y

Zoltan, L., & Szántó, L. (2003). Bats of the Carpathian Region. *Acta Chiropt*. 5, 155–160. https://doi.org/10.3161/001.005.0115

Supplementary materials

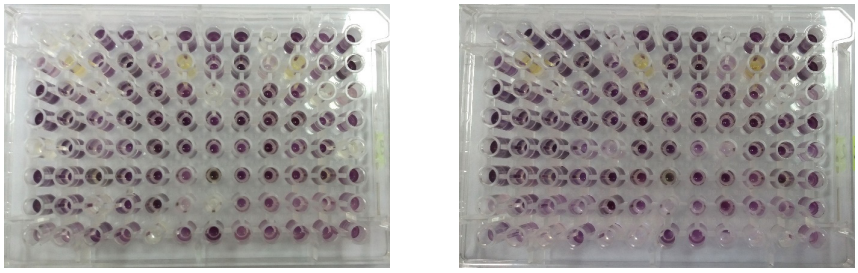

PCDF2-LIMON PCDF3-APA

Figure S1. Random selection of pictures showing the degradation patterns within Biolog® EcoPlates™ after an incubation period of 200 hours (PC – Closani Cave)

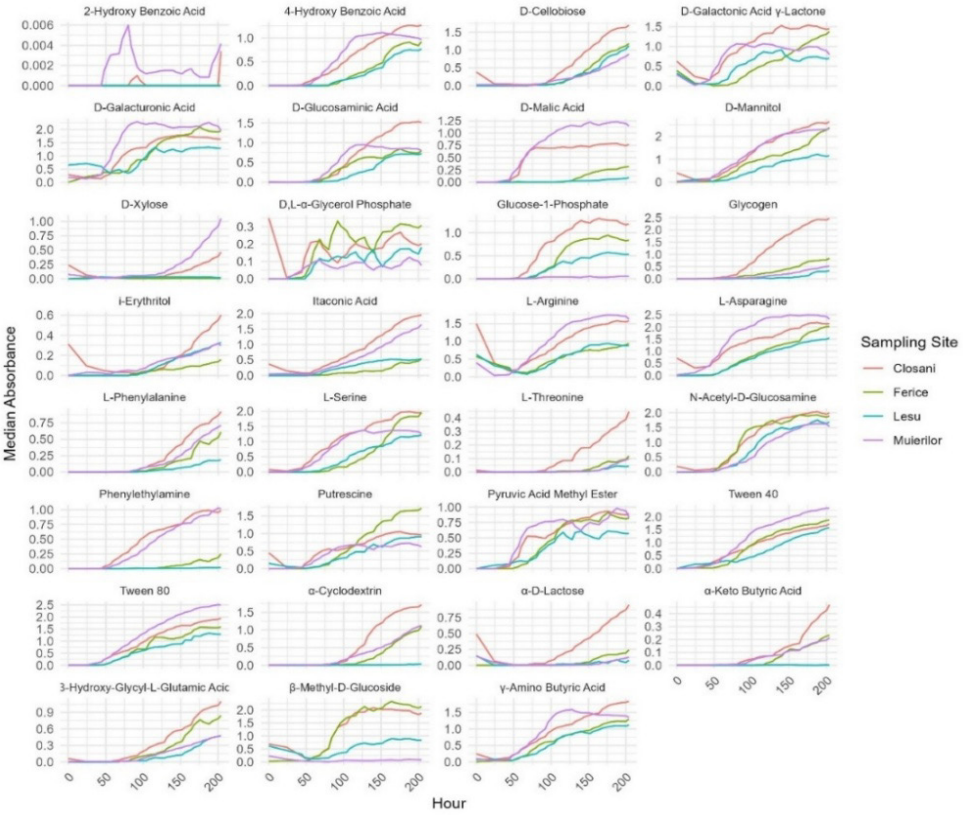

Figure S2. Median absorbance over time by carbon and sampling site for water samples only.

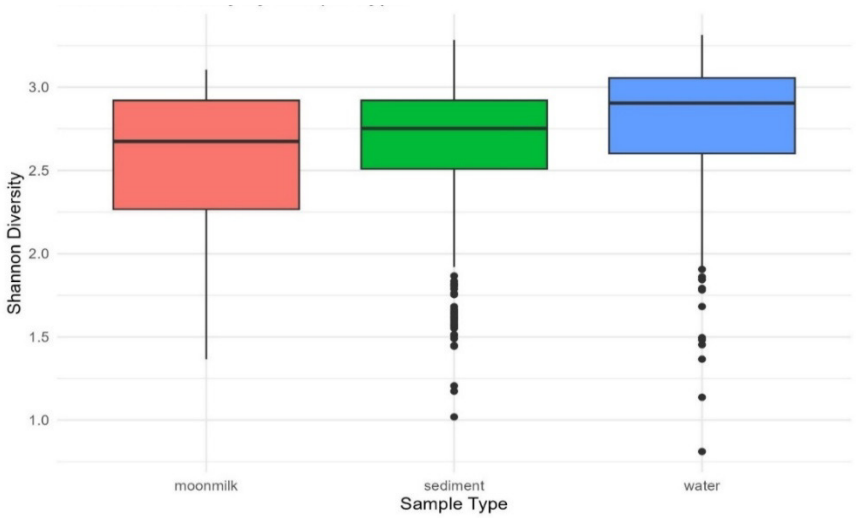

Figure S3. Shannon diversity (metabolic diversity) index of microbial communities in moonmilk, sediment, and water samples. Water samples show the highest diversity, followed by moonmilk and sediments. Boxplots display median, interquartile range, and outliers.

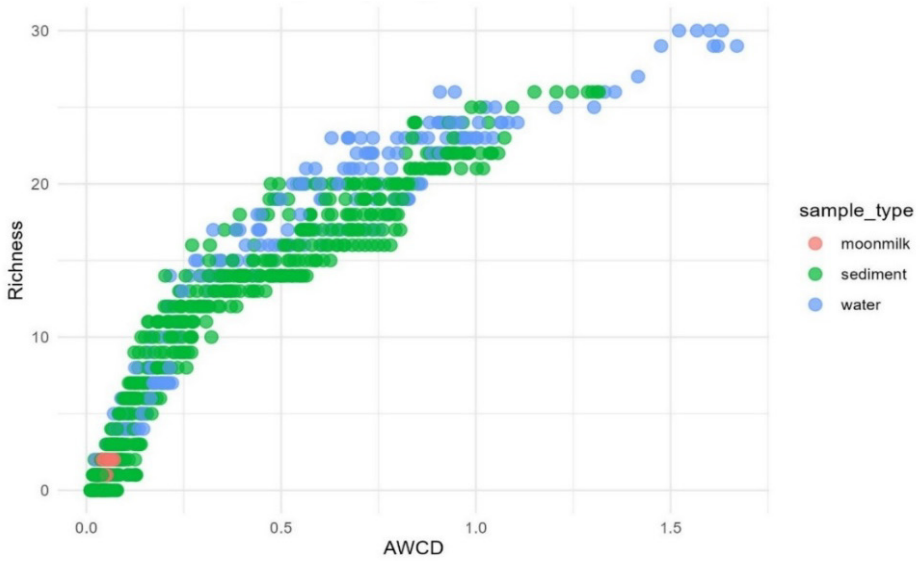

Figure S4. Scatter plot of AWCD versus richness of substrate degradation for sediments, moonmilk, and water samples, measured over time (0–204 hours).

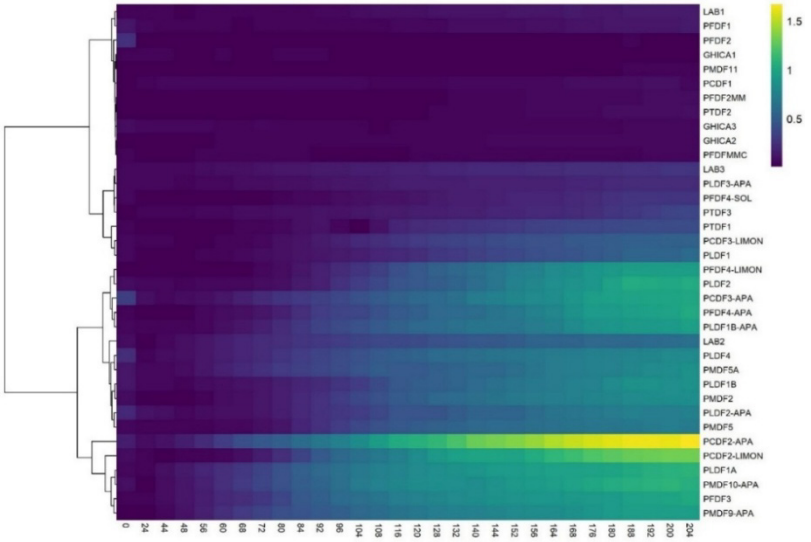

Figure S5. Heatmap of the average-well color development by sample and hour with clustering. See Table 1 for corresponding sample types and codes.

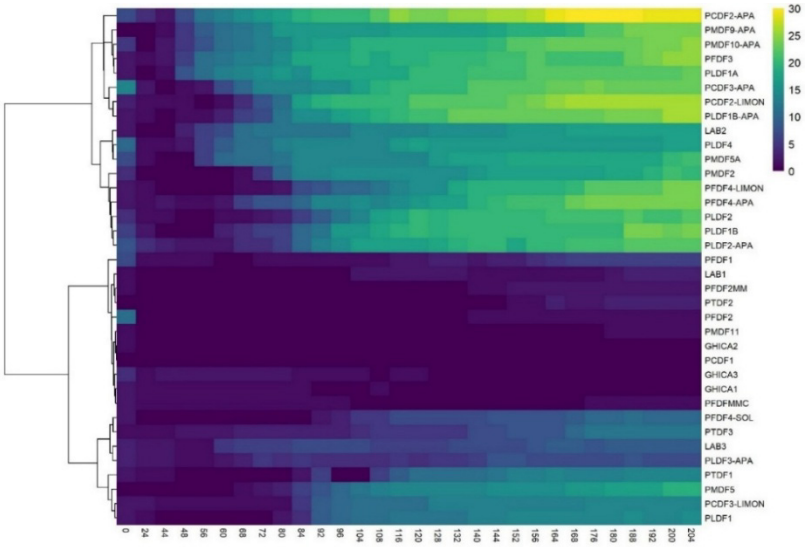

Figure S6. The heatmap showing the clustering of substrate richness by sample and hour. All the sample types are included in the analysis. The color scale represents species richness, with yellow indicating higher richness and dark purple representing lower richness. Hierarchical clustering was applied to both samples (rows) and time points (columns), revealing distinct temporal and sample-specific patterns in microbial diversity. See Table II.1 for corresponding sample types and codes.

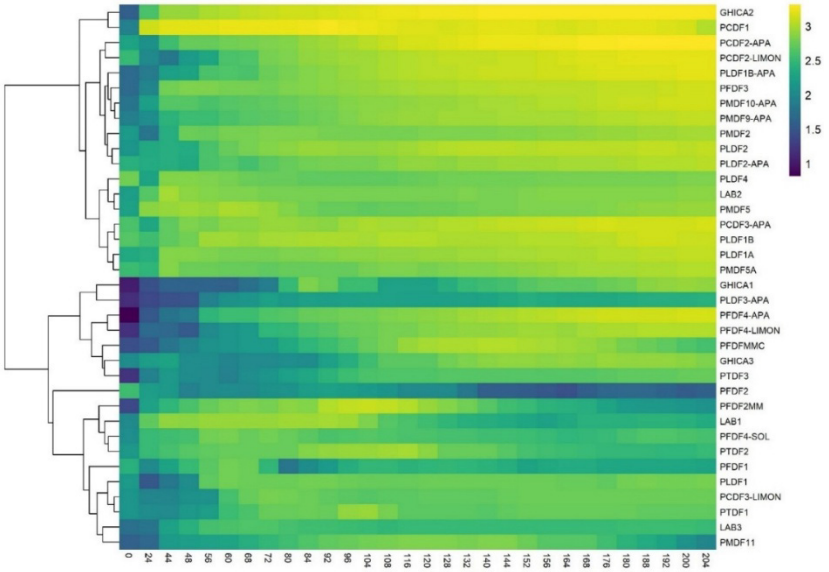

Figure S7. Dendrogram heatmap showing the clustering of Shannon diversity across different samples over time. The color scale represents Shannon diversity, with yellow indicating higher diversity and purple representing lower diversity. Hierarchical clustering was applied to both samples (rows) and time points (columns), revealing distinct temporal and sample-specific patterns in microbial diversity.

Table S1. Maximum AWCD values for water, sediment, and moonmilk samples across the sampling sites.

Site	Max AWCD (Water)	Max AWCD (Sediment)	Max AWCD (Moonmilk)
Cloșani	1.67	1.32	-
Ferice	1.01	1.01	0.07
Leșu	0.95	1.07	-
Muierilor	1.08	0.84	-
Topolnița	-	0.41	-

Table S2. List of geochemical parameters excluded from the PCA analysis, including elements (Al, Fe, S, Mn, As, Cr, Co, Ni, Cu, Zn) and water-specific parameters (DIC, DOC, SO_4^{2-}, NO_3^-, Cl^-, PO_4^{3-}), excluded for either low concentrations or incompatibility between sediment and water sample data.

Parameters																
	Al	**Fe**	**S**	**Mn**	**As**	**Cr**	**Co**	**Ni**	**Cu**	**Zn**	**DIC**	**DOC**	**SO_4^{2-}**	**NO_3^-**	**Cl^-**	**PO_4^{3-}**
sediments																
Sample ID	mg/kg	mg/kg	mg/kg	mg/kg	mg/kg	mg/kg	mg/kg	mg/kg	mg/kg	mg/kg	-	-	-	-	-	-
PMDF2	3903	4617	68.4	214	52.7	4.0	1.3	4.6	11.0	60.3	-	-	-	-	-	-
PMDF5	14847	27613	196	158	15.6	38.0	3.4	9.3	467	242	-	-	-	-	-	-
PMDF11	14370	14303	286	570	33.5	17.0	3.1	12.3	19.8	784	-	-	-	-	-	-
PMDF5A	16427	23567	322	195	8.2	6.0	1.8	6.4.0	35.1	56.0	-	-	-	-	-	-
PTDF1	24903	33967	92.7	586	6.1	66.0	12.7	29.3	22.6	83.3	-	-	-	-	-	-
PTDF2	25773	34367	37	635	5.5	59.0	12.9	28.2	21.0	64.6	-	-	-	-	-	-
PTDF3	14866	23100	206	81.2	5.3	8.5	1.7	5.0	3.4	9.2	-	-	-	-	-	-
LAB1	33362	30139	27.6	1097	5.1	49.7	19.7	51.7	51.2	156	-	-	-	-	-	-
LAB2	24540	22837	46.7	186	13.5	42.2	6.7	40.2	28.9	489	-	-	-	-	-	-
LAB3	38107	28104	39.6	138	11.9	34.0	5.2	32.5	21.5	153	-	-	-	-	-	-
GHICA1	62997	55572	61.1	313	13.9	93.7	8.2	69.7	46.4	148	-	-	-	-	-	-
GHICA2	63089	53824	85.8	305	14.1	89.7	8.2	72.8	47.1	154	-	-	-	-	-	-
GHICA3	57706	45181	47.3	304	13.1	89.0	8.1	73.1	49.6	156	-	-	-	-	-	-
PCDF1	27557	39667	30.9	945	6.2	44.0	14.1	30.0	32.7	96.5	-	-	-	-	-	-
PFDF1	28283	32257	59.0	622	20.2	38.0	7.7	27.0	15.8	130	-	-	-	-	-	-
PFDF2	25933	31157	31.8	998	17.2	38.0	10.6	31.5	17.1	111	-	-	-	-	-	-

Table S2 continued

Parameters																
	Al	**Fe**	**S**	**Mn**	**As**	**Cr**	**Co**	**Ni**	**Cu**	**Zn**	**DIC**	**DOC**	**SO_4^{2-}**	**NO_3^-**	**Cl^-**	**PO_4^{3-}**
PFDF3	40033	32097	67.8	686	19.7	46.0	11.0	23.9	17.6	170	-	-	-	-	-	-
PFDFMMC	12768	6089	24.5	128	29.6	13.4	1.8	17.6	1.6	31.3	-	-	-	-	-	-
PFDF2MM	3286	1853	86.2	66.3	5.6	5.6	1.2	6.0	0.3	14.7	-	-	-	-	-	-
PLDF1	9543	16157	36	411	23.8	13	5.5	13.9	5.5	28.5	-	-	-	-	-	-
PLDF1A	19853	26813	734	161	13.4	5	1.5	5.0	5.4	16.3	-	-	-	-	-	-
PLDF1B	18113	25193	176	832	53.3	21	8.3	27.8	26.0	134	-	-	-	-	-	-
PLDF4	12183	22273	128	745	51.0	19	7.3	25.1	28.5	134	-	-	-	-	-	-
PLDF2	18173	27787	801	272	13.8	4.7	1.8	5.9	8.7	51.4	-	-	-	-	-	-
water																
	µg/L	µg/L	-	µg/L	µg/L	µg/L	µg/L	µg/L	µg/L	µg/L	mg/L	mg/L	mg/L	mg/L	mg/L	mg/L
PMDF9-APA	<0.2	30.0	NA	0.20	0.50	1.00	<0.2	<0.2	0.7	5.1	16.9	3.3	13.5	61.5	1.9	13.5
PMDF10-APA	<0.2	30.0	NA	0.20	0.80	1.20	<0.2	0.4	0.9	3.5	19.8	2.1	28.0	78.5	2.7	28.0
PCDF2-APA	7.8	6800	NA	0.30	0.30	<0.2	<0.2	0.3	0.4	7.4	18.9	1.6	7.5	1.9	0.8	7.5
PCDF3-APA	<0.2	160	NA	0.40	<0.20	<0.2	<0.2	0.4	0.3	11.9	19.9	2.5	5.1	1.4	0.8	5.1
PFDF4-APA	<0.2	100	NA	0.70	0.70	<0.2	<0.2	<0.2	0.3	5.5	48.6	0.2	6.4	1.2	1.0	6.4
PLDF1B-APA	<0.2	10.0	NA	0.40	0.90	<0.2	<0.2	0.3	0.3	4.6	17.0	0.8	4.6	4.3	0.8	4.6
PLDF2-APA	<0.2	10.0	NA	0.30	1.40	<0.2	<0.2	<0.2	0.1	2.7	19.5	0.9	4.7	4.2	0.7	4.7
PLDF3-APA	<0.2	20.0	NA	0.30	0.70	1.50	<0.2	<0.2	0.3	10.2	24.2	1.0	7.7	2.3	0.7	7.7
PMDF9-APA	<0.2	30.0	NA	0.20	0.50	1.00	<0.2	<0.2	0.7	5.1	16.9	3.3	13.5	61.5	1.9	13.5

STUDIA UNIVERSITATIS BABEŞ-BOLYAI BIOLOGIA, 70, 1, 2025 (p. 287-302)
doi:10.24193/subbbiol.2025.1.13

Forage, preen or fight? A study of interspecific water bird interactions at Crișul Repede River

Ana-Teodora Ștefan[1]✉, Cristina Craioveanu[2], Alexandru Nicolae Stermin[2]

[1] Faculty of Science, Department of Biology, Lund University, Lund, Sweden; [2] Centre for Systems Biology, Biodiversity and Bioresources 3B, Babeș-Bolyai University, Cluj-Napoca, Romania
✉***Corresponding author, E-mail: an5837st-s@student.lu.se***

Article history: Received 18 March 2025; Revised 7 June 2025; Accepted 11 June 2025; Available online 25 June 2025

Abstract. Analyzing the behavior of birds offers insight into the conservation of biodiversity, a heavily discussed subject in the fields of ecology as well as ornithology. As it has been previously proven (Rushton *et al.*, 1994), slow-flowing areas of rivers represent important habitats for birds all throughout the year and the conservation of this type of habitats has been known to have a positive effect on the population of many water bird species (Rolls *et al.*, 2012). Therefore, this study explores the dynamic of interspecific interactions between water birds in open water areas from the Afon Peța portion of the Crișul Repede River in Bihor, Romania. We collected data over 8 months, from October 2022 to May 2023 and identified 23 bird species and three types of interactions between them: cooperation for foraging, for grooming, and aggression. The frequency of various interactions was directly proportional to the number of individuals observed on the area, however, we found no connection to the month or the season. Additionally, we detected no preference regarding the interaction partner species. We found a strong correlation between the number of individuals and the number of interactions in all species. The results obtained through this study will help broaden the knowledge about common aquatic bird species in the area, as well as the dynamic of behaviours over the course of three seasons.

Keywords: aggression, cooperation, Crișul Repede River, interspecific behaviour, water birds.

Introduction

Birds have been an object of fascination for people for centuries, as evidenced by Aristotle's belief that Redstarts become Robins as soon as winter begins (Lohmann, 2018). Since the debut of experimental work conducted on birds in the late 1800's (Birkhead & Charmantier, 2009), the number of published studies has been increasing exponentially (Bibby, 2003), many conservation biologists using them as great indicators for assessing the state of the environment (Grimes, 2005). Along with the appearance of ornithology came animal behavior, with pioneers such as C. Lloyd Morgan and Tinbergen publishing their work (Birkhead & Charmantier, 2009). The study of behavior in animals has been a crucial tool in conservation biology by allowing us to predict migrations (Chapman *et al.*, 2011) and the spread of invasive species (Cote *et al.*, 2010), one study focusing on developing a distribution model of bird populations in regard to interspecific interactions (Zurell, 2017). This type of behavior refers to a form of communication between two individuals from different species (Dhondt, 2012; Abrams, 2001), yet they are often short in duration and difficult to observe in nature and, as a result, there is a general lack of studies in this area.

The conservation of riverine habitats has been tightly linked to many benefits for humans and ecosystems alike; we can only benefit from regulating and cultural ecosystem services if we maintain the habitat quality (Arthington *et al.*, 2009). By preserving riverine habitats, we are ensuring connectivity between the habitats, as well as refugia for many species (Rolls *et al.*, 2012). Slow-slowing rivers play a crucial part in regulating nutrient cycling and sediment transport, all of which contribute to increasing biodiversity in freshwater ecosystems (Tickner *et al.*, 2020).

The purpose of this paper is to explore the dynamic of the interspecific interactions within water bird communities during passage and wintering seasons. In this context, the aims of our study were: i) the identification of interspecific interactions in the observed species, ii) the analysis of interspecific interactions in relation to the observation period and the qualitative and quantitative dynamics of avifauna.

Materials and methods

Study area

The Crişul Repede River's spring is in the Gilăului Mountains in the Apuseni Mountains (N-W Romania). It belongs to the hydrographic network of the Tisa River, forming the big three Crişuri rivers after which the Crişana area was

named, along with the Crişul Alb and Crişul Negru rivers (Telcean *et al.*, 2007). The Crişul Repede river that flows throughout the Apuseni Mountains is passing through Dealurile de Vest and Câmpia de Vest (Posea, 1977). Therefore, the drainage slope varies from steep in the mountain region to a very gentle one in the vicinity of Oradea (Măhăra, 2010). Here, the river meanders and the waterflow slows down, creating lakes such as the Afon Peţa Lake (Blaj *et al.*, 1979) (Fig. 1).

Figure 1. Map of the study area showing Afon Peţa lake with four observation points (Google Earth image generated at 07.09.2023)

The studied area is situated in the Sântion town from Bihor county, next to Balta Sântion, a fishing pond. The portion has been analyzed from 4 observation points (**Fig. 1**), depending on the visibility and presence or absence of the species. The observation area has a surface of 55 m^2 and has a perimeter of approximately 1,39 km; the observation points were chosen in order to maximize visibility over the water surface. Near the river bank, there is a patch of reed that is used by the birds as a refuge, covering about 5% of the study area. Surrounding the Crişul Repede, some *Rosa canina* bushes can be found, separating the agricultural corn fields from the river, as well as meadows that locals use for cattle grazing.

Sampling

For data collection, 51 single visits have been made in the Afon Peţa part of the Crişul Repede river, for which the following materials have been used: an observation sheet for each visit, Vortex Diamondback HD 8x42 binoculars, Canon PowerShoot ZOOM monocular camera, ornithological identification guide (Svensson, 2009). The data was collected in 2 sessions, one in the morning (anywhere between 08-11) and one in the afternoon (between 13-16).

Each monitoring visit began with a water bird species inventory from the studied area, followed by the counting of individuals in each species. An ethogram was completed over the course of 60 minutes, following the direct observations, the species and their behaviors observed being written on the

sheet along with the meteorological, and date and time aspects. The interactions fit into one of the two categories: aggression (A) or cooperation, the latter being divided into cooperation for feeding (CoF), CoG (for grooming), CoA (for attack), and CoD (for defence). In order to collect the data, we have organized four field visits per month, of which two in the morning and another two in the afternoon, the study taking place from October 2022 to May 2023.

A series of criteria was taken into consideration for an interaction to be placed into a category. For instance: aggression (A) implies that an individual will stake an attack stance (by raising their wings, extending the neck towards the enemy, and opening the bill). Cooperation for feeding (CoF) takes place when two individuals from different species are feeding simultaneously in close proximity to one another, similar to the grooming cooperation (CoG). For cooperation for attack (CoA) to take place, multiple species must aggress, at the same time and place, another species. For an interaction to be considered cooperation for defence (CoD), it has to imply an attack on another species, and a counterattack response from individuals that belong to another species than the aggressed one.

Data analysis

Bird interactions were recorded as interaction counts. We summarized the number of all interactions per species over 8 months of observations. We classified the types of interactions into the four observed categories: aggression (A), Cooperation for feeding (CoF), Cooperation for grooming (CoG), and Cooperation for aggression (CoA). Additionally, we categorized species into "instigator" and "reactor" depending on the role they assumed in the interaction behavior.

To check for differences between species, we computed the percentage of interactions per species and the role (instigator/reactor) in which they were observed. We also computed the percentage of interactions per type of interaction with other present species in each species that interacted the most. Interaction preference was tested only in the case of those species that significantly interacted more than others due to the larger number of values for interaction counts usable in statistical tests. Data was checked for normal distribution with the help of the Shapiro-Wilk test. For non-normally distributed data, we used the Kruskal test to check whether there are significant differences, followed, in case of significant results, by a Dunn post-hoc test with Benjamini-Hochberg adjusted p-values. We also performed a correlation analysis between the two components of interactions (instigation/reaction) and between the number of individuals and the number of interactions by using Spearman's rank correlation test. All data analyses were performed in RStudio (Posit team, 2024).

Results and discussions

During the study period, there have been observed a total of 23 species of birds (Table 1). In order to assess the species' dynamic, their monthly presence was noted, with the highest number of species per month appearing during April, with 18 species (Fig. 2). One possible explanation for the large number of birds during April 2022 (which represents the period between the cold and warm season) is the overlap (partially or completely) of migratory periods, the numbers of migratory populations being cumulated with those of sedentary populations (Dimitrie, 1984). The second most prolific month was January, with 13 observed species, closely followed by November with 12 bird species that spend winter in the slow-flowing rivers of Bihor. During October, February, March and May, 11 species inhabited the area, with the lowest number registered being recorded in December. The lack of diversity during these months is likely due to the competition between species, caused by limited sources of food, which leads to the maximizing of survival chances of the existing species (Dhondt, 2012).

Table 1. A complete list of species present during the study, including the shortened version of the names used during the statistical analysis.

Name of the species	Code
Actitis hypoleucos	Acti hypo
Anas penelope	Anas pene
Anas platyrhynchos	Anas plat
Anas querquedula	Anas quer
Anser fabalis	Anse faba
Ardea alba (Casmerodius albus)	Casm albu
Ardea cinerea	Arde cine
Aythya ferina	Ayth feri
Aythya fuligula	Ayth fuli
Chroicocephalus ridibundus	Chro ridi
Cygnus cygnus	Cygn cygn
Cygnus olor	Cygn olor
Egretta garzetta	Egre garz
Fulica atra	Fuli atra
Gallinula chloropus	Gall chlo
Himantopus himantopus	Hima hima
Larus michahellis	Laru mich
Nycticorax nycticorax	Nyct nyct
Phalacrocorax carbo	Phal carb
Podiceps cristatus	Podi cris
Sterna hirundo	Ster hiru
Tachybaptus ruficollis	Tach rufi
Vanellus vanellus	Vane vane

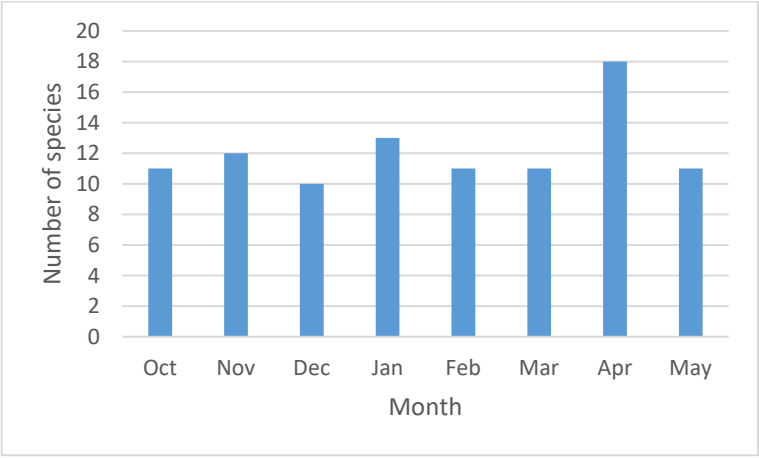

Figure 2. The species' dynamic over the course of 8 months.

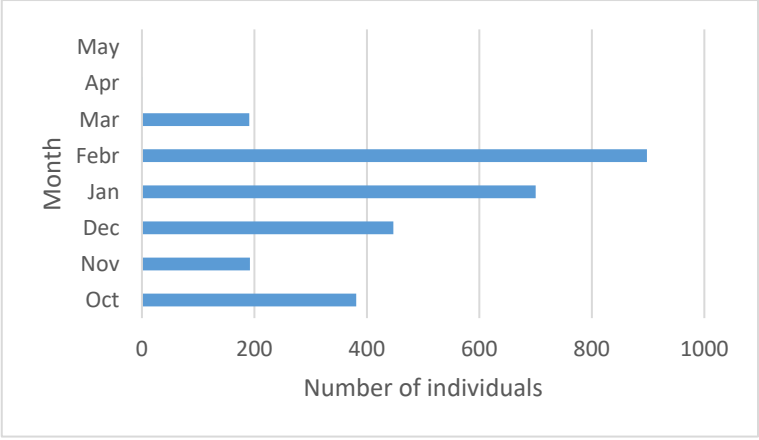

Figure 3. Numerical evolution of the Eurasian Coot population.

Out of the 23 species, three have been consistently present in the study area, with the most abundant being the Eurasian Coot (*Fulica atra*), 168 individuals being observed in one visit. The Black-headed Gull (*Chroicocephalus ridibundus*) is remarkable in numbers due to it having the largest number of individuals/species in one sitting (180 individuals). The third most notable species is the Tufted Duck (*Aythya fuligula*) with 32 birds observed at one time. Nevertheless, the Eurasian Coot population numbers have decreased drastically since February (Fig. 3); the Black-headed Gulls have presented a consistent numerical decrease over the entire course of the study (Fig. 4). Contrary to the coots, the Tufted Ducks have made their debut to Afon Peţa in December and

had an exponential growth until their decline in May, when no individuals were observed (Fig. 5). However, such changes in the number of individuals may also be due to the expected fluctuations in food over time (Keller *et al.*, 2009).

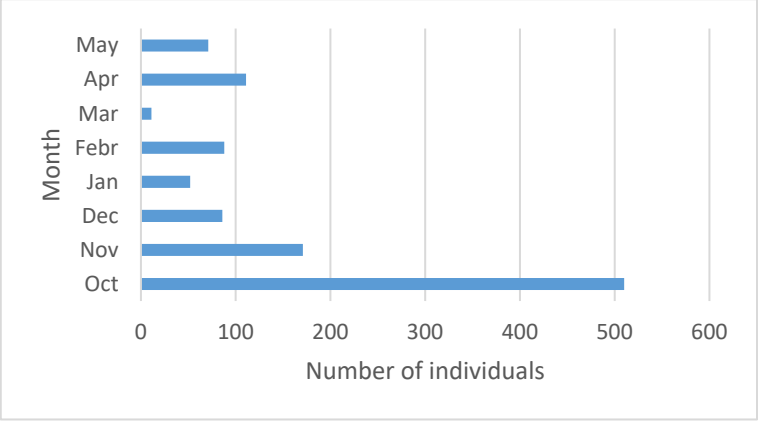

Figure 4. Numerical evolution of the Black-headed Gull population.

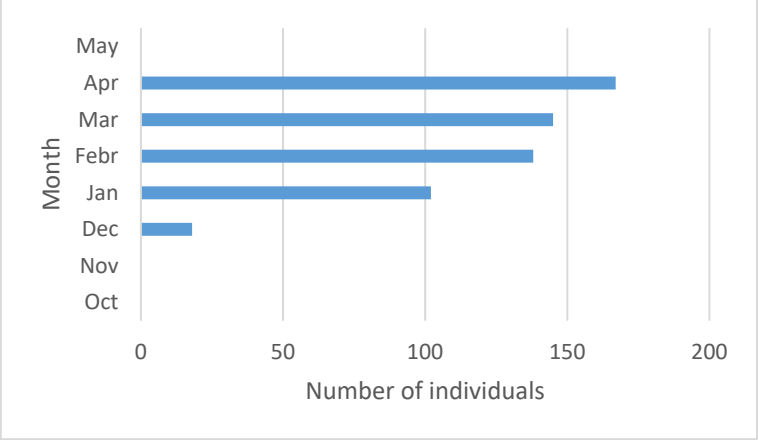

Figure 5. Numerical evolution of the Tufted Duck population.

There are two major limiting factors to be taken into consideration when analyzing animal behaviours: space and food availability. As the density of individuals increases, the average reproductive rate will decrease; it has also been shown that habitat heterogeneity within the territories occupied by individuals will affect each individual differently, therefore the species that compete for a territory will vary (Dhondt *et al.*, 1992; Ferrer *et al.*, 2006, Martinez *et al.*, 2008). Food is a limited resource during the wintering season, which

incites interspecific competition, having effects on the survival of individuals and implicitly on the size of the population that can reproduce (Dhondt, 2012). The bird species present in the area are part of different feeding guilds depending on the water depth at which they feed; in this context, surface-level feeders are terns and gulls, shallow water feeders are herons, egrets and Mallards, with the diving species observed being cormorants, the Tufted Duck, Common Pochard and the Eurasian Coot (Liordos & Kontsiotis, 2020). Thus, the feeding cooperation between several species which have different niches presents numerous benefits for birds, such as reducing the risk of predation, which has been studied by several authors (Lima, 1986, 1993; Pulliam and Caraco, 1984). An indirect result is reduced individual vigilance due to the safety provided by the group, which explains an increase in feeding rate (Beauchamp, 1998).

Of the 23 species observed, only 17 manifested interspecific interaction behaviors with other bird species. The Eurasian Coot and Tufted Duck represented the species with the most observed total interactions, manifesting three of four interaction types. At the same time, the Black-headed Gull and Yellow-legged Gulls (*Larus michahellis*) were the species where we observed all four interaction types (Fig. 6). The Little Egret (*Egretta garzetta*) and the Grey Heron (*Ardea cinerea*) were observed to interact very rarely and only with one interaction type (Fig. 6).

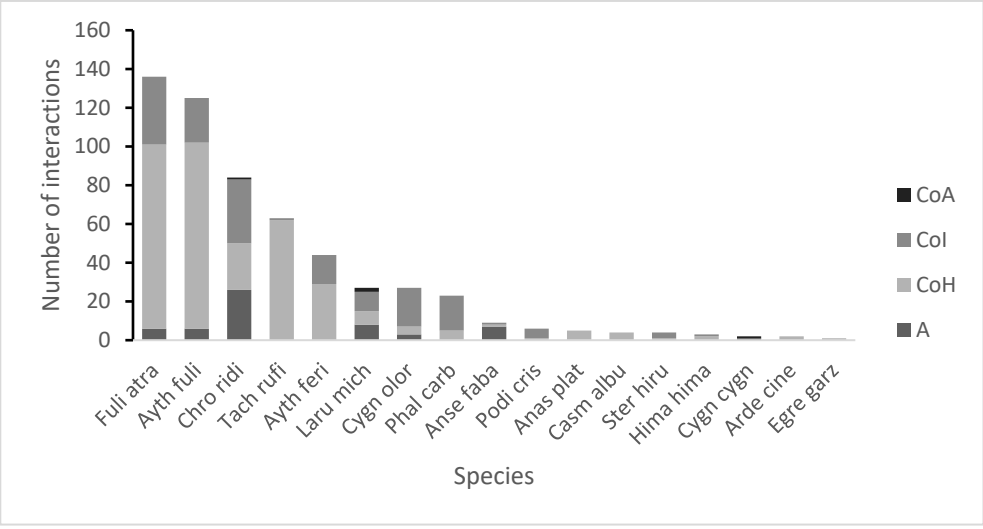

Figure 6. Total number of interspecific interactions and proportion of each interaction type per bird species observed during the passage, overwintering, and reproduction period 2022-2023. (CoA – cooperation for aggression, CoG – cooperation for grooming, CoF – cooperation for feeding, A – aggression)

We analyzed the species' preferences during interactions and concluded that the Tufted Duck had significantly more interactions as an instigator than the Great Crested Grebe, the Common Moorhen, the Mallard, and the Grey Heron (Fig. 7). The Eurasian Coot had significantly more interactions as instigator than Common Moorhens, Great Egrets and Mallards. Black-headed Gulls had significantly more interactions as instigators than Moorhens and Great Egrets (Fig. 7). Tufted Ducks consume aquatic plants at the bottom of the basin, and they are excellent divers, but spend less time the longer they dive (Stephenson *et al.*, 1986). Moreover, they spend most of their time feeding (Sutherland, 2009), similar to coots. An important result of the present study is the finding of a link based on continuous cooperation between Coots and Tufted Ducks between December and April, different trophic niches representing a plausible explanation for this result. Analyzing the ecology of coots, it has been shown that they spend ¾ (about 70%) of their time feeding to cope with intensive metabolic processes (Baaziz and Samraoui, 2008; Benlaharche and Boulakhssaim, 2018), but also that they feed more often in disturbed environments (Hafner *et al.*, 2004). The feeding behavior of the species has been documented in numerous studies (Horsfall, 1981; Draulans and Vanherck, 1987; Irwin and O'Halloran, 1997; Alouche, 1988; Pelsy-Mozzimann, 1999; Tamiser and Dehorter, 1999), from which we can describe 3 types of feeding: on the surface, through short-term diving or "grazing" (when the coots consume plant material from the shore); in early and mid-winter they forage on the surface and from February they start grazing on shore grasses, which is more energy efficient (Cramp and Simmons, 1980), also in preparation for the mating season.

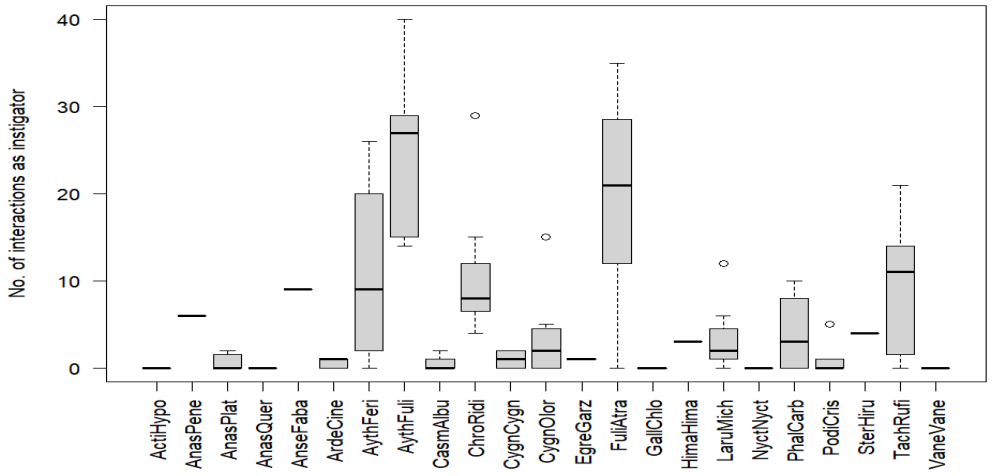

Figure 7. Number of interactions observed for each species in the role of instigator during eight months of observations. Boxplots represent the median (thick line inside the box), interquartile (box), minimum and maximum values (whiskers), and outliers (circles).

Thus, considering the time allocated to this behavior, but also the fact that coots are rarely aggressive during the winter period (Baaziz and Samraoui, 2008), it can be explained why it is the species that cooperates most often for food. Furthermore, their tendency to feed quantitatively more in autumn and less in winter (Paulus, 1988) has also been observed, intriguing in this context is the finding that coots tend to feed more so in environments where human influence is more intense (Hafner *et al.*, 2004).

In comparison to the rate of instigating behaviors manifested by the species, coots had significantly more interactions as reactors than Mallards, Grey Herons, Great Egrets, Moorhens, and Crested Grebes (Fig. 8). Coots had significantly more interactions as reactor than Great Crested Grebes, Common Moorhens, Great Egrets and Mallards. Black-headed Gulls had significantly more interactions as reactor than Mallards, Great Egrets and Common Moorhens (Fig. 8). Black-headed Gulls were present throughout the entire study period, the interspecific competition initiated by this species being based only on food, and after a period of feeding, their aggressiveness decreases significantly, so the seagulls do not have preferences for the places where they groom. Thus, a study that aimed to analyze the effects of the vegetation structure on Black-headed Gulls shows that the number of aggressions increases when the species is in an area with sparse and tall vegetation, with aggression occurring mainly in juveniles (Bukacińska and Bukaciński, 1993). Also, territory size has been shown to be influenced by interspecific interactions (Orians and Willson, 1964; Murray, 1971), so aggression could secure a territory in the case of interspecific competition (Reed, 1982). The most attacks initiated by this species were recorded in October, with the number of interactions decreasing every month. A possible explanation is abundant food, which can cause intense competition due to niche overlap with other species (Dhondt, 2012). Moreover, it is possible that individuals choose places densely populated with other bird species precisely to find food sources, preferring to tolerate other species at any other time of the day but when feeding. The connection between this behavior and the feeding of the species is explained by the dynamics of grooming behaviors during the 8 months, the frequency of joint grooming with other species decreasing along with the amount of food available on Crişul Repede.

The components of the interaction behavior: "instigation" and "reaction" were strongly and significantly correlated (Spearman Rank correlation: Rho = 0.937, $P < 0.001$), meaning overall that species showing more interactions interacted in both roles equally. Overall, some species (Tufted Duck, Black-headed Gull and Eurasian Coot) manifest significantly more interactions than others (Figs. 7 and 8).

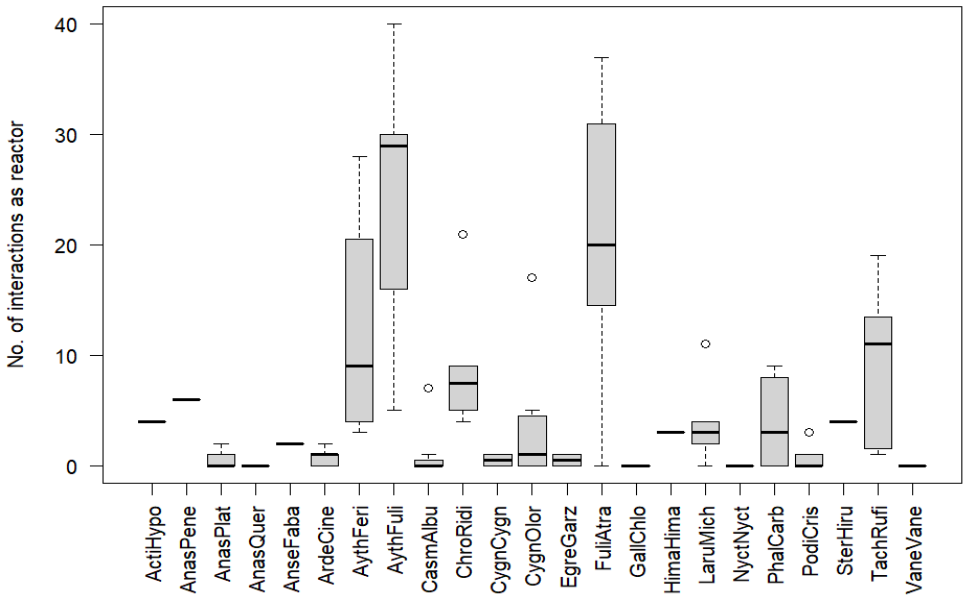

Figure 8. Number of interactions observed for each species in the role of reactor during eight months of observations. Boxplots represent the median (thick line inside the box), interquartile (box), minimum and maximum values (whiskers), and outliers (circles).

Considering all species and the whole observation period, the most frequent interaction observed was cooperation for feeding (CoF, 54.20% ± 37.51 SD), followed by cooperation for grooming (CoG, 30.07% ±30.74 SD), aggression (A, 12.28% ± 22.35 SD), and cooperation for aggression (CoA, 3.45% ± 12.13 SD). Tufted Ducks preferred to cooperate for feeding in 76.80% of the cases, while cooperation for grooming and aggression was observed in 18.40% and 4.80%, respectively. Black-headed Gulls was observed to perform a similar percentage of the interaction types CoG (39.32%,) A (30.95%,) and CoF (28.57). However, it also displayed cooperation for aggression (CoA, 1.19%) to a small extent. Eurasian Coots preferred to cooperate for feeding in 69.85% of the observed cases while also displaying cooperation for grooming (CoG, 25.74%) and aggression (A, 4.41%) to a smaller extent (Fig. 9).

We found a strong positive correlation between the number of individuals and the number of interactions in all species (Spearman's rank correlation: Rho = 0.62, $P < 0.001$), meaning that the more individuals were present on the lake, the more interactions we found, and is also the first indicator that individual densities tend to rule over species preferences.

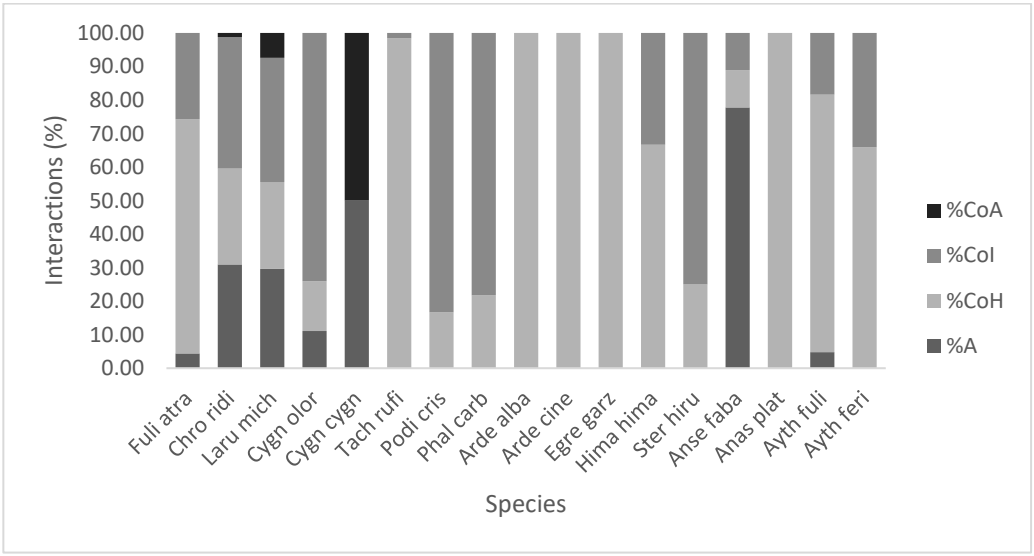

Figure 9. Barplot showing the percentage of interaction types performed by each species during the eight months of observations (CoA – cooperation for aggression, CoG – cooperation for grooming, CoF – cooperation for feeding, A – aggression).

For the three most interactive species (Eurasian Coot, Black-headed Gull, Tufted Duck), this relationship was also true with various correlation coefficients: Eurasian Coot– Spearman's rank correlation: Rho = 0.47, P = 0.002; Black-headed Gull – Spearman's rank correlation: Rho = 0.47, P = 0.002; Tufted Duck– Pearson's correlation: r = 0.36, P = 0.037.

We found no significant differences between months when all types of interactions were considered (Kruskal test: all P values > 0.05), which can be explained by the fact that abundant food in spring and summer does not generate interspecific competition, but the lack of food in winter should (DuBowy, 1988). However, since the temperatures during the winter of 2022 were abnormally high (up to 15^{0}C during the day), it is possible that more food sources, including smaller lakes that usually froze, became available to the species, leading to a similar quantity and quality of food throughout winter and spring/autumn. Moreover, we found no significant differences between months when just CoF was considered (Kruskal test: $\chi 2 = 10.50$, df = 7, P = 0.162), which supports our hypothesis.

For the most interactive species, we found no significant differences between the proportions of all types of interactions with other species (ANOVA or Kruskal test P > 0.05 in all cases), indicating there is no preference for interacting with a particular species in one specific way.

Conclusions

After observing the water bird community in the Afonul Peța part of the Crişul Repede river for 8 months, the 23 species engaged in 3 out of the 4 types of interactions we have analyzed. The most interactive species were the Eurasian Coot, Black-headed Gull and Tufted Duck, with the most often encountered interaction type being the cooperation for feeding (CoF), closely followed by cooperations for grooming, defence interactions being the rarest of all. Tufted Ducks and Eurasian Coots are the two most common instigators for interactions, while Coots and Black-headed Gulls are the main reactor species. Surprisingly, interactions did not differ significantly throughout the months and seasons, and species generally did not interact with a preferred species more than with the others. For future research, we believe that more studies should focus on interspecific interactions in water birds, especially using data from several years of study in the current context of climate change and global warming. Moreover, it would be beneficial for future studies to look at the community as a whole rather than to observe two of the species in the area, since it might provide a more cohesive view on the context of the interactions taking place in the area.

References

Abrams, P. A. (2001). Describing and quantifying interspecific interactions: A commentary on recent approaches. *Oikos. 94(2)*. 209–218. https://doi.org/10.1034/j.1600-0706.2001.940201.x

Arthington, A. H., Naiman, R. J., McClain, M. E., & Nilsson, C. (2009). Preserving the biodiversity and ecological services of rivers: New challenges and research opportunities. *Freshwater Biol*. *55(1)*. 1–16. https://doi.org/10.1111/j.1365-2427.2009.02340.x

Baaziz, N., Samraoui, B. (2008). The Status and Diurnal Behaviour of Wintering Common Coot Fulica Atra L in the Hauts Plateaux, Northeast Algeria. *Eur. J. Res. 23(3)*. 495-512

Beauchamp, G. (1998). The effect of group size on mean food intake rate in birds. *Biol. Rev. 73*. 449-72

Benlaharche, R., Boulakhssaim, M. (2018). The wintering behaviour of common coot Fulica atra L. in the Hauts Plateaux, Northeast Algeria. *Int. J. Bios. 12*. 230-241

Bibby, C. J. (2003). Fifty years of *Bird Study*. *Bird Study. 50(3)*. 194–210. https://doi.org/10.1080/00063650309461314

Birkhead, T. R., & Charmantier, I. (2009). History of Ornithology. In *eLS. John Wiley & Sons*, https://doi.org/10.1002/9780470015902.a0003096

Blaj, G., Szanto, Ş., Chira, I. (1979). Județele patriei. Bihor: Monografie. [in Romanian] Ed. *Sport-Turism*, Bucureşti, pp. 25–26

Bukacińska, M., & Bukaciński, D. (1993). The effect of habitat structure and density of nests on territory size and territorial behaviour in the black-headed gull (Larus ridibundus L.). *Ethology 94(4)*. 306–316. https://doi.org/10.1111/j.1439-0310.1993.tb00447.x

Chapman, B. B., Hulthén, K., Blomqvist, D. R., Hansson, L.-A., Nilsson, J.-Å., Brodersen, J., Anders Nilsson, P., Skov, C., & Brönmark, C. (2011). To boldly go: Individual differences in boldness influence migratory tendency. *Ecol. Lett. 14(9).* 871–876. https://doi.org/10.1111/j.1461-0248.2011.01648.x

Cote, J., Fogarty, S., Weinersmith, K., Brodin, T., & Sih, A. (2010). Personality traits and dispersal tendency in the invasive mosquitofish (*Gambusia affinis*). *P. Roy. Soc. B-Biol. Sci. 277(1687)*. 1571–1579. https://doi.org/10.1098/rspb.2009.2128

Cramp, S., Simmons, K.E.L. (1980). Handbook of the Birds of Europe, the Middle East and North Africa, Hawks to Bustards, Vol. 2. *Oxford University Press*. Oxford

Dhondt, A. A. (2012). Interspecific competition in birds. *Oxford University Press*. Oxford

Dhondt, A. A., Kempenaers, B., Andriaensen, F. (1992). Density-dependent clutch size caused by habitat heterogeneity. *J. Anim. Ecol. 61*. 643-8

Draulans, D., Vanherck, L. (1987). Food and foraging of Coot Fulica atra on fish ponds during autumn migration. *Wildfowl 38*, 63-69

DuBowy, P. J. (1988). Waterfowl Communities and Seasonal Environments: Temporal Variability in Interspecific Competition. *Ecology 69(5)*. 1439–1453. doi:10.2307/1941641

Ferrer, M., Newton, I., Casado, E. (2006). How to test different density-dependent fecundity hypothesis in an increasing or stable population. *J. Anim. Ecol. 75*, 111-17

Grimes, L. (2005). The state of the world's birds 2004: indicators for our changing world. BirdLife International, Cambridge, UK, pp. 73

Hafner, H., Johnson, A., Kayser, Y., Lefebvre, G., Mathevet, R., Pineau, O., Poulin, B., Sadoul, N., Barbraud, C. Tamisier, A., Isenmann, P. (2004). Les oiseaux de Camargue et leur habitat, Une histoire de cinquante ans 1954-2004, [in French]. *Meta-Éditions*, Paris

Horsfall, J. A. (1981). The time budget of the Coot Fulica atra. D. Phil. thesis, Oxford

Irwin, S., O'Halloran, J. (1997). The wintering behaviour of the Coot Fulica atra L. at Cork lough, South-west Ireland. *Biol. Environ. 97*, 157-162

Keller, I., Körner-Nievergelt, F., Jenni, L., & Suter, W. (2009). Within-winter movements: A common phenomenon in the Common Pochard (Aythya ferina). *J. Ornithol. 150(3)*, 501–510. https://doi.org/10.1007/s10336-009-0374-z

Lima, S. L. (1986). Predation risk and unpredictable feeding conditions: determinants of bodymass in birds. *Ecology 67*. 377-85

Lima, S. L. (1993). Ecological and evolutionary perspectives on escape from predatory attack: a survey of North-American birds. *Wilson Bull. 105*, 1-47.

Liordos, V., Kontsiotis, V. J. (2020). Identifying important habitats for waterbird conservation at a Greek Regional Nature Park. *Avian Res. 11*, Article 12. https://doi.org/10.1186/s40657-020-00224-7

Lohmann, K. J. (2018). Animal migration research takes wing. *Curr. Biol. 28(17)*. R952–R955. https://doi.org/10.1016/j.cub.2018.08.016

Măhăra, G., Chiriac, A., Bradu, M. (2010). Caracterizarea fizico-geografică. In: Monografia Judeţului Bihor. [in Romanian]. Ed. *Universităţii din Oradea*. Oradea. pp. 22-23

Martinez, J. A., Calvo, J. F., Martinez, J. E., Zuberogoitia, I., Zabala, J., Redpath, S. M. (2008). Breeding performance, age effects and territory occupancy in a Bonelli's Eagle Hieraaetus fasciatus population. *Ibis 150*, 223-33

Murray, B. G. (1971). The ecological consequences of interspecific territorial behavior in birds. *Ecology 52(3)*. 414–423. https://doi.org/10.2307/1937624

Orians, G. H., Willson, M. F, (1964). Interspecific territories of birds. *Ecology 45(4)*. 736–745. https://doi.org/10.2307/1934921

Paulus, S. L. (1988). Time-activity budgets of non-breeding Anatidae: a review. *University of Minnesota Press*, Minneapolis, pp. 135-152

Pelsy-Mozimann, F. (1999). Condition corporelle et stratégies d'hivernage des foulques macroules hivernant en Camargue: Isolement de deux Populations. [in French] PhD thesis. Université Lyon

Posea, A., Berindei, I., Măhăra, G., Pop, G. P. (1977). Crişul Repede. Ţara Beiuşului: Cercetări în Geografia României. [in Romanian]. Ed. *Ştiinţifică şi Enciclopedică*. Bucureşti. pp. 235–236

Posit team (2024). RStudio: Integrated Development Environment for R. Posit Software, PBC, Boston, MA. URL http://www.posit.co/

Pulliam, H. R., Caraco, T. (1984). Living in groups: is there an optimal group size?. In J.R. Krebs and N.B. Davies, *Behavioural Ecology: An Evolutionary Approach*. Oxford. 122-47.

Reed, T. M. (1982). Interspecific territoriality in the chaffinch and great tit on islands and the mainland of Scotland: Playback and removal experiments. *Anim. Behav. 30(1)*. 171–181. https://doi.org/10.1016/s0003-3472(82)80252-2

Rolls, R. J., Leigh, C., & Sheldon, F. (2012). Mechanistic effects of low-flow hydrology on riverine ecosystems: Ecological principles and consequences of alteration. *Freshw. Sci. 31(4)*. 1163–1186. https://doi.org/10.1899/12-002.1

Rushton, S. P., Hill, D., & Carter, S. P. (1994). The abundance of river corridor birds in relation to their habitats: A modelling approach. *J. App. Ecol. 31(2)*. 313. https://doi.org/10.2307/2404546

Stephenson, R., Butler, P. J., Woakes, A. J. (1986). Diving behaviour and heart rate in tufted ducks (*Aythya fuligula*). *J. Exp. Biol. 126(1)*. 341–359. https://doi.org/10.1242/jeb.126.1.341

Sutherland, I. T. (2009). Foraging behaviour of wild tufted duck *Aythya fuligula* in winter. *Wildfowl 59*. 53–61

Svensson, L. (2017). Ghid pentru Identificarea Păsărilor (2nd edition). [in Romanian]. Societatea Ornitologică Română

Telcean, I. C., Cupşa, D., Covaciu-Marcov, S. D., & Sas, I. (2007). The fishfauna of the Crişul Repede river and its threatening major factors. *Acta Agraria Debreceniensis (25)*. 13–18

Tickner, D., Opperman, J. J., Abell, R., Acreman, M., Arthington, A. H., Bunn, S. E., Cooke, S. J., Dalton, J., Darwall, W., Edwards, G., Harrison, I., Hughes, K., Jones, T., Leclère, D., Lynch, A. J., Leonard, P., McClain, M. E., Muruven, D., Olden, J. D., … Young, L. (2020). Bending the curve of global freshwater biodiversity loss: An emergency recovery plan. *BioScience 70(4)*. 330–342. https://doi.org/10.1093/biosci/biaa002

Zurell, D. (2017). Integrating demography, dispersal and interspecific interactions into bird distribution models. *J. Avian Biol. 48(12)*. 1505–1516. https://doi.org/10.1111/jav.01225

STUDIA UNIVERSITATIS BABEŞ-BOLYAI BIOLOGIA, 70, 1, 2025 (p. 303-326)
doi:10.24193/subbbiol.2025.1.14

MΦ macrophage – N0 neutrophil dialogue in the presence of TNF-α affects the endothelium

Sergiu-Marian Vatamanu[1]✉, Monica Țucureanu[2], Andreea Mihăilă[2], Elena Butoi[2] and Anca Farkas[1,3]

[1]Department of Molecular Biology and Biotechnology, Faculty of Biology and Geology, Babeș-Bolyai University, 400084 Cluj-Napoca, Romania; [2]Institute of Cellular Biology and Pathology "Nicolae Simionescu", 050568 Bucharest, Romania; [3]Centre for Systems Biology, Biodiversity and Bioresources, Babeș-Bolyai University, 400006 Cluj-Napoca, Romania.
✉Corresponding author, E-mail: sergiu.marian.vatamanu@stud.ubbcluj.ro

Article history: Received 31 March 2025; Revised 28 May 2025; Accepted 29 May 2025; Available online 25 June 2025

Abstract. Tumor necrosis factor-alpha (TNF-α) plays a pivotal role in the bi-directional dialogue between macrophages and neutrophils during the pre- and post- lesional stages of atherogenesis. This pro-inflammatory cytokine orchestrates a complex interplay between these immune cells, leading to the activation and recruitment of additional leukocytes, and the modulation of endothelial cell function, which collectively drive plaque formation and progression. Elevated levels of TNF-α result in the upregulation of adhesion molecules on the surface of endothelial cells. The cross-talk between macrophages and neutrophils, mediated by TNF-α, also leads to the release of soluble factors that have profound effects on the endothelium. Notably, these factors induce endothelial cell apoptosis via mechanisms involving caspase-3 activation, further contributing to the dysfunction and eventual denudation of the endothelial layer, a hallmark of atherogenesis. At molecular level, TNF-α exposure significantly upregulates the expression of pro-inflammatory mediators in macrophages, including interleukin-1 beta (IL-1β), inducible nitric oxide synthase (iNOS), and the activation of key signaling pathways such as the activation of mitogen-activated protein kinase (MAPK) signaling pathway and stress-activated protein kinase/c-Jun N-terminal kinase (SAPK/JNK). This bi-directional dialogue not only sustains chronic inflammation, but also amplifies the

pathogenic processes underlying atherosclerosis, suggesting that targeting TNF-α and its downstream effects could represent a therapeutic strategy to mitigate disease progression. In this study, we aimed at investigating the dialogue between macrophages and unpolarized neutrophils, by assessing the biomarkers leading to cells activation and their differentiation towards a pro-inflammatory phenotype. The effects of TNF-α were explored in the context of inflammation in the arterial wall, for a better understating of atherogenesis. The study results indicated a low intensity inflammatory response, characterized by the up-regulation of key molecules involved in cell signaling for differentiation towards an inflammatory phenotype but not in the production of significant amounts of cytokines and enzymes.

Keywords: atherosclerosis, endothelial cells, macrophages, neutrophils, TNF-α

Introduction

Atherosclerosis, a chronic inflammatory condition underlying cardiovascular disease, involves complex interactions between different types of cells in the arterial wall (Farahi *et al*., 2021). The two-way dialogue between macrophages and neutrophils is a crucial determinant of disease initiation and progression by vascular inflammation and atherosclerotic plaque development (Hansson *et al*., 2015). Macrophages and neutrophils, essential components of the innate immune system, contribute to atherosclerotic plaque formation by releasing cytokines, chemokines, and other signaling molecules (Hou *et al*., 2023; Zhang *et al*., 2023). Tumor necrosis factor-alpha (TNF-α), a key pleiotropic cytokine, plays a central role in regulating this dialogue, shaping the atherosclerotic microenvironment (Zhang *et al*., 2009; Gough *et al*., 2020).

TNF-α, a master regulator of inflammation, mediates and amplifies the macrophage – neutrophil crosstalk in atherosclerosis through its multiple effects. TNF-α modulates the adhesive interactions between these immune cells and the endothelium, promoting their recruitment to the inflamed arterial wall (Ikuta *et al*., 1991; Iademarco *et al*., 1995). TNF-α stimulates the secretion of pro-inflammatory factors and vascular adhesion molecules. In addition to atherosclerosis, this communication also plays a key role in myocardial infarction, following the hypoxic injury to the cardiac muscle (Tian *et al*., 2015).

Attracted by cytokines and cellular debris, the first cells to arrive at the site of the hypoxic injury are neutrophils, as they play an active role in promoting the initial phases of inflammation by secreting soluble factors and

reactive oxygen species (Frodermann *et al*., 2017; Horckmans *et al*., 2017; Chalise *et al*., 2021). Neutrophils sensitize the endothelium, favoring the migration of other immune cell types from the vascular compartment to the extravascular compartment (Dimasi *et al*., 2013). Circulating monocytes adhere to the endothelium and traverse the vascular compartment arriving in the subendothelial compartment, where they differentiate into resident macrophages, exposed to signaling molecules produced by neutrophils and cellular debris, further differentiating into a pro-inflammatory phenotype (Butterfield *et al.,* 2006; Čejková *et al*., 2016). The pro-inflammatory phenotype is characterized by the production of pro-inflammatory signaling molecules such as interleukin 1 beta (IL-1β), TNF-α, and inducible nitric oxide synthetase (iNOS). In addition, there are many other molecules with pro-inflammatory properties involved (Wang *et al*., 2020; Kadomoto *et al*., 2022).

The mechanisms involved in macrophage activation are intensively studied (Feng *et al*., 1999; Moore *et al*., 2010; Parameswaran and Patial, 2010), but not yet fully understood. It appears that a major role in macrophage activation is played by the transcriptional protein Nuclear Factor κB (NF-κB), which regulates gene expression of pro-inflammatory cytokines. NF-κB binds to specific DNA sequences in the promoter region of the target genes and stimulate or inhibit their transcription (Takashiba *et al*., 2010). Another key transcriptional factor involved in macrophage activation is activating protein-1 (AP-1) which is usually activated by the mitogen-activated protein kinase (MAPK) phosphorylation cascade, including the extracellular signal-related kinase (ERK) and the stress-activated protein kinase/c-Jun N-terminal kinase (SAPK/JNK) (Biggs *et al*., 1999; Rao, 2001). After the differentiation of macrophages towards a pro-inflammatory phenotype, there is a sudden increase in cytokine production. More interestingly, macrophages change their shape from round-like cells to a more spindle-like morphology, suggesting that pro-inflammatory macrophages might have migratory properties, which can lead to plaque microenvironment remodeling or some degree of subendothelial remodeling (Lee, 2019).

During the dynamic dialogue, after the secretion of cytokines, an amplification of the inflammatory response takes place due to the autocrine signaling effects of TNF-α on macrophages, which become even more activated (Xie *et al*., 1998). The soluble factors released by macrophages as well as by neutrophils have different effect on the endothelium, depending on the degree of resolution of the inflammatory processes in the subendothelial microenvironment (Xu *et al.,* 2022). At high concentrations, TNF-α exhibits cytotoxic effects on endothelial cells and on other immune cell types involved in atherogenesis (Larrick *et al*., 1990). Other authors have noticed that the exposure of endothelial cells to high

concentrations of cytokines leads to cell death by apoptosis. There is evidence suggesting that endothelial cell apoptosis is the main initiator of atherosclerotic plaque rupture and thrombus formation, as the non-thrombogenic surface of the blood vessel is disrupted (Polunovsky *et al*., 1994; Kavurma *et al*., 2005).

Despite extensive research, several gaps in knowledge related to the role of TNF- α in macrophage – neutrophil signaling remain to be elucidated. The cell-specific signaling pathways, the context-specific outcomes influencing the pro-inflammatory versus regulatory effects of the cytokine, the temporal dynamics and the crosstalk with other cytokines are underexplored research pathways, important for advancing therapeutic strategies.

The dialogue between macrophages and neutrophils, mediated by TNF-α, is particularly important for endothelial cells in atherosclerosis, since it directly affects endothelial integrity, activation and function. The immortalized line of human umbilical endothelial cells Ea.hy926 proved to be suitable for research of vein or artery endothelium in different pathologies (Deng *et al*., 2017). Recent investigations have shown that the dialogue between pro-inflammatory macrophages and smooth muscle cells found within the arterial wall leads to the remodeling of the vascular wall as a consequence of up-regulation of metalloproteases and production of extracellular matrix components by the smooth muscle cells, which leads to the narrowing of the lumen and the destabilization of the atherosclerotic plaque (Macarie et al., 2025). Other studies have shown that the dialogue between macrophages and neutrophils generates different outcomes depending on the phenotype of these cells at the time of the dialogue. Neutrophils from patients with different conditions are temporally polarized into pro-inflammatory (N1) and anti-inflammatory (N2) subpopulations. When exposed to activated neutrophils type N1, macrophages acquire a pro-inflammatory phenotype with improved efferocytotic properties, while exposure to soluble factors released by N2 neutrophils leads to an anti-inflammatory phenotype (Macarie *et al*., 2018; Mihăilă *et al*., 2024).

The present study aims to explore the molecular changes that takes place during the cross-talk between unpolarized neutrophils (N0) and resting macrophages (MΦ), to ascertain whether the secretome triggers an inflammatory response in endothelial cells. Also, for mimicking the inflammatory conditions found within the vascular wall in the atherosclerotic lesion site during the cross-talk, the cells were exposed to different concentrations of TNF-α or lipopolysaccharides (LPS) to further investigate the complex interplay and cellular differentiation towards a pro-inflammatory phenotype.

Materials and methods

Chemicals and reagents

Monoclonal antibodies, anti-iNOS (#2982), anti-NF-κB (#3033), anti-SAPK/JNK (#9252), anti-phosphorylated SAPK/JNK (#9255), anti-phosphorylated ERK1/2 (#4377), anti-caspase-3 (#9662) and anti-β-tubulin (#2146) were purchased from Cell Signaling Technologies (Danvers, Massachusetts, USA). Anti-ICAM-1 (710278) was purchased from Thermo Scientific (Waltham, Massachusetts, USA), anti-IL-1β (MAB 601) and anti-ERK1/2 (MAB1576) were procured from R&D Systems (Minneapolis, Minessota, USA), anti-TNF-α (SC-52746) was purchased from Santa Cruz (Dallas, Texas, USA), anti-caspase-1 (MAB-6215) was purchased from Novus Biologicals (Centennial, Colorado, USA). Human IL-1β ELISA kit (DuoSet) was purchased from R&D Systems (Minneapolis, Minnesota, USA). Human recombinant TNF-α and LPS were purchased from Sigma-Aldrich (St. Louis, Missouri, USA), culture media were provided by Corning Life Sciences (Corning, New York, USA) and Gibco (Waltham, Massachusetts, USA). Cell culture microplates were purchased from TPP AG (Trasadingen, Switzerland) and the co-culture inserts were from Falcon Plastics (Brookings, South Dakota). Other reagents and materials were from Sigma-Aldrich (St. Louis, Missouri, USA), Eppendorf (Hamburg, Germany), Bio-Rad (Hercules, California, USA), and Gibco (Waltham, Massachusetts, USA).

Cell cultures

THP-1, HL-60 and EA.hy926 cell lines used in this study were purchased from ATTC (American Type Culture Collection, Manassas, USA). Frequently used in cancer and drug research, THP-1 cells (ATCC TIB-202™) are immortalized human monocytes from the peripheral blood of a patient with acute monocytic leukemia. THP-1 cells were grown in suspension in RPMI-1640 culture media supplemented with 10% heat-inactivated FBS and were split 1:5 twice a week. Monocytes (1 x 10^6 cells) were plated in a 24-well plate and differentiated towards resting macrophages (МΦ) by exposure to 100 nM phorbol myristate acetate (PMA) for 3 days. As suggested by other authors (Butoi *et al*., 2016), PMA activation induces an unpolarized МΦ macrophage phenotype or a certain degree of classical activation (M1 phenotype). HL-60 (ATCC CCL-240™) is an immortalized line of pro myeloblasts isolated from a 36-year-old white woman with acute promyelocytic leukemia by leukapheresis. Briefly, HL-60 human neutrophils were grown in suspension in RPMI 1640 culture medium and were split 1:5 twice a week. Undifferentiated macrophages were co-cultured with neutrophils in RPMI-1640, without serum and antibiotics.

The entire co-culture system was exposed to different concentrations (10-100 ng/mL) of TNF-α or 1μg/mL LPS for 24h at 37°C and 5% CO_2. After 24h, the conditioned medium was collected under sterile conditions. EA.hy926 endothelial cells (ATCC CRL-2922™) were maintained in DMEM supplemented with 10% FBS and 1% PSA at 37°C under 5% CO_2. The cultures were starved of FBS 24h before exposure to conditioned medium. EA.hy926 cells were indirectly co-cultured using conditioned media resulting from macrophage – neutrophil cross-talk in the presence of TNF-α or LPS.

Experimental design: the co-culture system

Human neutrophils were plated on the filter inserts (lumenal side) in RPMI at a density of 10^6 neutrophils/insert. Human monocytes THP-1 were plated on the bottom of the transwell co-culture chamber (basolateral side) at a density of 10^6 cells/well and cultured in RPMI-1640 for macrophages differentiation, by exposure to 100 nmol/L PMA. After 3 days, the co-culture system was constructed by placing the inserts with neutrophils (N0) on the top of the microplate wells. The co-cultures were incubated for 24h at 37°C into an atmosphere enriched with 5% CO_2. Control groups were maintained in serum-free RPMI-1640. At the end of the cell co-culture period, the conditioned media resulting from the cross-talk was collected and used for further investigations and treatment of EA.hy926 endothelial cell monolayers.

The experimental groups were:

- MΦ: negative control group consisting of resting macrophages;
- MΦ + N0: resting macrophages co-cultured with unpolarized neutrophils;
- LPS: resting macrophages co-cultured with unpolarized neutrophils treated with 1 μg/mL LPS;
- LPS: resting macrophages co-cultured with unpolarized neutrophils treated with 10 ng/mL TNF-α;
- LPS: resting macrophages co-cultured with unpolarized neutrophils treated with 50 ng/mL TNF-α;
- LPS: resting macrophages co-cultured with unpolarized neutrophils treated with 100 ng/mL TNF-α.

Cell differentiation and microscopic evaluation

THP-1 cells were exposed to 100nM PMA for 72h to induce differentiation. After 24h of culture in the presence of PMA, the cells adhered to the polystyrene surface were examined by microscopy. Untreated endothelial cells and endothelial cells exposed to conditioned media from unpolarized macrophages (MΦ) were

used as negative controls. Experimental groups were exposed to conditioned media from TNF-α treated leucocytes (MΦ + N0). Cell morphology was examined under an DMi1 inverted microscope with phase contrast (Leica, Weltzar, Germany).

Western blot analysis

The protein expression of cytokines and other signaling molecules was assessed in the total extract of macrophages, neutrophils, and endothelial cells obtained by homogenizing the cells in Laemmli electrophoresis sample buffer (Sx2). Obtained cell lysates were incubated at 95°C for 5 minutes and then sonicated for 10 seconds on ice. The samples were kept on ice to inhibit protein degradation by exogenous and endogenous proteases. We determined the total protein concentration/sample by amido black staining and measured the absorbance using a microplate reader (TecanM200Pro) at 620 nm. 1µL of each sample was applied on a nitrocellulose membrane and then the membrane was washed with a fresh solution of 50% MeOH and stained for 10 seconds with 0.1% amido black solution. The obtained stained spots were collected in 400 µL 0.1M NaOH and vortexed for 10 seconds. Equal quantities of proteins were electroblotted through a 10% polyacrylamide gel and were then transferred onto a nitrocellulose membrane (Sigma-Aldrich, St. Louis, Missouri, USA). The membranes were blocked in 1% fish skin gelatin, 1% BSA, and 0.1% Tween-20 at room temperature for 1h before incubation with primary antibodies overnight at 4°C. Following washing three times with TBST, the membranes were incubated with the secondary antibody at room temperature for 1h. The following molecules were analyzed: pNF-κB, SAPK/JNK, ERK, iNOS, TNF-α for macrophages and VCAM-1, ICAM-1, vinculin, integrin αVβ5 and caspase-3 for endothelial cells, respectively. The blots were developed using SuperSignal West Pico chemiluminescent substrate (Thermo Fisher Scientific, Whaltman, Massachusetts, USA) and quantified by densitometry employing gel analyzer system Luminescent image analyzer LAS-4000 (Fujifilm, Tokyo, Japan) and ImageJ software version 1.54 (National Institutes of Health, Bethesda, Maryland, USA) (Schneider *et al*., 2012).

IL-1β quantification by ELISA

IL-1β antigens were quantified in the collected conditioned medium using the ELISA kit (R&D systems, Abingdon, UK), according to the manufacturer's instructions. Briefly, strips were coated with the capture antibody overnight at room temperature. Following incubation with the capture antibody, the strips were washed 3 times with washing buffer. Then, the plates were blocked with diluent reagent for one hour at room temperature. The detection antibody and

streptavidin HRP was added, and later, the substrate. After substrate addition, the plate was incubated in the dark at room temperature for 20 minutes, and the reaction was stopped using 2N H_2SO_4. Optical density of each well was read using a microplate reader (Tecan M200 Pro) at $\lambda = 450$ nm.

Statistical analysis

All experiments were performed in duplicates and statistics was applied using the Microsoft Office 2017 Excel software. The data obtained were expressed as mean values ± standard deviation (SD). For ELISA, statistical evaluation was carried out by one-way ANOVA followed by Dunnett's multiple comparisons test using GraphPad Prism version 10.0.0 for Windows, GraphPad Software (Boston, Massachusetts, USA).

Results

The present study explored the dialogue between unpolarized neutrophils and macrophages, by assessing the biomarkers leading to cells activation and their differentiation towards a pro-inflammatory phenotype. In this regard, EA.hy926 endothelial cells were exposed to the conditioned media resulting from macrophage – neutrophil cross-talk and various concentrations of TNF-α. The experimental design was based on a co-culture system using HL-60 neutrophils and resting macrophages (MΦ) differentiated from THP-1 monocytes, respectively (Figure 1A).

Microscopic evaluation of activated leucocytes and endothelial cells

Cell differentiation and activation was assessed microscopically. THP-1 cells grow in suspension and do not adhere to the plastic surface of the culture plates. To induce terminal differentiation to unpolarized MΦ macrophages or partially polarized toward an M1 pro-inflammatory phenotype, THP-1 cells were exposed to PMA. After 24h of culture in the presence of PMA, the cells adhered to the polystyrene surface of the cell culture plate and showed a specific spindle-like morphology, suggesting the activation and change in phenotype (Figure 1B). Microscopic evaluation revealed the formation of apoptotic bodies in the experimental groups treated with conditioned media from TNF-α treated leucocytes (Figure 1C). The presence of apoptotic cells in the endothelium monolayer suggested that the conditioned medium from the macrophage – neutrophil dialogue contained soluble pro-apoptotic signaling molecules that could affect the endothelial cells by promoting apoptosis. These images

demonstrate the hallmark sequential features of apoptotic cells detected by phase-contrast microscopy, including blebs, echinoid spikes, and surface blisters (Willingham, 1999) (Figure 1D).

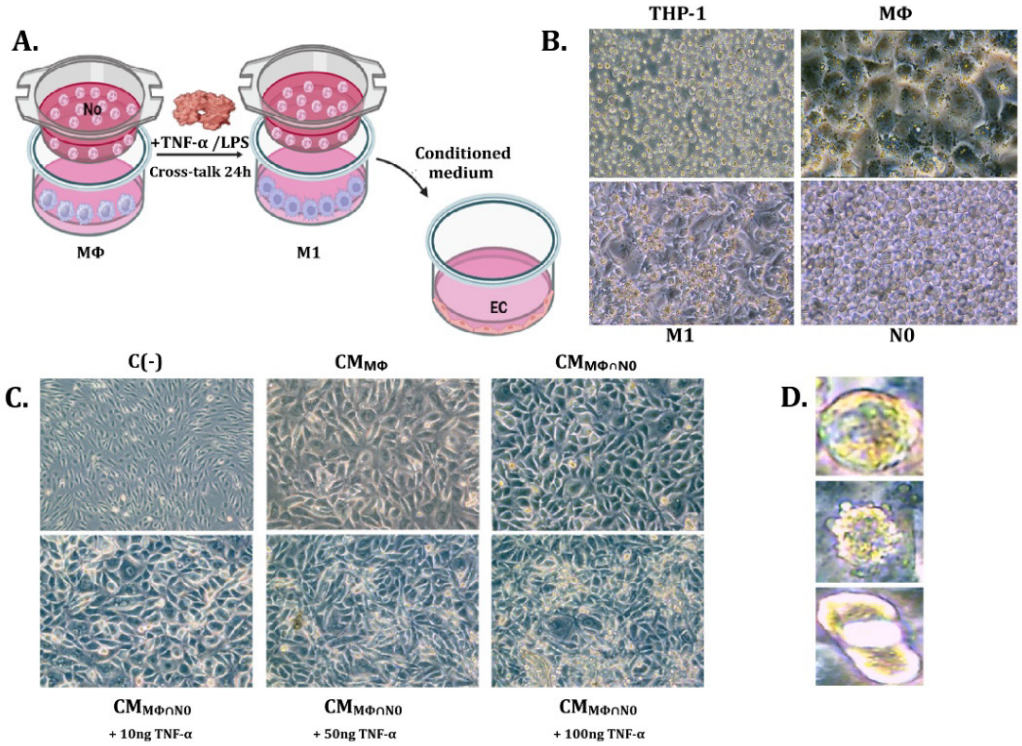

Figure 1. A. Co-culture design: endothelial cells (EC) were exposed to the conditioned media resulting from macrophage – neutrophil cross-talk and various concentrations of TNF-α or lipopolysaccharides (LPS). **B.** Induction of differentiation of THP-1 cells by PMA stimulation. THP-1 cells were incubated for 24h without or with 100 nM PMA. Undifferentiated macrophages were polarized towards an inflammatory phenotype (M1) by exposure to neutrophils (N0) and different concentrations of TNF-α, observed in phase contrast microscopy. **C.** Endothelial cells show a specific spindle-shaped-like morphology in phase contrast microscopy. Morphology of macrophages at the end of the 24h co-culture with HL-60 neutrophils, revealed polarized, spindle-shaped macrophages suggesting the activation and change in phenotype. Microscopic aspects in phase contrast microscopy showing the accumulation and presence of apoptotic cells in the endothelium monolayer, suggesting that conditioned media (CM) coming from M/N dialogue contains soluble pro-apoptotic signaling molecules that can affect the endothelial cells by promoting apoptosis. **D.** Morphology of apoptotic bodies in endothelial cell culture: the images demonstrate sequential features of apoptotic cells, including blebs, echinoid spikes, and surface blisters, detected by phase-contrast microscopy.

Macrophage activation by soluble factors released after cross-talk and TNF-α exposure

To get an insight into the molecular mechanisms involved in macrophage activation, we determined the relative expression levels of NF-κB, ERK, and SAPK/JNK, proteins involved in the activation of genes encoding cytokines.

Our results showed that, compared to basal expression, the relative expression level of the phosphorylated nuclear factor κB (pNF-κB) is upregulated upon exposure to TNF-α. This increase in expression is proportional to the TNF-α concentration, indicating a dose-dependent relationship between NF-κB activation and the levels of TNF-α. In the context of macrophage – neutrophil interaction, there is a slight up-regulation, exhibiting high variability. Additionally, LPS does not seem to induce a stronger response than MΦ. Therefore, TNF-α is a potent activator of NF-κB, whereas LPS and N0 have a weaker effect on NF-κB activation in macrophages (Figure 2A).

The SAPK/JNK pathway also demonstrated significant activity under high concentrations of TNF-α, observed in the relative expression and activation levels of the p54 and p46 isoforms. For p54, an increase in phosphorylation was observed in the presence of TNF-α and LPS, with the highest upregulation occurring at 50 and 100 ng/mL TNF-α, suggesting a dose-dependent activation. Meanwhile, exposure to LPS and 10 ng/mL TNF-α resulted in a more moderate response. For p46, phosphorylation did not appear to be affected by TNF-α exposure, as expression levels remain similar across concentrations, with a slight decrease compared to MΦ. MΦ exhibited high variability, which may indicate a spontaneous activation of p46 in some replicates. Therefore, we found that p54 is more strongly activated in the context of macrophage – neutrophil interaction compared to p46. TNF-α and LPS significantly induced p54 activation, whereas p46 activation did not appear to be affected, suggesting that this subunit is either less active in this context or is regulated by alternative signaling pathways (Figure 2B).

In the case of ERK, the relative expression and activation levels of the ERK1 (p44) and ERK2 (p42) isoforms were investigated. ERK1 phosphorylation was not influenced by the cross-talk between macrophages and neutrophils or by exposure to TNF-α. Electrophoretic analyses revealed that the relative expression level of ERK1 does not exceed basal conditions, whereas ERK2 showed preferential activation. The interaction between macrophages and neutrophils appeared to significantly upregulate ERK2 activation. Additionally, LPS induced an inflammatory response that, while weaker, is still more pronounced than the basal expression level observed in MΦ macrophages. Moreover, ERK2 activation appeared to be dependent on TNF-α concentration. ERK pathway was prominently activated by TNF-α. Phosphorylation of ERK1/2 led to downstream effects that promote pro-inflammatory cytokine production

and contributed to the broader inflammatory response. The dose-dependent activation of the ERK pathway suggested that multiple signaling cascades are converging to amplify macrophage activation in response to TNF-α (Figure 2C).

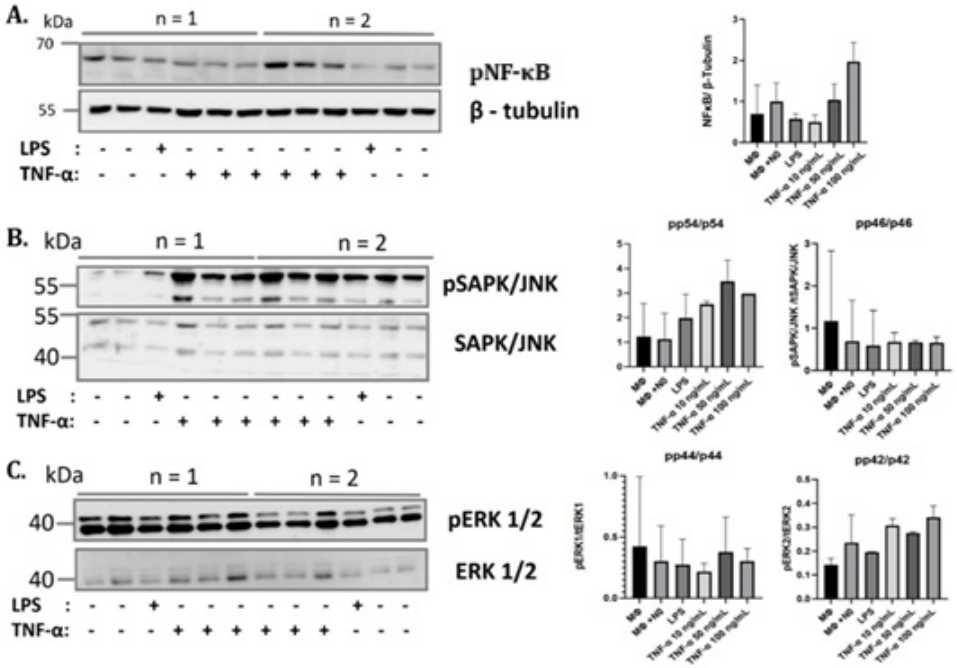

Figure 2. Relative expression levels of NF-κB (**A**), SAPK/JNK (**B**), ERK (**C**), in macrophages before and after exposure to neutrophils and TNF-α. p54 revealed a dose-dependent relationship based on the TNF-α concentrations between 10 and 50 ng/mL TNF-α. At 100ng/mL, TNF-α displayed cytotoxic effects which could interfere with the real expression level of p54. p46 did not exhibit the same pattern. ERK2 also showed the same dose-dependent pattern, while ERK1 did not. NF-κB was highly up-regulated after cross-talk and exposure to high TNF-α concentrations.

Macrophage identity and pro-inflammatory phenotype

For the analysis of macrophage activation, the relative expression levels of proinflammatory molecules characteristic to M1 macrophages were determined. Electrophoretic investigations revealed significant changes in the expression levels of key pro-inflammatory markers, specifically iNOS and TNF-α, following cross-talk with neutrophils in the presence of varying concentrations of TNF-α. A dose-dependent increase in iNOS expression was observed in macrophages co-cultured with neutrophils under stimulation with different TNF-α concentrations,

indicating a strong induction of the macrophages' antimicrobial and inflammatory functions. At low TNF-α concentrations, iNOS levels showed a modest elevation compared to the control. Low TNF-α concentrations, neutrophils and LPS failed to induce a strong activation of iNOS, comparing to basal levels. TNF-α production by macrophages significantly increased in response to the combined stimuli of neutrophil interaction and 10 ng/mL TNF-α exposure.

However, expression levels of TNF-α confirmed the autocrine signaling effect of macrophages (Figure 3). Overall, the study results revealed that macrophages, upon interacting with neutrophils and in the presence of TNF-α, exhibited a substantial upregulation of iNOS and TNF-α. The observed dose-dependent relationship with TNF-α concentration indicated that this cytokine plays a critical role in modulating macrophage identity towards a pro-inflammatory state.

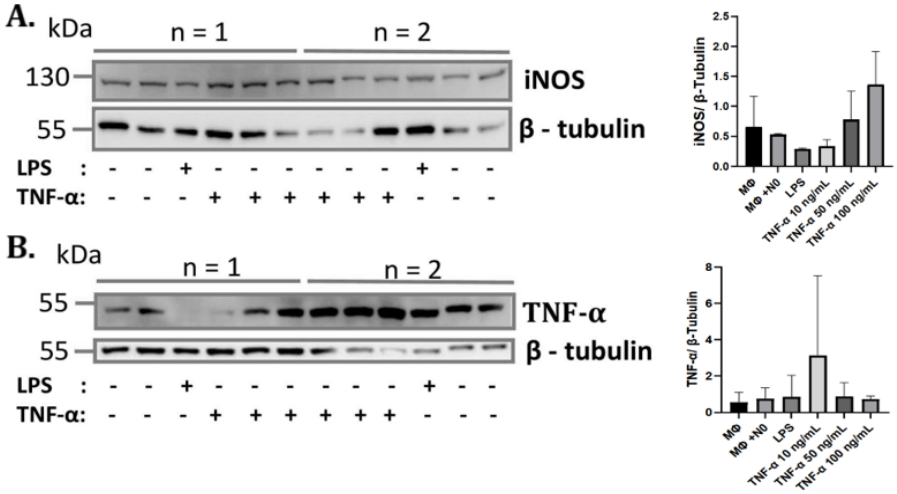

Figure 3. The relative expression levels of iNOS (**A**) are highly up-regulated in macrophages exposed to high TNF-α concentrations while TNF-α (**B**) is highly expressed in macrophages exposed to 10ng/mL TNF-α, as a peak of cytokine production after autocrine signaling effects of TNF-α.

We aimed to investigate the production of IL-1β in response to the cross-talk between macrophages and neutrophils, both in the presence and absence of TNF-α. THP-1 cells and immortalized neutrophils were co-cultured under various conditions, and IL-1β levels in the conditioned medium were quantified by ELISA assay. In the absence of TNF-α stimulation, both THP-1-derived macrophages and neutrophils did not produce IL-1β, indicating that neither cell type alone nor in co-culture without additional stimulation significantly induces IL-1β production. However, when macrophages were exposed to TNF-α, a modest increase in IL-

1β level was observed. This increase was more pronounced when macrophages were co-cultured with neutrophils (MΦ+N0), suggesting that the interaction between these cell types enhances IL-1β production, even under basal conditions. Interestingly, the production of IL-1β in response to TNF-α was not dose-dependent. Macrophages and neutrophils co-cultured and stimulated with 50 ng and 100 ng of TNF-α produced only slight increases in IL-1β levels. In contrast, the experimental group exposed to 10 ng TNF-α exhibited a substantial increase in IL-1β production, indicating a peak in cytokine release at this concentration (Figure 4). This suggested that there is an optimal concentration of TNF-α that maximally induces IL-1β production in this co-culture system.

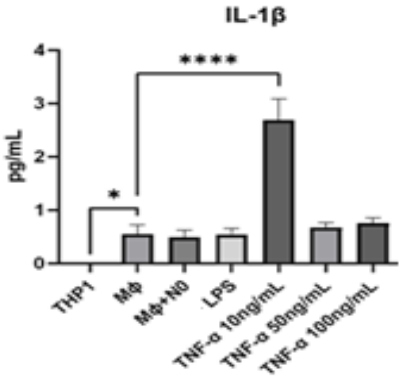

Figure 4. ELISA quantification of IL-1β revealed up-regulated levels of IL-1β in the case of macrophages co-cultured with neutrophils in the presence of 10 ng/mL TNF-α, this demonstrates a dose-dependent relation between IL-1β secretion and TNF-α concentration. Unstimulated macrophages and neutrophils showed little to no IL-1β production whereas for THP-1 cells there was no production of IL-1β. Data are expressed as the mean ± SD of three experiments for each set of experimental conditions * $p < 0.1$ and **** $p < 0.0001$ vs control.

Soluble factors released after the cross-talk enhance the adhesive properties of endothelial cells

Hypothesizing that the dialogue between the two cell types can lead to increased adhesion properties, we examined the relative protein expression levels of integrin αVβ5, VCAM-1, ICAM-1 and vinculin, well-known markers of cell adhesion. An increased expression of integrin αVβ5 in response to higher concentrations of TNF-α was observed (Figure 5A), suggesting that endothelial cells become more adhesive, promoting interactions with circulating immune cells or other cell types during inflammatory responses. VCAM-1, another critical adhesion molecule, is involved in the binding of leukocytes to the endothelium. Its upregulation was also observed (Figure 5B), further supporting the hypothesis

that TNF-α enhances endothelial cell adhesiveness through multiple pathways, reinforcing the role of endothelial cells in mediating inflammatory processes. Interestingly, ICAM-1, another adhesion molecule, did not show a significant change in expression levels despite the presence of TNF-α (Figure 5C). This could indicate a more selective or context-dependent role of ICAM-1 in TNF-α-induced adhesion processes, or perhaps that its expression is regulated by other factors or under different conditions. Vinculin also did not exhibit significant changes (Figure 5D). Therefore, we observed that while TNF-α upregulates integrin αVβ5 and VCAM-1, it might not directly affect the intracellular components linked to adhesion, such as vinculin, or that vinculin's role is more stable and less susceptible to modulation by TNF-α alone.

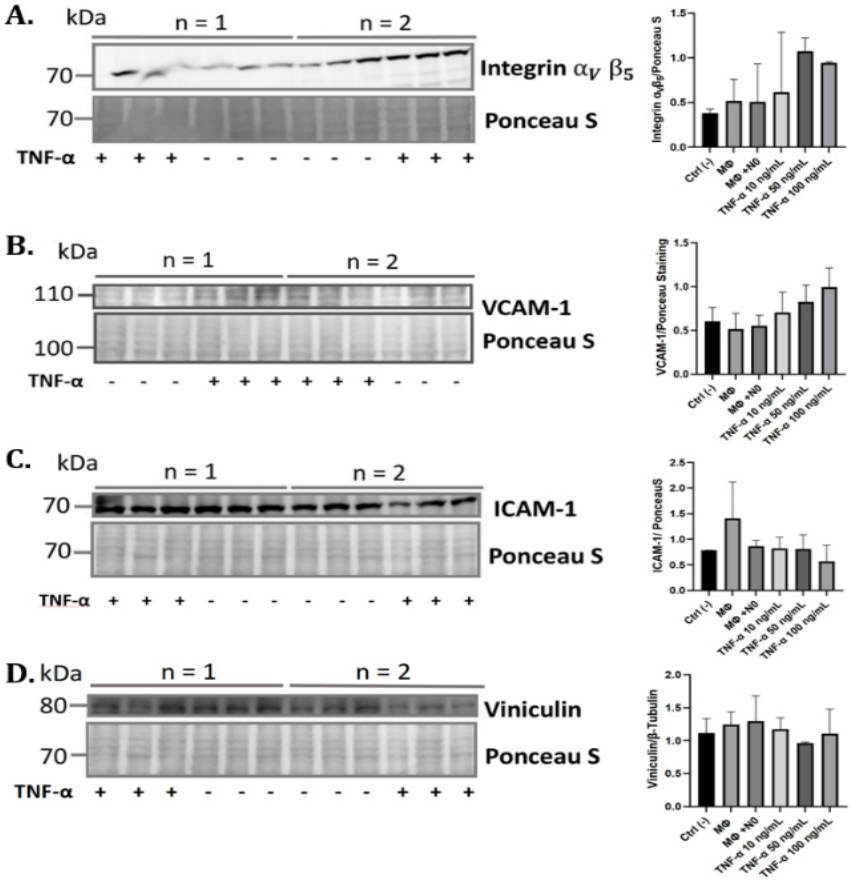

Figure 5. Electrophoretic investigations of endothelial cells exposed to the conditioned medium containing soluble factors released after the neutrophil-macrophage cross-talk revealed up-regulated levels of integrin αVβ5 (**A**), VCAM-1 (**B**), but not ICAM-1 (**C**) and vinculin (**D**).

The selective upregulation of integrins and VCAM-1 in response to TNF-α, without corresponding increases in ICAM-1 and vinculin, highlights the complex regulatory mechanisms governing endothelial cell adhesion. This selective enhancement of adhesion molecule expression may be crucial for the specific recruitment and attachment of leukocytes during inflammation, ensuring a targeted and efficient immune response. Additionally, these findings underscore the importance of considering the specific pathways activated by cytokines like TNF-α, as they may differentially regulate adhesion molecules and intracellular components involved in endothelial cell adhesion.

Soluble factors released after cross-talk induced apoptosis in endothelial cells

As a result of the bi-directional dialogue between macrophages and neutrophils, soluble factors are released by both cell types and they have major effects on the endothelium. Following this dialogue, in the presence or absence of TNF-α, these cell types undergo activation, and in particular, macrophages switch to a secretory phenotype releasing soluble cytokines. Our investigations showed that the conditioned culture medium contained TNF-α as a result of autocrine signaling of macrophages, IL-1β and iNOS. All three molecules exhibit profound effects on the endothelium. However, the dialogue between these cell types in an inactive state was not sufficient to induce a strong inflammatory response. The conditioned medium resulting from the classic dialogue still had effect on the endothelium, but its magnitude was not comparable to the effects produced by conditioned medium coming from co-cultures exposed to high concentrations of TNF-α. Endothelial cells exposed to high concentrations of TNF-α underwent cell death through a mechanism involving the activation of caspase-3 (Figure 6).

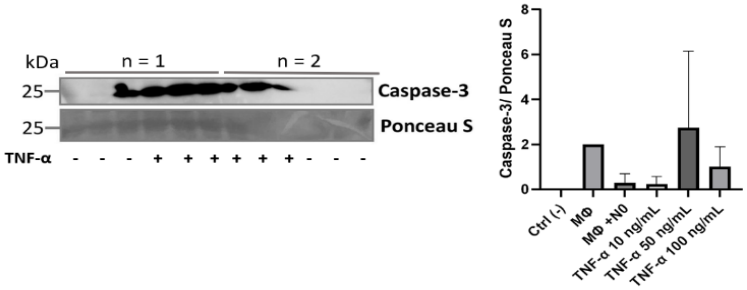

Figure 6. Electrophoretic investigations of the relative expression level of caspase-3 in endothelial cells exposed to conditioned medium derived from macrophage – neutrophil dialogue. It can be observed that upon exposure to conditioned media the endothelial cells present a sudden increase in caspase-3 levels at 50 ng/mL TNF-α, suggesting the activation of apoptotic pathways that would ultimately lead to endothelial cell death.

These results corroborate well with the microscopic observations showing an increase in the number of apoptotic bodies in endothelial monolayers, proportional with the increase of soluble factors released by the macrophage – neutrophil dialogue. Macrophage – neutrophil dialogue and TNF-α exposure induce endothelial cells apoptosis, suggesting that during the acute inflammatory stages of atherogenesis, the vessel lumen might suffer denudation leading to plaque instability and rupture.

Discussion

In this study, we demonstrated that the dialogue between macrophages with undecided fates and neutrophils leads to an inflammatory response in the presence of TNF-α, releasing pro-inflammatory molecules as a result of intracellular signaling processes that activate transcription factors controlling their expression.

The macrophages and neutrophils secretome, exerts pro-apoptotic and pro-inflammatory effects on endothelial cells. Macrophages, phagocytic cells of the innate immune system, originate from circulating monocytes that cross the vascular wall and reach the sub-endothelial space, where they differentiate (Moore *et al*., 2011). Upon exposure to stress factors, macrophages further differentiate into pro-inflammatory macrophages that release pro-inflammatory molecules into the extracellular space (Lee, 2019). These immune cells undergo morphological and functional differentiation upon exposure to soluble factors released by neutrophils and TNF-α (Parameswaran and Patial, 2010). The exposure triggers a signaling cascade that leads to macrophage activation, typically initiated by the interaction of TNF-α with the tumor necrosis factor receptor-1 (TNFR-1) expressed on the macrophage surface. Following ligand-receptor interaction, TNF receptor-associated death domain protein (TRADD) is recruited, along with an entire signal transduction complex, which interacts with NF-κB, leading to its activation (Hayden *et al*., 2014).

Our results show that NF-κB is activated upon exposure to neutrophils to LPS, and different concentrations of TNF-α, the activation being dose-dependent and proportional to TNF-α concentration. SAPK/JNK, a widely investigated kinase in the context of cellular signaling in inflammation (Dérijard *et al*., 1994; Yan *et al*., 2024) is involved in a phosphorylation cascade that activates transcription factors like c-Jun and c-Fos, which form the AP-1 complex that regulates cytokine gene expression (Yin *et al*., 2009). SAPK/JNK has two distinct isoforms, p54 and p46, encoded by different genes and presenting alternative splicing variants, that leads to high variability. p46 is more commonly associated

with fast responses, whereas p54 may have prolonged roles. Specifically, p54 is strongly activated by cellular stress, inflammation, and cytokines such as TNF-α and IL-1β, whereas p46 can be regulated by stimuli such as growth factors (EGF, NGF), cytoskeletal signaling via Rho GTPases, hypoxia, and metabolic stress (Chan *et al*., 1997). Both p54 and p46 can phosphorylate the same transcription factors (c-Jun, ATF2) but with varying efficiency. In some instances, p46 is more likely involved in cell survival, while p54 plays a greater role in apoptosis and inflammation. There is evidence that p46 may have spontaneous activity in macrophages differentiated from THP-1 cells, which may explain the high expression of p42 under basal conditions in our experimental design (Tournier *et al*., 2001). THP-1-derived macrophages express both p46 and p54, but their basal levels vary depending on the used stimuli (PMA, LPS, TNF-α). Additionally, it has been observed that p46 may exhibit higher basal activity than p54 in certain cell types, including macrophages (Tournier *et al*., 2000). Under specific conditions, p46 activation can occur without exogenous stimulation, for example, in the presence of FBS, which contains residual growth factors (Xia *et al*., 2000).

Regarding ERK, the activation of p44 (ERK1) and p42 (ERK2) isoforms is involved in a phosphorylation cascade and subsequently activates transcription factors (Wortzel and Seger, 2011). Although ERK1 and ERK2 are often considered functionally equivalent, recent findings (Wong *et al*., 2021) indicate that ERK2 plays a more dominant role in certain cellular contexts. ERK2 is more involved than ERK1 in cell proliferation and survival, which may be relevant in the context of TNF-α exposure as it induces both an inflammatory response and compensatory survival mechanisms. Higher ERK2 activity can be explained by the presence of the upstream kinase MEK1/2, which is influenced by TNF-α exposure and macrophage – neutrophil interactions (Trouba *et al*., 2004). Additionally, the lower ERK1 activity could be due to its transient presence or its degradation due to a highly regulated expression.

Our previous results showed that pro- or anti-inflammatory neutrophils can induce a pro- or anti-inflammatory profile of macrophages (Macarie *et al*., 2025). In the present study, we aimed to evaluate whether the dialogue between unpolarized macrophages and neutrophils could possibly lead to inflammation. To characterize the secretome resulting from macrophage – neutrophil dialogue in the presence of TNF-α, we evaluated the relative expression levels of hallmark pro-inflammatory molecules in macrophages, specifically iNOS and TNF-α.

iNOS is an enzyme involved in nitric oxide production, predominantly expressed in macrophages, endothelial cells, and hepatocytes in response to pro-inflammatory stimuli (Nathan and Xie, 1994). By producing NO, these enzymes contribute to vasodilation and increased vascular permeability. Besides its pro-inflammatory effects, iNOS can induce cell apoptosis through interactions with

free radicals (Nitsch *et al*., 1997). Unlike its counterparts eNOS and nNOS, which produce small, constitutive amounts of NO, iNOS generates large amounts of NO (Persichini *et al*., 2006). Our results showed that iNOS is strongly expressed by macrophages interacting with neutrophils and exposed to 50 or 100 ng/mL TNF-α, with a proportional increase in iNOS expression relative to TNF-α concentration.

TNF-α, the cytokine central to this study, is well known for both its pro-inflammatory and anti-inflammatory effects. However, in this context, a pro-inflammatory effect is evident. TNF-α expression is strictly controlled by NF-κB, which, once activated, stimulates TNF-α production and secretion, leading to autocrine signaling in macrophages that amplifies the inflammatory response via a feedback loop (Xaus *et al*., 2000). Additionally, NO activity from iNOS further enhances NF-κB activation, leading to even greater TNF-α expression. To characterize the secretome, we also quantified the relative level of IL-1β. Macrophages interacting with neutrophils and exposed to 10 ng/mL TNF-α produced the highest levels of IL-1β. However, overall IL-1β production remained low with minor variations. It was evident that N0, THP-1, and MΦ cells either did not express or expressed very low levels of IL-1β, while LPS and higher TNF-α concentrations induced a slight increase in IL-1β production. These findings indicate that the secretome resulting from macrophage – neutrophil dialogue contains pro-inflammatory molecules such as IL-1β, iNOS, and TNF-α. It is likely that this secretome includes additional pro-inflammatory molecules beyond those identified.

Based on previous determinations, we decided to explore the effects of IL-1β, TNF-α, and iNOS on the expression of cell adhesion molecules. After exposing endothelial cells to these pro-inflammatory conditions, which are also common in atherogenesis, we evaluated the relative expression levels of VCAM-1, ICAM-1, integrin αVβ5, and vinculin. Our results indicate that TNF-α plays a central role in regulating adhesion molecule and anchoring protein expression in endothelial cells exposed to macrophage – neutrophil dialogue. VCAM-1 and integrin αVβ5 were upregulated in a dose-dependent manner upon TNF-α exposure. We observed that endothelial cells treated with conditioned media from MΦ and MΦ+N0 exhibited lower VCAM expression than basal levels, possibly indicating either suppression of inflammatory effects due to the presence of anti-inflammatory molecules or a paradoxical effect of TNF-α. Unlike VCAM-1, ICAM-1 showed relatively stable expression levels, with increased expression only in response to conditioned media from MΦ, suggesting that MΦ secretes molecules that selectively induce ICAM-1 expression. Vinculin, a molecule involved in endothelial focal adhesions, interaction with extracellular matrix and cytoskeletal stability (James *et al*., 2024), exhibited relatively stable expression, suggesting that TNF-α does not dramatically affect the structure and organization of endothelial focal adhesion points. In the case of integrin αVβ5, we observed increased relative expression compared to the control and MΦ, with the conditioned

media from macrophage – neutrophil dialogue inducing a smaller increase compared to TNF-α alone. Integrins are transmembrane receptors that facilitate cell-extracellular matrix adhesion, as well as cell-cell interactions (Banerjee et *al*., 2022). However, low vinculin and ICAM-1 levels may also indicate an experimental design limitation, as decreasing expression could be artificial due to endothelial cell apoptosis induced by high concentrations of pro-inflammatory molecules and serum starvation. Recent studies also show that conventional 2D plastic culture systems are typically hypoxic, meaning that hypoxia, along with other factors, inevitably leads to cell death (Tan *et al*., 2024).

All these findings demonstrate that macrophage – neutrophil dialogue can lead to endothelial cell activation, while this cross-talk in the presence of TNF-α inevitably results in the upregulation of cell adhesion molecules. After data analysis and microscopic observations showing an accumulation of spherical, apoptotic cells, we decided to evaluate caspase-3 expression, a well-known apoptosis-related caspase. Our results indicate that caspase-3 is expressed in a TNF-α dose-dependent manner and that macrophage – neutrophil dialogue can induce apoptosis.

Conclusions

In this study, we aimed to mimic vascular inflammation conditions *in vitro* to investigate the cross-talk between macrophages and neutrophils. The secretome resulting from the interaction between these two immune cell types had significant effects on endothelial cells. Following cellular cross-talk and exposure to pro-inflammatory molecules, macrophages become activated through signaling pathways that lead to the phosphorylation of NF-κB, activation of SAPK/JNK, and ERK pathways and also differentiated into a pro-inflammatory phenotype characterized by increased expression and production of iNOS, TNF-α, and IL-1β. In the presence of TNF-α, VCAM-1 and integrin αvβ5 adhesion molecules were upregulated, while ICAM-1 and vinculin did not show significant changes. In addition to the increased expression of specific adhesion molecules, endothelial cells underwent apoptosis due to the cytotoxic effects of high TNF-α concentrations. This was confirmed both by microscopic examination and electrophoretic analysis of endothelial monolayers. Our study provides clear evidence that the cross-talk between the two immune cell types can lead to endothelial cell activation and even death. The outcomes of the study highlight the importance of the interaction and of the signaling molecule TNF-α as potential targets for the development of novel molecular therapies aimed at reducing arterial wall inflammation in various pathologies such as atherosclerosis.

Acknowledgements. This work was performed during a research stage of Vatamanu Sergiu Marian in Biopathology of Inflammation Laboratory, Institute of Cellular Biology and Pathology "Nicolae Simionescu" Bucharest under the guidance of Dr. Elena Butoi and with the help of Ph.D. Andreea Mihăilă and Ph.D. Monica Țucureanu.

Author contributions: S.M.V. and E.B. – conceptualization, experimental design; S.M.V., A.M. and M.Ț – methodology, analysis, data curation; S.M.V – original draft preparation; A.F. – supervision, writing.

References

Banerjee S, Nara R, Chakraborty S, Chowdhury D & Haldar S. (2022). Integrin regulated autoimmune disorders: Understanding the role of mechanical force in autoimmunity. *Front Cell Dev Biol*. 10, 852878. https://doi.org/10.3389/fcell.2022.852878

Biggs TE, Cooke SJ, Barton CH, Harris MP, Saksela K & Mann DA. (1999). Induction of activator protein 1 (AP-1) in macrophages by human immunodeficiency virus type-1 NEF is a cell-type-specific response that requires both hck and MAPK signaling events. *J Mol Biol.* 290, 21-35. https://doi.org/10.1006/jmbi.1999.2849

Butoi E, Gan AM, Tucureanu MM, Stan D, Macarie RD, Constantinescu C, Calin M, Simionescu M & Manduteanu I. (2016). Cross-talk between macrophages and smooth muscle cells impairs collagen and metalloprotease synthesis and promotes angiogenesis. *Biochim Biophys Acta*. 1863(7 Pt A), 1568-1578. https://doi.org/10.1016/j.bbamcr.2016.04.001

Butterfield TA, Best TM & Merrick MA. (2006). The dual roles of neutrophils and macrophages in inflammation: A critical balance between tissue damage and repair. *J Athl Train*. 41(4), 457-465.

Chalise U, Becirovic-Agic M & Lindsey ML. (2021). Neutrophil crosstalk during cardiac wound healing after myocardial infarction. *Curr Opin Physiol.* 100485. https://doi.org/10.1016/j.cophys.2022.100485

Chan ED, Winston BW, Jarpe MB, Wynes MW & Riches DW. (1997). Preferential activation of the p46 isoform of JNK/SAPK in mouse macrophages by TNF alpha. *Proc Natl Acad Sci USA.* 94(24), 13169-13174. https://doi.org/10.1073/pnas.94.24.13169

Čejková S, Králová-Lesná I & Poledne R. (2016). Monocyte adhesion to the endothelium is an initial stage of atherosclerosis development. *Cor et Vasa*. 58(4), e419-e425. https://doi.org/10.1016/j.crvasa.2015.08.002

Deng X, Zhang J, Liu Y, Chen L & Chao Y. (2017) TNF-α regulates the proteolytic degradation of ST6Gal-1 and endothelial cell-cell junctions through upregulating expression of BACE1. *Sci Rep.* 7, 40256. https://doi.org/10.1038/srep40256

Dérijard B, Hibi M, Wu IH, Barrett T, Su B, Deng T, Karin M & Davis RJ. (1994). JNK1: A protein kinase stimulated by UV light and Ha-Ras that binds and phosphorylates the c-Jun activation domain. *Cell* 76(6), 1025-1037. https://doi.org/10.1016/0092-8674(94)90380-8

Dimasi D, Sun WY & Bonder CS. (2013). Neutrophil interactions with the vascular endothelium. *Int Immunopharmacol.* 17(4), 1167-1175. https://doi.org/10.1016/j.intimp.2013.05.034

Farahi L, Sinha SK and Lusis AJ (2021). Roles of macrophages in atherogenesis. *Front Pharmacol.* 12, 785220. https://doi.org/10.3389/fphar.2021.785220

Feng GJ, Goodridge HS, Harnett MM, Wei XQ, Nikolaev AV, Higson AP & Liew FY. (1999). Extracellular signal-related kinase (ERK) and p38 mitogen-activated protein (MAP) kinases differentially regulate the lipopolysaccharide-mediated induction of inducible nitric oxide synthase and IL-12 in macrophages: *Leishmania phosphoglycans* subvert macrophage IL-12 production by targeting ERK MAP kinase. *J Immunol.* 163(12), 6403-6412

Frodermann V & Nahrendorf M. (2017). Neutrophil-macrophage cross-talk in acute myocardial infarction. Eur Heart J. https://doi.org/10.1093/eurheartj/ehw085

Gough P & Myles IA. (2020) Tumor necrosis factor receptors: Pleiotropic signaling complexes and their differential effects. *Front Immunol.* 11, 585880. https://doi.org/10.3389/fimmu.2020.585880

Hansson GK, Libby P, Tabas I. (2015). Inflammation and plaque vulnerability. *J Intern Med.* 278(5), 483-493. https://doi.org/10.1111/joim.12406

Hayden MS & Ghosh S. (2014). Regulation of NF-κB by TNF family cytokines. *Semin Immunol.* 26(3), 253-266. https://doi.org/10.1016/j.smim.2014.05.004

Horckmans M, Ring L, Duchene J, Santovito D, Schloss MJ, Drechsler M, Weber C, Soehnlein O & Steffens S. (2017). Neutrophils orchestrate post-myocardial infarction healing by polarizing macrophages towards a reparative phenotype. *Eur Heart J.* 38(3), 187-197. https://doi.org/10.1093/eurheartj/ehw002

Hou P, Fang J, Liu Z, Shi Y, Agostini M, Bernassola F, Bove P, Candi E, Rovella V, Sica G, Sun Q, Wang Y, Scimeca M, Federici M, Mauriello A & Melino G. (2023). Macrophage polarization and metabolism in atherosclerosis. *Cell Death Dis.* 14, 691. https://doi.org/10.1038/s41419-023-06206-z

Iademarco MF, Barks JL & Dean DC. (1995). Regulation of vascular cell adhesion molecule-1 expression by IL-4 and TNF-alpha in cultured endothelial cells. *J Clin Invest.* 95(1), 264-271. https://doi.org/10.1172/JCI117650

Ikuta S, Kirby JA, Shenton BK, Givan AL & Lennard TW. (1991). Human endothelial cells: effect of TNF-alpha on peripheral blood mononuclear cell adhesion. *Immunol.* 73(1), 71-76.

James J, Fokin AI, Guschin DY, Wang H, Polesskaya A, Rubtsova SN, Clainche CL, Silberzan P, Gautreau AM & Romero S. Vinculin-Arp2/3 interaction inhibits branched actin assembly to control migration and proliferation. *Life Sci Alliance*. 8(2), e202402583. https://doi.org/10.26508/lsa.202402583

Kadomoto, S, Izumi K & Mizokami A. (2022). Macrophage polarity and disease control. *Int J Mol Sci.* 23, 144. https://doi.org/10.3390/ijms23010144

Kavurma MM, Bhindi R, Lowe HC, Chesterman C & Khachigian LM. (2005). Vessel wall apoptosis and atherosclerotic plaque instability. *J Thromb Haemost*. 3(3), 465-472. https://doi.org/10.1111/j.1538-7836.2005.01120.x

Larrick JW & Wright SC. (1990). Cytotoxic mechanism of tumor necrosis factor-alpha. *FASEB J*. 4(14), 3215-3223. https://doi.org/10.1096/fasebj.4.14.2172061

Lee K. (2019). M1 and M2 polarization of macrophages: A mini-review. *Med Biol Sci Eng.* 2, 1-5. https://doi.org/10.30579/mbse.2019.2.1.1

Macarie RD, Tucureanu MM, Ciortan L, Vadana M, Mihaila A, Naie ML, Gan AM, Mandruteanu I & Butoi E. (2025). Molecular mechanisms of communication between innate immune cells and vascular cells in cancer and cardiovascular diseases. *SEE J Immunol*. 8. https://doi.org/10.3889/seejim.2025.6137

Macarie RD, Vadana M, Ciortan L, Tucureanu MM, Ciobanu A, Vinereanu D, Manduteanu I, Simionescu M & Butoi E. (2018). The expression of MMP-1 and MMP-9 is up-regulated by smooth muscle cells after their cross-talk with macrophages in high glucose conditions. *J Cell Mol Med*. 22(9), 4366-4376. https://doi.org/10.1111/jcmm.13728

Mihăilă A, Ciortan L, Tucureanu, M, Simionescu M & Butoi E. (2024). Anti-inflammatory neutrophils reprogram macrophages toward a pro-healing phenotype with increased efferocytosis capacity. *Cells* 13(3), 208. https://doi.org/10.3390/cells13030208

Moore KJ & Tabas I. (2011). Macrophages in the pathogenesis of atherosclerosis. *Cell.* 145(3), 341-355. https://doi.org/10.1016/j.cell.2011.04.005

Nathan C & Xie QW. (1994). Nitric oxide synthases: Roles, tolls, and controls, *Cell.* 78(6), 915-918. https://doi.org/10.1016/0092-8674(94)90266-6

Nitsch DD, Ghilardi N, Mühl H, Nitsch C, Brüne B & Pfeilschifter J. (1997). Apoptosis and expression of inducible nitric oxide synthase are mutually exclusive in renal mesangial cells. *Am J Pathol*. 150(3): 889-900.

Parameswaran N & Patial S. (2010). Tumor necrosis factor-α signaling in macrophages. *Crit Rev Eukaryot Gene Expr.* 20(2), 87-103. https://doi.org/10.1615/critreveukargeneexpr.v20.i2.10

Persichini T, Cantoni O, Suzuki H & Colasanti M. (2006). Cross-talk between constitutive and inducible NO synthase: An update. *Antiox Red Signal*. 8, 949-954. https://doi.org/10.1089/ars.2006.8.949

Polunovsky VA, Wendt CH, Ingbar DH, Peterson MS & Bitterman PB. (1994). Induction of endothelial cell apoptosis by TNFα: Modulation by inhibitors of protein synthesis. *Exp Cel Res.* 214(2), 584-594. https://doi.org/10.1006/excr.1994.1296

Rao KM (2001). MAP kinase activation in macrophages. *J Leukoc Biol.* 69(1), 3-10. https://doi.org/10.1189/jlb.69.1.3

Schneider CA, Rasband WS & Eliceiri KW. (2012). NIH Image to ImageJ: 25 years of image analysis. *Nat Methods*. 9, 671–675. https://doi.org/10.1038/nmeth.2089

Takashiba S, Van Dyke TE, Amar S, Murayama Y, Soskolne AW & Shapira L. (1999). Differentiation of monocytes to macrophages primes cells for lipopolysaccharide stimulation via accumulation of cytoplasmic nuclear factor kappaB. *Infect Immun*. 67(11), 5573-5578. https://doi.org/10.1128/IAI.67.11.5573-5578.1999

Tan J, Virtue S, Norris DM, Conway OJ, Yang M, Bidault G, Gribben C, Lugtu F, Kamzolas I, Krycer JR, Mills RJ, Liang L, Pereira C, Dale M, Shun-Shion AS, Baird HJ, Horscroft JA, Sowton AP, Ma M, Carobbio S, Petsalaki E, Murray AJ, Gershlick DC, Nathan JA, Hudson JE, Vallier L, Fisher-Wellman KH, Frezza C, Vidal-Puig A & Fazakerley DJ. (2024). Limited oxygen in standard cell culture alters metabolism and function of differentiated cells. *EMBO J*. 43(11), 2127-2165. https://doi.org/10.1038/s44318-024-00084-7 Erratum in: *EMBO J.* 43(19), 4439. https://doi.org/10.1038/s44318-024-00230-1

Tian M, Yuan YC, Li JY, Gionfriddo MR & Huang RC. (2015). Tumor necrosis factor-α and its role as a mediator in myocardial infarction: A brief review. *Chronic Dis Transl Med.* 1(1), 18-26. https://doi.org/10.1016/j.cdtm.2015.02.002

Tournier C, Hess P, Yang DD, Xu J, Turner TK, Nimnual A, Bar-Sagi D, Jones SN, Flavell RA & Davis RJ. (2000). Requirement of JNK for stress-induced activation of the cytochrome c-mediated death pathway. *Science.* 288(5467), 870-874. https://doi.org/10.1126/science.288.5467.870

Tournier C, Dong C, Turner TK, Jones SN, Flavell RA & Davis RJ. (2001). MKK7 is an essential component of the JNK signal transduction pathway activated by proinflammatory cytokines. *Genes Dev.* 15(11), 1419-1426. https://doi.org/10.1101/gad.888501

Trouba K & Germolec D. (2004). Micromolar concentrations of sodium arsenite induce cyclooxygenase-2 expression and stimulate p42/44 mitogen-activated protein kinase phosphorylation in normal human epidermal keratinocytes. *Toxicol Sci*. 79, 248-257. https://doi.org/10.1093/toxsci/kfh132

Wang Y, Zhao M, Liu S, Guo J, Lu Y, Cheng J & Liu J. (2020). Macrophage-derived extracellular vesicles: diverse mediators of pathology and therapeutics in multiple diseases. *Cell Death Dis.* 11(10), 924. https://doi.org/10.1038/s41419-020-03127-z

Willingham MC. (1999). Cytochemical methods for the detection of apoptosis. *J Histochem Cytochemistry.* 47(9), 1101-1109. https://doi.org/10.1177/002215549904700901

Wong E, Xu F, Joffre J, Nguyen N, Wilhelmsen K & Hellman J. (2021). ERK1/2 has divergent roles in LPS-induced microvascular endothelial cell cytokine production and permeability. *Shock.* 55(3), 349-356. https://doi.org/10.1097/SHK.0000000000001639

Wortzel I & Seger R. (2011). The ERK cascade: Distinct functions within various subcellular organelles. *Genes Cancer*. 2(3), 195-209. https://doi.org/10.1177/1947601911407328

Xaus J, Comalada M, Valledor AF, Lloberas J, López-Soriano F, Argilés JM, Bogdan C & Celada A. (2000). LPS induces apoptosis in macrophages mostly through the autocrine production of TNF-alpha. *Blood.* 95(12), 3823-3831. https://doi.org/10.1182/blood.V95.12.3823

Xia Y, Makris C, Su B, Li E, Yang J, Nemerow GR & Karin M. (2000). MEK kinase 1 is critically required for c-Jun N-terminal kinase activation by proinflammatory stimuli and growth factor-induced cell migration. *Proc Natl Acad Sci USA*. 97(10), 5243-5248. https://doi.org/10.1073/pnas.97.10.5243

Xie B, Laouar A & Huberman E, (1998). Autocrine regulation of macrophage differentiation and 92-kDa gelatinase production by tumor necrosis factor {alpha} via {alpha}5{beta}1 integrin in HL-60 cells. J Biol Chem. 273(19), 11583-11588. https://doi.org/10.1074/jbc.273.19.11583

Xu S, Lyu QR, Ilyas I, Tian XY & Weng J. (2022). Vascular homeostasis in atherosclerosis: A holistic overview. *Front Immunol.* 13, 976722. https://doi.org/10.3389/fimmu.2022.976722

Yan H, He L, Lv D, Yang J & Yuan Z. (2024). The role of the dysregulated JNK signaling pathway in the pathogenesis of human diseases and its potential therapeutic strategies: A comprehensive review. *Biomol.* 14(2), 243. https://doi.org/10.3390/biom14020243

Yin Y, Wang S, Sun Y, Matt Y, Colburn NH, Shu Y & Han X. (2009). JNK/AP-1 pathway is involved in tumor necrosis factor-alpha induced expression of vascular endothelial growth factor in MCF7 cells. *Biomed Pharmacother*. 63(6), 429-435. https://doi.org/10.1016/j.biopha.2009.04.045

Zhang H, Park Y, Wu J, Chen Xp, Lee S, Yang J, Dellsperger KC & Zhang C. (2009). Role of TNF-α in vascular dysfunction. *Clin Sci (Lond)*. 116(3), 219-230. https://doi.org/10.1042/CS20080196

Zhang X, Kang Z, Yin D & Gao J. (2023). Role of neutrophils in different stages of atherosclerosis. *Innate Immun.* 6, 97-109. https://doi.org/10.1177/17534259231189195

STUDIA UNIVERSITATIS BABEŞ-BOLYAI BIOLOGIA, 70, 1, 2025 (p. 327-336)
doi:10.24193/subbbiol.2025.1.15

Antimicrobial effects produced by gold nanoparticles obtained with extracts of *Allium sativum* and *Allium ursinum*

Ioana Andreea Barbu[1,2], Rahela Carpa[1,3]✉, Oana Maria Biro[4] and Marcel Pârvu[1]

[1] Faculty of Biology and Geology, Babes-Bolyai University, 1 M. Koganiceanu Str., 400084 Cluj-Napoca, Romania; [2] Doctoral School of Integrative Biology, Babes-Bolyai University, 400015 Cluj-Napoca, Romania; [3] Institute for Research-Development-Innovation in Applied Natural Sciences, Babes-Bolyai University, 30 Fântânele Str., 400294 Cluj-Napoca, Romania; [4] Faculty of Physics, Babes-Bolyai University, 1 M. Koganiceanu Str., 400084 Cluj-Napoca, Romania
✉***Corresponding author, E-mail: rahela.carpa@ubbcluj.ro.***

Article history: Received 16 May 2025; Revised 29 May 2025; Accepted 29 May 2025; Available online 25 June 2025

Abstract. Gold nanoparticles (AuNPs) obtained by green synthesis using plant extracts from the genus *Allium* have attracted significant scientific interest due to their potential applications as antimicrobial agents in the biomedical field. This study investigates the antimicrobial potential of AuNPs obtained by green synthesis using extracts of *Allium sativum* and *Allium ursinum*. These plant extracts are rich in sulfur compounds (allicin), flavonoids and polyphenols, which not only facilitate the formation of nanoparticles, but also confer them increased antimicrobial properties. The nanoparticles thus obtained were characterized by spectroscopic methods (UV-Vis) and were tested for antimicrobial activity. Microbiological tests performed *in vitro* demonstrated an antimicrobial activity of the nanoparticles against Gram-positive (*Staphylococcus aureus*) and Gram-negative (*Escherichia coli*) bacteria but also against *Candida albicans* and *Candida parapsilosis*. The results support the idea that gold nanoparticles functionalized with *Allium* extracts may constitute a promising alternative in the development of natural antimicrobial compounds with applications in medicine, the food industry and the pharmaceutical field.

Keywords: *Allium sativum, Allium ursinum,* antimicrobial, nanoparticles

Introduction

The synthesis of metal nanoparticles (NPs) often requires the use of toxic materials and high costs, limiting their clinical use. Nanoparticles of various multifunctional metals and metal oxides have been produced, such as gold, silver, platinum, zinc oxide, nickel oxide, iron oxide, cesium oxide, magnesium, and several others (Ezhuthupurakkal *et al.,* 2017; Cui *et al.,* 2021; Uddin *et al.,* 2021; Chowdhury *et al.,* 2025). Recently, green synthesis methods have helped to overcome these problems. Extracts from plants, algae, yeast, actinomycetes, fungi and even bacteria are used in green synthesis methods (Abdelsattar *et al.,* 2024; El-Gebalya *et al.,* 2024; Bogale *et al*., 2025). The use of metal oxide nanoparticle materials that possess antimicrobial characteristics presents a significant benefit: a better equilibrium between therapeutic benefits and adverse effects when compared to traditional antibiotics (Ma *et al.,* 2024). Plants contain a variety of therapeutically beneficial bioactive compounds or phytochemicals, such as alkaloids, flavonoids, terpenoids, saponins, amino acids, tannins, steroids, glycosides and polyphenols, vitamins, and minerals providing routes for the synthesis of easier and non-toxic nanoparticles (Tan *et al.,* 2023; Chowdhury *et al.,* 2025). Nanoparticles derived from noble metals like gold, silver, and platinum have been widely applied in various fields, including medicine, cosmetics, biological sensors, and catalysis (Yulizar *et al.,* 2017). Currently, nanoparticles of gold, iron, zinc, cobalt, and silver are widely utilized in the early diagnosis and treatment of various diseases caused by pathogens, viruses, and parasites. They also show significant potential in addressing refractory conditions such as cancer (Rabiee *et al.,* 2020; Baran *et al.,* 2023).

In plant-based synthesis methods, phytochemicals extracted from different plant parts—such as fruits, leaves, flowers, or roots—using either hot or cold extraction serve as reducing agents for metal ions while also stabilizing the metallic core. The synthesis process can be controlled by adjusting the ratio of reducing/stabilizing agents to metal salts, as well as modifying ambient conditions like temperature and pH. This allows the precise control of nanoparticle size and shape (Tan *et al.,* 2023).

Garlic (*Allium sativum*) has been valued since ancient times for its culinary, seasoning, medicinal, nutraceutical, and insecticidal properties. Traditional remedies utilizing garlic for various health conditions are well-documented across different cultures and historical texts. The health advantages of garlic arise from the combined effects of its complex chemical components. It is a rich source of essential minerals, including potassium, phosphorus, sulfur, zinc, selenium, and germanium, along with major amino acids and moderate amounts

of vitamins A and C (Suleria *et al.,* 2015, Subbanna *et al.,* 2020). Garlic is a rich source of bioactive compounds, particularly organosulfur compounds and thiols, which constitute up to 2.3% of its total nutritional composition. Allicin (allyl 2-propenethiosulfinate, diallyl thiosulfinate, or S-allyl cysteine sulfoxide) is the most abundant thiosulfinate in fresh garlic, making up approximately 70% (w/w). It is an unstable, volatile molecule formed through an enzymatic reaction catalyzed by alliinase, which converts its precursor amino acid into allicin (Suleria *et al.,* 2015).

Garlic extract and its isolated bioactive compounds serve as excellent reducing and capping agents in the synthesis of various metal and metal oxide-based nanoparticles. This effectiveness stems from garlic's rich composition of phytochemicals, particularly organosulfur compounds, which offer superior chemical interactions with metal and metal oxide components compared to other plant-based bioactives. A key advantage of nano-based formulations is their ability to release active ingredients gradually and in a controlled manner at the targeted site. The antimicrobial properties of garlic extract are primarily attributed to allicin, a highly abundant dithiosulfinate. Allicin modifies sulfhydryl groups, inhibiting essential sulfhydryl-containing enzymes in bacterial cells, ultimately leading to cell death (Subbanna *et al.,* 2020).

In addition to *A. sativum* extract, *A. ursinum* is also noteworthy. The allicin component of *A. ursinum* extract is comparable to that of garlic extract, giving it antimicrobial properties (Barbu *et al.,* 2023). Due to the proven antimicrobial properties of these extracts, but also to the numerous existing studies in which gold nanoparticles were synthesized using *A. sativum* extracts, this study aims the synthesis and testing gold nanoparticles using both extracts. To our knowledge, gold nanoparticles using hydroalcoholic extract of *A. ursinum* have not been tested before.

Materials and methods

Extracts preparation

Bulbs of *Allium sativum* were collected from a private garden, while leaves of *Allium ursinum* were gathered from the "Alexandru Borza" Botanical Garden in Cluj-Napoca. In both cases, samples were obtained from mature plants cultivated under natural conditions without any special treatment. The preparation of the extracts followed protocols previously described in the literature (Barbu *et al.,* 2023).

Au-Nanoparticles biosynthesis and characterization

For the gold nanoparticles synthesis, a protocol by Coman *et al*. (2013) was followed. 25 ml of a 0.2 mM $HAuCl_4x4H_2O$ solution was brought to a boil and 50 µl of *A. sativum* extract were added to the boiling solution under vigorous stirring. A rapid colour change could be observed in about 30s. The mixture was left to boil for another 5 minutes. In the case of *A. ursinum*, because of the difference in extract concentrations, 120 µl were added to the tetrachloroaurate solution and the mixture was left to boil for 15 minutes. The amounts were chosen based on author recommendations as well as several incremental tries starting at 30 µl for *A. sativum* and at 60 µl for *A. ursinum*, all these solutions having a blue colour and being deemed unstable (Coman *et al.,* 2013).

The *Allium* AuNPs were characterised through UV-Vis spectroscopy. The UV-Vis absoption spectra were recorded on a Jasco V-630 spectrophotometer. The measurements were performed in the 400-1000 nm wavelength range, with a spectral resolution of 1 nm, using quartz cuvettes with 1 cm optical path.

Antimicrobial activity

The antimicrobial activity of the nanoparticles was evaluated by disk-diffusion method against *Escherichia coli* ATCC 25922, *Staphylococcus aureus* ATCC 25923, and two *Candida* species: *Candida albicans* ATCC 10231 and *Candida parapsilosis* ATCC 22019 on Mueller–Hinton agar (MH) in which 5 mm wells were made using a sterile cut pipette tip. A 0.5 McFarland standard suspension of each pure microbial culture was evenly inoculated onto the agar surface using a sterile swab. Sterile cotton discs, 5 mm in diameter, were placed in the wells, and 150 µL of each AuNP suspension, along with 150 µL of 30% alcohol as a control, was pipetted onto the discs. Sulfamethoxazole, cefuroxime and voriconazole were used as controls. The plates were incubated at 37 °C for 24 hours, after which the zones of inhibition were measured. All tests were conducted in triplicate, and results are reported as the mean ± standard error (Barbu *et al.,* 2023).

Results

Characterization of AuNPs by UV-Vis spectrometry

The *A. sativum* AuNPs have a maximum peak at 539 nm, while the *A. ursinum* have the plasmonic band at 571 nm as shown in Figure 1. Both peaks are in accordance with the ones indicated in literature for gold nanoparticles, the red-shift indicating larger nanoparticles were formed with *A. ursinum* extract (Huang and El-Sayed, 2010). The *A. sativum* nanoparticles have a much

sharper peak, indicating less polydispersity than the *A. ursinum* ones, which have a broader band. The *A. ursinum* ones display a double colour in solution, indicating the possibility of existence of at least two different shapes that interact differently with light.

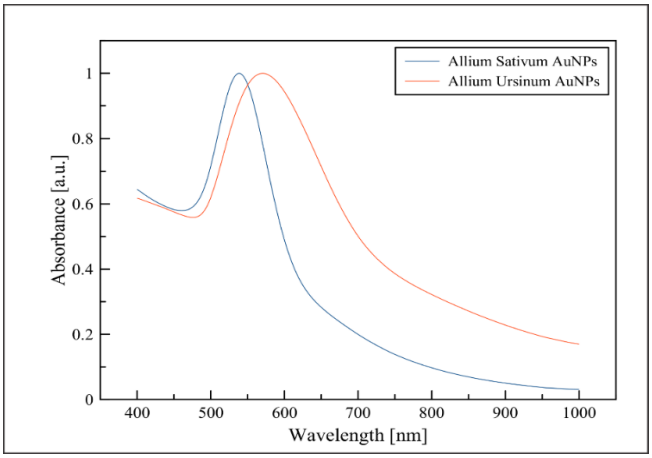

Figure 1. UV-Vis spectra of AuNPs biosynthesized using a bulb extract of *A. sativum* and leaves extract of *A. ursinum*

Stability of nanoparticles in time was assessed by comparing the UV-Vis spectra at day 0 and day 20. The broadening of the bands indicate the aggregation of the nanoparticles, and thus a lack of stability in time. The AuNPs from *Allium sativum* perform more effectively than those from *Allium ursinum*, which have almost completely dissolved within 20 days.

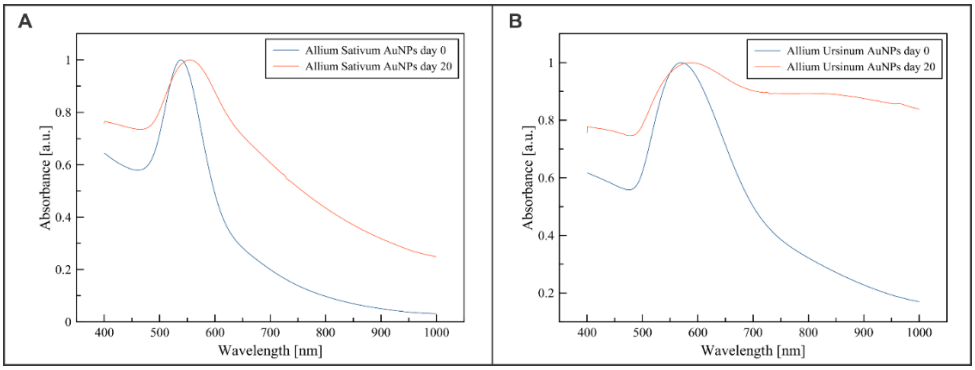

Figure 2. A. UV-Vis spectra of *A. sativum* AuNPs on day 0 and day 20; **B.** UV-Vis spectra of *A. ursinum* on day 0 and day 20.

Antimicrobial activity

Gold nanoparticles showed better effects on the two tested bacterial species than on the *Candida* species, as illustrated in Figure 3. The nanoparticles synthesized using *A. sativum* extract had similar effects on both bacterial species, with inhibition zones of 14 mm for *E. coli* and 13 mm for *S. aureus*. The effects on *E. coli* are even comparable to those of cefuroxime, used as a control. Nanoparticles obtained using *A. ursinum* extract showed weaker effects on S. aureus compared to sulfamethoxazole, used as control, with inhibition zones of 11 mm and 20 mm, respectively. For the two tested *Candida* species, the effects of the gold nanoparticles synthesized with both extracts were lower compared to voriconazole, used as control, showing inhibition zones of 7–8 mm versus 25–35 mm.

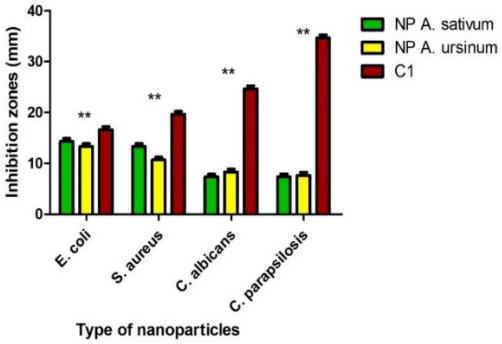

Figure 3. The antimicrobial effect of AuNPs obtained with *Allium sativum* and *A. ursinum* extracts on *S. aureus* (C1 – sulfamethoxazole), *E. coli* (C1 – cefuroxime), *C. albicans* and *C. parapsilosis* (C1 – voriconazole). The values represent the mean of three measurements ± standard deviation; ** $p < 0.005$, according to one-way ANOVA.

Discussion

Silver and gold nanoparticles, classified as noble metallic nanoparticles, have attracted significant attention due to their outstanding biological and physicochemical properties (Dauthal and Mukhopadhyay 2016; Saeed *et al.,* 2023).

In UV–Vis spectroscopy, the surface plasmon resonance (SPR) peak of gold nanoparticles typically lies between 510–580 nm, depending on size, shape, and surrounding medium (Huang and El-Sayed 2010). The red-shifted SPR band indicates larger or more irregularly shaped nanoparticles, consistent with findings from Sharma *et al.* (2009) and Jain *et al.* (2007) who showed that anisotropic AuNPs (e.g., rods, triangles) absorb light at higher wavelengths compared to spherical ones (Jain et al. 2007; Sharma, Yngard, and Lin 2009).

The *A. sativum*-AuNPs had a sharper and narrower peak, indicating a monodisperse or uniform size distribution. In contrast, the *A. ursinum* extract produced a broader, less defined peak, suggesting higher polydispersity. This finding aligns with previous results of Bastus *et al.* (2011), which demonstrated that monodisperse nanoparticles produce sharper SPR peaks, while heterogeneous mixtures result in broader bands. The phytochemical composition of *A. sativum* (especially the higher concentration of allicin and other sulfur-containing compounds) may have led to better capping and size control during nanoparticle formation (Bastús, Comenge, and Puntes 2011).

The *A. ursinum*-AuNP solution showed a dual color, suggesting a mixture of particle shapes. In literature, this is often linked to the presence of anisotropic nanoparticles, which can display multiple SPR modes. For instance, gold nanorods or triangular prisms can show both transverse and longitudinal absorption peaks, leading to solution colors ranging from violet to blue-green (Link and El-Sayed 2000). Mixed shapes can also arise when the reaction kinetics are slower or less controlled, possibly due to lower phytochemical concentrations or weaker reducing/stabilizing agents in *A. ursinum* (Huang & El-Sayed 2010).

The UV–Vis spectral analysis supports that both *Allium sativum* and *Allium ursinum* can mediate the green synthesis of gold nanoparticles, but with notable differences in nanoparticle characteristics. *A. sativum*-derived AuNPs exhibit smaller size, lower polydispersity, and greater homogeneity, likely due to more efficient capping and reducing action of its bioactive sulfur compounds. In contrast, *A. ursinum* results in larger, more diverse nanoparticle populations, possibly due to variations in phytochemical content or weaker stabilization capacity. These differences may influence the physicochemical behavior nanoparticles and biological activity, reinforcing the importance of extract composition in green nanoparticle synthesis.

The antimicrobial activity of gold nanoparticles (AuNPs) synthesized using *Allium* species extracts are similar to previous findings emphasizing previous studies emphasizing the broad-spectrum antibacterial potential of biogenic AuNPs, particularly against Gram-negative and Gram-positive bacteria. In this study, AuNPs showed greater efficacy against *E. coli* and *S. aureus* than against *Candida* species. Gabriel *et al.* (2022) tested different concentrations of nanoparticles with *Allium*, and their study showed that as the concentration increased, the inhibition zone also increased. At concentrations of 100 mg/mL, they obtained inhibition zones of 19 mm for *E. coli* and 17 mm for *S. aureus.* The results obtained in our study are comparable to those of Gabriel *et al.* (2022) at the concentration of 40 mg/mL (*S. aureus* 15 mm, *E. coli* 14 mm, and *S. aureus* 13 mm, *E. coli* 13 mm, respectively).

Meanwhile, AuNPs synthesized with *A. ursinum* extract exhibited a weaker antibacterial effect on *S. aureus* (11 mm inhibition zone), lower than that of sulfamethoxazole (20 mm). The lower efficacy may be linked to differences in nanoparticle characteristics, such as larger particle size or greater polydispersity, as inferred from the broader UV-Vis absorbance band observed in *A. ursinum*-derived AuNPs (Huang and El-Sayed 2010; Franci *et al.,* 2015). Larger or more polydisperse nanoparticles often show reduced antimicrobial potency due to decreased surface area-to-volume ratios and less efficient cellular interactions (Sondi and Salopek-Sondi 2004).

In contrast, both nanoparticle formulations demonstrated poor antifungal activity, with inhibition zones between 7–8 mm against *Candida* species, much lower than those observed with voriconazole (25–35 mm).

Conclusions

Our study confirms that biologically synthesized gold nanoparticles, especially those obtained with *A. sativum* extract*,* are promising antibacterial agents, but further optimization (e.g., size control, functionalization) may be necessary to enhance their antifungal and antibacterial effectiveness.

Acknowledgements. This research was funded by Babes-Bolyai University, the doctoral grant of Ioana Andreea Barbu.

References

Abdelsattar, A.S., Kamel, A.G., Eita, M.A., Elbermawy, Y., & El-Shibiny, A. (2024). The cytotoxic potency of green synthesis of zinc oxide nanoparticles (ZnO-NPs) using *Origanum majorana*. *Mat Lett,.* 367, 136654. https://doi.org/10.1016/j.matlet.2024.136654

Baran, M.F., Keskin, C., Baran, A., Hatipoğlu, A., Yildiztekin, M., Küçükaydin, S., Kurt, K.; Hoşgören, H.; Sarker, M.M.R.; Sufianov, A., Beylerli, O., Khalilov, R., & Eftekhari, A. (2023). Green Synthesis of Silver Nanoparticles from *Allium cepa* L. Peel Extract, Their Antioxidant, Antipathogenic, and Anticholinesterase Activity. *Molecules,* 28, 2310. https://doi.org/10.3390/molecules28052310

Barbu, I. A., Ciorîță, A., Carpa, R., Moț, A. C., Butiuc-Keul, A., & Pârvu, M. (2023). Phytochemical Characterization and Antimicrobial Activity of Several *Allium* Extracts. *Molecules*, 28 (10): 3980. https://doi.org/10.3390/molecules28103980

Bastús, N. G., Comenge, J., & Puntes, V. (2011). Kinetically Controlled Seeded Growth Synthesis of Citrate-Stabilized Gold Nanoparticles of up to 200 nm: Size Focusing versus Ostwald Ripening. *Langmuir J,* 27 (17): 11098–105. https://doi.org/10.1021/la201938u

Bogale, B.L., Adamu, T.B., Kebede, M.A., Ayana, M.T., Kebede, W.W., & Fetene T. (2025). Green and facile synthesis of silver nanoparticles (Ag NPs) using *Rhamnus prinoides* (Gesho) leaf extract for antibacterial, antioxidant and photocatalytic activities. *Next Nanotechnology, 7*: 100163 https://doi.org/10.1016/j.nxnano.2025.100163

Coman, C., Leopold, L. F., Rugină, O. D., Barbu-Tudoran, L., Leopold, N., Tofană, M., & Socaciu, C. (2013). Green Synthesis of Gold Nanoparticles by *Allium sativum* Extract and Their Assessment as SERS Substrate. *J Nanopart Res, 16* (1): 2158. https://doi.org/10.1007/s11051-013-2158-4

Chowdhury, M.A.S., Islam, M.M., Jamal, M. (2025). Green synthesis of nickel oxide nanoparticles using *Allium cepa* stalks and investigation of their antibacterial activity. *Results Chem, 16*, 102328. https://doi.org/10.1016/j.rechem.2025.102328

Cui, Z., Hu, J., Jiang, X., Zhang, D., Fang, C. (2021). Asymmetric Au/(PdAg alloy) nano-allium giganteums for their enhanced electrocatalytic performances to ethanol oxidation reaction*. J. Alloys Comp, 855*, 2, 157385. https://doi.org/10.1016/j.jallcom.2020.157385

Dauthal, P., & Mausumi, M. (2016). Noble Metal Nanoparticles: Plant-Mediated Synthesis, Mechanistic Aspects of Synthesis, and Applications. *Ind Eng Chem Res, 55* (36): 9557–77. https://doi.org/10.1021/acs.iecr.6b00861

El-Gebalya, A.S., Sofya, A.R., Hmeda, A.A., Youssef, A.M. (2024). Green synthesis, characterization and medicinal uses of silver nanoparticles (Ag-NPs), copper nanoparticles (Cu-NPs) and zinc oxide nanoparticles (ZnO-NPs) and their mechanism of action: A review. *Biocatal Agric Biotech, 55,* 103006. https://doi.org/10.1016/j.bcab.2023.103006

Ezhuthupurakkal, P.B., Polaki, L.R., Suyavaran, A., Subastri, A., Sujatha, V., Thirunavukkarasu, C. (2017). Selenium nanoparticles synthesized in aqueous extract of *Allium sativum* perturbs the structural integrity of Calf thymus DNA through intercalation and groove binding. *Mat Sc Eng C, 74*, 597–608. http://dx.doi.org/10.1016/j.msec.2017.02.003

Franci, G., Falanga, A., Galdiero, S., Palomba, L., Rai, M., Morelli, G., & Galdiero, M. (2015). Silver Nanoparticles as Potential Antibacterial Agents. *Molecules*, *20* (5): 8856–74. https://doi.org/10.3390/molecules20058856

Huang, X., & El-Sayed. M. A. (2010). Gold nanoparticles: Optical properties and implementations in cancer diagnosis and photothermal therapy. *J Adv Res*, *1* (1): 13–28. https://doi.org/10.1016/j.jare.2010.02.002

Jain, P. K., Huang, X., El-Sayed, I.H., & El-Sayed, M. A., (2007). Review of Some Interesting Surface Plasmon Resonance-Enhanced Properties of Noble Metal Nanoparticles and Their Applications to Biosystems. *Plasmonics, 2* (3): 107–18. https://doi.org/10.1007/s11468-007-9031-1

Link, S., & El-Sayed, M. A. (2000). Shape and size dependence of radiative, non-radiative and photothermal properties of gold nanocrystals. *Int Rev Phy Chem*, *19* (3): 409–53. https://doi.org/10.1080/01442350050034180

Ma, W., Zhu, G., Zhang, Y., & Guo, J. (2024). Green synthesis of ZnO NPs with long-lasting and ultra-high antimicrobial activity. *Surfaces and Interfaces, 50*, 104506. https://doi.org/10.1016/j.surfin.2024.104506

Rabiee, N., Mojtaba Bagherzadeh, Mahsa Kiani, Amir Mohammad Ghadiri, Kaiqiang Zhang, Zhong Jin, Seeram Ramakrishna, & Mohammadreza Shokouhimehr. (2020). High Gravity-Assisted Green Synthesis of ZnO Nanoparticles via *Allium ursinum*: Conjoining Nanochemistry to Neuroscience. *Nano Exp*, *1* (2): 020025. https://doi.org/10.1088/2632-959X/abac4d

Saeed, Z., Pervaiz, M., Ejaz, A., Hussain, S., Shaheen, S., Shehzad, B., & Younas, U. (2023). Garlic and ginger extracts mediated green synthesis of silver and gold nanoparticles: A review on recent advancements and prospective applications. *Biocatal Agric Biotech, 53,* 102868. https://doi.org/10.1016/j.bcab.2023.102868

Sharma, Virender K., Ria A. Yngard, & Yekaterina Lin. (2009). Silver Nanoparticles: Green Synthesis and Their Antimicrobial Activities. *Adv Colloid Interface Sc*, *145* (1–2): 83–96. https://doi.org/10.1016/j.cis.2008.09.002

Sondi, I., & Branka S.-S. (2004). Silver Nanoparticles as Antimicrobial Agent: A Case Study on *E. coli* as a Model for Gram-Negative Bacteria. *J Colloid Interface Sc*, *275* (1): 177–82. https://doi.org/10.1016/j.jcis.2004.02.012

Suleria, H. A. R., Masood, S.B., Nauman, K., Saira, S., Ali, R., Muhammad, A., & Munawar, A. (2015). Garlic (*Allium sativum*): Diet Based Therapy of 21st Century–a Review, *Asian Pac J Trop Dis, 5* (4): 271-278 https://doi.org/10.1016/S2222-1808(14)60782-9

Tan, G., Tevlek, A., & Aydin, H. M.. (2023). Comparison of garlic and onion extract-derived gold nanoparticles: Characterization and anticancer activity. *J Drug Deliv Sc Tech*, *84*, 104542. https://doi.org/10.1016/j.jddst.2023.104542

Uddin, S., Safdar, L. B., Anwar, S., Iqbal, J., Laila, S., Abbasi, B. A., Saif, M. S., Ali, M., Rehman, A., Basit, A., Wang, Y., & Quraishi, U. M. (2021). Green Synthesis of Nickel Oxide Nanoparticles from *Berberis balochistanica* Stem for Investigating Bioactivities. *Molecules*, *26*(6), 1548. https://doi.org/10.3390/molecules26061548

Yulizar, Y., Ariyanta, H. A., & Abduracman, L. (2017). Green Synthesis of Gold Nanoparticles Using Aqueous Garlic (*Allium sativum* L.) Extract, and Its Interaction Study with Melamine. *Bull Chem React Eng Catal, 12* (2): 212–18. https://doi.org/10.9767/bcrec.12.2.770.212-218